REPORT SERIES IN AEROSOL SCIENCE
N:o 163 (2015)

Proceedings of the 1st Pan-Eurasian Experiment (PEEX) Conference and the 5th PEEX Meeting

Editors: Markku Kulmala, Sergej Zilitinkevich, Hanna K. Lappalainen, Ella-Maria Kyrö and Jenni Kontkanen

Helsinki 2015

ISSN 0784-3496
ISBN 978-952-7091-16-6 (electronic publication)
Aerosolitutkimusseura ry – Finnish Association for Aerosol Research FAAR
http://www.atm.helsinki.fi/FAAR/

PREFACE

These are Conference Proceedings of the 1st Pan-Eurasian Experiment (PEEX) Conference and the 5th PEEX Meeting.
The Eurasian Pan-Eurasian Experiment (PEEX) is a multidisciplinary, multi-scale program focused on solving Grand Challenges in northern Eurasia and China focusing in arctic and boreal regions. It is a bottom-up initiative by several European, Russian and Chinese research organizations. The PEEX approach emphasises that solving challenges related to climate change, air quality and cryospheric change requires large-scale coordinated co-operation of the international research communities.

https://www.atm.helsinki.fi/peex/

Helsinki, February 2015

Markku Kulmala
Sergej Zilitinkevich
Hanna K. Lappalainen

TABLE OF CONTENTS

BUILDING THE METADATABASE OF PEEX OBSERVATIONAL INFRASTRUCTURE

P.K. ALEXEYCHIK[1], H. LAPPALAINEN[1]., N. ZAYTSEVA[2]., J. KUJANSUU[1] and T. PETÄJÄ[1]

[1]Department of Physics, University of Helsinki

[2]Institute of Geography, Russian Academy of Sciences

Keywords: PEEX, SITES, INFRASTRUCTURE, MEASUREMENTS.

INTRODUCTION

Pan-Eurasian Project (PEEX) is a joint multinational initiative in climate and environmental studies over the Eurasian continent (Kulmala et al. 2011, Lappalainen et al. 2014). The focus areas include the establishment of a coherent research infrastructure, forecasting the effects of the climate change and developing mitigation strategies for the Northern states. The infrastructure aspect of the project has a high priority as the foundation of all future activities. It is recognized that the observational and research infrastructure extent is very uneven across the PEEX domain, and that steps need to be taken in order to harmonize it.

MATERIALS AND METHODS

As the first approach to the problem of the infrastructure harmonization, the building of the PEEX metadatabase was begun. The metadatabase summarizes the observational facilities included in PEEX and provides details about their organization, measurement equipment and a number of other features. One of the important aspects of the metadatabase is the classification of the PEEX observational infrastructures according to their development in *atmospheric* and *environmental* directions. Each facility is assigned two numbers ranging from 0 to 3 depending on how equipped it is for the two classes of observational activities. Aerosol, meteorological and absolute concentration measurements contribute to the *atmospheric* rating, while the *environmental* rating is based on the sum of soil, vegetation and water observations.

RESULTS

The number of PEEX sites included at the moment is 284, most of which are classified according to the above-mentioned scheme (Figure 1). While the PEEX metadatabase is currently in preparation, its preliminary version already gives certain indications about the PEEX observational infrastructure. The general distribution of the sites can be assessed in comparison with the non-PEEX sites, included here for demonstrational purposes (Figure 2). This representation allows identifying the areas of higher or lower development of the infrastructure.

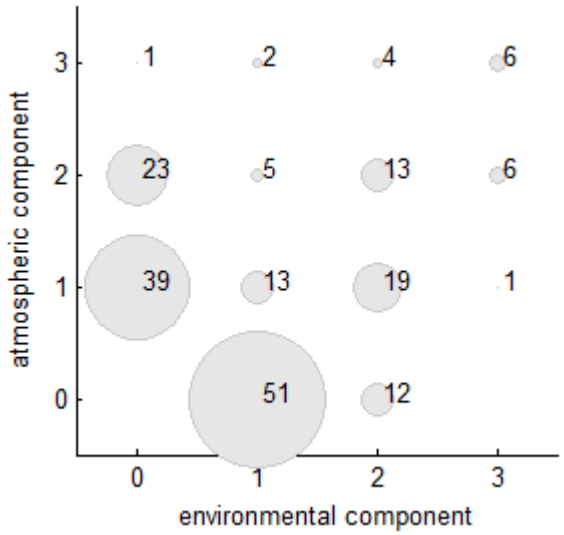

Figure 1. PEEX site classification according to the atmospheric and environmental components of the measurement equipment. The numbers indicate the of sites characterized by the development indices, with the circle sizes proportional to the site number.

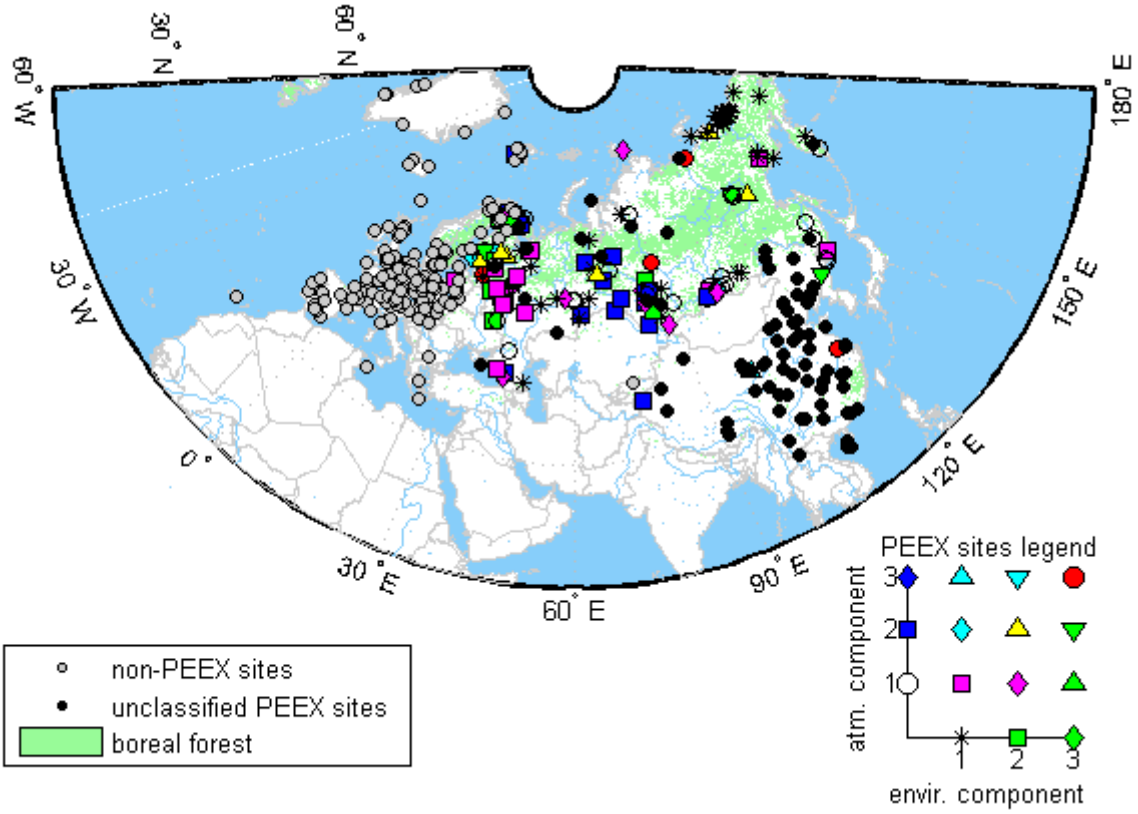

Figure 2. Spatial distribution of PEEX and non-PEEX sites in Eurasia.

The PEEX project encompasses a great expanse of land in Eurasia with good coverage in both the Southern and Northern latitudes (Figure 3).

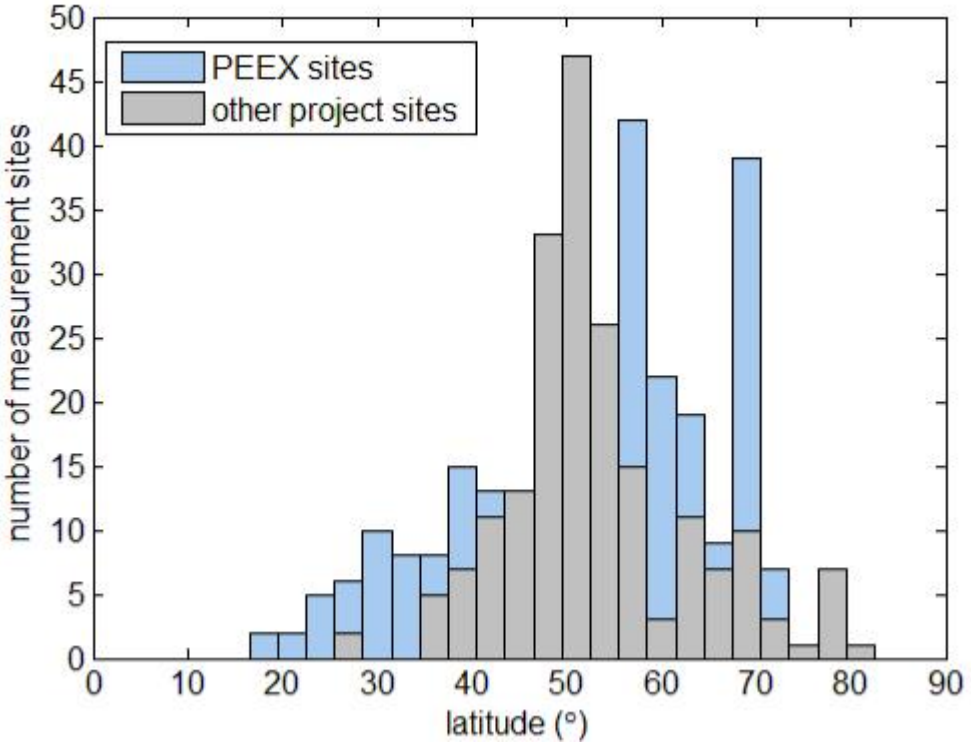

Figure 3. latitudinal distribution of PEEX and non-PEEX sites.

More detailed information can also be retrieved from the metadatabase, for example, the distribution of the sites with eddy-covariance systems (Figure 4) or aerosol observations (Figure 5).

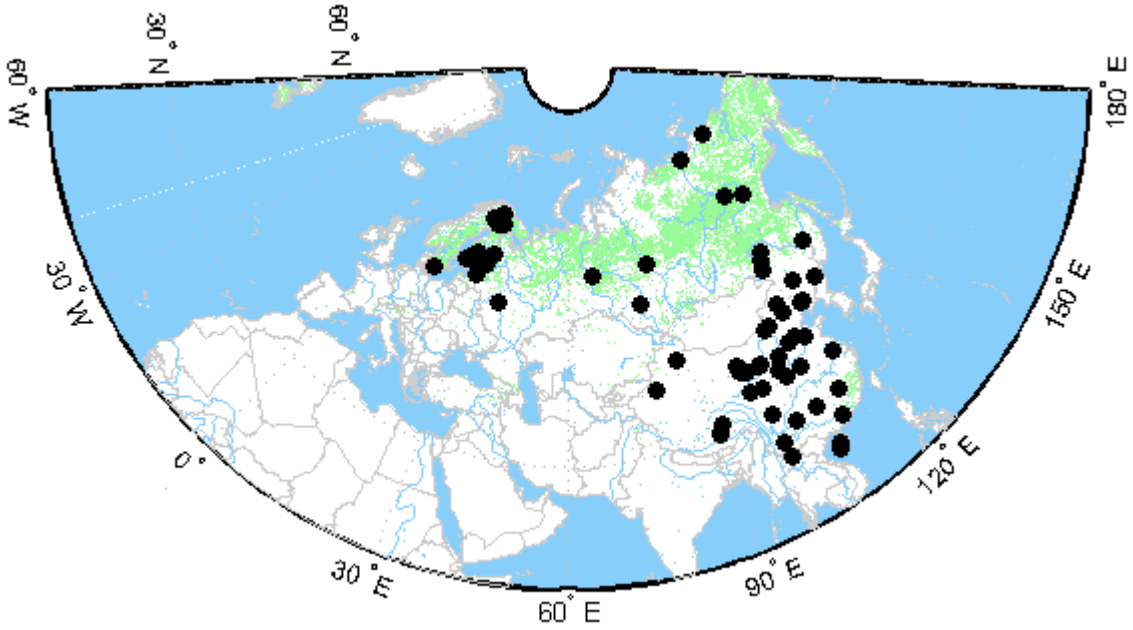

Figure 4. Spatial distribution of the PEEX sites equipped with eddy-covariance systems.

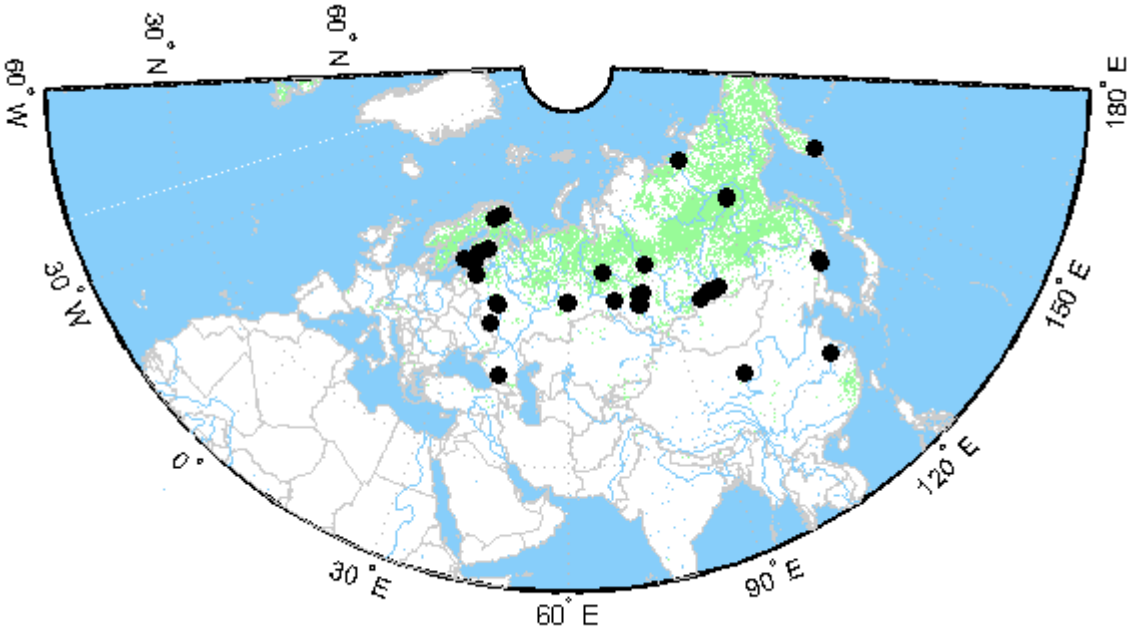

Figure 5. Spatial distribution of the PEEX sites equipped with aerosol measurement instruments.

REFERENCES

Kulmala M., Alekseychik P., Paramonov M., Laurila T., Asmi E., Arneth A., Zilitinkevich S. & Kerminen V.-M. (2011). On measurements of aerosol particles and greenhouse gases in Siberia and future research needs. *Boreal Env. Res*. 16: 337-362.

Lappalainen H., Petaja T., Kujansuu J., Kerminen V.-M., Shvidenko A. & Back J. (2014). Pan-Eurasian Experiment (PEEX) - a research initiative meeting the grand challenges of the changing environment of the northern Pan-Eurasian arctic-boreal areas . *J. Geography, Environment, Sustainability* 2(7): 13-48.

DYNAMICS OF THE ATMOSPHERIC BOUNDARY LAYER ELECTRICITY

S.V. ANISIMOV*, K.V. APHINOGENOV and S.V. GALICHENKO

Borok Geophysical Observatory IPE RAS, Borok, Yaroslavl region, 152742, RF

Keywords: ATMOSPHERIC ELECTRICITY, ATMOSPHERIC BOUNDARY LAYER, LIGHT AEROIONS CONCENTRATION.

INTRODUCTION

It is generally assumed that quasi-stationary state of the global electric circuit specified by permanent activity of thunderstorm generators, which make potential difference between electrodes of concentric-spherical capacitor founded by conductive layers of lower ionosphere, ocean upper layer and Earth's crust. Electrical state of the atmosphere depends of ionosphere potential, atmospheric column resistance, vertical electric current density, electric field strength, polar electric conductivities of air, thunderstorm electrical energy lifetime and vertical profiles of these electrical quantities. [Anisimov et al, 2008; Chalmers, 1974; Anisimov, 2003; Mareev et al, 2009; Roble et al, 1986; Williams, 2009; Anisimov et al, 2014b]. The sum of atmospheric electrodynamical processes includes electrical interaction both global and regional current systems, concentrated in near-ground atmospheric layer, planetary boundary layer, troposphere, middle atmosphere and different regions of ionosphere and magnetosphere [Anisimov et al, 2008]. Electrodynamics of middle latitude near-ground atmosphere forms as a sum of electrical charges separation, generation and transport physical processes in wide space-time scales range. The goal of this work aims at dynamics of electrical field and electrical conductivity of near-ground atmosphere investigation in wide time range, including turbulent aeroelectric pulsations, self-similarity characteristics and intermittency. Research base was founded by long-term amplitude-time series, wich were given as a result of high time resolution permanent stationary and field ground-based middle latitude aeroelectrical observations.

EXPERIMENTAL SETUP AND FILED GROUND-BASED OBSERVATIONS

Precision and reliable measurements of lower atmosphere electrical quantities are necessary basis of Earth electrical environment investigations. Borok Geophysical Observatory has implemented stationary observations of air electricity since 1985. Observatory investigations aimed at solving classical tasks of atmospheric electricity (such as investigations of annual, seasonal and diurnal variations) and development of new directions connected with investigation of global electric circuit, interactions of geospheric shells, aeroelectrical pulsations dynamics and geomagnetic field pulsations structures.

* Contact information: Sergey Anisimov, Borok Geophysical Observatory IPE RAS, Borok, Yaroslavl region, 152742, Russian Federation; E-mail: anisimov@borok.yar.ru

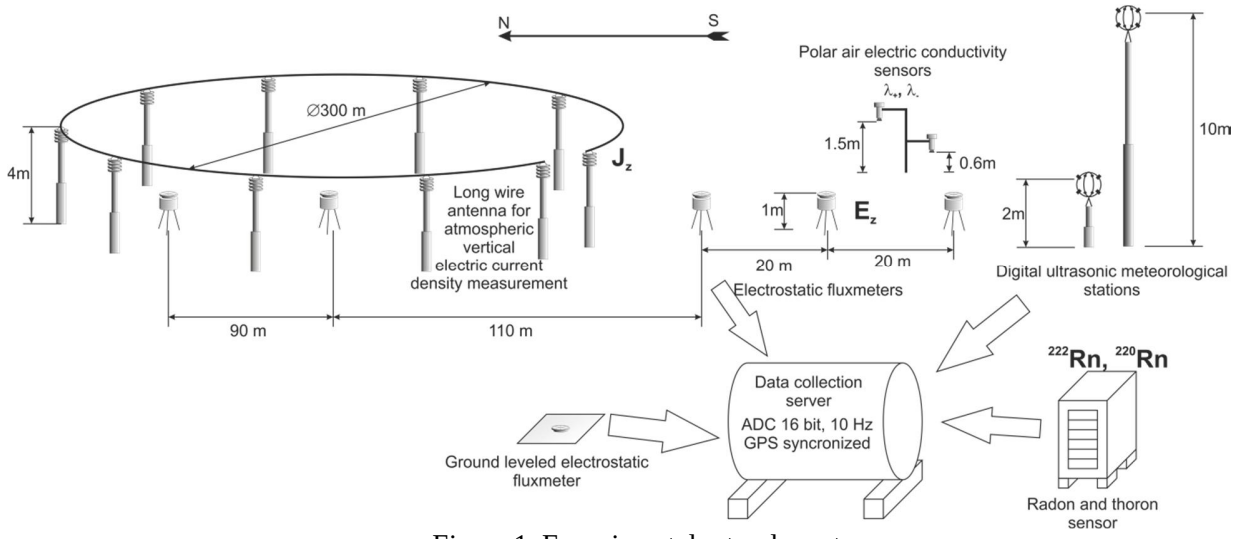

Figure 1. Experimental setup layout

Figure 1. shows the layout of experimental setup of summer seasonal observations of year 2013. Electrodynamical conditions of atmospheric surface layer were investigated by syncronous remote sensing of air electical field strength variations using electrostatic fluxmeters ("field mill"). Measurements were provided at experimental ground of Borok Geophysical Observatory IPE RAS (58°04'N; 38°14'E).

Five electric field strength sensors (electrostatic fluxmeter) were installed along a line south-north according to scheme at 1m height. One electrostatic fluxmeter was installed at a ground level for reduction ratio determination, wich was necessary to translate values of electric field strength measured at 1m height to equivalent values at the ground level. Vertical atmospheric electric current density was measured using a long-wire antenna (a current collector). The current collector represents a conductive ring of 300m in diameter mounted at insulators. Sensitivity of that current collector was not less than 0.1 pA/m^2. For the measurement of positive and negative electric air conductivities bipolar air conductivity sensors based on gerdien tube were used. Sensitivity of these sensors was not less than 0.1 fS/m, and air ion mobility range was more than 1.6 $cm^2/V{\cdot}s$. Field full-scale observations data were registered by the information collection system with 10 samples per second digitization rate.

Altitude profiles of wind velocity and direction were registered using an acoustic dopler locator (SODAR) "VOLNA-3" from 60m to 800m height and 5m resolution. The acoustic dopler locator works permanently in the stationary measurement complex of the observatory (Figure 2). Meteorological observations were realized using two digital ultrasonic meteorological units "METEO-2H" installed on heights 2m and 10m above a ground surface. Meteorological units provide true data with 10 samples per second rate. Measurement of solar irradiance in wavelength interval from 300nm to 2800nm the Kipp&Zonen CMP3 pyranometer was used. Sensitivity of the pyranometer is 5-20 $\mu V/(W/m^2)$ and measurement range is 0-2000 W/m^2. Monitoring of radon (^{222}Rn) and thoron (^{220}Rn) volume activity was realized using seismic radon station "SRS-05". Sensitivity of the radon station is not less than $0.5{\cdot}10^{-4}$ $Bq{\cdot}s^{-1}{\cdot}m^{-3}$. Measurement range is $20\text{-}5{\cdot}10^{4}$ Bq/m^3. Averaging time is 30 minutes.

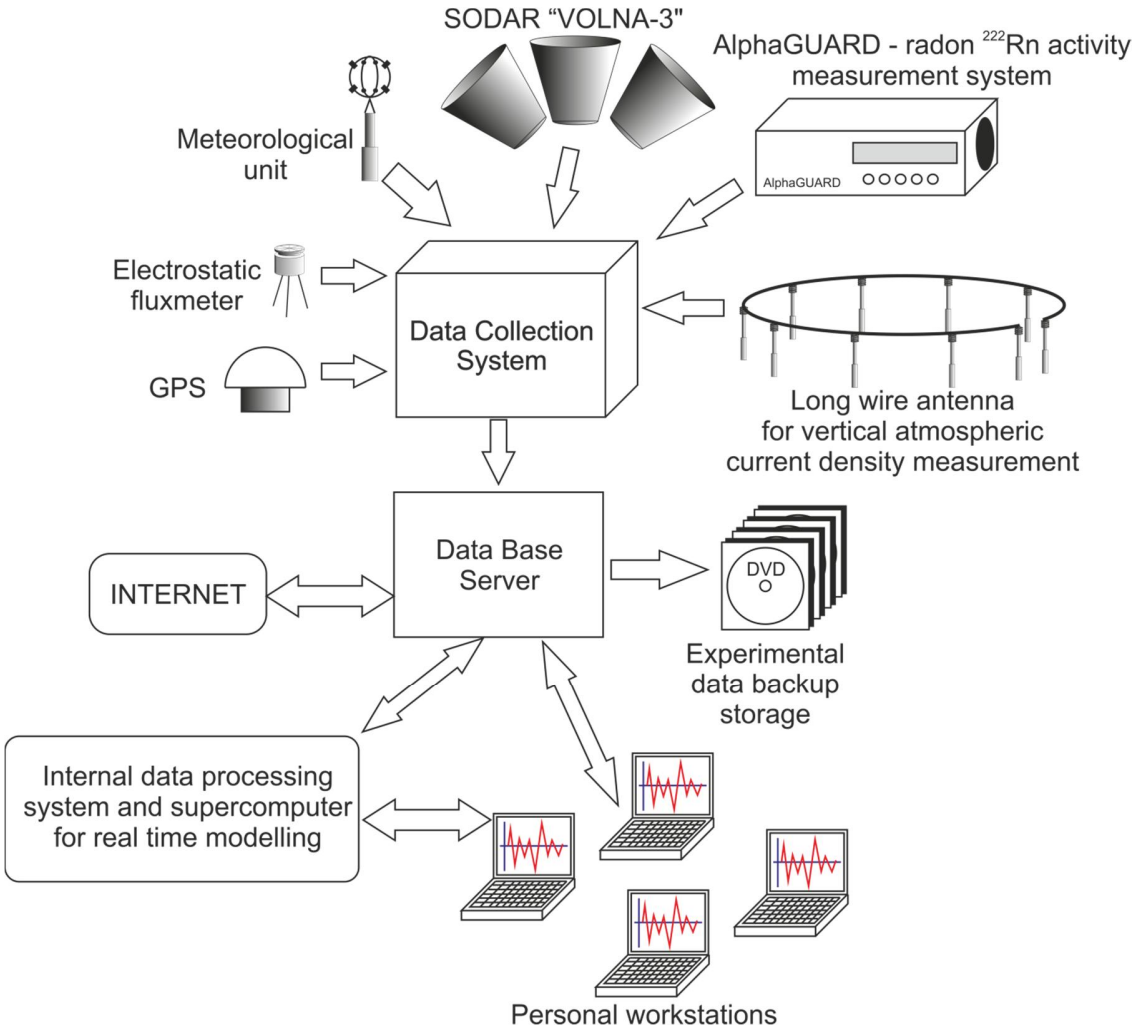

Figure 2. Scheme of the stationary permanent atmospheric electricity observation system

Figure 2 shows the scheme of the stationary permanent atmospheric electricity observation system in Borok Geophysical Observatory. The stationary observation system hardware includes an electrostatic fluxmeter, a long-wire antenna for vertical atmospheric current density measurement, the acoustic dopler locator “VOLNA-3”, the radon (^{222}Rn) monitoring system AlphaGUARD, digital ultrasonic and classical meteorological units. Meteorological units provide registration of air temperature, air humidity,atmospheric pressure, wind velocity and its direction. All the information is stored in digital form by a data collection system. The data collection system was built using precision ADCs with 16 bit and 10Hz resolution. Digital data are transmitted to the data base server, wherein automatically sorted and subjected to initial treatment for publishing on the Internet. Periodically data are stored in DVD disks as a backup. The data base server works interconnected with supercomputer, wich is using for real time modelling of aeroelectrical processes.

EXPERIMENTAL DATA PROCESSING AND ANALYSIS RESULTS

Figure 3 shows an example of experimental data variations from a field ground-based measurement complex.

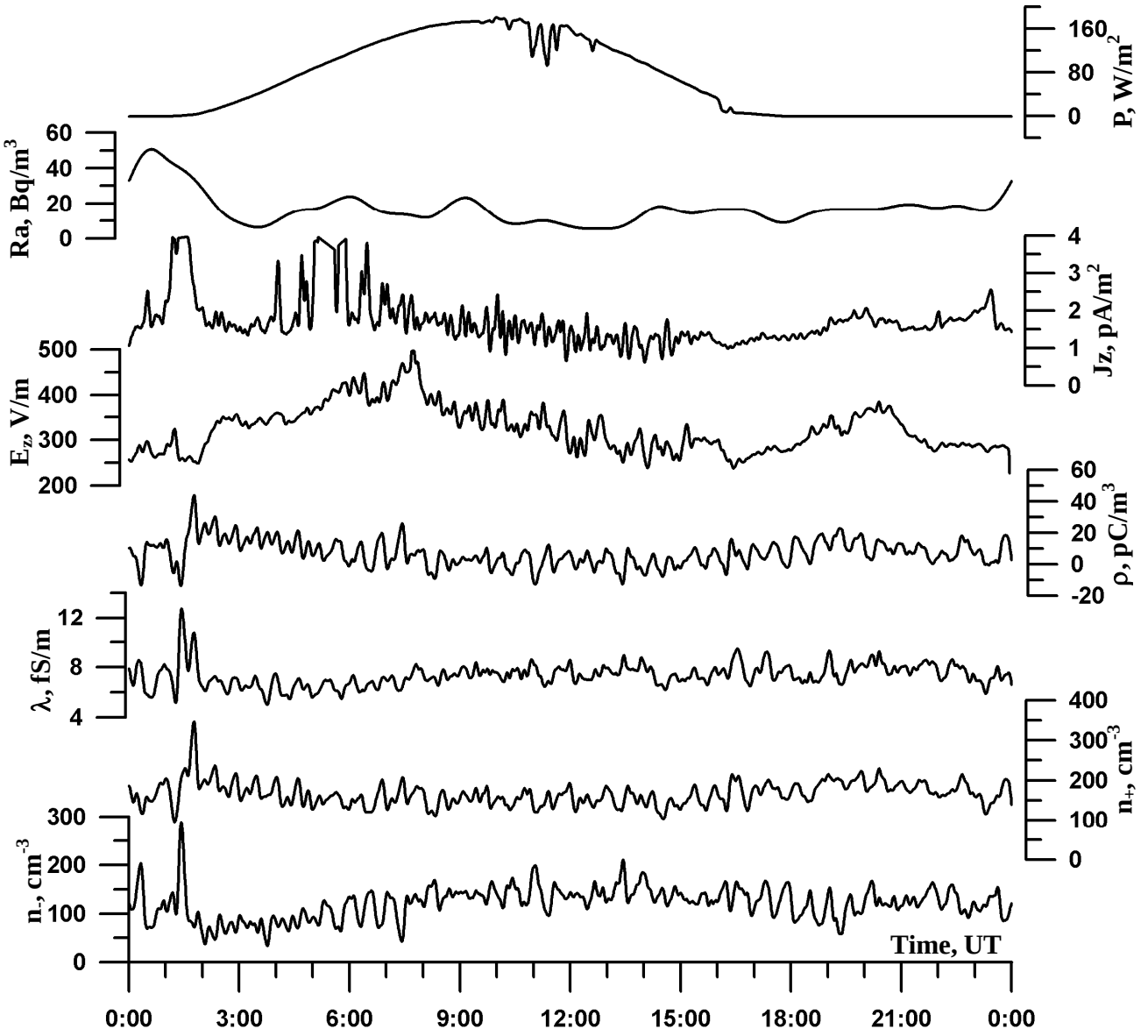

Figure 3. Variations of light ion concentrations (n_+, n_-), air electrical conductivity (λ), space charge density (ρ), electrical field strength (E_z), vertical air electrical current density (J_z), radon ^{222}Rn activity (Ra) and solar irradiance (P). (30.07.2012). All data averaged by 30 sec.

The figure contains plots of light ion concentration, electrical air conductivity, space charge at light ions, electrical field strength, vertical electrical current density, volume radon activity and solar irradiation variations.

Figure 4 contains diurnal variations plots of space charge density concentrated on light ions for summer and winter time. Data averaged by one hour. It is shown that there is an expressed maximum at 04:00UT in space charge variations for summer time case. This time corresponds to the intensive ground surface warming by solar radiation. Average daily value of space charge density is 15 (±10) pC/m^3. At winter time ground surface was shielded by snow. In the particular case the thickness of snow cover was 50 cm.

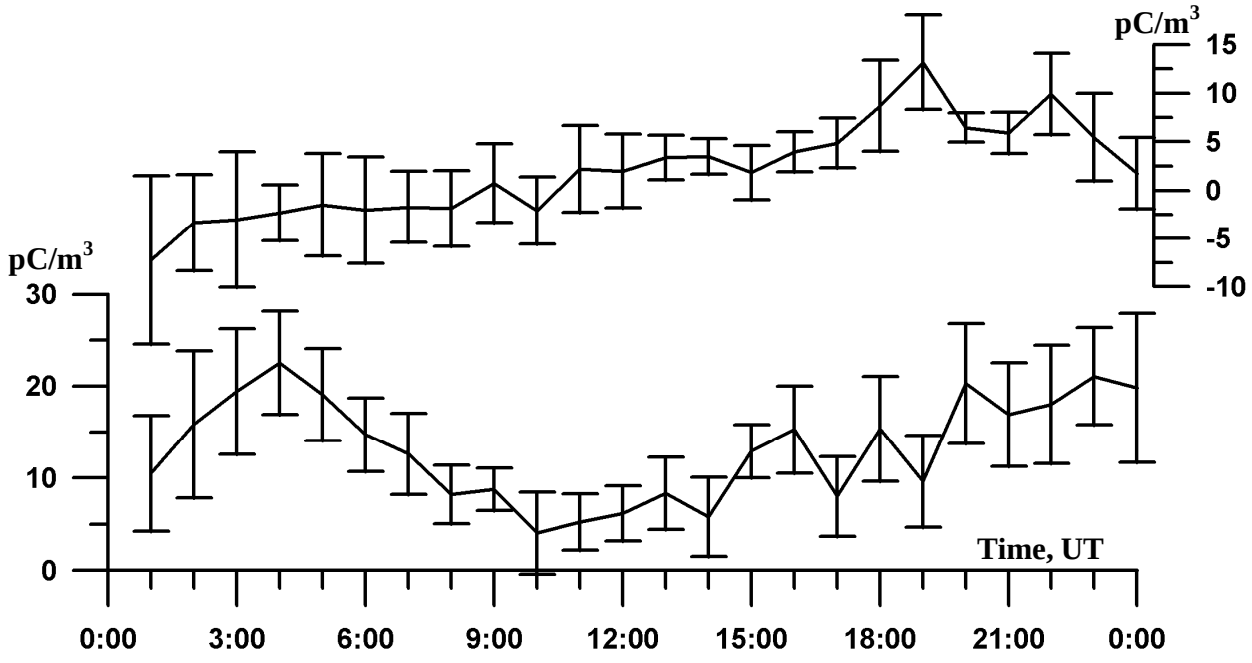

Figure 4. Daily varitations of space charge density for winter (top plot) and summer time (bottom plot). One hour averaging of six days for winter time case and seven days for summer time case

A snow cover blocks radon transmission in the atmosphere and its effect to the ionization of surface atmospheric layer is greatly reduced. Average daily value of space charge density for winter time is 2 (± 10) pC/m^3.

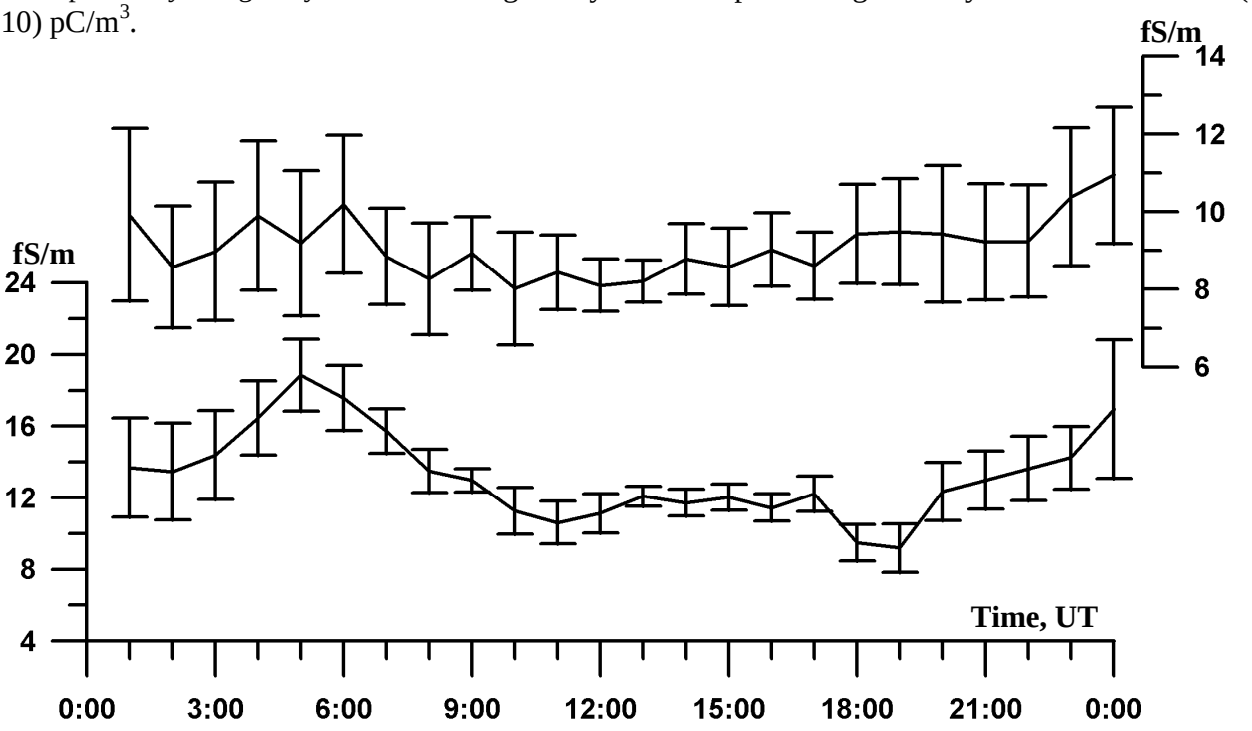

Figure 5. Daily variations of air electrical conductivity for winter (top polt) and summer time (bottom plot).

One hour averaging of six days for winter time case and seven days for summer time case

Figure 5 presents diurnal variations of atmospheric surface layer electrical conductivity according to data of summer and winter seasons. It is an expressed maximum at 05:00UT in air electric conductivity variations for summer time, wich is also associated with intensive ground surfase heating by the sun. There are no expressed maximums in the diurnal variations of winter time air electric conductivity. Average daily value of air electric conductivity for summer time is 14 (±6) fS/m, and for winter time is 9 (±1.5) fS/m. Figure 6 shows diurnal variations of atmospheric surface layer polar electric conductivities according to data of summer and winter seasons.

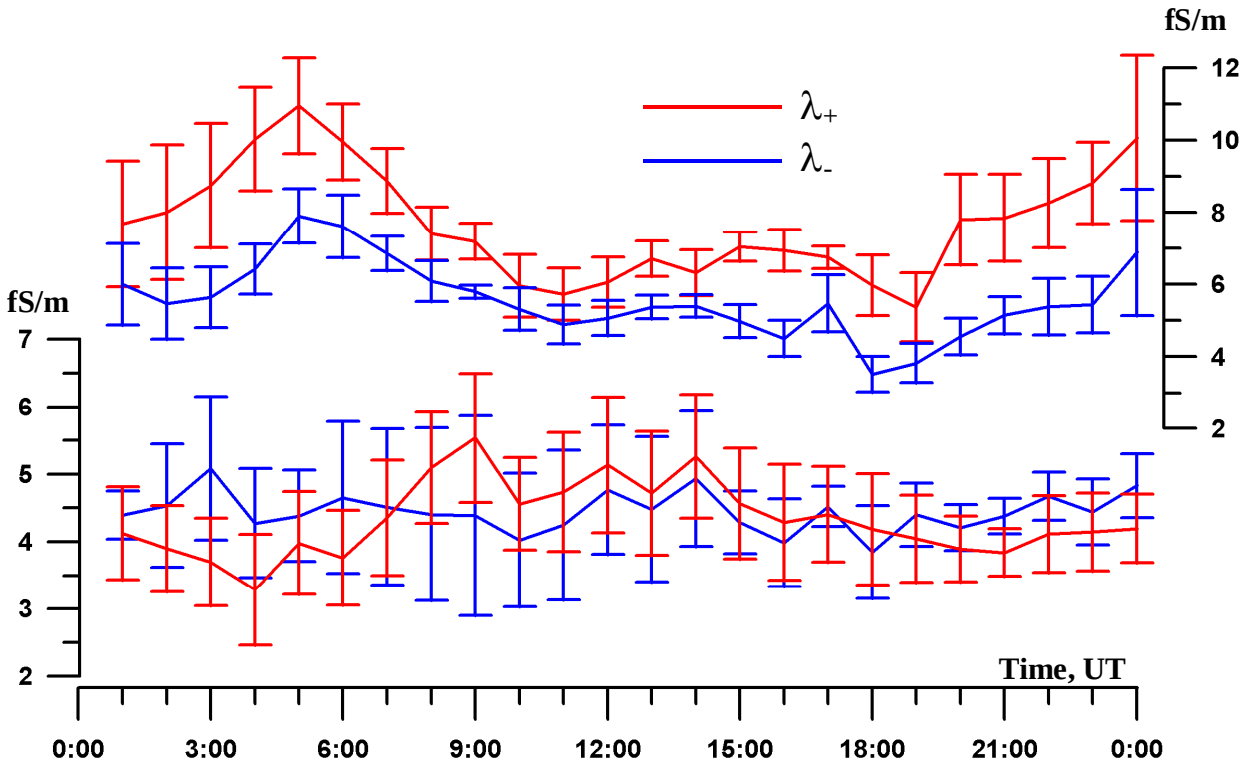

Figure 6. Diurnal variations of polar air electric conductivities for summer (top plot) and winter (bottom plot) time. One hour averaging of six days for winter time case and seven days for summer time case.

Decay of radioactive gases from the blowes of the earth is the main factor of atmospheric surface layer ionization [Smirnov, 1992]. Radon (^{222}Rn) and thoron (^{220}Rn) emanations are major factors of atmospheric surface layer ionization. Variations of radon volume activity near ground surface show significant correlation with air electrical conductivity at 0.6m height. Correlation quotient between ^{222}Rn volume activity and λ on average is 0.6 for time averaging of 30 minutes. For time averaging of 3 hours mean value of correlation quotient is 0.9. Figure 7 presents diurnal variations of air electric conductivity (λ) and radon volume activity (^{222}Rn) according to data from 09, 17-20, 28, 30 of August 2013. There was a maximum value of ^{222}Rn volume activity at night time, and minimum during day time.

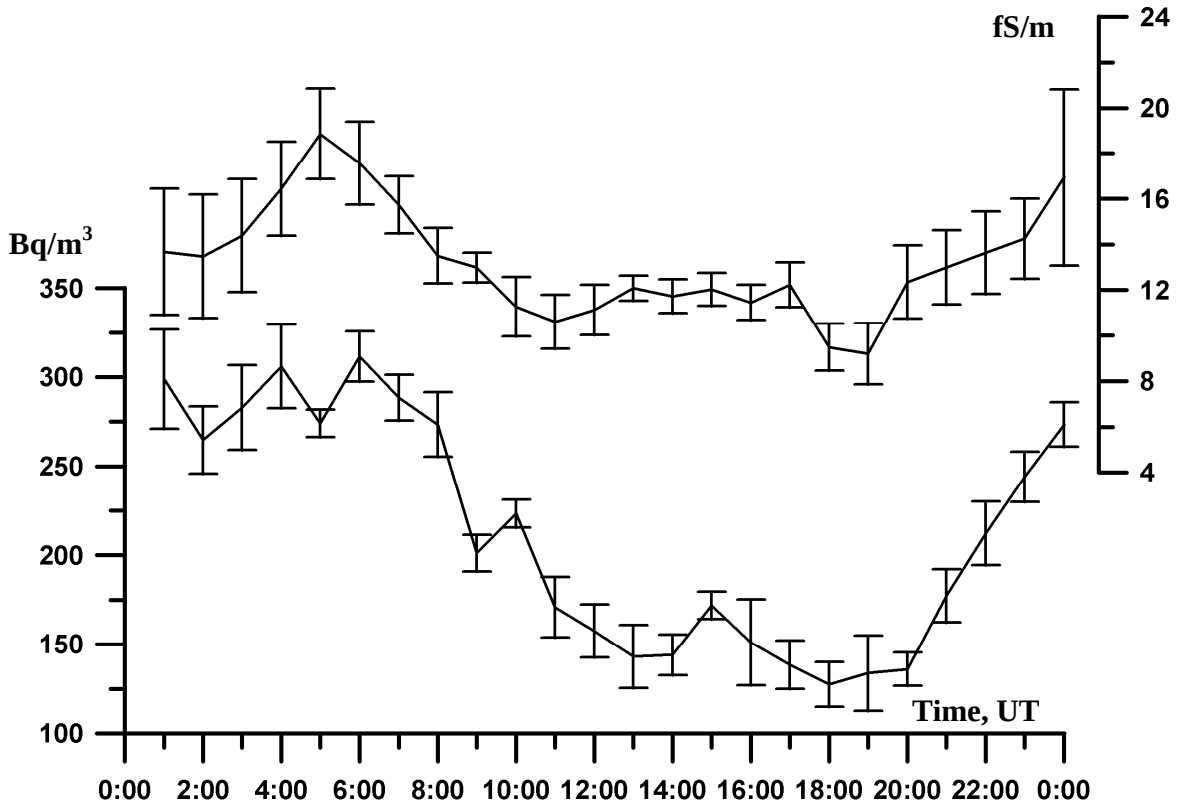

Figure 7. Diurnal variations of ^{222}Rn activity (bottom plot) and electric air conductivity (top plot). One hour averaging of seven days.

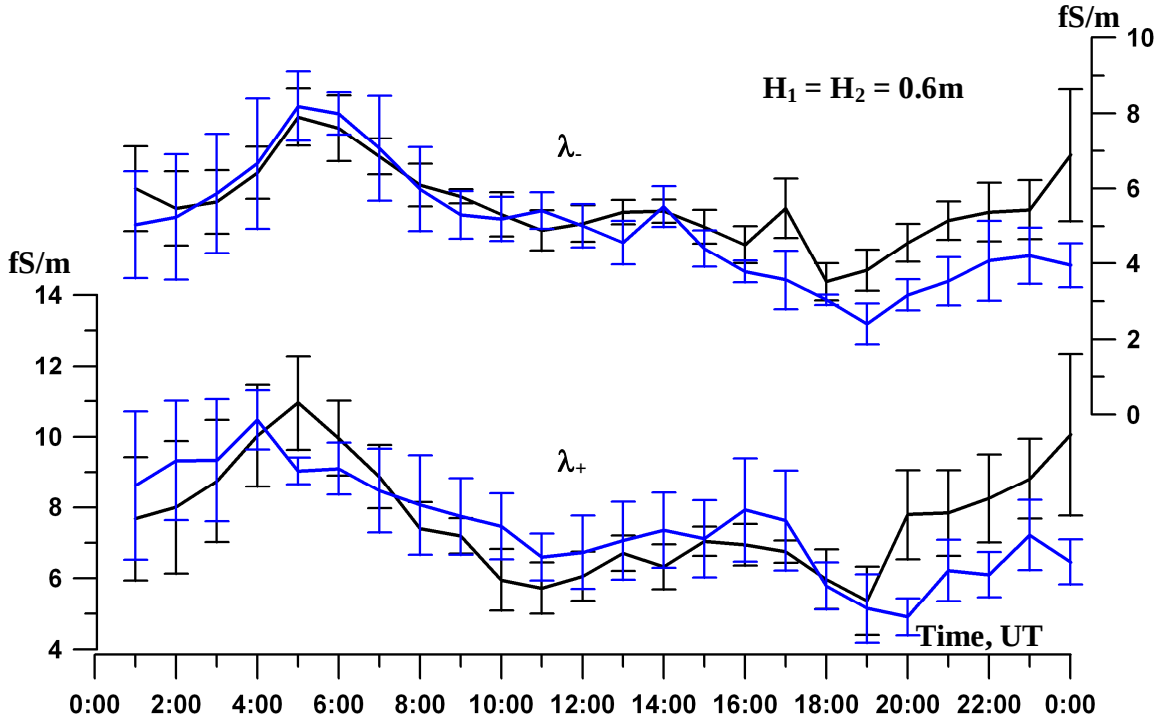

Figure 8. Diurnal variations of polar electric air conductivities at 0.6m height above the ground surface. One hour averaging of seven days.

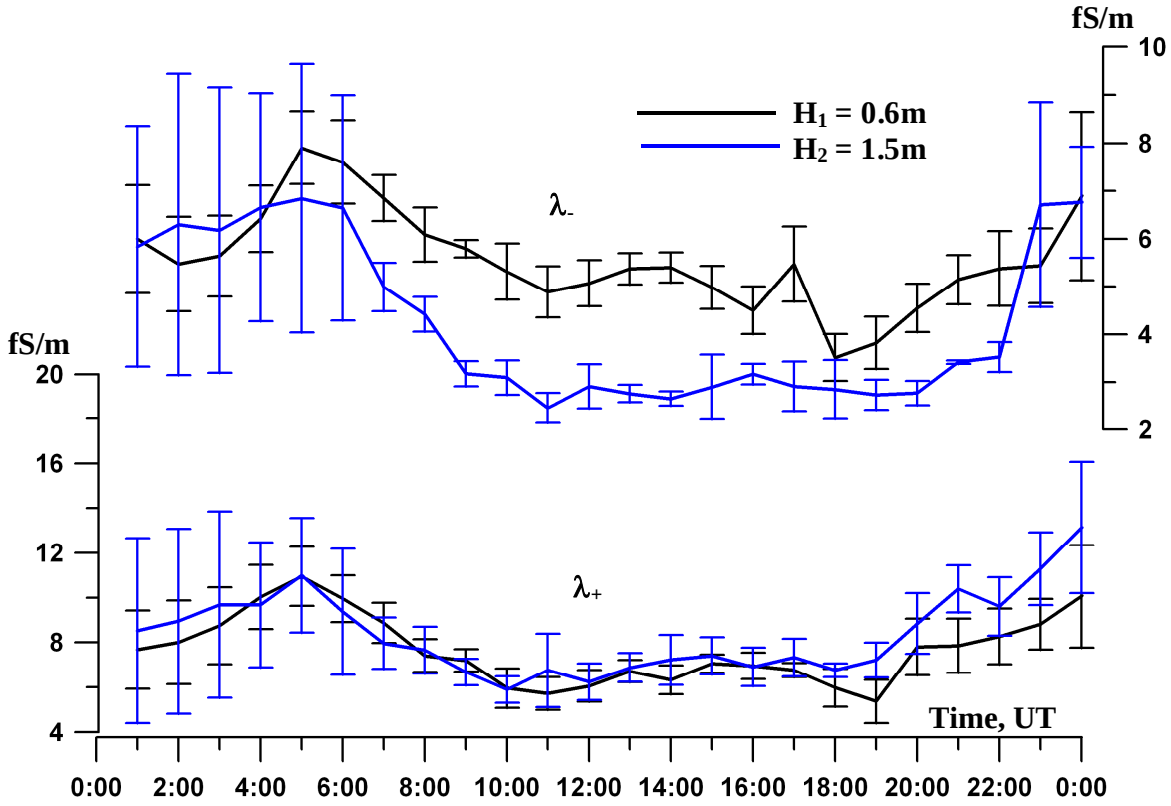

Figure 9. Diurnal variations of polar electric air conductivities at 0.6m (black plot) and 1.5m (blue plot) heights above the ground surface. One hour averaging of seven days.

During summer field ground-based observations of year 2013 synchronous measurements of polar air electric conductivities variations at heights 0.6m and 1.5m above the ground surface were provided. Initially both of the sensors were placed at 0.6m above the ground surface and at a distance of 1m from each other. Figure 8 shows diurnal variations of polar air electric conductivities registered by the sensors wich were installed at 0.6m height. Correlation quotient between data froms sensors is 0.96. At the next stage, one of the sensors has been raised to a height 1.5m, and the second sensor was at height 0.6m. Figure 9 presents diurnal variations of polar air electric conductivities at heights 0.6m and 1.5m. It is shown that air electric conductivities at night time at such heights have about absolute values, however at day time negative air electric conductivity at height 1.5m is two times less, than the same air conductivity at height 0.6m. Presumably this is due to the influence of turbulent convection and activity arising from the ground and atmosphere warming by the sun, such situation is typical only for periods of fair weather conditions.
Figure 10 shows forming of aeroelectrical structures in space charge density concentrated at light ions and electric field strength [Anisimov et al, 2014a].

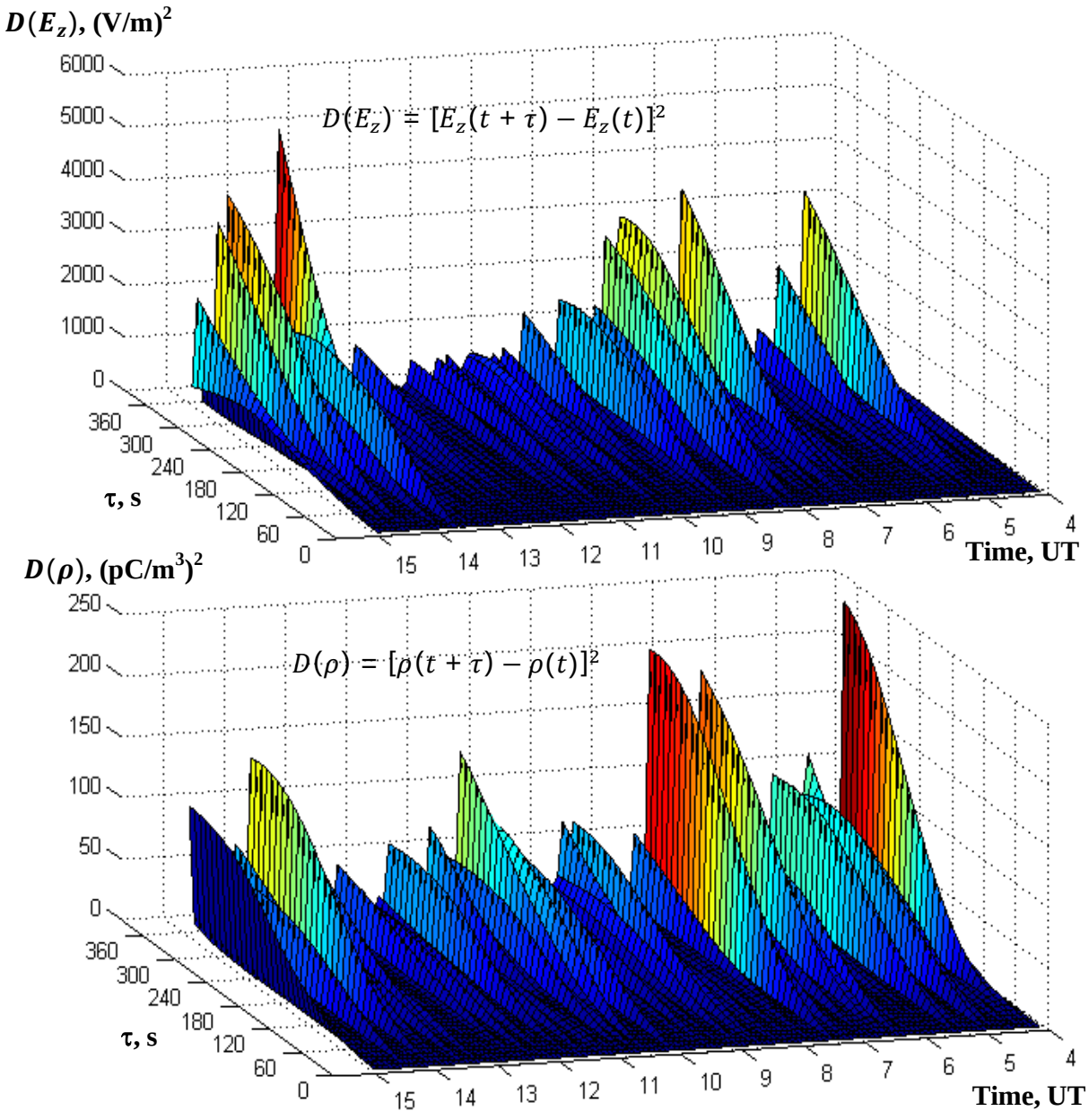

Figure 10. Structures in electrical field strength (top plot) and space charge density (bottom plot) on 28.07.2012 at Borok Observatory.

Figure 11 shows variations spectral density of space charge, concentrated at light ions. Time interval at 24 hours with 1 second meaning was choosen for calculation. It is shown that space charge density spectra is self-similar. The power of spectra decay is close to (-1.6).

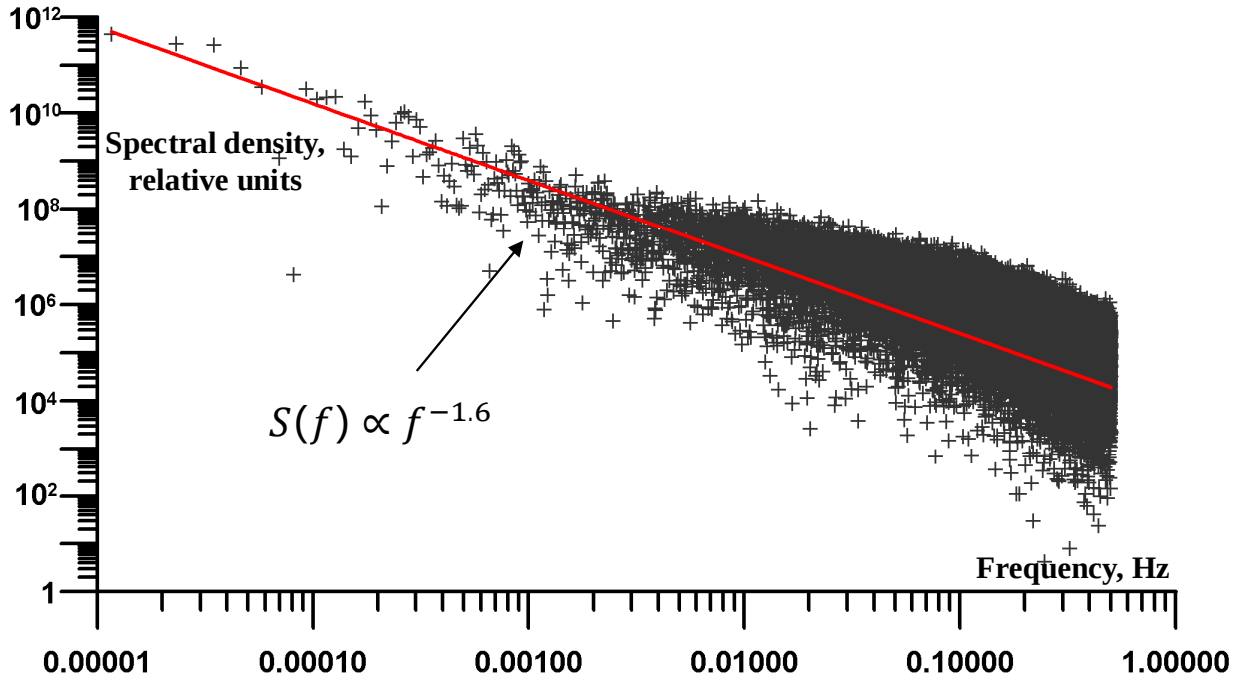

Figure 11. Spectral density of space charge variations on 09.08.2013 at Borok Observatory.

Spectral density of space charge variations is presented at Figure 12. The power of spectra decay for period from 10 to 500 seconds are close to -5/3. The power of spectra decay for period from 2 to 10 seconds is different at day and night conditions. At daytime power of spectra decay for this period is mostly close to -5/3. But at nighttime power of spectra decay varies from -1.9 to -3.1.

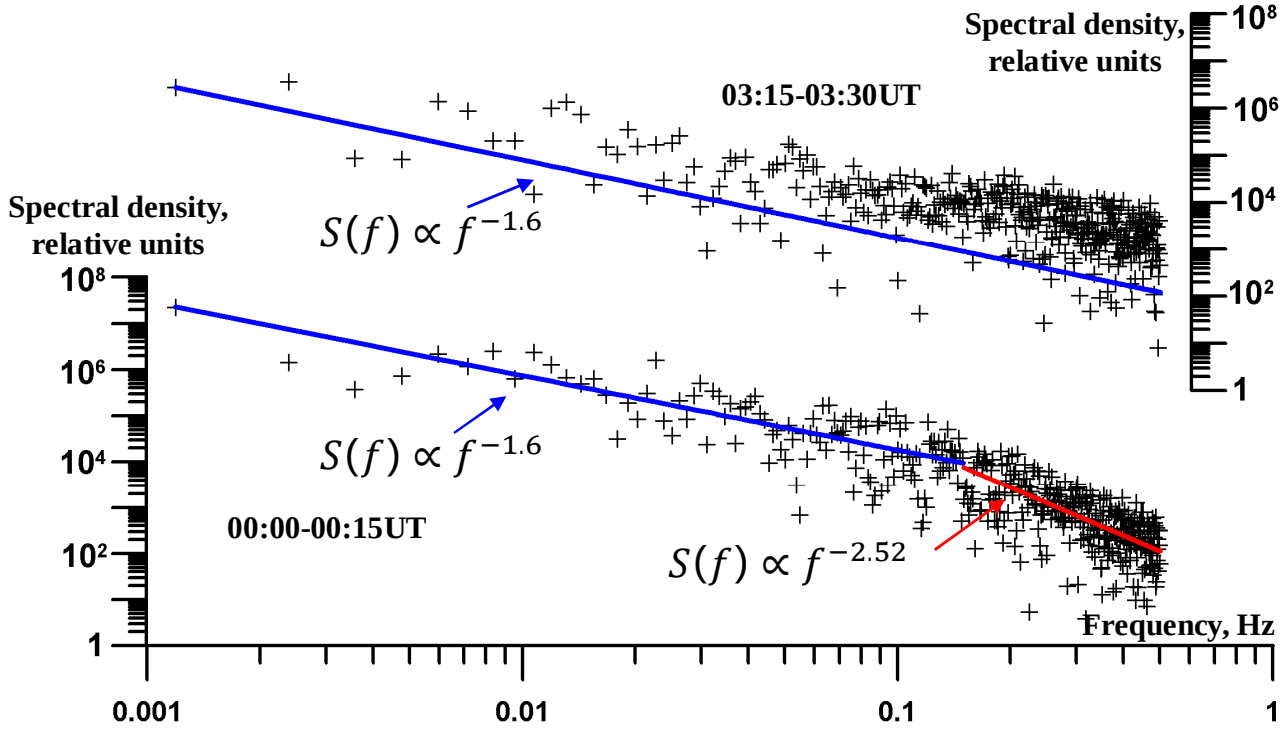

Figure 12. Spectral density of space charge for day and night on 03.08.2012 at Borok Observatory.

CONCLUSIONS

Thus, the results of statistical processing of amplitude-time series obtained during ground aeroelectric observations of 2011-2013 years (performed at midlatitude Borok observatory and included observations of electrical field strength, light ion concentration and atmospheric surface layer electrical conductivity) suggest that:

- Light ion concentration changes during the day. At night time when turbulence is suppressed by stable stratification light ion concentration mainly more than at day time. This can be explained by accumulation of radioactive gases and their progeny near the ground surface due to weak convection.
- There is maximum of space charge density concentrated at light ions during sunrise. More intensive forming of middle and heavy ions fractions due to hydratation and clusterization at surface warming and water vaporization conditions is a possible reason of light ions total positive charge growth at morning hours [Smirnov, 2010]. Hydrate complexes concentration growth causes asymmetric electrical charge redistribution between ion fractions and negative charge gaining by heavy fraction [Smirnov, 2010].
- Presence of coherent aeroelectrical structures is a typical feature of turbulent aeroelectrical pulsations and space charge density [Anisimov et al, 2014a, Anisimov et al, 2014b].
- Light air ion concentration variations and space charge density are connected with radon activity variations [Anisimov et al, 2013].
- Space charge density variations spectra is self-similar. The power of spectra decay for period interval from 10 to 10000 seconds is close to -5/3. The power of spectra decay for period from 2 to 10 seconds is different at day and night conditions. At day time the power of spectra decay for this period is mostly close to -5/3. But at night time the power of spectra decay varies from -1.9 to -3.1. [Anisimov et al, 2013]

ACKNOWLEDGMENTS

This work has been supported by Russian Foundation for Basic Research (Grants 12-05-00820, 13-05-12060) and grant from the Government of the Russian Federation under contract No. 14.B25.31.0023.

REFERENCES

Anisimov, S.V., Mareev, E.A., 2008: Geophysical studies of the global electric circuit. *Izv. Phys. Solid Earth* **44 (10)**, 760–769;

Chalmers J.A., 1974: Atmospheric electricity, Gidrometeoizdat, St. Peterburg, 420 pp

Anisimov S.V., 2003: The global electric circuit and lower atmospheric electricity (key point) *Proc. 12-th Int. Conf. on Atmospheric Electricity. - Versailles, France*, 693-696;

Mareev E.A., Anisimov S.V., 2009: Lifetime of the thunderstorm electric energy in the global atmospheric circuit and thunderstorm energy characteristics. *Atmospheric Research* **91**, 161–164, **doi:**10.1016/j.atmosres.2008.05.010;

Roble R.G., Tzur I., 1986: The Global Atmospheric-Electrical Circuit. *in: Krider, E.P., Roble, R.G. (Eds.), The Earth's Electrical Environment*. Natl. Acad. Press, Washington, 206-231;

Williams E.R., 2009: The global electrical circuit: a review. *Atmospheric Research* **91**, 140–152;

Anisimov S.V., Shikhova N.M., 2014a: Intermittency of turbulent aeroelectric field. *Atmospheric Research* **135-136**, 255-262

Smirnov V.V., 1992: Ionization in the Troposphere, Gidrometeoizdat, St. Peterburg, 312 pp

Smirnov V.V., 2010: Electrization of aerosol wetted in bipolary ionized air. *Izvestya, Physics of atmosphere and oceans*, **vol. 46, No. 3**, 321-331

Anisimov S.V., Galichenko S.V., Shikhova N.M., 2014b: Space charge and electric flows in the exchange layer: An experimental and numerical study. *Atmospheric Research* **135-136**, 244-254

Anisimov S.V., Aphinogenov K.V., Shikhova N.M., 2013: Dynamics of undisturbed midlatitude atmospheric

electricity: from observations to scaling. *Radiophysics and Quantum Electronics*, **vol. 56, issue 11-12,** 787-804

MODELING ELECTRICAL PROPERTIES OF DRY CONVECTIVE BOUNDARY LAYER

S.V. ANISIMOV, S.V. GALICHENKO and N.M. SHIKHOVA

Borok Geophysical Observatory of Schmidt Institute of Physics of the Earth, Russian Academy of Sciences, Borok, Yaroslavl region, 152742, Russia

Keywords: CONVECTIVE BOUNDARY LAYER, ATMOSPHERIC ELECTRICITY.

INTRODUCTION

The planetary boundary layer is the lower part of the global electric circuit. This part is very thin in comparison with the distance between high-conductive Earth's surface and ionosphere that works as global capacitor plates. Nevertheless, the contribution of boundary layer electric columnar resistance to the columnar resistance of full depth of atmosphere is essential (Harrison and Bennett, 2007). The atmospheric convectively-driven boundary layer is a particular type of turbulent boundary layer forced mainly by surface heating. Electrodynamics processes within the CBL are strongly influenced by turbulent buoyant convection of ionizing and electrically charged components of air. Ionization of air is the main mechanism of electric space charge generation. The ion production rate due to ^{222}Rn and its progeny is space- and time-dependent in the CBL. Electric conductivity of air directly depends on the number density of light atmospheric ions. Therefore, conditions of ion production, their recombination, and attachment to aerosol particles have a substantial effect on electrical phenomena in the CBL. Boundary layer forced by increasing buoyancy flux deepens (Stull, 1988; Garratt, 1992). It forms well-mixed part of the boundary layer and causes vertical spreading ^{222}Rn and its progeny which have been trapped within the nocturnal stable boundary layer (Vinuesa et al., 2007). As a result, vertical profiles of mean conductivity, charge density, and electric field intensity change with changes of ion production rate.

The calculations of convection electric currents in unstable boundary layer based on second-order turbulence closure showed that turbulent transport of charge acts as a local generator which modifies the electrical structure of the CBL (Willett, 1979). In order to study the variability of electric field during morning transition, several experiments with tethered balloon were performed (Marshall et al., 1999). It was found space charge by the ground to be increased after sunrise in some cases. Later low lying electric charge was spreading up to several hundred meters that vertical profiles of electric field intensity were significantly modified. Recently, the Lagrangian stochastic model has been proposed to calculate the electric field disturbances due to turbulent transport of space charge heterogeneities within the boundary layer (Anisimov et al., 2013a).

This paper introduces the concepts of Lagrangian stochastic modeling of electrodynamics of the CBL including morning transition period. We focus on the computation and analysis of mean and variations of vertical profiles of ionization rate, light ions, single-charged aerosol particles, electric space charge, electric field, and vertical conduction and convection currents.

METHODS

One of the sources of the atmospheric electric field is space charge originated from combined action of air ionization and separation of produced electric charges. The external electric currents maintain the global potential difference thereby they supply the quasistationary conduction current flowing through the fair weather regions of atmosphere. Within the CBL in addition to conduction current, strong vertical turbulent transport of electric charge takes place. In order to derive the air conductivity and space charge density varying with space and time, we need to know the number densities of light atmospheric ions and other

charged particles. For simplicity, we take into account only light ions and aerosol particles with the unit elementary charge. The balance equations for light negative and positive atmospheric ions are

$$\frac{\partial n_-}{\partial t} + (\boldsymbol{v}\nabla)n_- = q(\boldsymbol{r},t) - n_-\left[\alpha n_+ + \sum_{D_a}\left(\beta_{-0}(D_a)N_{0a} + \beta_{-+}(D_a)N_{+a}\right)\right] + \mu_-\nabla(n_-\boldsymbol{E}),$$

$$\frac{\partial n_+}{\partial t} + (\boldsymbol{v}\nabla)n_+ = q(\boldsymbol{r},t) - n_+\left[\alpha n_- + \sum_{D_a}\left(\beta_{+0}(D_a)N_{0a} + \beta_{+-}(D_a)N_{-a}\right)\right] - \mu_+\nabla(n_+\boldsymbol{E}). \quad (1)$$

Left hand sides (1) hold the substantial derivatives, $\boldsymbol{v}$ is the flow velocity; right hand sides hold $q(\boldsymbol{r},t)$ that is the ionization rate, recombination rate with the coefficient α, rate of ions depletion due to ion-aerosol attachment with the size-dependent coefficients β_{+0} , β_{+-} , β_{-0} , β_{-+} which correspond to adsorption of light ions by neutral aerosol particles and particles with opposite sign of charge. N_{0a} , N_{+a} , N_{-a} are the number densities of neutral, positively, and negatively charged aerosol particles with the diameter D_a correspondingly. The last terms in rhs of (1) describe the drift of ions with the mobility μ in the electric field $\boldsymbol{E}$. The equations for charged aerosol particles

$$\frac{\partial N_+}{\partial t} + (\boldsymbol{v}\nabla)N_+ = \frac{n_+}{\tau_{+0}} - \frac{n_-}{\tau_{-e}}, \quad \frac{\partial N_-}{\partial t} + (\boldsymbol{v}\nabla)N_- = \frac{n_-}{\tau_{-0}} - \frac{n_+}{\tau_{+e}} \quad (2)$$

hold in rhs the terms which correspond to charging of neutral particles and discharging of charged particles resulting from attachment of light ions; τ_{+0} , τ_{-0} ,τ_{+e} , τ_{-e} are the lifetimes of light ions. These lifetimes are derived by replacement of summation in (1) for integration of attachment coefficients with the aerosol particle size distribution function

$$\sum_{D_a}\beta_{\pm0}(D_a)N_{0a} = \int_{D_1}^{D_2}\beta_{\pm0}(D)\,f_0(D)dD = \tau_{\pm0}^{-1} \quad . \quad (3)$$

The main contribution to (3) gives the size interval from D_1=10^{-6} cm to D_2=10^{-3} cm. The neutral aerosol particle size normalized distribution function is assumed to have the form

$$f_0(D) = \begin{cases}\left[1.5 - D_1/\tilde{D} - 0.5\cdot(\tilde{D}/D_2)^2\right]^{-1}\cdot N_0/\tilde{D}, & D < \tilde{D} = 10^{-5}\ cm\\ \left[1.5 - D_1/\tilde{D} - 0.5\cdot(\tilde{D}/D_2)^2\right]^{-1}\cdot (N_0/\tilde{D})\cdot(\tilde{D}/D)^3, & D \ge \tilde{D},\end{cases} \quad (4)$$

where N_0 is the number density of aerosol particles with the diameters from D_1 to D_2. The attachment coefficient for ion and charged aerosol particle is given by (Smirnov, 1992)

$$\beta_\pm(D) = 2\pi\bar{D}_\pm D\left(\frac{1+\sqrt{\pi\gamma_\pm(D)}}{1+8\bar{D}_\pm/D\bar{c}_\pm}\right), \quad (5)$$

where $\beta_+=\beta_{+-}$, $\beta_-=\beta_{-+}$; $\bar{D}_\pm$ is the mean diffusion coefficient for ion; $\bar{c}_\pm$ is the mean thermal velocity of ion; $\gamma_\pm$ is the dimensionless parameter of adsorption

$$\gamma_\pm(D) = \frac{e^2}{2\pi\varepsilon_0 DkT}, \quad (6)$$

where e is the elementary charge, T is the absolute temperature. For a relation between attachment coefficients one may receive the parameterization based on the results of laboratory experiments and theoretical estimations given in Hoppel (1985), Hoppel and Frick (1986)

$$\beta_{\pm0}(D) \approx \beta_\pm(D)\exp\left[\frac{5.5\cdot10^{-6}}{D}\right], \quad (D \text{ in cm}). \quad (7)$$

Substituting (5) to (7), (4) and (7) to (3), and integrating, we obtain

$$\tau_{\pm0}^{-1} = \bar{\beta}_{\pm0}N_0\ , \quad (8)$$

where $\bar{\beta}_{\pm0}$ is the mean attachment coefficient for light ions and neutral aerosol particles. Because of light ion attached to the particle with the diameter greater than 10^{-6} cm increases its size insignificantly

(Smirnov, 1992), we make assumption that the charged aerosol particle size normalized distribution function has the analogous to (4) form

$$f_{\pm}(D)=\begin{cases}\left[1.5-D_1/\tilde{D}-0.5\cdot(\tilde{D}/D_2)^2\right]^{-1}\cdot N_{\pm}/\tilde{D}, & D<\tilde{D}=10^{-5}\ cm\\ \left[1.5-D_1/\tilde{D}-0.5\cdot(\tilde{D}/D_2)^2\right]^{-1}\cdot(N_{\pm}/\tilde{D})\cdot(\tilde{D}/D)^3, & D\geq\tilde{D}.\end{cases} \tag{9}$$

Therefore, (5) and (9) give

$$\tau_{\pm e}^{-1}=\sum_{D_a}\beta_{\pm}(D_a)N_{\mp a}=\int_{D_1}^{D_2}\beta_{\pm}(D)\,f_{\mp}(D)dD=\overline{\beta}_{\pm}N_{\mp}, \tag{10}$$

where $\overline{\beta}_{\pm}$ is the mean attachment coefficient for light ions and charged aerosol particles. According to Gauss's law

$$\nabla\boldsymbol{E}=\frac{e}{\varepsilon_0}\left(n_+-n_-+N_+-N_-\right). \tag{11}$$

To compute the mean vertical profiles of electrodynamics quantities within the CBL, we use horizontal-averaged one-dimensional form of (1), (2), and (11) thereafter. It is assumed the vertical conduction current density J_z to be a high-independent above the CBL and it can be expressed as

$$J_z(t)=\frac{V_i(t)}{\int\sigma^{-1}(z,t)dz}, \tag{12}$$

where $V_i(t)$ is the potential difference between Earth's surface and ionosphere, $\sigma(z,t)$ is the air conductivity

$$\sigma=e\left(\mu_+n_+ + \mu_-n_-\right). \tag{13}$$

From the continuity equation we have

$$J_z(t)=\left(\varepsilon_0\frac{\partial E_z}{\partial t}+\sigma E_z\right)\Big|_{z=h(t)}, \tag{14}$$

where $h(t)$ is the height of the growing CBL. The expression (14) is the boundary condition from which E_z on the CBL top is extracted. The lower boundary conditions are the time series of $n_+(t)$ and $n_-(t)$ obtained from in-situ field observations (Figure1) (Anisimov et al., 2013b). For $\sigma(z)$ above the CBL and $V_i(t)$ we use conventional parameterization (e. g. Gish, 1944). Ionization rate $q(z,t)$ is sum of rates due to cosmic rays, radiation of ground, ^{222}Rn and ^{220}Rn decaying families (Hoppel et al.,1986; Bazilevskaya et al., 2008).

The set of equations (1) and (2) in Lagrangian form does not include advective terms. It allows replace space integration by Monte-Carlo simulation the ensemble of particles in a turbulent flow given the probability density function of the random velocities advecting the particles along stochastic trajectories. Each Lagrangian trajectory or tracer is associated with a rather small finite volume of air which contains a sufficient amount of ionizing atoms such as ^{222}Rn, ^{220}Rn, and their progeny, light ions, and aerosol particles. Following the general rules for constructing of Lagrangian stochastic models to describe the dispersion of tracers in the ABL, we exploit the set of stochastic differential equations for random vertical velocity and displacement (Thomson, 1987; Rodean, 1996)

$$\begin{aligned}dW&=a(Z,W,t)dt+b(Z,W,t)d\varsigma,\\ dZ&=Wdt,\end{aligned} \tag{15}$$

where $a(Z, W, t)dt$ is the deterministic velocity forcing function, $b(Z, W, t)d\varsigma$ is the random velocity forcing with the quantity $d\varsigma$ being a component of a Gaussian white noise. For $a(Z, W, t)$ and $b(Z, W, t)$ are used expressions obtained in (Baerentsen and Berkowicz, 1984; Thomson, 1987; Luhar and Britter, 1989) and which must be parameterized by the vertical profiles of the variance of the vertical velocity $\sigma_w^2(z,t)$, third moment of the vertical velocity $\overline{w}^3(z,t)$, and mean turbulent kinetic energy dissipation $\varepsilon(z,t)$. Over the past decade a lot of expressions for the vertical profiles of convective turbulence statistics are evaluated and proposed from large eddy simulation (LES), laboratory experiments and natural observations (e. g.

Franzese et al., 1999; Cassiani et al., 2005; Essa and Embaby, 2007). About all of these vertical profiles are the functions both of Deardorff convective velocity scale w_* and dimensionless height z/h with h being the height of mixed layer top. It implies that the turbulent statistics profiles are time-dependent since the CBL deepens. The convective velocity scale is

$$w_* = (ghH_0 / \Theta_v)^{1/3}, \quad (16)$$

where g is the gravity acceleration, H_0 is the kinematic turbulent heat flux at the surface, and Θ_v is the reference virtual temperature. To date several approaches are developed to describe the evolution of the CBL in terms of a few thermodynamic and energetic parameters. These approaches are based on different models of mixed layer and entrainment zone structure and dynamics. LES has played a significant role in the studies of the CBL and has given the possibility to evaluate some characteristics of the CBL evolution through comparison of LES output with the predictions of bulk or probabilistic models of the CBL (Fedorovich et al., 2004; Sorbjan, 2007; Tombrou et al., 2007; Gentine et al., 2013). Combining the Lagrangian part with the electrodynamic part by means of time decoupling of the turbulent convective transport from the processes of ionization, ion-ion recombination, ion-aerozol attachment, and drift of ions in self-consistence electric field, we get the vertical profiles of space charge, electric field, air conductivity, vertical conduction and convection current densities with high space-time resolution.

RESULTS AND DISCUSSION

Vertical profiles of electrodynamics quantities in the CBL

At sunrise, the solar heating causes heat transfer from ground to adjacent layer of air. The heating of low-lying air are known to be responsible for the developing of convective instability. Intensive vertical mixing tends to equalize the radioactive nuclei concentrations and, consequently, the air conductivity. The absorption of light positive ions by aerosol particles prevents their drift in electric field but does not affect on their turbulent mixing. Thus, after sunrise observed number density of light positive ions decrease, at the same time total space charge and electric field may increase (Marshall et al., 1999; Anisimov et al., 2013b). Figure 2 shows the calculated electric field at the lower level of computational grid in comparison with the observed electric field. In Fig. 3 both the mean of modeled electric field and its dispersion agree with observed reasonably well.

Figures 3 and 4 show the sequence of computed electric field and conduction current density vertical profiles correspondingly. From modeled results we can conclude that adjacent to ground layer acts as the reservoir of electric charge for the convection current. When the vertical gradient of positive space charge is negative close to ground or the gradient of negative space charge is positive, the convection current is positive there and vice versa. As modeling shows the convection current density can be of the same order of magnitude as the conduction current density.

CONCLUSIONS

The model we presented includes the balance equations for light atmospheric ions, neutral and charged aerosol particles, balance equations for ^{222}Rn and ^{220}Rn decaying families (not shown), stochastic differential equations accounting for convective turbulent transport of constituents, prognostic equation for the height of mixed layer top (not shown), equations for air conductivity, current density, and electric field, dynamic boundary conditions as well. We have seen that the Lagrangian approach allows simulate many of key properties of the CBL such as nonstationarity, nonlocality both of dispersion and processes which determine electric quantities. It has been found the convection current to be dependent from the vertical distribution of electric space charge and may have positive or negative vertical direction.

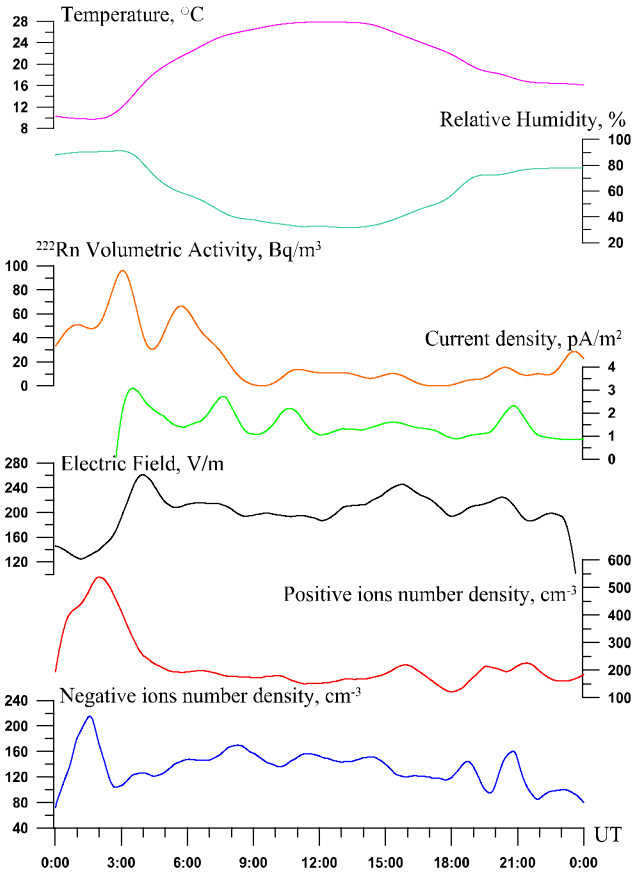

Figure 1. Example of hourly sliding averaged quantities observed on July 29, 2012 at Borok Observatory.

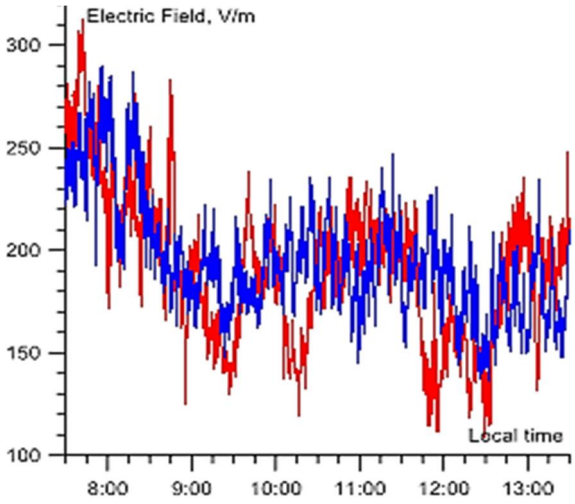

Figure 2. Example of the electric field near the surface: blue – observed on July 29, 2012 at Borok Observatory; red – calculated at the lower level of computational grid.

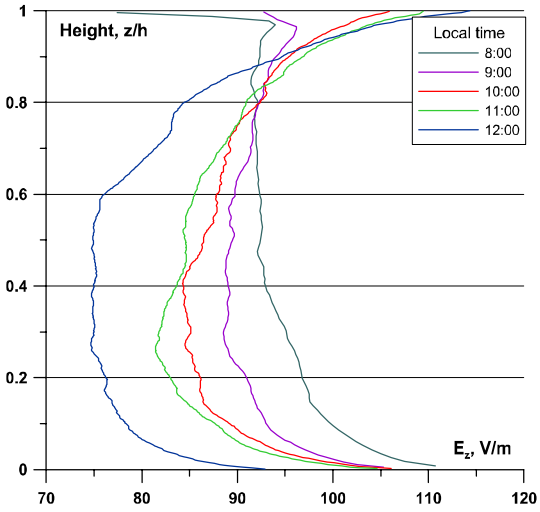

Figure 3. The 5-minutes sliding averaged vertical profiles of electric field.

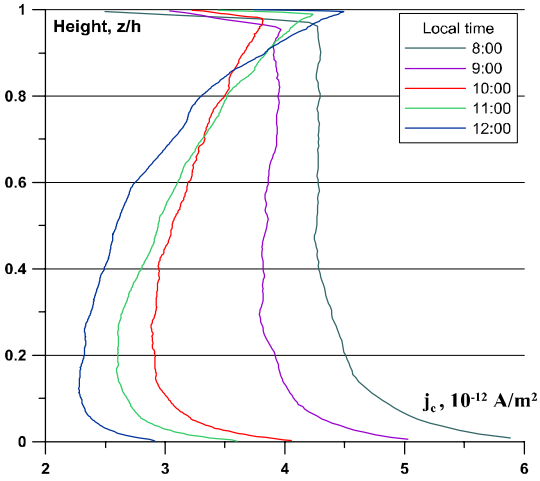

Figure 4. The 5-minutes sliding averaged vertical profiles of conduction current density.

ACKNOWLEDGEMENTS

This work was supported by the Russian Foundation for Basic Research (grants № 12-05-00820, №13-05-12060) and grant from the Government of the Russian Federation under contract No. 11.G34.31.0048.

REFERENCES

Anisimov S.V., S.V. Galichenko, N.M. Shikhova, 2013a: Space charge and aeroelectric flows in the exchange layer: An experimental and numerical study. *Atmospheric Research*, doi: 10.1016/j.atmosres. 2013.01.012.

Anisimov S.V., N.M. Shikhova, K.V. Aphinogenov, 2013b: Dynamics of undisturbed atmospheric electricity of middle latitudes: from observations to scaling. *Radiophycs and Quantum Electronics*, **56**, 11-12, 787-804.

Baerentsen J.H., R. Berkowicz, 1984: Monte Carlo simulation of plume dispersion in the convective boundary layer. *Atmos. Environment*, **18**, 701-712.

Bazilevskaya G.A., I.G. Usoskin, E.O. Flückiger, R.G. Harrison, L. Desorgher, R. Bütikofer, M.B. Krainev, V.S. Makhmutov, Y.I. Stozhkov, A.K. Svirzhevskaya, N.S. Svirzhevskky, G.A. Kovaltsov, 2008: Cosmic ray induced ion production in the atmosphere. *Space Sci. Rev*. **137**, 149–173.

Cassiani M., P. Franzese, U. Giostra, 2005: A PDF micromixing model of dispersion for atmospheric flow. Part II: application to convective boundary layer. *Atmos. Environ*ment, **39**, 1471–1479.

Essa K.S.M., M. Embaby, 2007: New formulations of eddy diffusitivity for solution of diffusion equation in a convective boundary layer. *Atmos. Res.*, **85**, 77-83.

Garratt J.R. 1992: *The Atmospheric Boundary Layer*. Cambridge University Press, Camridge, UK, 316 pp.

Gentine P., A.K. Betts, B.R. Lintner, K.L. Findell, C.C. van Heerwaarden, A. Tzella, and F. D'Andrea, 2013: A probabilistic bulk model of coupled mixed layer and convection. Part I: clear-sky case. *J. Atmos Sci*., **70**, 1543-1556.

Gish O.H., 1944: Evaluation and interpolation of the columnar resistance of the atmosphere. *J. Geophys. Res.*. **49**, 159-168.

Fedorovich E., R. Conzemius, and D. Mironov, 2004: Convective entrainment into a shear-free, linearly stratified atmosphere: Bulk models reevaluated through large eddy simulations. *J. Atmos Sci*., **61**, 281-295.

Franzese P., A.K. Luhar, M.S. Borgas, 1999: An efficient Lagrangian stochastic model of vertical dispersion in the convective boundary layer. *Atmos. Environment*, **23**, 1911-1924.

Harrison, R. G., and A. J. Bennett, 2007: Cosmic ray and air conductivity profiles retrieved from early twentieth century balloon soundings of the lower troposphere. *J. Atmos. Solar-Terr. Phys.*, **69**, 515-527.

Hoppel W.A. 1985: Ion-aerosol attachment, ion depletion and charge distribution on aerosols. J. *Geoph. Res.*, **90**, 5917–5923.

Hoppel W.A., G.M. Frick, 1986: Ion-aerosol coefficients and the steady-state charge distribution on aerosols in a bipolar ion environment. *Aerosol Sci. Tech*., **5**, 1–21.

Hoppel W.A., R.V. Anderson, J.C. Willett, 1986: Atmospheric electricity in the planetary boundary layer, in The Earth's electrical environment. Krider, E.P. and Roble, R.G., eds., Natl. Acad. Press., Washington, USA, 149–165.

Luhar A.K., R.E. Britter, 1989: A random walk model for dispersion in inhomogeneous turbulence in a convective boundary layer. *Atmos. Environment*, **33**, 2337-2345.

Marshall T.C., W.D. Rust, M. Stolzenburg, W.P. Roeder, P.R. Krehbiel, 1999: A study of enhanced fair-weather electric fields occurring soon after sunrise. *J. Geophys. Res.*, **104**, 24455–24469.

Rodean H., 1996: *Stochastic Lagrangian models of turbulent diffusion*. American Meteorological Society, Boston, 84 pp.

Smirnov V.V., 1992: *Ionization in the troposphere*. Gidrometeoizdat, Saint-Petersburg, RF, 312 pp. (in russian)

Sorbjan Z., 2007: A numerical study of daily transitions in the convective boundary layer. *Bound.-Layer Met*. **123**. 365–383.

Stull R.B., 1988: *An introduction to Boundary Layer Meteorology*. Kluwer, Dordrecht, 670 pp.

Thomson D.J., 1987: Criteria for the selection of the stochastic models of particle trajectories in turbulent flows. *J. Fluid Mech*., **180**, 529-556.
Tombrou M., A. Dandou, C. Helmis, E. Akylas, G. Angelopoulos, H. Flocas, V. Assimakopoulos, N. Soulakellis, 2007: Model evaluation of the atmospheric boundary layer and mixed-layer evolution. *Bound.-Layer Met.* **124**. 61–79.
Vinuesa J.-F., S. Basu, and S. Galmarini, 2007: The diurnal evolution of ^{222}Rn and its progeny in the atmospheric boundary layer during the WANGARA experiment. *Atmos. Chem. Phys.*, **7**, 5003-5019.
Willett J.C., 1979: Fair weather electric charge transfer by convection in unstable planetary boundary layer. *J. Geophys. Res*., **84**, 703–718.

EVALUATING MODEL-SIMULATED SHORT-LIVED CLIMATE POLLUTANTS IN THE HIGH LATITUDE PAN-EURASIAN REGION

S.R ARNOLD[1], S.A. MONKS[1], D.V. SPRACKLEN[1], C.E. SCOTT[1], T. PETÄJÄ[2], J-D. PARIS[3], M. ARSHINOV[4], B. BELAN[4], E. ASMI[5], L.J. CARPENTER[6], A.C. LEWIS[6], K.A. READ[7], J.D. LEE[7], L.K. EMMONS[8], M. ANDREAE[9], J. WINDERLICH[9], A. SKOROKHOD[10], Y. BORISOV[11], A. MAKSHTAS[12], V. SOKOLOV[12] and O. POPOVICHEVA[13]

[1]Institute for Climate and Atmospheric Science, School of Earth & Environment, University of Leeds, United Kingdom.

[2]Division of Atmospheric Science, Department of Physics, University of Helsinki, Finland.

[3]Laboratoire des Sciences du Climat et de l'Environnement, IPSL, CNRS-CEA-UVSQ, Gif sur Yvette, France.

[4]V.E. Zuev Institute of Atmospheric Optics, Russian Academy of Sciences, Siberian Branch, Tomsk, Russia.

[5]Finnish Meteorological Institute, Climate and Global Change, Helsinki, Finland.

[6]Department of Chemistry, University of York, York, United Kingdom.

[7]National Centre for Atmospheric Science (NCAS), University of York, York, United Kingdom

[8]National Center for Atmospheric Research, Boulder, CO, USA

[9]Biogeochemistry Department, Max Planck Institute for Chemistry, Mainz, Germany

[10]A.M. Obukhov Institute of Atmospheric Physics, Russian Academy of Sciences, Moscow, Russia.

[11]Central Aerological Observatory, Dolgoprudny, Moscow region, Russia

[12] Arctic and Antarctic Research Institute, St. Petersburg, Russia/

[13]Moscow State University, Russia.

Keywords: SHORT-LIVED CLIMATE POLLUTANTS, OZONE, AEROSOLS, CHEMICAL TRANSPORT MODEL

Temperature observations show that the boreal high latitudes have warmed rapidly in the past few decades compared to the northern hemisphere as a whole (Hartmann et al., 2013). Model calculations suggest that changes in short-lived climate pollutants (SLCPs) such as ozone and aerosol may have contributed significantly to this warming over the past century (Shindell and Faluvegi, 2009). Arctic tropospheric budgets of SLCPs are impacted by long-range transport of trace gases and aerosols from Europe, Asia and N. America, but also by local sources such as gas flaring, shipping and boreal fires. Past studies have shown that global chemical transport models demonstrate poor and highly varied skill in simulating aerosol, tropospheric ozone and precursors (CO) at remote Arctic surface stations when compared with limited available data. (Shindell et al., 2008). Recently, the POLARCAT Model Intercomparison Project (POLMIP) showed that significant model biases persist through the depth of the European and North American high latitude troposphere in both spring and summer for ozone, organic compounds and reactive

nitrogen (Monks et al., 2014; Emmons et al., 2014; Arnold et al., 2014). These limited evaluations give us low confidence in the ability of global models to correctly simulate Arctic atmospheric composition and climate response to future changes in mid-latitude emissions.

Evaluation of models over the Siberian high latitudes is challenging due to a paucity of available observations, despite the potential importance of this region as a route for European pollution export to the Arctic. In this work, we will show preliminary evaluation of 10 global chemical transport models from the POLMIP project using a limited collection of surface, aircraft and satellite observations over the sparsely observed high latitude pan-Eurasian region. We will compare the performance of the models in this region with their performance over the North American and European Arctic. We will also use the model simulations to derive optimum locations for the development of future monitoring activities in high latitude Eurasia with an aim of better constraining SLCP sources and sinks in this region. A key component of any enhancement in observations in the region will be their full integration into global datasets such as WMO GAW and inter-comparability with European and North American observations. To gain confidence that small changes in both time and space are significant we propose a number of essential experimental inter-comparisons that may be required to support effective model evaluation.

REFERENCES

Arnold, S. R., Emmons, L. K., Monks, S. A., Law, K. S., Ridley, D. A., Turquety, S., Tilmes, S., Thomas, J. L., Bouarar, I., Flemming, J., Huijnen, V., Mao, J., Duncan, B. N., Steenrod, S., Yoshida, Y., Langner, J., and Long, Y., Biomass burning influence on high latitude tropospheric ozone and reactive nitrogen in summer 2008: a multi-model analysis based on POLMIP simulations, Atmos. Chem. Phys. Discuss., 14, 24573-24621, doi:10.5194/acpd-14-24573-2014, 2014.

Emmons, L. K., Arnold, S. R., Monks, S. A., Huijnen, V., Tilmes, S., Law, K. S., Thomas, J. L., Raut, J.-C., Bouarar, I., Turquety, S., Long, Y., Duncan, B., Steenrod, S., Strode, S., Flemming, J., Mao, J., Langner, J., Thompson, A. M., Tarasick, D., Apel, E. C., Blake, D. R., Cohen, R. C., Dibb, J., Diskin, G. S., Fried, A., Hall, S. R., Huey, L. G., Weinheimer, A. J., Wisthaler, A., Mikoviny, T., Nowak, J., Peischl, J., Roberts, J. M., Ryerson, T., Warneke, C., and Helmig, D.: The POLARCAT Model Intercomparison Project (POLMIP): overview and evaluation with observations, Atmos. Chem. Phys. Discuss., 14, 29331-29393, doi:10.5194/acpd-14-29331-2014, 2014.

Hartmann, D.L., et al, 2013: Observations: Atmosphere and Surface. In: Climate Change 2013: The Physical Science Basis. Contribution of Working Group I to the Fifth Assessment Report of the Intergovernmental Panel on Climate Change [Stocker, T.F., D. Qin, G.-K. Plattner, M. Tignor, S.K. Allen, J. Boschung, A. Nauels, Y. Xia, V. Bex and P.M. Midgley (eds.)]. Cambridge University Press, Cambridge, United Kingdom and New York, NY, USA.

Monks, S. A., Arnold, S. R., Emmons, L. K., Law, K. S., Turquety, S., Duncan, B. N., Flemming, J., Huijnen, V., Tilmes, S., Langner, J., Mao, J., Long, Y., Thomas, J. L., Steenrod, S. D., Raut, J. C., Wilson, C., Chipperfield, M. P., Schlager, H., and Ancellet, G., Multi-model study of chemical and physical controls on transport of anthropogenic and biomass burning pollution to the Arctic, Atmos. Chem. Phys. Discuss., 14, 25281-25350, doi:10.5194/acpd-14-25281-2014, 2014.

Shindell, D. and Faluvegi, G.: Climate response to regional radiative forcing during the twentieth century, Nat. Geosci., 2, 294-300, 2009.

Shindell, D. T., Chin, M., Dentener, F., et al., A multi-model assessment of pollution transport to the Arctic, Atmospheric Chemistry and Physics, 8, 5353-5372, 2008.

NEW INSIGHTS ON THE NEW PARTICLE FORMATION EVENTS OBSERVED IN THE BOREAL ZONE OF WEST SIBERIA DERIVED FROM RECENT FOUR-YEAR CONTINUOUS OBSERVATIONS

M.YU. ARSHINOV[1], B.D. BELAN[1], D.K. DAVYDOV[1], A.V. KOZLOV[1], A.S. KOZLOV[2] and V.G. ARSHINOVA[1]

[1]V.E. Zuev Institute of Atmospheric Optics, Russian Academy of Sciences, Siberian Branch, (IAO SB RAS), Tomsk, Russia.

[2]V.V. Voevodsky Institute of Chemical Kinetics and Combustion, Russian Academy of Sciences, Siberian Branch, (ICK&C SB RAS) Novosibirsk, Russia.

Keywords: NEW PARTICLE FORMATION, FORMATION AND GROWTH RATES, SIBERIA.

INTRODUCTION

The new particle formation (NPF) itself was firstly reported by John Aitken more than one century ago (Aitken, 1898). At the same time, a phenomenon of NPF bursts was discovered relatively recently, but the data obtained to date showed that it is observed frequently in a variety of environments (Kulmala et al., 2004a; Hirsikko et al., 2011). Bursts occur more often in South Africa (Vakkari et al., 2011) and in tropical forests of South-East Australia (Suni et al, 2008), practically during the whole year. Also they are frequently observed in clean continental areas with forested ecosystems (Dal Maso et al., 2005, 2007) and coastal background sites (O'Dowd et al., 2002, 2007). The role of Siberia is of great importance to understand the climate change due to it covers about 10% of Earth's land surface. Assuming that increasing global temperature and CO_2 fertilization can likely lead to an extension of the annual photosynthesis period and forest growth, Kulmala et al. (2004b) suggested a possible feedback mechanism linking forests, aerosols and the climate effect of CO_2 through the intensification of metabolic processes causing enhanced non-methane BVOC emission and organic aerosol production as well. Taking into account that the major part of boreal forests is located in Siberia, this possible feedback makes this region one of the most key domains for the Pan-Eurasian Experiment (PEEX) not only because of studying GHG budget, but also because of it can be an important source of natural secondary aerosols. In spite of the importance of Siberian region for understanding of the surface-atmosphere exchange processes, continuous and comprehensive measurements of aerosols and GHGs over Siberia are still lacking.

EXPERIMENTAL

In recent years, IAO SB RAS decided to establish two monitoring stations for continuous measurements of aerosols and trace gas species (CO_2, CH_4, O_3, NO_x, SO_2, and CO) in order to fill up the gap in data. The first one is a so-called TOR-station (56°28'41"N, 85°03'15"E), and another one – Fonovaya Observatory (56°25'07"N, 84°04'27"E).

Measurements of aerosol size distributions have been carrying out since March 2010 at TOR-station and since May 2011 at Fonovaya Observatory by means of the improved versions of Novosibirsk diffusional aerosol spectrometers (Ankilov et al., 2002; Reischl et al., 1991) and the GRIMM aerosol spectrometers (#1.109 and #1.108). This enables continuous measurements of aerosol size distribution in a wide range to be performed with a better time resolution than it was done before (Dal Maso et al., 2008).

RESULTS AND DISCUSSION

Maximal concentrations observed at both stations were about tens of thousands per cm^3. The mean particle number concentration during the measurements at TOR-station was 4575 cm^{-3} (SD=4568 cm^{-3}, median=3330 cm^{-3}), and 2947 cm^{-3} (SD=3079 cm^{-3}, median=2403 cm^{-3}) at Fonovaya observatory. According to Jaenicke (1993), such values are typical for the remote continental and rural areas.

The dataset accumulated to date allowed us to classify new particle formation events observed in Siberia in accordance with criteria proposed by Dal Maso et al. (2005) and Hammed et al. (2007). Typical NPF events and non-events recorded in the Siberian air shed are shown in Fig.1. Analysis of the classified size spectra enabled a frequency and seasonal dependency of the new particle formation events to be revealed (Fig. 2). It showed that NPF events in Siberia are more often observed during spring (from March to May) and early autumn (secondary frequency peak in September). On average, NPF evens took place on 23-28 % of all days. This percentage is a little bit higher than one reported earlier by Dal Maso et al. (2008). Statistics improved in recent years showed that a seasonal pattern of the NPF frequency is very similar to one observed at SMEAR II Station (Hyytiälä, Finland; Dal Maso et al. 2005, 2007).

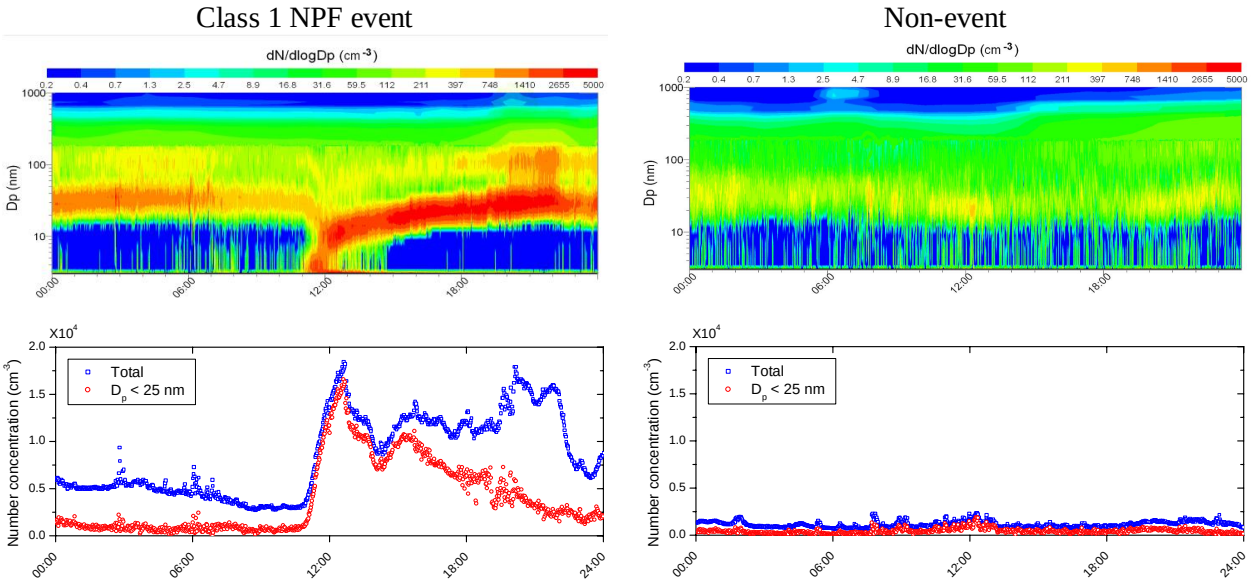

Figure 1. An example of aerosol size distribution evolution during NPF events and non-events observed in the atmosphere of West Siberia.

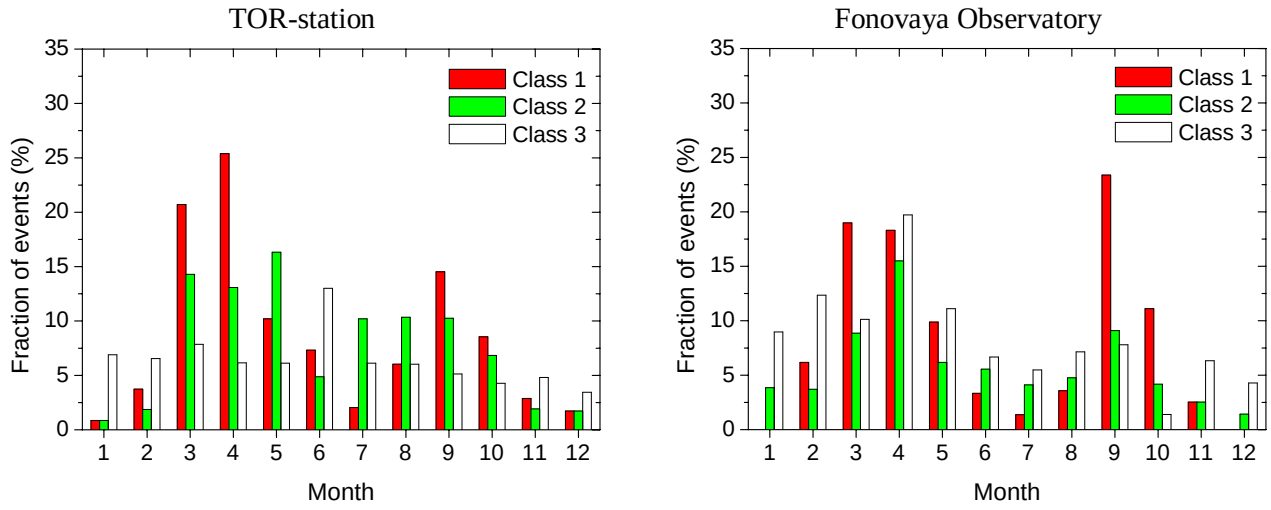

Figure 2. Seasonal dependency of NPF event frequency observed at two West Siberian stations obtained in accordance with the classification proposed by Hammed et al. (2007).

Particle formation rates were calculated based on the principles explained by Kulmala et al. (2004a). Formation rates (FR) of particles with diameters below 25 nm are summarized in Table 1. It can be seen that FR varies in wide range from 0.1 to 10 cm^{-3} s^{-1}. Mean values of FR for the entire period of observations (including August, 2014) were 1.7 $cm^{-3}s^{-1}$ (median = 1.13 cm^{-3} s^{-1}) at TOR-station and 0.88 cm^{-3} s^{-1} (median = 0.69 cm^{-3} s^{-1}) at Fonovaya Observatory. Enhanced values of FR are usually observed from spring to autumn.

	TOR-station, FR (cm^{-3} s^{-1})				Fonovaya Observatory FR (cm^{-3} s^{-1})			
Month	min	max	mean	median	min	max	mean	median
1	0.81	2.26	1.54	1.54	0.3	0.67	0.47	0.44
2	0.4	1.95	0.98	0.82	0.22	0.66	0.34	0.30
3	0.11	6.93	1.18	0.72	0.23	1.96	0.79	0.67
4	0.24	5.08	1.47	1.28	0.22	2.71	1.10	0.93
5	0.12	10.63	2.11	1.55	0.46	3.5	1.39	1.31
6	0.33	7.51	2.20	1.73	0.32	1.54	0.74	0.74
7	0.44	9.56	3.55	3.03	0.25	2.89	1.04	0.77
8	0.26	7.2	2.09	1.24	0.38	1.78	0.96	0.91
9	0.17	4.02	1.29	0.89	0.27	1.93	0.87	0.75
10	0.2	2.58	1.05	0.96	0.15	2.04	0.57	0.41
11	0.22	1.26	0.70	0.82	0.1	0.54	0.32	0.31
12	0.6	3.65	2.40	2.67	0.19	0.19	0.19	0.19

Table 1. Monthly mean, median and extreme values of formation rates FR (cm^{-3} s^{-1}) during NPF events of Class 1 and Class 2.

Growth rates were estimated by the increase of the geometric mean diameter of particles during the formation burst events (Dal Maso et al., 2005). Mean growth rates observed at TOR-station and Fonovaya Observatory were 6.5 nm h^{-1} (median = 5.0 nm h^{-1}) и 8.3 nm h^{-1} (median = 6.4 nm h^{-1}), respectively. Monthly mean values of GR over the entire period of observations are given in Table 2

	TOR-station, GR (nm h^{-1})				Fonovaya Observatory GR (nm h^{-1})			
Month	min	max	mean	median	min	max	mean	median
1	1.89	4.13	3.01	3.01	1.34	3.80	2.48	2.29
2	1.38	24.57	8.07	3.39	0.91	6.56	3.08	2.91
3	1.30	12.51	4.82	3.38	1.59	9.50	5.18	4.55
4	0.87	24.59	5.97	4.88	2.40	53.04	10.64	7.08
5	1.31	23.80	7.99	6.05	2.88	22.29	11.64	11.77
6	1.91	19.31	8.76	7.46	2.01	22.11	8.35	6.54
7	1.22	29.18	6.70	3.70	4.25	26.33	12.16	10.24
8	0.26	27.68	6.86	5.30	1.35	27.37	8.53	7.55
9	1.41	16.17	5.66	4.33	1.79	20.10	8.20	7.20
10	1.61	10.70	5.09	4.87	2.03	27.52	9.41	6.22
11	0.34	6.65	3.87	5.03	3.03	4.86	3.84	3.74
12	4.96	22.99	11.12	8.27	7.15	7.15	7.15	7.15

Table 2. Monthly mean, median and extreme values of growth rates GR (nm h^{-1}) during NPF events of Class 1 and Class 2.

CONCLUSIONS

Continuous measurements of aerosol size distribution carried out in West Siberia in recent years enabled the NPF event statistics to be improved. Analysis of the obtained dataset showed that NPF bursts are observed two times more often than it was reported for Siberia before (Dal Maso et al., 2008). Seasonal pattern of the burst occurrence is more similar to that observed at Nordic field stations (Dal Maso et al., 2007). At the same time, formation and growth rates observed during NPF events in Siberia are higher than those estimated for Scandinavian sites.

ACKNOWLEDGEMENTS

This work was supported by the Branch of Geology, Geophysics and Mining Sciences of RAS (Program No. 5); State contracts of the Ministry of Education and Science of Russia No. 14.604.21.0100, (RFMTFIBBB210290) and No. 14.613.21.0013 (RFMEFI61314X0013); and Russian Foundation for Basic Research (grant No. 14-05-00590).

REFERENCES

Aitken, J. A. (1898). On some nuclei of cloudy condensation, *Trans. Roy. Soc. of Edinburgh.* **XXXIX**. Part I. No 3. 15–25.

Ankilov, A., Baklanov, A., Colhoun, M., Enderle, K.H., Gras, J., Julanov, Y., Kaller D., Lindner, A., Lushnikov, A.A., Mavliev, R., McGovern, F., Mirme, A., O'Connor, T.C., Podzimek, J., Preining, O., Reischl, G.P., Rudolf, R., Sem, G.J., Szymanski, W.W., Tamm, E., Vrtala, A.E., Wagner, P.E., Winklmayr, W., Zagaynov, V. (2002). Intercomparison of number concentration measurements by various aerosol particle counters, *Atmospheric Research* **62**, 209–237.

Dal Maso, M., Kulmala, M., Riipinen, I., Wagner, R., Hussein, T., Aalto, P. P., and Lehtinen, K. E. J. (2005). Formation and growth of fresh atmospheric aerosols: eight years of aerosol size distribution data from SMEAR II, Hyytiälä, Finland, *Boreal Environ. Res.* **10**, 323–336.

Dal Maso, M., Sogacheva, L., Aalto, P., Riipinen, I., Komppula, M., Tunved, P., Korhonen, L., Suur-uski, V., Hirsikko, A., Kurten, T., Kerminen, V., Lihavainen, H., Viisanen, Y., Hansson, H., and Kulmala, M. (2007). Aerosol size distribution measurements at four Nordic field stations: identification, analysis and trajectories analysis of new particle formation bursts, *Tellus B* **59**, 350–361.

Dal Maso, M., Sogacheva, L., Anisimov, M. P., Arshinov, M., Baklanov, A., Belan, B., Khodzher. T. V., Obolkin, V. A., Staroverova, A., Vlasov, A., Zagaynov, V. A., Lushnikov, A., Lyubovtseva, Y. S., Riipinen, I., Kerminen, V.-M., and Kulmala, M. (2008). Aerosol particle formation events at two Siberian stations inside the boreal forest, *Boreal Environ. Res.* **13**, 81–92.

Hamed, A., Joutsensaari, J., Mikkonen, S., Sogacheva, L., Dal Maso, M., Kulmala, M., Cavalli F., Fuzzi S., Facchini, M. C., Decesari, S., Mircea, M., Lehtinen, K. E. J., and Laaksonen, A. (2007). Nucleation and growth of new particles in Po Valley, Italy, *Atmos. Chem. Phys.* **7**, 355–376.

Hirsikko, A., Nieminen, T., Gagné, S., Lehtipalo, K., Manninen, H. E., Ehn, M., Hõrrak, U., Kerminen, V.-M., Laakso, L., McMurry, P. H., Mirme, A., Mirme, S., Petäjä, T., Tammet, H., Vakkari, V., Vana, M., and Kulmala, M. (2011). Atmospheric ions and nucleation: a review of observations, *Atmos. Chem. Phys.* **11**, 767–798.

Jaenicke, *R.* (1993) Tropospheric aerosols, in: Aerosol-Cloud-Climate Interactions, edited by P.V. Hobs. – Academic Press, San Diego, CA; 1–31.

Kulmala, M., Vehkamäki, H., Petäjä, T., Dal Maso, M., Lauri A., Kerminen, V.-M., Birmili, W., and McMurry, P. H. (2004a) Formation and growth rates of ultrafine atmospheric particles: a review of observations, *J. Aerosol Science* **35**, 143–176.

Kulmala, M., Suni, T., Lehtinen, K. E. J., Dal Maso, M., Boy, M., Reissell, A., Rannik, Ü., Aalto, P., Keronen, P., Hakola, H., Bäck, J., Hoffmann, T., Vesala, T., and Hari, P. (2004b) A new feedback mechanism linking forests, aerosols, and climate, *Atmos. Chem. Phys.* **4**, 557-562.

O'Dowd, C. D., Hämeri, K., Mäkelä, J.M., Kulmala, M., Pirjola, L., Berresheim, H., Jennings, S.G., Hansson, H-C, de Leeuw, G., Allen, A.G., Hewitt, C.N., Stroh, A., and Viisanen, Y. (2002). A dedicated study of New Particle Formation and Fate in the Coastal Environment (PARFORCE): Overview of objectives and achievements, *J. Geophys. Res.* **D107**, 8108.

O'Dowd, C. D., Yoon, Y. J., Junkerman, W., Aalto, P., Kulmala, M., Lihavainen, H., and Viisanen, Y. (2007). Airborne measurements of nucleation mode particles I: coastal nucleation and growth rates, *Atmos. Chem. Phys.* **7**, 1491–1501

Reischl, G.P., Majerowicz, A., Ankilow, A., Eremenko, S. and Mavliev, R. (1991). Comparison of the Novosibirsk Automated Diffusion Battery with the Vienna Electro Mobility Spectrometer, *J. Aerosol Science* **22**, 223-228.

Suni, T., Kulmala, M., Hirsikko, A., Bergman, T., Laakso, L., Aalto, P. P., Leuning, R., Cleugh, H., Zegelin, S., Hughes, D., van Gorsel, E., Kitchen, M., Vana, M., Hõrrak, U., Mirme, S., Mirme, A., Sevanto, S., Twining, J., and Tadros, C. (2008). Formation and characteristics of ions and charged aerosol particles in a native Australian Eucalypt forest, *Atmos. Chem. Phys.* **8**. 129–139.

Vakkari, V., Laakso, H., Kulmala, M., Laaksonen, A., Mabaso, D., Molefe, M., Kgab,i N., and Laakso, L. (2011). New particle formation events in semi-clean South African savannah, *Atmos. Chem. Phys.* **11**, 3333–3346.

COMPARATIVE STUDY OF SIBERIAN METHANE FLUXES DURING THE TWO YAK AEROSIB AIRBORNE CAMPAIGNS OF 2012 AND 2013

E. ARZOUMANIAN[1], J.-D. PARIS[1], A. PRUVOST[1], S. PENG[1], S. TURQUETY[2], A. BERCHET[1], I. PISON[1], M. ARSHINOV[3] and B. BELAN[3]

[1]Laboratoire des Sciences du Climat et de l'Environnement, CEA-CNRS-UVSQ, IPSL, Gif-sur-Yvette, France.

[2]Laboratoire de Météorologie Dynamique, IPSL, Ecole Polytechnique, Palaiseau, France.

[3]Institute of Atmospheric Optics, SB-RAS, Tomsk, Russia.

Methane (CH_4) is the second most important anthropogenic greenhouse gas. It is also naturally emitted by a number of processes, including microbial activity in wetlands, permafrost degradation and wildfires. Our current understanding of the extent and amplitude of its natural sources, as well as the large scale driving factors, remain highly uncertain (Kirschke et al., Nature Geosci., 2013). Furthermore, high latitude regions are large natural sources of CH_4 in the atmosphere. Observing boreal/Arctic CH_4 variability and understanding its main driving processes using atmospheric measurements and transport model is the task of this work. YAK-AEROSIB atmospheric airborne campaigns (a joint French-Russian research program) have been performed in order to provide observational data on the composition of Siberian air. This work will be focused on the two summer campaigns of 2012 and 2013. Flights were performed in the tropospheric layer up to 9 km connecting the two cities of Novosibirsk and Yakutsk. A chemistry-transport model (CHIMERE), combined with datasets for anthropogenic (EDGAR) emissions and models for wetlands (ORCHIDEE) and wildfire (APIFLAME), is used to quantify CH_4 fluxes in the region. Furthermore, a lagrangian particle dispersion model (FLEXPART) is used in order to determine the origin of polluted air plumes. Recent results concerning CH_4 fluxes and its atmospheric variability in the Siberian territory derived from a modeled-based analysis will be shown and discussed.

ACKNOWLEDGEMENTS

This work was funded by CNRS (France), the French Ministry of Foreign Affairs, CEA (France), Presidium of RAS (Program No. 4), Brunch of Geology, Geophysics and Mining Sciences of RAS (Program No. 5), Interdisciplinary integration projects of Siberian Branch of RAS (No. 35, No. 70, No. 131), Russian Foundation for Basic Research (grants No 14-05-00526, 14-05-00590).

REFERENCES

Kirschke, S., P. Bousquet, P. Ciais, M. Saunois, J.G. Canadell, E.J. Dlugokencky, P. Bergamaschi, D. Bergmann, D.R. Blake, L. Bruhwiler, P. Cameron-Smith, S. Castaldi, F. Chevallier, L. Feng, A. Fraser, M. Heimann, E.L. Hodson, S. Houweling, B. Josse, P.J. Fraser, P.B. Krummel, J.-F. Lamarque, R.L. Langenfelds, C. Le Quéré, V. Naik, S. O'Doherty, P.I. Palmer, I. Pison, D. Plummer, B. Poulter, R.G. Prinn, M. Rigby, B. Ringeval, M. Santini, M. Schmidt, D.T. Shindell, I.J. Simpson, R. Spahni, L.P. Steele, S.A. Strode, K. Sudo, S. Szopa, G.R. van der Werf, A. Voulgarakis, M. van Weele, R.F. Weiss, J.E. Williams, and G. Zeng (2013). Three decades of global methane sources and sinks, *Nature Geosci.*, **6**, 813-823.

LONG-TERM AEROSOL MEASUREMENTS IN RUSSIAN ARCTIC

E. ASMI[1], V. KONDRATYEV[1,2], D. BRUS[1], T. LAURILA[1], H. LIHAVAINEN[1], M. AURELA[1], J. HATAKKA[1], Y. VIISANEN[1], T. UTTAL[3], V. IVAKHOV[4] and A. MAKSHTAS[5]

[1]Finnish Meteorological Institute, Atmospheric Composition Research, Helsinki, Finland.

[2]Yakutia Department of Hydrometeorology and Environmental Monitoring, Tiksi, Russia.

[3]National Oceanic and Atmospheric Administration, Boulder, USA.

[4]Voeikov Main Geophysical Observatory, St. Petersburg, Russia.

[5]Arctic and Antarctic Research Institute, St. Petersburg, Russia.

Keywords: ARCTIC AEROSOL, AEROSOL SIZE DISTRIBURION, LONG-TERM MEASUREMENTS, DMPS.

INTRODUCTION

The Arctic and northern boreal regions of Eurasia are experiencing rapid environmental changes due to pressures by human activities. Shindell and Faluvegi (2009) suggested that over two thirds of the Arctic surface temperature increase during the last decades is attributed to changes in concentrations of sulphate and black carbon (BC) aerosols. Contrary to most of the planet, on snow and ice -covered regions the clouds can cause a positive climate forcing; increasing the aerosols can in fact enhance warming of the surface (Walsh and Chapman, 1998; Mauritsen et al., 2011). There is also some recent experimental evidence that at pristine polar regions the aerosol-cloud feedback can be extremely sensitive to aerosol numbers (Asmi et al., 2012). In polar regions of particular importance is also the snow and ice albedo reduction by BC and organics containing particles which can influence snow coverage by warming the atmosphere, reducing surface-incident solar energy, and reducing snow reflectance after deposition (Flanner et al., 2009; Hirdman et al., 2010; Kohn et al., 2011; AMAP, 2011).

Global estimates of aerosol direct and indirect radiative effects largely rely on model calculations as well as on remote sensing techniques, which provide global coverage (IPCC, 2013). It is well realized that models encounter many problems in predicting the polar aerosol quantities and properties, their composition and annual cycles (e.g. Liu et al., 2005; Bourgeois and Bey, 2011, Liu et al., 2012). Most importantly, the observations at polar regions are sparse and often lacking sufficient temporal scales for model development and comparison studies.

In this work, we provide long-term high-quality observations from Arctic Siberia by introducing the first four years of continuous aerosol number size distribution observations from Siberian Arctic Climate Observatory in Tiksi. We present the aerosol seasonal variability in terms of particle modal features and number and mass concentrations and analyze the sources affecting these aerosol properties.

METHODS

Tiksi meteorological observatory in northern Siberia (71°36´N; 128°53´E) on the shore of the Laptev Sea has been operating since 1930s. Recently, it was upgraded and joint in the network of the International Arctic Systems for Observing the Atmosphere (IASOA, www.IASOA.org). The project is run in collaboration between National Oceanic and Atmospheric Administration (NOAA) with the support of the

NSF, Roshydromet (AARI and MGO units), government of the Republic of Sakha (Yakutia) and the Finnish Meteorological Institute (FMI). FMI activities in Tiksi were initiated in summer 2010 by aerosol size distribution measurements in the size range of 7 nm – 10 µm. These are measured with a twin-Differential Mobility Particle Sizer (DMPS) -system and with an TSI Aerodynamic Particle Sizer (APS).

CONCLUSIONS

The monthly statistics of aerosol data series are presented in Figure 1. Similar inter-annual cycle repeats from year-to-year, with the minimum number concentration observed in late autumn and maxima in spring and summer. Number concentration values are typical to a clean remote site. In seasonal cycle, the monthly median total aerosol number concentration in Tiksi extends from 184 cm^{-3} (in November) to 724 cm^{-3} (in July). For the local maximum in March a median value of 481 cm^{-3} is obtained. In mass concentration, only one annual maximum occurs being in early spring, where as in summer the particle mass is low.

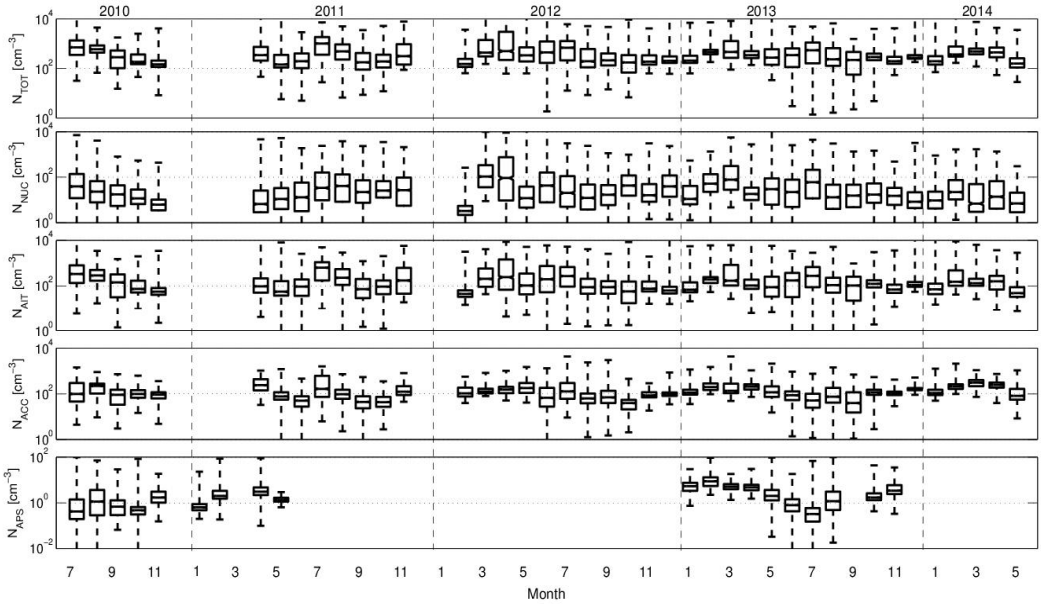

Figure 1. Four-year data series of aerosol number concentration in different size ranges, from up to down: total, nucleation mode (7-25 nm), Aitken mode (25-100 nm), accumulation mode (100-500 nm) and coarse mode (>0.5µm) concentrations in units of particles cm^{-3}. Bars present monthly medians and quartiles and whiskers the extreme values measured, for months with sufficient amount of data available.

The seasonal cycles in number and mass can be largely explained by long-range transported anthropogenic and regional biogenic sources. Arctic haze and long-range transported particles originating from lower latitudes dominate in early spring increasing the accumulation and coarse mode concentrations and particle mass. This is typical to all Arctic observatories. In addition, the winter meteorological conditions during stable inversions were seen to lead to some occasional local and/or regional pollution events. In summer, biogenic emissions from Siberian tundra and boreal forests increased the number of smaller, nucleation and Aitken mode particles. Increase of larger particle number was solely observed in continental air masses. In fact, the impact of temperature dependent natural emissions for aerosol and cloud condensation nuclei numbers was found to be exceptionally strong in Tiksi. Concentration of particles of diameters >100 nm showed exponential temperature dependence stronger than previously found in any other remote site of similar measurements (ref to: Paasonen et al., 2013). Therefore, in addition to the biogenic precursor emissions, the frequent Siberian forest fires are suggested to play a role even up in the Arctic during the warmest months. Evidence of this was also found using simultaneous

black carbon and gaseous precursor measurements, as well as the combined air mass analysis and satellite retrievals. A detailed source analysis will be presented in the meeting.

Our results give valuable new information on inter-annual cycles of aerosols in the Eurasian side of the Arctic, as explained by different anthropogenic and natural sources affecting them.

ACKNOWLEDGEMENTS

This work was supported by the Academy of Finland project Greenhouse gas, aerosol and albedo variations in the changing Arctic (project number 269095) and Centre of Excellence (project number 272041), KONE foundation (grant number 46-6817) and Magnus Ehrnooth foundation grant for "Natural climate feedbacks of aerosols in the Arctic". We gratefully acknowledge their support.

REFERENCES

AMAP (2011) The Impact of Black Carbon on Arctic Climate. By: Quinn, P.K. et al., Arctic Monitoring and Assessment Programme (AMAP), Oslo, 72 pp.

Asmi, E. et al. (2012) Aerosol cloud activation in summer and winter at puy-de-Dôme high altitude site in France, Atmos. Chem. Phys., 12, 11589–11607.

Bourgeois, Q. and Bey, I. (2011) Pollution transport efficiency toward the Arctic: Sensitivity to aerosol scavenging and source regions, J. Geophys. Res., 116, D08213.

Flanner, M. G. et al. (2009) Springtime warming and reduced snow cover from carbonaceous particles, Atmos. Chem. Phys., 9, 2481–2497.

Hirdman, D. et al. (2010) Longterm trends of black carbon and sulphate aerosol in the Arctic: changes in atmospheric transport and source region emissions, Atmos. Chem. Phys., 10, 9351-9368.

IPCC, 2013: Climate Change 2013: The Physical Science Basis. Contribution of Working Group I to the Fifth Assessment Report of the Intergovernmental Panel on Climate Change [Stocker, T.F., D. Qin, G.-K. Plattner, M. Tignor, S.K. Allen, J. Boschung, A. Nauels, Y. Xia, V. Bex and P.M. Midgley (eds.)]. Cambridge University Press, Cambridge, United Kingdom and New York, NY, USA, 1535 pp, doi:10.1017/CBO9781107415324.

Koch, D. et al. (2011) Coupled aerosol-chemistry-climate twentieth-century transient model investigation: Trends in short-lived species and climate responses.J. Clim., 24, 2693–2714.

Liu, X. et al. (2012) Toward a minimal representation of aerosols in climate models: description and evaluation in the Community Atmosphere Model CAM5, Geosci. Model Dev., 5, 709–739.

Liu, X. et al (2004) Global modeling of aerosol dynamics: Model description, evaluation and interactions between sulfate and non-sulfate aerosols, J. Geophys. Res., 110, D18206.

Mauritsen, T. et al. (2011) An Arctic CCN-limited cloud-aerosol regime, Atmos. Chem. Phys., 11, 165-173.

Paasonen, P. et al. (2013) Warming-induced increase in aerosol number concentration likely to moderate climate change, Nat. Geosci., 6, 438--442, doi:10.1038/ngeo1800.

Shindell, D. and Faluvegi, G. (2009) Climate response to regional radiative forcing during the twentieth century. Nature Geosci. 2, 294–300.

Walsh, J. E. and Chapman, W. L. (1998) Arctic cloud-radiation-temperature associations in observational data and atmospheric reanalysis, J. Climate, 11, 3030–3045.

CHARACTERIZATION OF THE NORTHERN SNOW ALBEDO WITH SATELLITE OBSERVATIONS

K. ATLASKINA[1], F. BERNINGER[2] and G. de LEEUW[1,3]

[1]Atmopshere Sciences Division, Department of Physics, University of Helsinki

[2]Department of Forest Sciences, Faculty of Agriculture and Forestry, University Helsinki, Finland

[3]Finnish Meteorological Institute, Helsinki, Finland

Keywords: CLIMATE CHANGE, SURFACE ALBEDO, SATELLITE DATA.

INTRODUCTION

Climate models predict changes in land surface albedo in boreal and Arctic areas of the Northern Hemisphere (NH) due to shrinking snow cover, rising temperatures and expanding shrubs and forests. If a highly reflective snow-covered surface is replaced by aged snow, a darker more vegetated or snow-free surface, more solar radiation will be absorbed and the temperature will rise, triggering a positive feedback loop: greater radiation absorption enhances further warming. This feedback effect of greater warming with decreasing snow or ice cover is referred to as 'Arctic Amplification' (Screen and Simmonds, 2010). Indeed, the snow cover extent in the NH has reduced during the past decades (Brown and Robinson, 2011) with the strongest decrease observed during the spring season. Air temperatures have increased more in the northern latitudes than in tropics (Screen, 2014) and affected snow cover extent in the NH (Brown and Robinson, 2011). In warmer conditions, increased snow cover temperatures enhance snow grain growth (Wiscombe and Warren, 1980). Vegetation productivity in subarctic regions has recently increased (arctic greening) and is associated with summer warmth enhancement which in turn is connected to sea ice retreat (Dutrieux et al., 2012). Dark vegetation over a snow covered surface results in a decrease in reflectivity. Precipitation pattern changes will alter snow properties and thus the surface albedo: fresh snow has a higher albedo than aged snow with a larger grain size. Aged snow has also been exposed for longer time to impurities, such as dark aerosol particles or vegetation litter depositing on top of the snow layer and has therefore a lower albedo than freshly fallen snow (e.g. Hansen and Nazarenko, 2004). All these processes together change the surface albedo and, thus the radiation balance, affecting the climate system on global and local scales. Due to the large difference in albedo of snow-covered and snow-free surfaces, albedo changes have the largest impact on the radiative balance during the snowmelt period.

The goal of this work is to study a possible relation between satellite-derived surface albedo in the spring (March, April and May) and factors which may affect it. In this study we looked at the effects of snow cover fraction (SCF), air temperature, precipitation amount and frequency, and vegetation greenness. The area of interest lies in the NH, north of 50°N (NH_{50}) and covers all land territories, except Greenland and Iceland.

METHODS

Satellite and gridded station observations for the years 2000-2012 were analyzed. The Moderate Resolution Imaging Spectroradiometer (MODIS) MCD43C3 combined product from two sensors onboard the Terra and Aqua satellites was used. Short-wave (0.3-5.0 μm) black-sky albedo and SCF data, both with a resolution of 8 days on a spatial grid of 0.05 degrees, were selected. The MOD13C2 Enhanced Vegetation Index (EVI), which relates to the photosynthetic absorption of radiation by vegetation and can be interpreted as biomass, was used to study the effect of vegetation on surface albedo. It is a monthly product on a 0.05 degrees grid. Climate Research Unit (CRU) time-series (TS) data on air temperature, precipitation amount and occurrence was also used. It is gridded to the 0.5 degree temporal and monthly time resolution dataset from over 4000 weather stations around the world.

For direct comparison, all data were reprojected and resampled to the 25km EASE-grid (Equal-Area Scalable Earth Grid) which is widely used in the analysis and visualization of data in polar areas. Additionally, MODIS surface albedo and SCF data were averaged to monthly means. All data pixels where SCF was less than 1% were discarded from the analysis.
Areas with permanent and complete (100%) SCF were divided into several geographical regions, such as Arctic Archipelago, Taymir Peninsula, Siberia, Scandinavia, Northern Canada and Labrador Peninsula.
Because albedo might not have a linear dependence on the studied variables, we chose Spearman's rank correlation over linear Pearson correlation in our calculations.

RESULTS

We found that SCF is the strongest variable affecting the surface albedo in the land areas of NH_{50} during the spring season. Changes in albedo are tightly connected to changes in SCF throughout spring season. Significant high positive correlation was found over most of the territories of NH_{50}, where SCF changes were detected (Figure 1). Averaged over the whole study domain, albedo and SCF also show strong positive correlation with correlation coefficients varying from 0.75 in March to 0.96 in May. However, we have also found that in large areas in both North America and Eurasia the albedo may change by up to ±0.2 in conditions of constant 100% SCF. Hence, we postulate that other factors, such as air temperature, precipitation pattern or vegetation, affect surface albedo changes.

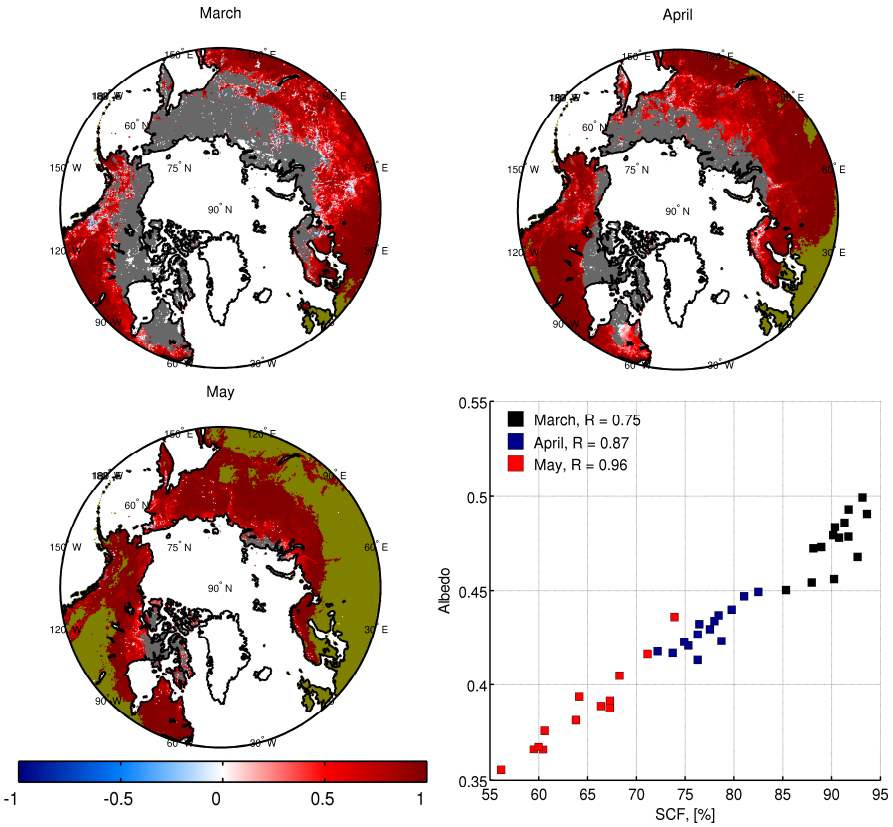

Figure 1. Maps of Albedo – SCF correlation coefficients for March, April and May determined for the years 2000-2012. Grey areas show areas with constant SCF throughout the study period. The scatterplot shows the relation between the albedo, averaged over study domain, and SCF for each of the spring months separately. Correlation coefficients are listed in legend.

From the factors we looked at, the air temperature has the largest effect on the spring-time surface albedo for areas where SCF does not change. Our analysis shows that there is a threshold of about -15°C for temperature, above which temperature affects the snow albedo: if the monthly mean exceeds this value,

further warming decreases albedo (Figure 2). Correlation maps (not shown) support this finding. For the areas where the mean monthly temperature is warmer than about -15°C, the correlation coefficient is found to be negative. This threshold is much lower than usually considered in climate models with temperature dependent snow albedo parameterization schemes (e.g. Pedersen and Winther, 2005).

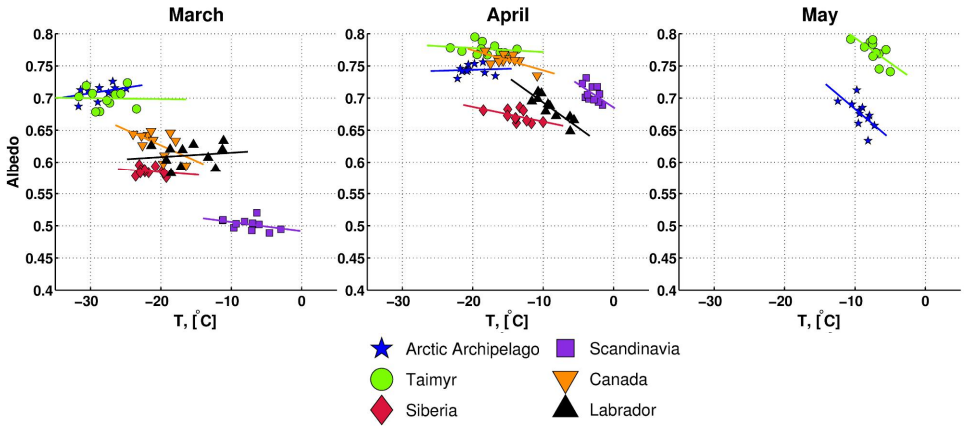

Figure 2. Relation between albedo and mean air temperature for the study regions. Straight lines show linear fits to data. Note that the areas of the regions are changing from month to month because of the requirement of constant 100% SCF.

The precipitation amount has been found to be important in Northern Canada in March, while in the Arctic Archipelago and Taymir Peninsula the precipitation occurrence affects albedo in April (Table 1). Despite of anticipation of positive correlation between precipitation amount or occurrence and albedo, there are vast areas where precipitation is negatively correlated with albedo (Figure 3). A possible reason for this observation could be the increased occurrence of rain or wet snow, rather than solid precipitation.
The strongest trend in greening has been observed in subarctic areas. However, no significant correlation has been found on the regional level, with the exception of Northern Canada, with a significant negative correlation in March (R = -0.81) and a positive correlationin April (R = 0.79) (Table 1).

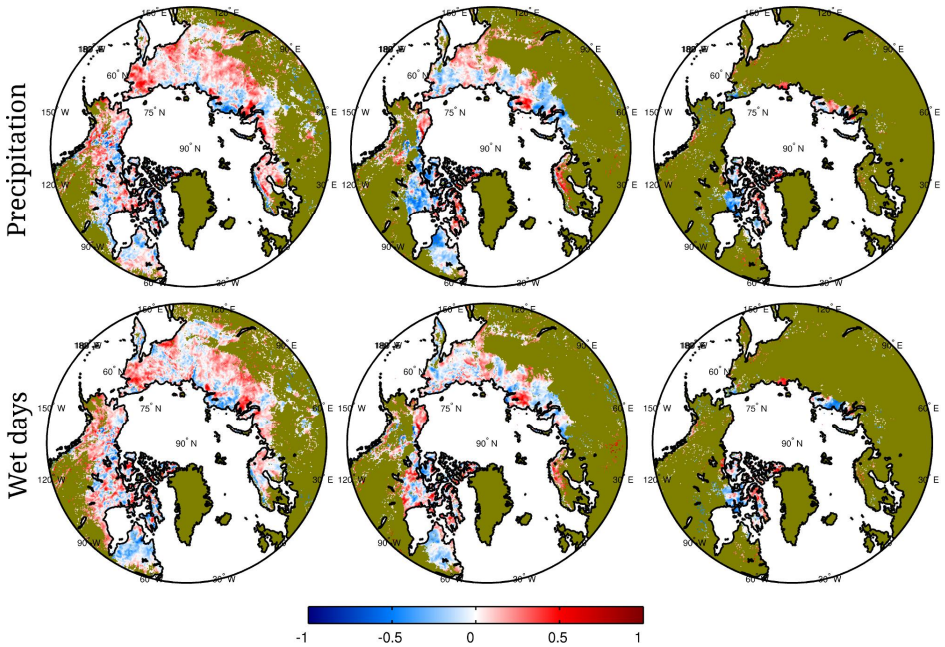

Figure 3. Albedo and precipitation amount (top panel) and number of days with precipitation (bottom panel) correlation coefficients maps.

	March				April				May			
	T °C	Prec	Wet days	EVI	T °C	Prec	Wet days	EVI	T °C	Prec	Wet days	EVI
Arctic Arch.	0.34	-0.4	-0.03	0.22	0.16	0.57	**0.7**	-0.18	**-0.73**	-0.15	-0.42	-0.15
Tajmyr	0.0	-0.57	-0.28	0.19	-0.28	0.53	**0.65**	-0.14	**-0.8**	0.35	0.12	-0.26
Siberia	-0.26	-0.14	-0.28	0.22	-0.56	-0.32	-0.39	-0.32	-	-	-	-
Scand.	-0.49	0.11	0.06	-0.49	-0.54	0.47	0.5	-0.36	-	-	-	-
Canada	-0.44	**0.52**	0.55	**-0.81**	-0.26	**-0.62**	0.01	**0.79**	-	-	-	-
Labrador	0.17	0.58	**0.69**	0.04	**0.88**	0.21	0.07	0.38				

Table 1. Pearson correlation coefficients for albedo and studied parameters for each of the regions falling into a constant SCF area. Significant correlation coefficients (p-value < 0.05) are shown in bold.

ACKNOWLEDGEMENTS

This work is supported by Cryosphere-Atmosphere Interactions in a Changing Arctic Climate (CRAICC) project which is part of the Top-level Research Initiative and by the Centre on Excellence in Atmospheric Science funded by the Finnish Academy of Sciences Excellence (project no. 272041).

REFERENCES

Brown, R. D., and D.A. Robinson (2011). Northern Hemisphere spring snow cover variability and change over 1922–2010 including an assessment of uncertainty, *The Cryosphere*, **5**, 219-229.

Dutrieux, L. P., Bartholomeus, H., Herold, M., and J. Verbesselt (2012). Relationships between declining summer sea ice, increasing temperatures and changing vegetation in the Siberian Arctic tundra from MODIS time series (2000–11). *Environ. Res. Lett*, **7**, 44028.

Hansen, J. and L. Nazarenko (2004). Soot climate forcing via snow and ice albedos, *Proceedings of the National Academy of Sciences of the United States of America,* **101**, 423-428.

Pedersen, C. A., and J.-G. Winther (2005). Intercomparison and validation of snow albedo parameterization schemes in climate models, *Climate Dynamics*, **25**, 351-362.

Screen, J. A. (2014). Arctic amplification decreases temperature variance in northern mid- to high-latitudes, *Nature Climate Change*, **4**, 577-582.

Screen, J. A. & Simmonds, I. (2010) The central role of diminishing sea ice in recent Arctic temperature amplification. *Nature* **464**, 1334_1337.

Wiscombe, W. J. and S. G. Warren (1980). A Model for the Spectral Albedo of Snow, I: Pure Snow, *J. Atmos. Sci*., **37**, 2712–2733.

CH_4 AND CO_2 EXCHANGE ON PERMAFROST TUNDRA IN TIKSI. SIBERIA

M. AURELA[1], T. LAURILA[1], J.-P. TUOVINEN[1], J. HATAKKA[1], M. LINKOSALMI[1], T. VIRTANEN[2], J. MIKOLA[2], E. ASMI[1], V. IVAKHOV[4], V. KONDRATYEV[5], T. UTTAL[6] and A. MAKSHTAS[7]

[1]Finnish Meteorological Institute, Helsinki, Finland.

[2]Department of Environmental Sciences, University of Helsinki, Helsinki, Finland.

[3]Department of Environmental Sciences, University of Helsinki, Lahti, Finland

[4]Voeikov Main Geophysical Observatory, St.Petersburg, Russia.

[5]Tiksi Hydrometeorological Service, Tiksi, Russia.

[6]National Oceanic and Atmospheric Administration, Boulder, U.S.A.

[7]Arctic and Antarctic Research Institute, St.Petersburg, Russia.

Keywords: ARCTIC TUNDRA, CH_4 FLUXES, CO_2 EXCHANGE, GHG BALANCE, PERMAFROST.

INTRODUCTION

The predicted environmental changes in the Arctic (permafrost thaw; changes in hydrology and vegetation) are suggested to have a marked effect on the CO_2 and CH_4 dynamics. Especially methane, as a strong greenhouse gas, may have a significant positive feedback to climate warming in the permafrost areas. It would be important to incorporate these GHG sources into the climate models, but more long-term flux measurements in the Arctic are needed to understand the dynamics behind their atmosphere-biosphere exchange. The Finnish Meteorological Institute (FMI) has started continuous long-term measurements of the fluxes and concentrations of the most important greenhouse gases, carbon dioxide and methane in Tiksi, in northern Siberia. The efforts of the FMI are part of a collaboration project with National Oceanic and Atmospheric Administration (NOAA) and Roshydromet (Yakutian Hydrometeorological Service, Arctic and Antarctic Research Institute and Main Geophysical Observatory units). The atmospheric research activities in Tiksi started as International Polar Year 2007/2008 project ”The International Arctic Systems for Observing the Atmosphere (IASOA)”. In this presentation we will provide first estimates of the annual balances of CO_2 and CH_4 exchange in Tiksi, study the responses of fluxes to different environmental and phenological variables and compare the results from this permafrost system to results obtained in non-permafrost soils in northern Finland.

METHODS

The Tiksi flux measurement station (71º35.656’N, 128º53.273’E, 7m a.s.l.) is situated in the vicinity of the Tiksi observatory on the shore of the Laptev Sea and close to the Lena river estuary. The measurement area covered by eddy covariance measurements consist of a mosaic of different vegetation and land cover types along with the hydrological gradient from a drier upland to a wetter valley. The permafrost in the area is continuous and the typical depth of the active layer in August is 40-50 cm. The mean annual temperature and precipitation at Tiksi observatory are -12.7 ºC and 323 mm, respectively.

Continuous eddy covariance flux measurements of CO_2 and energy started in July 2010, and in June 2012, the system was extended to cover the CH_4 fluxes as well. The EC instrumentation consisted of USA-1 (METEK) sonic anemometer, LI-7000 (Li-Cor) CO_2/H_2O analyzer and RMT-200 CH_4 analyzer (Los Gatos Research). The surface area covered by eddy covariance measurements consisted of a mosaic of different vegetation and land cover types along with the hydrological gradient from a drier upland to a wetter valley. The community structure, biomass, areal cover and leaf area index of the vegetation and the pH, organic matter (OM) content, temperature and permafrost depth of the soil have been studied in the measurement area in two field campaigns (17-23 July 2012, 1 July – 17 August 2014). For the upscaling purposes the EC footprint was categorized into seven vegetation types: bog, wet fen, dry fen, tussock tundra, grass meadow, shrub moss tundra heath and lichen tundra heath. High resolution (2m) Quickbird and WorldView2 images will be utilized to produce land use map for the area.

The supporting meteorological and hydrological measurements were recorded at 30min frequency in three different locations representing dry, wet and intermediate surfaces. The measurements included air temperature and humidity, different radiation components (net radiation, global radiation, PPFD, albedo), soil temperature and humidity, water table depth and soil heat flux. Precipitation and snow depth were measured at the near-by Tiksi observatory.

RESULTS

The EC measurements of CO_2 and energy fluxes have been running continuously since June 2010 with an exception of a 3 month break during the first winter. The CO_2 uptake rates during the peak summer were similar to those observed in a wetland in northern Finland, but during the winter time the CO_2 fluxes averages close to zero, while in northern Finland small but steady CO_2 efflux takes place throughout the winter.

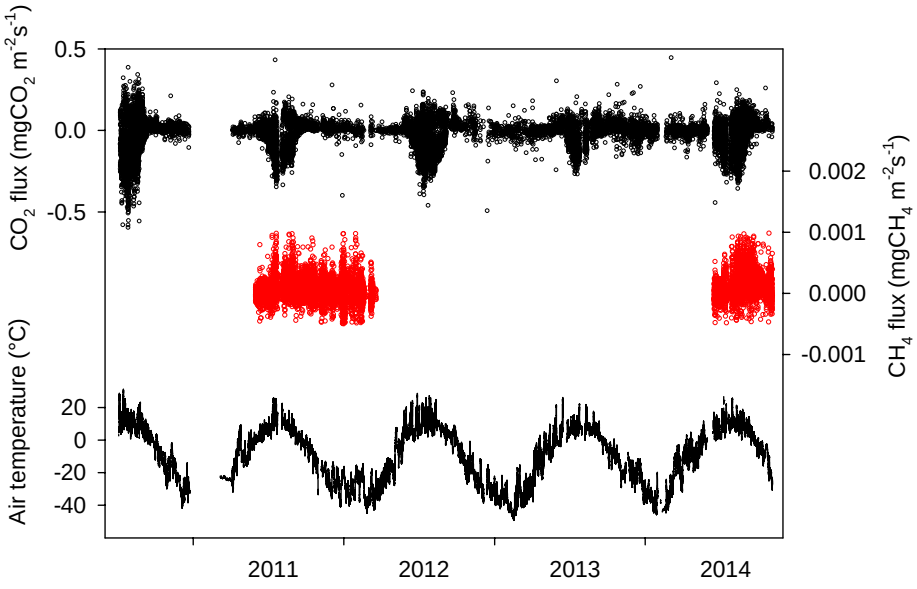

Figure 1. Half-an-hourly CO_2 and CH_4 fluxes at Tiksi. The negative values represent downward fluxes i.e. uptake by ecosystem.

The CH_4 fluxes were started in July 2011 but due to series of instrumental problems there was a long break in the measurements until they were re-started in June 2014 (Fig. 1). The CH_4 fluxes show distinctive differences in the fluxes representing different vegetation classes and hydrological conditions with higher fluxes from the wetter southern sector and to small uptake on the dry upland in north (Fig. 2).

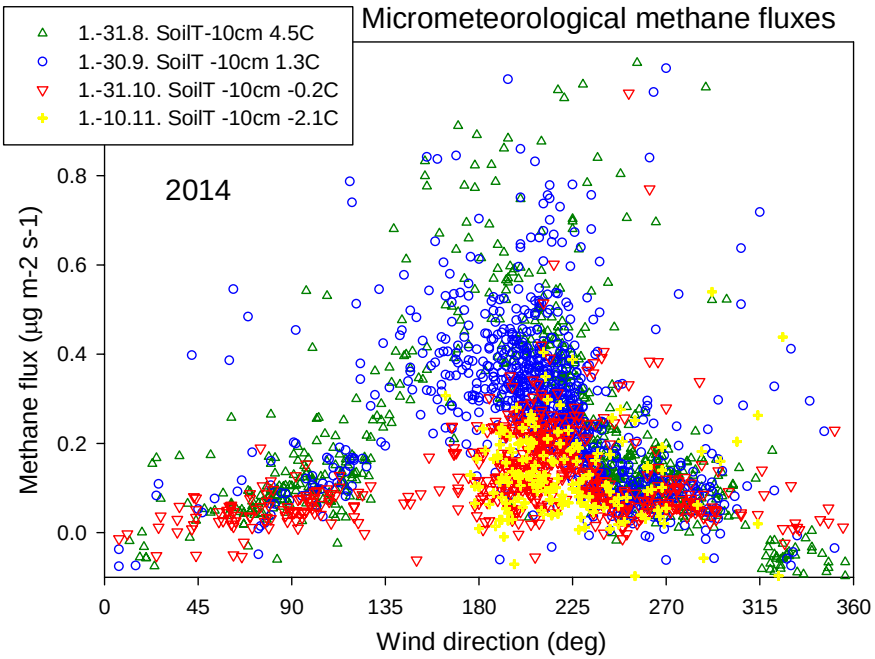

Figure 2. CH_4 emission in different wind directions during summer 2014. The highest fluxes are observed for southerly winds from the wet sedge area at the valley bottom.

ACKNOWLEDGEMENTS

This work was supported by the Academy of Finland (project no. 269095: Greenhouse gas, aerosol and albedo variations in the changing Arctic), European Commission (Changing permafrost in the Arctic and its Global Effects in the 21st Century, PAGE21) and Nordic Council of Ministers (DEFROST, a Top Research Initiative within NORDFORSK).

A STUDY OF AEROSOL ACTIVATION AT THE CLOUD EDGE WITH HIGH RESOLUTION NUMERICAL SIMULATIONS

N. BABKOVSKAIA[1], M. BOY[1], S. SMOLANDER[1], S. ROMAKKANIEMI[2], U. RANNIK[1] and M. KULMALA[1]

[1] University of Helsinki, Department of Physics, University of Helsinki, PO Box 48, Erik Palmenin aukio, 1, 00014 University of Helsinki, Finland.

[2]Department of Applied Physics, University of Eastern Finland, P.O.Box 1627, 70211 Kuopio, Finland.

Keywords: aerosol, DNS, cloud

INTRODUCTION

Atmospheric aerosol particles are affecting the Earth's radiative balance both by scattering solar radiation and by acting as cloud condensation nuclei (CCN). CCNs are a subset of all particles that are able to form cloud droplets in specific atmospheric conditions. Radiative properties of clouds are dependent on the number of cloud droplets and according to Twomey (1974) an increase in the CCN concentration leads to an increase in the cloud droplet number concentration (CDNC). Makkonen and co-workers (2012) showed, that on a global scale, a decrease in CCN in the year 2100 resulting from more efficient reduction of sulphur dioxide emissions, could lead to a decrease in CDNC by 20 %. The change in CDNC combined with the decrease of the direct aerosol effect would lead to a change in aerosol forcing from present-day to year 2100 of up to 1.4 W m^{-2}. Other important parameters for the concentrations of cloud droplets are the updraft velocity prevailing at the cloud base during cloud droplet formation (with high updrafts more cloud droplets can activate), the number concentration and the chemical composition of the cloud condensation nuclei.

The CDNC does not only dependent on the activation at the cloud base, but the cloud is a dynamic system with spatially and temporally varying properties. More cloud droplets may form due to in-cloud activation or due to entrainment of air from the cloud edges that might lead to formation of fresh cloud droplets. On the other hand, cloud droplets may evaporate because of mixing at the cloud boundaries or in-cloud dynamics. The latter of these can be important in stratus type clouds with long in-cloud residence time of the air parcel. The mixing at cloud boundaries takes place in all clouds, and the type of mixing is dependent on the meteorological conditions and mixing time scales. In homogeneous mixing, all particles loose water, but their number concentration is not affected. In heterogeneous mixing part of the droplet population experiences complete evaporation and shrinks back to aerosol particles. It is dependent on the time scales and moisture content of the entraining air and also the size of the droplets evaporating. Different phenomena related to aerosol cloud interactions and cloud dynamics involve large range of scales. Microphysics of aerosol-cloud interactions can be studied by process models, or so called box models, which are mainly used to study how and which aerosol particles are able to form cloud droplets. On the other end of scales are global models, which are needed to assess how changes in cloud properties affect the global radiation budget. Between these scales exist cloud resolving (CRM), or large eddy models (LES), that can be used to study cloud dynamics and for example the effect of aerosols on drizzle formation. In our research group Large Eddy Simulation model is actively used to investigate the effect of turbulence on the formation and growth processes, and to reveal a more realistic turbulent flow in the boundary layer. However, even in CRM the scale (resolution > 1 m) is such that all small scale turbulence needs to be parametrized.

A tool to provide this parametrization is direct numerical simulation (DNS), which can be used to study for example cloud boundaries in the scales from a few centimetres up to a few meters at most. Recently, in order to study the activation process at the cloud edge, the following model was proposed by our research

group (Babkovskaia et al., 2015). In this model the gas is compressible; thermal conductivity and diffusion coefficients of every species and of a mixture are described by the accurate expressions (Babkovskaia et al., 2011); thermal flux, change of energy by evaporation/condensation and viscous heating are included in the energy equation, and the solute effect is taken into account. To study the activation of aerosol particles we consider the condensation and evaporation of the aerosol particles covered by liquid water. We take 80 size classes of the cloud droplets with the droplet size logarithmically distributed in a range from 0.08 to 10 μm.

METHODS

We use the direct numerical simulation high-order public domain finite-difference PENCIL Code for compressible hydrodynamic flows. The code advances the equations in a non-conservative form. The degree of conservation of mass, momentum and energy can then be used to assess the accuracy of the solution. The code uses six-order centered finite differences. For turbulence calculation we normally use the RK3- 2N scheme for the time advancement. This scheme is of Runge-Kutta type, third order. On a typical processor, the cache memory between the CPU and the RAM is not big enough to hold full three-dimensional data arrays. Therefore, the Pencil Code has been designed to evaluate first all the terms on the right-hand sides of the evolution equations along a one-dimensional subset (pencil) before going to the next pencil. This implies that all derived quantities exist only along pencils. Only in exceptional cases do we allocate full 3-dimensional arrays to keep derived quantities in memory. The code is highly modular and comes with a large selection of physics modules. It is widely documented in the literature and used for many different application (Dobler et al., 2006; http://pencil-code.googlecode.com and references therein).

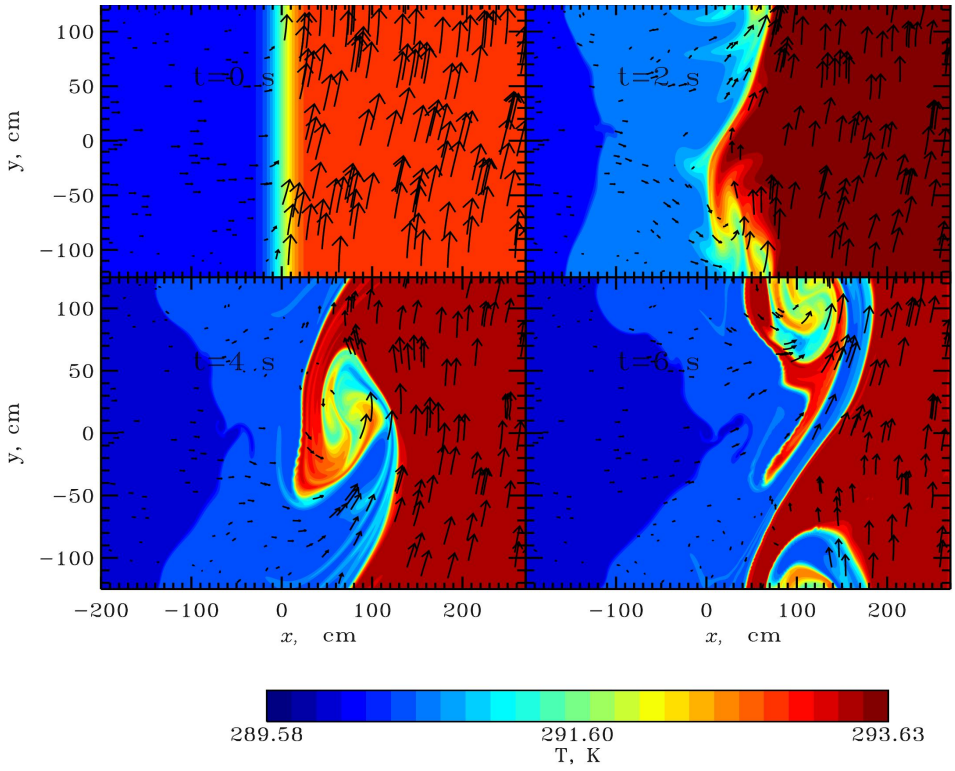

Fig.1 Velocity (showed by arrows) and temperature distributions at t=0, 2, 4, 6 s.

CONCLUSIONS

We study the aerosol activation process at a cloud edge in the computational domain of the size 500 cm x 250 cm x 250 cm. In Fig. 1 we show the structure of the motion at t=0, 2, 4 and 6 s. We assume that the dry air flux is coming into the domain (with velocity Ux=10 cm/s) in the middle part and going out near the boundaries. Moist air moves in horizontal direction with velocity Uy=100 cm/s. We consider the flux of aerosol particles, through the boundary between dry and moist air and analyse the effect of aerosol dynamics on the turbulent fields and vice versa.

Since the Kolmogorov scale is much smaller than the typical grid cell size of numerical simulation in atmospherics science (*O(1)* mm), we use the Smagorinsky model for the subgrid scale turbulence. To analyse the validity of the Smagorinsky approximation for the description of turbulent motion of air with aerosol particles, we compare the number of activated particles in 2D and 3D models with different resolutions. We find that the differences between the results of 2D simulations with different grid cell sizes are much larger than those between 2D and 3D simulations with the same cell size. Therefore, we conclude that a high resolution 2D model gives more realistic result for the simulations of activated particles than a similar 3D model with lower resolution.

We analyze the distributions of supersaturation and the concentration of activated particles in the domain at times t=0 s, 1 s, 2 s, 4 s. We show that the small scale turbulence plays an important role in particle activation. In a high resolution case, activation is limited at the cloud edge, whereas this is opposite in a case of lower resolution. Finally, we investigate the interactions between turbulence and microphysics. We find that aerosol dynamics increases the supersaturation in most parts of the domain by 16 %, and in some places even by 46 %. Activation of particles decreases the air temperature by about 0.03 K, and evaporation increases it by about 0.26 K.

ACKNOWLEDGEMENTS

We thank the Helsinki University Centre for Environment (HENVI), the Academy of Finland (251427, 139656) and computational resources from CSC – IT Center for Science Ltd are all gratefully acknowledged.

REFERENCES

Babkovskaia, N., Boy, M., Smolander, S., Romakkaniemi, S., Rannik, U., Kulmala, M., (2015). Atmospheric Research, **153,** 49 (*is accepted for publication*).

Babkovskaia, N., Haugen, N., Brandenburg, A. (2011). J. Comput. Phys., **230**, .

Dobler, W., Stix, M., Brandenburg, A. (2006). Astrophys. J., **638**, 336.

Haugen, N. E., Brandenburg, A. (2006). Phys. Fluids, **18**, 1.

Makkonen, R., Asmi, A., Kerminen, V.-M., Boy, M., Arneth, A., Hari, P. and Kulmala, M. (2012). J. Atmos. Chem. Phys., **12**, 1515.

The PENCIL Code, http://pencil-code.googlecode.com (2001).

Twomey, S. (1977). J. Atmos. Sci., **34**, 1149.

DOES NORTHERN HEMISPHERE TERRESTRIAL SNOW COVER VARY INTRASEASONALLY?

B.S. BARRETT[1] and G.R. HENDERSON[1]

[1]Oceanography Department, U.S. Naval Academy, Annapolis, Maryland, United States

Keywords: HIGH-LATITUDE TERRESTRIAL SNOW, INTRASEASONAL VARIABILITY, MADDEN-JULIAN OSCILLATION.

INTRODUCTION

High-latitude terrestrial snow is a complex component of the Earth climate system. Part of its complexity comes from its sensitivity to the atmosphere on a range of spatial and temporal scales. Snow cover acts as a buffer to modify energy exchange between the surface and the atmosphere. It also serves as a storage term in water balance, affecting both streamflow and runoff. Connecting snow cover to variability in atmospheric circulation remains a challenging problem (e.g., Derksen and LeDrew, 2000). For example, while the presence or absence of snow modifies energy exchanges with overlying air masses, the air masses themselves are responsible for depositing and ablating snow cover. Furthermore, snow has high surface albedo in open areas, low thermal conductivity, and plays important role in both global energy and hydrology balances. However, despite its importance to a wide spectrum of the sciences, the *intraseasonal* variability, on 30-60 day time scales, of snow has received little attention. This is in spite of the known atmospheric circulation response to tropical convection on time scales of the Madden-Julian Oscillation (MJO; Madden and Julian, 1972). The primary hypothesis of this work is that anomalies in tropical convection modulate atmospheric circulation in high-latitudes and subsequently modify surface snow during the winter season (see Fig. 1 for a detailed depiction of this hypothesis). By testing variability of changes of snow depth by phase of the MJO, possible relationships and variability on intraseasonal time scales can be explored.

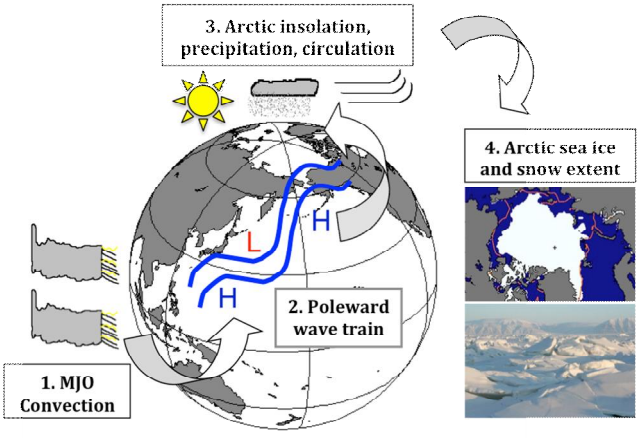

Figure 1. Possible pathway for intraseasonal variability of high-latitude terrestrial snow cover.

METHODS

Measuring terrestrial surface snow is a challenging dimension of the problem. Several variables exist to quantify surface snow: snow cover (the presence, or absence, of snow at a point), snow depth (the deepness of snow at a point), snow mass, volume, and density (the quantity of snow at a point), and even snow water equivalent (the quantity of frozen water at a point). Each of these variables has strengths and weaknesses, including in measurements. In-situ measurements often provide the best assessment of snow at a point, but in high-latitude regions, these are rare. Remote measurements, such as those from geostationary and polar-orbiting satellites, provide more temporal and spatial coverage, but often suffer from gaps including cloudy regions or regions with variable surface cover or topography. For this study, the first snow variable tested was snow depth, as it was considered to be the most rigorous. Subsequent work will test snow water equivalent.

The analyses in this study were based on publicly available datasets. To quantify snow variability, daily snow depth data from 1980-2013 were taken from the European Center for Medium-Range Weather Forecasting (ECMWF) interim (ERA-interim; Dee *et al.* 2011). For this study, only the month of October was analyzed. October was selected because that is the start of the winter snow season over high-latitude areas. Daily snow depth changes were passed into a self-organizing map (SOM) neural network with nine nodes. The SOM net then organized each day into the node most closely matching observed snow depth change. To gain an understanding of the state of the Arctic atmosphere under different phases of the MJO at both surface and mid-tropospheric levels, daily data from the National Centers for Environmental Prediction (NCEP)–Department of Energy (DOE) reanalysis 2 (Kanamitsu *et al.* 2002) were examined. Variables included in the atmospheric analysis were surface air temperature, 500-hPa geopotential height, mean sea level pressure, 2-m surface temperature, and 10-m winds, for the period 1980 to 2013. Daily composite anomalies of pressure, height, temperature and wind were calculated for October by phase of the MJO using the methodology described below.

CONCLUSIONS

Given that Arctic sea ice was found to vary intraseasonally by Henderson *et al.* (2014), and that Arctic atmospheric circulation was found to vary intraseasonally by Vecchi and Bond (2004) and Yoo *et al.* (2012), among others, it is likely that MJO projects also onto high-latitude terrestrial snow. Figure 2 shows preliminary results that indicate the variability of snow depth change by nodes in the SOM.

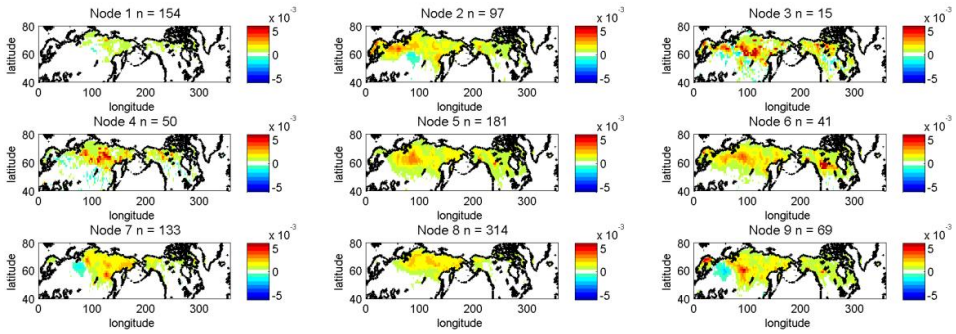

Figure 2: Mean snow depth changes as organized by a self-organizing map (SOM) neural network.

Node 1 indicates minimal snow depth change over high latitudes, while Node 9 indicates a dipole in snow depth change, with negative snow depth change over western Russia and positive snow depth change over central and eastern Russia. Each node is also associated with different occurrences of the eight active (and the inactive) MJO phases. Figure 3 shows the occurrence of each MJO phase in each SOM node. Yoo *et al.* (2012) found that one to two weeks after phases 4-6 was associated with below-normal temperatures over North America.

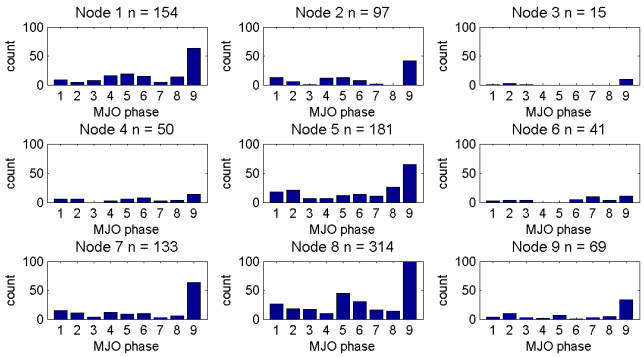

Figure 3: MJO phase occurrences for each SOM node.

Nodes 1, 2, and 8 were found to have the highest occurrences of those MJO phases, although mean snow depth change over North America was mostly neutral in those nodes. The complexity of the interaction between SOM nodes and MJO phases suggests additional work is needed to understand the MJO's role in modulating high-latitude snow cover.

ACKNOWLEDGEMENTS

This work was supported by the U.S. National Science Foundation grant PLR-1203843.

REFERENCES

Dee, D.P., and 35 co-authors (2011). The ERA-Interim reanalysis: Configuration and performance of the data assimilation system. *Quarterly Journal of the Royal Meteorological Society* **137**, 553-597.

Derksen, C., and E. LeDrew (2000). Variability and change in terrestrial snow cover: data acquisition and links to the atmosphere. *Progress in Physical Geography* **24**, 496-498.

Henderson, G.R., B.S. Barrett, and D.M. LaFleur (2014). Arctic sea ice and the Madden-Julian Oscillation (MJO). *Climate Dynamics*, **43**, 2185-2196.

Kanamitsu, M., W. Ebisuzaki, J. Woollen, S.-K. Yang, J.J. Hnilo, M. Fiorino, and G.L. Potter (2002). NCEP–DOE AMIP-II Reanalysis (R-2). *Bulletin of the American Meteorological Society* **83**, 1631–1643.

Madden, R.A., and P.R. Julian (1972). Description of global-scale circulation cells in the tropics with a 40–50 day period. *Journal of the Atmospheric Sciences* **29**, 1109–1123.

Vecchi G.A., and N.A. Bond (2004). The Madden–Julian Oscillation (MJO) and northern high latitude wintertime surface air temperatures. *Geophysical Research Letters* **31**, L04104.

Yoo C., S. Lee, and S.B. Feldstein (2012). Mechanisms of Arctic Surface Air Temperature Change in Response to the Madden–Julian Oscillation. *Journal of Climate* **25**, 5777–5790.

CHINA ENVIRONMENTAL AND CONTAMINATION HISTORIES: INSIGHTS FROM ATMOSPHERIC TRACE ELEMENTS IN THE PURUOGANGRI ICE CORE (TIBETAN PLATEAU)

E. BEAUDON[1], P. GABRIELLI[1,2], R. SIERRA-HERNANDEZ[1], A. WEGNER[3] and L. G. THOMPSON[1,2]

[1]Byrd Polar Research Center, the Ohio State University, Columbus, OH, United States

[2]School of Earth Science, the Ohio State University, Columbus, OH, United States

[3]Alfred Wegener Institute, Bremerhaven, Germany

Asia is facing enormous challenges including large-scale environmental changes, rapid population growth and industrialization. The inherent generated pollution contributes to half of all Earth's anthropogenic trace metals emissions that, when deposited to glaciers of the surrounding mountains of the Third Pole region, leave a characteristic chemical fingerprint. Records of past atmospheric deposition preserved in snow and ice from Third Pole glaciers provide unique insights into changes of the chemical composition of the atmosphere and into the nature and intensity of the regional atmospheric circulation systems. The determination of the elemental composition of aeolian dust stored in Tibetan Plateau glaciers can help to qualify the potential contamination of glacial meltwater as a part of the greater fresh Asian water source. The 215 m long Puruogangri ice core retrieved in 2000 at 6500 m a.s.l. in central Tibetan Plateau (Western Tanggula Shan, China) provides one of the first multi-millennium-long environmental archives (spanning the last 7000 years and annually resolved for the last 400 years) obtained from the Tibetan Plateau region. The Puruogangri's area is climatologically of particular interest because of its location at the boundary between the westerly (dry) and the monsoon (wet) dominated atmospheric circulation (the monsoon strength being driven by Eurasian spring snow cover). The major objective of this study is to determine the concentration of trace and ultra-trace elements in the Puruogangri ice core between 1600 and 2000 AD in order to characterize the atmospheric aerosols entrapped in the ice. Particular attention is given to assess the amount of trace elements originating from anthropogenic sources during both the pre-industrial and industrial periods. The distinction between the anthropogenic contribution and the crustal background may rely on the precise decoupling of the dry and wet seasons signals, the former being largely influenced by dust contribution.

POLLUTION OF THE AIRBASIN OF AN INDUSTRIAL CENTER

B.D. BELAN, D.K. DAVYDOV, A.V. FOFONOV, G.A. IVLEV, A.V. KOZLOV, D.A. PESTUNOV, D.V.SIMONENKOV,T.M. RASSKAZCHIKOVA, T.K. SKLYSDNEVA, N.V. UZHEGOVA, G.N. TOLMACHEV and M.YU. ARSHINOV

V.E. Zuev Institute of Atmospheric Optics, Siberian Branch, Russian Academy of Sciences, Tomsk, Russia.

Keywords: NDUSTRIAL CENTER, URBAN, SUBURBAN, HEAT ISLAND, AIR POLLUTION, MOBILE MEASUREMENT STATION.

INTRODUCTION

Research of patterns of air pollution field formation and transformation in large industrial centers has been thriving for the last 10–15 years. It has been considered for a long time that a city is well ventilated on a regular day with moderate wind, and increased concentration of air pollution is observed only near the industrial areas or along the plume of contaminants. A lot of studies show that the polluting admixtures produced in the city area are not transported outside but can be converted furthermore by various processes. As a result of combining such factors as industrial objects accumulation in limited space, orography, artificial and natural reservoirs etc., a local circulation arises in city areas (Penenko and Korotkov 1998, Penenko and Tsvetova, 2002).

The peculiarity of urban local circulation is the arousal of returned airflows leeward of the city opposite to the main airflow. This returned air circulation locks industrial emissions in the city area. A haze consisting of gases and aerosols appears above the city. It is called “pollution cap”. A peculiar characteristic of such a circulation is that it persists not only with a light wind but with a moderate one too. It is disrupted by atmospheric fronts but is renewed within 24 hours.

Thus, an “urban column” is formed above the city. Since the air temperature inside the column is higher than that of the city surroundings, the air begins to rise. At the beginning the urban column has a vertical shape and then under the influence of the main airflow it begins to bend (Landsberg, 1983). At a considerable distance from the city it becomes horizontal and spreads near the upper edge of the atmospheric boundary layer. This layer is separated from the free atmosphere by entrainment zone and its height depends on the season.

The goal of this paper was to determine experimentally the local air circulation effect on air composition of the industrial cities of Siberian region. In this paper we analyzed summer period and compared it with the results obtained for other seasons. The winter period was extensively studied by Matveev (2000).

DATA AND METHODOLOGY

During this investigation we used the AKV-2 mobile station designed by the Institute of Atmospheric Optics SB RAS. The station equipment enables the following continuous measurements to be carried out: air temperature and humidity; wind speed and direction; total solar radiation; NO, NO_2, O_3, SO_2, CO, CO_2 concentration; aerosol size distribution in two ranges: 0,4-10 μm by use of the modernized AZ–6 optical counter and 3–200 nm with the diffusion aerosol spectrometer. The accuracy of all given measurements by the AKV–2 station has been described in detail by Arshinov et al. (2005).

Aerosol chemical composition was determined by particulate matter sampling onto FPP filters and subsequent analytical analysis. In general, the AKV–2 station doesn't differ much from similar ones designed by other institutions.

The possibility of conducting en route measurements with the AKV–2 mobile station has allowed us to proceed from route based observations to the areal ones. This, in turn, allows the use of modern software packages for air pollutant mapping of the territory of a specific city. We had validated this method in Tomsk in July 2005 (Belan et al., 2007). To compare the air composition in other cities we had carried out measurements in February–March, 2004 and in August, 2005 along the route shown in Fig. 1. En-route measurements were performed in every large industrial city.

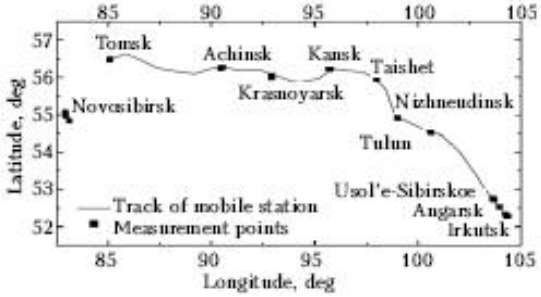

Figure 1. The route of the mobile station in February–March, 2004.

In addition to the continuous observations during the station motion, in Angarsk, Usol'e-Sibirskoe, Tulun, Nizhneudinsk, Taishet, Kansk, Krasnoyarsk, and Achinsk, we had carried out measurements during stops at the city entry, near the downtown, and at the exit. This method is classical. These observations were aimed at estimating the contribution of urban circulation to pollution accumulation in the city area and the change of thermodynamic regime. The main feature of this method is that the measurements were had to carry out as soon as possible in the three points. Fig. 2 illustrates the positions of the stops in Achinsk. In other cities, the measurements were performed by the same scheme.

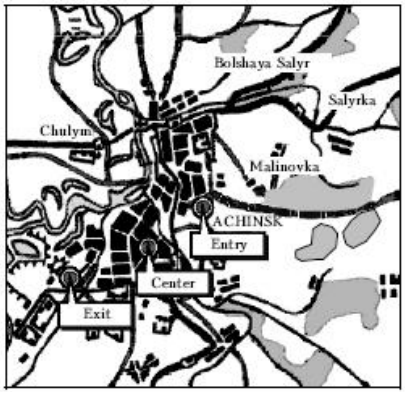

Figure 2. Scheme of measurement sites in Achinsk on February 29, 2004 (07:00–11:00 LT).

RESULTS AND DISCUSSION

The measurement data obtained in all of the above-mentioned cities have revealed the presence of pollutant accumulation processes and change of the thermodynamic regime on their territory. Of course, there is no ideal correspondence with a theory. Nonetheless, certain general regularities do exist.

If we look at Fig. 3, which presents the gas and aerosol concentrations, temperature, and relative humidity observed in Achinsk, we can see that in the central part where usually admixtures are accumulated, the SO_2, NO_2, CO, and aerosol concentrations are a several times higher than in the city periphery. On the contrary, the ozone content in center is much lower. This is normal, having in mind that the ozone is not injected to air by enterprises and engines, but rather is formed from precursors immediately in the

atmosphere (Penenko and Aloyan, 1985). In the presence of high aerosol concentration, ozone molecules O_3 start to interact with aerosol particles and are destructed.

Ambient air temperature was 2,5°C higher at the center than in the eastern/western periphery of the city. The relative humidity deserves a special note. The point is that it is still unclear whether it is normally higher in the city or outside it. Oke (Oke, 1982) argues that the city has additional water vapor sources: enterprises, untight communications, motor vehicles. On the other hand, he also showed that in winter time the snow is removed from the city streets, and much of its territory is covered with asphalt. Therefore, the natural source in the form of surface evaporation is less effective here. Therefore, knowing the relationship between absolute and relative humidity at a fixed air temperature (Matveev, 2000), it is possible to draw the following conclusion. If with the increase of air temperature at the center of the city the relative humidity proportionally decreases, this indicates that there are no additional sources of water vapor. Otherwise, in the case of proportional covariation, the water vapor sources are present. Returning to Fig. 3, we see that in Achinsk there took place a proportional decrease of relative humidity. Therefore, the city has no additional moisture sources.

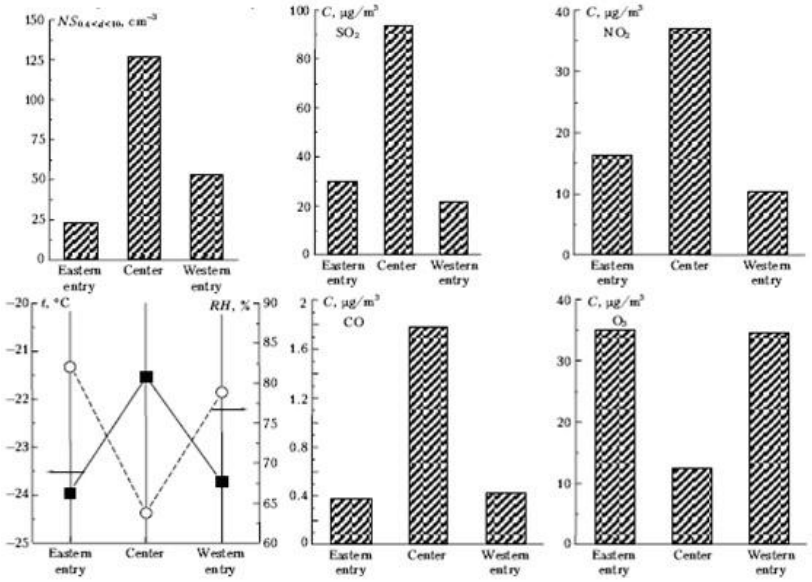

Figure 3. Concentrations of sulfur and nitrogen dioxide, carbon monoxide, ozone, aerosol number concentration (NS), air temperature, and relative humidity in center of Achinsk and its periphery on February 29, 2004.

The plots analogous to those in Fig. 3 have been made for all cities in which we have carried measurements for both summer and winter periods. Their analysis would occupy too much space; therefore, we compiled the tables containing the differences between parameters at city center and its periphery:

$$\Delta X = Xc - Xp$$

From this formula it is clear that any quantity with plus (minus) sign will have higher value at the center (on the periphery) of the city.

Wintertime data are given in Table 1, and summertime data in Table 2. It should be noted that, in contrast to winter, summertime measurements were conducted twice in most of the cities, on the way to and back.

City	t°C	RH, %	CO, mg/m^3	O_3, μ/m^3	SO_2, μ/m^3	NO_2, μ/m^3	NS, sm^{-3}	Note
Irkutsk	1.74	-9.5	0.23	-29.4	35.4	29.1	6.9	
Angarsk	0.13	0.8	0.30	-22.9	23.0	12.2	10.3	

Usol'e-Sibirskoe	0.78	8.9	-0.36	22.7	-49.9	-20.0	-2.5	Surbub in industrial zone
Tulun	0.90	2.9	0.21	-7.5	34.2	15.9	8.5	
Nizhneudinsk	-0.48	0.7	0.04	-10.8	6.8	0.3	3.6	
Taishet	-1.27	8.3	2.32	-16.2	11.6	3.3	50.8	Smog
Kansk	1.57	-8.8	-0.03	13.1	-24.5	-9.3	-11.3	Surbub in industrial zone
Krasnoyarsk	6.80	2.2	-0.18	-1.5	63.0	7.8	4.5	Smog
Achinsk	2.19	-15.1	1.36	-22.1	71.9	26.7	73.2	
Novosibirsk	1.65	0.3	0.35	-39.9	77.5	29.8	10.7	
Akademgorodok Novosibirsk	0.56	7.9	-0.07	-1.1	34.3	17.4	0.3	

Table 1. Differences in admixture concentrations and meteorological quantities between the centers and peripheries of Siberian cities in February–March, 2004.

City	t°C	RH, %	CO, mg/m^3	O_3, μ/m^3	SO_2, μ/m^3	NO_2, μ/m^3	NS, sm^{-3}	Note
Angarsk	-0.6	6.4	2.5	-29	-6.1	33	260	11.08
Usol'e-Sibirskoe	0.2	-4.6	-1.2	34	-5.0	-12	-11	08.08
Usol'e-Sibirskoe	4.0	-16.6	-3.8	1	3.8	12	-18	11.08
Tulun	-0.3	2.2	0.1	9	4.0	0.3	26	07.08
Tulun	0.0	3.2	0.1	-10	3.9	2.4	28	11.08
Nizhneudinsk	-0.6	-3.0	0.1	9	-3.0	0.4	2	07.08
Nizhneudinsk	-0.5	2.4	1.1	-7	4.0	2.2	0	11.08
Taishet	0.1	5.2	0.1	-17	7.2	2.6	57	07.08
Taishet	-0.4	-4.0	-0.2	-2	-3.0	3.2	9	11.08
Kansk	0.3	4.3	0.2	-14	-14.0	10.8	-16	06.08
Kansk	-0.1	-10.5	0.1	12	-2.9	1.4	-40	12.08
Krasnoyarsk	1.0	-6.0	0.2	-1	3.2	4.0	28	05.08
Krasnoyarsk	1.5	-9.9	0.1	7	-9.8	2.4	10	12.08
Achinsk	-1.2	0.7	0.2	2	-	-14	-150	06.08
Achinsk	1.8	-7.6	0.1	-1	-	5.3	27	12.08
Mariinsk	1.9	-12.1	0.3	20	-	-3.9	3	05.08
Mariinsk	-0.2	-1.4	0.1	11	1.1	-4.0	1	13.08
Novosibirsk	-0.1	3.5	0.2	-14	0.9	9.0	111	01.07

Table 2. Differences in admixture concentrations and meteorological quantities between the centers and peripheries of Siberian cities in August, 2005.

From data of Table 1 it is seen that in most cases the air temperature is higher at the center than on the periphery of the city (9 out of 11 cities). It is also seen that, the bigger the city, the larger the temperature difference. Obviously, in this situation the number of enterprises, motor vehicles, and heat leakage from buildings are important.

The relative humidity varies from city to city in a wide range. Nonetheless, from Table 1 we can conclude that on the territory of eight out of eleven cities, there are additional sources of water vapor.

Carbon monoxide in the city is mainly produced by automobile engines. Naturally, its density is higher in the central part of the cities. This is reflected in Table 1. Exceptions are Usol'e-Sibirskoe where the peripheral point turned out to be near industrial zone, and Krasnoyarsk, in which the measurements at the center were conducted at nighttime. Seemingly, the peripheral measurements were carried out in period of a heavier traffic. The difference in Kansk and Novosibirsk's Akademgorodok is close to the measurement error of these parameters.

As was already noted above, ozone in the central part of the cities suffers destruction in fresh emissions and frequently recovers to the periphery. From Table 1 it is seen that this pattern is observed in nine cities out eleven under consideration. Two cities, in which the background points undergo impact of the industrial zone, the pattern is reverse.

Sulfur and nitrogen dioxide, whose sources are emissions of different origin, typically have increased concentration at the city centers and decreased concentrations towards the periphery. Exceptions, again, occur for two cities in which the background measurements were conducted in industrial zone.

Concentration of particles with $d \geq 0.4$ μm is presented in the last column of Table 1. Data in this column also demonstrate increased values in the central part of the cities and decreased values in the periphery, of course, with the exception of the cases when the background was measured in the region of industrial zone.

Thus, the industrial emissions and automobile exhausts in most of the industrial cities of Siberia in winter turn out to be the source of increased admixture concentrations in the atmosphere of the cities. Moreover these pollutants do not disperse, but even are accumulated.

From Table 2 it follows that, in contrast to winter period (Landsberg, G.E., 1983), in summer the differences in concentrations and meteorological quantities between the city center and periphery are much more variable. The main interseasonal difference is the absence of a stable regularity in the distribution of the differences, which was the case for winter. Obviously, this is due to better dispersal of the contaminants from the atmosphere of this region in summer.

CONCLUSION

The experimental studies conducted have revealed that in winter in the industrial cities of Siberia the existing specific local circulation favors creation of specific fields of admixture distribution. The admixture concentration is higher in the central city parts and decrease toward the periphery. This same is also true for thermodynamic air characteristics.

In summer, owing to more effective atmospheric ventilation, the effects of local circulation substantially weaken. As a result, the distinct admixture accumulation in the central parts of the cities may not always be revealed.

ACKNOWLEDGEMENTS

This work was supported by Presidium of the Russian Academy of Sciences (Program No. 4), the Branch of Geology, Geophysics and Mining Sciences of RAS (Program No. 5); interdisciplinary integration projects of the Siberian Branch of the Russian Academy of Science No. 35, No. 70 and No. 131; State contracts of the Ministry of Education and Science of Russia No. 14.604.21.0100, (RFMTFIBBB210290) and No. 14.613.21.0013 (RFMEFI61314X0013); and Russian Foundation for Basic Research (grants No. 14-05-00526, No. 14-05-00590, No. 14-05-93108).

REFERENCES

Arshinov, M.Y., Belan, B.D., Davydov, D.K., Ivlev, G.A., Kozlov, A.V., Pestunov, D.A., Pokrovskii, E.V., Simonenkov, D.V., Uzhegova, N.V., Fofonov, A.V. (2005). AKV-2 mobile station and its use in Tomsk city as an example, *Atmos. Oceanic Opt.* **18**, 575–580.

Belan, B.D., Ivlev, G.A., Kozlov, A.S., Marinaite, I.I., Penenko, V.V., Pokrovskii, E.V., Simonenkov, D.V., Fofonov A.V., Khodzher T.V. (2007), Comparison of air composition over industrial cities of Siberia, *Atmos. Oceanic Opt.* **20**, 387–396.

Landsberg, H. E. *The urban climate*, International Geophysics Series, Vol. 28. Academic Press, New York. 1981, 275.

Landsberg, G.E. (1983) *Urban climate*, 248.

Matveev, L.T., (2000). *Atmospheric Physics*. Gidrometeoizdat, Saint Petersburg, 360.

Oke, T.R. (1987) *Climates of Boundary Layer*, Psychology Press, 435.

Penenko, V.V.and Aloyan A.E. (1985) *Models and methods for environmental protection problems*, Nauka, Novosibirsk, 256.

Penenko, V.V. and Korotkov, M.G. (1998). Application of numerical models for forecasting of emergency and ecologically unfavorable situations in the atmosphere, *Atmos. Oceanic Opt.* **6**, 492–496.

Penenko, V.V. and Tsvetova, E.A. (2002). Methods and models for assessment of ecological risks, *Atmos. Oceanic Opt.* **5-6**, 370–376.

ATMOSPHERE-LAND COUPLING AT HIGH LATITUDES: IMPACT ON NEAR SURFACE TEMPERATURE AND CO_2

A. BELJAARS, G. BALSAMO, E. DUTRA and I. SANDU

European Centre for Medium-range Weather Forecasts (ECMWF)
Shinfield Park, Reading, RG2 9AX, United Kingdom.

Keywords: BOUNDARY LAYER, SNOW, VEGETATION COUPLING, DIURNAL CYCLE.

INTRODUCTION

Many models, including the ECMWF model, show strong sensitivity to the parameterization of the stable boundary layer. The sensitivity is reflected in the night time temperature, the amplitude of the diurnal temperature cycle, the structure of the wind profile (wind direction, surface wind, low level jet), the surface stress, impact on the large scale flow, the magnitude of Arctic amplification in climate models, and the night time build-up of CO_2 in carbon models. Similarity theory supported by observations is well established for the stable boundary layer. It is widely accepted for the surface layer with Monin Obukhov similarity, and can be extended to the outer layer through local scaling (Nieuwstadt 1984). This is fully consistent with a closure scheme that expresses turbulent diffusion coefficients into shear, the distance above the surface as length scale and stability functions dependent on the Ri-number (Louis 1979). However, very few models use functions that are purely observationally based. With an observationally based formulation it is very difficult to control the diurnal cycle of temperature and to obtain optimal large scale scores (Beljaars 2001). The reason for this discrepancy is not well understood. Possible explanations are: (i) similarity theory only applies to the fully turbulent stable boundary layer and not to the intermittent low wind regime, (ii) similarity theory applies to homogeneous terrain only, whereas real terrain is nearly always sloping or covered with inhomogeneous vegetation, and (iii) meso-scale variability may contribute to the vertical transport or enhance turbulence.

This is the reason that many models use so-called “long tail” stability functions to have more diffusion in general and also some mixing at high Richardson numbers where traditional similarity theory has virtually no turbulent transport. One of the complications is a positive feedback between turbulent diffusion and stability. In case of surface cooling through radiation, the increased temperature gradient leads to an increase of the heat flux towards the surface, but stronger stability opposes such an increase. The result can be a so-called “run-away” cooling of the surface. In that case turbulent diffusion stops altogether and a radiative equilibrium between the atmosphere and the surface is established. The “long tail” stability functions are efficient in controlling such run-away cooling. Similar issues exists for the simulation of CO_2, where models can have a too strong accumulation of CO_2 in the lowest model layer at low wind speeds when observationally based stability functions are used.

This short paper gives an overview of experience at ECMWF with stable boundary layer parameterization issues. The main features of the ECMWF scheme are described in Beljaars and Viterbo (1998) wit recent upgrades in Köhler et al. (2011), and Sandu et al. (2013). As illustration, Fig. 1 shows the latitude dependence of the January 2011 night time temperature errors. It is clear that the errors increase with latitude, which suggests that the most stable regime is the most sensitive to errors. This is also clear from the long term evolution of mean night time temperature errors over Europe as illustrated in Fig. 2. The model changes which had a big impact were in 1996 and 2007, both related to turbulent diffusion in stably stratified flow. In 1996 the diffusion coefficient for heat was increased and in 2007 the diffusion above the surface layer was reduced. The latter was detrimental for the temperature forecasts but was necessary to avoid the destruction of stratocumulus through excessive diffusion in inversions. This illustrates the multi-faceted aspects of the turbulent diffusion parameterization.

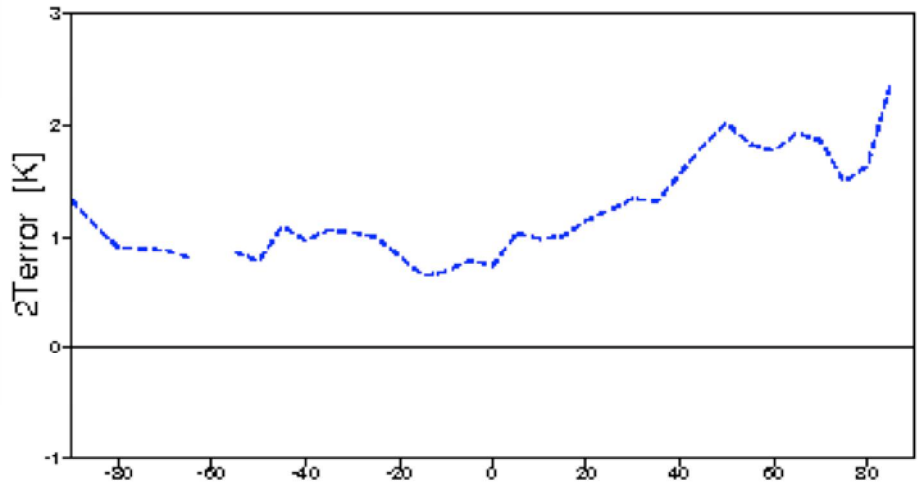

Figure 1. Zonal mean absolute night time temperature error at 2m over land as a function of latitude of the operational ECMWF system verified against the analyses for January 2011 (the analysis is a gridded representation of the SYNOP observations). The night time temperature has been obtained by selecting a verification time of 0, 6, 12 or 18 UTC (dependent on longitude and latitude) to be closest to the minimum temperature for each location. Daily 24, 30, 36 and 42-hour forecasts have been used.

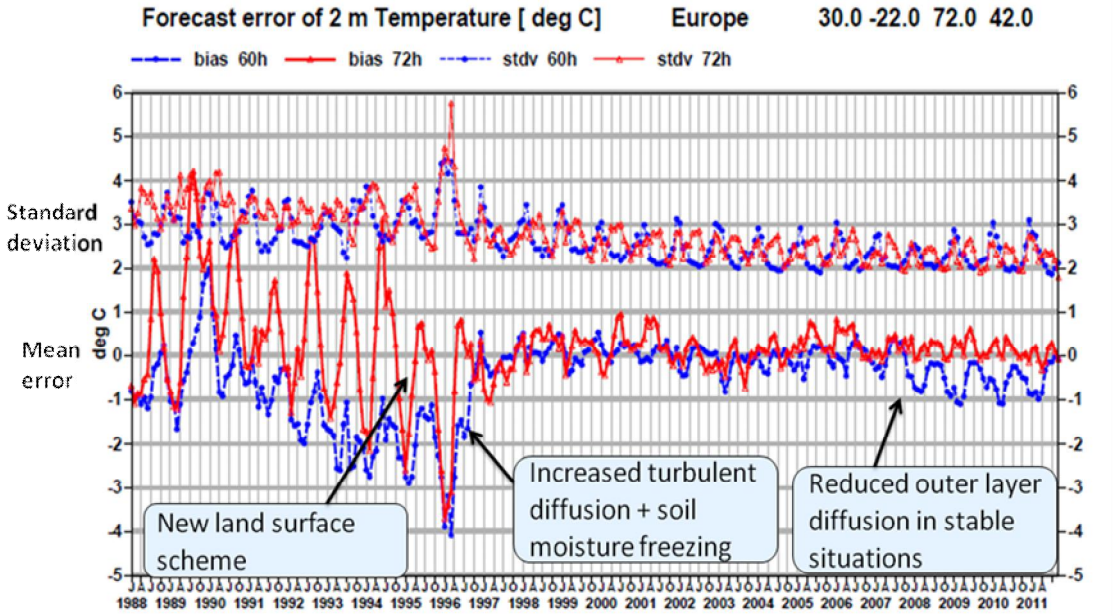

Figure 2. Historic evolution of 2m temperature errors of the operational ECMWF system. These are monthly values of mean and standard deviation of errors for step 60 and 72 hour forecasts, initialized daily at 12 UTC, verifying at 0 UTC (blue) and 12 UTC (red) respectively. The verification is against about 800 SYNOP stations over Europe (30°N-72°N/ 22°W-72°E).

THERMAL COUPLING BETWEEN ATMOSPHERE AND LAND SURFACE

The thermal coupling between atmosphere and the deep surface, has an atmospheric component and a surface component with the radiative forcing in the middle at the so-called skin layer (see Beljaars 2011 for more details). The latter is the layer that intercepts or emits the radiation and can be the vegetation

canopy, a litter layer on top of the soil, a snow layer or a combination of these in heterogeneous terrain. At night the skin layer cools through radiation and it depends on the strength of the turbulent coupling

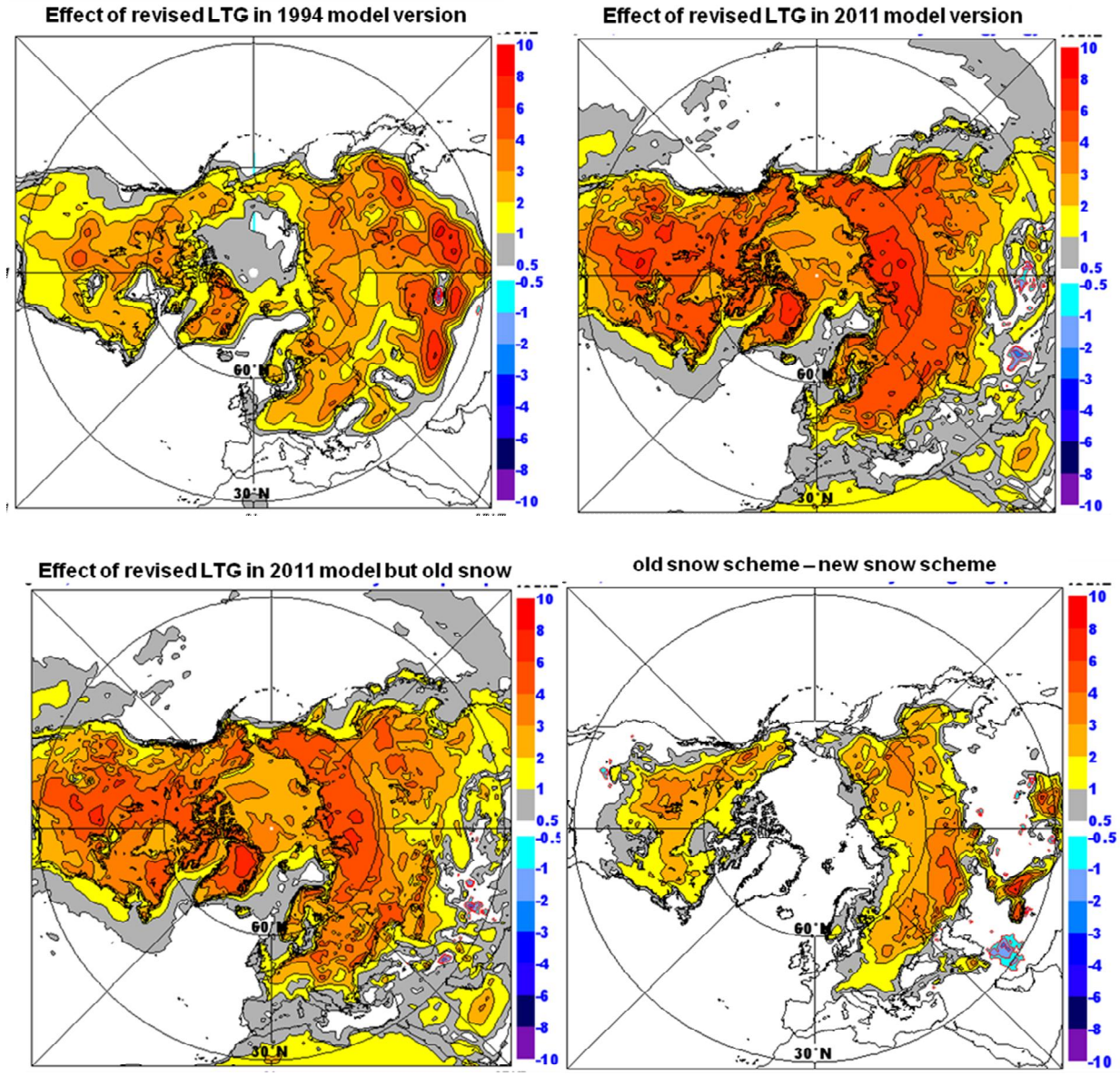

Figure 3. Effect (in terms of mean temperature change) of the model change as indicated by the figure title on averaged January 1996 temperature. These sensitivity experiments were performed by starting a long integration from 1 October 1995 and applying relaxation to the 6-hourly operational analyses above 500 m from the surface. This is an efficient way of doing "deterministic" seasonal integrations without constraining the stable boundary layer.

with the atmosphere as well as the thermal coupling with the underlying soil to what extent the near surface temperature will drop. These processes are affected by many empirical parameters and processes: turbulent diffusion in the stable boundary layer (dependent on shear, stratification and meso-scale variability), the surface roughness lengths for momentum and heat, coupling between the vegetation layer and the soil (expressed in the ECMWF model by a vegetation type dependent conductivity), the soil diffusion coefficient, the presence of snow (including thickness and density), the occurrence of soil water freezing/thawing, and terrain heterogeneity.

A clear example is the change in 1996 in which the stability functions were changed from “LTG” (long tails) to “Revised-LTG” (even longer tails) and in which the process of soil water freezing was introduced. Both, the increased diffusion for heat and the additional thermal inertia of the soil due to the freezing process, reduced the winter cold bias. The top left panel of Fig. 3 shows the impact of the revised boundary layer scheme as published by Viterbo et al. (1999) with the 1994 version of the model. This experiment was repeated with the 2011 version of the model by implementing the original LTG and revised-LTG versions. The impact of revised-LTG versus LTG is shown in the top right panel of Fig. 3. Comparing the two top panels of Fig. 3, it is clear that the same boundary layer change has a much bigger impact in the 2011 model version than in old 1994 version. It is impossible to say which model element is responsible as many model changes were made over the years. However, very likely candidates are the new soil hydrology scheme (Balsamo et al. 2009) and the new snow scheme (Dutra et al. 2010). In the latter, snow is a much better insulator and therefore the winter temperatures are lower. The impact of revised-LTG with the old snow scheme (bottom left panel) is also smaller than with the new snow scheme (top right). Unfortunately, the effect of revised-LTG could not be tested with the old hydrology scheme.

It is clear that realistic diurnal cycles can be achieved in different ways, namely by adjusting the coupling strength in the atmosphere through turbulent diffusion and by the coupling strength to the underlying soil. All this, obviously depends on wind speed, presence and density of snow, and soil state (dry/wet/frozen). To diagnose the coupling aspects, the heat fluxes over six hours before reaching the minimum temperature are plotted as a zonal average over land as a the result of an average of daily short range forecasts with the ECMWF NWP model (Fig. 4). The sign convention for the fluxes is positive for downward fluxes. We will focus here on the Northern Hemisphere latitude dependence and the wind speed dependence of long wave cooling (Lnet) , sensible heat flux (H) and ground heat flux (G0). Short wave radiation (Snet) in this phase of the diurnal cycle is zero, and the latent heat flux (LE) is negligible. The long wave cooling (red) decreases strongly with latitude mainly because at high latitudes the temperature is lower and therefore the long wave emission is less. This also applies to the wind speed dependence, for strong winds (dashed) the temperature is higher than for low winds (solid) and therefore the cooling is stronger. Surprisingly, the sensible heat flux (green) is nearly constant with latitude and the ground heat flux (brown) follows the radiation. For strong winds the sensible heat flux is higher because there is more mixing in the boundary layer, but for ground heat flux the wind dependence is fairly small. It should be noted that this zonal averaging is over different types of terrain, and snow cover, so no conclusions can be drawn for a particular location.

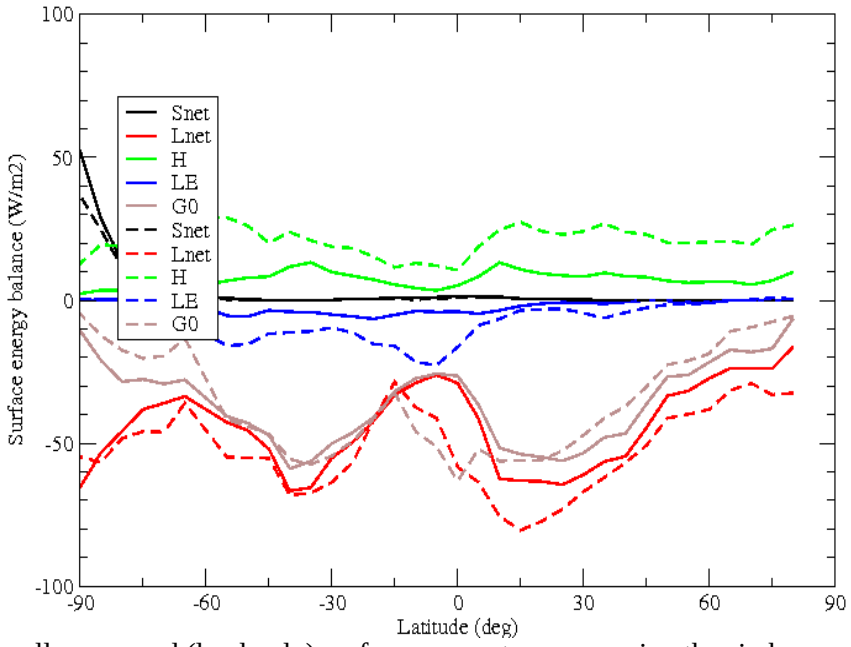

Figure 4. Zonally averaged (land only) surface energy terms covering the six hours preceding the minimum temperature. Data has been averaged over a month of daily 24, 30, 36 and 48-hour forecasts

selecting the forecast range for each longitude that is the closest to the minimum temperature (Operations, Feb 2009). The solid and dashed lines are for wind speeds smaller and larger than 3 m/s respectively. The sign convention is: positive for downward fluxes.

CONCLUSIONS

The model analysis above clearly illustrates that temperature forecasts at high latitudes depend strongly on the details of the turbulent coupling between atmosphere and surface and between surface and underlying soil. The ratios of turbulent heat flux and ground heat flux are documented for the ECMWF model, but it is by no means clear whether these are realistic. Given the lack of verification on this aspect it is very well possible that reasonable diurnal temperature cycles are achieved for the wrong reason. This will also have consequences for the strength of the Artic amplification in climate models. Different models with different relative coupling strengths may have similar results for the current climate but have different projections for future scenarios.

A possible way forward is to characterize the turbulent fluxes in relation to long wave cooling from observations in a similar way as in Betts (2006). By lack of direct sensible heat flux observations, the observed depth of the stable boundary layer (from radio sondes) can be used to estimate the amount of heat necessary to cool such a layer. The study should be done for a wide range of surface characteristics and wind speeds, and similarly for model output. Although the characterization of relations between diurnal cycles and fluxes can be done on climate model output, there is an advantage in using NWP models because exactly the same cases can be used for the model and the observations. In NWP it is possible to stay within the predictable range, which filters "noise" from synoptic variability. Furthermore, there is an advantage to include CO_2 in the analysis of diurnal cycles, because it gives a different perspective on turbulent mixing compared to heat flux (Betts 2006; Law et al. 2008).

REFERENCES

Balsamo, G., A. Beljaars, K. Scipal, P. Viterbo, B. van den Hurk, M. Hirschi and A.K. Betts, A.K. (2009): A revised hydrology for the ECMWF model: verification from field site to terrestrial water storage and impact in the Integrated Forecast System, *J. Hydr. Meteor*., **10**, 623-643.

Beljaars, A.C.M. and P. Viterbo (1998): The role of the boundary layer in a numerical weather prediction model, in: *Clear and cloudy boundary layers*, A.A.M. Holtslag and P. Duynkerke (eds.), Royal Netherlands Academy of Arts and Sciences, p. 287-304, Amsterdam, North Holland Publishers.

Beljaars, A.C.M. (2001): Issues in boundary layer parameterization for large scale models, ECMWF seminar on: *Key issues in the parameterization of subgrid physical processes*, p. 71-88, 3-7 Sept., Reading.

Beljaars, A. (2011): The stable boundary layer in the ECMWF model, In: *ECMWF Workshop on diurnal cycles and the stable boundary layer*, p1-10, http://old.ecmwf.int/publications/library/do/references/list/163

Betts, A. K. (2006): Radiative scaling of the nocturnal boundary layer and the diurnal temperature range, *J. Geophys. Res.*, **111**, D07105.

Dutra, E., G. Balsamo, P. Viterbo, P. Miranda, A. Beljaars, C. Schär and K. Elder (2010): An improved snow scheme for the ECMWF land surface model: description and offline validation, *J. Hydr. Meteor*., **11**, 899-916.

Köhler, M., M. Ahlgrimm, A. Beljaars, (2011): Unified treatment of dry convective and stratocumulus-topped boundary layers in the ECMWF model, *Quart. J. Roy. Meteor. Soc.*, **137**, 43-57.

Law, R.M., W. Peters, C. Rödenbeck, C. Aulagnier, I. Baker, D.J. Bergmann, P. Bousquet, J. Brandt, L. Bruhwiler, P.J. Cameron-Smith, J.H. Christensen, F. Delage, A.S. Denning, S. Fan, C. Geels, S. Houweling, R. Imasu, U. Karstens, S.R. Kawa, J. Kleist, M.C. Krol, S.-J. Lin, R. Lokupitiya, T. Maki, S. Maksyutov, Y. Niwa, R. Onishi, N. Parazoo, P.K. Patra, G. Pieterse, L. Rivier, M. Satoh, S. Serrar, S. Taguchi, M. Takigawa, R. Vautard, A.T. Vermeulen, and Z. Zhu (2008): TransCom model simulations of

hourly atmospheric CO2: Experimental overview and diurnal cycle results for 2002, *Global Biogeochem. Cycles*, **22**, GB3009.

Louis, J.-F. (1979): A parametric model of vertical eddy fluxes in the atmosphere, *Bound.-Layer Meteor.*, **17**, 187-202.

Nieuwstadt, F.T.M. (1984): The turbulent structure of the stable nocturnal boundary layer, *J. Atmos. Sci.*, **41**, 2202-2216.

Sandu, I., A. Beljaars, P. Bechtold, T. Mauritsen and G. Balsamo (2013): Why is it so difficult to represent stably stratified conditions in numerical weather prediction (NWP) models?, *J. Adv. Mod. Earth Sys.*, **5**, 117-132.

Viterbo, P., A. Beljaars, J.-F. Mahfouf, and J. Teixeira, (1999): The representation of soil moisture freezing and its impact on the stable boundary layer, *Quart. J. Roy. Meteor. Soc*., **125**, 2401-2426.

GOING BEYOND CARBON: THE EFFECTS OF FOREST MANAGEMENT ON CLIMATE - A CASE STUDY FOR FINLAND BASED ON THE HENVI FOREST PROJECT

F. BERNINGER[1], T. KALLIOKOSKI[1], K. MINKKINEN[1], L. VALSTA[1], A. MÄKELÄ[1], J. BÄCK[1], N. KUUSINEN[1], A. VÄHÄTALO[1] M. BOY[2], D. MOGENSEN[2], L. ZHOU[2] and E. NIKINMAA[1]

[1]Department of Forest Sciences, POBox 27, 00014 University of Helsinki

[2]Department of Physics, POBox 64, 00014 University of Helsinki

Keywords: FORESTRY, AEROSOL, ALBEDO, VOC, SUBSTITUTION EFFECT.

INTRODUCTION

The role of forests in the global carbon cycle has been explored in depths and has received large attention. However, the effects of forests on the global climate and not restricted to carbon but there are numerous feedbacks of forest ecosystems to the global climate system. These include albedo, emissions of VOC leading to direct aerosol forcing and cloud formation. The effects of albedo are, in addition, usually opposite to the effects of carbon and might, therefore, change the total effects of forests on the climate system.

Furthermore, a large proportion of global forests are managed in some way. From an atmospheric modeling point of view forest management is certainly the worlds larges “geo-engineering project” (in terms of area). Apart from forest carbon stocks, also the proportion of open areas and affect deeply stand biomasses and the proportion of different tree species. This means that in addition to the carbon balance forest management will thus critically change albedo, VOC emissions and other parts of the surface model.

The path of carbon, fixed by trees does not finish when trees are cut in forest operations. Some of the carbon, the so called logging residues, are left on the site to decompose. However, these woody residues might also be used for bioenergy which usually leads to a more rapid emissions of carbon in the logging residues and a subsequent reduction in forest carbon stocks. CO_2 emissions from bioenergy might be smaller or bigger than emissions from fossil fuels, depending on the type of biomass used and the fossil fuel that is used as a baseline.

A third dimension of the carbon balance of the forest sector depends on the use of the wood by the industry and consumers. Wood and wood products contain carbon and there is evidence that a growing stock of carbon is accumulated in wood products as wooden houses or furniture. This carbon stock is relatively large and might be increasing depending how society and economy develop. A more obscure, but potentially important effect of forestry is the called substitution effect. The substitution effect describes the carbon emissions incurred or avoided by using wood derived products instead of non-wood based products. It is based on a comparison of the life cycle analysis of wood products and alternative products.

In this talk we present for the first time a comprehensive analysis of the aforementioned effects of forestry in Finland on climate warming. The effects are put to the same scale and societal scenarios in the forest sector are compared.

METHODS

Scenario simulations and carbon balances
The potential GPP of Finnish Forests was modeled with simple canopy carbon exchange model, PRELES (Mäkelä et al. 2008). The simulated GPP values, both in the reference period and in future climate (SRESA2, inmcm3.0 climate mode), were used to force OptiPipe model (Valentine and Mäkelä 2012) to obtain new NPP values. Within this model, temperature sum and soil nitrogen availability were linked. Soil organic matter decomposition was modeled using the Yasso model (Liski et al. 2005). The obtained growth change were fed into the MOTTi growth simulator (Hynynen et al. 2005) for the development of growth predictions for the whole of Finland. Simulations were done for three different intensities for forestry (65, 100, 130 x 106 m3 yr-1 wood production). The functions to calculate albedo effects, VOC/aerosol effects, the accumulation of carbon in wood products as well as the substitution effect are described below.

Albedo measurements
Albedo effects of forest management were calculated by linear unmixing from MODIS satellite products based on stand volume and tree species. The measurements compared positively to in situ measurements of albedo (Kuusinen et al. 2012). Albedos were changed into radiative forcing using a radiative transfer model.

Aerosol modeling
Aerosol effects of different forest structures were calculated using the SOSAA model. As input we used the VOC emission parameters for clear cuts and three different ages for each of the three tree species investigated here. Direct Aerosol forcing was calculated offline by the SOSAA model using the climate data and background concentrations of SO2 and other gases of importance for Hyytiälä (Boy et al 2012). Forcing values were interpolated for different ages using linear interpolations between different stand ages. Indirect forcing of aerosols by cloud formation was estimated according to Kurthen (Kurten et al., 2003).

Carbon sequestration in wood products and substitution effects
Carbon sequestration in wood products was calculated using product allocation and decay functions of Karjalainen et al. (1994). These were separate for sawnwood derived products and pulpwood derived products. Carbon emissions were assumed to occur during both manufacturing or wood products and when wood products are withdrawn from the product cycle.

The substitution benefits of wood products were assumed to occur at the time when alternative products are manufactured which was set to equal the time when wood products are manufactured. The values were based on studies for sawnwood and for packaging based on values of the Meta-analysis of Sarthre and O'Connor as well as the work of Pingoud et al., (Sathre and O'Connor 2010, Pingoud et al. 2010).

CONCLUSIONS

Our results indicated that carbon dominated the climate impacts of forestry. The annual cut was a central variable that determines the carbon storage of the forest ecosystems and higher annual cuts reduced the total carbon storage in the ecosystems. Forest shifted from being a carbon sink to a carbon source depending on the annual cut.

Albedo effects were much smaller. It seemed that there were limited possibilities to use stand density and stand rotation time to impact the albedo forcing. However, changes in tree species from conifers to broad-leafs seemed to involve large changes in atmospheric forcing. Non-carbon effects, namely albedo and aerosols seem to cancel each other out in current climate, while in future climate aerosols have larger effect than albedo. This shift is seen especially in deciduous trees The opposite signs of the albedo and aerosol effects may be an indicator that both depend on light absorption of leaves. Albedo values are

proportional to the light reflected, while photosynthesis, which drives VOC emissions, is roughly proportional to the amount of light absorbed by the foliage

The effect of substitution of non-wood products was large and dominated the responses. This is due to the fact that the manufacturing of wood products is, on average, far less energy intensive than the manufacturing of alternative non-wood products. However, the size of the substitution effect is relatively uncertain and depends on consumers habits and building practices.

Altogether the work shows that the forests have a large potential for climate change mitigation. Non-carbon effects, namely albedo and aerosols seem to cancel each other out. The large substitution effect shows that research on the carbon balance of the end use of wood requires further attention and that the use of sawnwood or industrial for bioenergy should be avoided if the wood can be used for manufacturing.

ACKNOWLEDGEMENTS

We acknowledge help for the Aerosol forcing calculations from Dr. Timo Nousiainen from FMI and Päivi Haapanala. The work was financed by the Academy of Finland Center of Excellence grant 272041 and the University of Helsinki HENVI -Forest grant. The abstract has been first presented as presentation to the FCOE annuala meeting in October 2014 and has been submitted to the reports in Aerosol sciences there.

REFERENCES

Boy, M.; Sogachev, A.; Lauros, J.; , Zhou, L.; Guenther, A. & Smolander, S. (2011) SOSA - a new model to simulate the concentrations of organic vapours and sulphuric acid inside the ABL - Part I: Model description and initial evaluation, *Atmospheric Chemistry and Physics*, **11**, 43-51

Hynynen, J., A. Ahtikoski, J. Siitonen, R. Sievänen, and J. Liski, (2005) Applying the motti simulator to analysethe effects of alternative management schedules on timber and non-timber production, *Forest Ecology and Management*, **207** (1-2 SPEC. ISS.), 5–18.

Karjalainen, T., S. Kellomaki, and A. Pussinen (1994) Role of wood based products in absorbing atmospheric carbon, *Silva Fennica*, **28**, 67–80.

Kurten, T., et al., (2003) Estimation of different forest-related contributions to the radiative balance using observations in southern Finland. *Boreal Environment Research*, **8**, 274–285.

Kuusinen, N., E. Tomppo, and F. Berninger (2013) Linear unmixing of modis albedo composites to infer subpixel land cover type albedos, *International Journal of Applied Earth Observation and Geoinformation*, **23** ,324–333.

Liski, J., T. Palosuo, M. Peltoniemi, and R. Sievänen (2005) Carbon and decomposition model yasso for forest soils. *Ecological Modelling*, **189** 168–182, 2005.

Mäkelä, A., et al., (2008) Developing an empirical model of stand GPPwith the LUE approach: Analysis of eddy covariance data at five contrasting conifer sites in europe, *Global Change Biology*, **14** 92–108.

Pingoud, K., J. Pohjola, and L. Valsta (2010) Assessing the integrated climatic impacts of forestry and wood products, *Silva Fennica*, **44**, 155–175.

Sathre, R., and J. Oconnor (2010) Meta-analysis of greenhouse gas displacement factors of wood product substitution, *Environmental Science and Policy*, **14**, 104–114.

Valentine, H. T., and A. Mäkelä, (2012) Modeling forest stand dynamics from optimal balances of carbon and nitrogen, *New Phytologist*, **194,** 961–976.

TEMPORAL - SPATIAL VARIABILITY OF THE THERMAL REGIME OF THE NEAR-SURFACE PERMAFROST AT TIKSI OBSERVATORY

P.V. BOGORODSKII, A.P. MAKSHTAS and V.YU. KUSTOV

Arctic and Antarctic Research Institute, St.Petersburg, Russia.

Keywords: PERMAFROST, ACTIVE LAYER, MEASUREMENTS, MODELING.

The data of five-year measurements of the active soil layer temperature started in the autumn 2009 at Tiksi Observatory are presented with the features of climatic and landscape characteristics of the region. The active layer thermal structure is described. The reasons for its possible evolution are analyzed and their basic statistical characteristics are given. The experimental data are compared with estimates of seasonal thawing depth dynamic for 1936 - 2012, calculated with empirical relationships and the modified version of Kudryavtsev model, where thermophysical properties of vegetation and ground are parameterized as input. The results indicate a gradual reduction of the active layer thickness during 1930s -1960s, replaced later by growth, continuing to the present. The calculated values of the active layer characteristics are in a good agreement with estimations for the Tiksi area.

AEROSOL AND CLOUD PROPERTIES MEASURED DURING PALLAS CLOUD EXPERIMENT - PACE 2012

D. BRUS, E. ASMI, M. AURELA, U. MAKKONEN, K. NEITOLA, J. SVENSSON, A.-P. HYVÄRINEN, T. RAATIKAINEN, A. HIRSIKKO, H. HAKOLA, R. HILLAMO and H. LIHAVAINEN

Finnish Meteorological Institute, Erik Palménin aukio 1, P.O. Box 503, 00101 Helsinki, Finland.

Keywords: CCN, CLOUDS, AEROSOL COMPOSITION, BC.

INTRODUCTION

Clouds constitute perhaps the largest source of uncertainty in predicting the behaviour of the Earth's climate system. Vulnerable Arctic region is slowly heading towards a new climatic state with substantially decreased permanent ice cover. However, due to poorly understood feedback mechanisms, the rate of Arctic climate response to changes is very hard to predict with current global models. Arctic clouds are supposed to have central role in these feedback processes (Vavrus, 2004). Many of the climatically important cloud properties, including the reflectivity, lifetime and precipitation patterns of clouds, depend strongly on atmospheric aerosol particle properties, like chemical composition or number concentration. The essential cloud microphysical parameters in studying aerosol-cloud-climate interactions are the total number concentration and effective radius of cloud droplets, cloud liquid water content and the relative dispersion of a cloud droplet population (Komppula *et al*., 2005; Lihavainen *et al*., 2008).

METHODS

The 4th Pallas cloud experiment was carried out six weeks, between September 17th and October 30th 2012, at Finnish Meteorological Institute's Pallas-Sodankylä Global Atmosphere Watch (GAW) station in northern Finland (Hatakka *et al.*, 2003). The measuring site - Sammaltunturi station (67°58′N, 24°07′E) - resides on a top of the second southernmost fjeld, a round topped treeless hill, in a 50-km-long north and south chain of fjelds at an elevation of 565 m a.s.l. Sammaltunturi station is, due to topography of the surrounding terrain, a great place for ground-based observations of low level orographic clouds. Thus providing an opportunity to investigate not only the cloud droplet activation of aerosol particles, but also directly the cloud particle phase (Kivekas *et al.*, 2009; Anttila *et al.*, 2012).

The measurements included wide range of instrumentation: aerosol number size distribution with differential mobility particle sizers (DMPS), total number particle counters (CPC, TSI 3010, Airmodus A20), particle absorption with Aethalometer (model AE 31, Magee Scientific), Multi-Angle Absorption Photometer (MAAP, Thermo Scientific) and the Single Particle Soot Photometer (SP2, DMT), and particle scattering with the integrating Nephelometer (model 3563, TSI). The ambient RH was measured with Vaisala HUMICAP sensor, and visibility and temperature were measured with Vaisala FD12P weather sensor.

In addition to the above mentioned equipment, the aerosol CCN and hygroscopic properties were measured with the HTDMA (Hygroscopicity Tandem Differential Mobilitity Analyzer) and the Cloud Condensation Nuclei Counter (CCNc, DMT model CCN-100). In situ cloud properties were measured with a Forward Scattering Spectrometer Probe (FSSP, 3-47μm, model SPP-100, DMT) and the Cloud, Aerosol and Precipitation Spectrometer (CAPS, DMT), which includes three instruments: the Cloud Imaging Probe (CIP, 12.5 μm-1.55 mm), the Cloud and Aerosol Spectrometer (CAS-DPOL, 0.51-50 μm) with depolarization feature, and the Hotwire Liquid Water Content Sensor (Hotwire LWC, 0 - 3 g/m3).

Mass and chemical composition of non-refractory submicron particulate matter was characterized with an Aerosol Chemical Speciation Monitor (ACSM, Aerodyne) and the chemical composition of gas and aerosol phase was measured with an online ion chromatograph for Measuring AeRosols and GAses (MARGA 2S ADI 2080, Metrohm Applikon Analytical BV).

Trajectrory analysis was done with NOAA HYSPLIT model using GDAS meteorological data at three heights (100, 500, 1000 m a.g.l.). The air mass source regions were divided into five categories: Arctic, Eastern, Southern, Western and Local, (Fig. 1.). Based on weighted fractions of air masses over the source regions, for each trajectory the region of the highest weight was considered to represent this air mass type.

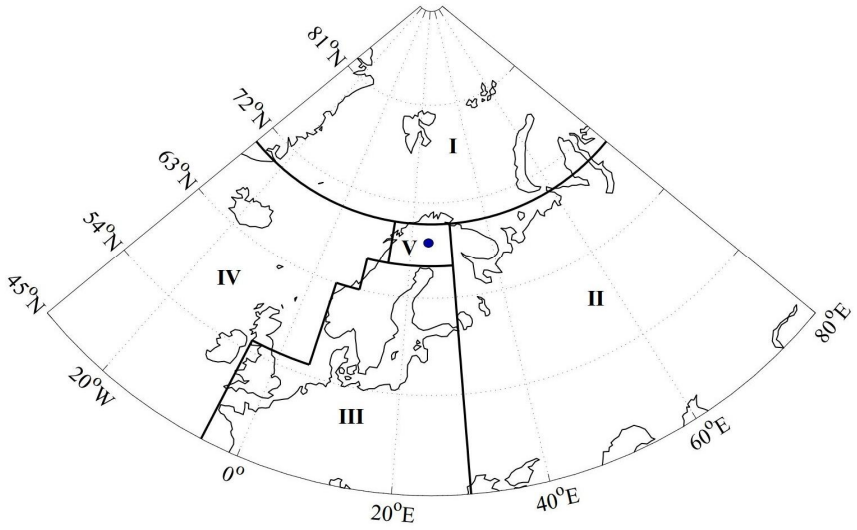

Figure 1. Map of air mass sectors: I (Arctic), II (East), III (South), IV (West) and V (Local).
Table summarizes statistics over each sector for all three heights.

G.L.A [m]	Local	Arctic	East	South	West
100	0.28	0.39	0.15	0.08	0.10
500	0.18	0.42	0.14	0.09	0.17
1000	0.12	0.37	0.16	0.15	0.19
Avg	0.19	0.39	0.15	0.11	0.15
Std	0.08	0.03	0.01	0.04	0.05

Table 1. Weighted coverage of air mass type for particular sectors.

CONCLUSIONS

PaCE 2012 campaign is summarized in figures 2.and 3. Figure 2 shows total CN and CCN concentrations together with κ and *GF* values obtained with CCNc and HTDMA, respectively. Lower part of Fig. 2 covers the aerosol chemical composition divided according to sectors of air mass origin (at 500 m a.g.l.). Meteorology, cloud droplet concentrations and derived parameters like MVD, ED and LWC are shown in Fig 2.

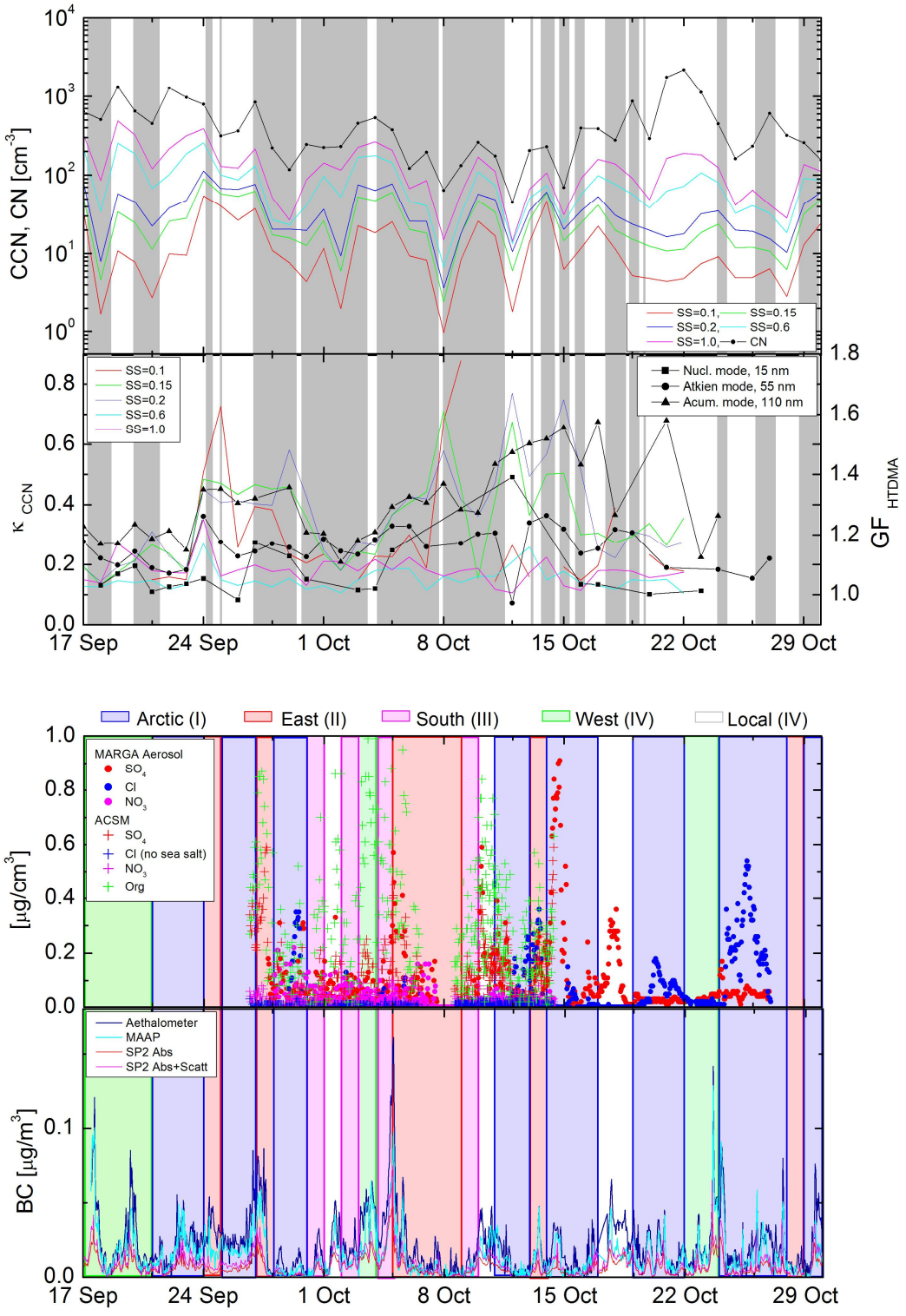

Figure 2. Total CN and CCN concentrations at five supersaturation levels 0.1, 0.2, 0.3 0.6 and 1.0 (upper panel) together with κ and *GF* values obtained with CCNc and HTDMA. Grey areas represent cloud events determined from visibility measurements. Aerosol chemistry according to air mass sectors of origin, (lower panel): ACSM and MARGA, lower panel black carbon (BC) concentration measured by Aethalometer, MAAP and SP2 (absorbing and mixed particles separately).

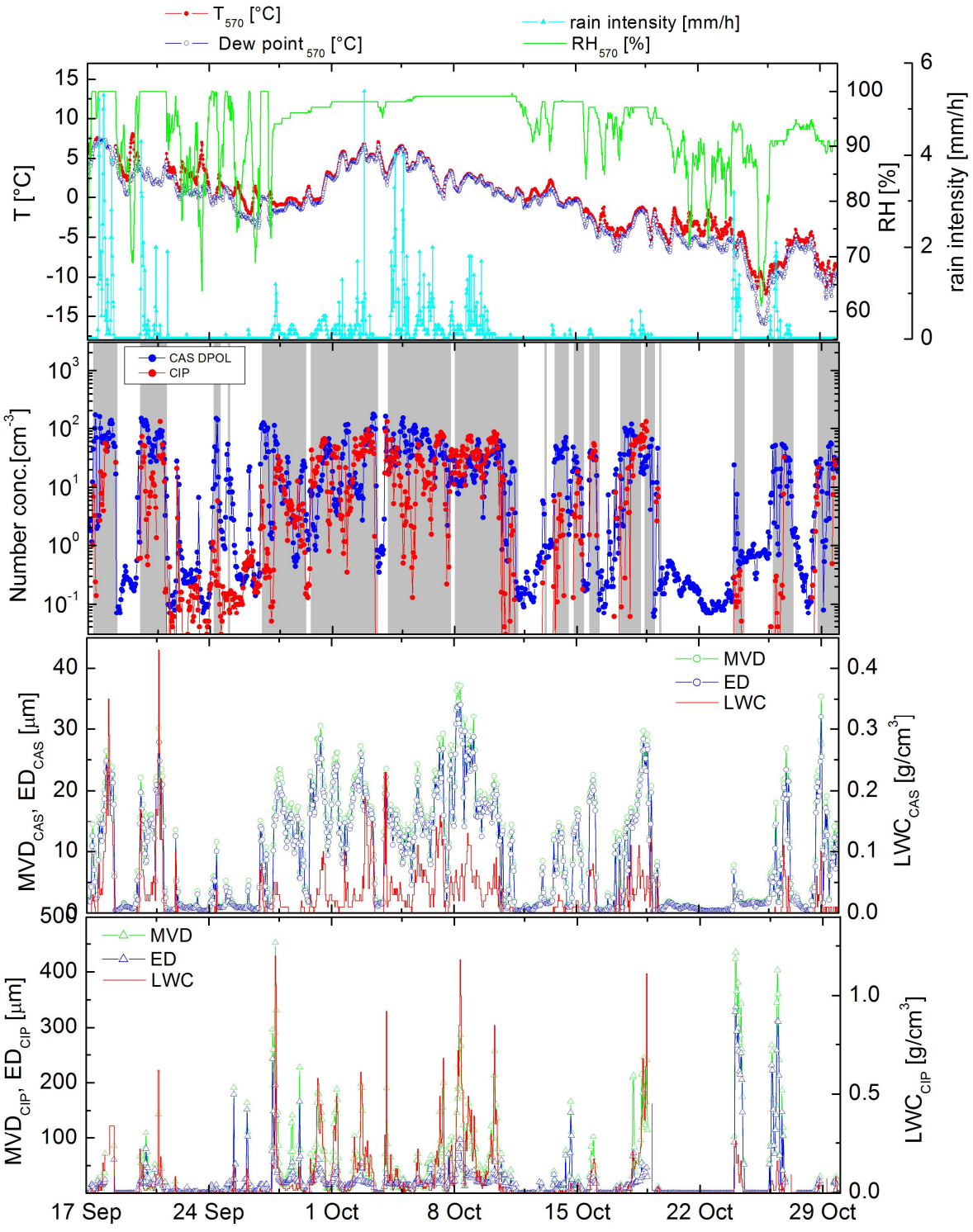

Figure 3. Meteorological parameters (temperature, dew point, relative humidity, and rain intensity), and cloud droplets concentrations measured with CAS-DPOL and CIP probes (upper two panels). Derived parameters: mean volume diameter (MVD), equivalent diameter (ED) and liquid water content (LWC) for each probe separately (lower two panels).

ACKNOWLEDGEMENTS

This work was supported by the Academy of Finland Centre of Excellence (project number 272041), KONE foundation (grant number 46-6817) and Nordforsk Contract number 26060, CRAICC Amendment on CRAICC-PEEX Collaboration.

REFERENCES

Vavrus, S. (2004). The impact of cloud feedbacks on Arctic climate under greenhouse forcing, *J. Climate*, **17**, 603.

Komppula, M. *et al.,* (2005). Measurements of cloud droplet activation of aerosol particles at a clean subarctic background site, *J. Geophys. Res.*, **110**, D06204.

Lihavainen, H. *et al.*, (2008). Measurements of the relation between aerosol properties and microphysics and chemistry of low level liquid water clouds in Northern Finland, *Atmos. Chem. Phys.*, **8**, 6925

Hatakka, J. *et al.,* (2003). Overview of the atmospheric research activities and results at Pallas GAW station, *Boreal Environ. Res.*, **8**, 365.

Kivekas, N. *et al.*, (2009). Physical and chemical characteristics of aerosol particles and cloud-droplet activation during the Second Pallas Cloud Experiment (Second PaCE), *Boreal. Environ. Res.*, **14**, 515.

Anttila, T. *et al.,* (2012). Relationships between particles, cloud condensation nuclei and cloud droplet activation during the third Pallas Cloud Experiment, *Atmos. Chem. Phys.*, **12**, 11435.

TRENDS IN ECOSYSTEM ACTIVITY IN VÄRRIÖ STRICT NATURE RESERVE, EASTERN LAPLAND

J. BÄCK[1], T. PETÄJÄ[2], A. MIKOLA[1], P. HARI[1], P. KOLARI[1, 2], S. DENGEL[2], J. ITÄMIES, E. PULLIAINEN[1], E.-M. KYRÖ[2] and M. KULMALA[2]

[1]Department of Forest Sciences, University of Helsinki, Finland.

[2]Department of Physics, University of Helsinki, Finland.

[3]Department of Biology, University of Oulu, Finland

Keywords: CLIMATE CHANGE, PHENOLOGY, BUD BURST, BERRY YIELDS, SNOW DEPTH, PHOTOSYNTHESIS, SMEAR I STATION.

INTRODUCTION

Climate change is already having a significant impact on the Arctic and subarctic nature. The Arctic regions have been warming at about twice the global-average rate during the recent decades, and in the 2000's at least five summers were probably warmer than any other summer during the past 600 years in high northern latitudes (Tingley & Huybers 2013, IPCC 2013). The amplified Arctic warming is expected to continue, with significant impacts on the Arctic ecosystems and human societies in those regions. As a result of warming, the growing season is already lengthening at high northern latitudes (Menzel *et al.*, 2006), stimulating ecosystem productivity and implying large increases in biomass and increased carbon uptake capacity. Due to the improved productivity, tree lines are advancing and the previously open tundra is gradually turned into a shrub-land or forest. This "Arctic greening" (Myneni *et al.*, 1997, Xu *et al.*, 2013) promotes several climate feedback mechanisms via changes in surface albedo, GHG (greenhouse gas) sinks and sources, aerosol precursor emissions, hydrological cycle and cloud properties. With long datasets of ecological events, we aim at analysing the changes over the past decades, and link them to ecosystem and atmospheric processes measured at our field site in eastern Lapland.

METHODS

We utilize the climatic, photosynthetic and phenological data collected in a systematic manner at Värriö Subarctic Research Station since 1967, and analyse the potential of these measured indices to reveal changes in timing or length of growing season and photosynthetically active period, species interrelations and the consequent impacts on ecosystem and atmospheric processes. The phenological events, e.g. timing of bud-burst, flowering, leaf senescence, berry yields, arrival of migrating birds and changes in nocturnal insect populations are compared with climatic variables such as mean, minimum and maximum temperatures, snow depth, lake ice-out and precipitation. Scots pine (*Pinus sylvestris* L.) gas exchange (incl. photosynthesis) and growth, and atmospheric composition are also analysed to reveal potential links to long-term ecosystem and climate changes.

PRELIMINARY RESULTS AND DISCUSSION

The climate show a steady increase in both minimum and maximum temperatures and precipitation over the study period. The first analyses indicate that at the same time, bud burst of silver birch (*Betula pubescens*) and flowering of bilberry (*Vaccinium myrtillus*) have been clearly advancing since 1980. Further, the berry yields (both fresh and dry weights) have been highest in the last years of 2000s. These results may reflect an increased productivity and prolonged growing season at the site, which has already been detected in the stepwise advancing treeline (Aakala *et al.*, 2014). However, a large proportion, over 60% of nocturnal moth species feeding with other than vascular plants were associated negatively with

climate variables, indicating a potential for population sensitivity to climate change. In order to see whether the long-term changes in phenology indices can also be detected in the feedbacks between ecosystems and atmosphere, the continuous atmospheric and ecophysiological measurements at the SMEAR I measurement station (Station for Measuring Ecosystem Atmosphere Relations), done since early 1990's, will be further analysed.

ACKNOWLEDGEMENTS

This work has been supported by the Finnish Center of Excellence in Atmospheric Science - From Molecular and Biological processes to The Global Climate, the Nordic Center of Excellence CRAICC and the University of Helsinki. The staff and trainees of Värriö Research Station haves done extremely valuable work in collecting and maintaining the datasets over the decades, and deserve our warm acknowlegdements.

REFERENCES

Aakala, T., Hari, P., Dengel, S., Newberry S.L., Minuzuma, T. & Grace, J. (2014) A prominent stepwise advace of the tree line in north-east Finland. *Journal of Ecology* DOI: 10.1111/1365-2745.12308

Hunter M.D., Kozlov M.V., Itämies J., Pulliainen E., Bäck J., Kyrö E.-M. & Niemelä P. (2014) Current temporal trends in moth abundance are counter to predicted effects of climate change in an assemblage of subarctic forest moths. *Global Change Biology*, DOI: 10.1111/gcb.12529.

IPCC (2013) Climate Change 2013: The Physical Science Basis. Contribution of Working Group I to the Fifth Assessment Report of the Intergovernmental Panel on Climate Change [Stocker, T.F., D. Qin, G.-K. Plattner, M. Tignor, S.K. Allen, J. Boschung, A. Nauels, Y. Xia, V. Bex and P.M. Midgley (eds.)]. Cambridge University Press, Cambridge, United Kingdom and New York, NY, USA, 1535 pp.

Menzel et al. (2006) European phenological response to climate change matches the warming pattern. *Global Change Biol.* 12, 1969-1976

Myneni RB, Keeling CD, Tucker CJ, Asrar G, Nemani RR (1997) Increased plant growth in the northern high latitudes from 1981 to 1991. *Nature* 386: 698-702.

Tingley M.P. & Huybers P. (2013) Recent temperature extremes at high northern latitudes unprecedented in the past 600 years. *Nature* 496, 201−205.

Xu et al. (2013) Temperature and vegetation seasonality diminishment over northern lands. *Nature Clim. Change* 3, 581−586.

GLOBAL PRECIPITATION MISSION AND IN-SITU OBSERVATION IN PEEX

V. CHANDRASEKAR[1,2,3] AND D. MOISSEEV[1]

[1]University of Helsinki, Finland.

[2]Finnish Meteorological Institute, Finland.

[3]Colorado State University, USA.

Keywords: PEEX, GLOBAL PRECIPITATION MAP.

INTRODUCTION

The Global Precipitation Measurement (GPM) is an international satellite mission to provide next-generation observations of rain and snow worldwide every three hours. NASA and the Japanese Aerospace Exploration Agency (JAXA) launched the spacecraft on February 27th, 2014, carrying advanced instruments, including advanced radars and radiometers that will set a new standard for precipitation measurements from space. The GPM core observatory provides extensive coverage for the PEEX region covering up to 65 deg N latitude. The GPM Core will carry two major instruments namely, the GPM Microwave Imager (GMI) and Dual-frequency Precipitation Radar (DPR). These instruments will collect improved observations that will allow scientists to better "see" inside clouds. The GMI has the capability to measure the amount, size, intensity and type of precipitation, from light rain and snowfall. The DPR will return three-dimensional profiles and intensities of liquid and solid precipitation. These data will reveal the internal structure of storms within and below clouds. With the advanced observations from the GMI and DPR, we will be able to study the internal structure of precipitation throughout their life cycles, and view how they change over time. This paper will discuss opportunities for targeted studies that are specific to the PEEX region with an eye towards the performance of the GPM retrievals in the PEEX regime, using distributed ground observations in the PEEX.

SIMULTANEOUS OBSERVATIONS OF GPM AND GROUND OBSERVATIONS IN FINLAND

Finland provides excellent opportunities for simultaneous satellite and ground Observations in the GPM era. Fig 1, shows the layout of Finnish meteorological weather radar network (Source FMI). The inner circles in the figure show the coverage of snow (120 KM circles), whereas the summer coverage is up to 250 Km from the radar, the outer coverage circle. Fig 1 also shows the map of Finland. More recently, FMI has been going through a nationwide upgrade of radars to dual-polarization. With this upgrade we can examine the microphysical processes responsible for precipitation in the PEEX region.

The dual- frequency radar on board the GPM satellite makes measurements of reflectivity at two independent frequencies, i.e., Ku-band and Ka-band. The GPM program has developed several algorithms to provide retrievals of precipitation from these observations. Fig 2 shows a schematic of the downward looking GPM radar. The disks represent sampling volumes. It can be seen that the GPM observations over the PEEX region gives a broad area coverage that can be compared against the ground observations.

The GPM algorithms rely on the surface reference technique (SRT) to estimate path attenuation and correct the measured reflectivity measurements. Therefore GPM is also continuously monitoring the surface also. In addition to the FMI radars, the University of Helsinki radar (Kumpula Dual-polarized Doppler radar), is a research radar that is designated a TIER1 radar of the GPM program. As TIER1 radar, the Kumpula radar will conduct coordinated scans with the GPM satellite routinely.

Kumpula radar receive an alert about the approach of the GPM core within a given distance to the radar site in advance. Information provided is referred to the point of closest approach point to the radar location. Position of that point is provided both in geographical coordinates latitude and longitude, and with respect the Kumpula radar, in terms of ground range d and azimuth θ. Satellite heading direction along with timing of the closest approach is also provided. Such data allow to design Kumpula radar scanning in correspondence to satellite overpasses, in which scanning is totally related to the geometry of observation of the two sensors and not to the location of the observed phenomenon. Actually, optimizing scanning taking into account the phenomenon ongoing, such as a convective cells, or a shallow snow event that could be interesting to scan, means adapting the design rule to an arbitrary direction instead of the azimuth of the closest approach point and considering an arbitrary sector to be scanned.

SUMMARY

This paper will present the plans for coordinated large scale GPM observations over the PEEX region, while demonstrating the coordinated activities with FMI weather service radars as well as Kumpula research radar. Not mentioned in detail is the future plan for coordinated observations over the Hyytiälä Field Station, where there will be vertically pointing C band radar along with cloud radar. The purpose of the paper is to demonstrate the coordinated observations, and to look for opportunities to extend the coordination to the broader PEEX region.

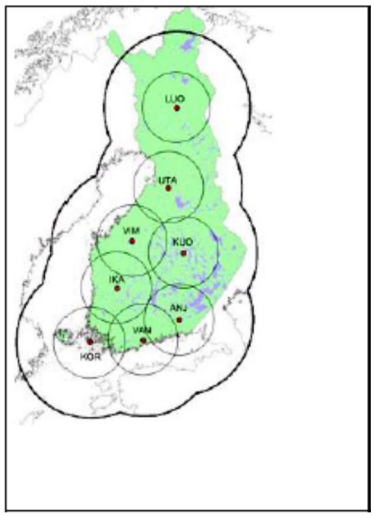

Figure 1. Layout of the FMI radars.

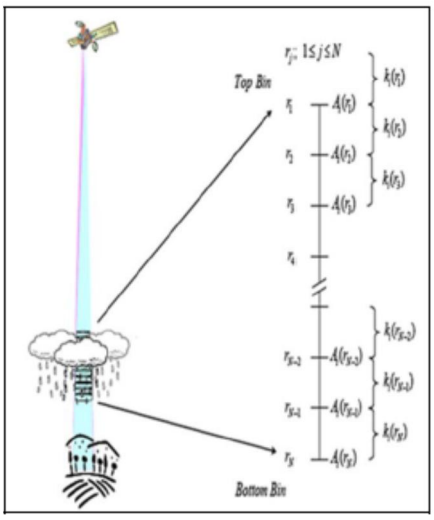

Figure 2. Schematic of the downward looking GPM radar.

ACKNOWLEDGEMENTS

This work was supported by the NASA GPM program as well as University of Helsinki and FMI.

ENVIRONMENTAL RADIOACTIVITY AND AIR IONS IN THE LOWER ATMOSPHERE

X. CHEN[1], J. PAATERO[2], V.-M. KERMINEN[1], A. FRANCHIN[1], H. MANNINEN[1], T. PETÄJÄ[1] and M. KULMALA[1]

[1]Department of Physics, University of Helsinki, Finland

[2]Finnish Meteorological Institute, Helsinki, Finland

Keywords: RADON, COSMIC RADIATION, IONISATION.

INTRODUCTION

Ionising radiation released by natural radioactivity supplies the energy for the ionisation and excitation in the lower atmosphere. It is responsible for air ion production and, therefore, a key player in air conductivity, which is known as an indicator of air quality (Cobb, 1973). On the other hand, the energy expended in exciting trace gases in the atmosphere could contribute to the formation of neutral aerosol particles. Together with the charged fraction, these aerosol particles affect climate, human health and visibility (Poschl, 2005). Although vast investigations have been carried out in the field of natural radioactivity and in the field of air ions, the connection between natural ionising radiation and air ion formation is still poorly understood. We, therefore, aim at investigating the relation between natural radioactivity and air ion formation as well as atmospheric electricity.

METHODS

This work is based on the environmental radioactivity and air ion measurements at Hyytiälä SMEAR II station (61°50´40´´N, 24°17´13´´E), located in southern Finland in a boreal forest (Hari and Kulmala, 2005). The environmental radioactivity at this site is monitored by a pair of Geiger-Müller counters for the beta emissions of radon decay (Paatero et al., 1994) and total gamma detector (Hirsikko et al., 2007). Both of these instruments are deployed and owned by the Finnish Meteorological Institute (FMI). Air ions are measured with a Balanced Scanning Mobility Analyser (BSMA), Symmetric Inclined Grid Mobility Analyser (SIGMA) and Neutral and Air Ion Spectrometer (NAIS) (Kulmala et al., 2012).

This first phase of the work seeks for reasons for the observed variations in natural ionising radiation and corresponding ion pair production, i.e. ion source rate. Then, by further comparing the ion source rate to the observed air ion concentration, an assessment on air ion balance will be performed. Finally, with the results of the assessment, possible improvement and refinement on the theory of air ion balance will be investigated.

RESULTS AND DISCUSSIONS

Variations in natural ionising radiation in Hyytiälä SMEARI II station have been studied based on ambient data collected during 2000-2013. Seasonal and diurnal cycles in radon activity concentration and gamma dose rate were observed. The ion source rate derived from natural ionising radiation followed the same patterns as the natural ionising radiation. The median radon activity concentration was 2.2 Bq/m^3 for 2000-2007, corresponding to an ion source rate of about 1.3 $cm^{-3}s^{-1}$. The gamma dose rate varied between 0.07 and 0.16 μSv/h for 2000-2013, which gave a median ion source rate of 9.1 $cm^{-3}s^{-1}$. The low gamma dose rate in winter and early spring was mainly due to the attenuation of the terrestrial fraction of gamma radiation by snow cover (Figure 1). This is the main contribution to the seasonal variation in gamma radiation, though the cosmic fraction is also affected by the solar activity on an 11-year cycle (Bazilevskaya et al., 2008).

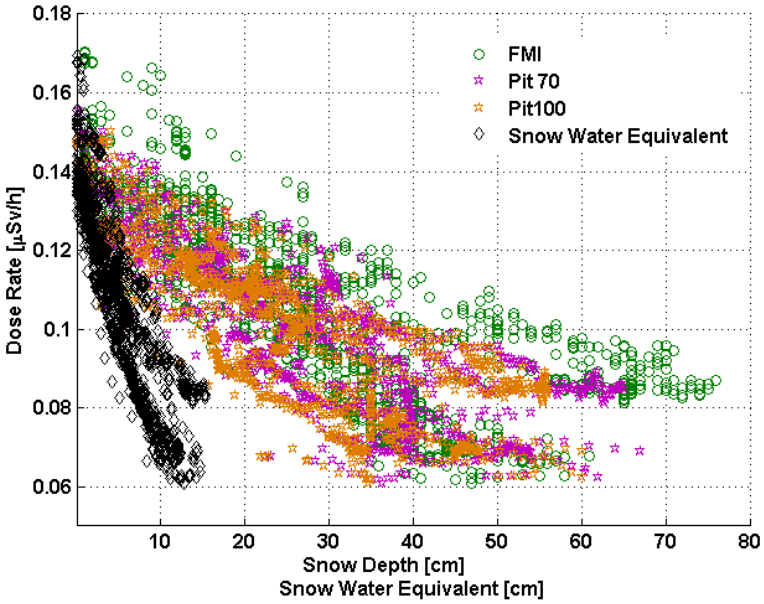

Figure 1. The attenuation of gamma radiation by snow cover. Green: snow depth data from the Finnish Meteorological Institute (FMI). Pink and orange: Station measurements of snow depth at two different locations. Black: snow water equivalent data modelled by the Finnish Environment Institute (SYKE).

The patterns in radon activity concentration can be affected by the stability of the atmosphere (Griffiths et al., 2013). Higher radon activity concentrations were observed when winds blew from the southeast direction. Soil conditions were found to influence the radon activity concentration. The diurnal cycles in the radon activity concentration resulted from the development of the boundary layer, which also made the diurnal features in total gamma radiation in summer distinguishable. The midday boundary layer was typically thicker in summer time than in other seasons (McGrath-Spangler and Denning, 2013).

CONCLUSIONS

Variations in natural ionising radiation in Hyytiälä SMEARI II station were studied based on ambient data collected during 2000-2013. The seasonal and diurnal cycles in radon activity concentration and gamma dose rate were presented. The ion source rate derived from natural ionising radiation followed the same patterns as the natural ionising radiation. The low gamma dose rate in winter and early spring was mainly due to the attenuation caused by snow cover. The patterns in radon activity concentration could be connected to the stability of the atmosphere.

The source areas of radon observed in the Hyytiälä SMEAR II station, along with further investigations connecting the natural ionising radiation with measured air ion concentration and atmospheric electricity, are under progress. With an overall understanding on the balance between the supplied energy by environmental ionising radiation and expended energy in the formation of air ions, i.e. air ion balance, energy lost in the excitation of gaseous molecules in the atmosphere can be estimated and the contributions of natural radioactivity to the production of neutral aerosol particles may then be evaluated. Furthermore, this work could open up possibilities to test various feedback mechanisms in relation to the changes in climate system.

ACKNOWLEDGEMENTS

This study was supported by Academy of Finland Centre of Excellence programs (project no. 272041 and 1118615). The authors appreciate the Senior Coordinator Tapani Säynätkari from the Finnish Environment Institute for providing the modelled data on snow water equivalent.

REFERENCES

Bazilevskaya, G. A., et al. (2008), Cosmic Ray Induced Ion Production in the Atmosphere, *Space Sci Rev 137*, 149–173, doi:10.1007/s11214-008-9339-y.

Cobb, W. E. (1973), Oceanic aerosol levels deduced from measurements of the electrical conductivity of the atmosphere, *Journal of Atmospheric Science*, *30*, 101-106.

Griffiths, A. D., S. D. Parkes, S. D. Chambers, M. F. McCabe, and A. G. Williams (2013), Improved mixing height monitoring through a combination of lidar and radon measurements, *Atmospheric Measurement Techniques*, *6*(2), 207-218, doi:10.5194/amt-6-207-2013.

Hari, P., and M. Kulmala (2005), Station for measuring ecosystem-atmosphere relations (SMEAR II), *Boreal Environment Reseach*, *10*, 315-322.

Hirsikko, A., J. Paatero, J. Hatakka, and M. Kulmala (2007), The ^{222}Rn activity concentration, external radiation dose and air ion production rates in a boreal forest in Finalnd between March 2000 and June 2006, *Boreal Environment Reseach*, *12*, 265 - 278.

Kulmala, M., et al. (2012), Measurement of the nucleation of atmospheric aerosol particles, *Nature protocols*, *7*(9), 1651-1667, doi:10.1038/nprot.2012.091.

McGrath-Spangler, E. L., and A. S. Denning (2013), Global seasonal variations of midday planetary boundary layer depth from CALIPSO space-borne LIDAR, *Journal of geophysical research: Atmospheres*, *118*, 1226–1233, doi: doi:10.1002/jgrd.50198.

Paatero, J., J. Hatakka, R. Mattsson, and I. Lehtinen (1994), A comprehensive station for monitoring atmospheric radioactivity, *Radiation Preotection Dosimetry*, *54*(3), 33-39.

Poschl, U. (2005), Atmospheric aerosols: composition, transformation, climate and health effects, *Angewandte Chemie*, *44*(46), 7520-7540, doi:10.1002/anie.200501122.

ANALYSES SNOW AND ICE THICKNESS FROM HIGH RESOLUTION THERMISTOR TEMPERATURE PROFILES

B. CHENG[1], T. VIHMA[1] and J. ZHAO[2]

[1]Finnish Meteorological Institute (FMI), 00101, Helsinki Finland.

[2]National Marine Environmental Forecasting Centre (NMEFC), 100081, Beijing, China.

Keywords: SNOW, ICE, TEMPERATURE, THICKNESS.

INTRODUCTION

The thickness of snow and ice is important element in the cryosphere system. The accurate snow and ice thickness is obtained by drill-hole measurements. In remote area snow and ice thicknesses are often obtained by ice mass balance buoy (IMB).

The classical ice mass balance buoy was developed by the USA Cold Region Research and Engineering Laboratory (CRREL). The CRREL IMB equipped with sophisticated acoustic sounders to measure the positions of the surface and bottom in order to determine the thickness of snow and ice. This type of ice mass balance buoys have been widely used to monitor snow and ice thickness in the Arctic Ocean (e.g. Perovich, et al, 2003).

The Scottish Association for Marine Sciences (SAMS) has developed a novel innovated ice mass balance buoy (SIMB), also known as Sea-Ice Mass Balance Array (SIMBA) (Jackson et al., 2013). The SIMB measures the vertical temperature profile of air-snow-ice-water system using a high-resolution ice thermistor chain with 2 cm sensor interval. Additionally, two short heating cycles (of the order of 1-2 minutes) is applied successively on thermistor chain once a day. The real time air-snow-ice-water temperature and heating cycle temperature profiles are used to analyses the snow and ice thickness. The cost cutting design of SIMB makes it feasible to be deployed in a large numbers in the remote area, e.g. Arctic, and it is applicable for snow and ice monitoring in seasonal ice covered seas and lakes. However, analysis the snow and ice thickness from the measured temperature profiles is not a trivial task.

In this study we describe FMI's's SIMB deployment program. We also reveal a procedure toward development of a reliable algorithm for snow and ice thickness analyses from SIMB measured temperature profiles.

DEPLOYMENT OF SIMB

The first SIMB test trail deployment has been carried out in winter 2009/2010 in lake Orajärvi, Sodankylä northern Finland. Since then the SIMBS have been deployed regularly in lake Orajärvi in winter 2011/2012 onward (Fig.1). The physical configuration of deployment has been updated from time to time in order to ensure best possible data quality (Fig. 2). The SIMBs have been deployed in the Baltic Sea since 2012/2013 winter season in the coastal land fast ice zone to monitor the snow and ice evolution.

For safety reasons, the SIMBs are often deployed when ice thickness is at least 20 cm. The in situ snow and ice thickness as well as freeboard level are measured. For convenience later on of the snow and ice thickness detection, we also record sensor positions at ice surface, freeboard level and ice bottom (derived from ice thickness measurement). The thermistor chain borehole remained exposed (e.g. Fig.1) to ensure a proper refreezing of it. This is important, especially if the SIMB is deployed in thick ice field (> 2 m thickness) in the Arctic Ocean.

Figure 1. The initial deployment of SIMB in lake Orajärvi, Sodankylä in December 2011.A wooden frame is attached with thermistor string deployed vertically through the air-snow-ice and water. (Photo by Pekka Kosloff).

Figure 2. The updated SIMB deployment in lake Orajärvi, Sodankylä in 2013/2014 ice season. A wooden stick marked with scale is attached with thermistor string vertically distributed in along air-snow-ice-water. The SIMB is lifted with a fiberglass frame to ensure better iridium data transmission. (Photo by Jyrki Mattanen).

DATA ANALYSES

Under cold condition, the temperature distribution in-snow and in-ice can be assumed linear (Leppäranta, 1993). One could apply a linear interpoation/expolateriation to retrive the snow and ice thickness. Figure 3 gives temperature profiles of one SIMB measured in March (red line) and April (blue) in Svalbard 2013 (Gunnar Spreen, personal communication). A number of sensors are located in the air, so those sensors readings are approximately the same, i.e. the vertical temperature gradient was small. Base on the same principle, a number of sensors have been placed in the water, so these sensors should yield quite same

temperature values as well. Furthermore we know that the thermal heat conductivity of snow is roughly 15% of that of sea ice, so the temperature gradients in snow and ice differ from each other. Assuming the heat flux continuation between air/snow; snow/ice and ice/water interfaces, one can obtain the snow and ice thickness by identifying the cross point of the temperature gradient lines. In this case, the detected initial snow thickness in March was 12 ± (2~4) cm and the ice thickness was 56± (2~4) cm. In April the snow and ice thickness were 16 ± (2~4) cm and 90 ± (2~4). We implicitly assume the inaccuracy of sensor position was 2-4 cm, i.e. 2 sensors interval. The ice grew some 28 cm from March 5 to April 13 at the ice bottom. The independent *in situ* measurements confirmed the analyses above are reasonable well (initial snow and ice thickness were 7cm and 55cm, respectively, Gunnar Spreen, personal communication).

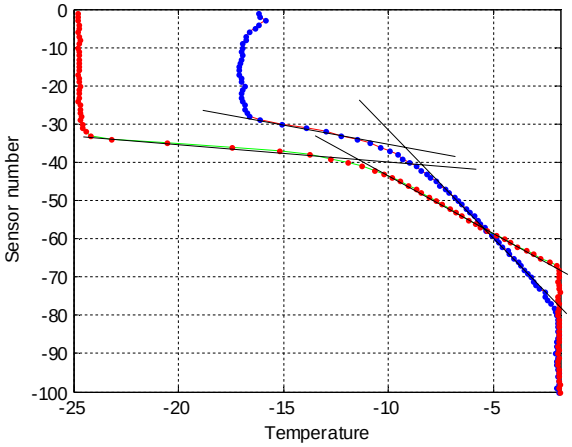

Figure 3. Temperature profiles of one SIMB measured in Svalbard on March 5 (red dotted line) and April 13 (blue dotted line). The black lines are interpolated /extroplated linear temperature gradients.

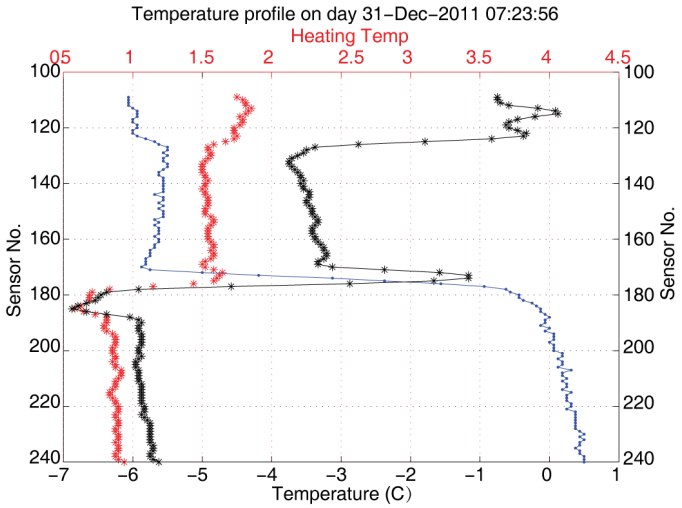

Figure 4. Vertical temperature profiles from one SIMB deployed in the Orajärvi lake in 2011/2012 winter season. The *in situ* temperature profile is the blue line; One-miute heating temperature was in red and two-minutes heating temperature was the black line.

For better estimation of the positions of interfaces, the heating cycle temperature profiles are needed. The temperature readings, in particular the heating cycle temperature may subject to perturbution technically. In order to redue such uncertainty, we made 3-pints moving average to reduce the perturbution noise level. Figue 4 shows the temperature profile measured in lake. The temperature gradient calculation indicated that sensor 171 is located at the air-snow interface; sensir 181 is at the snow/ice interface and sensor 190 is

about the ice/water interface. Such interface analyses lead to a 20 cm snow thickness and 18 cm ice thickness, respectively. The time series of snow and ice thickness obtained from this interface detection procedure is given in Figure 5.The snow and ice thickness derived mainly from *in situ* temperature profiles (Cheng et al., 2014) is also plotted for comparsion. Bare in mind that the blue lines snow and ice thickness are derived solely from temperature data even without knowing initial snow and ice thickness. Compared with borehole thickness measurement, the new proceudre works more systematically and can be used as a starting point to develop an automatic thickness retrieval algorithm.

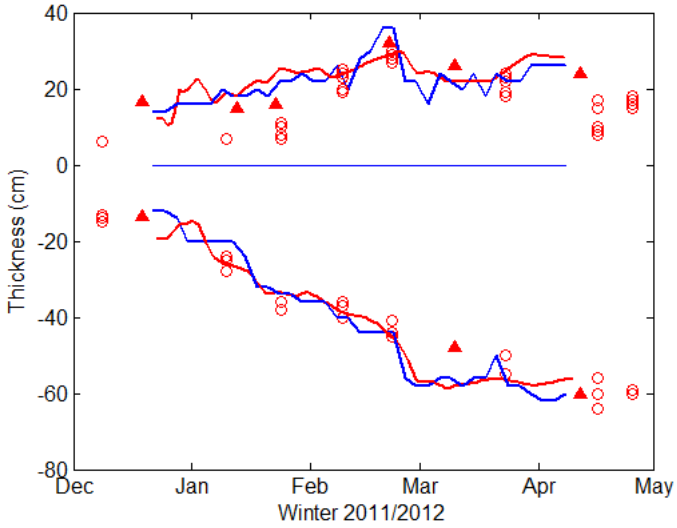

Figure 5. The snow and ice thickness derived mainly from *in situ* temperature profiles (red lines) in previous study and those from the *in situ* temperature and heating cycle temperature profiles (blue lines) in this study. The snow/ice interface is set as zero reference level. The symbols are snow and ice thicknesses measured near the SIMB site (▲) and at regular sites (○) some 1km away from SIMB site.

CONCLUSIONS

SIMB is a compact device with better mobility and easy to be deployed and maintained. A large number of SIMB can be deployed to investigate the spatial distribution of snow and ice thickness. The SIMB can also be used to monitor temperature and thickness of snow and ice in real time, i.e. applicable for snow and ice operational service. In cold condition, *in situ* temperature profiles can be used solely to derive reasonable well snow and ice thickness. The heating cycle temperature profile helps to determine the snow and ice thickness. Sensitivity study suggested that the interface detection is not affected by point moving average procedure that used to reduce the heating cycle temperature noise.

Finally, we want to emphasise that our latest SIMB deployment reveals that placing a segment (e.g. 20 cm) of the thermistor string horizontally at the ice surface is probably not a very good idea. The perpendicular of sensor chain may to some extent increase the risk of temperature sensor malfunction. A clear vertical deployment of thermal chain is therefore recommended (Fig. 2).

ACKNOWLEDGEMENTS

This work was also supported by the Academy of Finland (contract 259537).

REFERENCES

Cheng, B., T. Vihma, L. Rontu, A. Kontu, Pour H. Kheyrollah, C. Duguay and J. Pulliainen (2014). Evolution of snow and ice temperature, thickness and energy balance in Lake Orajärvi, northern Finland, Tellus A 2014, 66, 21564, http://dx.doi.org/10.3402/tellusa.v66.21564

Jackson, K., J.Wilkinson, T. Maksym, D. Meldrum, J. Beckers, C. Haas, and D. MacKenzie (2013). A novel and low cost sea ice mass balance buoy. J. Atmos. Ocean. Tech. 30(11), 2676 - 2688. DOI: 10.1175/JTECH-D-13-00058.1.

Leppäranta M. (1993) A review of analytical sea ice growth models. Atmosphere–Ocean. 31(1): 123-138.

Perovich, D. K., T. C. Grenfell, J. A. Richter-Menge, B. Light, W. B. Tucker III, and H. Eicken (2003). Thin and thinner: Sea ice mass balance measurements during SHEBA, J. Geophys. Res., 108 (C3), 8050, doi:10.1029/2001JC001079, 2003

URBAN AEROSOL PROPERTIES OF THE ATMOSPHERE IN MOSCOW AND OTHER CITIES OF RUSSIA ACCORDING TO AERONET AND MODIS MEASUREMENTS

N. YE. CHUBAROVA[1], YE.P. MALININA[1], A.A. POLYUKHOV[1] and M.A. SVIRIDENKOV[2]

[1]Lomonosov Moscow State University, Faculty of Geography, 119991, Moscow, Russia.

[2]Obukhov Institute of Atmospheric Physics RAS, Moscow, 119017, Russia

Keywords: URBAN AEROSOL PROPERTIES, MODIS, AERONET, RUSSIA.

INTRODUCTION

The impact of urban aerosol on climate change and human health is very significant, however, aerosol properties in heavy populated industrial cities are characterized by the most complicated nature. There is only limited information about the urban aerosol over Russia. Thus, the objective of this study is to analyze the urban aerosol properties of the atmosphere according to available AERONET and MODIS datasets over large cities of Russia, which are characterized by the large emissions of aerosol precursors and particulate matter.

METHODS

The information on urban aerosol properties in Moscow region was obtained from the AERONET measurements at the Meteorological Observatory of Moscow State University (Moscow MSU MO) located in the centre of Moscow during the 2001- 2013 period, and since 2006 - at the Obukhov IAP RAS Zvenigorod Scientific Station (ZSS) (Chubarova, Smirnov, Holben, 2011, Chubarova et al, 2011). In order to assess the degree of urban aerosol pollution of other large Russian cities we also used the data on aerosol optical thickness AOT at 550 nm from the satellite radiometer MODIS with a spatial resolution of $1° \times 1°$ for the 2000 – 2013 warm periods. The validation of these data over different Russian regions according to AERONET data has revealed their satisfactory quality and the ability for their application in characterizing the urban aerosol pollution. For quantifying the urban aerosol pollution effect we used the aerosol optical thickness difference between the AOT over city and in background conditions (ΔAOT550). For assessing the background conditions we used the 5% percentile AOT value obtained within the square of 7x7° in the nearby region. We analyzed 50 large Russian cities, which are located in different geographical conditions and have various sorts of emission of different levels. In addition, in order to assess the dominating aerosol components in different cities the data of annual reports on air pollution in Russian cities were used for different years. The data on emissions and concentrations of the main pollutants were analyzed over the 1988-2011 period.

The quality of AERONET data has been thoroughly analyzed. We revealed the additional uncertainties of AERONET measurements due to insufficiency of the standard cloud-screening procedure and the necessity of additional account for NO_2 correction in large cities. The application of standard cloud-screening algorithm provides the uncertainty for monthly mean aerosol optical thickness of about 0.04-0.05, which significantly exceeds the stated nominal measurement error of 0.01. To avoid this problem we proposed the additional cloud filter procedure, which has been validated for many years in the MSU MO. The additional NO_2 correction of aerosol optical thickness and other aerosol retrievals (volume particle distribution, single scattering albedo, etc.) was estimated for Moscow conditions. In addition to the standard NO_2 correction considered in AERONET, the optical thickness of non accounting NO_2 content was estimated to be about 0.01 for channel 340nm, 0.015 - for channels 380 and 440nm, and 0.006 – for channel 500 nm. We proposed the simple approach for its account for other cities using the information on NOx emissions.

Taking into account for these corrections the aerosol properties in Moscow were analyzed over 2001-2013. The annual 50% quantile of AOT at 500nm was equal to 0.16 varying from 0.08 in December to 0.23 - in August. Moscow aerosol was characterized by slightly absorbing properties with single scattering albedo of 0.89 in visible region. Volume aerosol size distribution usually had fine and coarse modes and a noticeable prevalence of fine mode fraction with an effective radius of about 0.15 micrometers. We also characterized the specific conditions of forest and peat bog fires in 2002 and 2010, when the aerosol properties had changed dramatically. During forest fires in 2010 AOT at 500 nm reached the highest observed level of AOT500=6.4. In these smoky conditions there was a tendency of fine mode aerosol effective radius significant increasing from 0.18 to 0.25μm with the growth of AOT. Single scattering albedo in visible region increased up to 0.95 but notably dropped in UV region (less 0.8) according to other radiative measurements at the Moscow MSU MO. There was a high correlation of different aerosol parameters between Moscow and Zvenigorod that confirmed that natural processes are the dominant factor in changing the aerosol properties of the megalopolis. At the same time, in some periods the urban aerosol pollution can reach high values of 0.4 at 550nm. According to the measurements over 2006-2013 period the average difference in AOT at 500nm between Moscow MSU MO and ZSS was about +0.02. There was no statistically significant difference between the single scattering albedo values at these sites, however, there was a pronounced tendency of its decreasing in Moscow. The analysis of the interannual AOT variability shows its statistically significant 20% decrease since 2001 in Moscow (Fig.1) mainly due to fine mode aerosol fraction decreasing.

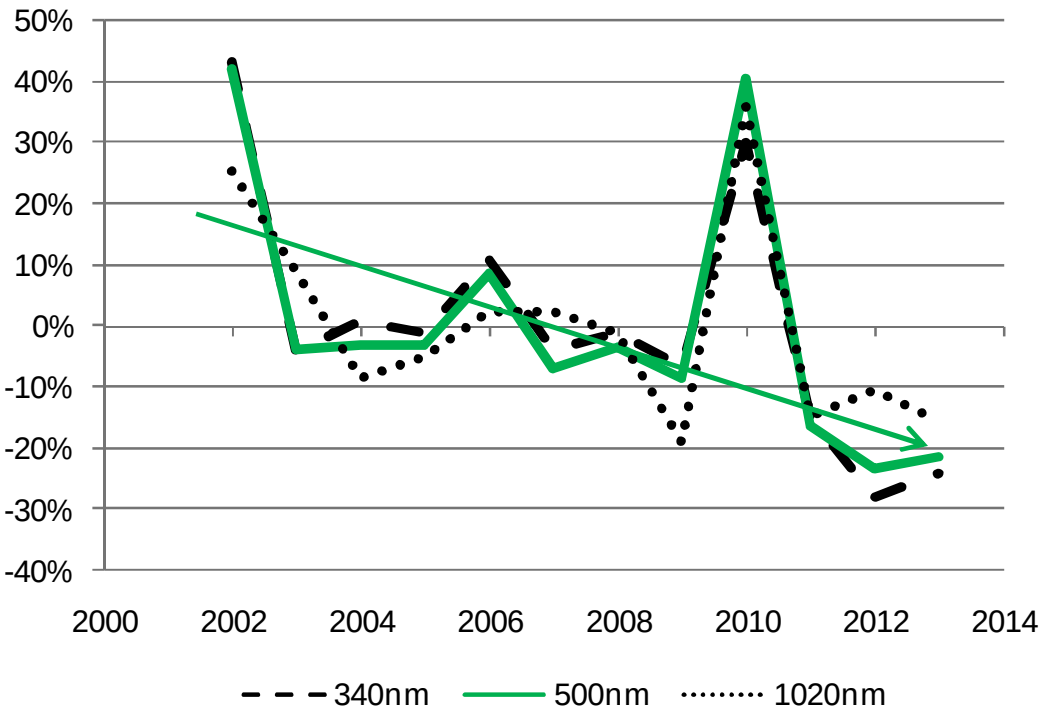

Figure 1. Interannual relative changes in annual mean aerosol optical thickness at different wavelengths in Moscow. Moscow MSU MO AERONET level 2 dataset with the additional application of cloud and NO_2 corrections.

The analysis of the urban aerosol pollution of other Russian cities was fulfilled using the MODIS dataset of AOT at wavelength of 550nm, collection 5 during warm periods to avoid the problems with bad quality of AOT retrievals over partly snow surfaces. According to the proposed method of evaluation the mean

effect of urban aerosol pollution over Russian cities varies from 0.01 to 0.08 with mean value of ΔAOT550=0.03±0.005. There was a statistically significant dependence of the urban aerosol pollution on the emission rate of the particulate matter over each city (Fig.2), however the relationship was not very tight.
We also saw a pronounced dependence of the ΔAOT550 on aerosol content in background conditions, that can indirectly reveal the favourable conditions for the aerosol generation over the particular regions of Russia.

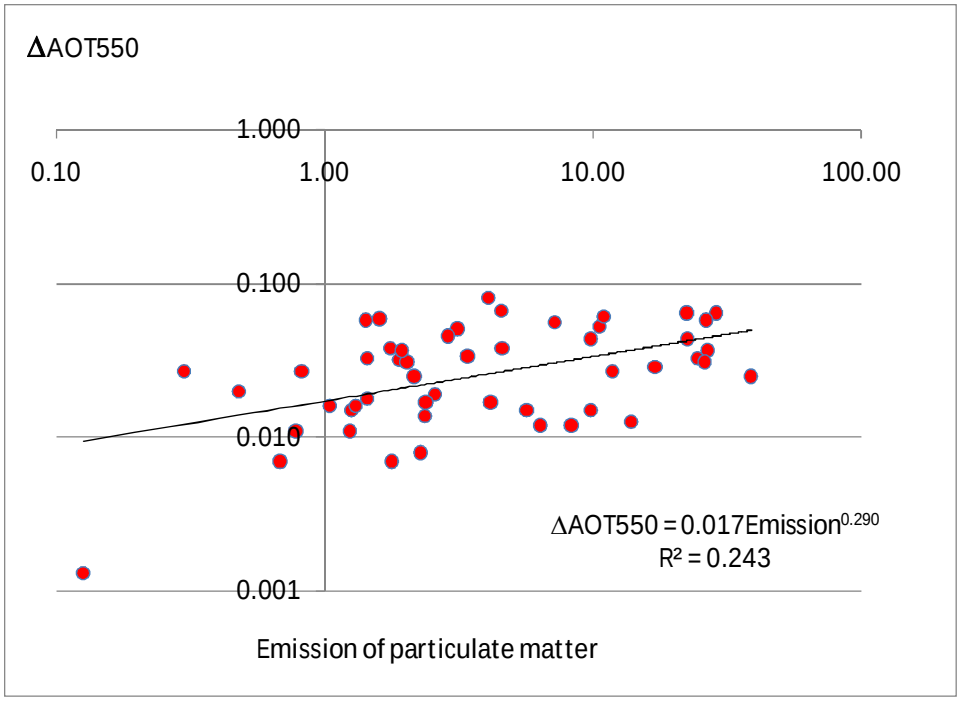

Figure 2. Urban aerosol pollution (ΔAOT550) over Russian cities as a function of particulate matter emission.

The analysis of the data on emissions and concentrations of the main pollutants over the 1988-2011 period together with ΔAOT500 variability have been made. For each city the ratio of sulfur dioxide to nitrogen dioxide emissions was evaluated to assess temporal variability and the dominating aerosol properties in various geographical regions. Different areas over Russia were revealed with dominating SO_2 or NOx regimes of pollution.
As a result, the radiative forcing of urban aerosol pollution for different cities was evaluated. Depending on the geographical location, as well as on the level of aerosol pollution the radiative forcing varied from -4. Wm-2 to -0.4Wm-2. The negative sign of the radiative forcing showed the cooling effect of urban aerosol.

CONCLUSIONS

Some assessments were fulfilled to reveal the temporal and spatial variability of aerosol urban pollution over Russia. More accurate estimates were made for Moscow region using the data from two collocated ground ARONET stations. According to them we have revealed the absolute value of urban aerosol optical thickness of about +0.02 in visible region, the existence of two aerosol modes – both fine and coarse, and a tendency to smaller single scattering albedo.

The application of the satellite MODIS AOT retrievals provided the estimates of urban aerosol pollution of 50 large cities, which were characterized by the mean value of $\Delta AOT550=0.03\pm0.005$. Some assessments of the type of emissions and their temporal trends were also fulfilled. The preliminary estimates of radiative forcing due to urban aerosol pollution varied within -0.4-÷- 04 Wm-2. They demonstrated the cooling urban aerosol effects.

ACKNOWLEDGEMENTS

The work was partially supported by the grant RFBR #13-05-00956.

REFERENCES

Chubarova N., Smirnov A., Holben B.N.(2011). Aerosol properties in Moscow according to 10 years of AERONET measurements at the Meteorological Observatory of Moscow State University, *Geography, environment, sustainability*, **4**, № 1, 19-32.

Chubarova N.Y., Sviridenkov M.A., Smirnov A., Holben B.N. (2011). Assessments of urban aerosol pollution in Moscow and its radiative effects, *Atmospheric Measurement Techniques*, **4**, 367-378

SATELLITE REMOTE SENSING OF AEROSOL AND CLOUD PROPERTIES OVER EURASIA

G. DE LEEEUW[1,2], L. SOGACHEVA[1], P. KOLMONEN[1], G. SAPONARO[1], T.H. VIRTANEN[1], E. RODRIGUEZ[1], K. ATLASKINA[2] and A.-M. SUNDSTRÖM[2]

[1]Finnish Meteorological Institute, Helsinki, Finland

[2]Department of Physics, University of Helsinki, Finland.

Keywords: SATELLITE REMOTE SENSING, AEROSOL, CLOUDS, AOD.

INTRODUCTION

Satellite remote sensing provide the spatial distribution of aerosol and cloud properties over a wide area. Polar orbiting satellite provide on the order of 14 orbits per day and the swath width of instruments used for observations of atmospheric properties such as aerosol or cloud parameters or atmospheric trace gases may vary from a few hundred kilometres to ca. 2300 km. Their importance is, among others, that they use optical techniques to obtain information on aerosol properties and hence the results are of direct relevance to climate because particles are observed in the optically active size range. These particles are also important for air quality, since they contribute particulate matter concentrations included in PM1 or PM2.5. The column- integrated aerosol extinction, aerosol optical depth or AOD, which is primarily reported from satellite observations, is used as a proxy for cloud condensation nuclei (CCN) and hence contains information on the ability of aerosol particles to form clouds. Hence, connecting this information with direct observations of cloud properties provides information on aerosol-cloud interactions.
On the other hand, particles smaller than about 100 nm are important for many processes but cannot be observed from satellites. In that case, atmospheric trace gases which can serve as aerosol precursors, as well as other proxies such as UV radiation and AOD, which serves as a proxy for condensation sink, can be sued from satellites to provide information on new particles formed through nucleation.

Whereas all these processes can be studies in great detail from ground-based measurements involving a large instrument suite to provide information on a wide variety of parameters, satellites are very limited as regards the number of parameters they can provide and the detail of their properties. Satellites measure only a few signals, in particular the intensity of the upwelling solar radiation reflected by atmospheric constituents (clouds, aerosols, trace gases) and the Earth surface, in several wavebands or as a wide spectrum over a certain wavelength range, sometimes at more than one viewing angle and sometimes with polarization information. This limited information allows only few degrees of freedom of the information which can be retrieved. With this difference in mind, the complementarity of satellite and in situ ground based observations needs to be explored, where satellites are very important to provide information over the vast areas where no ground-based information is available. This applies, for instance, over the larger part of the Eurasia, the study domain of PEEX.

SATELLITE DATA

Retrieval algorithms for aerosol and clouds have been developed for the (Advanced) Along Track Scaning Radiometer (A)ATSR, consisting of a series of instruments of which we use the second and third one: ATSR-2 which flew on the ERS-2 satellite (1995-2003) and AATSR which flew on the ENVISAT satellite (2002-2012) (both from the European Space Agency, ESA). The ATSR instruments provide two views: one near-nadir and the other at 55 degrees forward. Each view provides the radiances at the top of the atmosphere (TOA) in 7 wavebands from the visible (VIS) to the thermal infrared (TIR). The TIR wavebands are mainly used for cloud detection, in combinations with a number of tests including shorter wavelengths. The VIS and NIR (near-infrared) wavebands are sued for aerosol retrieval. Over land the

dual view algorithm is used, in which the effect of the land surface reflectance is accounted for by using the ratio of both views in the 1.6 µm band, assuming that the effect of aerosols on the TOA reflectance is small. Together with some other assumptions, the dual view algorithm provides very good information on the aerosol properties over land with a quality which is similar to that of other satellites which are commonly used as the 'standard' for aerosol retrieval (in particular MODIS, MISR). However, ATSR has a smaller swath and thus less coverage than MODIS, and a bit better than MISR. Over ocean only a single view is used (forward) and also here the quality of the data is competitive with that of other instruments. The advantage of the ATSR-2/AATSR combination is that it provides a time series of 17 years, longer than any other of the currently available quality products (MODIS, MISR, SeaWiFS). This time series will be further expanded with those from the Sea and Land Surface Temperature Radiometer (SLSTR) on the ESA/EU GMES Sentinel-3 mission which is planned to be launched in the autumn of 2015.

The Dual View algorithm provides aerosol data on a global scale with a default resolution of 10x10km^2 (L2) and an aggregate product on 1^o x1^o (L3). Optional, a 1x1 km^2 retrieval products is available over smaller areas for specific studies. Since for the retrieval of AOD no prior knowledge is needed on surface properties, the surface reflectance can be independently retrieved using the AOD for atmospheric correction.

For the retrieval of cloud properties, the SACURA algorithm has been implemented in the ADV/ASV aerosol retrieval suite. Cloud properties retrieved from AATSR data are cloud fraction, cloud optical thickness, cloud top height, cloud droplet effective radius, liquid water path. In addition to AATSR data we also use MODIS cloud properties publicly available from the internet.

Information on trace and greenhouse gases is available form instruments such as SCIAMACHY, OMI, GOME-2, IASI. These instruments fly on different satellites. Information provided is, for instance, UV radiation and concentrations of gases such as NO2, SO2, VOCs and greenhouse gases.

APPLICATIONS TO THE PEEX STUDY AREA

Aerosol and cloud properties are applied for different studies over the PEEX area. Using the simultaneous retrieval of aerosol and cloud properties allows for study of the transition from the aerosol regime to the cloud regime, such as changes in effective radius or AOD (aerosol optical depth) to COT (cloud optical thickness). Such studies are being made with aerosol and cloud properties retrieved for single AATSR pixels (nominal 1x1 km^2 sub-nadir) which reveals information on the aerosol retrieval techniques and the processes which may play a role in the transition zone.

In another studies large data sets are used for statistical studies on aerosol cloud interaction in an area over Fennoscandia, the Baltic Sea and adjacent regions over the European mainland. This area spans several regimes with different influences on aerosol cloud interaction such as a the transition from relative clean air over Fennoscandia to more anthropogenically polluted air further south, and the influence maritime air over the Baltic and oceanic air advected from the North Atlantic. The aim of the study is to study the effect of these different regimes on aerosol-cloud interaction using a large aerosol and cloud data set provided by MODIS.

The air over Finland, as an example, is rather clean with AOD which is usually on the order of about 0.05, except in period with transport of more polluted over the area, such as from Central Europe or Russia. In particular the signature of forest fires generated aerosol can be easily detected through the large aerosol plumes and their spatial extend. The presence of this aerosol type can be further confirmed by the presence of trace gases or the enhanced fraction of absorbing aerosol. In ADV we use a mixture of aerosol components which allows to vary the ssa (single scattering albedo). The retrieval method works such that, after an initial guess of the aerosol composition obtained from using a modelling based aerosol data base, the aerosol components are varied to optimize the AOD at three wavelengths (over land) by minimizing the difference between the observed and modelled AODs. The modelled AOD are obtained from

continuous vary the mixing fractions of four components. Thus the retrieval provides the optimum mixing fractions of the components together with a measure for the AOD level. With each component being characterized by the coefficients describing their lognormal size distribution and a specified refractive index, the AOD can be calculated at each wavelength. However, in principle also other aerosol properties could be calculated from these data, such as ssa. This method has been applied to the forest fire episode near Moscow in 2010 and the results have been evaluated.

In another study, the AOD over the boreal forest has been correlated with the occurrence over forest fires, as determined from satellite observations (a satellite fire product). These two parameters are well correlated and a clear seasonal signature is present. One problem in such studies is the discrimination between areas with high AOD and clouds. This is true for both forest fires, desert dust and anthropogenic pollution.

Anthropogenic pollution occurs in several parts of the PEEX study area, and in particular near densely populated areas and megacities, but also in industrialized areas and areas with dense traffic. The aerosol in such areas is quite different from that produced over the boreal forest and has different effects on air quality and climate. Studies have been made on the effects of aerosols on air quality and on the radiatin balance in China. The current time AATSR series allow for the study of temporal trends over specific areas and contrast effects of megacities and more rural areas.

As mentioned above, the scattering efficiency of aerosol particles smaller than about 100 nm is very small and therefore no information on such particles can be obtained from satellite observations. However, using satellite-derived proxies information can be obtained on nucleation mode particles (Kulmala et al., 2011; Sundström et al., 2014). During the ALANIS project the use of satellite proxies over Finland has been studied and results have been compared with GLOMAP model calculations.

CONCLUSIONS

The rationale for the application of satellite observation over the vast EURASIAN PEEX study area has been outlined above. Satellites can provide information on a variety of phenomena over the boreal forest and more industrialized area in EURASIA, including the local generation of aerosols by nucleation using proxies, the transport of aerosols from elsewhere and their effects on air quality and climate, both direct and indirect through aerosol cloud interaction. Aerosols and cloud also affect the surface radiation level and thus the biosphere by limiting radiation. Together with other satellite observations by other PEEX participants on land and water surfaces, forests, vegetation, snow and ice, satellites are crucial in the PEEX project. They provide the spatial extent which cannot possibly be covered by ground-based or airborne observations. In this way they fill the gaps between the planned supersites and other stations. Furthermore, since the same instruments are used over a long period of time and over the same area, a consistent source of information on phenomena over the boreal forest is provided. The long time series show the temporal variation and can be sued for trend analysis. An example is the trend in the albedo of snow-covered surfaces in the Northern hemisphere. Other work includes snow albedo and the effect of soot on snow properties.

ACKNOWLEDGEMENTS

This work was supported by This work was supported by the Centre on Excellence in Atmospheric Science funded by the Finnish Academy of Sciences Excellence (project no. 272041), the CRAICC (Cryosphere-atmosphere interactions in a changing Arctic climate), which is part of the Top-level Research Initiative (TRI) of the joint Nordic research and innovation initiative, the ESA-ESRIN projects Aerosol-cci (project AO/1-6207/09/I-LG), STSE-ALANIS Atmosphere-Land-Interaction Study, Theme 3 Aerosols (Contract No 4200023053/10/I-LG), and Globemission (ESA-ESRIN Data Users Element (DUE), project AO/1-6721/11/I-NB), the EU projects PEGASOS (EU FP7 ENV.2010.1.1.2-1) and MEGAPOLI (EU FP7 FP7-ENV-2007.1.1.2.1), and the Nessling Foundation.

REFERENCES

Kulmala, M., Arola, A., Nieminen, T., Riuttanen, L., Sogacheva, L., de Leeuw, G., Kerminen, V.-M., and Lehtinen, K. E. J.: The first estimates of global nucleation mode aerosol concentrations based on satellite measurements, *Atmos. Chem. Phys.*, 11, 10791-10801, doi:10.5194/acp-11-10791-2011, 2011.

Mei, L., Xue, Y., de Leeuw, G., Guang, J., Wang, Y., Li, Y., Xu, H., Yang, L., Hou, T., He, X., Wu, C., Dong, J., and Chen, Z.: Integration of remote sensing data and surface observations to estimate the impact of the Russian wildfires over Europe and Asia during August 2010, Biogeosciences, 8, 3771-3791, doi:10.5194/bg-8-3771-2011, 2011.

Toledano, C., V. Cachorro, M. Gausa, K. Stebel, V. Aaltonen, A. Berjón, J. P. Ortiz de Galisteo, A.M. de Frutos, Y. Bennouna, S. Blindheim, C. L Myhre, G. Zibordi, C. Wehrli, S. Krazter, B. Hakansson, T. Carlund, G. de Leeuw, A. Herber (2012). Overview of sun photometer measurements of aerosol properties in Scandinavia and Svalbard, Atmospheric Environment 52 (2012) 18-28, DOI: 10.1016/j.atmosenv.2011.10.022.

E. Rodríguez, E., C. Toledano, V. Cachorro, A. De Frutos, G. de Leeuw, M. Gausa and B. Holben (2012). Comparison of aerosol optical properties at the sub- arctic stations ALOMAR-Andenes, Abisko and Sodankylä in late spring and summer 2007. Atmospheric Research, Volume: 107 Pages: 20-30 DOI: 10.1016/j.atmosres.2011.12.003.

Sundström, A.-M., P. Kolmonen, L. Sogacheva and G. de Leeuw(2012). Aerosol retrievals over China with the AATSR Dual-View Algorithm. *Remote Sensing of Environment*, Volume 116, 15 January 2012, Pages 189-198.

Aaltonen, V., E. Rodriguez, S. Kazadzis, A. Arola, V. Amiridis, H. Lihavainen, and G. de Leeuw (2011). On the variation of aerosol properties over Finland based on the optical columnar measurements (2012). *Atm. Res.*, 116, 46-55 (http://dx.doi.org/10.1016/j.atmosres.2011.07.014).

Mei, L.L., Y. Xue, G. de Leeuw, W. von Hoyningen-Huene, A. A. Kokhanovsky, L. Istomina, J. Guang, J.P. Burrows (2013). Aerosol optical depth retrieval in the Arctic region using MODIS data over snow. Remote Sensing of Environment 128 (2013) 234–245.

Mei, L.L., Y. Xue, A.A. Kokhanovsky, W. von Hoyningen-Huene, L. Istomina, G. de Leeuw, J.P. Burrows, J. Guang and Y. Jing (2013). Aerosol optical depth retrieval over snow using AATSR data. *International Journal of Remote Sensing*, 34:14, 5030-5041.

Li, Y., Y. Xue, G. de Leeuw, C. Li, L. Yang, T. Hou and F. Marir (2013). Retrieval of Aerosol Optical Depth and Surface Reflectance over Land from NOAA AVHRR Data. Remote Sensing of Environment 133 (2013) 1–20.

Hollmann, R., C. Merchant, R. Saunders, C. Downy, M. Buchwitz, A. Cazenave, E. Chuvieco, P. Defourny, G. de Leeuw, R. Forsberg, T. Holzer-Popp, F. Paul, S. Sandven, S., Sathyendranath, M. van Roozendael, W. Wagner (2013).The ESA climate change initiative: satellite data records for essential climate variables. Bulletin of the American Meteorological Society Oct. 2013, 1541-1552. ; e-View: doi: http://dx.doi.org/10.1175/BAMS-D-11-00254.1.

Holzer-Popp, T., de Leeuw, G., Griesfeller, J., Martynenko, D., Klüser, L., Bevan, S., Davies, W., Ducos, F., Deuzé, J. L., Graigner, R. G., Heckel, A., von Hoyningen-Hüne, W., Kolmonen, P., Litvinov, P., North, P., Poulsen, C. A., Ramon, D., Siddans, R., Sogacheva, L., Tanre, D., Thomas, G. E., Vountas, M., Descloitres, J., Griesfeller, J., Kinne, S., Schulz, M., and Pinnock, S.: Aerosol retrieval experiments in the ESA Aerosol_cci project, Atmos. Meas. Tech., 6, 1919-1957, doi:10.5194/amt-6-1919-2013, 2013.

de Leeuw, G., T. Holzer-Popp, S. Bevan, W. Davies, J. Descloitres, R.G. Grainger, J. Griesfeller, A. Heckel, S. Kinne, L. Klüser, P. Kolmonen, P. Litvinov, D. Martynenko, P.J.R. North, B. Ovigneur, N. Pascal, C. Poulsen, D. Ramon, M. Schulz, R.Siddans, L. Sogacheva, D. Tanré, G.E. Thomas, T.H. Virtanen, W. von Hoyningen Huene, M.Vountas, S. Pinnock (2013). Evaluation of seven European aerosol optical depth retrieval algorithms for climate analysis, Remote Sensing of Environment (2013), http://dx.doi.org/10.1016/j.rse.2013.04.023. (proofed 03Oct2013)

Virkkula, A., Levula, J., Pohja, T., Aalto, P. P., Keronen, P., Schobesberger, S., Clements, C. B., Pirjola, L., Kieloaho, A.-J., Kulmala, L., Aaltonen, H., Patokoski, J., Pumpanen, J., Rinne, J., Ruuskanen, T., Pihlatie, M., Manninen, H. E., Aaltonen, V., Junninen, H., Petäjä, T., Backman, J., Dal Maso, M., Nieminen, T., Olsson, T., Grönholm, T., Aalto, J., Virtanen, T. H., Kajos, M., Kerminen, V.-M., Schultz, D. M., Kukkonen, J., Sofiev, M., De Leeuw, G., Bäck, J., Hari, P., and Kulmala, M.: Prescribed burning of logging slash in the boreal forest of Finland: emissions and effects on meteorological quantities and soil properties, Atmos. Chem. Phys., 14, 4473-4502, doi:10.5194/acp-14-4473-2014, 2014..

H.K. Lappalainen1, T. Petäjä, J. Kujansuu, V. –M. Kerminen, A. Shvidenko, J. Back, T. Vesala, T. Vihma, G. de Leeuw, A. Lauri, T. Ruuskanen, V. B. Lapshin, N. Zaitseva, O. Glezer, M. Arshinov, D.V. Spracklen, S. R. Arnold, S. Juhola, H. Lihavainen, Y. Viisanen, N. Chubarova, S. Chalov, N. Filatov, A. Skorokhod, N. Elansky, E. Dyukarev, I. Esau, P. Hari, V. Kotlyakov, N. Kasimov , V. Bondur, G. Matvienko, A. Baklanov, E. Mareev, Y. Troitskaya, A. Ding, H. Guo, S. Zilitinkevich, M. Kulmala (2014). J. Geography, Environment and Sustainability, 13-48.

Rosenfeld, D., M. O. Andreae, A. Asmi, M. Chin, G. de Leeuw, D. Donovan, R. Kahn, S. Kinne, N. Kivekäs, M. Kulmala, W. Lau, S. Schmidt, T. Suni, T. Wagner, M. Wild, J. Quaas (2013). Observations of aerosol-cloud-precipitation-climate interactions. *Rev. Geophys*. Available online: doi: 10.1002/2013RG000441.

Sundström, A.-M., Arola, A., Kolmonen, P., Xue, Y., de Leeuw, G., and Kulmala, M.: On the use of satellite remote sensing based approach for determining aerosol direct radiative effect over land: a case study over China, Atmos. Chem. Phys. Discuss., 14, 15113-15147, doi:10.5194/acpd-14-15113-2014, 2014. (submitted 28March 2014, accepted 02Oct2014).

Tomasi, C., A.A. Kokhanovsky, A. Lupi, C. Ritter, A. Smirnov, N.T. O'Neill, R.S. Stone, B.N. Holben, S. Nyeki, C. Wehrli, A. Stohl, M. Mazzola, C. Lanconelli, V. Vitale, K. Stebel, V. Aaltonen, G. de Leeuw, E. Rodriguez, A.B. Herber, V.F. Radionov, T. Zielinski, T. Petelski, S.M. Sakerin, D.M. Kabanov, Y. Xue, L.-L Mei, L. Istomina, R. Wagener, B. McArthur, P.S. Sobolewski, R. Kivi, Y. Courcoux, P. Larouche, S. Broccardo and S.J. Piketh (2015). Aerosol remote sensing in polar regions, Earth-Science Reviews 140 (2015) 108–157.

Sogacheva, L., Kolmonen, P., Virtanen, T. H., Rodriguez, E., Sundström, A.-M., and de Leeuw, G.: Determination of land surface reflectance using the AATSR dual-view capability, Atmos. Meas. Tech. Discuss., 7, 7451-7494, doi:10.5194/amtd-7-7451-2014, 2014.

Rodríguez, E., Kolmonen, P., Virtanen, T. H., Sogacheva, L., Sundström, A.-M., and de Leeuw, G.: Retrieval of aerosol absorption properties using the AATSR satellite instrument: a case study of wildfires over Russia 2010, Atmos. Meas. Tech. Discuss., 7, 9839-9868, doi:10.5194/amtd-7-9839-2014, 2014.

Sundström, A.-M., Nikandrova, A., Atlaskina, K., Nieminen, T., Vakkari, V., Laakso, L., Beukes, J. P., Arola, A., van Zyl, P. G., Josipovic, M., Venter, A. D., Jaars, K., Pienaar, J. J., Piketh, S., Wiedensohler, A., Chiloane, E. K., de Leeuw, G., and Kulmala, M.: Characterization of satellite based proxies for estimating nucleation mode particles over South Africa, Atmos. Chem. Phys. Discuss., 14, 25825-25867, doi:10.5194/acpd-14-25825-2014, 2014.

INTRODUCTION TO A FLAGSHIP SITE SORPES IN EAST CHINA AND AN OVERVIEW OF MAIN RESULTS OBTAINED DURING 2011-2014

A. DING[1,2], C. FU[1,2], W. NIE[1,2,3], X. YANG[1,2], J. SUN[1,2], T. PETÄJÄ[3], V.-M. KERMINEN[3] and M. KULMALA[3]

[1]Institute for Climate and Global Change Research & School of Atmospheric Sciences, Nanjing University, 210023, Nanjing, China

[2]Collaborative Innovation Center of Climate Change, Jiangsu Province, China

[3]Department of Physics, University of Helsinki

This study will give an introduction to a latest developed SMEAR-type "flagship" site SORPES and give a summary about the main results and key findings obtained during the past three years (2011-2014). The SORPES- Station for Observing Regional Processes of the Earth system is a research and experiment platform developed by Nanjing University (NJU) in collaboration with the University of Helsinki. The overall objective of this platform is to characterize the temporal variation of key parameters related to climate change and to understand the interactions of different regional processes of the Earth system in eastern China, a region strongly influenced by monsoon weather and by intensive human activities. The SORPES sites focus on four major processes: land surface processes, air pollution–climate interaction, ecosystem–atmosphere interaction, and hydrology and water cycle. With 3-yr continuous measurements, several key findings have been obtained, including chemistry of ozone, HONO, and fine particle, air pollution-weather interactions, aerosol size and new particle formation, and inter-annual variability of pollutants and the linkage to Asian Monsoon etc. (Ding et al., 2013ab, Hermman et al., 2014, Nie et al., 2014, Xie et al., 2015, Qi et al., 2015, Ding et al., 2015).

REFERENCES

Ding, Aijun, Fu, C. B.; Yang, X. Q.; et al., Ozone and fine particle in the western Yangtze River Delta: an overview of 1 yr data at the SORPES station, Atmos. Chem. Phys.(Impact factor: 5.298) , 13,11, 5813-5830,2013.

Ding, Aijun, C.B. Fu, X.Q. Yang, J.N. Sun, T. Peteja, V.-M. Kerminen, T. Wang, Y. N. Xie., E. Herrmann, L.F. Zheng, W. Nie, Q. Liu, X.L. Wei and M. Kulmala: Intense atmospheric pollution modifies weather: a case of mixed biomass burning wither fossil fuel combustion pollution in the eastern China, Atmos. Chem. Phys. (Impact factor: 5.298) ,13,10545-10554, 2013.

Ding, Aijun, Fu, C. B. et al., Interannual variation of ozone and fine particles in the western Yangtze River Delta, manuscript in preparation, 2015.

Herrmann, E., Ding, A. J., Kerminen, V.-M., Petaja, T., Yang, X. Q., Sun, J. N., Qi, X. M., Manninen, H., Hakala, J., Nieminen, T., Aalto, P. P., Kulmala, M., and Fu, C. B.:

Aerosols and nucleation in eastern China: first insights from the new SORPES-NJU station, Atmos. Chem. Phys., 14, 2169-2183, doi:10.5194/acp-14-2169-2014, 2014.

Nie, Wei, Aijun Ding*, Y.N.Xie, Z. Xu, H. Mao, V. Kerminen, L.F. Zheng, X.M. Qi, X.Q. Yang, J.N. Sun, E. Herrmann, T. Petaja, M. Kulmala, C.B Fu, Influence of biomass burning plumes on HONO chemistry in eastern China, Atmos. Chem. Phys. Discuss., 14, 6, 7859-7887, 2014 (*in press* on Atmos. Chem. Phys.).

X.M. Qi, W. Nie, A.J. Ding, T. Petaja, V.-M. Kerminen, E. Herrmann, Y.N. Xie, L.F. Zheng, H. Manninen, P. P. Aalto, J.N. Sun, Z.N. Xu, X.G. Chi, X. Huang, M. Boy, A. Virkkula, X.Q. Yang, C.B. Fu, and M. Kulmala, Aerosol size distribution and new particles formation in western Yangtze River Delta of China: two-year measurement at the SORPES station, manuscript submitted to Atmos. Chem. Phys., 2015.

Xie, Y.N. A.J. Ding*, W. Nie, X.M. Qi, H.T. Mao, V.-M. Kerminen, T. Petaja, X. Huang, X.G. Chi, A.Virkkula, L.F. Zheng, Erik Herrmann, J.N. Sun, X.Q.Yang, M. Kulmala, and C.B.Fu, Enhanced sulfate formation by nitrogen dioxide: two in-situ evidences with different mechanisms observed at SORPES station, manuscript submitted to Atmos. Chem. Phys., 2015.

VERTICAL MIXING OF AEROSOL IN THE PLANETARY BOUNDARY LAYER AT NY-ÅLESUND, SVALBARD

O. Drofa[1], C. Lanconelli[1], A. Lupi[1], M. Mazzola[1], F. Tampieri[1], A. P. Viola[1], V.Vitale[1],
S. Becagli[2], F. Giardi[2], R. Udisti[2],
M.Maturilli[3], A.Schultz[3],
J. Strom[4], P. Tunved[4], R. Krejci[4] and H. C. Hansson[4]

[1]CNR ISAC, Bologna and Rome, Italy

[2]Chemistry Department "Ugo Schiff", University of Florence, Florence, Italy

[3]AWI, Potsdam, Germany

[4]Department of Applied Environmental Science (ITM), Stockholm University, Stockholm, Sweden

Keywords: Aerosol, Artic Planetary Boundary Layer, Vertical mixing.

INTRODUCTION

Aerosol is an important component of the atmosphere. Its vertical distribution in the planetary boundary layer (PBL) is an index of the mixing that occurs between the tracers transported in the free atmosphere and those of local origin.

The present paper aims to investigate the influence of the boundary layer structure and dynamics on the vertical distribution of aerosol. The main issue is related to the height of PBL: the question is whether some decoupling occurs between the surface layer and the atmosphere aloft when the PBL is shallow or the mechanical mixing due to the synoptic circulation provides an overall vertical homogeneity of the concentration of the aerosol irrespective of the stability conditions.

To this end, the aerosol concentration and size distribution measured near the surface are compared to the ones measured at 500 m height. The surface turbulent fluxes are examined, and the radiosoundings and the meteorological simulations from the NWP model BOLAM are used to evaluate the stability and the dynamics of the first km of the atmosphere above the measuring station.

DATA, MODELS AND METHODOLOGY OF ANALYSIS

The Climate Change Tower: meteo and surface flux data

The Department of Earth System Science and Environmental Technologies of the Italian Nationl Reaserach Council has recently financed the construction of the Amundsen-Nobile Climate Change Tower (CCT). The tower was installed at the end of 2009 about 2 Km NW off the village of NyÅlesund (located at about 79 N, 12 E), in the Svalbard Islands (Norway), in the framework of the so called Climate Change Tower Integrated Project (CCT-IP). The tower is 34 m height and provides a platform for different atmospheric monitoring activities. Since the beginning of the project the tower was equipped with 4 thermo-hygrometers and 4 propeller anemometers at the heights of 2.0, 4.8, 10.3 and 33.4 m, with a 4-components net radiometer at the top of the tower and a couple of pyranometer-pyrgeometer installed at 25 m measuring the outgoing radiation, with a sonic range sensor, an infrared camera and 2 PT100 resistance thermometers measuring the snow

height, skin and internal temperatures, respectively, and a flux plate at the snow-ground interface. Since March 2010 a set composed by a sonic anemometer (model Gill R3-50) and a fast hygrometer (Campbell Scientific KH2O) was installed at an height of 7.5 m.

Aerosol data

Aerosol measurements were performed at Mount Zeppelin laboratory (474 m.s.l), just SW the CCTower (hereinafter Z), equipped with a DMSP (Differential Mobility Particle Sizer), able to analyze particles in 32 classes in the range $0.003 - 0.9\,\mu$m (Tunved et al., 2013), with an acquisition time of 20 minutes, and at Gryvebadet Laboratory (hereinafter G), with a Scanning Mobility Particle Sizer (TSI 3034), which analyzes particles in 52 classes in the range $0.01 - 0.49\,\mu$m (Hogrefe et al., 2006), with an acquisition time of 10 minutes. The actual size distribution measurements have been compared in the spring/summer months of 2013 (from April to August).

From the size spectra, the Geometric Mean Diameter GMD has been computed. GMD is an useful tool to describe the modal characteristics of the aerosol size distribution and gives a simple parameterization to represent and compare various aerosol population. The whole Geometric Mean Diameter is defined as the weighted mean of the size distribution (Krishna Moorthy et al., 2011) :

$$GMD = \exp\left(\sum \frac{N_j \log(D_j)}{N}\right) , \tag{1}$$

where N is the total number of particles per unit volume (number concentration) and N_j is the number concentration of the particles in the diameter range D_j, D_{j+1}.

Atmospheric modeling

In the present work, the Numerical Weather Prediction (NWP) model BOLAM (Buzzi et al., 2003) was used. BOLAM is an hydrostatic, limited area model, based on the primitive equations with wind, temperature, water vapor mixing ratio, surface pressure and five microphysical species as prognostic variables; it is based on a lat-lon rotated, staggered Arakawa-C grid (in this work, the resolution is 0.06×0.06 degree, i.e. about 7 km), with hybrid, terrain following vertical coordinate (with 60 levels), and uses a 3-D Weighted Average Flux (WAF) advection scheme for the basic variables and a semi-Lagrangian advection scheme for the microphysical variables. The radiation scheme is based on Ritter and Geleyn (1992) and the parameterization of European Center for Medium-Range Weather Forecast (ECMWF) (Morcrette, 1991); the TKE-l vertical diffusion scheme (Zampieri et al., 2005) is based on Mellor-Yamada closure of order 2; it uses the Kain-Fritsch convection parametrisation scheme. The microphysical scheme takes into account cloud water, cloud ice, rain, snow and hail (Drofa and Malguzzi, 2004). There is a vegetated surface and deep soil scheme, taking into account the water phase transitions. Objective analyses of the meteorological parameters produced by the Integrated Forecasting System (IFS) of ECMWF are used as initial and boundary conditions for Bolam simulations. These data are available every 6 hours and are provided on a grid of 0.15×0.15 degrees in a rotated coordinate system with the same rotation parameters used for BOLAM simulation: the origin of coordinate system is located in the observation point (NyÅlesund). IFS-ECMWF data are provided at all available atmospheric model levels (hybrid vertical coordinate) and at 4 available levels under surface. The used domain is large enough to solve the problem of relatively long interval (6 hours) between two checkpoints of the global analysis data used.

Backward trajectories are computed using the Lagrangian model FLEXPART (Stohl et al., 2005). In the present work the version 8.2 is used. FLEXPART runs using as input the BOLAM simulations

at high resolution both in space (about 7 km) and in time (1 hour between two checkpoints). The backward trajectories are computed for each one-day long case-studies, with hourly frequency, from 0 to 23 UTC. The meteorological simulation starts at 00 UTC of the previous day and runs for 48 hours to cover the whole backward trajectory period.

THE CASE STUDIES

We have selected five months for the analysis: from April 2013 to August 2013, characterized by different weather and PBL features and by the full availability of data. Moreover, detailed analysis of one day is reported, chosen in order to put into evidence some special features.

Monthly analysis

The analysis of the atmospheric circulation regime in the region considered here shows that the synoptic conditions on Svalbard Island are generally determined by the Polar vortex. During the period under investigation a pressure trough is usually located to the West of the region of interest, thus a south-westerly wind condition prevails.

At the beginning of the period, the transition of polar atmospheric circulation from winter to summer regime is observed. In April the Polar vortex is situated in the Eastern Hemisphere, with one of its dipole located close to Svalbard islands, North of them. Svalbard islands are close to the trough axis of a Rossby wave. In this situation a northern advection prevails at the concerning point. During the month of May the transition to summer circulation regime terminates. The Polar vortex center migrates to the Pole and gets weaker. Svalbard Islands fall in the vicinity of the ridge axis of a Rossby wave, and south-western advection dominates in this region. It must be noted that during the season transition period the observed advection velocity is relatively low. An analogous situation is observed in June: moderate south-western advection prevails over Svalbard Islands. In July the seasonal weakening of the Polar depression is at its peak and the Polar vortex advection is slow and close to the westerly direction. During the month of August a gradual regeneration of the Polar vortex takes place. The through of the Polar depression is located over Greenland and a forced south-west air stream is observed in the Svalbard region in presence of week local cyclonic circulation West of Iceland.

As far as the stability is concerned, the standard index is the Obukhov length L, based on the kinematic fluxes of momentum u_*^2 and of heat $\langle w\theta \rangle$ measured from the sonic anemometer placed at an height $z = 7.5\,\mathrm{m}$:

$$L = -\frac{\Theta}{\kappa\ g}\frac{u_*^3}{\langle w\theta \rangle}\ , \tag{2}$$

where Θ is a reference potential temperature, $\kappa = 0.4$ the von Karman constant and g the gravity acceleration.

During April stable conditions prevail, while in the summer period unstable conditions occurr more frequently. As shown in Fig. 1, it results that a full range of stabilities near the ground is exploited in the examined periods.

To compare the aerosol measurements in the two stations, the scatterplots of the number concentration measured at Z vs. the one measured at G, *i.e.* $N_Z = \alpha_N\ N_G$, has been evaluated for the four examined months: it results that the number concentration in the upper station is about one half of the one measured in the lower one, with good correlations. For the detail of the months, see Table 1. Also the scatterplots of the Geometric Mean Diameter has been evaluated: $GMD_Z = \alpha_{GMD}\ GMD_G$. This quantity is the same in the two stations within the 10%, with a fair correlation coefficient (higher in April, lower in the summer months). The picture that arises

is that the aerosol population is quite similar in the two sites, at least as far the main physical characteristics are concerned.

Month	α_N	R_N	α_{GMD}	R_{GMD}
April	0.407	0.702	1.169	0.941
May	0.496	0.734	1.107	0.647
June	0.448	0.722	1.066	0.814
July	0.541	0.639	1.081	0.699
August	0.474	0.802	0.993	0.742

Table 1: Comparison between the number concentration N and the mean diameter GMD measured at Z and G for the four examined months. α represents the coefficient of the linear fit, R the correlation coefficient.

A further analysis can be made selecting the cases in terms of stability: the scatterplots of N and GMD have been made for stable conditions ($z/L > 0.5$), unstable ($z/L < -0.5$) and near neutral (z/L in between): see the scatterplots in Fig. 2 and the values in Table 2. It results that α_{GMD} is not sensitive to variations of stability, and maintains the same value as for the various months. The number concentration at the two stations is slightly more similar in convective conditions (at Z about 50% of the value at G) than in stable ones (about 40%), as expected. However, the influence of the surface stability can be considered quite small in determining the relative concentration at the two stations.

Stability	α_N	R_N	α_{GMD}	R_{GMD}
unstable: $z/L < -0.5$	0.50	0.83	1.19	0.95
near neutral: $\|z/L\| < 0.5$	0.44	0.84	1.20	0.94
stable: $z/L > 0.5$	0.41	0.85	1.18	0.97

Table 2: Comparison between the number concentration N and the mean diameter GMD measured at Z and G for different stability conditions, during the full period under investigation.

The case of 21 April 2013

This case presents a synoptic situation typical of the considered region: it is characterized by the presence of an intense South-Easterly advection, associated with the jet stream of the Polar vortex. One dipole of the Polar depression is located South-West of the Svalbard Islands and forces the jet stream to take course over the region. An analogous air stream situation takes place at the surface: over the considered region an anticyclone to the North-Est and a dipolar cyclone to the South-West are evident from the mean sea level pressure field, thus an intensive southerly current is observed in the wind field at 10 m over the surface. In these conditions an intense wind friction is observed at the surface, when a strong wind in the low troposphere from the flat sea surface encounters the sharp orographical obstacle of the islands, leading to an intense dynamical mixing of low troposphere layer.

Looking at the details of the time series (see Fig. 3), it results that there is an abrupt change in the wind intensity at about 10:00 at G, while the intensity increases slowly at Z (the directions are similar, from South to South-East). Correspondingly, the number concentration increases in both the stations, with a remarkable time sincronization. The heat flux is negligible in the morning, then becomes negative, corresponding to unstable conditions; at the same time the downwards short wave radiative flux increases. The momentum flux increases as the wind intensity does. The ratio of turbulent kinetic energy (TKE) at the Z and G heights simaulated by BOLAM indicates that

the TKE is always lower of at least one order of magnitude at the upper level, i.e. the simulated boundary layer depth can be argued to be lower than 500 m.

The backward trajectories ending at 1500 m and 500 m over the surface at the observation site are shown in Fig. 4, together with the wind fields at three time instants, representative of the whole period of trajectory simulation of the case-study, that starts at 0 UTC of 20/04/2013 and finishes at 23 UTC of 21/04/2013. In the maps of the trajectories at 1500 m level the wind field at 850 hPa is presented, while the maps of trajectories at 500 m level show the wind field at 950 hPa. Light brown symbols show the wind 12 hours before beginning of case-study day (12 UTC 20/04/2013), violet symbols show the wind at the beginning of the case-study day (0 UTC 21/04/2013), and dark green symbols show the wind in the middle of case-study day (12 UTC 21/04/2013).

The trajectories at the two levels are in broad agreement; they are suddenly changing direction of provenience from South-West to South-East and the particle velocities are increasing due to the change of synoptical scale air flows. Minor displacements on the vertical direction occurs, so the corresponding plots are not presented here.

CONCLUSIONS

Although different local conditions occurr during the examined periods (in terms of surface turbulent fluxes), the vertical distribution of the aerosol shows minor changes. Moreover, the number concentration ratios appear to be weakly dependent on the surface stability.

The case study support the same conclusion, i.e. that in spite of the fact that the estimated depth of the PBL (from BOLAM simulations) is less than the height of station Z, and that surface fluxes change during the day, the aerosol behaviour is quite similar in the two observing stations.

Thus, the large scale transport results to be the dominant factor in determining the concentration and size of the aerosol in the entire layer examined here, of depth of about 500 m, while the vertical distribution turns out to be only weakly affected by the local heat and momentum fluxes measured near the ground.

ACKNOWLEDGEMENTS

The present study was developed as a part of the Climate Change Tower Integrated Project (CCT-IP), and with the support of the Italian Ministero Affari Esteri (MAE) by a research project within the Executive Programme of Scientific and Technological Cooperation between the Italian Republic and the Republic of Korea. The authors gratefully acknowledge the colleagues Kjetil Törseth and Mona Johnsrud of the Norwegian Institute for Air Research (NILU), for supplying the wind data recorded at the Zeppelin station, and the DTA (Dipartimento Scienze del Sistema Terra e Tecnologie per l'Ambiente) of the Italian National Research Council (CNR) for the logistic help.

REFERENCES

Buzzi, A., M. D'Isidoro, and S. Davolio, 2003: A case-study of an orographic cyclone South of the Alps during the MAP SOP. *Q. J. Roy. Meteor. Soc.*, **129**, 1795–1818.

Drofa, O. and P. Malguzzi, 2004: Parameterisation of microphysical processes in a non-hydrostatic prediction model, *Proc. - 14th Intern. Conf. on Clouds and Precipitation (ICCP). Bologna, 19-23 July 2004.*

Hogrefe, O., G. G. Lala, B. P. Frank, J. J. Schwab, and K. L. Demerjian, 2006: Field evaluation of a TSI 3034 Scanning Mobility Particle Sizer in New York City: Winter 2004 intensive campaign. *Aerosol Sci. Technol.*, **40**, 753–762.

Krishna Moorthy, K., V. Sreekanth, J. Prakash Chaubey, G. M. M., S. S. Babu, S. Kumar Kompalli, S. P. Bagare, B. C. Bhatt, V. K. Gaur, and N. S. Singh, 2011: Fine and ultrafine particles at near free-tropospheric environment over the high altitude station Hanle, in Trans-Himalayas: new particle formation and size distribution. *Journal of Geophysical Research*, **116**, D20212.

Morcrette, J. J., 1991: Radiation and cloud radiative properties in the ecmwf operational weather forecast model. *J. Geophys. Res.*, **96D**, 9121–9132.

Ritter, B. and J. F. Geleyn, 1992: A comprehensive radiation scheme for numerical weather prediction models with potential applications in climate simulations. *Monthly Weather Review*, **120**, 303–325.

Stohl, A., C. Forster, A. Frank, P. Seibert, and G. Wotawa, 2005: Technical note: The Lagrangian particle dispersion model FLEXPART version 6.2. *Atmos. Chem. Phys. Discuss.*, **5**, 2461–2474.

Tunved, P., J. Strom, and R. Krejci, 2013: Arctic aerosol life cycle: linking aerosol size distributions observed between 2000 and 2010 with air mass transport and precipitation at Zeppelin station, Ny-Alesund, Svalbard. *Atmospheric Chemistry and Physics*, **13**, 3643–3660.

Zampieri, M., P. Malguzzi, and A. Buzzi, 2005: Sensitivity of quantitative precipitation forecasts to boundary layer parameterization: a flash flood case study in the western mediterranean. *Natural Hazards Earth System Science*, **5**, 603–612.

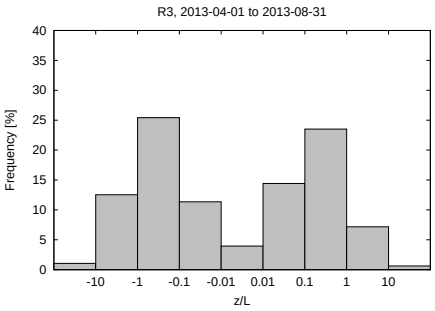

Figure 1: z/L measured in the surface layer, from April to August 2013.

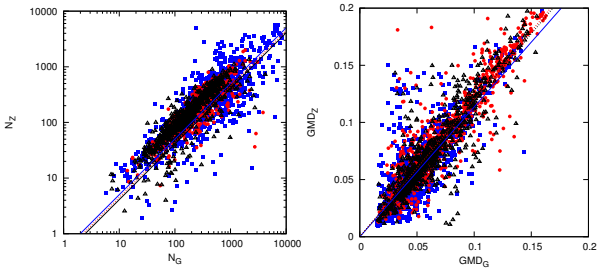

Figure 2: Scatterplots of the number concentration and of the Geometric Mean Diameter measured in the two stations, for the entire period April to August 2013, separating stable, almost neutral and unstable cases.

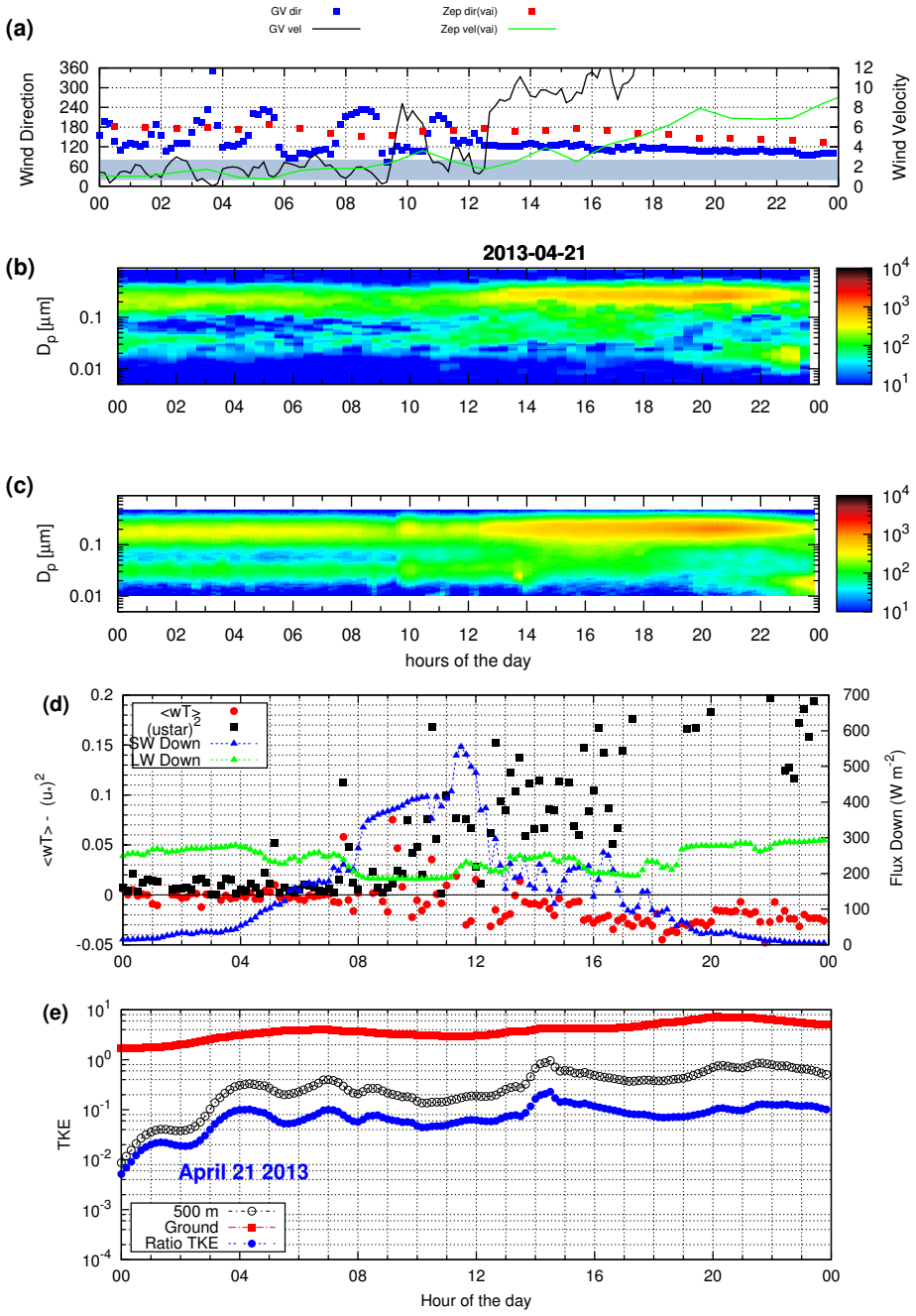

Figure 3: Case study 21 April 2013. The time series are reported for: (a) wind speed and direction measured at CCT (close to G: black line and blue symbols), and at Z (green line and red symbols). The gray area indicates directions from the village of NyÅlesund, between 20 and 80 degrees, presumably a human-contaminated sector; (b) Aerosol Size Distribution (ASD) recorded at Z: in ordinate, the particle diameter D_j, the color scale corresponds to the number concentration N_j; (c) same ASD at G; (d) shortwave and longwave downwelling fluxes (respectively blue and green symbols) measured at CCT, heat flux (red symbols) and momentum flux (black symbols); (e) TKE evaluated at the surface (black symbols) and at 500 m a.s.l. (red symbols), together with their ratio (blue symbols), from BOLAM simulations.

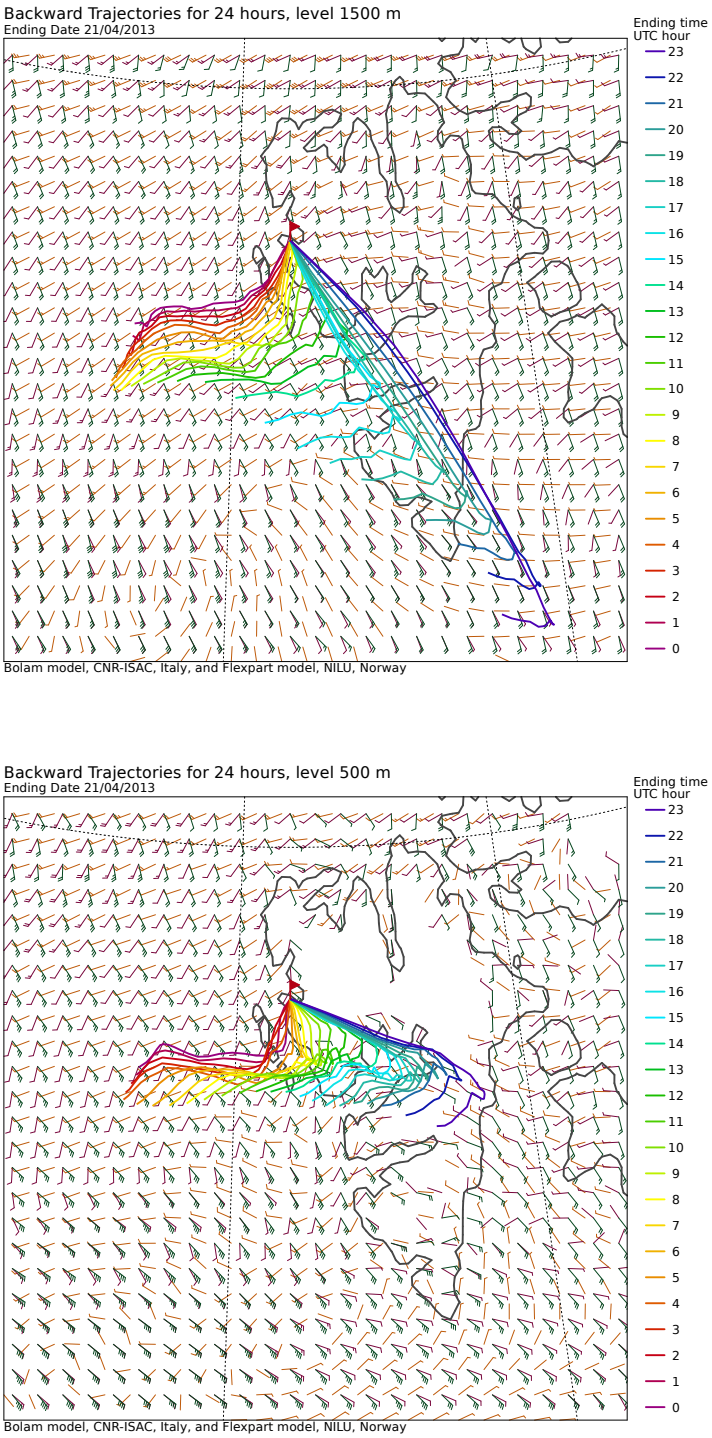

Figure 4: Case study 21 April 2013. Backward trajectories at 1500 m (upper panel) and 500 m (lower panel) levels at 12 UTC 20/04/2013 (light brown symbols), at 0 UTC 21/04/2013 (violet symbols), at 12 UTC 21/04/201 (dark green symbols).

FROZEN TECHNOGENIC GROUND IN THE NAZAROVO COAL PIT DUMP, THE SOUTHERN PART OF THE WESTERN SIBERIA

D.S. DROZDOV and S.A. LAUKHIN

Earth Cryosphere Institute SB RAS (ECI SB RAS), Tyumen, Russia

Russian State Geological prospecting University (MGRI-RSGPU), Moscow, Russia

Tyumen State Oil and Gas University, Tyumen, Russia

Keywords: FROZEN C GROUND, TECHNOGENIC PERMAFROST, CRYOLITHOZONE, MINING, THICK EMBANKMENT, CRYOGENIC PROCESSES PERMAFROST DEGRADATION.

INTRODUCTION, THE KEY-SITE LOCATION

The Nazarovo coal pit is situated in the South-Eastern part of the West Siberian Plain (56°02' N, 90°30' E) near the city of Krasnoyarsk (figure 1). In is almost 500 km southward of the contemporary boundary of the island permafrost, which doesn't occur further than 60° N (Vasilchuck, 2013). In spite of this the technogenic permafrost has been found at various depth intervals and in the embankments of various age approximately in 10% of engineering-geological boreholes drilled in the dumps of Nazarovo coal pit (the ground had been moved by railroad (figure 2) or by digger).

Figure 1. The key-site location (white square)

At the most part of Nazarovo depression the mean annual air temperatures are about 0°C and the ground temperatures on a depth of zero amplitude in the natural conditions are some +2…+3.5°C. Thereafter, there are no conditions for the permafrost conservation in the dumps, so its complete degradation can be expected. Thus the technogenic perennially frozen ground of this region are of interest mostly from the viewpoint of their behavior during the thawing as a factor contributing to the ground bearing capacity retrogression, the development of ground subsidence process and the destruction of the recultivated landscape (Drozdov, 2005).

THE MAIN FACTORS OF THE TECHNOGENIC PERMAFROST DEGRADATION

The main type of the technogenic permafrost degradation in Nazarovo coal pit is its thawing. The duration of the thawing process is affected by:

- The thickness of ground overlying the frozen deposits; the larger the thickness – the longer the thawing process.
- The composition and the water content of the technogenic permafrost; the more disperse is the ground and the higher is its water content – the less is the rate of permafrost degradation.
- The composition and the water content of the embankment overlying the technogenic permafrost; the more ripped and drained is the embankment – the less is the rate of permafrost degradation.
- The thickness and temperature of permafrost; the larger the thickness and the lower the temperature – the slower the thawing.
- The complex of the external conditions – the mean annual air temperatures, the amount of precipitation in the frost-free season, the presence of the vegetable cover and the thickness of the snow cover well correlated with the heat flux into the ground (Nifontov *et al.*, 1973; Kudryavtsev, 1979).

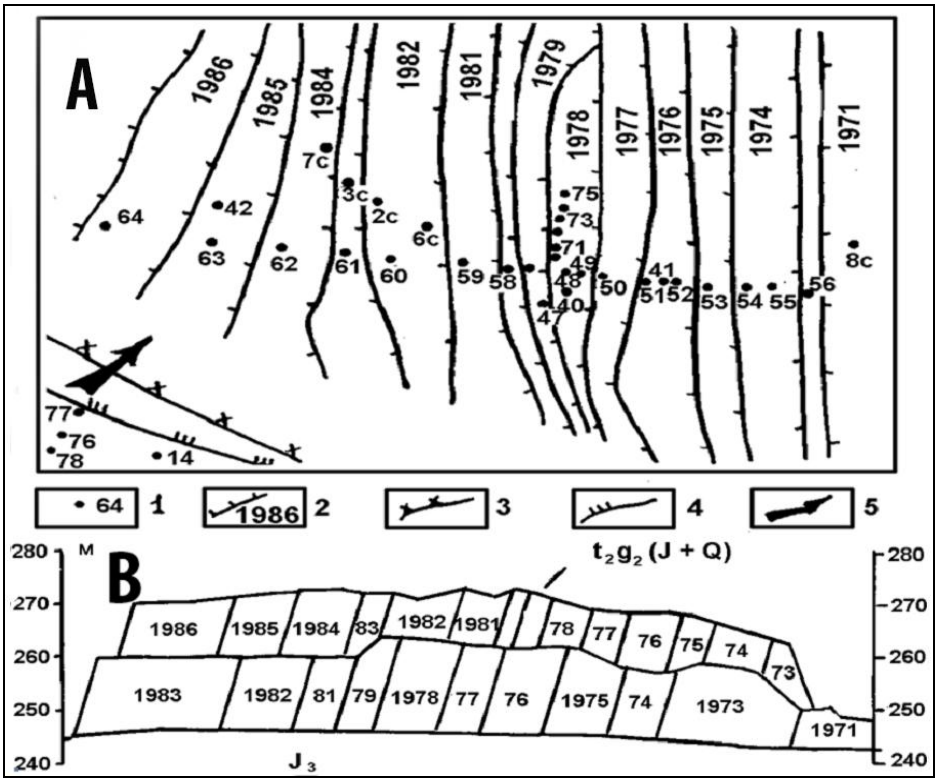

Figure 2. Diagram of the formation of dumps of the Nazarovo coal pit: A – layout of the upper layer of dumps and the borehole distribution; B – dump's section lengthwise the profile of engineering-geological boreholes 1 – number of borehole; 2 – dump bench and the year of embankment; 3 – coal pit edge; 4 – overburden edge; 5 – overall direction of the overburden transportation to the ground. Notes: the boreholes were tested in 1984-1986.

TWO TYPES OF THE TECHNOGENIC PERMAFROST IN THE NAZAROVO DUMP

THE NON-ICE-RICH PERMAFROST

Two types of frozen strata of various origin and structure have been found in the dumps during the operation of a coal deposit. The first type is usually characterized by the thickness of 10 m and more; the top of permafrost occurs at the depth 4-7 m, sometimes – 10-12 m; the temperature throughout the whole frozen layer is -0.1…-0.3°C. The cryostructure of rocks is massive, the water content W≅0.23, the soil skeleton density $\rho_d^2 \cong 1.6$ gr/cm^3. This frozen ground does not differ from the unfrozen ones by the habitus, water content and density. The formation of the frozen ground of this type had taken place in the process of the piling due to the digging up of the seasonally frozen soil and moving it to new position during the winter-spring period (boreholes 63 and 64, figure 3).

Sometimes it could be buried the seasonal permafrost of the lower-level embankment while upper-level one is piled onto it. Usually this happens the so-called railroad dumps (borehole 62, fig. 3).

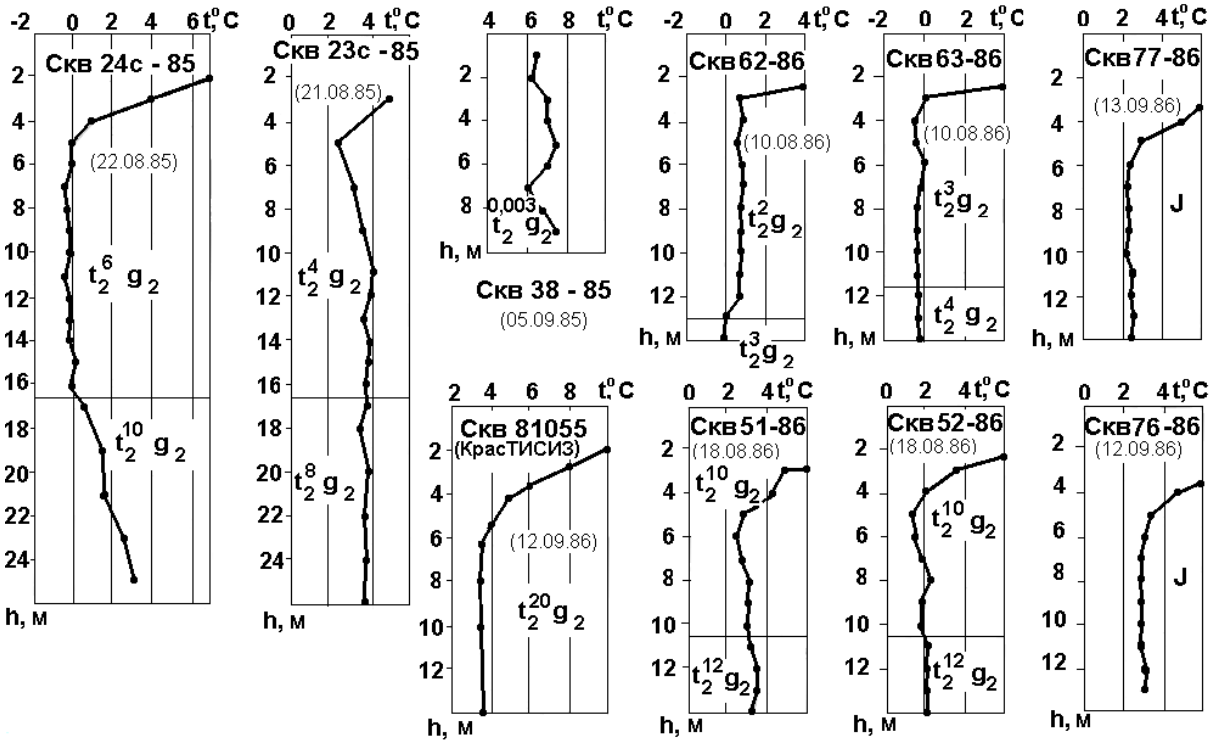

Figure 3. Typical diagram of ground temperature in the engineering-geological boreholes on the dumps of Nazarovo coal pit: $C_{KB}51\text{-}86$ – borehole number and year of drilling; $t_2^X g_2$ – technogenic geosystem index where ^{X} – age of dump at the moment of testing, years

The serious surface deformations do not occur during the thawing of permafrost of this type except the insignificant thermosubsidences provoking by the reduction in mechanical strength of rocks and their consolidation. Such a subsidence per se does not cause much damage but the formed depressions can turn to become the places of accumulation of the atmospheric waters and the development of the concomitant processes. Due to the relatively deep occurrence and the considerable thickness of the permafrost the thawing process can be prolonged and will be activated only in the case of heat transfer by the ground waters. Thus, in

order to compensate the thermosubsidence the winter dumps ought to be made beforehand somewhat higher than the spring-summer-autumn ones (Drozdov and Spiridonov, 1988).

THE ICE-RICH PERMAFROST

The second type of the technogenic frozen strata is characterized by the lesser thickness (usually the first meters), the small depth of occurrence (the first meters as well), the higher ice content (Wc=0.4) and the presence of ice lenses with the thickness up to 1 m. The permafrost degrades actively due to the small thickness and depth of occurrence. The high ice content ensures the essential subsidence. As a result 0.5-3.5 m depressions appear. Their "thermokarst" origin is verified by the borehole's drilling. The ice, the frozen soil and the thawed cavities have been met in the bottom of "thermokarst" depressions and nearby them. The forms of subsidence in plan are the most diverse.

The presence of the ice of various structure testifies that the permafrost of this type occurs as a result of filling-up of the vast holes during the grading in the winter time when the "burial" of the large frozen pools or snow accumulations takes place. Herewith, the underlayed and the overlayed ground and soils (if they have not still frozen) freeze as well due to their contact with ice. The volume of freezing depends on the ground temperature, temperatures of ice and snow at the moment of filling-up, on the lithological composition and water content of rocks, on the thickness of embankment.

SPATIAL DISTRIBUTION OF HAZARDOUS FROZEN PATCHES

The maximal number of subsidences has been observed on the levelled excavation dumps where the conditions favorable for snow and water accumulation had been created among the waste heaps. Thus, the surface of the excavation dumps levelled at the early 1980ies is the alternation of the flat elevations on the place of the topped-off waste heaps (the permafrost of the first type is observed) and the low areas (up to 0,5-1,5 m) – the depressions previously filled up with the ground from the tops of waste heaps. On the whole, in this case the surface settling is the result of the displacement of the redeposit ground mass. The most depressed areas are the result of subsidence upon the ice-rich permafrost.

The most contrast manifestations of the thermosubsidence have been observed on the inner railroad dumps made in a low-thick layer over the deposits of the previously leveled excavation blades. There the thawing of permafrost of the second type with the formation of the crater-gap occurs. The mechanism of formation of the craters – subsidence – seems to be the following: the gradual thawing of the permafrost accompanied by the decreasing of its volume and the ice lens melting. At that, the water migration from the zone of greater water content (in the place of permafrost occurrence) to the zone of lesser water content (partially due to the gravitational forces, partially due to the capillary forces) takes place resulting in the further decreasing of the rock volume due to the infiltration consolidation. In the process of ice melting and permafrost thawing the overlaying rocks are subsiding occupying the vacant space and compacting the underlaying ground been previously in the frozen state. On the dump surface the depression in micro relief forms where the atmospheric moisture begins to accumulate. Percolating through the ground, the moisture stimulates the process of permafrost degradation and the formation of relief depression. On the edges of depression above the ice (snow) lens the cracks appear in rocks. During the whole ice melting and the permafrost degradation the surface settlement is determined by the rate of filtration consolidation. If the entry of moisture into the crater is more than or equal to the filtration discharge, then the consolidation will be slow. In case of moisture deficit, the crater will be dry for the most time and the rocks under it will not be water-saturated, though their water content will be higher than the water content in the surrounding massive and the consolidation could be more rapid.

While the engineering-geological mapping with the allocation of different types of the technogenic sediments (Afonin et al. 1990; Goral'chuck et al. 1991; Drozdov 1992) the observed damage of the dumps of Nazarovo pit by the permafrost degradation initiating "thermokarst" and the subsequent surface settlement has been assessed up less than 5% of total area. At that the potential damage can be assessed by the results of drilling as 10% of the dump's square. Some revealed regularities permit contouring the potentially hazardous areas. Thus the prisms of the railroad dumps (figure 4) potentially contain the technogenic permafrost in the segments filled-up in the winter-spring time (December-March). The thermokarst hazard is real for each prism in the zone equal approximately to one thirds of its width.

CONCLUSIONS

The technogenic permafrost forms at mines and pits while extracting mineral resources and redepositing of the large masses of overburdens during winter-spring period. In those regions where the background ground temperatures on the depth of zero seasonal amplitude insignificantly exceed the 0°C (+2…+3.5°C) the degradation of permafrost goes on during the first ten years retarding the reclamation of the territories and leading to the deformation of the recultivated surfaces. About 10 % of the dump's area can be damaged by the processes dependent on the permafrost degradation. They are concentrated in the dumps filled-up or leveled in the winter-spring time. Thus the probability of thermokarst here is up to 30 %.

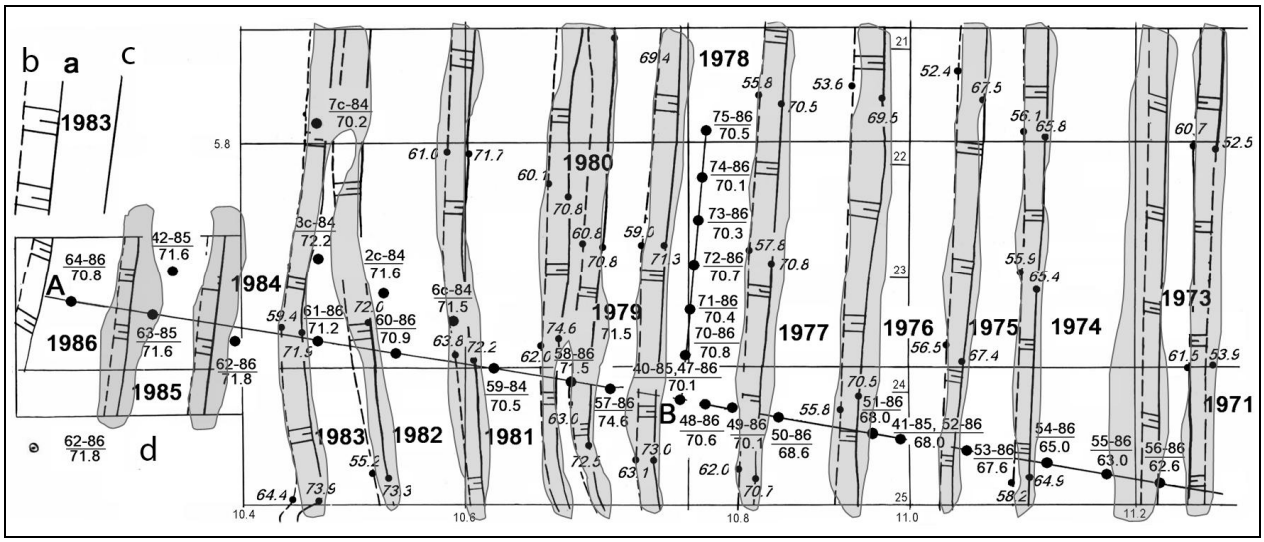

Figure 4. Layout of the railroad dumps of Nazarovo coal pit and the zone of technogenic permafrost distribution in the upper layer of the dump (grey color): dump bench along: a – edge, b – base; c – year of embankment; d – engineering-geological borehole (numerator – number and year of drilling, denominator – mark of the mouth); italic numbers – marks of the surface.

The technogenic permafrost in the capacity of geosystems of technogenic dumps occurs in two essential forms: 1) the frozen ground slightly varying from the unfrozen one by water content and density, 2) the ice and the ground ice formed during the burial of frozen pools, ponds and snowbanks. In the first case the degradation of the technogenic permafrost results in the insignificant thermosubsidence replacing afterwards by the processes of the noncryogenic compaction of the ground. In the second case the thermokarst takes on the large-scale, sometimes disastrous forms with the full destruction of the surface and the reclamation fullfiled in the standard time.

The particular problem of the reclamation damage is the total watering and the decreasing of the strength properties of the dump's massive during the restoration of the ground water level at the displacement of the working zone of the pit and the crater of depression away from the pit drainage.

ACKNOWLEDGEMENTS

The research is supported by the Fundamental Programs VIII.75.1 and VIII.72.2; Integration Projects SB RAS-FEB RAS №9 and SB RAS №144, ONZ RAS № 12; Government Work for Board of Education and Science № 9093 and № 1082; RF President Grants NSH-5582.2012.5; RFBR-RGO-13-05-41509 RGO, RFBR 13-05-00811, 13-08-91001-ANF-a; International Programs TSP, LCLUC, CALM, SWIPA; VSEGINGEO Institute.

REFERENCES

Afonin, A.P., Dudler, E.V., Ziangirov, R.S., Lychko, Yu.M., Spiridonov, D.V. and Drozdov, D.S. (1990). Classification of the technogenic ground. *Engineering geology* **1**: 115-121.

Drozdov, D.S. and Spiridonov, D.V. (1987). Mapping of the geological bodies formed as a result of technogenesis, in *Methods of hydrogeological and engineering-geological mapping* (VSEGINGEO, Moscow), 125-136

Drozdov, D.S. (1992). Allocation of the technogenic geological bodies during the engineering-geological mapping and geoecological researches, in, *Geoecological researches during the engineering-geological surveys* (VSEGINGEO Moscow) 28-35.

Drozdov, D.S. (2005). Generation and degradation of technogenic frozen ground outside the permafrost zone (Southern Siberia, Nazarovo coal-field). In, *Priorities in the Earth Cryosphere Research*. (Pushchino, Russia) 256-257.

Drozdov, D.S. and Spiridonov, D.V. (1988). Regime engineering-geological observations during the complex hydro-geological and engineering-geological mapping in the areas of the intense technogenesis, in, *Investigation of the regime of exogenous geological processes in the areas of intensive economic development*. (VSEGINGEO, Moscow), 80-84.

Goral'chuk, M.E., Drozdov, D.S. and Spiridonov, D.V. (1991). Methods of research and mapping of the technogenic changes in the rock properties during the engineering-geological researches, in, *Engineering-geological and geocryological researches in geoecology*. (VSEGINGEO, Moscow), 136-146.

Kudryavtsev, V.A. (ed.) (1979). *Total General geocryology*. (Moscow State University, Moscow) 464.

Nifontov, F.P., Rogov, N.S. and Pulyaev, V.N. (1973). Engineering-geological conditions of the building of the large pits in Siberia. In, *Tomsk State university*. (Tomsk State university, Tomsk) 72-77.

Vasil'chuk, Yu.K. (2013). Modern southern limit of permafrost in Western Siberia Lowland. *Earth's Cryosphere*. **XVII(I)**:17-27.

ICE NUCLEATION PROPERTIES OF PARTICLES FROM NORTHERN EURASIA

J. DUPLISSY[1], Q. NGUYEN[2], E.S. THOMSON[3], V. HEMMILÄ[4], M. KULMALA[4], T. PETÄJÄ[4], M. SIPILÄ[4], M. BILDE[2] AND E. SWIETLICKI[5]

[1]Helsinki Institute of Physics, University of Helsinki, 00014, Helsinki, Finland

[2]Department of Chemistry and iNANO, Aarhus University, 8000 Aarhus, Denmark

[3]Department of Chemistry and Molecular Biology, Atmospheric Science, University of Gothenburg, 41296, Gothenburg, Sweden

[4]Department of Physics, University of Helsinki, 00014 Helsinki, Finland

[5]Department of Physics, Lund University, Box 118, 222 11 Lund, Sweden

Keywords: Ice Nuclei Chamber, PINC, ZINC, ice nuclei, CRAICC

INTRODUCTION

The importance of ice crystals in clouds for our climate is manifold: Their presence, number and shape influences the optical properties of clouds, the formation of precipitation and their lifetime. All of these aspects have an impact on the radiation balance and therefore on climate. Within the CRAICC project (Cryosphere-atmosphere interactions in a changing Arctic climate) we aim to investigate the ice nuclei properties of aerosols present in the arctic region, covered by the PEEX project, by continuous measurements at different Nordic field stations.

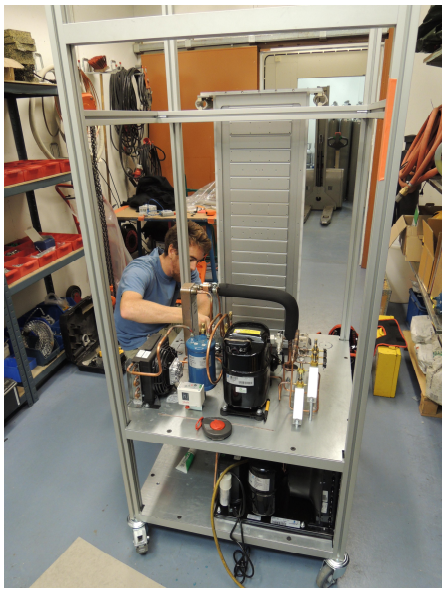

Figure 1.Installation of the 1 m long ice nucleation chamber close to the refrigeration unit.

METHODS

Two new ice nucleation chambers are currently built based on the concept of the laboratory instrument ZINC (Zurich Ice Nucleation Chamber) and PINC (Portable Ice Nucleation Chamber), both being developed at ETHZ, Switzerland. The field instrument PINC has already successfully participated in a

couple of laboratory campaigns (Chou et al, 2013; Kanji et al, 2013; Wex et al, 2014; Hiranuma et al, 2014) as well in field campaign (Chou et al, 2011). Our improved PINC has two portable refrigerant compressors to directly cool the walls of the chamber without the use of an intermediate cooling liquid. In this configuration, the instrument is able to measure ambient ice nuclei (IN) concentrations at conditions as cold as -40°C and relative humidities exceeding water saturation. Our improved PINC has a longer ice nucleation chamber (1 meter) similar to the ZINC.

CONCLUSIONS

A successful collaboration between ETHZ and the CRAICC partners has led to technology transfer for the manufacture of the two Ice Nucleation Chambers. An inter-comparison prior to their first campaign is scheduled in spring 2015. The status of the ice chambers, their operational field modes as well as their improvement will be presented during this meeting.

ACKNOWLEDGEMENTS

This work was supported by CRAICC, the Finnish Center of Excellence and the Swedish Research Councils

REFERENCES

Chou et al. (2011), *Atmos. Chem. Phys*., 11, 725-4738
Chou et al. (2013), *Atmos. Chem. Phys*., 13,761-772
Hiranuma et al. (2014), *Atmos. Chem. Phys*. Disc., 14, 22045–22116
Kanji et al. (2013), *Atmos. Chem. Phys*., 13, 9097-9118
Wex et al. (2014), *Atmos. Chem. Phys. Disc*., 14, 22321–22384

CHAMBER MEASUREMENTS AND MATHEMATICAL MODELLING OF CO_2 EXCHANGE OF A MESO-OLIGOTROPHIC FEN AT WEST SIBERIA

E.A. DYUKAREV

Institute of monitoring of climatic and ecological system SB RAS, Akademicheskii 10/3, Tomsk, Russia

Keywords: Peatlands, carbon balance, carbon dioxide fluxes, mathematical modelling, West Siberia.

INTRODUCTION

West Siberia peatlands are important components of the terrestrial carbon cycle and store about70 Pg of carbon in peat soil (Sheng 2004). Although the size of the carbon reservoir is considerable, the role of peatlands in the global carbon budget is not studied\investigated deep enough.

The carbon budget of a peatland ecosystem is the net result of the balance of net primary production (NPP) by photosynthetic fixation of CO_2, total ecosystem respiration (ER) by autotrophic and heterotrophic CO_2 emission from soil, together with methane emission by microbiologic peat decomposition and export of dissolved organic matter by runoff. Numbers of environmental factors play important roles in governing the rate of net CO_2 exchange in peatlands and expected climate change can affect these regulating factors (Bubier et al., 2003, Golovatskaya 2009).

The present climate warming in the Northern hemisphere (IPCC 2013; Ippolitov et al. 2014) can increase ecosystem carbon uptake by reducing cold-temperature constrains on plant carbon assimilation and growth (Hudson et al, 2011). Soil warming accelerates carbon losses due to exponential effect of temperature on soil respiration. Possible changes in temperature and humidity may alter the peatland carbon budget significantly. Determination of carbon exchange rates between peatlands and the atmosphere, as well as the ecological and climatic controls on this exchange under existing climatic changes are important scientific objectives.

The purpose of this study was to develop a mathematical model for estimation of CO_2 exchange fluxes of a meso-oligotrophic fen at West Siberia, to calibrate the model using field observations data on CO_2 fluxes obtained using automatic transparent chamber and infra-red gas analyzer.

MATERIALS AND METHODS

The measurement site is located in the south of West Siberia (Russia) at small oligotrophic bog “Timiryazevskoe”(56°26'N 84°50'E) near the Tomsk city. The bog area is about 14,5 ha, maximal peat depth – 8 m, average peat depth – 2,7 m, total peat storages – 421 300 m^3. 70% of the bog area occupied by pine-shrub-sphagnum community with stunted pine trees, about 25% - by meso-oligotrophic sedge-sphagnum fen. Discontinuous moss cover of *Sphagnum fuscum, Sph. angustifolium, Sph. magellanicum* composes vegetation of the fen. Herbs and sedges cover about 50% of the area and represented by *Eriophorum vaginatum, Carex rostrata, Carex limosa, Scheuchzeria palustris* species.

An automated soil CO_2 flux system LI‑8100A (Li-Cor Biogeoscience, USA) with transparent long-term chamber LI-8100-104 has been used for carbon dioxide emission measurements from May to September 2014. Measurements were conducted two times in a month during daytime only. Intense field campaigns were held in August 15-17 and August 21-25 for a round day observation of CO2 fluxes.

The chamber was installed at plastic cylindrical basement deepened to the peat to 15 cm. The vegetation cover under the chamber consists of mosses only. Carbon dioxide fluxes was estimated by the rise of CO_2 concentration in the chamber. Exposition time for CO_2 accumulation within the chamber was 5 minutes,

but only two first minutes were used for total flux calculation. Measurements were automatically repeated each 20 minutes. Simultaneous observations of air, surface and peat temperatures, incoming photosynthetically active solar radiation, air pressure, air water content, water table level and precipitation were made.

RESULTS

The vegetation cover under the chamber consists of mosses only. The net CO_2 exchange of terrestrial ecosystems (NEE) is determined by the difference between C uptake due to photosynthesis (Ph) and C loss due to ecosystem respiration (ER). Total ER consist of soil (R) and plants respiration (H). NEE is defined negative when the absolute value of Ph exceeds the absolute value of ER and there is a net removal of carbon dioxide from the atmosphere. NEE is defined positive when the absolute value of ER exceeds the absolute value of Ph and carbon dioxide is released to the atmosphere. Measured CO_2 fluxes have clear diurnal variations with maximum at night time and minimum at day time (Fig.1 see NEE_obs).

Observed day-time NEE fluxes usually negative and reach -0.45 μmol m^{-2} s^{-1} (at 09:00 23.08.2014). Photosynthesis rate registered by chamber method is reduced by about 30% due to shading mosses by the chamber during the employment of the chamber. Maximal nigh-time fluxes (ER) were registered at 00:40 24.08.2014 (2.8 μmol m^{-2} s^{-1}). Diurnal amplitude of net CO_2 flux is about 2.1 μmol m^{-2} s^{-1} is attributed to daytime photosynthetic assimilation of CO_2 by mosses.

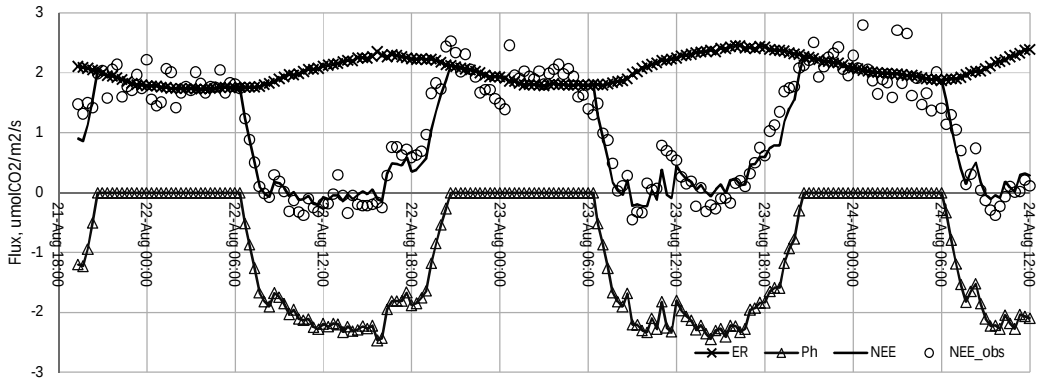

Figure 1. Observed NEE flux (NEE_obs) and modeled ecosystem respiration (ER), photosynthesis rate (Ph), net ecosystem exchange (NEE) fluxes in August 2014.

MODELLING

For modelling of CO_2 fluxes, model based on photosynthetically active radiation (PAR in μmol m^{-2} s^{-1}), surface temperature (T in °C), were used. NEE was empirically modelled using the following forms:

$$NEE = ER - Ph; \qquad ER = R + H = R_0 \cdot \exp(k_R \cdot T); \qquad Ph = \alpha \cdot PAR \cdot P_{max} / (\alpha \cdot PAR + P_{max})$$

NEE – net ecosystem exchange, ER – total ecosystem respiration, R – soil respiration, H – plant dark respiration, Ph – assimilation of CO_2 during photosynthesis. The respiration model is based on an Arrenius-type exponential relation between total ecosystem and surface temperature (T), where R_0 is defined as the ecosystem respiration at reference temperature, k_R is the sensitivity coefficient.

Photosynthesis was depended on incoming PAR using the well know hyperbolic form, where $\cdot P_{max}$ is the maximal CO_2 fixation rate at unlimited PAR, $\alpha\cdot$- the apparent quantum yield, interpreted as the ecosystem light use efficiency. Coefficients for Ph model were determined from daytime period (PAR > 15 μmol m^{-2} s^{-1}) data only, coefficients for the ER were determined for the round day data.

Empirical coefficients of the model was estimated using above described observations of CO_2 fluxes and meteorological parameters using the MATLABT software package. We have found the following values of the coefficients: $R_0 = 1.281$ μmol m^{-2} s^{-1} ; $k_R = 0.027$ T^{-1} ; $\alpha = 0.0222$ μmol^{-1} m^2 s ; $P_{max} = 2.668$ μmol m^{-2} s^{-1}.

There is good agreement between the model output and the observations in day time but not so good during night period (Fig. 1). Observed night time variations of soil respiration is much more than modeled ones. It is known (Koskinene et al., 2014) that chamber method overestimated carbon dioxide respiration flux during calm summer the nights when a CO_2 concentration gradient from soil/moss system to atmosphere builds up. Soil respiration model should be improved by taking into account gas diffusion process within soil and the soil-moss CO_2 gradient.

Daily variation of ecosystem respiration is about 0.7 μmol m^{-2} s^{-1} with maximum rate values at 17:00 and minimum at 6:00. Maximal daytime assimilation of CO_2 due to photosynthesis occurs around the 16:00 and its rate is about 2.5 μmol m^{-2} s^{-1}. Using the suggested model, we were able to separate estimations for of soil/plant respiration and photosynthesis rate.

The annual growing cycle of vegetation activity is strongly related to radiation and temperature variations. Basing on this scheme, we calculate ER, Ph values for period with positive air temperatures (form 15 May till 15 September 2014). The maximal photosynthesis rate were regulated using second order dependence with air temperature to take into account efficiency of light utilization depression at temperatures displaced from the plant growing optimum.

Calculations of the ER, Ph and NEE for warm period of 2014 was made using estimations for model empirical coefficients obtained for observation data from May to September. Carbon assimilation by mosses observes during whole summer, but in May and September assimilation fluxes reduces significantly. The ecosystem respiration generally followed seasonal course similar to its obvious driving temperature.

Daily averaged carbon fluxes (Fig. 2) at the studied ecosystem usually positive, i.e. carbon is removing from the peatland to the atmosphere. The sum of the ER is 544 gCm^{-2}, the total photosynthetic assimilation for the warm period is 176.9 gCm^{-2}, that result in 77.1 gCm^{-2} for NEE value. Here we did not take into account sedges, occupying about 50% of the fen area. Accumulation of carbon in sedges will shift the total carbon balance to negative values (Golovatskaya, 2009).

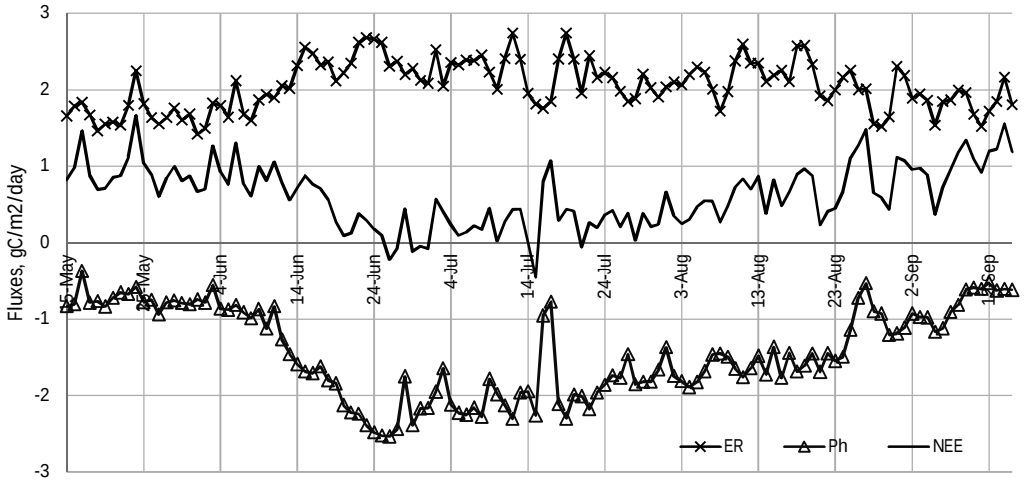

Figure 2. Modeled daily rates of CO_2 exchange during warm period 2014. Ecosystem respiration (ER), photosynthesis rate (Ph), gross primary production (GPP) and net ecosystem exchange (NEE).

CONCLUSIONS

Using the suggested model calibrated by field chamber measurements, we were able to separate estimations for the ecosystem respiration and photosynthesis rate, and calculate total summer time net ecosystem exchange for meso-oligotrophic fen.

REFERENCES

Bubier J.L., Crill P.M., Mosedale A., Frolking S., Linder E. (2003) Peatland responses to varying interannual moisture conditions as measured by automatic CO_2 chambers. *Global Biogeochem Cycles* **17**(2), 1066.

Golovatskaya E.A., Dyukarev E.A. (2009). Carbon budget of oligotrophic bog in southern taiga in Western Siberia. *Plant and Soil* **315**, 19-34.

Hudson J.M.G., Henry G.H.R., Cornwell W.K. (2011) Taller and larger: shifts in Arctic tundra leaf traits after 16 years of experimental warming. *Glob Chang Biol*. **17**, 1013–1021.

IPCC, 2013: Climate Chang 2013: *The Physical Science Basis. Contribution of Working Group I to the Fifth Assessment Report of the Intergovernmental Panel on Climate Change* [Stocker, T.F., D/ Qin, G.-K. Plattner, M.Tignor, S.K. Allen, J. Boschung, A.Nauels, Y. Xia, V. Bex and P.M. Midgley (eds.)], (Cambridge University Press, Cambridge, United Kingdom and New York, NY, USA), 1535 p.

Koskinen M., Minkkinen K., Ojanen P., Kamarainen M., Laurila T., Lohila A. (2014) Measurements of CO_2 exchange with an automated chamber system throughout the year: challenges in measuring night-time respiration on porous peat soil. *Biogeosciences*. **11**, 347–363.

Loginov S.V., Ippolitov I.I. Kharyutkina E.V. (2014). The relationship of surface air temperature, heat balance at the surface, and radiative balance at the top of atmosphere over the Asian territory of Russia using reanalysis and remote-sensing data. *Int. J. of Remote Sensing* **35**(15), 5878-5898.

Sheng Y., Smith L.C., MacDonald G.M., Kremenetski K.V., Frey K.E., Velichko A.A., Lee M., Beilman D.W., Dubinin P. (2004) A high–resolution GIS–based inventory of the west Siberian peat carbon pool. *Global Biogeochem Cycles,* **18**, GB3004.

UNDERSTANDING AND FORECASTING WEST AFRICA OCEAN DYNAMICS: COMMUNICATING FORECAST UNCERTAINTY AND LESSONS LEARNED

O.A. EDIANG[1] and A.A. EDIANG[2]

[1]Marine Division, Nigerian Meteorological Agency, PMB1215 OSHODI Lagos, Nigeria
Email: ediang2000@yahoo.com

[2]The Nigerian Maritime Administration and Safety Agency, 6 Burmal Road, Apapa, Lagos,Nigeria.
Email: ediang2005@yahoo.com

Keywords: MARINE ENVIRONMENT, NIGERIA AND GHANA, COASTAL DEGRADATION, DATA ANALYSIS, OCEAN DYNAMICS.

This paper examines the chain of interactions between climate change, forecasting and Ocean Dynamics in West Africa. The paper relies mainly on secondary data generated by individuals, government and non-governmental bodies. From these sources, the paper reveals that climate change results in Nigeria and Ghana is having a very real impact and needs urgent attention. Extreme weather as a manifestation of climate change is increasingly problematic for the people along the coastline of West Africa Countries. *The complex coastal surfaceand deep Ocean of Nigeria and Ghana plays a great role in the formation and modification as well as distribution of weather in both countries.*

For this study, the aim of this investigations to get a better understanding of improving marine and ocean data and products for science and society and how it is related to the probable changes of water levels during Ocean storm surges along the West Africa coast, taken Nigeria and Ghana as a case study, depending on parameters that might change in a future climate. The results will help to identify vulnerabilities of e.g the shore protection along the Nigerian and Ghana coasts and give us a chance to work on adaptation and risk mitigation necessitated under possible climate change.

Some evidences of climate change in the Nigerian and Ghana coast have been observed in communities, institutions and individual have suffered various degrees of devastation from coastal flooding where at least 20% of the population is at risk of coastal flooding which give rise to displacement of people and damage to lives and properties more then any other disaster (Adewale, 2012, Boateng, 2006; IPCC, 2007; Armah, A.K., Amlalo, D.S., 1998, Appeaning et al.,2008,Nkah 2009).

This paper conclude with an attempt to investigate the risks of loss of life and damage to capital assets due to Ocean storm surges and coastal floods are likely to become larger in the future. This is because exposure, due to socioeconomic development and the frequency of such events are projected to increase. From available data from satellite technology imageries, and other remote sensing, social media etc, the projected population growth in flood prone areas is expected to be higher between 1950-2040. This leads to an increase in potential fatalities of 68%. The combined impact of rise in sea level and population growth shows that the expected number of fatalities could quadruple by 2040. i.e a combination of climate and socioeconomic change may increase expected looses.

ATMOSPHERIC MASS SPECTROMETRY GROUP AT THE UNIVERSITY OF HELSINKI: OVERVIEW AND RECENT RESULTS

M. EHN, T. RUUSKANEN[+] and M. SIPILÄ
and the MS group: J. DUPLISSY, O. GARMASH, L. HEIKKINEN, V. HENRIKSSON, T. JOKINEN, H. JUNNINEN, M. KAJOS, J. KANGASLUOMA, T. LAURILA, L. MAULDIN, J. PATOKOSKI, T. PETÄJÄ, P. RANTALA, M. RISSANEN, N. SARNELA, S. SCHALLHART, S. SCHOBESBERGER, O. PERÄKYLÄ, A. PRAPLAN, C. YAN, M. ÄIJÄLÄ, D. WORSNOP

Division of Atmospheric Sciences, Department of Physics, University of Helsinki, Helsinki, Finland
[+] and Palmenia Centre for Continuing Education, University of Helsinki, Finland

Keywords: MASS SPECTROMETRY, ATMOSPHERIC AEROSOL, VOLATILE ORGANIC COMPOUNDS, ELVOC.

INTRODUCTION

The Atmospheric Mass Spectrometry Group at the Division of Atmospheric Sciences at the University of Helsinki focuses on developing and deploying state-of-the-art mass spectrometric techniques for gas and aerosol phase analysis in conjunction with other state of art gas and aerosol instrumentation. Research interests span a range of scientific topics, including volatile (mainly organic) emissions, atmospheric oxidants and oxidation products, small molecular clusters, as well as larger aerosol particles. We aim for a comprehensive understanding of how primary emissions are converted to condensable species, clusters, secondary aerosol particles, and eventually to cloud condensation nuclei.

The core research areas are described below in more detail:
- Volatile organic compounds (VOCs): Understanding the biosphere-atmosphere exchange of VOCs and their atmospheric behavior, especially in boreal regions.
- Atmospheric oxidants: Detailed measurements of the hydroxyl radical (OH) and stabilized Criegee intermediates help us understand the relative importance of different species for the oxidative capacity of the atmosphere.
- Organic oxidation products: Semi-, low- and extremely low-volatility organic compounds (SVOC, LVOC, ELVOC) contribute to secondary organic aerosol (SOA), which forms a major fraction of atmospheric aerosol particle mass. The relative roles of these species in SOA formation and growth of newly formed particles governs the final amount of particles available to act as cloud condensation nuclei (CCN), thereby affecting Earth's climate.
- Aerosol particle precursors and clusters: In addition to ELVOC, sulfuric acid, ammonia, amines and iodide oxides are examples of vapors that we have measured in direct relation to cluster formation and new particle formation both in laboratory and field.
- Aerosol particle composition: The composition of particles larger than about 50 nm is influenced by both local sources as well as long-range transport in the atmosphere. The concentration and composition of these particles governs the amount of directly available CCN, but also strongly influences how new particles are able to form.

METHODS

The main instrumentation applied in our group is high-resolution time-of-flight (TOF) mass spectrometry, which forms the common tool for the group members. However, the detailed applications of the TOFs vary greatly, as each instrument is optimized for measurements of specific compounds.
- The PTR-MS (quadrupole, Lindinger et al., 1998) and the PTR-ToF-MS (Jordan et al., 2008) use proton transfer from the hydronium ion H_3O^+ at low pressure (~2.2 mbar) to detect VOCs and the latter one also to measure trimethylamine. - The acetate ToF-CIMS (Bertram et al., 2011) ionizes organic and inorganic

acids by proton transfer to the acetate ion $C_2H_3O_2^-$ at a pressure of ~100 mbar. Mainly SVOCs, have been studied using this method.
- The atmospheric pressure interface TOF (APi-TOF, Junninen et al., 2010) has been successfully deployed to measure positive and negative natural ions, produced e.g. by galactic cosmic rays or the radioactive decay of radon. This technique is extremely sensitive to strong acids (in negative ion mode) and strong bases (in positive ion mode), and has been able to detect large ionic clusters during atmospheric as well as laboratory produced aerosol particle formation events, helping to understand particle formation mechanisms.
- The nitrate chemical ionization CI-APi-TOF has been used to detect sulfuric acid and ELVOC species, both important particle precursors. In addition, the conversion of SO_2 to H_2SO_4 has been utilized to measure (indirectly) oxidants such as OH and Criegee intermediates. Also neutral clusters of sulfuric acid-amines (in laboratory) as well as iodine oxidizes (both laboratory and field) have been observed with the nitrate-CI-APi-TOF. We have also developed a bisulphate – sulphuric acid cluster based CI-APi-TOF that is capable of detecting ammonia and amines with extremely high sensitivity (Sipilä et al., in preparation).
Measurements have been performed in a wide range of surroundings, including boreal, coastal, and marine environments, at remote, rural and urban sites. Long-term ambient data sets from the boreal forest are on-going with PTRMS and nitrate-CI-APi-TOF. Chamber facilities at CERN (Kürten et al., 2014). Research Center Jülich, Germany (Mentel et al., 2009), and TROPOS, Leipzig, Germany (Jokinen et al., 2014) have been successfully utilized in several campaigns to study VOC oxidation and particle formation. Also laboratory investigations within the Division's facilities have been performed, mainly using flow tubes.

SELECTED RESEARCH HIGHLIGHTS

We reported on the formation of ELVOCs at significant yields from typical boreal VOCs, and their important role for organic aerosol formation in a recent publication in Nature (Ehn et al., 2014). This seminal work has motivated several follow-up studies, two of which have been accepted in high-level journals (Rissanen et al., 2014; Jokinen et al., 2014), on the formation mechanisms of ELVOC.

At the CLOUD chamber in CERN, our mass spectrometers have been in crucial roles when revealing details of the particle formation process from organic precursors (Riccobono et al., 2014; Schobesberger et al., 2013) (see abstract by S. Schobesberger) and from sulphuric acid – dimethyl amine system (Almeida et al., 2013). With CI-APi-TOF we also discovered the molecular steps of cluster formation up to cluster sizes containing ~40 molecules in sulphuric acid – dimethyl amine system (Kürten et al., 2014). This is the first direct, well established observation of molecule by molecule proceeding neutral nucleation process in close ambient conditions.

Besides laboratory observations, we have also discovered the atomic composition of freshly formed neutral clusters in coastal environment of Mace Head, Ireland (Sipilä et al., in preparation). Laboratory work continues to resolve the exact molecular steps of that clustering (or nucleation) process.
We have applied the CI-APi-TOF for sCI detection in Hyytiälä and been able to quantify the sCI concentrations and production rate as well as estimate their lifetime (see abstract by Sarnela et al., 2014). Also we have studied sCI chemistry with a wide scope and quantified their capability to react with SO_2, water and organic acids (Sipilä et al., 2014 and references therein).

Using the PTR-ToF-MS, we have observed that agricultural trimethylamine is mainly due to mixture of faeces and urine in farm yards and concluded that ruminant farms are a source of amines that can increase the regional aerosol formation budget (Sintermann et al., 2014). In addition the influence of data-analysis method on VOC flux results was studied at an Italian mixed forest (see abstract by Schallhart et al., 2014).
The long term PTR-MS measurements at SMEAR II, Hyytiälä have been used for OVOC method intercomparison (see abstract by Kajos et al., 2014), to observation of OVOC deposition (see abstract by Rantala et al., 2014) and for evaluation of flux methods (Rantala et al., 2014).

We have found out that the surface-layer-gradient (SLG) method is the method of choice for long term measurements at low-flux conditions typical for boreal forests (Rantala et al., 2014). SLP method performs better than disjunct-eddy-covariance (DEC) or surface-layer-profile (SLP) and has smaller detection limits and better data coverage than the DEC method. The long lived VOCs, including methanol, acetonitrile, acetaldehyde, acetone, benzene and toluene, arrive at Hyytiälä from ten main sources, mainly from episodic forest fires and continuous anthropogenic emissions (Patokoski et al, 2014).

ACKNOWLEDGEMENTS

This study was supported by Academy of Finland Centre of Excellence programs (project no. 272041, 251427 and 1118615).

REFERENCES

Almeida, J., et al. Molecular understanding of sulphuric acid–amine particle nucleation in the atmosphere, *Nature* 502, 359–363, 2013.

Bertram, T. H., et al. A field-deployable, chemical ionization time-of- flight mass spectrometer. *Atmos. Meas. Tech*, 4, 1471-1479. doi:10.5194/amt-4-1471-2011, 2011.

Ehn, M., et al. A large source of low-volatility secondary organic aerosol. *Nature*, 506, 476{479. doi:10.1038/nature13032, 2014.

Jokinen, T., et al. Rapid autoxidation forming highly oxidized RO2 radicals in the atmosphere, *Angewan. Chem.*, 2014 (in press).

Junninen, H., et al. A high-resolution mass spectrometer to measure atmospheric ion composition. *Atmos. Meas. Tech.* 3(4): 1039-1053, 2010.

Kürten A., et al., Neutral molecular cluster formation of sulfuric acid–dimethylamine observed in real time under atmospheric conditions , *Proc. Natl. Acad. Sci.*, doi:10.1073/pnas.1404853111, 2014.

Mentel, T. F., et al. Photochemical production of aerosols from real plant emissions, *Atmos. Chem. Phys.*, 9, 4387-4406, doi:10.5194/acp-9-4387-2009, 2009.

Patokoski, J. et al. Sources of atmospheric VOCs with long lifetime at a rural boreal forest site, SMEAR II. Submitted to Atmospheric Environment.

Rantala, P.,et al. Continuous flux measurements of VOCs using PTR-MS — reliability and feasibility of disjunct- eddy-covariance, surface-layer-gradient, and surface-layer-profile methods. Boreal Env. Res. 19 (suppl. B): 87–107, 2014

Riccobono, F. et al. Oxidation products of biogenic emissions contribute to nucleation of atmospheric particles, *Science* 344, 717-721, 2014.

Schobesberger, S., et al. Molecular understanding of atmospheric particle formation from sulfuric acid and large oxidized organic molecules, Proc. Natl. Acad. Sci. USA 110, 17223-17228, 2013.

Sipilä, M. et al., Reactivity of stabilized Criegee intermediates (sCI) from isoprene and monoterpene ozonolysis toward SO2 and organic acids, Atmos. Chem. Phys. Discuss., 14, 3071-3098, 2014 (accepted to ACP).

Sintermann, J., et al. Trimethylamine emissions in animal husbandry. Biogeosciences Discuss., 11, 6519-6553, 2014.

AGING OF BIOMASS BURNING AEROSOL AFTER LONG- RANGE TRANSPORT FROM LARGE SCALE WILDFIRES IN THE PEEX REGION

K. ELEFTHERIADIS[1], E. DIAPOULI[1], S. VRATOLIS[1] and O. POPOVICHEVA[2]

[1]ERL, Institute of Nuclear & Radiological Sciences & Technology, Energy & Safety, N.C.S.R. "Demokritos", 15310, Athens, Greece

[2]Scobeltsyn Institute of Nuclear Physics, Moscow State University, 119991, Moscow, Russia

Keywords: WILDFIRES, LONG-RANGE TRANSPORT, AGING, INDIVIDUAL PARTICLE ANALYSIS, OPTICAL PROPERTIES.

INTRODUCTION

Smoke aerosol emitted by large scale wildfires in the European part of Russia and Ukraine, was transported to Athens, Greece during August 2010 and detected the Demokritos GAW/ACTRIS suburban background station. Due to the low emissions during this period of summer in the Athens Metropolitan area, large increases in PM10 and carbonaceous aerosol concentrations provided strong evidence of incoming aerosol from a different source area.

METHODS

Measurements were conducted for physico-chemical characterization of the aged aerosol and included on-line monitoring of PM10 and carbonaceous particles mass concentrations, as well as aerosol optical properties. In addition TSP filter samples were analyzed for major inorganic ions, while morphology and composition of particles was studied by individual particle analysis. Results supported the long-range transport of smoke plumes from Ukraine and Russia burning areas indicated by back trajectory analysis. An increase of 50% and 40% on average in organic (OC) and elemental carbon (EC) concentrations respectively, and more than 95% in carbonate carbon (CC) levels was observed for the biomass burning (BB) transport period of August with respect to the previous month of July. Mean 24-hr OC/EC ratio was found in the range 3.2 – 8.5 (fig.1)

Individual particle analysis of the samples collected during BB-transport event in Athens revealed elevated number of soot externally mixed with fly ash Ca- rich particles. This result is in agreement with the increased OC and CC levels measured, thus pointing towards the main components comprising the aged BB aerosol microstructure.

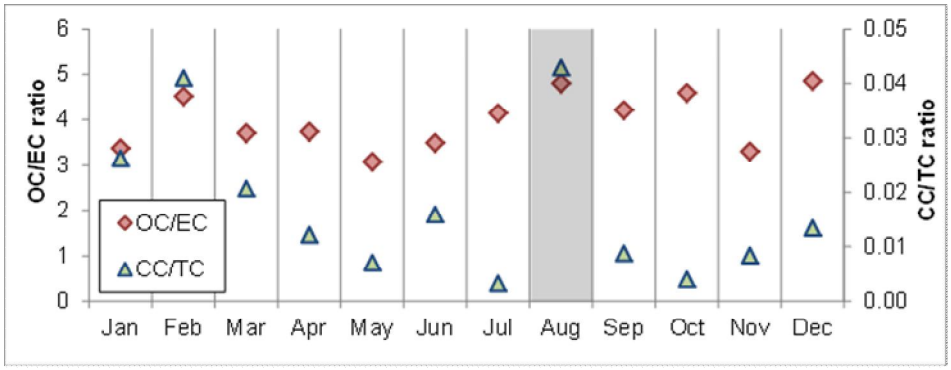

Figure 1. Monthly variation of OC/EC and CC/TC concentration ratios, during 2010.

CONCLUSIONS

It was found that aging of biomass burning aerosol and mixing with co-emitted dust leads to increase of

single scattering albedo (SSA), indicating abundance of light scattering constituents and/or shift of size distributions towards larger particles. Increase in particle size was further supported by a decreasing trend in absorption Angström exponent (AAE) derived from the wavelength dependence of Absorption coefficient (fig. 2), while the aging of the organic fraction appears to eliminate the higher AAE which is normally characteristic of biomass burning aerosol.

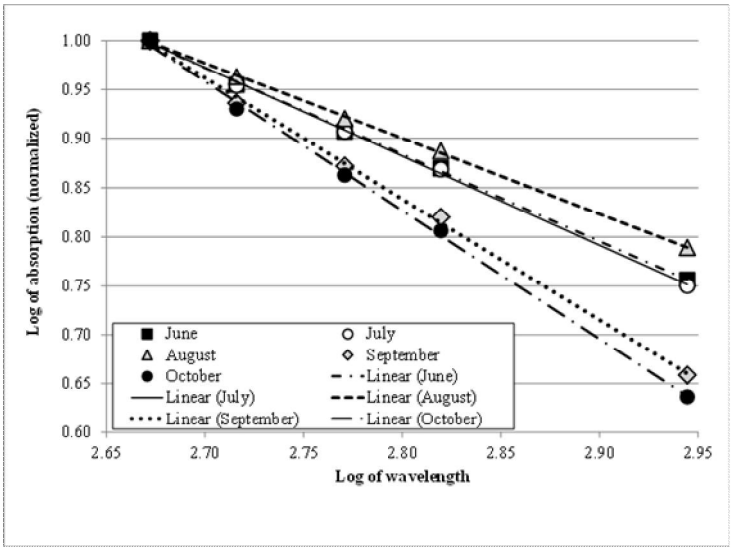

Figure 2. Wavelength-dependence of absorption coefficient during June – October 2010.

ACKNOWLEDGEMENTS

The work was partly supported by the EnTeC FP7 Capacities programme (REGPOT-2012-2013-1,FP7, ID:316173). Financial support of RFBR-NSC№12-05-92002 and RFBR№12-05-00395 projects is also acknowledged

REFERENCES

Popovicheva O.B., Kireeva E.D., Persiantseva N.M., Timofeev M.A., Kistler M., Kopeikin V.M., Kasper-Giebl A. (2014) Physicochemical characterization of smoke aerosol during large-scale wildfires: Extreme event of August 2010 in Moscow. *ATMOS ENVIRON*, doi : 10.1016/j.atmosenv.2014.03.026.

THE CLIMATE ROLE OF SHALLOW STABLY STRATIFIED ATMOSPHERIC BOUNDARY LAYERS

I. ESAU[1] and R. DAVY[1]

[1]Nansen Environmental and Remote Sensing Centre / Bjerknes Centre for Climate Research, Thormohlensgt. 47, 5006, Bergen, Norway.

Keywords: ATMOSPHERIC BOUNDARY LAYER, EARTH'S CLIMATE, ATMOSPHERIC STRATIFICATION, TURBULENCE.

INTRODUCTION

The surface air temperature, T, is readily observed and frequently used to characterize the earth's climate system (Hartmann et al., 2013). Its change could be expressed through an energy-balance model as

$$\Delta T = C^{-1}Q \quad (1)$$

where Q is the heat flux divergence (climate forcing) and C is the system's heat capacity (Sellers, 1969; North and Kim, 2015). The climate research is mainly concerned with the climate response on natural and anthropogenic changes in Q, whereas it often assumes a passive role of the heat capacity in the climate processes. Only in the last few years, the problem of the varying C was reopened for discussion in connection with so called the climate "hiatus" problem (e.g. Kosaka and Xie, 2013).

Arguably, the major impact on the century to millennia time scales should be attributed to the heat capacity of the upper ocean. The upper ocean is a slow system with respect to the atmosphere. It integrates the atmospheric temperature fluctuations, smoothes them and transfers their effects on larger time and spatial scales (Donohoe et al., 2014). Kosaka and Xie (2013) were able to simulate those climatic aspects of the air-sea interactions and attribute the weaker global warming to these effects. Their simulations however failed to reproduce the observed temperature trends over the continents. It suggests that the atmospheric boundary layer (ABL) has other mechanisms to modify the temperature response on the climate forcing. The ABL is a fast system with small heat capacity. It impacts the temperature variations through selective and asymmetric response on the variations in the climate forcing. As it follows from Eq. (1), the largest ΔT will be observed in the ABL states with the smallest C. Since C is proportional to the layer thickness, h, the climate forcing should cause the strongest response in the most shallow ABL.

Indeed, the analysis of the observed diurnal, seasonal and geographical asymmetries in the temperature variability and trends revealed the largest changes in the nocturnal, wintertime and continental temperatures over the historical period of instrumental observations (Vose et al., 2005). In earlier publications, these asymmetries were attributed to a diverse array of local factors such as changes in cloudiness, precipitation and soil moisture, agricultural and irrigation systems' development (Bonan, 2000), urbanization etc (Lim et al., 2005). Esau et al. (2012) pointed out that the proposed explanations attribute the changes in the maximum temperatures whereas the observed amplified variability of the minimum temperatures remained unexplained. They proposed a complementary explanation involving the ABL thickness as a parameter to control the temperature response on the instant forcing anomaly. Such a control has been theoretically suggested in Zilitinkevich and Esau (2009).

In this study, we further develop the analysis of Esau et al. (2012), McNider et al. (2012) and Davy and Esau (2013). In particular, our statistical analysis of the ECMWF ERA-Interim data demonstrates the emergence of the ABL thickness as a major parameter to control the temperature response in the cold climates dominated by the downward sensible heat flux and the stable stratification of the lower atmosphere.

METHODS

ERA-Interim reanalysis data over the period 1 Jan 1979 to 31 Dec 2010 were obtained from the ECMWF website. Daily pressure, precipitation, snowfall and total cloud cover at 3 hour intervals and the daily minimum and maximum temperature at a height of 2 m were obtained at a resolution of 1.5^o x 1.5^o. The land-sea mask for the dataset was applied to select for over-land grid points. The temperature and cloud cover data were filtered for days without strong pressure changes ($P_{max}-P_{min}>10$ hPa), high precipitation (>10 mm) or high snowfall (>100 mm). This was done to select for days where ABL processes were the principle determinant of the near-surface temperature. Anomalies and means were calculated for the daily minimum, maximum, mean temperatures. Monthly and seasonal values were determined by taking the mean of the daily anomalies and means. For each grid point a first order polynomial was fit, using least-squares fitting, to these anomalies to obtain the trend in each variable. The statistical significance of these fits was calculated using the two-tailed Student's t-test. These trends were filtered for statistical significance using a maximum accepted p-value of 0.05. The presented analysis is obtained using all northern hemisphere locations: latitudes greater than thirty degrees north.

RESULTS

Although Eq. (1) looks rather simple, its stochastic interpretation faces serious difficulties. The statistical correspondence between the anomalies of $C \propto h$ and Q is generally unknown. It may vary in different climates and from season to season. Hence, in order to establish the ABL role in the climate system, one should demonstrate that the statistical dependence (signal) between the temperature variations and h is stronger than the impact of other factors, which are considered here as noise.

At the first step of our analysis, we establish the statistical relationships between the diurnal minimum and maximum temperatures, the ABL thickness and the surface sensible heat flux in the ERA-Interim data. Figure 1 reveals statistical correspondence between the negative surface sensible heat flux, which defines the stably stratified ABL, and both the diurnal minimum temperature and ABL thickness. Using the same data, Esau et al. (2012) demonstrated that the large temperature trends are predominantly found in the areas, which are dominated by the shallow ABL. Davy and Esau (2013) additionally showed that these excessive trends are trapped in the lower atmosphere, whereas the trends in the free atmosphere above the ABL do not have such a differentiation.

At the next step of the analysis, we quantitatively assess the statistical correspondence between the temperature trends and the ABL thickness in the frameworks of the model in Eq. (1). Figure 2 reveals no correspondence (correlation coefficient less than 0.2) between the temperature trends and the ABL thickness in relatively deep ABLs with $h > h_0$. In this part of the parameter space, the temperature trends are determined by other factors, which have been extensively discussed in literature. The strong reciprocal dependence (the corr. coef. 0.6) on the ABL thickness emerges for $h < 0.8h_0$. It indicates that the ABL becomes the major factor of the climate variability overriding the other effects in shallow ABL with $h < 400$ m. The correspondence between the shallow and stably stratified ABL is well known from the theoretical analysis (Zilitinkevich et al., 2007).

In order to quantify the relative contribution of different suggested climate factors to the observed temperature trends, we conducted a linear multi-factor regression analysis in the form

$$\dot{T} / \dot{T}_0 = \sum_i b_i F_i / F_{i0} \qquad (2)$$

where b_i are non-dimensional regression coefficients and F_i are the corresponding climate factors normalized by their climatological norms. We analysed the regressions onto the reciprocal ABL thickness (1/BLH), cloud cover (CC), soil moisture (q_soil) and precipitation (Precip). Figure 3 shows that the ABL thickness is the largest component of the regression in all seasons with exception of summer. In particular,

the dependence on h is strongly pronounced in the autumn and in the annually averaged data. As it is expected and has been presented in literature (Zhou et al., 2009; Tang, and Leng, 2012), the summer regressions are controlled by the hydrological factors such as cloud cover, precipitation and soil moisture.

CONCLUSIONS

Analysis of the ERA-Interim data over the period 1979-2010 supports the hypothesis that the surface air temperature trends over the continental areas are significantly (as much as by the factor of two) amplified in the shallow stably stratified atmospheric boundary layers. This amplification is controlled by the ABL thickness, which impact overrides the other climate factors when $h < 400$ m. Such shallow ABL is found mostly in situations with the downward surface sensible heat flux, and therefore, with the local temperature minimums. Unlike the previously proposed explanation of the observed asymmetric temperature changes, the ABL thickness mechanism links the amplified temperature changes with the climate forcing impact on the minimum temperatures, which occur in the periods and in the areas when and where the shallow stably-stratified ABL establishes.

ACKNOWLEDGEMENTS

This work was supported by the Bjerknes Centre for Climate Research funding and the Norwegian projects: CLIMARC: Climate variability and change in the Eurasian Arctic in the 21st century; and BjerknesARC (227137) - Bjerknes Compensation Mechanism: Historical perspective, geographical pattern, and Arctic multi-decadal predictability.

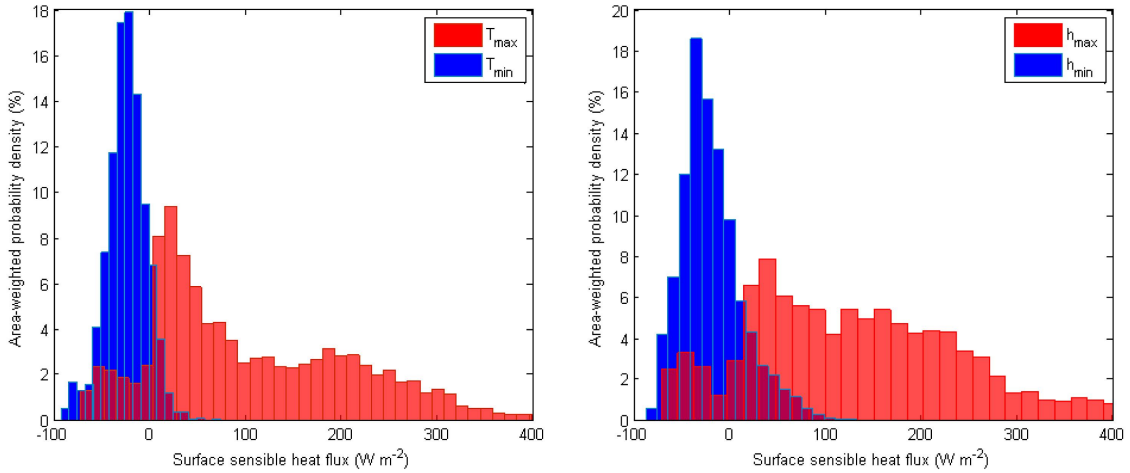

Figure 1. Land-area weighted probability density functions of the diurnal minimum and maximum (a) temperature and (b) ABL thickness as a function of surface sensible heat flux. Source: ERA-Interim.

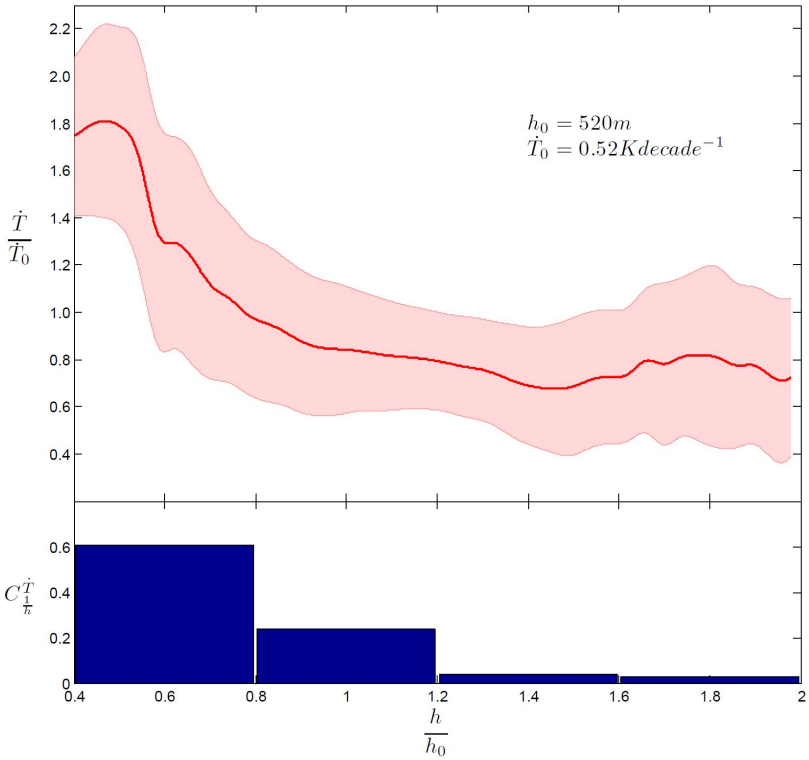

Figure 2. (Upper panel) The surface air temperature trends (normalized by their hemispheric average value), $\dot{T}/\dot{T}_0$, dependence on the respective ABL thicknesses (normalized by their hemispheric average value), h/h_0. The dependences were calculated for each continental grid point north of 30°N. The red curve is the average for all dependences in the corresponding intervals of h/h_0. The shading shows the intervals of three standard deviations. (Lower panel) The corresponding correlation coefficients between $\dot{T}$ and h. The correlations were defined within the intervals of h/h_0 as given by the boxes. Source: ERA-Interim.

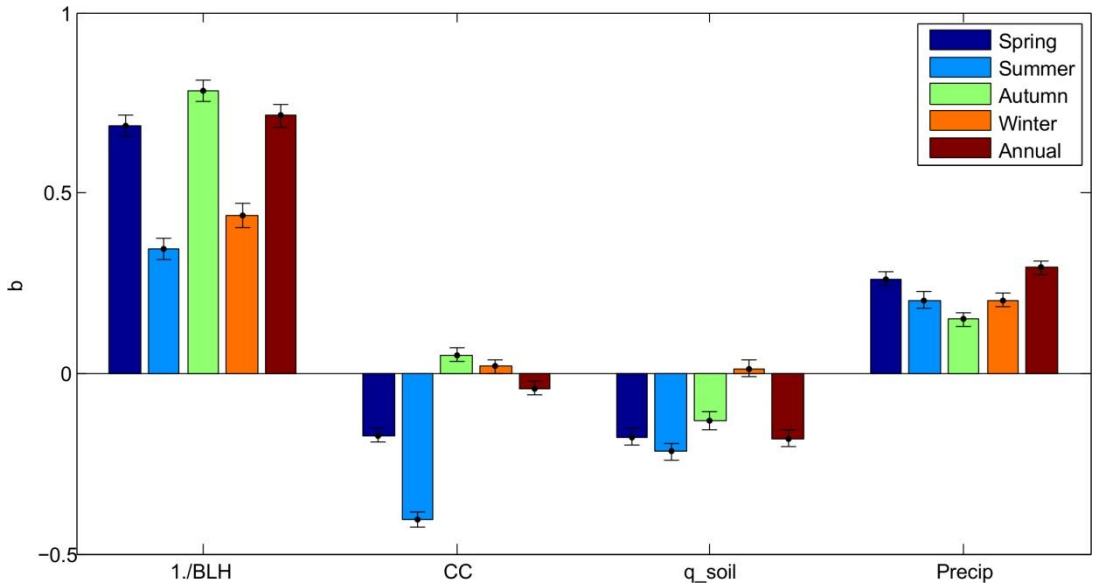

Figure 3. The regression coefficients, b_i, for each of the four components of the multi-linear regression model (Eq. 2) for each season and for the full annual cycle. The error bars represent the 95% confidence interval on the coefficients.

REFERENCES

Hartmann, D.L., A.M.G. Klein Tank, M. Rusticucci, L.V. Alexander, S. Brönnimann, Y. Charabi, F.J. Dentener, E.J. Dlugokencky, D.R. Easterling, A. Kaplan, B.J. Soden, P.W. Thorne, M.Wild and P.M. Zhai (2013): Observations: Atmosphere and Surface. In: *Climate Change 2013: The Physical Science Basis. Contribution of Working Group I to the Fifth Assessment Report of the Intergovernmental Panel on Climate Change* [Stocker, T.F., D. Qin, G.-K. Plattner, M. Tignor, S.K. Allen, J. Boschung, A. Nauels, Y. Xia, V. Bex and P.M. Midgley (eds.)]. Cambridge University Press, Cambridge, United Kingdom and New York, NY, USA, pp. 119–158, doi:10.1017/CBO9781107415324.0

Bonan, G. (2000). Observational evidence for reduction of daily maximum temperature by croplands in the Midwest United States. J. Clim., 14, 11, 2430-2442

Davy, R. and I. Esau (2013). Surface air temperature response in global climate models, Atmos. Sci. Lett., 15, 13-20, doi: 10.1002/asl2.456

Donohoe, A., Frierson, D.M.W., and D.S. Battisti (2014). The effect of ocean mixed layer depth on climate in slab ocean aquaplanet experiments, Climate Dynamics, 43(3-4), 1041-1055

Esau, I., R. Davy and S. Outten (2012). Complementary explanation of temperature response in the lower atmosphere, Environ. Res. Lett., 7, 044026

Sellers, W.D. (1969). A Global Climatic Model Based on the Energy Balance of the Earth-Atmosphere System. J. Appl. Meteor., 8, 392–400

North, G.R. and K.-Y. Kim (2015). Climate and climate change: Energy balance climate models, Encyclopedia of Atmospheric Sciences, 69-72

Kosaka, Y. and S.-P. Xie (2013). Recent global-warming hiatus tied to equatorial Pacific surface cooling, Nature, 501, 403–407, doi:10.1038/nature12534

Lim, Y.-K., M. Cai, E. Kalnay, L. and Zhou (2005): Observational evidence of sensitivity of surface climate change to land types and urbanization. Geophys. Res. Lett., 32, L22712, doi: 10.1029/2005GL024267

McNider, R.T., Steeneveld, G.J., Holtslag, A.A.M., Pielke, R.A., Sr., Mackaro, S., Pour-Biazar, A., Walters, J., Nair, U. and Christy, J. (2012). Response and sensitivity of the nocturnal boundary layer over land to added longwave radiative forcing. J. Geophys. Res., 117 (D14): D1410

Tang, Q., and G. Leng (2012). Damped summer warming accompanied with cloud cover increase over Eurasia from 1982 to 2009. Environ. Res. Lett., **7**, 014004

Vose, R.S., Easterling, D.R., Gleason B. (2005). Maximum and minimum temperature trends for the globe: an update through 2004. Geophys Res Lett 32:L23822. doi:10.1029/2005GL024379

Zilitinkevich, S., I. Esau, and A. Baklanov (2007). Further comments on the equilibrium height of neutral and stable planetary boundary layers, Quarterly J. Royal Meteorol. Soc.,133, 265-271

Zilitinkevich, S. and I. Esau (2009). Planetary boundary layer feedbacks in climate system and triggering global warming in the night, in winter and at high latitudes, Geography, Environment and Sustainability, 1(2), 20-34

Zhou, L. A. Dai, Y. Dai, R. S. Vose, C.-Z. Zou, Y. Tian, and H. Chen (2009). Spatial dependence of diurnal temperature range trends on precipitation from 1950 to 2004. Climate Dynamics, 32, 429 - 440

SUBFOSSIL CLADOCERA OF BOLSHOY KHARBEY LAKE (NORTHERN RUSSIA) AS INDICATORS OF ECOLOGICAL AND CLIMATIC CHANGES

L.A. FROLOVA[1], E.B. FEFILOVA[2], A.A. FROLOVA[1] and O.N. TUMANOV[1].

[1]Kazan Federal University, Kremlyovskaya 18, 420008, Kazan, Russia.

[2]Institute of Biology, Komi Scientific Centre Ural Branch of Russian Academy of Sciences, Kommunisticheskaya 28, 167982, Syktyvkar, Russia.

Keywords: CLADOCERANS, TUNDRA LAKE, ECOSYSTEM DYNAMIC.

INTRODUCTION

Northern ecosystems are the most vulnerable to increasing anthropogenous influence owing to their specific characteristics. Climate change is most strongly expressed in the Arctic and northern ecosystems are most unstable and especially sensitive to external ecological influences (Kienast *et al.*, 2011; Rautio & Nevalainen 2013). The situation in a water ecosystem is reflected by zooplankton and benthos communities (Rudaya *et al*, 2012). Cladocera (Branchiopoda, Crustacea) fossil assemblages in lacustrine sediments are increasingly important for reconstructing past ecological and climate change (Korhola *et al*.2005; Korhola & Rautio, 2001; Frolova *et al*, 2014). We investigated subfossil Cladocera assemblages from short sediment cores (~ 150 years) from the lake of Kharbey lake system, eastern part of Bolshezemel'skaya tundra in the northeast of Europe 67°31-36′ N, 62°51-56′ E and 129.8 m above sea level.

METHODS

The Lake Bolshoi Kharbei is the major lake in the Kharbei lake and river system. It belongs to the Pechora River basin, and is situated in the east of theBolshezemelskaya tundra region (67°31'15.75" to 67°36'9.59" N; 62°50'43.49" to 62°55'20.95" E). The surface area of the lake is 21.3 km^2; the maximum depth is 18 m. The nearest source of possible human-induced pollution is the industrial area of the city of Vorkuta and coalmines situated in this area (~80 km away from the lake).

For the paleoecological study a short 25 cm sediment core was collected using a UWITEC impact corer in the southern part of the Lake Bolshoi Kharbei (67º 31.832´N, 062º 52.669´ E) in August 2012 from the depth of 6 m. Simultaneously with collecting hydrobiological and paleoecological samples, we measured water temperature, pH, dissolved oxygen concentration (with a Multi 340i/SET portable analyzer, Germany), and transparency (with a Secchi disk), and collected water samples for chemical analysis. The following parameters were determined later: mineralization, ionic composition, biogenic (organic) matter and microelements.

Twenty-five slices of 1 cm thickness were cut for cladoceran analysis. Each subsample of wet bottom sediment was dissolved in 10% KOH and heated to 75°C for 30 min. Between 100 and 186 Cladocera individuals were counted per sample. Identification was based on both modern identification guides for recent and subfossil Cladocera (Szeroczyńska, Sarmaja-Korjonen, 2007; Korosi, Smol, 2012) and the guides for identifying contemporary Cladocera (Kotov *et al*., 2010). TILIA version 2.0.b.4 was used to generate a cladoceran percentage diagram. The program CONISS was used to perform a stratigraphically constrained incremental sum-of-squares cluster analysis to identify the major zones throughout core (Grimm, 2004).

RESULTS

Among the subfossil cladoceran communities of the Lake Bolshoi Kharbei, 18 taxa were identified to the species level, one to the subspecies level, and two to the genus level (Figure 1). Three of them: *Graptoleberis testudinaria* (Fisher), *Disparalona rostrata* (Koch), and *Pleuroxus trigonellus* (O.F. Müller)

have not been found in any previous studies of the Lake. This is the first finding of *D. rostrata* in the Bolshezemelskaya tundra region. The subfossil communities did not include *L. frontosa* and *H. gibberum* that always occur in hydrobiological samples of the study lake. It is well known that external skeleton of these obligate planktonic cladocerans is rapidly decomposed and do not stay in bottom sediments (Hann, 1989). Representatives of the planktonic genus *Daphnia* might have remained unidentified for the same reason. *Bosmina* species, *Ch. sphaericus*, and *A. affinis* were abundant both in zooplankton and zoobenthos communities studied with hydrobiological methods and in the subfossil communities of the Lake Bolshoi Kharbei.

Cluster analysis identified four zones in the core of bottom sediments of the Lake Bolshoi Kharbei that differed in the structure of subfossil cladoceran communities (Figure 1).

Zone I covers the earliest study period (before 1890 AD), was characterized by the clear dominance of the genus *Bosmina* and *Ch. sphaericus* over the other taxa.

In zone II (between 1890 and 1941 AD) *Bosmina* and *Ch. sphaericus* still dominated, but the contribution of planktonic-benthic fauna was growing, which might be indirect evidence of changes in hydrological parameters of the Lake and enhanced development of phytobenthos in that time period (Korhola et al., 2000; DeSellas et al., 2008). In this zone, similarly to zone I *B. cf. longispina* prevailed over *B. longirostris* among *Bosmina* species, but in the layers closer to the surface, the abundance of *B. longirostris* increased while the abundance of the other planktonic species decreased (Figure 1).

The abundance of *B. longirostris* in the subfossil communities continued to grow in the Zone III (corresponding to the period between 1941 and 1993 AD) (Figure 1). The abundances of the both species of subfossil *Bosmina* were similar. The both taxa alternately dominated in different layers of this zone. Only in the Zone III we found remains of the rare for the Bolshezemelskaya tundra region species *C. rectirostris*, *D. rostrata*, and *G. testudinaria*. These are moderately thermophilic cladocerans, indicators of the warm-water conditions (Nevalainen, Luoto, 2010).

Finally, in the Zone IV (after 1993 AD), the abundance of *B. longirostris* first increased dramatically but then dropped sharply (Figure 1).

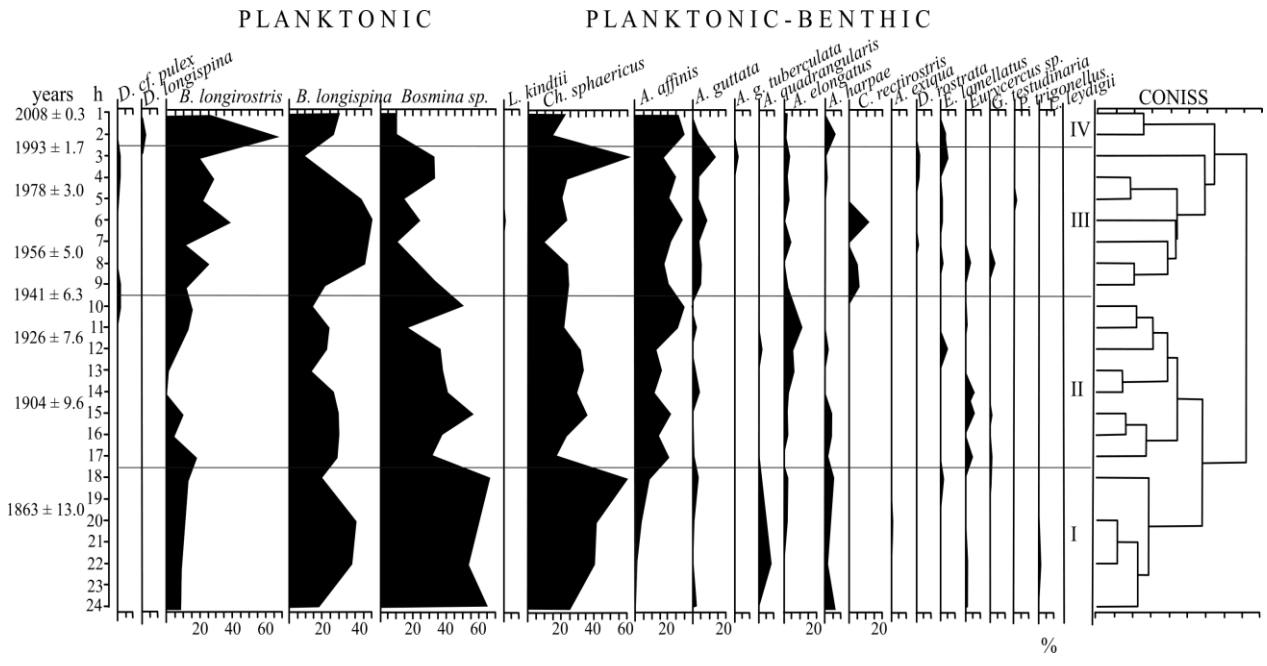

Figure 1. Cladoceran diagram from lake Bolshoi Kharbei, northeastern European Russia.

Results of the study of subfossil cladoceran community of the Lake Bolshoi Kharbei are in a good agreement with the data on dynamics of climatic and human-induced environmental conditions in the study area and with the dynamics of cladoceran populations and communities in the Lake during the

period of the hydrobiological investigations. Increase in the abundances of some species (*D. longispina*, *B. longirostris*, *C. rectirostris*, and *D. rostrata*) from the middle of the zone II to the upper layers of sediments must be associated with the air temperature warming during the analyzed time intervals (since 1937 AD), that have been particularly pronounced after 1965 AD.

CONCLUSIONS

Consequences of warming and other human-related impacts were revealed in cladoceran communities of the investigated Lake Bolshoi Kharbei situated the eastern part of European tundra. The structure of the benthic cladoceran communities of the Lake had changed before the area was urbanized and commercially developed, probably due to transboundary human impacts. Planktonic cladoceran communities were more sensitive to warming: they showed increase in the abundance of thermophilic species and the species indicative of eutrophication. Since no chemical eutrophication has been revealed in the Lake ecosystem, these changes in zooplankton are associated with thermal eutrophication.

ACKNOWLEDGEMENTS

This work was funded by the subsidy allocated to Kazan Federal University for the state assignment in the sphere of scientific activities. O.N.T was partially supported by RFBR, research project No 15-05-04442 – a. L.A.F was supported by Russian Government Program of Competitive Growth of Kazan Federal University.

REFERENCES

DeSellas, A.M., Paterson, A.M., Sweetman, J.N., J.P. Smol (2008). Cladocera assemblages from the surface sediments of southcentral Ontario (Canada) lakes and their relationships to measured environmental variables, Hydrobiol. **600**,105–119.

Frolova, L., Nazarova, L., Pestryakova, L. and U. Herzschuh (2014). Subfossil cladoceran remains from sediment in thermokarst lakes in northeastern Siberia, Russia, J. Paleolim. **52**, 1, 107-119, DOI 10.1007/s10933-014-9781-7.

Frolova, L.A., Nazarova, L.B., Pestryakova, L.A. and U. Herzschuh (2013). Analysis of the effects of climate-dependent factors on the formation of zooplankton communities that inhabit Arctic lakes in the Anabar River basin, Contemp. Prob. Ecol. **6**, 1, 1-11. DOI: 10.1134/S199542551301006X

Grimm, E.C. (2004) *TG View 2.0.2 (Software)*, Illinois State Museum, Springfield, Illinois.

Kienast, F., Wetterich, S., Kuzmina, S., Schirrmeister, L., Andreev, A., Tarasov, P., Nazarova, L., Kossler, A., Frolova, L. and V. Kunitsky (2011). Paleontological records prove boreal woodland under dry inland climate at today's Arctic coast in Beringia during the last interglacial, Quat. Sc. Rev. **30**, 17/18, 2134-2159.

Korhola, A, Olander, H and T. Blom (2000). Cladoceran and chironomid assemblages as qualitative indicators of water depth in subarctic Fennoscandian lakes. J Paleolimnol. **24,** 43–54.

Korhola, A. and M. Rautio (2001). Cladocera and other branchiopod crustaceans. In: J.P. Smol, H.J.B. Birks & W.M. Last (eds.), Tracking Env. Change Using Lake Sediments **4**: Zool. indic. Kluwer Academic Publishers, 5-41.

Korhola, A., Tikkanen, M. and J. Weckstro¨m (2005). Quantification of Holocene lakelevel changes in Finnish Lapland using a cladocera – lake depth transfer model, J. Paleolim. **34,** 175–190.

Korosi, J. B. and J. P. Smol (2012). An illustrated guide to the identification of cladoceran subfossils from lake sediments in northeastern North America, The Chydoridae. Springer Science+Business Media B.V.

Kotov, A.A., Sinev, A.Y., Glagolev, S.M. and N.N. Smirnov (2010). *Water fleas (Cladocera)*. In: Alexeev V.R., Tsalolokhin S.Y. (eds.), Key book for zooplankton and zoobenthos of fresh waters of European Russia, KMK, Moscow, 151-276.

Nevalainen, L. and T.P. Luoto (2010) Temperature sensitivity of gamogenesis in littoral cladocerans and its ecological implications, J. Lim. **69**, 120-125.

Rautio, M. and L. Nevalainen (2013).Cladocera, Encyclopedia of Quat. Sciences **3**, 271-280.

Szeroczyńska, K. and K. Sarmaja-Korjonen (2007). *Atlas of Subfossil Cladocera from Central and Northern Europe*. Friends of the Lower Vistula Society, 84.

Rudaya, N., Nazarova, L., Nourgaliev, D., Palagushkina, O., Papin, D. and L. Frolova **(**2012). Mid-late Holocene environmental history of Kulunda, southern West Siberia: vegetation, climate and humans. Quat. Sc. Rev. **48**, 32-42.

Solovieva, N., Jones, V.J., Nazarova, L., Brooks, S.J., Birks, H.J.B., Grytnes, J.A., Appleby, P.G., Kauppila, T., Kondratenok, B., Renberg, I. and V. Ponomarev (2005) Palaeolimnological evidence for recent change in lakes from the northern Urals, arctic Russia, J. Paleolim. **33**, 463-482.

PROACTIVE AND INTEGRATIVE ADAPTATION TO CLIMATE CHANGE IN FUTURE EARTH

C. FU, H. MAO, A. DING and W. GUO

Institute for Climate and Global Change Research, Nanjing University, Nanjing, Jiangsu, China

Global change research has entered a new phase in the 21st century, from understanding the governing principles and mechanisms driving the earth system (i.e. natural variability and anthropogenic influence) to predicting and coping with future changes. The most imminent goals in this phase are: 1) reduce/slow down negative impacts of climate and environmental changes, and 2) adapt to inevitable changes. This study presents an overview of humankind's adaptation to climate change and the evolution of global and climate change research, which serves as the foundation of the science of climate change adaptation. Future directions in global change research are recommended with an emphasis on a proactive and integrative approach to future climate change adaptation. As one of the core research areas, climate change and its socioeconomic impacts will be forecasted in response to natural and anthropogenic forces on decadal to longer time scales and on regional to global spatial scales, and based on such information, a most effective climate change adaptation framework will be developed. Polar and semi-arid regions as well as monsoon Asia have been suggested to be most sensitive to climate change and are hence proposed for case studies to demonstrate how this adaptation framework proposed here can be applied in practice.

ARCTIC SEA ICE AND EAST ASIAN MONSOONS

Y. GAO[1,2], D. GAONG[3], D. GUO[1] and F. LI[1]

[1]Nansen-Zhu International Research Center, Institute of Atmospheric Physics, Chinese Academy of Science, Beijing, 100029, China

[2]Nansen Environmental and Remote Sensing Center/Bjerknes Center for Climate Research, Bergen 5006, Norway

[3]State Key Laboratory of Earth Surface Processes and Resource Ecology, Beijing Normal University, Beijing 100875, China

Observational data and coupled atmosphere–ocean (AOGCM) and atmosphere-only (AGCM) model simulations are used to investigate how spring Arctic sea ice impacts the East Asian summer monsoon (EASM). Consistent with early studies, observational data from 1979 to 2009 show that spring Arctic sea ice is significantly linked to the EASM on inter-annual timescales. Data analysis reveal that sea surface temperature (SST) changes in the North Pacific may serve as a bridge for the inter-seasonal connection between spring Arctic sea ice and the EASM. Large-scale atmospheric circulation and precipitation changes are consistent with the SST changes. The mechanism found in the observational data is confirmed by the numerical experiments and can be described as follows: spring Arctic sea ice anomalies cause atmospheric circulation anomalies, which, in turn, cause SST anomalies in the North Pacific. The SST anomalies can persist into summer and then impact the summer monsoon circulation and precipitation over East Asia. The mediating role of SST changes is highlighted by the result that only the AOGCM, but not the AGCM, reproduces the observed sea ice-EASM. The similar mechanism also links the spring Arctic Oscillation with the EASM for the period of 1979 to 2009.

ASSESSMENT OF VARIABILITY OF WIND WAVES PARAMETERS ON THE BLACK SEA

F.N. GIPPIUS[1], V.S. ARKHIPKIN[1] and G.V. SURKOVA[2]

[1]Department of Oceanology, Faculty of Geography, Lomonosov Moscow State University, Moscow, Russia

[2]Department of Meteorology and Climatology, Faculty of Geography, Lomonosov Moscow State University, Moscow, Russia

Keywords: WIND WAVES, BLACK SEA, NCEP/NCAR REANALYSIS, SWAN MODEL.

INTRODUCTION

The interest in wave regime studies is due to more and more rapt attention paid to marine areas from both the scientific and applied points of view. The Black Sea and its coasts are intensely used for shipping, recreation and other human activities. These aspects determine the need of wind waves studies on the Black Sea.

More or less fundamental research of the wave climate of the Black Sea started in the second half of the XX century in the USSR with the development of the stochastic approach of wind waves studies. The results of such studies are summarized in several monographs, such as (Rzheplinskiy, 1969) and (Simonov and Altman, 1991). Studies of Efimov and Komarovskaya (2009) and Polonsky et al. (2011) are examples of investigations in extreme and climatic parameters of the whole sea. Another traditional research field is coastal studies, e.g. in bays and straits, such as (Ivanov et al., 2009; Alekseev et al., 2013).

The present paper highlights some results of a modelling study of wind wave parameters and their variability in the Black sea during more than 60 years basing on the NCEP/NCAR reanalysis data (Kalnay et al., 1996), which was not applied yet as forcing for wave simulations covering the entire sea. The goal of this study was to assess modern climatic parameters of wind waves on the Black Sea and to determine their spatial, annual and seasonal variability.

DATA AND METHODS

An accurate bathymetry dataset is needed to create a digital model of the bottom topography. In order to create a reliable dataset a hydrographic chart of the Black Sea issued by the Main Naval and Oceanographic Administration of the Russian Ministry of Defense in 1996 was used. The scale of this chart is 1:2500000. Isobaths corresponding to depths of 20, 50, 100, 200, 500, 1500 and 2000 m are plotted on the chart as well as 514 separate points with corresponding depth values.

The scanned image of this map was processed by means of the Golden Software MapViewer package. As a result, a database containing geographic coordinates of points and corresponding depth values was created. Afterwards geographic coordinates of all collected points were transformed to cartesian ones and the irregularly distributed depth values were interpolated onto the nodes of a rectangular grid with a spatial resolution of 5×5 km. In order to avoid computational errors, small bays and capes having sizes roughly equal to the grid cell size were smoothed. Thus, a 129×242 cells matrix was created, which was used as the computational grid in the study. The same database was previously applied for numerical hydrodynamic studies of the Black Sea (Arkhipkin et al., 2013).

Continuous wind forcing is needed for the calculation of wave parameters. For this purposes wind speed series (decomposed to u and v components) at 10 m height above the sea surface were selected from the

NCEP/NCAR reanalysis. This reanalysis contains hindcasted values of various meteorological parameters dating back to 1948. The temporal resolution of this dataset is 6 hours, while the spatial one is 1.875° in the longitudinal direction and 1.9046° in the latitudinal one. Data corresponding to the study domain were selected and interpolated on the computational grid. This reanalysis was chosen first of all due to its enormous temporal extend, which is significantly larger than most other analogues.

Wave parameters were calculated by means of the third-generation spectral wave model SWAN (Booij et al., 1999; Ris et al., 1999). This model is widely used all over the world for the calculation of wave parameters on various scales (e.g. Gorrell et al., 2011; Rusu et al., 2008; Zijlema, 2010; Van Ledden et al., 2009). It was also implemented in several Black Sea studies (e.g. Akpinar et al., 2012; Polonsky et al., 2011; Valchev et al., 2012). Version 40.81 of the model was applied. Calculations were carried out in third-generation mode. Exponential wave growth was described according to Komen et al. (1984). Bottom friction was parameterized by a constant JONSWAP spectrum (Hasselmann et al., 1973). Besides this, triad wave-wave interactions and diffraction were considered. The computations were carried out continuously for every year. “Hot-files” containing wave parameters calculated during the three last days of a year were created to launch the computations for the next year. The directional resolution was of 1°. In the frequency-space there were 21 logarithmically distributed divisions between 0.7 and 1 Hz. The time step of the computations was of 30 minutes. At every time step values of significant wave height, wave period, mean length and direction were calculated at the nodes of the computational grid. By-turn, these parameters were stored in the model’s output file every 3 hours.

Point №		1	2	3
Coordinates		43° N, 31° E	43° N, 34° E	43° N, 37° E
Maximal observed 5-day average SWH		3.2363	2.8370	2.6223
Maximal calculated 5-day average SWH		1.9205	2.0455	1.5582
Average observed 5-day average SWH		0.8908	0.8569	0.8211
Average calculated 5-day average SWH		0.6368	0.6576	0.5745
Minimal observed 5-day average SWH		0.0708	0.1293	0.1389
Minimal calculated 5-day average SWH		0.1300	0.1427	0.1568
Deviation between observed and calculated 5-day average SWH	Maximal	1.6690	1.5245	1.5400
	Average	0.3423	0.3144	0.3256
	Standard deviation	0.3061	0.2817	0.3006
	Minimal	0.0007	0.0039	0.0017
Correlation coefficient (95% confidence)		0.7258	0.7149	0.7022

Table 1. General statistical parameters of calculated against observed SWH values

In order to validate the calculations satellite altimetry data was used. The altimeter products were produced and distributed by Aviso (http://www.aviso.altimetry.fr/), as part of the Ssalto ground processing segment. This data consists of 5-days averaged SWH values with a spatial resolution of 1°. Three offshore locations corresponding to nodes of the Aviso grid were selected for validation. Simulated SWH values at these locations were averaged over the same time periods as the Aviso data. Data corresponding to the entire year 2010 was selected for the validation.The comparison demonstrated that modelled SWH is usually somewhat lower than observed one – the average deviation between these values varies between

0.31 and 0.34 at various points. The overall patterns of observed and modelled SWH are similar – the mean correlation coefficient between AVISO and SWAN data is of 0.71. The mentioned deviations may be caused by the coarse resolution of the wind forcing and possible underestimations of reanalyzed wind speed values itself. Moreover, the relief surrounding the Black Sea also has an impact on the offshore wind conditions, which can be not represented in the reanalysis in the most accurate way. Similar modelling features with low-resolution forcing as the input are discussed by Akpinar et al. (2012).

RESULTS AND DISCUSSION

Maximal significant wave heights (SWH, over 6.5 m) as well as wave lengths (over 55 m) and periods (over 7 s) correspond to autumn and winter. Besides, areas with most expressed waves in winter correspond to the southwestern region of the Black Sea, whereas these areas in autumn – to the northeastern one. In spring and summer wind waves are not as intense as during other seasons – maximal SWH does not exceed 6 and 4.5 m, respectively. The area of most heavy storminess moves to the central parts of the sea and to the southern Crimean coast during these seasons.

The overall maximal wave parameter distribution is shown on Fig. 1. As already mentioned above, two areas with most expressed storminess are determined in the Black Sea – the south-western and the north-eastern ones.

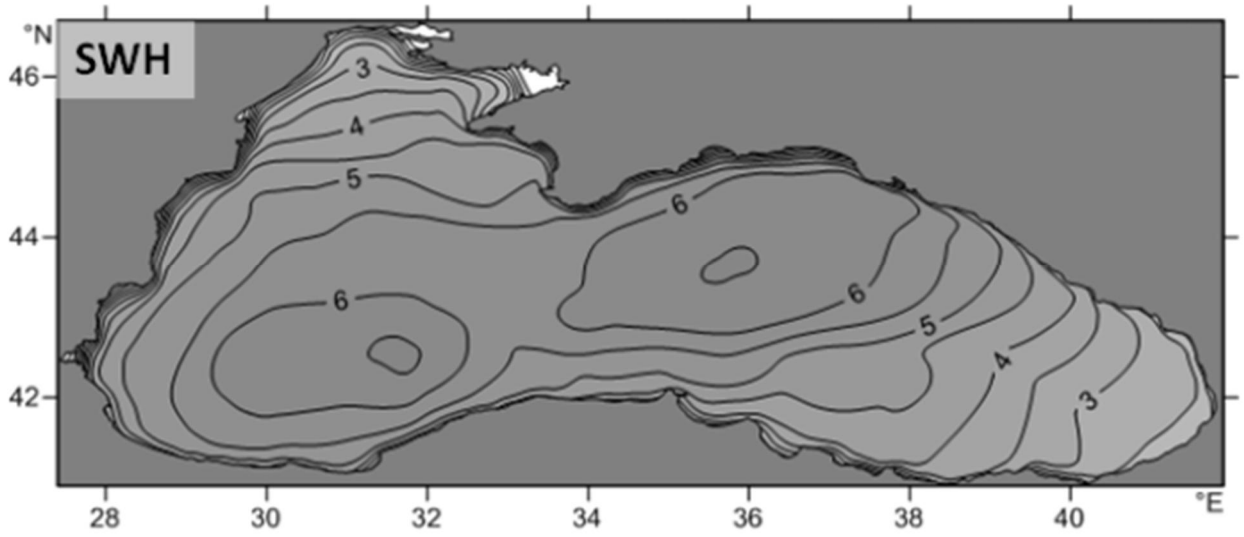

Figure 1. Maps of calculated significant wave height maxima [m].

The spatial distribution of the storminess intensity can be explained by the atmospheric circulation which is responsible for the wind pattern. There are two prevailing types of the large-scale sea level pressure (SLP) fields causing storms over the Black Sea (Surkova et al., 2013). These types are revealed by clustering analysis (k-means) from the set of SLP fileds only for storm days with SWH≥4 m. One SLP pattern is characterized by the trough of atmospheric pressure spreading from the eastern Mediterranean towards the Black Sea and often forming a local cyclone over the Black Sea. Its further movement to the north is blocked by the vast high pressure centre over Eastern Europe. Under the influence of the southern trough, northeasterly, easterly and southeasterly winds are predominant over the Black Sea. When an independent Black Sea cyclone is generated at the periphery of the trough, the pattern of wind direction over the sea is more complicated and can be opposite in different parts of the sea. For the second type, there is also a cyclone over the Black Sea or nearby, but the large-scale configuration of the atmospheric pressure field differs from the first regime. The appearance of the cyclone is accompanied by a quick propagation of a trough from Scandinavia and the Baltic Sea. At the same time, high atmospheric pressure

prevails to the west of the Black Sea region. Such a situation may lead to strong northwestern, western and south-western winds (Surkova et al., 2013).

Storm cyclones over the Black Sea are connected with the global atmosphere circulation patterns. A connection with the NAO index (November-March) shows that periods with the lowest NAO index are accompanied by higher storminess (Fig. 2). Thus, the correlation coefficients between the NAO index and the storm duration and quantity are -0.35 and -0.25, respectively. It may be interpreted as decreasing of the influence of Azor anticyclone's ridge over the Mediterranean and Black Sea giving the opportunity of local cyclones intensification.

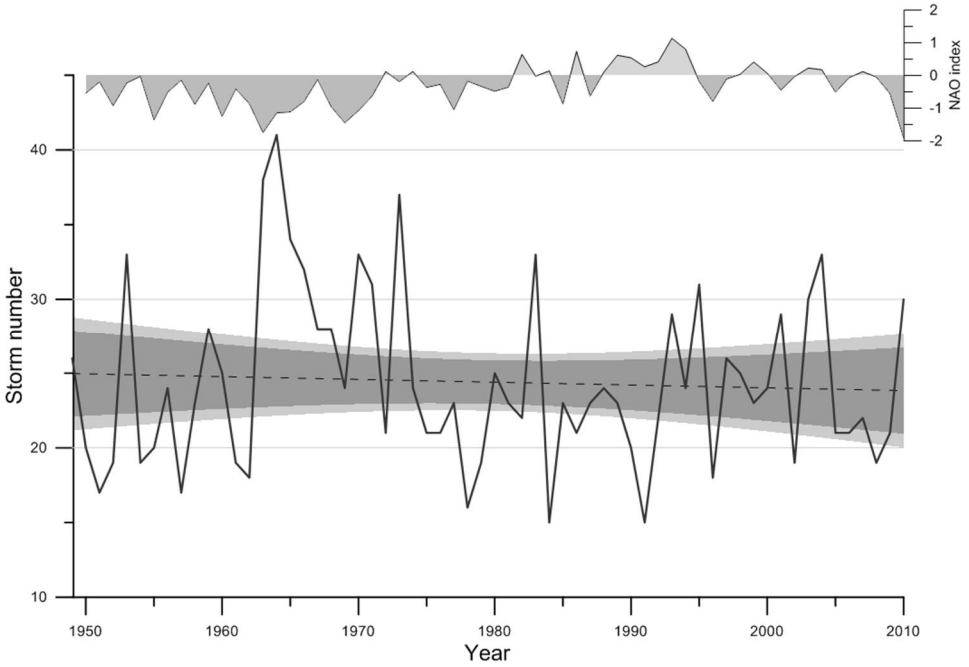

Figure 2. Interannual variability of storm events per year, its linear trend (-0,02 storms/year), 95% (dark grey) and 99% (light grey) confidence intervals.

The interannual variability of total storm duration and of the number of storms over the period 1949–2010 was analyzed. The linear trends of these series show a negligible decrease of both annual duration and quantity of storms – -0,62 h/year and -0,02 storms/year. At the same time it is possible to determine a period of relative high storminess in the Black Sea. This period spans from the early 1960-s until approximately the middle of the 1970-s. Other stormy years corresponding to negative NAO values are 1995, 2001, 2005 and 2010.

Such results generally match the data on storminess trends at the western coast of the Black Sea described in a research by Valchev et al. (2012), where also a decreasing trend of storminess activity is stated. Moreover, the alternation of relative calm and stormy periods as well as the increase of storminess in approx. 1960–1975 is a typical feature not only for the Black Sea, but also for other European seas, e.g. the North and Baltic seas as shown in (Matulla et al., 2008).

ACKNOWLEDGEMENTS

This work was supported by the Russian ministry of education and science under grant № G.34.31.0007 and by the Russian scientific foundation under grant №14-37-0 38.

REFERENCES

Akpinar, A., and Kömürcü M. I. (2012). Wave energy potential along the south-east coasts of the Black Sea, *Energy* **42**, 289-302, doi: 10.1016/j.energy.2012.03.057

Alekseev, D. V., Ivanov, V. A., Ivancha, E. V., Fomin, V. V., and Cherkesov, L. V. (2013). Estimation of the effect of protective piers on wind wave parameters in the Sevastopol Bay, *Russian Meteorology and Hydrology* **38**, No. 4, 248-255, doi: 10.3103/S1068373913040067.

Arkhipkin, V. S., Kosarev, A. N., Gippius, F. N., and Migali., D. I. (2013). Seasonal variations of climatic fields of temperature, salinity and water circulation in the Black and Caspian seas, *Moscow University Bulletin*, **5(5)**, 33–44 (in Russian).

Booij, N., Ris, R. C., and Holthuijsen, L. H. (1999). A third-generation wave model for coastal regions. 1. Model description and validation, *Journal of Geophysical Research* **140**, No. C4, 7649-7666.

Efimov, V.V., and Komarovskaya, O.I. (2009). Atlas of extreme wind waves in the Black Sea. EKOSI-Gidrofizika, Sevastopol (in Russian).

Gorrell, L., Raubenheimer, B., Steve Elgar, and Guza, R.T. (2011). SWAN predictions of waves observed in shallow water onshore of complex bathymetry, *Coastal Engineering* **58**, 510–516, 2011, DOI: 10.1016/j.coastaleng.2011.01.013

Ivanov, V. A., Fomin, V. V., Cherkesov, L. V., and Shul'ga, T. Ya. (2009). Influence of the Kerch Strait on surge phenomena and currents induced by cyclonic disturbances in the Sea of Azov, *Physical Oceanography* **19**, No. 4, 197–210, DOI: 10.1007/s11110-009-9051-9

Polonsky, A.B., Fomin, V.V., and Garmashov, A.V. (2011). Characteristics of wind waves of the Black Sea, *Reports of the National Academy of Sciences of Ukraine*, 8, 108–112 (in Russian).

Ris, R. C., Holthuijsen, L. H., and Booij, N. (1999). A third-generation wave model for coastal regions. 2. Verification, *Journal of Geophysical Research* **104**, No. C4, 7667-7681.

Rusu, E., Pilar. P, and Guedes Soares, C. (2008) Evaluation of the wave conditions in Madeira Archipelago with spectral models, *Ocean Engineering* **35**, 1357–1371, DOI: 10.1016/j.oceaneng.2008.05.007

Rzheplinkskij, G. (1969). Wind and Wave Atlas of the Black Sea. Gidrometeoizdat, Leningrad, 1969 (in Russian).

Simonov A.I. and Altman, E.N. (eds, 1989). Project 'The USSR seas'. Hydrometeorology and hydrochemistry of the USSR seas, Vol 4. Black Sea, No. 1: hydrometeorological conditions. Gidrometeoizdat, St. Petersburg, (in Russian).

Surkova, G.V., Arkhipkin, V.S., Kislov, A.V. (2013). Atmospheric circulation and storm events in the Black Sea and Caspian Sea, *Centr. Eur. J. Geosci.* **5(4)**, 548–559, doi: 10.2478/s13533-012-0150-7.

Valchev, N. N., Trifonova, E. V., and Andreeva, N. K. (2012). Past and recent trends in the western Black Sea storminess, *Natural Hazards and Earth System Sciences* **12**, 961-977, doi:10.5194/nhess-12-961-2012

Van Ledden, M., Vaughn, G., Lansen, J., Wiersma, F., and Amsterdam, M. (2009). Extreme wave event along the Guyana coastline in October 2005, *Continental Shelf Research* **29**, 352-361, DOI: 10.1016/j.csr.2008.03.010

Zijlema, M. (2010). Computation of wind-wave spectra in coastal waters with SWAN on unstructured grids, *Coastal Engineering* **57**, 267–277, DOI: 10.1016/j.coastaleng.2009.10.011

METHANE EMISSION FROM TUNDRA LAKES IN WESTERN SIBERIA

L.L. GOLUBYATNIKOV and V.S. KAZANTSEV

A.M.Obukhov Institute of Atmospheric Physics,
Laboratory of Mathematical Ecology, Moscow, Russia.

Keywords: METHANE EMISSION, LAKES, TUNDRA, WESTERN SIBERIA.

INTRODUCTION

Among the natural sources of methane, lakes are second in intensity of its emission into the atmosphere. The area of the global network of lakes is about 4.2×10^6 km^2 or about 3% of the surface area of continents (Downing *et al.*, 2006). Experimental studies shown that methane is emitted from lakes into the atmosphere continuously during the warm period when lakes are free of ice (Kling *et al.*, 1992). The intensity of methane emissions from lakes depends significantly on the reserves of organic matter at their bottoms: the methane emission is more intense from lakes whose bottom sediments are rich by the organic matter (Fedorov *et al.*, 2005; Golubyatnikov and Kazantsev, 2013).

The global methane emission from lakes is estimated at 8-50 MtCH_4/yr (Bastviken *et al.*, 2004; Anderson *et al.*, 2010), which is 4-24% of the global methane emission from natural sources. It should be noted that the methane emission from lakes exceeds that from the World Ocean surface, which is estimated at 5-7 MtCH_4/yr.

The biogeochemical processes of methane generation and oxidation in tundra lakes are yet not very well studied experimentally. The published studies show the estimates of methane emissions from tundra lakes in Alaska, northern European Russia, and north-eastern Russia. There is little published evidence for the methane fluxes from tundra lakes in Western Siberia. The aim of our research is to evaluate annual methane flux from tundra lakes in Northern Siberia from the experimental measurements.

METHODS

Field experiments were carried out in summer 2010 and 2013 at four sites located in the tundra zone of the Yamal-Nenets Autonomous Okrug: Yasavei (67°21'N, 78°54'E, southern tundra, 2010), Gyda (70°54'N, 78°32'E, boundary of arctic and typical tundra, 2010), Yarneto (67°22'N, 78°37'E, southern tundra, 2013), and Yarayakha (69°31'N, 77°06'E, typical tundra, 2013). Five lakes were studied at each site. These lakes are typical for the northwestern Siberia: shallow (1.5-2.5 m in depth), small in area (from 1000 m^2 to 1.8 km^2) with sandy–slimy and peaty bottoms.

We used static chambers with base size of 40×40 cm and height of 30 cm floated on water surface. The chambers had a light-reflecting coating. Each observation included collecting 4 samples in a 8-10 minute time step. The gas samples were taken using the syringes. Methane concentration in samples was analyzed using a gas chromatograph equipped with a flame ionization detector.

The annual emission of methane from the surfaces of lakes is calculated on the basis of the experimentally measured specific flux of methane, the area of lakes, and the length of the emission period. We chose the median value of the corresponding distribution as an estimate of the specific flux of methane from the lakes in each tundra subzone. On the basis of a hydrological map we determined lake areas for each tundra subzone. We determined the basic climate characteristics of the tundra subzones in Western Siberia on the basis of data obtained at meteorological stations located in the region under study.

CONCLUSIONS

Lakes of the tundra ecosystems of western Siberia occupy about 17×10^3 km^2, which is 5% of the area of the region under consideration. The largest portion of these lakes (about 6%) belongs to the typical tundra of Western Siberia. In arctic and southern tundra lakes occupy 3% and 5% of their areas, respectively.
In this work the period with a daily mean surface air temperature of not less than 5°C (vegetation period) is taken as a period of methane emission. According to meteorological data, the period of methane emission in the tundra zone of Western Siberia lasts from 67 to 100 days.

On the basis of experimental data we obtained that over the warm season the methane emission from tundra lakes in Western Siberia is about 14 $KtCH_4$ per year (Fig.1). Southern tundra lakes of Western Siberia make the main contribution (about 63%) to methane emissions from the region lakes. Contribution of arctic tundra and typical tundra lakes in methane emissions from the territory under study is about 4% and 33%, respectively.

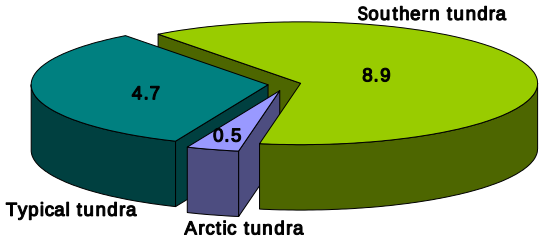

Figure 1. The annual methane emissions ($KtCH_4$) from tundra lakes of Western Siberia.

ACKNOWLEDGEMENTS

This work was supported by the Russian Foundation of Basic Research (projects 14-05-00193, 15-35-20533), the Basic Research Program (Department of Earth Sciences, Russian Academy of Sciences) "Impact of Modern Climate Change and Environmental on Processes in Atmosphere and Cryosphere".

REFERENCES

Anderson, B., K. Bartlett, S. Frolking, et al. (2010). *Methane and Nitrous Oxide Emissions from Natural Sources*, (EPA, Washington, DC).

Bastviken, D., J. Cole, M. Pace and L. Tranvik (2004). Methane emissions from lakes: dependence of lake characteristics, two regional assessments and a global estimate, *Global Biogeochem. Cycles* **18**, GB4009.

Downing, J. A., Y. T. Prairie, J. J. Cole, et al. (2006). The global abundance and size distribution of lakes, ponds, and impoundments, *Limnol. Oceanogr.* **51**, 2388-2397.

Fedorov, Yu. A., N. S. Tambieva, D. N. Gar'kusha and V. O. Khoroshevskaya (2005). *Methane in Water Ecosystems*, (Kopitsentr, Rostov-on-Don, Russia).

Golubyatnikov, L.L. and V.S. Kazantsev (2013). Contribution of tundra lakes in western Siberia to the atmospheric methane budget, *Izvestiya, Atmospheric and Oceanic Physics* **49,** 395-403.

Kling, G. W., G. W. Kipphut and C. Miller (1992). The flux of CO_2 and CH_4 from lakes and rivers in Arctic Alaska, *Hydrobiologia* **240**, 23-46.

Al SPECIATION IN MELTWATER ON RECLAMATION PLOTS NEAR A CU-NI-SMELTER (MODELLING AT DIFFERENT TEMPERATURES)

T.T. GORBACHEVA, S.I. MAZUKHINA, S.V. IVANOV and T.A. CHEREPANOVA

Institute of the North Industrial Ecology Problems, INEP, Akademgorodok, 14a, 184209, Apatity, Russia

Keywords: AL SPECIATION, MELTWATER CHEMISTRY MODELLING, AEROTECHNOGENIC LOAD, DIFFERENT TEMPERATURES.

INTRODUCTION

The Russian Arctic is known for numerous deposits of polymetallic ores (Dodin *et al.*, 2010). Among the issues dealt with in the national strategy of research and development in the Arctic, currently implemented as the Program «Arctic in the XXI century», an important one is forecasting of possible environmental impacts of resource development and proposing measures for land rehabilitation. The problem of land degradation is bound to be getting worse in view of expected urban growth on the area.

Notwithstanding the availability of technologies for reclamation of degraded land, reviewed by Mulligan *et al.* (2001) and Kapelkina (2012), the tough problem in the Arctic is lack of natural soil for replacing of contaminated soil. Among soil substitutes there should be considered compost, i.e. a soil-like substrate, obtainable from sewage sludge.

Although compost has proved effective in reclamation of land damaged by the metallurgical industry of Murmansk region (Kikuchi and Gorbacheva, 2006; Kikuchi *et al.*, 2006, 2011), it cannot be expected to perform as successfully in other Arctic and Subarctic regions. Research in this area is to take into account the local specifics such as features of the ecosystem, the soil nutritional regime, and the effect of low temperatures. Naturally, it should also involve a compilation of best practices of degraded land rehabilitation.

The forest ecosystems in the Arctic and Subarctic regions are mainly affected by local aerial technogenic contamination. Of these, the Kola Peninsula (66–70°N and 28°30'–41°30'E) is considered to be extremely polluted; its soil and ground vegetation degenerated to the extent of forming industrial barren land by depositing metal pollutants from copper-nickel smelters. The term «industrial desert (barren)» means bleak, open landscapes emerging around the point sources of industrial pollution by deposited airborne pollutants, with small patches of vegetation cover (usually about 10% or less relative to control) and surrounded by bare land with an illuvial horizon, or even bedrock, exposed as a result of intensive soil erosion (Kozlov and Zvereva, 2007).

Nowadays, the copper-nickel smelters on the Kola Peninsula are surrounded by dry, sandy and stony ground within a radius of 10–15 km. An experiment on remediation of disturbed forest land, aimed also at recovery of otherwise unusable sewage sludge, has been carried out on this industrial barren (67º51’N and 34º48’E) on an area of 4 ha. Forecasting of pollutants speciation and toxicity involved analysis of the chemical composition of meltwater, since the period of snow accumulation is long (up to 180 days of a year).

After snow melting, the entire substrate layer is drained with meltwater and is potentially subjected to contaminants accumulated in the snow cover. The problems addressed in this work were the following: (i) transformation of meltwater after reclamation with sewage sludge compost; (ii) redistribution of Al forms after the reclamation activities.

It should be noted that the Al concentration in meltwater on industrial barren, estimated within a decade of 1993 to 2014, did not exceed 50 μg l^{-1}, which is far from toxicity level. Thus, according to Sjöstedt et al. (2009), Al is toxic to phytoplankton at a concentration of 300 μg l^{-1} at pH 8.5. Nevertheless, we considered it important to study the Al speciation in meltwater because Al can form anionic complexes with heavy metals, which enhances the migration activity of the latter resulting in higher water toxicity with a possible impact on the biota.

METHODS

A description of sampling plots selecting and analysis of the snow cover chemistry on reclamation plots compared to original barren was reported in our earlier publications (Kikuchi and Gorbacheva, 2006). Snow cores were sampled in a pit wall using a plastic collector (plastic tube and restricting Plexiglas plate) and polyethylene bags. Increments varied from 15–20 cm to the entire profile height depending on snow density. Each increment was transferred from the plastic tube to a polyethylene bag and transported to a chemical laboratory in a frozen state. The samples were melted in a plastic basin in the laboratory, and then the volume of each sample was recorded.

Snow samples were directly analysed using the following techniques – potentiometry for determining H^+, atomic absorption spectrometry for determining Al, Fe, Ca, Mg, K, Mn, Zn, Ni, Cu, Na, ion-exchange chromatography for determining SO_4^{2-}, Cl^- and NO_3^-, colorimetry for determining Si and P, and C determination was carried out by permanganate and bichromate oxidation with COD (chemical oxygen demand) reactor (Hach Co., USA) followed by reagent residue titration. Metal concentrations were mainly determined by FI-AAS (by Perkin-Elmer 360, Perkin-Elmer USA and AAS-30, Carl-Zeiss Jena, Germany) due to high level. A Perkin-Elmer AAnalyst 800 atomic absorption spectrometer equipped with a THGA graphite furnace with Zeeman-effect background correction and autosampler AS 800 was used for elemental analyses in the case of metal concentration lower FI-AAS limit of detection. Argon was used as the purge gas. Stock solutions of metals as the nitrate (1000 mg l^{-1}) were prepared from Merck concentrates. Test solutions were prepared daily by the appropriate dilution of certified reference standard (Russia). Quality check of water analysis was carried out at our laboratory on the basis of the present control standards according to manuals of the International Co-operative Program on Assessment and Monitoring of Air Pollution Effects on Forests (operated by the United Nations Economic Commission for Europe).

A great number of methods existing for the fractionation of aqueous aluminium have been reviewed by Wickstrom *et al.* (2000). However, all of them feature a common drawback, namely, a possible redistribution of Al forms due to the use of a lot of chemical reagents. Besides, some of the Al forms cannot be recorded because their aqueous concentrations are below the detection limit. In this work we have made an attempt of physical-chemical modelling of meltwater to estimate the Al speciation.

The results of direct analytical determination are combined with those of physical and chemical modeling based on Selector program complex within the framework of an *Al-B-Br-Ar-He-Ne-C-Ca-Cl-F-K-Mg-Mn-N-Na-P-S-Si-Sr-Cu-Zn-H-O-e* system (Karpov, 1981). The input to Selector program included pH, temperature and determined concentrations of Al, Fe, Ca, Mg, K, Mn, Zn, Ni, Cu, Na, SO_4^{2-}, Cl^-, NO_3^-, Si, P and C. In the test region, the annual mean temperature is about -1ºC, the maximum temperature (~15ºC) is generally recorded in July, and snowmelt takes place during April to June. Since modelling was applied to snowmelt in a cold region, we varied the temperature input data from 25^0C (the temperature of analytical determination) to 5^0C (the biological active temperature limit). Al speciation was modelled at 25^0C, 10^0C and 5^0C and the obtained results are given in Table 2. Moreover, the Selector made possible the *Eh* modelling as well.

CONCLUSIONS

The chemical contents of meltwater on original barren and reclamation plots have been found to differ considerably (Table 1) due to different mineralization of snow cover caused by the following factors:

1) Liming with dolomite (Ca, Mg) on reclamation plots to diminish the uptake of heavy metals;
2) Salination of reclamation plots with NaCl used for deicing of a nearby motorway;
3) Proximity of reclamation plots to a Cu-Ni-smelter (about 3 km from emission source) resulting in higher SO_4^{2-} concentration;
4) Dusting from eroded area adjoining the Cu-Ni smelter, resulting in higher Al and Fe concentrations.

Parameter	Unit	Plots	
		Industrial barren	Reclamation
pH		5.19	5.15
Ca	mg l^{-1}	0.59	**3.92**
Mg	mg l^{-1}	0.15	**0.55**
K	mg l^{-1}	0.05	0.75
Na	mg l^{-1}	0.70	**22.46**
NH_4^+	mg l^{-1}	0.43	0.19
Al	mg l^{-1}	0.002	**0.029**
Fe	mg l^{-1}	0.001	**0.08**
Mn	mg l^{-1}	0.002	0.05
Zn	mg l^{-1}	0.003	0.09
Ni	mg l^{-1}	0.281	1.04
Cu	mg l^{-1}	0.026	1.03
P	mg l^{-1}	0.005	0.01
SO_4^{2-}	mg l^{-1}	1.96	**15.05**
NO_3^-	mg l^{-1}	0.63	0.10
Cl^-	mg l^{-1}	2.02	**45.16**
C	mg l^{-1}	0.77	0.71
Si	mg l^{-1}	0.05	0.23

Table 1. Meltwater chemistry

Irrespective of differences between the plots, the distribution of Al forms there was noted to be similar. As shown by the Al speciation data, this element migrates with meltwater mainly as $Al(OH)^{2+}$ (about 47%) and Al^{3+} (about 30%). Kinetic studies of chemical speciation by the Chelex-100 batch technique have revealed that, in snow, aluminum is present both as aqua ions and as simple complexes of inorganic ligands, whereas in surface water it is probably bound to macromolecule complexants and/or colloidal substances (Lu *et al.*, 1994). Since the concentration of organic matter in meltwater is low, the Al organic-mineral compounds can only form after the water penetrates through the soil-like substrate. The share of positive ions of Al ($Al(OH)_2^+$, $AlSO_4^+$) in meltwater did not exceed 20% in total. Neutral forms of Al ($Al(OH)_3^0$, $HAlO_2^0$) were always in very low concentrations.

The results of Eh modelling were essentially different. In all cases Eh of meltwater on reclamation plots was negative (about -100 mV). This may have been caused by the presence of reducing agents, such as ammonia, organic acids, and carbohydrates, in the snow cover of reclamation plots. Their source could be artificial ground with sewage sludge as base. Probably, there is another reducing agent, namely SO_2, which is a major component of Cu-Ni smelter emissions.

Parameter	*Plot with reclamation measures* *Temperature*			Control plot (25°C)
	25°C	10°C	5°C	
pH	5.15	5.25	5.30	5.19
Eh, V	-0.09	-0.08	-0.08	0.91
Speciation		*%*		
AlO_2^-	0.14	0.01	0.01	0.21
$Al(OH)^{2+}$	47.38	37.06	32.36	47.73
$Al(OH)_2^+$	14.64	5.26	3.55	16.94
$Al(OH)_3^0$	2.01	0.30	0.15	2.66
$Al(OH)_4^-$	0.11	0.01	0.01	0.16
$AlSO_4^+$	0.01	0.01	0.01	0.03
$Al(SO_4)_2^-$	*	*	*	*
Al^{3+}	32.82	56.84	63.66	28.49
$HAlO_2^0$	2.91	0.50	0.26	3.78

* - less 0.01%

Table 2. Al speciation (%) in meltwater

As has been revealed by modelling, lower temperatures tend to increase the meltwater pH on reclamation plots (from 5.15 at 25°C to 5.30 at 5°C). Apparently, this results from decreasing of Al compounds hydrolysis ($Al^{3+} + H_2O = Al(OH)^{2+} + H^+$). A similar explanation can be offered for the tendency to Al forms re-distribution in response to temperature decrease. For instance, the share of Al monomeric forms increases from 33% at 25°C to 64% at 25°C for Al^{3+}. There is no evidence of the effect of temperature lowering on *Eh*.

The obtained data are of practical importance for predicting of both changes in migratory activity of pollutants under conditions of decreasing aerotechnogenic load, which is now being observed on the Kola Peninsula, and possible effects of reclamation activities in the Arctic zone.

ACKNOWLEDGEMENTS

This research project is supported by Monchegorsk Forestry Enterprise and Severonikel Company, and organized by the Institute of the North Industrial Ecology Problems of the Russian Academy of Sciences (RAS). A part of the work was supported by the RAS Program «Fundamental Scientific Research for the Development of the Arctic Zone of the Russian Federation». The authors also wish to thank Mrs. N.I. Nikolaeva for English review.

REFERENCES

Dodin D.A., Kaminsky V.D., Zoloev K.K., Koroteev V.A. (2010): A strategy of assimilation and study of Russian Arctic and Subarctic mineral-product base in condition of passage to steady development. *Litosphere,* **6**, 3–24. (in Russian)

Kapelkina L.P. (2012): Natural revegetation and remediation of disturbed lands of the North. *Advances in current natural sciences,* **11**, 98–102. (in Russian)

Karpov I.K. (1981) Physical and chemical computer modelling in geochemistry. Novosibirsk: Nauka, 247. (in Russian)

Kikuchi R. and Gorbacheva Tamara T. (2006) Vegetation Recovery after Environmental Damage by Metallurgic Industry in the Arctic Region: Transformation of Soil Chemistry in Restored Land. *Conservation and Recycling of resources: New Research.* New York: Nova Science Publishers. Editors: Christian V. Loeffe. ISBN: 1-60021-125-9, 93–118.

Kikuchi R., Gorbacheva T.T. and Gerardo R.(2011): Application of phytoremediation from experimental stage to practical stage: comparative study in the southern part and the northern part of the

European region. *Handbook of Phytoremediation.* Editors: Ivan A. Golubev. ISBN: 978-1-61728-753-4. NY: Nova Science Publishers, Chapter 2, 613–630.

Kikuchi R., Gorbacheva T.T., Gerardo R. (2006): A pilot-scale example of phytoremediation in the arctic area: comparison of zones placed at different distances from a metal emission source. *Environmental biotechnology*, **2**, 37–45.

Kozlov M.V., Zvereva E.L. (2007): Industrial barrens: extreme habitats created by non-ferrous metallurgy. *Rev Environ Sci Biotechnol*, **6**, 231–259.

Lu Y., Chakrabarti C.L., Back M.H., Grégoire D.C., Schroeder W.H. (1994): Kinetic studies of aluminum and zinc speciation in river water and snow. *Analytica Chimica Acta*, **293**, 95–108.

Mulligan C.N., Yong R.N., Gibbs B.F. (2001): Remediation technologies for metal-contaminated soils and groundwater: an evaluation. *Engineering Geology*, **60**, 193–207.

Sjöstedt C., Wällstedt T., Gustafsson J.P, Borg H.(2009): Speciation of aluminium, arsenic and molybdenum in excessively limed lakes. *Science of The Total Environment*, **407**, 5119–5127.

WEB-GIS BASED VIRTUAL RESEARCH ENVIRONMENT FOR NORTH EURASIA CLIMATIC STUDIES

E.P. GORDOV[1], V.N. LYKOSOV[2] and V.N. KRUPCHATNIKOV[3]

[1]Institute of Monitoring of Climatic and Ecological Systems SB RAS and Tomsk State University, Tomsk, Russia.

[2] Institute of Numerical Mathematics RAS and MSU Research Computing Center, Moscow, Russia.

[3]Siberian Research Institute of Hidrometeorology, Novosibirsk, Russia.

Keywords: VIRTUAL RESEARCH ENVIRONMENT, WEB-GIS, REGIONAL CLIMATE CHANGE.

INTRODUCTION

Volumes of environmental data archives are growing immensely due to recent models, high performance computers and sensors development as well as due to initiation of a set of large scale complex global and regional climatic studies. It makes impossible their comprehensive analysis in conventional manner on workplace using in house computing facilities, data storage and processing software at hands. One of possible answers to this challenge is creation of virtual research environment (VRE), which should provide a researcher with an integrated access to huge data resources, tools and services across disciplines and user communities and enable researchers to process structured and qualitative data in virtual workspaces [1]. VRE should integrate data, network and computing resources providing interdisciplinary climatic research community with opportunity to get profound understanding of ongoing and possible future climatic changes and their consequences. Presented are first steps and plans for development of virtual research environment prototype [2] as an element of future environmental VRE aimed at regional climatic and ecological monitoring and modeling as well as at continuous education and training support.

METHODS

Georeferenced datasets are currently actively used for modeling, interpretation and forecasting of climatic and ecosystem changes on different spatial and temporal scales. Due to inherent heterogeneity of environmental datasets as well as their huge size (up to tens terabytes for a single dataset) a special software supporting studies in the climate and environmental change areas is required [2].

Recently developed experimental software and hardware platform Climate (http://climate.scert.ru/) is used as an approach test bench. VRE under development will integrate on the base of geoportal distributed thematic data storage, processing and analysis systems and set of models of complex climatic and environmental processes run on supercomputers. VRL specific tools are aimed at high resolution rendering on-going climatic processes occurring in Northern Eurasia and reliable and found prognoses of their dynamics for selected sets of future mankind activity scenaria.

Currently VRE prototype is accessible via developed geoportal at the same link (http://climate.scert.ru/) and integrates the WRF and «Planet Simulator» models, basic reanalysis, instrumental measurements data and support profound statistical analysis of storage and modeled on demand data. In particular, one can run the integrated models, preprocess modeling results data, using dedicated modules for numerical processing perform analysys and visualize obtained results. New functionality recently has been added to the statistical analysis tools set aimed at detailed studies of climatic extremes occurring in Northern Asia.

Dedicated information-computational environment for supporting climate services, including integrated analysis, visualization and dissemination of heterogeneous georeferenced climatological and meteorological data, is presented. It is based on combination of Web and GIS technologies according to Open Geospatial Consortium (OGC) standards, and involves many modern solutions such as object-oriented programming model, modular composition, and JavaScript libraries based on GeoExt library (http://www.geoext.org), ExtJS Framework (http://www.sencha.com/products/extjs) and OpenLayers software (http://openlayers.org).

The main advantage of the system lies in it's capability to perform integrated analysis of time series of georeferenced data obtained from different sources (in-situ observations, model results, remote sensing data) and to combine the results in a single map [3, 4] as WMS and WFS layers in a web-GIS environment. Also analysis results are available for downloading as binary files from the graphical user interface or can be directly accessed through web mapping (WMS) and web feature (WFS) services for a further processing by a user. Data processing is performed on distributed computational cluster comprising data storage systems and corresponding computational nodes.

Several geophysical datasets represented by NCEP/NCAR Reanalysis II, JMA/CRIEPI JRA-25 Reanalysis, ECMWF ERA-40 Reanalysis, ECMWF ERA Interim Reanalysis, MRI/JMA APHRODITE's Water Resources Project Reanalysis, DWD Global Precipitation Climatology Centre's data, GMAO Modern Era-Retrospective analysis for Research and Applications, reanalysis of Monitoring atmospheric composition and climate (MACC) Collaborated Project, NOAA-CIRES Twentieth Century Global Reanalysis Version II, NCEP Climate Forecast System Reanalysis (CFSR), meteorological observational data for the territory of the former USSR for the 20th century, results of modeling by global and regional climatic models, and others are available for processing by the system.

VRL is also supporting thematic educational courses for students and post-graduate students of the Tomsk State University [5]. In particular, it allow students to perform on-line thematic laboratory work cycles on the basics of analysis of current and potential future regional climate change using Siberia territory as an example. We plan to expand the integrated models set and add comprehensive surface models.

CONCLUSIONS

VRL under development should provide specialists involved into multidisciplinary research projects with reliable and practical instruments for integrated research of climate and ecosystems changes on global and regional scales. With its help even a user without programming skills would be able to process and visualize multidimensional observational and model data through unified web-interface using a common graphical web-browser.

ACKNOWLEDGEMENTS

This work is partially supported by SB RAS project VIII.80.2.1, RFBR grants 13-05-12034 and 14-05-00502.

REFERENCES

1. Xiaobo Yang and Rob Allan (2006). Web-Based Virtual Research Environments (VRE): Support Collaboration in e-Science. *In* Proc. 2006 IEEE/WIC/ACM international conference on Web Intelligence and Intelligent Agent Technology (WI-IATW '06), Hong Kong (IEEE Computer Society, Washington DC), 184.
2. Gordov E.P., Lykosov V.N., Krupchatnikov V.N., Okladnikov I.G., Titov A.G., Shulgina T.M. (2013) *Computational and information technologies for monitoring and modeling of climate changes and their consequences,* (Nauka, Siberian branch, Novosibirsk, Russia).

3. T.M. Shulgina, E.P. Gordov, I.G. Okladnikov, A.G., Titov, E.Yu. Genina, N.P. Gorbatenko, I.V. Kuzhevskaya,A.S. Akhmetshin. (2013). Software complex for a regional climate change analysis, *Vestnik NGU. Series: Information technologies* **11**, Issue 1, 124.
4. I.G. Okladnikov, A.G. Titov, T.M. Shulgina, E.P. Gordov, V.Yu. Bogomolov, Yu.V. Martynova, S.P. Suschenko,A.V. Skvortsov (2013). Software for analysis and visualization of climate change monitoring and forecasting data, *Numerical methods and programming*, **14**, 123.
5. Yu.E. Gordova, E.Yu. Genina, V.P. Gorbatenko, E.P. Gordov, I.V. Kuzhevskaya, Yu.V. Martynova , I.G. Okladnikov, A.G. Titov, T.M. Shulgina, N.K. Barashkova (2013). Support of the educational process in modern climatology within the web-GIS platform «Climate», *Open and Distant Education*, **1(49)**, 14.

THE ROLE OF ANTHROPOGENIC ACTIVITIES IN CO2 AND CH4 EMISSION FROM SOIL TO ATMOSPHERE IN POLAR REGIONS OF EAST EUROPE

S.V.GORYACHKIN[1], D.V.KARELIN[1,2], A.V.DOLGIKH[1], D.I.LYURI[1], V.A.SHISHKOV[1] and E.P.ZAZOVSKAYA[1]

[1]Institute of Geography, Russian Academy of Sciences,
Staromonetny 29, Moscow, 119017, Russia.

[2]Department of Biology, Lomonosov Moscow State University, Moscow, Russia.

Keywords: CO2 EMISSION, HUMAN-INDUCED CHANGE, SPITSBERGEN, NORTHERN REGIONS OF RUSSIA.

INTRODUCTION

Nowadays, the global dangerous situation is related to the combination of two processes acting in one direction - climate warming and anthropogenic warming based on positive feedback from the output of the carbon balance (primarily CO2). At the same time, the role of specific types of anthropogenic impacts (plowing, fire, grazing, trampling, transport, chemical pollution and others) remains unclear. That can be estimated now only locally. The fragile character of the Arctic ecosystems with respect to both climate and anthropogenic factors is related to their functioning in condition of both extreme temperature and moisture content. The most convenient and the fastest way to integrated assessment of the functional state of natural ecosystems is the measurement of CO2 (and/or CH4) - emissions. In contrast to the climate impact assessment, to identify the anthropogenic contribution the short-term measurements of C-flows in different types of impacts are sufficient. Soil emission is about 70-80% of ecosystems' gross "breath" and largely determines the overall C-balance. This component is much easier and faster to be measured than the productivity and relevant calculation.

METHODS

The authors carried out 421 measurement of carbon dioxide emissions from the soil surface in the arctic tundra (Spitsbergen), south-tundra and northern taiga subzones of the European part of Russia with continuous and discontinuous permafrost. Since the measurements were carried out at different points, and almost simultaneously by the same method (Karelin, Zamolodchikov, 2008), it is possible to compare the absolute values of CO2 fluxes between them.

The method is based on direct measurements of CO2 by gas analyzer. On all the plots, opaque plastic cylinders (chambers) of 11.5 cm in the inner diameter were inserted into the soil to a depth of 5–10 cm and left there for two hours before the measurements. The time of separate measurements was about 1–3 min. An infrared closed_path gas analyzer LI_COR 6200 (Lincoln, Nebraska USA) was used. This analyzer gives estimates of the CO2 flux with an accuracy of 0.1 ppm in the range from 0 to 2000 ppm.

The flow of methane was measured by accumulative method on site for 1 -3 hours by gaseous chromatography.

The soil temperature (at the depth of 10 cm) and air temperature (0.5 m above the soil surface at each of the base cylinders) were determined with a portable electronic thermometer Checktemp_1 (the accuracy of 0.1°C; temperature range from –50 to +150°C) produced by Hanna Instruments. The volumetric soil water content inside the cylinders was measured with a field reflectometer HH2 Moisture Meter equipped with a ThetaProbe ML2x sensor (±1% accuracy) produced by Delta_T Devices Ltd. Each time, the volume of the

closed chamber was carefully measured with an accuracy of about 1 cm3. It was possible to include all the major well-known specific types of human impact to measure emissions in those geographic areas.

RESULTS

The measurements of carbon dioxide emissions from soils in the northern taiga (key plot "Pinezhsky" 64° 40 'N), tundra and southern shrub tundra (key plot "Naryan-Mar" 67°40' N and "Vorkuta" 67° 20 'N zone of sporadic permafrost), as well as in the Arctic tundra (key plot "Svalbard" 78°04' N, continuous permafrost zone) showed that local anthropogenic factors essentially change the soil carbon fluxes. Depending on the type of land use there can be observed an increase or decrease in emissions compared to its background levels in similar local ecosystems unaffected by human activity.

Thus, an increase in soil respiration values (from +17 to + 124%) in the northern taiga is typical for residential (settlement) areas, well fertilized recent vegetable gardens (age less than 20 years of development), garden with age more than 100 years of development, anthropogenic grasslands (fallows functioning as meadows). Reduction of soil respiration values was typical for recent gardens with no manure amendments (-11%) and forest fellings (-87%). On average, this increases the emission in this region at the same time increasing its variance (Fig. 1, 2).

For the southern tundra the increase of soil emission of CO2 in comparison with the natural background - +34% (peat palsas) to + 130% (settlement) noted in residential landscapes, reindeer grazing areas and in shrub-moss-lichen tundra on peat palsas. As a result, the reindeer grazing in the shrub-moss lichen tundra on loams and sands there is a decrease (-7% (on loam) to -61% (in the sand) of soil CO2 emissions. The similar results were obtained for the site "Vorkuta" for other forms of anthropogenic activity.

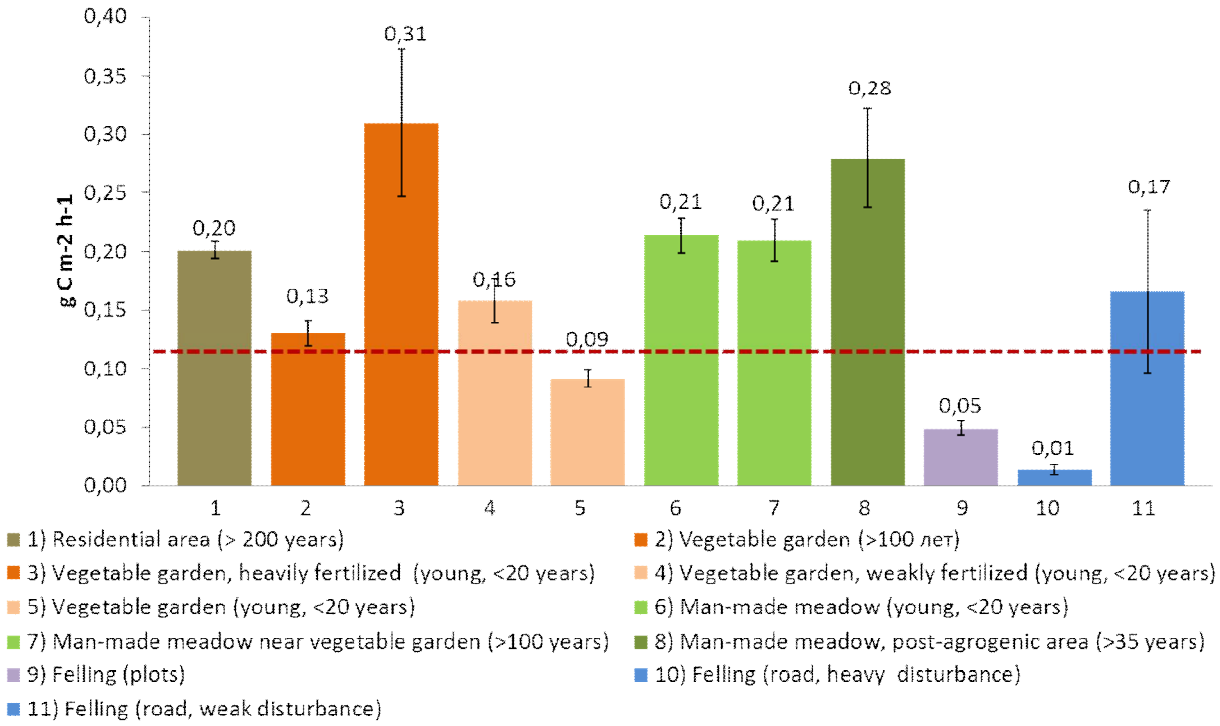

Fig. 1. Soil emissions of carbon dioxide (mean and standard error). Northern taiga subzone, a key plot "Pinezhsky" (N = 100, July - August 2014). As background biotope or control (see dotted line) shows the average level of emissions in spruce forest with *Polytrichum* and *Sphagnum* (0.13 g C m-2 h-1) and pine forest with *Cladina* (0.12).

In the sub-Arctic tundra able to assess the impact of a new kind - emission from the surface mine dumps (after coal mining). Arctic tundra subzone feature is that, on average, equally low background flows of CO2 emissions in the southern tundra, under the influence of specific human factors almost always been a shift in the direction of increasing emissions. Somewhat unexpected from these data similarity of background soil emissions and in the southern Arctic tundra may explains how well-known conservative soil emissions in general and local fertilizer Arctic landscape with coal dust as a result of many years of coal mining (additional inflow of nutrients).

The average value of anthropogenic emissions is proportional to its natural zoning background. In the northern taiga, where it is higher than in the tundra, the anthropogenic flows also, on average, are higher (Fig. 1, 2). However, as can be seen from the same figure, human factors and lead to a significant (and similar in these areas) increase the spatial dispersion of background threads. As in the case of the northern taiga and tundra of various types, the differences between the mean values of natural (background) and anthropogenic sources are significant. In the case of tundra landscapes the degree of enhancement of soil emission at equal dispersion is higher.

The highest values of CO2 emissions in the tundra zone (even compared to the most active on this indicator shrub hollows) were detected in industrial and settlement areas - in villages (0.241), coal tailings (0.235 g C m-2 h-1), as well as in areas of flooding along acting (0.220) and abandoned (60 years ago) railways (0.213). These values reach maximum emissions, which are recorded in the warmer climates of northern taiga. In the case of "natural" ornithogenic fertilizer in a soil under bird colonies in the tundra there can be achieved levels of 0.154 g C m-2 h-1, almost equal to the average level of emissions at a settlement in this area (0.164). This is the maximum we know the level of natural emissions.

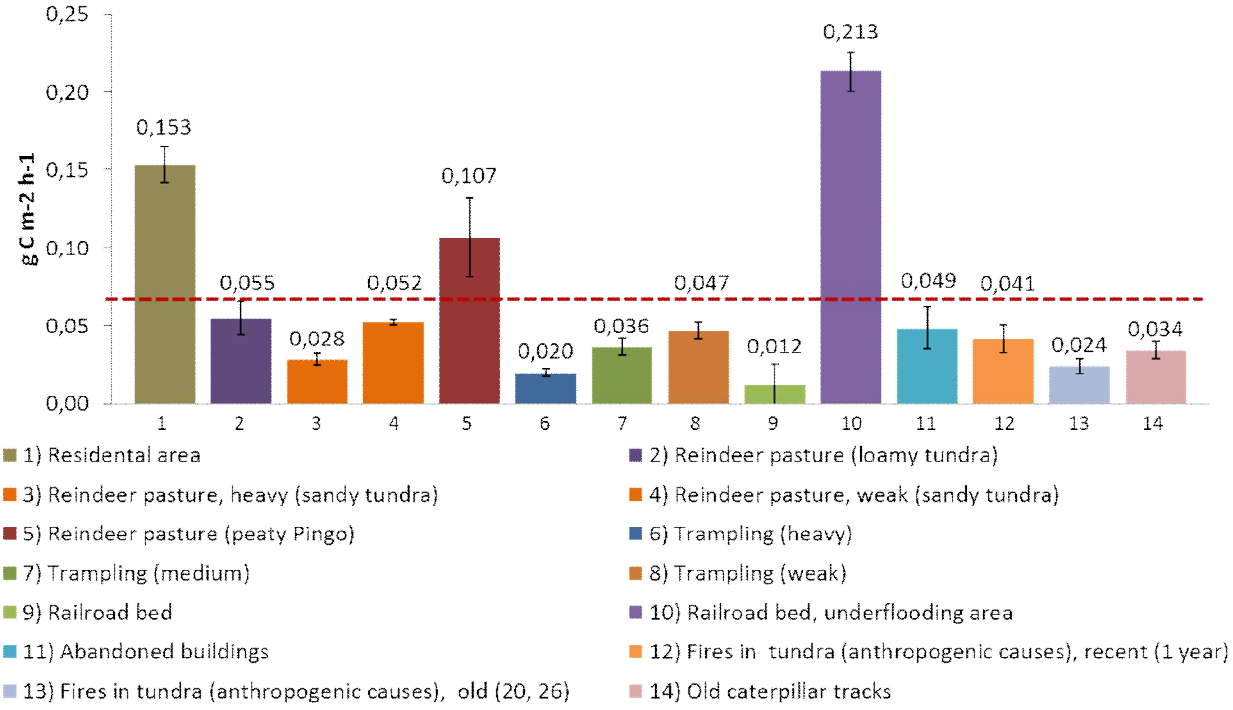

Fig. 2. Soil carbon dioxide emissions. Tundra, key areas "Naryan-Mar" (July-August 2014, N = 107) and "Vorkuta" (July-August 2014 N = 109). The average level of emissions in the three main types of the southern dwarfshrub, dwarfshrub- moss and lichen tundras (0.063 ± 0.01 g C m-2 h-1) was taken as background biotope or control (see dotted line).

In the case of flooding the cause of high emissions is the direct consequences of positive feedbacks: "protection from winter winds by a railway mound - an increase of snow cover depth - insulation and protection of the aerial parts of wintering plants - a gain of phytomass - increased respiration of roots and soil microbiota – growing of the observed emission". This is the famous "refuge effect", which is always observed in the tundra of different types, in the low-level mesorelief under a thick layer of snow, however in this case the anthropogenic factors behave as a magnifier of emissions. It can be considered as positive phenomenon as reinforced soil emission is a by-product effect of increasing of primary production, including roots, respiration which correlates with their weight, and the respiration of soil microbiota, in turn, depends on the activity of the roots (Karelin, Zamolodchikov, 2008).

The second group of anthropogenic factors leading to increased emissions is related to amendments of organic fertilizers or waste (kitchen gardens, fertilized grasslands, landfills, locations of fur farms and so on.) It gives a "negative" effect because it only contributes to the growth of the emissions not accompanied by carbon sequestration.

The suppression of emission level by anthropogenic factors (2-12 times in comparison with the background) is also often observed. In all cases it concerns to destruction of vegetation due to different specific reasons (felling and forest fires in the northern taiga, fire, trampling impacts of transport, reideer grazing in tundra and so on.). This extremely broad group of the observed forms of anthropogenic impact leads to a reduction of soil emissions in two ways: by reducing of primary production (physical destruction of vegetation), and the suppression of the actual process of soil degradation (deterioration of water and air conditions the root and microbial respiration, and soil fauna). It is also negative in its effects factors that help to reduce both CO2 fixation and growth of its emissions.

Anthropogenic changes in flows of methane were measured in the southern tundra (section "Vorkuta", July-August 2014). Note that we accept sinks and sources of these gases in the aboveground vegetation insignificant, so their soil fluxes in this case are considered as net carbon fluxes (net flux).

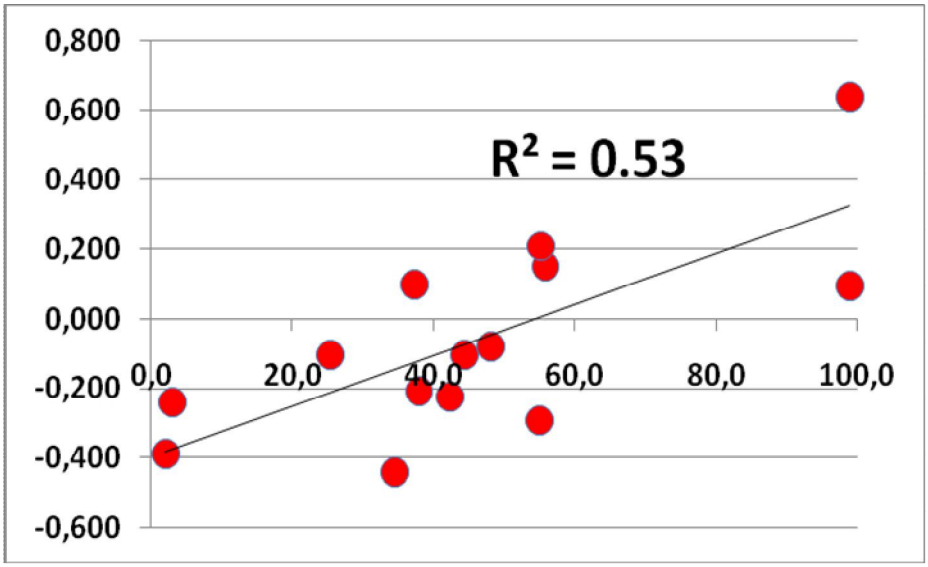

Fig. 3. Correlation of soil methane fluxes observed with the bulk soil moisture in all surveyed habitats (section Vorkuta, July 2014). Negative values indicate the flow, positive - the source for the atmosphere. Line and the coefficient of determination are linear regression.

Simultaneous measurements of methane fluxes, the second in importance after CO2 atmospheric carbon-containing gas, have shown that background relief hydromorphic depressions that normally are sources of

CH4 to the atmosphere (+0.64 mg C-CH4 m-2 day-1), in anthropogenically-modified objects are its weaker sources (+0.1: +0.2) or weak sinks with a mean of -0.15 mg C-CH4 m-2 day-1, whereas hills and microhighs, compared to the control, do not change the direction on the balance of methane, staying or sinks for the same quantity of flow (-0.22 and -0.16), or even increasing the flow (-0.4 g; burnt tundra in 2013). Only in 3 out of 14 habitats of methane fluxes did not differ significantly from zero.
Flows from the soil anthropogenic methane factors influenced mainly depending on the particular hydromorphous plot (Fig. 3). At the same time, more hydromorphic areas inhibited methane emissions, and more dry - enhances the sink. On average, under the influence of anthropogenic factors there has been a shift in the direction of reducing emissions or enhancing the flow of methane (positive effect).

So, our data from the tundra showed that there were not only sources of methane, but it sinks – and it is not an artifact. As shown by measurements of methane in the boreal wetland habitats (Glagolev et al., 2011), on the bogs of drier sites also seen preferential sink due to the greater activity of aerobic methanotrophic bacteria compared with the dominance of anaerobic methanogenic bacteria in the underwater part of peat layer. The presence of classical positive linear relationship between soil moisture and methane flux (Fig. 3) - further confirms the accuracy of the data.

CONCLUSIONS

The measurements of carbon dioxide emissions in the northern taiga, southern shrub tundra and arctic tundra showed that local anthropogenic factors lead to significant changes in carbon fluxes in this case. It may be, as an increase or decrease in emissions compared to background levels in similar local ecosystems unaffected by human activity. Depending on the combination of these factors, it can be described as the gain (or more fertilized accumulative cell) or decrease of CO2 emissions (mainly due to suppression of primary production). As for CH4, under the influence of anthropogenic factors there has been a shift in the direction of reducing emissions or enhancing the flow of methane (positive effect)

ACKNOWLEDGEMENTS

This work was supported by the Program "Searching basic studies for the development of the Arctic zone" of the Presidium of the Russian Academy of Sciences.

REFERENCES

Glagolev, M., I. Kleptsova, I. Filippov, S. Maksyutov, T. MacHida (2011). Regional methane emission from West Siberia mire landscapes, *Environmental Research Letters*. **6** (4), 045214
Karelin, D.V. and D.G. Zamolodchikov (2008). *Uglerodnyi obmen v kriogennykh ekosistemakh* (Carbon Exchange in Cryogenic Ecosystems), (Nauka,Moscow).

TOWARDS GLOBAL CHANGE MEASUREMENT NETWORK

HARI, P.[1], PETÄJÄ, T.[2], BÄCK, J.[1], KERMINEN, V.-M.[2], LAPPALAINEN, H.K.[2,3], VIHMA, T.[3], LAURILA, T.[3], VIISANEN, Y.[3],VESALA, T.[2] AND KULMALA, M.[2]

[1]Department of Forest Sciences, University of Helsinki, Finland

[2]Department of Physics, University of Helsinki

[3]Finnish Meteorological Institute, Helsinki, Finland

ABSTRACT

Anthropogenic emissions and actions are rapidly changing the global environment. These activities modify atmospheric aerosol and greenhouse gas concentrations resulting in regional and global climate change and disturbing food and fresh-water security. We outline the design of a global, hierarchical observation network that provides tools to tackle the inter-connected environmental and societal challenges, we are facing. The design relies on physical conservation laws of mass, energy and momentum, as well as on concentration gradients as drivers for the atmosphere-biosphere mass and energy exchange. The hierarchical network is composed of three level stations, i.e. (i) standard, (ii) flux/advanced and (iii) flagship stations. The standard stations are quite simple and the flagship stations are complicated and they utilise the cutting edge measuring techniques. There are very different ecosystems on the globe and measuring stations on each ecosystem type should take into consideration the special features of the ecosystems. The problems caused by the large scale, heterogeneity and complexity of the ecosystems should be solved in the planning of the network. The most comprehensive flagship stations allow the process-level understanding that can be expanded to continental and global scales with flagship and standard stations. In addition, advanced data analysis, earth system modelling and satellite remote sensing are needed to apply the results obtained at flag ship stations on the global level.

REGIONAL GREENHOUSE GAS BUDGETS OF NORTHERN EURASIA AS INFERRED FROM IN SITU OBSERVATIONS AND FROM SPACE

M. HEIMANN[1], C. RÖDENBECK[1], T. NUNEZ RAMIREZ and J. MARSHALL[1]

[1] Max-Planck-Institute for Biogeochemistry, Hans-Knöll-Str. 10, D-07745 Jena, Germany.

Keywords: Carbon cycle, carbon dioxide, methane, biogeochemistry.

INTRODUCTION

Currently, only about 50% of the CO_2 emitted from the burning of fossil fuels and from changes in land use accumulate in the atmosphere. The remainder is taken up by ocean and land in about similar proportions. A significant fraction of the terrestrial component of this sink is located in the extratropical northern hemisphere (Tans *et al.* 1990), however, the most important regional locations of this "northern hemisphere" sink are still very much uncertain. Locating and quantifying this sink, determining its controls and how it develops over time is a pressing question in Earth System science. Will warmer temperatures lead to longer vegetation periods and thus enhanced CO_2 uptake? or will warmer temperatures enhance soil respiration and turn the sink in the future into a net source? And what will be the contribution from the vast carbon stored in a thawing permafrost? What is the contribution of CH_4 emissions from boreal wetlands, from biomass burning and from fossil gas mining? Current models of terrestrial ecosystems show vastly different patterns of CO_2 uptake in Europe and in particular in boreal Eurasia. Answering these question requires a regional observation strategy, consisting of in situ measurements in key ecosystems, e.g. with eddy covariance flux towers, which are combined with high-precision atmospheric concentration measurements of the greenhouse gases, measured at remote stations, tall towers and/or from space.

METHODS AND RESULTS

While dense observational networks have been established both in western Europe, in the US and partially in Canada, the vast boreal forests of European Russia and Siberia are heavily under sampled. During several EU funded projects, and also with funding from the German Max-Planck-Society, the Max-Planck-Institute for Biogeochemistry (Heimann *et al.* 2014), together with Russian and European colleagues have established elements of a greenhouse gas observation system in Western Russia and Siberia, which complements the observation network developed in western Europe (Integrated Carbon Observation System, ICOS, http://www.icos-infrastructure.eu).

Here we review the regional budgets of CO_2 and CH_4 of western Russia and Siberia over the last 3 decades as inferred from existing atmospheric observations using the top-down inversion approach, and compare it with similarly estimated budgets for geographical Europe (Schulze *et al.*, 2009). Figure 1 shows e.g. the net surface-atmosphere flux of CO_2 over the northern hemisphere averaged over the years 1998–2012, estimated from concentration measurements from the atmospheric station network using the Jena inversion system (updated from (Rödenbeck *et al.*, 2003)). The atmospheric inversion system locates a major fraction of the northern hemisphere sink in western Siberia. However, this contrasts for the recent years with new information from space based total column observations (e.g. from the GOSAT system, http://www.gosat.nies.go.jp), which, if used in a top-down inversion system, while at the same time tend to reduce the sink in Siberia while decreasing the net emissions from Europe (Chevallier *et al.* 2014). The causes of the discrepancy

between the net CO_2 budgets inferred from the in situ station network and the space based column observations are currently not clear.

The interannual variability of surface-atmosphere fluxes of CO_2 and CH_4 over Siberia and Europe can be traced to climate fluctuations (such as the hot summers in Europe in 2003 and in western Russia in 2010, including substantial contribution from forest fires). Distinct signatures of substantial greenhouse gas emissions from thawing Siberian permafrost regions, however, are at present not discernible in the existing observations.

CONCLUSIONS

While providing tantalising results, the current greenhouse gas observing system for northern Eurasia is still far from providing robust regional information. The current in situ network is still very sparse and is operated by different agencies lacking a comprehensive mutual data exchange policy. New space based instruments, e.g. OCO-2 (http://oco.jpl.nasa.gov), TROPOMI (http://www.tropomi.eu) and the planned mission for active measurements of the CH_4 column, MERLIN (https://directory.eoportal.org/web/eoportal/satellite-missions/m/merlin) will improve the observation coverage, albeit with less accuracy. A coordinated observation strategy combining a multitude of observational data streams is needed to systematically keep track of the future development of the boreal budgets of CO_2 and CH_4 in Eurasia.

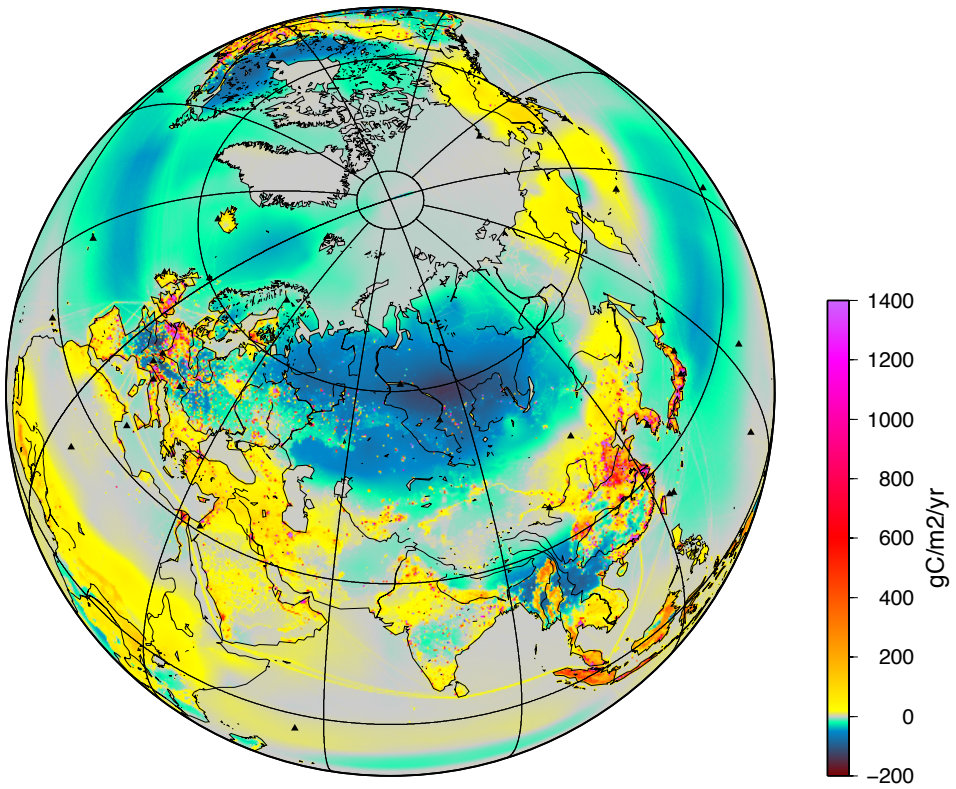

Figure 1: Net surface-atmosphere flux of CO_2 averaged over 1998-2012 estimated from the atmospheric concentration measurement station network (black triangles) using the Jena inversion system (Rödenbeck *et al.*, 2003).

REFERENCES

Chevallier, F. et al. (2014), P. I. Palmer, L. Feng, H. Boesch, C. W. O'Dell, and P. Bousquet, (2014). Toward robust and consistent regional CO_2 flux estimates from in situ and spaceborne measurements of atmospheric CO_2. *Geophys. Res. Lett.*, **41**, 1065–1070, doi:10.1002/2013GL058772.

Heimann, M., E.-D. Schulze, J. Winderlich, M. O. Andreae, X. Chi, C. Gerbig, O. Kolle, K. Kübler, J. Lavric, E. Mikhailov, A. Panov, S. Park, C. Rödenbeck, and A. Skorochod, (2014). The Zotino Tall Tower Observatory (ZOTTO): Quantifying large scale biogeochemical changes in central Siberia. *Nova Acta Leopoldina*, **117**, 51–64.

Rödenbeck, C., S. Houweling, M. Gloor, and M. Heimann, (2003). CO_2 flux history 19822001 inferred from atmospheric data using a global inversion of atmospheric transport. *Atmos. Chem. and Phys.*, **3**, 1919–1964.

Schulze, E.-D. S. Luyssaert, P. Ciais, A. Freibauer, I. A. Janssens, J. F. Soussana, P. Smith, J. Grace, I. Levin, B. Thiruchittampalam, M. Heimann, A. J. Dolman, R. Valentini, P. Bousquet, P. Peylin, W. Peters, C. Roedenbeck, G. Etiope, N. Vuichard, M. Wattenbach, G. J. Nabuurs, Z. Poussi, J. Nieschulze, and J. H. Gash, (2009). Importance of methane and nitrous oxide for EuropeÕs terrestrial greenhouse-gas balance. *Nat Geosci*, **2**, 842–850, doi:10.1038/ngeo686.

Tans, P. I. Y. Fung, and T. Takahashi, (1990). Observational constraints on the global atmospheric CO_2 budget, *Science*, **247**, 1431–1438.

GHG EFFLUX FROM BOREAL LAKES

J. J. HEISKANEN[1], I. MAMMARELLA[1], A. OJALA[2,3], H. MIETTINEN[3] and T. VESALA[1]

[1]Department of Physics, University of Helsinki, P.O. Box 48, FI-00014 University of Helsinki, Finland

[2]Department of Forest Sciences, University of Helsinki, P.O. Box 27, FI-00014 University of Helsinki, Finland

[3]Department of Environmental Sciences, University of Helsinki, Niemenkatu 73, FI-15140 Lahti, Finland

Keywords: LAKES, GREENHOUSE GAS, WIND, HEAT, FLUX, BOREAL ZONE.

INTRODUCTION

Lakes as net heterotrophic systems have an opposite role than oceans in global carbon balance. About 10 % of the terrestrial net ecosystem exchange is released back to the atmosphere from lakes. Most of the world's lakes and wetlands reside in the boreal zone – locally even 20 % of the land area can be covered by lakes (Raatikainen and Kuusisto, 1990) – making boreal lakes very important in the carbon cycle both in regional and global scale. The importance of lakes in global carbon cycle has only recently being understood, mostly due to hugely increased estimates of the amount of freshwaters and increased flux estimates. However, there are still big uncertainties in global lake-atmosphere GHG exchange estimates – and future predictions – due to lack of understanding of the underlying lake physics.

METHODS

The unique full ecosystem scale measurement platform called Lake-SMEAR which is connected to SMEARII station at the Hyytiälä Forestry Field Station of Helsinki University has been running since 2009 and was used for conducting the field studies. In conventional aquatic studies, the system under study is sampled weekly or even monthly whereas in our measuring platform in Lake Kuivajärvi everything is measured automatically and continuously. The measurements include direct flux measurements (eddy covariance) of carbon dioxide, water vapour and methane, continuous profiling of water column carbon dioxide concentration and temperature measurements throughout the water column with a thermistor chain. In addition to continuous CO_2 measurements, we have taken weekly samples of CH_4 and N_2O to derive their efflux with the floating chamber method.

CONCLUSIONS

From the perspective of global warming, the CO_2 emissions were by far the most significant and the relevance of the N_2O emissions was negligible on Lake Kuivajärvi, which is a typical boreal, humic lake, surrounded by managed forest (Miettinen et al. 2014). Also methane fluxes were small.

Atmospheric forcing, namely heat flux into the lake, causes temperature gradient in the water column, which wind forcing further augments by forming a thermocline (steep temperature gradient) between the surface and near-bottom waters. However, the optical properties of the water, namely water clarity, govern how the solar radiation penetrates the water column and thus play a crucial role in the formation and shape of the thermocline (Heiskanen et al., manuscript). This, in turn, affects surface water temperatures and thus influences near-surface turbulent fluxes.

Thermocline is a strong barrier preventing vertical gas exchange in the water column, which leads to oxygen depletion and further CO_2 and CH_4 accumulation in the bottom waters. Besides playing a key role in thermocline formation, wind also causes thermocline tilting which can result in the mixing of deep, CO_2 and CH_4 rich waters to the surface, which leads to increased GHG efflux (Heiskanen et al. 2014). This can also lead to spatial variability in surface water CO_2 concentrations, and if neglected, result as mean error of ~10 % in gas transfer velocities when derived from EC measurements (Heiskanen et al. 2014).

ACKNOWLEDGEMENTS

This study was funded through the Academy of Finland Center of Excellence program (project 272041), Academy of Finland ICOS project (263149), EU ICOS project (211574), Research Foundation of the University of Helsinki, EU GHG-Europe project (244122), EU-project GHG-LAKE, DEFROST (Nordforsk) project, Academy of Finland (project 218094), and University of Helsinki research funds through the project Vesihiisi.

REFERENCES

Heiskanen, J.J., Mammarella, I., Haapanala, S., Pumpanen, J., Vesala, T. and co-authors. 2014. Effects of cooling and internal wave motions on gas transfer coefficients in a boreal lake. Tellus Ser. B-Chem. Phys. Meteorol., 66, 22827.

Heiskanen, J. J., Mammarella, I., Ojala, A., Stepanenko, V., Erkkilä, K.-M., Miettinen, H. and co-authors. Sensitivity of two lake models to water clarity parameterization. Manuscript.

Miettinen, H., Pumpanen, J., Heiskanen, J., Aaltonen, H., Mammarella, I. and co-authors. 2014. Towards a more comprehensive understanding of lacustrine greenhouse gas dynamics – two year measurements of concentrations and fluxes of CO2, CH4 and N2O in a typical boreal lake surrounded by managed forest. Bor. Env. Res., 20, ISSN 1797-2469.

Raatikainen, M. and Kuusisto, E. 1990. Suomen järvien lukumäärä ja pinta-ala [The number and surface area of the lakes in Finland]. Terra. 102, 97-110. [In Finnish with English 1010 summary].

INFLUENCE OF EASTERLY AIR MASSES ON NMHC MIXING RATIOS IN NORTHERN FINLAND

H. HELLÈN, P. ANTTILA, R. KOUZNETSOV and H. HAKOLA

Finnish Meteorological Institute, Air Quality, P.O. Box 503, FI-00101 Helsinki, Finland

Keywords: NON-METHANE HYDROCARBONS, NMHC, VOC.

INTRODUCTION

Non-methane hydrocarbons (NMHC) are released to the air due to petrol exhaust and evaporation, stationary combustion, gas leaks, solvent use etc. Also nature releases large amounts of VOCs into the atmosphere (Tarvainen *et al.* 2007). In the air the reaction with hydroxyl radical is the main sink reaction for NMHCs, but ozone reaction is also important for alkenes (Atkinson 1994). In addition NMHCs react with nitrate (Atkinson 1994, Penkett *et al.* 1993) and chlorine (Finnlayson-Pitts et al., 1989) radicals. The atmospheric lifetimes of NMHCs are rather long varying from months to days during winter, but being much shorter in summer when there is enough light to produce hydroxyl radicals. In winter NMHCs accumulate in the northern latitudes and maximum concentrations are measured during dark winter months. In spring the VOC concentrations start decreasing, concomitant with ozone increase, due to efficient photochemical reactions and the minimum concentrations are reached in summer.

NMHC reactions with OH radical can result in ozone formation when enough nitrogen oxdides are present (Derwent *et al.* 2003). Emission reductions of ozone precursors in Europe have been followed by downward trend of episodic peak ozone levels (Derwent *et al.* 2003). However, background ozone levels have increased in central Europe (Simmonds *et al.* 2004). In Finland ozone concentrations increased in the years 1990-2000, although a decreasing trend was observed in the other Nordic countries (Laurila *et al.* 2004, Solberg *et al.* 2005). Between 1994 and 2007 mean summer concentrations of O_3 showed no significant trends at eight Finnish rural sites. Summertime peak concentrations increased slowly (but significantly) at the two northernmost stations while at the other background sites no significant trends were detected in the summertime peak concentrations (Anttila and Tuovinen 2010).

Light molecular weight hydrocarbons (C2-C6) have been measured in Finnish Lapland, at Pallas GAW (Global Atmosphere Watch) station, since 1994 based on canister sampling twice a week. These measurements were replaced by in-situ analysis using on-line gas-chromatograph in the beginning of 2010. The concentration trends have been studied earlier (Hakola *et al.* 2006) and the concentrations of the fast reacting species were found to have decreased by 10-40 % in 1994-2003, whereas the concentrations of the slowly reacting compounds ethane and propane showed no change or were increasing over the ten years of measurements. Higher concentrations were found in the air masses arriving Pallas from the Central Europe and from Russia while the marine air masses were the cleanest.

Here we study the trends of NMHCs during the twenty years (1994-2013) of measurement and the source areas using data from new in situ measurements.

METHODS

The measurements were conducted at Pallas-Sodankylä Global Atmosphere Watch station at Sammaltunturi station. The station is situated at the northernmost limit of the northern boreal forest zone (67° 58’N, 24°07’E). The station resides on a top of the fjeld at an elevation of 565 m above sea level.

In 1994-2011 NMHC samples were collected into evacuated stainless steel canisters twice a week and analyzed later in the laboratory using gas-chromatograph after concentrating in liquid nitrogen traps. The in-situ gas-chromatograph was taken into use in 2010. The system is Perkin-Elmer thermal desorption-gas chromatography system with flame ionization detection. The GC system is composed of dual columns configured with a heartcut device. The first column is a BP-1 methyl silicone column (50 m*0.22 mm*1 µm) followed by the heartcut device and alumina/Na_2SO_4 PLOT column (50 m*0.32 mm). The heartcut device is used to separate the analytes into two fractions; the more-volatile fraction elutes from the dimethyl siloxane column and is directed into the PLOT column for further chromatography and detection on FID2. After the volatile fraction has passed dimethylsiloxane column, the heartcut is switched to the other position and the later eluting compounds are directed to the FID1.

The linear trends in the concentration time series were estimated by Generalized Least Squares (GLS) regression with classical decomposition and autoregressive moving average (ARMA) errors as described the in Anttila and Tuovinen (2010).

To identify the source areas of ambient VOCs at Pallas we have used the footprint analysis for the hourly-averaged values of concentrations measured in wintertime in 2010-2012. The method is described in Meinander *et al.* (2013). Comparison of the sensitivity maps for "clean" and "polluted" samples allows one to identify the areas that of likely locations of powerful sources. The areas of high sensitivity for "clean" samples do not contain persistent powerful sources. Thus the likely source areas can be identified as those missing from "clean" maps, but are highly represented in "polluted" ones.

RESULTS AND DISCUSSION

All compounds showed typical seasonal variation with highest mixing ratios in winter and lowest in summer, when lifetimes are shortest due to higher abundance of OH radicals. During winter or spring months, the mixing ratios did not show any diurnal variations. This was expected due to remote location of the site and relatively long lifetime of the compounds. In summer all other alkanes except the longest living ethane had day minima and night maxima.

Ratios of isomeric pairs (i-butane and n-butane or i-pentane and n-pentane) are not expected to change during the transport due to OH oxidation since the reaction rate constants are very similar. Subsets of the data for the four seasons show no obvious change in the correlations indicating main sources staying the same throughout the year (Fig. 1). However, the ratio has increased a little in the end of 2000's compared to 1990's. Lifetime of n-butane is a bit lower than for i-butane and therefore in more remote air masses ratio is expected to be a bit higher and higher ratio may indicate more distant sources.

The trends in NMHC mixing ratios at Pallas during 1994-2013 were studied. A small downward trend can be seen for most alkanes and benzene, but decreasing trend is significant only for ethyne. This is not in accordance with reconstructed NMHC trends for Northern Hemispehere, which shows a clear downward trend (1-5 % $year^{-1}$) during that period (Helmig *et al.* 2014). According to the EMEP emission database also emissions of NMVOCs have decreased in European Union over 50% during the studied period. At a rural French site significant downward trend of benzene and i-pentane concentrations was observed in 1997-2006 (Sauvage *et al.* 2009). Persistent mixing ratios indicate that some other sources or source areas are dominating at Pallas compared to Central Europe. Lifetimes of these NMHCs are relatively long especially in winter (9-1000 days depending on the compound) and therefore they can transport long distances.

Despite of decreased emissions of ozone precursors in Europe, mean ozone concentration is not showing any downward trend at Pallas either. At Mace Head in Ireland background ozone levels have even increased in 1987-2003 (Simmonds *et al.* 2004). However, downward trend of episodic peak ozone levels have been observed in Europe (Derwent *et al.* 2003). Lack of downward trend of background ozone at Pallas is in accordance with the trend of background NMHCs.

Fig. 2 shows average footprints for “clean” and “polluted” air for different NMHCs. The comparison of “clean” and “polluted” patterns clearly show sensitivity in Eastern Europe for “polluted” footprints that correspond to a gap in sensitivity for “clean” samples. There are several large cities (e.g. Helsinki, St. Petersburg and Moscow), which are likely to be responsible for the pollution from that area. For compounds (butanes and pentanes) with shorter lifetime and therefore lower background concentration, source area is clearer than for compounds with higher background (e.g. ethane).

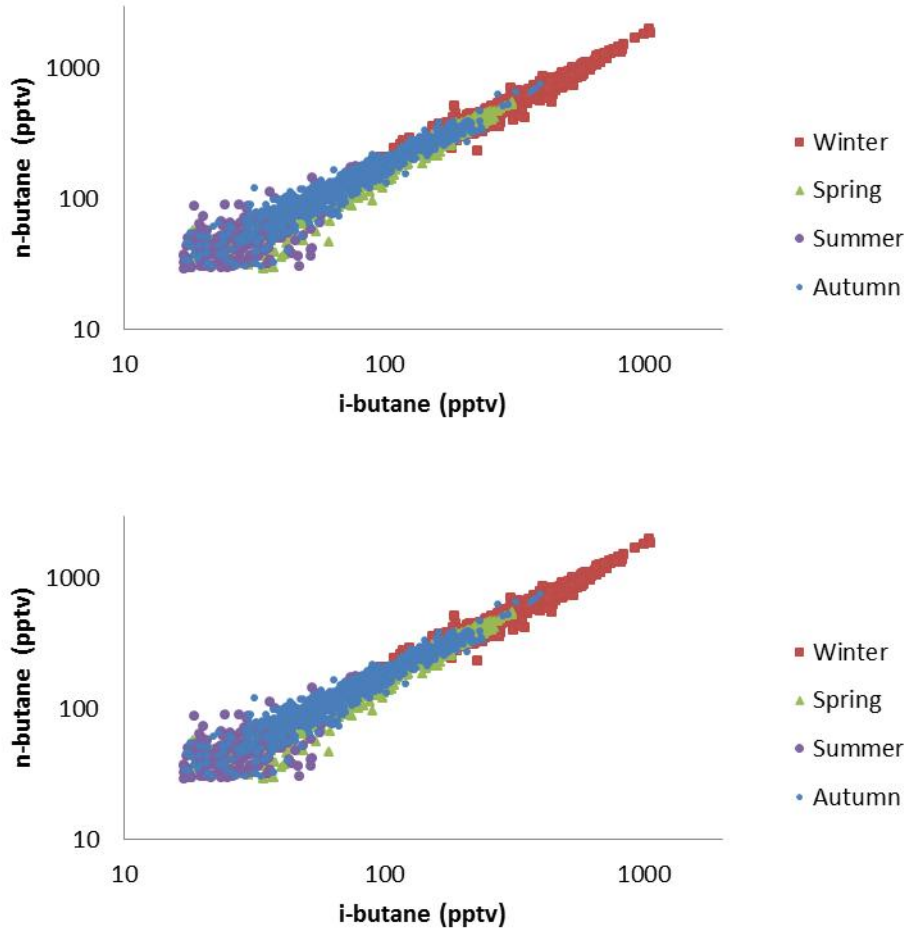

Fig. 1. Seasonal analysis of butane and pentane isomers for the year 2012 a) n-butane versus i-butane, b) n-pentane versus i-pentane

Northern part of Central Europe does not show any contribution to higher concentrations and there is actually higher sensitivity for “clean” air. As mentioned earlier, emissions of NMHCs in European Union area have decreased by 50 % in 1994-2012. However, this has not been the case in concentrations of most of alkanes at Pallas, where concentrations did not show any significant decreasing trend between 1994 and 2013 (Table 2). This could be explained by the South-East being the main source area for higher concentrations. Also in the earlier study at Pallas (Hakola *et al*. 2006), highest concentrations has been observed in air masses coming from East. However, air masses coming from Central Europe had high concentrations too. Those measurements were conducted in 1994-2003 and as mentioned above, emissions in Central Europe have been decreasing significantly during that time.

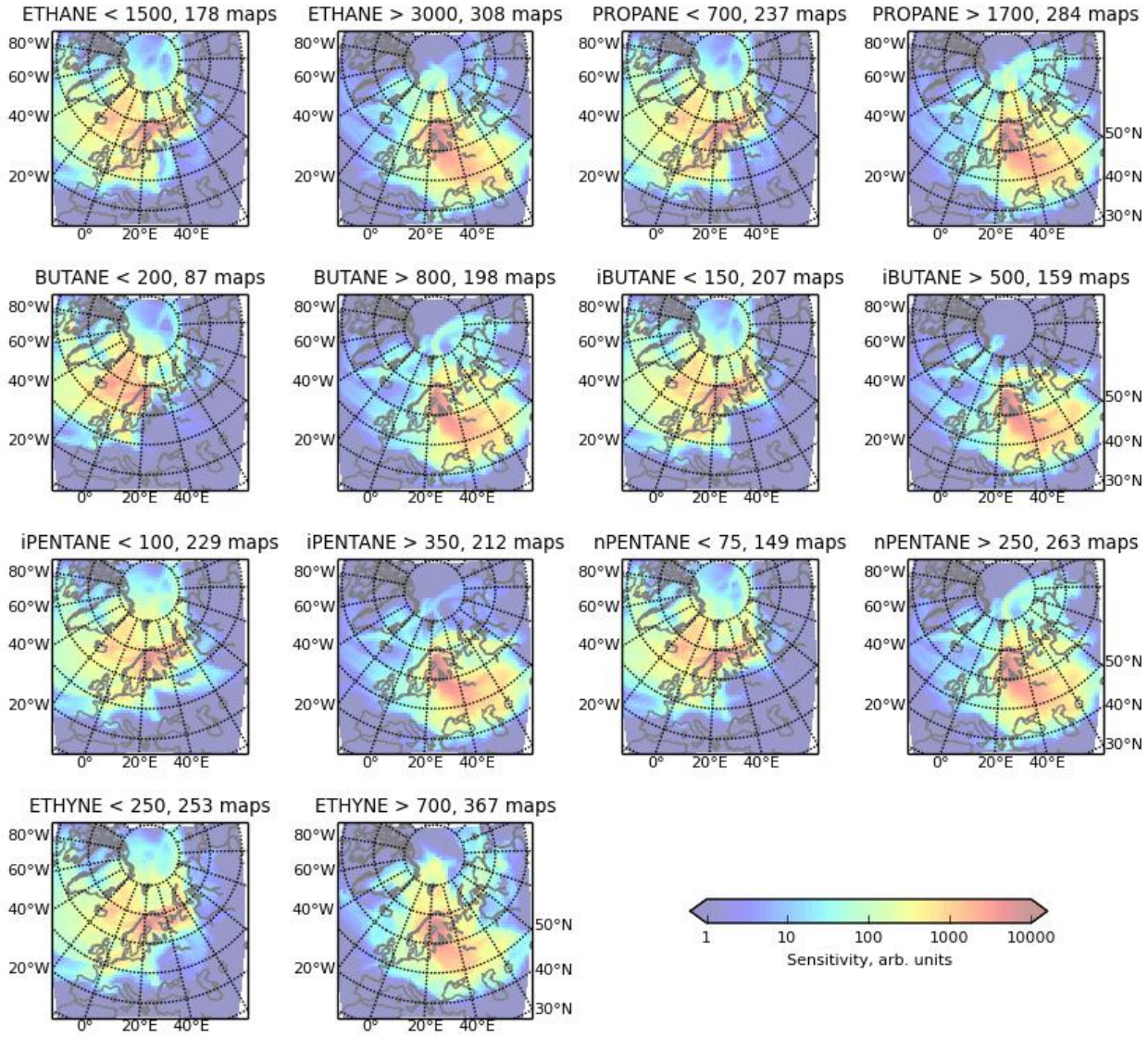

Fig. 2. The footprints for “clean” (left panel) and “polluted” (right panel) air masses

CONCLUSIONS

Emissions of NMHCs in Europe Union have decreased by 50 % in 1994-2012, but this is not seen in mixing ratios at Pallas. Significant downward trend was found only for ethyne in 1994-2013. Despite of decreased emissions of ozone precursors in Europe, ozone is not showing any downward trend at Pallas either.

Seasonal butane and pentane ratios indicated that main sources are staying the same throughout the year at Pallas. i/n-Butane ratio has increased since 1994, this may indicate that air masses are transported over longer distance.

Source area studies of NMHCs indicate that Central Europe is not a significant source area for NMHCs at Pallas anymore. Main source area is located in Eastern Europe to the South-West from Pallas. Increased Eastern emissions may explain the missing downward trend in the NMHC mixing ratios.

REFERENCES

Anttila, P. & Tuovinen, J.-P. 2010: Trends of primary and secondary pollutant concentrations in Finland in 1994–2007. *Atmos. Environ.* 44: 30–41.

Atkinson R. 1994. Gas-phase tropospheric chemistry of organic compounds. *J. Phys. Chem. Ref. Data.* Monograph 2: 216 p..

Derwent R.G., Jenkin M.E.m Saunders S.M., Pilling M.J., Simmonds P.G., Passant N.R., Dollard G.J., Dumitrean P. & Kent A. 2003: Photochemical ozone formation in orth west Europe and its control. *Atmos. Environ.* 37: 1983-1991.

Finlayson-Pitts B.J., Ezell M.J. and Pitts Jr. J.N. 1989: Formation of chemically active chlorine compounds by reactions of atmospheric NaCl particles with gaseous N_2O_5 and $ClONO_2$. *Nature*, 337, 241-244.

Hakola H., Tarvainen V. Laurila T., Hiltunen V., Hellén H. & Keronen P. 2003: Seasonal variation of VOC concentrations above a boreal coniferous forest. *Atmos. Environ.* 37, 1623-1634.

Hakola H., Hellén H. & Laurila T. 2006: Ten years of light hydrocarbon (C2-C6) concentration measurements in background air in Finland. *Atmos. Environ.* 40: 3621-3630.

Hellén H., Kouznetsov R., Anttila P. and Hakola H., 2014. Increasing influence of easterly air masses on NMHC concentrations at the Pallas-Sodankylä GAW station. Accepted *to Boreal Environ. Res.*, ISSN 1797-2469.

Helmig D., Petrenko V., Martinerie P., Witrant E., Röcmann T., Zuiderweg A., Holzinger R-., Hueber J., Thompson C., White J.W.C., Sturger W., Baker A., Blunier T., Etheridge D., Rubino M. & Tans P. 2014: Reconstruction of Northern Hemisphere 1950-2010 atmospheric non-methane hydrocarbons. *Atmos. Chem. Phys.* 14: 1463-1483.

Laurila T., Tuovinen J.-P., Tarvainen V., Simpson D., 2004: Trends and scenarios of ground-level ozone concentrations in Finland. Boreal Environment Research 9, 167-184.

Meinander O., Kazadzis S., Arola A., Riihelä A., Räisänen P., Kivi R., Kontu A., Kouznetsov R., Sofiev M., Svensson J., Suokanerva H., Aaltonen V., Manninen T., Roujean J.-L. and Hautecoeun O., 2013. Spectral albedo of seasonal snow during intensive melt period at Sodankylä, beyond the Arctic Circle. *Atmos. Chem. Phys.* 13: 3793-3810.

Penkett S.A., Blake N.J., Lightman P., Marsh A.R.W. and Anzwyl P., 1993: The seasonal variation of nonmethane hydrocarbons in the free troposphere over the North Atlantic Ocean: Possible evidence for extensive reaction of hydrocarbons with the nitrate radical. *J. Geophys. Res.*,**98**, 2865-2885.

Sauvage S., Plaisance H., Locoge N., Wroblewski A., Coddeville P & Galloo J.C. 2009: Long term measurement and source apportionment of non-methane hydrocarbons in three French rural areas. *Atmos. Environ.* 43: 2430-2441.

Simmonds P.G., Derwent R.G., Manning A.L. & Spain G. 2004: Significant growth in surface ozone at Mace Head, Ireland, 1987-2003. *Atmos. Environ.* 38: 4769-4778.

Solberg S., Bergström R., Langner J., Laurila T., Lindskog A., 2005: Changes in Nordic surface ozone episodes due to European emission reduction in the 1990s. Atmospheric Environment 39, 179-192.

Tarvainen V. Hakola H., Rinne J., Hellén H. & Haapanala S. 2007: Towards a comprehensive emission inventory of the Boreal forest. *Tellus* 59 B: 526-534.

AMINE MEASUREMENTS IN BOREAL FOREST AIR

M. HEMMILÄ, H. HELLÉN, U. MAKKONEN and H. HAKOLA

Finnish Meteorological Institute, PL 503, 00101 Helsinki, Finland

Keywords: AMINES, AMBIENT AIR, MARGA-MS.

INTRODUCTION

Amines are gaseous bases, whose general formula is RNH2, R2NH or R3N. Models have shown that they could affect to aerosol particle forming with sulfuric acid (Kurtén et al. 2008, Paasonen et al. 2012). Atmospheric aerosol particles affect the climate, because they can act as cloud condensation nuclei (CCN) (IPCC 2014). They also scatter and absorb the radiation of the sun. Amines also affect hydroxyl radical (OH) reactivity and via that to the atmospheric chemistry (Hellén et al. 2014, Kieloaho et al. 2013).
Amines have been collected earlier as filter samples and analyzed with high pressure liquid chromatography coupled to mass spectrometry (HPLC-MS, Kieloaho et al. 2013). In this method the samples were collected for 24 to 72h and analyzed later in the laboratory. We have developed a method for analysis of amines using on-line ion-chromatograph connected to a mass-spectrometer with 1-hour time resolution. In-situ analysis also avoids biases caused by transporting and pretreatment of the samples. The method was used for amine measurements in a boreal forest site during summer and autumn 2014.

METHODS

Measurements were done in SMEAR II station at Hyytiälä, Southern Finland (61o510´N, 24o170´E, 180 m a.s.l., Hari and Kulmala, 2005) from June to December 2014. For sampling and measuring we used MARGA (Monitor for AeRosols and Gases in Ambient air, Metrohm-Applikon, Schiedam, Netherlands) (ten Brink et al. 2007), which is an on-line ion chromatograph (IC) connected to sampling system. The MARGA system was connected to electrospray ionization quadrupole mass spectrometer (MS, Shimadzu LCMS-2020, Shimadzu Corporation, Kyoto, Japan) to improve sensitivity of amine measurements. This new set-up enabled amine concentration measurements in ambient air both in aerosol and gas phases. With MARGA-MS we analyzed 7 different amines: monomethylamine (MMA), dimethylamine (DMA), trimethylamine (TMA), ethylamine (EA), diethylamine (DEA), propylamine (PA) and butylamine (BA).
Sampling air flow was 16.7 l/min and sampling time 1 hour. Eluent for IC analysis was oxalic acid (3.2 mol/l) and its flow was 0.7 ml/min. We used concentration column (Metrosep C PCC 1 VHC/4.0) before the analytical column (Metrosep C 4 – 100/4.0). Detection limits were calculated from blank-values (Table 1).

Amine	**LOD (ng/m^3)**	**LOD (ppt$_v$)**
DEA	1.2	0.4
DMA	3.1	1.7
TMA	0.6	0.2
EA	0.9	0.5
MMA	1.1	0.8

Table 1. Detection limits (LOD) of different amines.

RESULTS AND DISCUSSION

We started measurements at SMEAR II in June 2014 and continued until December 2014. In preliminary data analysis we found out, that amine concentration levels in gas phase were higher in June than in July, whereas they were below detection limit in aerosol phase most of the time (Figs. 1, 2 and 3). Monthly mean concentrations are shown in Fig.4. DMA was the most abundant amine in gas phase, followed by BA, DEA and EA. The measured concentrations of gaseous amines followed temperature variation, which could mean that amines are produced and emitted from the environment or re-emitted from the surfaces as temperature rises after deposition during night-time. All amines had similar diurnal variation with maxima during afternoon and minima during night.

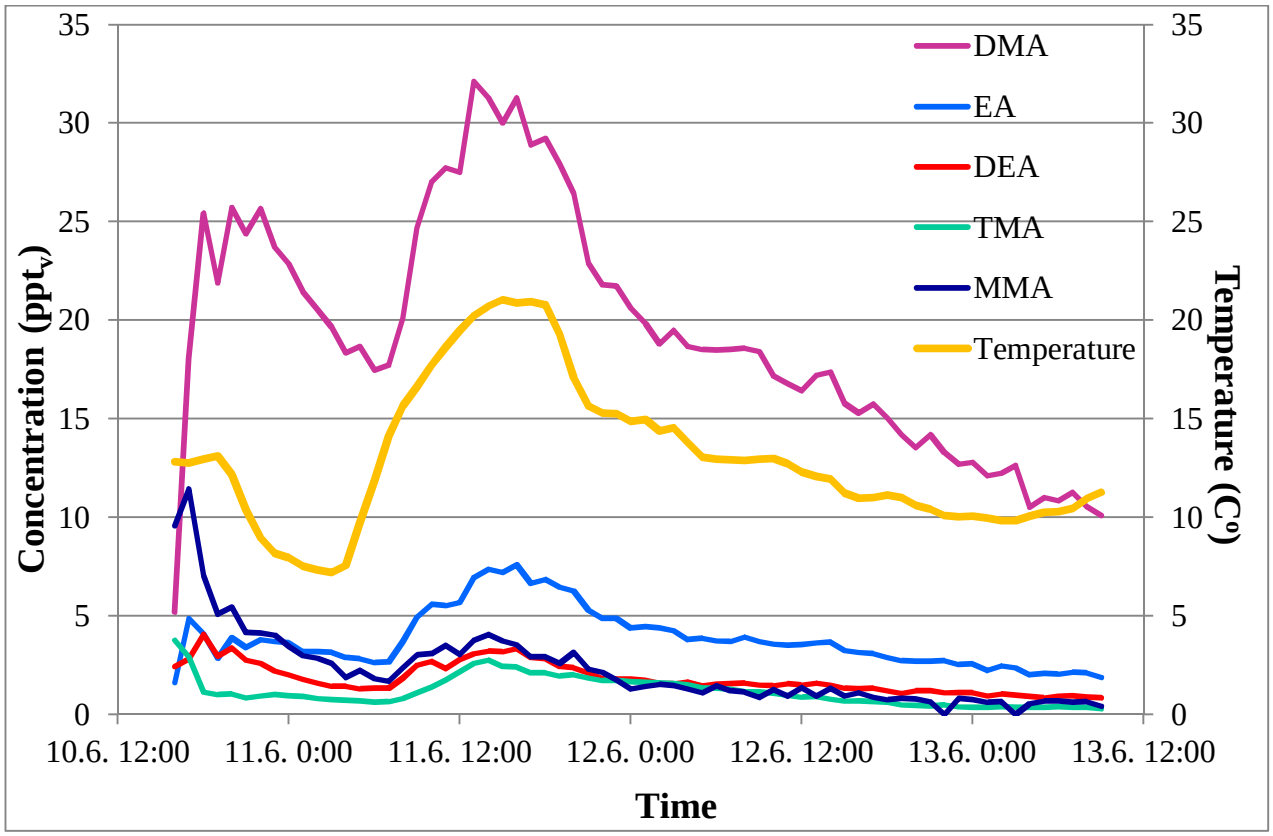

Figure 1. Concentrations (pptv) of gaseous dimethylamine (DMA), ethylamine (EA), diethylamine (DEA), trimethylamine (TMA), monomethylamine (MMA), and temperature in June 2014.

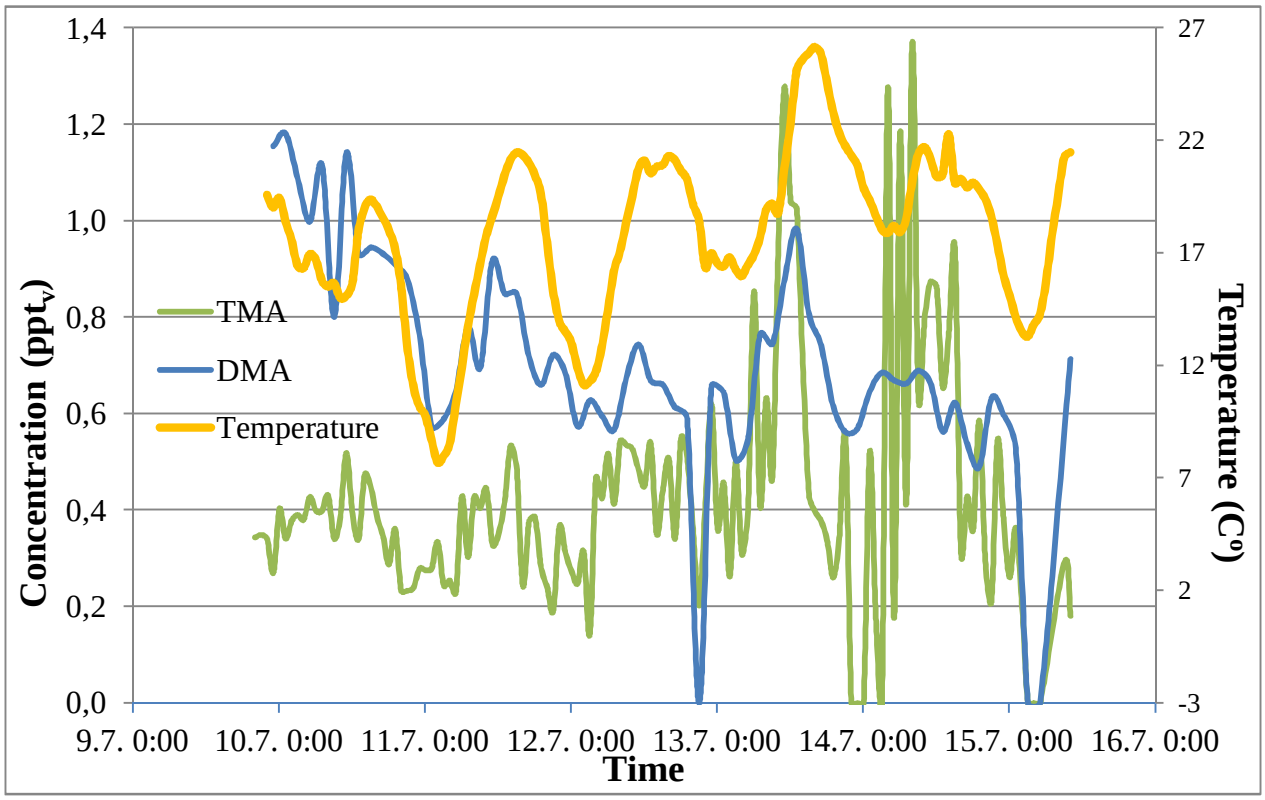

Figure 2. Concentrations (ppt$_v$) of gaseous DMA and TMA and temperature in July 2014.

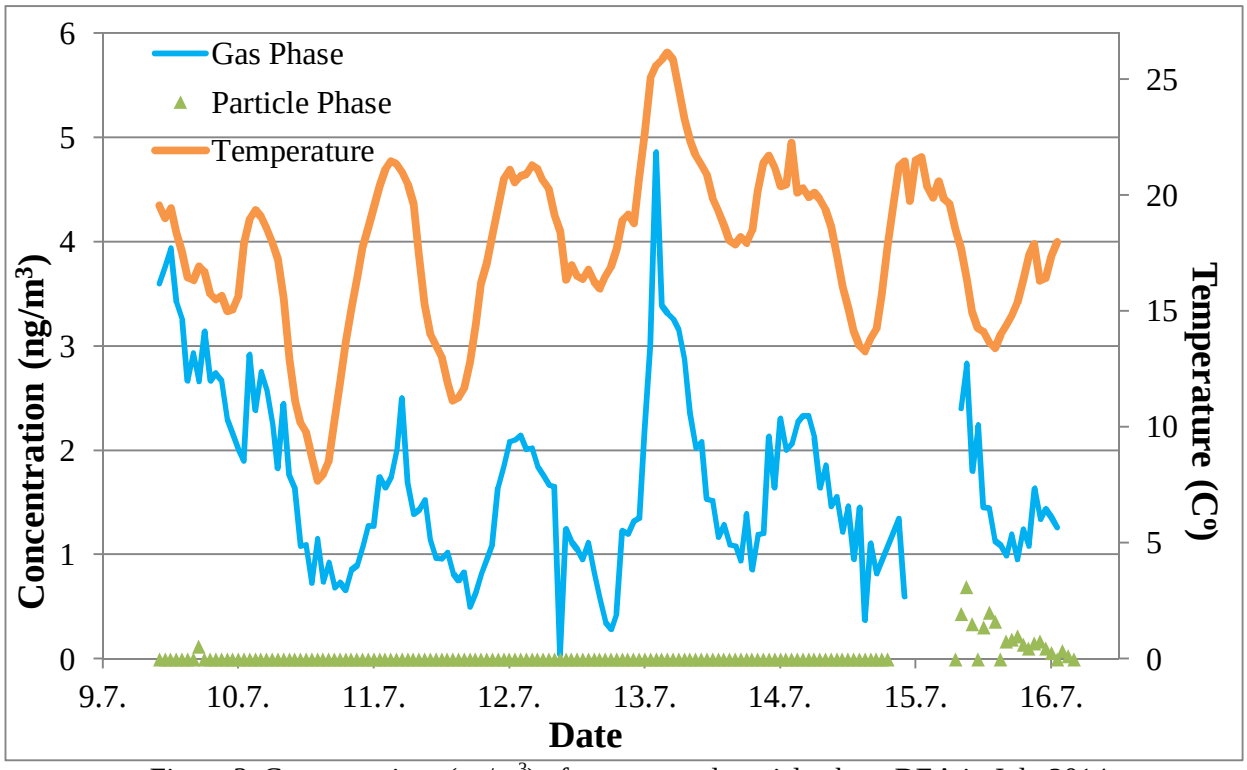

Figure 3. Concentrations (ng/m^3) of gaseous and particle phase DEA in July 2014.

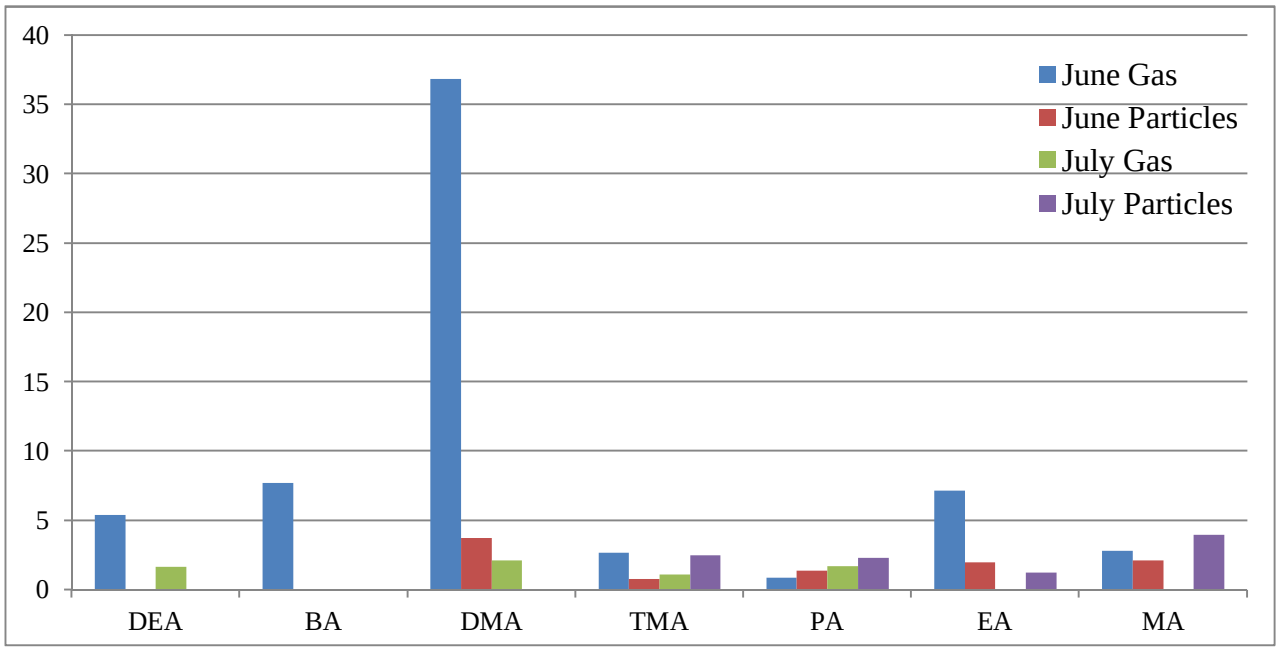

Figure 4. Monthly mean concentrations (ng/m3) of amines in 2014.

Kieloaho et al. (2013) also measured amine concentrations at SMEAR II in summer 2011 (Table 2). Their concentration levels were about the same as ours; the differences can be due to different meteorological conditions. The weather in summer 2014 was very exceptional; June was unusually cold and rainy, whereas July was warm and dry. Also the data reported by Kieloaho et al., covers longer season than our current measurements.

Amine	**Average concentration May-October 2011 (ppt_v) ***	**Average concentration June and July 2014 (ppt_v)**
DMA		10
EA		3.9
DMA+EA	42 ± 30	
DEA	6.5 ± 5.6	1.2

*adapted from Kieloaho et al., 2013

Table 2. Comparison of average amine concentrations in summer 2011 and 2014.

CONCLUSIONS

Concentrations of amines in ambient air were measured at SMEAR II, Hyytiälä with MARGA-MS starting in June 2014. In preliminary data-analysis we found out, that concentrations were higher in June than in July. The amines were found above detection limits mostly in gaseous phase and the compounds detected were MMA, DMA, TMA, EA and DEA. In the poster we will also present the autumn measurements.

ACKNOWLEDGEMENTS

The financial support of the Academy of Finland Centre of Excellence program (project no. 272041) and the Academy research fellow project by H. Hellén (275608) are gratefully acknowledged.

REFERENCES

Hari, P. and Kulmala, M., Boreal Environment Research, 10 (2005) 315-322.
Hellén, H, Kieloaho, A.-J. and Hakola, H., Atmospheric Environment, 94 (2014) 192-197.
IPCC, The Intergovernmental Panel on Climate Change: Climate Change 2013: The Physical Science Basis. Cambridge University Press, New York, 2013.
Kieloaho, A.-J., Hellén, H., Hakola, H., Manninen, H.E., Nieminen, T., Kulmala, M. and Pihlatie, M., Atmospheric Environment, 80 (2013) 369-377.
Kurtén, T., Loukonen, V., Vehkamäki, H. and Kulmala, M., Atmospheric Chemistry and Physics, 8 (2008) 4095-4103.
Paasonen, P., Olenius, T., Kupiainen, O., Kurtén, T., Petäjä, T., Birmili, W., Hamed, A., Hu, M., Huey, L. G., Plass-Duelmer, C., Smith, J. N., Wiedensohler, A., Loukonen, V., McGrath, M. J., Ortega, I. K., Laaksonen, A., Vehkamäki, H., Kerminen, V.-M., and Kulmala, M., Atmospheric Chemistry and Physics, 12 (2012) 9113-9133.
ten Brink, H. M., Otjes, R., Jongejan, P., and Slanina, J., Atmospheric Environment 41 (2007) 2768–2779.

EARTH OBSERVATION FOR ENVIRONMENTAL STUDIES ON THE SILK ROAD ECONOMIC BELT

G. HUADONG

[1]Institute of Remote Sensing and Digital Earth (RADI), Chinese Academy of Sciences (CAS), Beijing 100094, China; E-mail: hdguo@radi.ac.cn

Keywords: EARTH OBSERVATION, ENVIRONMENTAL ISSUES, SILK ROAD ECONOMIC BELT.

INTRODUCTION TO THE SILK ROAD ECONOMIC BELT

In Sep. 2013, China's President Xi Jinping proposed a strategic concept to jointly build "the Silk Road Economic Belt" during a visit to Kazakhstan. The Silk Road Economic Belt (SREB) is an economic cooperation region among China and countries in central and western Asia and Europe. The spatial domain is almost the same as that of the ancient Silk Road. The PEEX program mainly focuses on northern Eurasia, particularly the arctic and boreal regions. Figure 1 shows that SREB and PEEX have large overlapping areas. PEEX includes more northern regions and SREB covers more southern parts of Asia and Europe.

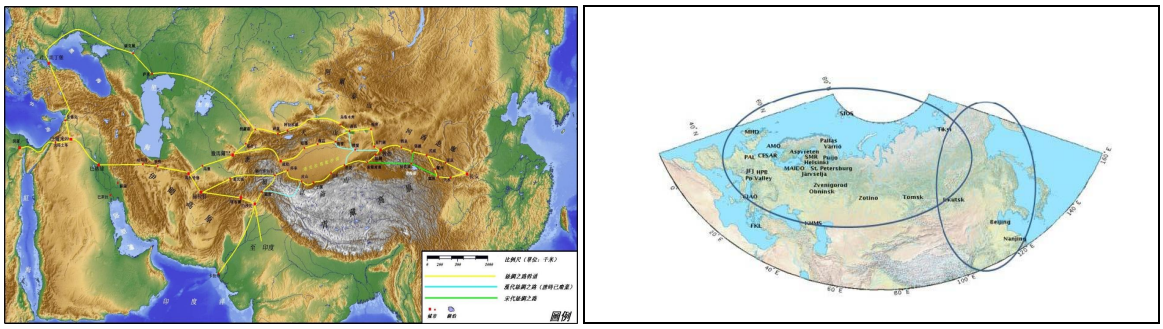

Figure 1. Spatial domain of the ancient Silk Road and PEEX study area

EARTH OBSERVING TECHNIQUES IN CHINA

China's Earth observation has made great progress and plays an important role in sustainable development. Currently, China has developed four series of remote sensing satellites, which include land resource satellites, environment satellites, ocean satellites, and meteorological satellites. More recently, high-resolution Earth observation satellites and Beidou navigation satellites have also been developed. China has successfully applied its Earth observation technologies to global environmental change, resource prospection, disaster assessment and mitigation, and urban environments.

ENVIRONMENTAL ANALYSIS OF SREB

Under the dual interactions between natural and human factors, the Silk Road Economic Belt faces more and more challenges with desertification, eco-environmental issues, water resources, and natural disasters, especially in Central Asia and western China. All of these factors have significantly limited the region's social and economic development. The paper presents and discusses remote sensing monitoring and analysis of ecological and environmental change, land use/land cover change, vegetation degradation, lake area and level change, snow area and SWE change, natural and culture heritage, and global environmental change monitoring. The spatial and temporal patterns of the environment and the potential development of SREB are also analysed.

PROSPECTIVE

The opportunities and challenges in the Silk Road Economic Belt from the aspect of Earth observation are discussed, and future work is introduced.

ACKNOWLEDGEMENTS

This work was supported by the Key Projects in the National Science & Technology Pillar Program (Grant No. 2012BAH27B05).

REFERENCES

Katy Unger-Shayesteh, Sergiy Vorogushyn, Daniel Farinotti, Abror Gafurov, Doris Duethmann, Alexander Mandychev, Bruno Merz, What do we know about past changes in the water cycle of Central Asian headwaters? A review, Global and Planetary Change 110 (2013) 4 – 25

Birgit Mannig, Markus Müller, Eva Starke, Christian Merkenschlager, Weiyi Mao, Xiefei Zhi, Ralf Podzune, Daniela Jacobe, Heiko Paeth, Dynamical downscaling of climate change in Central Asia, Global and Planetary Change 110 (2013) 26 – 39

APPLICATION OF OMI TROPOSPHERIC NO2 FOR AIR QUALITY MONITORING AT HIGH LATITUDES: SHIPPING AND LAND-BASED CASE STUDIES

I. IALONGO[1], J.J. HAKKARAINEN[2] and J. TAMMINEN[2]

[1]Finnish Meteorological Institute, Atmospheric Remote Sensing group
Helsinki, Finland.

Keywords: ATMOSPHERIC COMPOSITION, URBAN AIR QUALITY, SATELLITE REMOTE SENSING, NITROGEN DIOXIDE (NO_2).

INTRODUCTION

Satellite-based data are very important for air quality applications in those areas where air pollution information are not available from other sources. In particular, in Northern Europe an extensive characterization of the pollution levels in terms of satellite retrievals of tropospheric NO_2 is currently missing. On the other hand, the tropospheric NO_2 monitoring at high latitudes using satellite data is challenging because of the reduced light hours in winter and the snow-covered surface, which make the retrieval complex, and because of the reduced signal due to low Sun.

This work presents a detailed characterization of the tropospheric NO_2 columns focused on Northern Europe using the Ozone Monitoring Instrument (OMI) tropospheric NO_2 standard product.

METHODS

The tropospheric NO_2 Level 2 data were gridded on a 0.1×0.1 degrees latitude and longitude scale and averaged over seasonal time scales. Averaging over many days over a grid box smaller than the instrument pixel size, allows an increased effective spatial resolution. The OMI pixels corresponding to SZA (solar zenith angle) larger than 70° and with effective cloud fraction (OMCLDO2 product) larger than 30 % were removed before gridding the data. Only the OMI pixel with number from 6 to 24 were included in the analysis to take into account only central small pixels and to avoid the pixels corrupted by the row anomaly. The analysis focused on summer season (1 June–31 August)

The NO_2 emissions and lifetime in Helsinki were estimated from the average decay of the signal with the distance from the city center. Westerly winds were taken into account in the analysis, because the largest part of the data is collected under these conditions. The model proposed by Beirle et al. (2011) was used to fit the NO_2 line densities, which were derived integrating the NO_2 data in across-wind direction over 2 latitude degrees interval.

The OMI NO2 tropospheric columns were compared with the NOx emissions of marine traffic as derived from the model STEAM (Ship Traffic Emission Assessment Model), based on the messages provided by the automatic identification system (AIS), which enable the positioning of ships with high spatiotemporal resolution (Jalkanen et al., 2009).

CONCLUSIONS

The results showed that, despite the regional area of interest and the relatively small emission sources, it is possible to distinguish the signal from the main coastal cities and from the shipping lanes by averaging the data over seasonal time range.

The summertime NO_2 emission and lifetime values (E = (1.0 ± 0.1)*10^{28} molec. and τ = (3.0 ± 0.5) h, respectively) in Helsinki were estimated from the decay of the signal with distance from the city center.

The comparison between the ship emissions from model calculations and OMI NO_2 tropospheric columns in the central Baltic Sea area confirmed the applicability of satellite data also for ship emission monitoring. In particular, both the emission data and the OMI observations showed similar year-to-year variability, with a drop in year 2009, corresponding to the effect of the economical crisis.

REFERENCES

Beirle, S., Boersma, K. F., Platt, U., Lawrence, M. G., and Wagner, T.: Megacity emissions and lifetimes of nitrogen oxides probed from space, Science, 333, 1737–1739, doi:10.1126/science.1207824, 2011.

Jalkanen, J.-P., Brink, A., Kalli, J., Pettersson, H., Kukkonen, J., and Stipa, T.: A modelling system for the exhaust emissions of marine traffic and its application in the Baltic Sea area, Atmos. Chem. Phys., 9, 9209–9223, doi:10.5194/acp-9-9209-2009, 2009.

OBSERVATIONAL INFRASTRUCTURE IN EASTERN SIBERIA BY JAPANESE COLLABORATIVE STUDY

Y. IIJIMA[1], H. PARK[1], A.N. FEDOROV[2] and T.C. MAXIMOV[3]

[1]Research and Development Center for Global Change, Japan Agency for Marine-Earth Science and Technology, Yokosuka, Kanagawa, 237-0061, Japan.

[2]Melnikov Permafrost Institute, Siberian Division of Russian Academy of Science, Yakutsk, Russia.

[2]Institute of Biological Problem in Cryolithozone, Siberian Division of Russian Academy of Science, Yakutsk, Russia.

Keywords: PERMAFROST, SUPERSITE, OBSERVATIONAL NETWORK, EASTERN SIBERIA.

INTRODUCTION

The Arctic terrestrial system consists of elements such as permafrost, snow cover, soil/vegetation, and water. The warming and thawing permafrost have enormous feedbacks to the Arctic and global climate changes through interacting with changes in snow cover and vegetation which will consequently induce changes in greenhouse gas emissions and surface albedo. Our objectives, thus, are extended to clarify the role and function of the Arctic terrestrial system in the climate system, and assess the influence of changes in the Arctic on a global scale. To understand the terrestrial ecosystem throughout the circum-polar Arctic region, we refine and continue our observations at existing field sites in Arctic and Sub-Arctic regions in Russian Territory, where individual researchers collaborating with circum-polar countries have set up their own systems for long-term observations. We will also extend new sites to combine observations using a mobile system to monitor spatial variation and multiple site observations with simple soil temperature and moisture boreholes.

Based on these observational data, we will carry out interdisciplinary studies involving both observation-based and model-based researchers, and then develop terrestrial system models that can reproduce realistic changes in the thawing of frozen soil, vegetation, ecohydrological and carbon cycles.
In eastern Siberia, three supersites at Yakutsk, Elegii and Tiksi have the boreholes of soil temperature and moisture within active layer and energy, water and carbon flux systems. Borehole network and CALM (Circum-Polar Active Layer Monitoring) sites distribute in central Yakutia at both left and right banks of the Lena River. New soil temperature and moisture Yakutsk–Villuy–Chernoshevsky transect are set up since 2012. All of the sites are designed to get soil temperature and moisture profiles at active layer and near surface permafrost (4–10m depth). In addition, we plan to completely get soil physical parameters including soil organic matters, heat conductivity and capacity profile, and vegetation parameters (vegetation type, leaf area index) to smoothly collaborate with modelling studies.

IMPACT OF BIOGEOPHYSICAL AND BIOGEOCHEMICAL PROCESSES AND THEIR INTERACTIONS ON PERMAFROST SOIL CARBON STOCKS

A.K. JAIN and S. SHU

Department of Atmospheric Science, University of Illinois
105 S. Gregory Street, Urbana, IL 61801.

Keywords: PERMAFROST SOIL CARBON, LAND SURFACE MODEL, BIOGEOPHYSICS, BIOGEOCHEMISTRY.

INTRODUCTION

One of the major challenges in more detailed Earth system models (ESMs) is the treatment of the biophysical and biogeochemical processes and feedbacks and their impact on soil organic carbon (SOC) in the Northern high latitudes (NHL). As a result of this, there are large uncertainties in modelling both the permafrost extent (Koven *et al*., 2012), and the carbon stored therein (Todd-Brown *et al*., 2013). Such a range in modelling outcomes show a strong need to systematically analyse, and to reduce the uncertainties from contributing processes within a model itself. Achieving a reasonable distribution of permafrost carbon in climate models is important because of the strong influence on future global climate through permafrost carbon feedbacks (Burke *et al*., 2012). However, a larger suite of active terrestrial processes coupled with scarcity of observational data introduce many challenges for modelling these processes (Walsh *et al*., 2007). Nonetheless, several studies in the recent past have demonstrated improved permafrost modelling capabilities by incorporating soil/snow processes that critically influence the ground energetics in these environments, such as: deep soil layers and organic soils (Lawrence *et al*., 2008), and the effects of wind compaction and depth hoar formations (Schaefer *et al*., 2009) , as well as structural properties of vegetation (phenology, assimilated vegetation C allocation to leaves, stems, and roots and root dynamics), which can change in response to changes in environmental factors, such as atmospheric CO_2 concentration and climate. However, no study has yet evaluated the combined effects of the improvements of these biogeophysical and biogeochemical processes on for the entire Northern high-latitudes.

METHODS

We use a land surface model, the Integrated Science Assessment Model (ISAM), which is a coupled biogeophysical (water, and energy) and biogeochemical (C and N) model that calculates terrestrial fluxes of C, N , water and energy at $0.5^o \times 0.5^o$ spatial resolution at multiple temporal resolution ranging from half hourly to yearly time scales (Barman *et al*., 2014a,b; ElMasri *et al*., 2013; Song *et al*., 2013), to investigate the effects of feedbacks between the biogeochemical and biogeophysical processes on the model estimated soil organic carbon (SOC) for the NHL permafrost region. We not only focus on recent model improvements in the biogeophysical processes that are deemed important for the high latitude soils/snow; such as deep soil column, modulation of soil thermal and hydrological properties, wind compaction of snow, and depth hoar formation; on permafrost SOC; but also biogeochemical processes; such as dynamic phenology and root distribution, litter carbon decomposition rates and nitrogen amount remaining; on soil biogeochemistry. We select multiple sites to evaluate the model. We then carried out several model simulations to study the effects of feedbacks between biogeochemical and biogeophysical processes on SOC.

CONCLUSIONS

After accounting for dynamic biogeochemical processes, ISAM is able to capture the seasonal variability in leaf area index (LAI), and root distribution in the soil layers and the root response of soil water uptake and transpiration. The evaluation of the model results suggest that without accounting these processes, modelled growing season length (GSL) for NHL was almost two times higher as compared to measurements. To quantify the implication of these processes on the carbon and water fluxes, we compared the results of two different versions of ISAM, dynamic version which accounts for dynamic processes ($ISAM_{DYN}$) and static version which do not account for dynamic processes ($ISAM_{BC}$), with measurements from12 eddy covariance flux sites. The results show that $ISAM_{DYN}$, unlike $ISAM_{BC}$, is better able to capture the seasonal variability in GPP and energy fluxes. Our modelling analysis shows that by including the biophysical processes in addition to biogeochemical processes, the modelled NHL permafrost carbon increased by 30% from 328 to 447 GtC in the top one meter of soil which is in better agreement with observational estimates of 495 GtC (Northern Circumpolar Soil Carbon Database). Even though the inclusion of these processes generally reduced vegetation productivity and litter production due to a decrease in soil temperature and liquid water content, increased soil carbon stocks highlight the dominance of soil water/temperature stress on decomposition processes. While continued improvements are required in the treatment of biogeochemistry, here we demonstrate the importance of soil/snow biogeophysical and biogeochemical processes in modelling permafrost carbon stocks, as important drivers of soil biogeochemical processes.

ACKNOWLEDGEMENTS

This work was supported in part by the U.S. Department of Energy (DOE) Office of Science (DOE-DE-SC0006706).

REFERENCES

Barman, R., Jain, A. K., Liang, M. (2014a). Climate-driven uncertainties in terrestrial gross primary production: a site-level to global scale analysis. *Global Change Biology*, DOI: 10.1111/gcb.12474.

Barman, R., Jain, A. K., Liang, M. (2014b). Climate-driven uncertainties in terrestrial energy and water fluxes: a site-level to global scale analysis. *Global Change Biology*, DOI: 10.1111/gcb.12473.

Burke, E., C. Jones, and C. Koven, 2012: Estimating the permafrost-carbon climate response in the CMIP5 climate models using a simplified approach. *J. Climate*. 26, 4897-4909.

El-Masri, B., Barman, R., Meiyappan, P., Song, Y., Liang, M., and Jain, A. K. (2013). Carbon dynamics in the amazonian basin: Integration of eddy covariance and ecophysiological data with a land surface model. *Agr. Forest Meteorol.*, doi:10.1016/j.agrformet.2013.03.011, 2013.

Koven, C., W. Riley, and A. Stern, (2012): Analysis of permafrost thermal dynamics and response to climate change in the CMIP5 Earth System Models. J. Climate. 26, 1877-1900.

Lawrence, D. M., Slater, A. G., Romanovsky, V. E., and Nicolsky, D. J. (2008). Sensitivity of a model projection of near-surface permafrost degradation to soil column depth and representation of soil organic matter. *Journal of Geophysical Research*, 113(F2), F02011.

Schaefer, K., Zhang, T., Slater, A. G., Lu, L., Etringer, A., and Baker, I. (2009). Improving simulated soil temperatures and soil freeze/thaw at high-latitude regions in the simple Biosphere/Carnegie-Ames-Stanford approach model. *Journal of Geophysical Research: Earth Surface (2003–2012), 114*(F2)

Song, Y., Jain, A.K., & McIsaac, G.F. (2013).Implementation of dynamic crop growth processes into a land surface model: evaluation of energy, water and carbon fluxes under corn and soybean rotation. Biogeosciences Discuss., 10, 9897-9945.

Todd-Brown, K. E. O., Randerson, J. T., Post, W. M., Hoffman, F. M., Tarnocai, C., Schuur, E. A. G., and Allison, S. D. (2013). Causes of variation in soil carbon simulations from CMIP5 earth system models and comparison with observations. Biogeosciences,10(3), 1717-1736.

Walsh, J., Anisimov, O., Hagen, J., Jakobsson, T., Oerlemans, J., Prowse, T., Romanovsky, V. Savelieva, N., Serreze, M., Shiklomanov, A., Shiklomanov, I., Solomon,S. (2005). Cryosphere and hydrology. *Arctic Climate Impact Assessment*, 183-242.

MICROORGANISMS IN BEIJING'S PM2.5 AND PM10 POLLUTANTS

J. JIANG

School of Environment, Tsinghua University, Beijing, China.

INTRODUCTION

Particulate Matter (PM) has been shown to be a major air pollutant in Beijing (Cheng et al., 2013). Though PM physicochemical characteristics have been studied extensively, much less is known about what microorganisms are in the PM pollutants. When measuring bioaerosol, culture-based method is constrained to a limited number of cultivatable species. Though 16S or 18SrRNA gene sequencing has been used to characterize bacteria or fungi, they cannot provide information at species level which is necessary to understand the allergenic and pathogenic potentials of microorganisms.

METHODS

In this study, metagenomic methods were employed to analyze the microbial compositionsof Beijing's PM2.5 and PM10 pollutants. With sufficient sequencing depth, airborne microbes including bacteria, archaea, fungi and dsDNA viruses were identified at species level (Cao et al., 2014). Bacteria appeared to be the most abundant prokaryotic microorganisms. Among them, the most abundant phyla were *Actinobacteria, Proteobacteria, Chloroflexi, Firmicutes, Bacteroidetes* and *Euryarchaeota*.

RESULTS

The results showed that the majority of the microorganisms were soil-associated and nonpathogenic to human. Nevertheless, the sequences of several respiratory microbial allergens and pathogens were identified. Furthermore, their relative abundance appeared to have increased with increased concentrations of PM pollution.

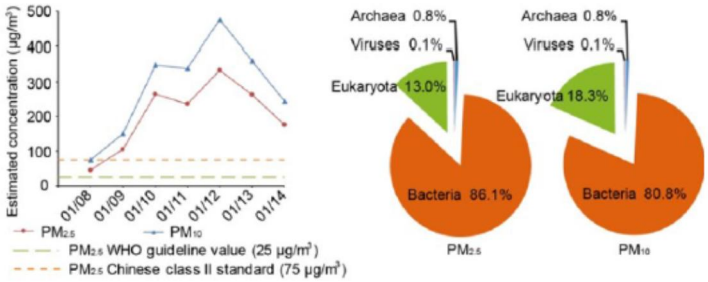

Figure 1. Daily average PM2.5 and PM10 concentrations during Jan 8-14, 2013 (left) and relative abundance of different microorganisms in PM samples (right).

ACKNOWLEDGEMENTS

Daily average PM2.5and PM10concentrations during Jan 8-14, 2013 (left)and relative abundance of different microorganisms in PM samples (right).

REFERENCES

Cheng, Z., Jiang, J., Fajardo, O.,Wang, S., Hao, J. (2013). *Atmos. Environ.*, **65**,186-194.
Cao, C., Jiang, W., Wang, B., Fang, J., Lang, J., Tian, G., Jiang, J., Zhu, T.F. (2014). *Environ. Sci. Technol.*, **48**, 1499-1507.

RUSSIAN SCIENCE AND TECHNOLOGY FORESIGHT AND PEEX AGENDA

N.S. KASIMOV[1], N.N. ALEKSEEVA[1], L.M. GOKHBERG[2] and A.V. SOKOLOV[2]

[1]Faculty of Geography, Lomonosov Moscow State University, Moscow, Russian Federation.

[2]Institute for Statistical Studies and Economics of Knowledge, National Research University – Higher School of Economics, Moscow, Russian Federation

Keywords: RUSSIAN LONG-TERM FORESIGHT, ENVIRONMENT, NATURAL RESOURCES, PEEX.

INTRODUCTION

State of environment is now considered as important interdisciplinary area of scientific and technological development that can make contribution to the nation's security, economic growth, and competitiveness. In Russia it has long been considered as second-rate as compared with the economic growth. Now efficient environmental management is listed among the priorities identified by the Government of the Russian Federation together with life sciences, energy sector, transport, ICT, etc . In contrast to other sectors, natural resources and environment sectors are characterized by comprehensive interdisciplinary solutions, long planning horizons, the inability to obtain rapid and clear economic benefits. That is why this sector still depends greatly on the government regulation in Russia.

The paper reveals key features and the results of national long-term science and technology (S&T) foresight of sectors associated with environment and natural resources. The urgent priorities of the research and development (R&D) for the next decade in Russia are close to PEEX research agenda.

METHODS

Russian S&T Foresight is aimed at identifying the most promising areas of science and technology development in Russia towards 2030 to ensure the implementation of the competitive advantages of the country (Ministry of Education and Science of the Russian Federation, 2013; Sokolov and Chulok, 2012). The foresight was undertaken at the moment when major changes occurred in Russian economy (particularly in the area of S&T) associated with transformation of scientific and innovation policy with expansion of the range of subjects and instruments used.

The foresight of environmental management represented a wide coverage of issues (global and national challenges, growing markets, analysis of perspective products and technologies, new emerging issues and barriers, assessment of the R&D level in Russia vis-a-vis leading countries in the world, etc) and methods (expert panels, surveys, bibliometric analysis, review of patent data, roadmapping, etc.).

As the foresight methodology requires the involvement of experts and stake-holders in the foresight process, the capacity building and networking was crucial for the research (Meissner, et al, 2013). S&T Foresight centres for expert support of the foresight activities were organized at various Russian universities. The Science & Technology Foresight Centre on Environmental Management was established at Lomonosov Moscow State University, it coordinates the network of the other research universities in Russia which are the centers of competences in key critical technologies (Kasimov, Alekseeva, 2013).

The other important instrument for the foresight studies was the involvement of the expert potential of the Technology platform “Technologies of Environmental Development” created under Russian Geographical Society in 2011. Its serves as a communication platform for business, academia, state governance and civil

society for the promotion of environmental technologies and eco-services in Russia. Now 285 companies, educational and scientific institutions, public organizations are the members of the Technology platform "Technologies of Environmental Development". The expert community participated in various foresight procedures including expert panels, brainstorming, surveys, questioning, workshops carried out jointly by Moscow State University and the Higher School of Economics. In total some 300 experts were invited to participate in the research. The study is based on the thorough analysis of expert opinions and their assessment of future applications and the development of demand for these applications.

RESULTS AND DISCUSSION

A large number of global challenges which will face humanity in the near future are linked to the environment and the unsustainable use of natural resources (OECD, 2012). The foresight process resulted with a set of global and national challenges, windows of opportunities and emerging threats for Russia, with breakthrough future technology along with a list of priority S&T areas related to the environment in Russia (Alekseeva, 2013). They were identified from the policymakers' perspective in order to support development of relevant strategies. Results were validated through a process of consultation, which involved: regular high-level expert panels, series of workshops and seminars, discussions at national and international scientific conferences, presentations at the sites of federal and regional authorities, domestic and foreign universities, research centers, and international organizations.

Windows of opportunity in the field of environment that may open in medium- and long-term perspective are as follows:

- Development of technologies for environmentally safe recycling of waste and disposal of toxic substances,
- Creating effective technologies of remote monitoring and evaluation of ecosystems,
- Creating super-computing technologies and information infrastructure,
- Development of methods of forecasting hydrometeorological processes,
- Development of methods of forecasting natural and technogenic emergency situations,
- Conducting complex exploration of the Arctic zone of Russia,
- Wide-range use of materials with new properties and technologies, development of "green" construction,
- Development of environment-friendly transport,
- Development of new technologies of production and deep processing of hydrocarbons.

Based on the expert research the following main markets in the area of environmental safety and management were identified:

1) Technologies for monitoring and forecasting of the environment, including natural and man-made emergencies;

2) Technologies for efficient development and use of natural resources;

3) Technologies for prevention and mitigation of environment pollution (including the impacts of accidents).

According to the experts, up to 2020 the most rapidly growing markets of Russia are as follows: equipment and materials for efficient extraction and processing of mineral resources; systems of early detection and prediction of natural and man-made emergencies; environmentally-friendly materials and products; software and geographic information systems (GIS). In the long term (2020-2030) the markets of water treatment and water reuse, environmentally safe waste management, as well as the markets of recycling and finished products based on the processing of waste and wastewater can significantly increase.

According to experts, two different global economic trends can create the best opportunities for the S&T development in Russia: 1) the greening of the economy and "green growth", and 2) the growth of offshore oil and gas production and the accelerated development of the Arctic zone of the Russian Federation. This

result reflects the really existing uncertainty in the choice of a long-term way of scientific and technological development, a kind of “bifurcation point” between innovative direction and the energy and raw materials based scenario of Russia's long-term technological development. Now both trends in Russia are developing in line. Currently, S&T development is concentrated in the areas which get sufficient financial support (from state or companies) and address the issues of environmental responsibility.

The recent foresight study revealed that the most booming areas of S&T development in Russia will be focused on the issues of exploration and development of the wide range of resources of the Arctic zone including large deposits of hydrocarbons and solid minerals on the Arctic shelf of Russia. According to the Strategy of the Development of the Arctic zone of the Russian Federation and National Security until 2020, the growth of shelf oil and gas production and the acceleration of the Arctic region development will allow to increase resources and raw materials availability and will create opportunities for developing transport system in the region including Northern Sea Route. The development of the Arctic zone of Russia will require the mobilisation of significant financial resources (Ernst & Young, 2013). As technological opportunities arise for the extraction of hydrocarbons, there may be some risk of increasing geopolitical competition in "disputed" areas.

The large-scale extraction of deposits in the Arctic presupposes the implementation of environmentally safe technologies of oil and natural gas production and processing. Among the fastest growing technologies are the systems of environmental monitoring, technologies and methods for bio-remediation of oil polluted soils, waste oil disposal from oil spills, remote sensing to justify placing of oil and gas facilities with improved environmental safety. There is the need of comprehensive development of mechanisms to offset damages caused by potential incidents which, according to the experts, at present cannot be covered by any insurance company. Climate change also poses serious risks, potentially causing the destruction of the mining industry infrastructure in the Arctic, which will with a high probability result in an environmental disaster.

Current and future R&D in the field “Inventory and utilisation of resources of the World Ocean, Arctic and Antarctic regions” are in line with PEEX activities. Among them we can mention:

- Technologies of integrated hydro-meteorological monitoring of natural hazards, including ice conditions in the Arctic zone
- Technologies of remote sensing, including environmental monitoring, for resource assessment and forecasting of the natural environment of the Arctic zone of the Russian Federation on the basis of a multi-purpose Russian space system "Arktika", as well as automated data collection and processing of information in remote areas in the Arctic zone of Russia.

While PEEX is investigating various types of natural ecosystems and urban environments, its scope is extensive enough to provide gap-filling and integrated scientific knowledge related to a wide range of research questions (Lappalainen et al, 2014). There are many challenges and threats that determine the urgent priorities of the R&D for the next decade in Russia which are close to PEEX research agenda. Environmentally safe technologies for the development of the Arctic zone of Russia are of priority importance as well as actions for adaptation to climate change and mitigation of effects of thawing permafrost.

The experts indicated a rather broad range of potential threats to Russia concerning environment within PEEX domain:

- Trans-boundary transport of pollutants in the northern areas;
- Need for rehabilitation areas with strong anthropogenic pollution and accumulated environmental damage in the Arctic zone of Russia;
- Thawing permafrost that causes deformation and disruption of the functioning of engineering structures and communications. Increased risks of industrial accidents and spills of hydrocarbons;
- Need to cope with the a favorable environment for disease vector, expanding the range of tick-borne encephalitis, borellioza, salmonellosis and other diseases;

- Depletion of biological resources due to habitat pollution and habitat losses as well as over-exploitation of some species;
- Spread of alien species, the displacement of native Arctic species by the invasive species from southern latitudes;
- Increased public attention to the ecological status of the Russian Arctic;

Experts indicate the deficiency of technological possibilities for the research, development and effective use of Arctic areas and resources at the moment. The crucial challenge is lacking of preparedness for the transition to innovative development of the Russian Arctic. Solution to the problem lies not only in the increased funding of the environmental activities by state-owned companies but in much better coordination by various agencies and organizations of the development of the resources in the Arctic zone of Russia.

Windows of opportunities indicated by the experts are as follows:

- Creating a unique forecasting system for hydrometeorological support at high latitudes on the basis of domestic satellite data and technology of model weather forecasts;
- Developing and improving of the models of permafrost behavior under different external conditions;
- Creating and applying a systematic, evidence-based package of measures to monitor engineering and permafrost conditions in the areas of industrial development within the permafrost zone;
- Creating a system for monitoring the soil temperature in the major settlements of the Arctic zone of Russia and the improvement technologies to strengthen ground under buildings and industrial enterprises;
- Continuous monitoring of environment and geochemical situation;
- Introduction of biological resources monitoring programs to assess the state of resources and amount allowable fishing;
- Development and implementation of methods for preventing the invasion process (search for biological counterparties), the development and improvement of quarantine and diagnostic equipment;
- Developing and implementing the National Strategy for rare and endangered species of the Arctic zone of Russia;
- Further development of a system of protected areas;
- Development, upgrading and implementation of effective environmental education programs.

CONCLUSIONS

In January 2014 the Prime Minister of the Russian Federation approved the Long-term Forecast for Scientific and Technological Development of Russia until 2030. The Foresight results were implemented in the State Program “Development of Science and Technology” for 2013-2020, Strategies and programs for the development of regional innovative clusters, technological platforms and companies. The Foresight–2030 has given support for the revision of the national list of S&T priorities and critical technologies.

Some of prospective thematic areas indicated in the Long-term Forecast for Scientific and Technological Development of Russia until 2030 are very close to PEEX scientific agenda and this creates sustainable platform for further collaboration and participatory research.

ACKNOWLEDGEMENTS

This work was supported by the Ministry of Education and Science of the Russian Federation.

REFERENCES

Alekseeva, N. (2013). Science and Technology Foresight 2030 in Russia: Environmental Management, *Geography, Environment, Sustainability*, **02** (v. 06), 94-96.

Ernst & Young (CIS) B.V. (2013) Neft' i gaz Arktiki. Retrived: 28.11.2014 from http://www.ey.com/Publication/vwLUAssets/Arctic_report_rus/$FILE/Arctic_report_rus.pdf

Kasimov, N.S., N.N. Alekseeva (2013). Systema nauchno-technologicheskogo prognozirovania po prioritetnomu napravleniyu Racional'noye prirodopolzovanie (System of S&T forecast of environmental management), *Vestnik MGU. Geography series*, **4**, 95-96. (in Russian)

Lappalainen, H.K., T. Petäjä, J. Kujansuu, et al (2014). Pan Eurasian experiment (PEEX) – a research initiative meeting the grand challenges of the changing environment of the Northern Pan-Eurasian Arctic-boreal areas, *Geography, Environment, Sustainability*, **02** (v. 07), 13-48.

Ministry of Education and Science of the Russian Federation (2013). Prognoz nauchno-technologicheskogo razviyia Rossiyskoy Federacii na period do 2030 goda (*Russian S&T Foresight up to 2030)*. Moscow: 80.

Sokolov A., A. Chulok (2012). Dolgosrochnyy prognoz nauchno-tekhnologicheskogo razvitiya Rossii na period do 2030 goda: klyuchevye osobennosti i pervye rezul'taty (Russian S&T Foresight–2030: Key Features and First Results), *Foresight-Russia*, **1** (v. 6), 12-25.

Meissner D., Gokhberg L., Sokolov A. (eds.) (2013). *Science, Technology and Innovation Policy for the Future: Potentials and Limits of Foresight Studies*. Heidelberg, New York, Dordrecht, London: Springer.

OECD (2012). *OECD Environmental Outlook to 2050. The Consequences of Inaction*. Paris: OECD Publishing. Retrived: 01.11.2014 from http://www.oecd-ilibrary.org/environment/oecd-environmental-outlook-to-2050_9789264122246-en;jsessionid=2vq54j2113bgd.x-oecd-live-02

GEOCHEMICAL PATTERNS IN A LARGE RIVER NETWORK DUE TO HYDROCLIMATIC DEVELOPMENT AND ANTHROPOGENIC IMPACTS: SELENGA-BAIKAL CATCHMENT

N.S. KASIMOV[1], S.R. CHALOV[1] and M.Y.LYCHAGIN[1]

[1]Lomonosov Moscow State University, Moscow, Leninskie gory, GSP-1, 119991.

Keywords: LAKES, WETLANDS AND LARGE RIVER SYSTEMS IN SIBERIAN REGION; CLIMATE CHANGE; ANTHROPOGENIC IMPACTS ON WATER.

INTRODUCTION

Many Asian rivers have been intensively used to boost economic growth, resulting in sudden and drastic changes in geochemical patterns. The present research considers the unregulated Selenga River and its basin. The Selenga River, which originates in Mongolia, contributes about 50 % of the total inflow into Lake Baikal. Together with the Angara and Yenisey rivers it forms the longest river network in Eurasia. Elevated sediment-associated chemical concentrations reported for the area (Chalov et al, 2014) tend to fall into one of two categories: those associated with soil/petrologic anomalies or those associated with anthropogenic inputs. The latter is related to mining, industrial and agricultural activities within the Selenga drainage basin, which affect the geochemical patterns in the rivers. At the same time, the region is reported to experience the warming trends with acceleration since the 1970s (Unger-Shayesteh et al., 2013), what has a profound impact on the components of hydrological system in the area. The catchment is still lacks of any type of soil and water conservation and sediment control programmes as far as reservoir constructions which are in the global perspective cause decreased sediment fluxes (e.g. Walling, Fang, 2003).

The key question for the understanding regional environmental change is to disentangle the influence of climate change from that of other changes in catchment condition. The present study is focused on temporal trends in geochemical fluxes. The noted spatial variability of water and suspended sediment composition was used to determine nature of change based on the catchment inventory and basin wide accounting segment combining climatic, hydrological and land use drivers.

METHODS

The present analysis is based on data from the national gauging network of the Selenga River Basin, which is implemented by the Russian and the Mongolian hydrometeorological surveys for their corresponding parts of the basin. The long-term hydrological changes in the selected rivers were calculated based on reference period 1975-1995 for the average values of 1996-2011:

$$\Delta Q = \frac{Q_{1996-2011}}{Q_{1975-1995}}$$

For the detailed investigation of geochemical patterns novel screening campaigns were conducted in June–September 2011-2014 in both the Russian and the Mongolian parts of the Selenga river basin. Discharge and suspended sediment concentration (SSC) data were combined to yield estimates of daily and monthly water discharges, suspended load averages at more than 150 locations. All samples (suspended and streambed sediments and filtered water) were analyzed for 62 elements by inductively-coupled plasma mass spectrometry ICP-MS (ICP-AES) using a semi-quantitative mode and a 10-fold automated dilution during the analysis. Elemental analyses were conducted on the filtered samples without additional treatment. For a fully quantitative analysis, the instrument is calibrated with a series of known standards for each element. Corrections are applied for potential interferences, and more comprehensive quality assurance/control measures are performed for each element. The contribution of various forms of transport to sediment-associated chemical constituents are

$r_{s\text{-}d} = C_{dissolved} / C_{suspended}$

where $C_{dissolved}$, $C_{suspended}$ are concentration of chemical elements in the dissolved and suspended phases. The spatial variability of geochemical fluxes was evaluated based on environmental surveys conducted in 2011- 2014. The surveys targeted sites located along the Tuul River (T), the Orkhon River (O), the Eg River (EG), the Yeroo River (ER), the Khangal River (H), the Selenga River (S) and the Kharaa River (Hr) in Mongolia (Fig. 1). In Russia the observational sites were located along the main stem of the Selenga River (S) and its main tributaries – Dzhida (D), Temnik (TM), Chikoy (CHK), Hilok (HK), Orongoy (OR), Uda (U), Itantsa (IT), Kiran (KR), Kudara, Zheltura (G), Udunga (UD), Suhara (SH), Tugnui (TG), Menza (MZ), Buy, Bryanka (BK), Ilka (IK), Chelutay, Kurba (KB), Kodun (KD), Kizhinga (KG), Ona (Fig. 1). In the present paper the analyses have been done for the selected case study catchments, covering the main hydrological and soil/petrologic conditions, as far as various types of human pressures.

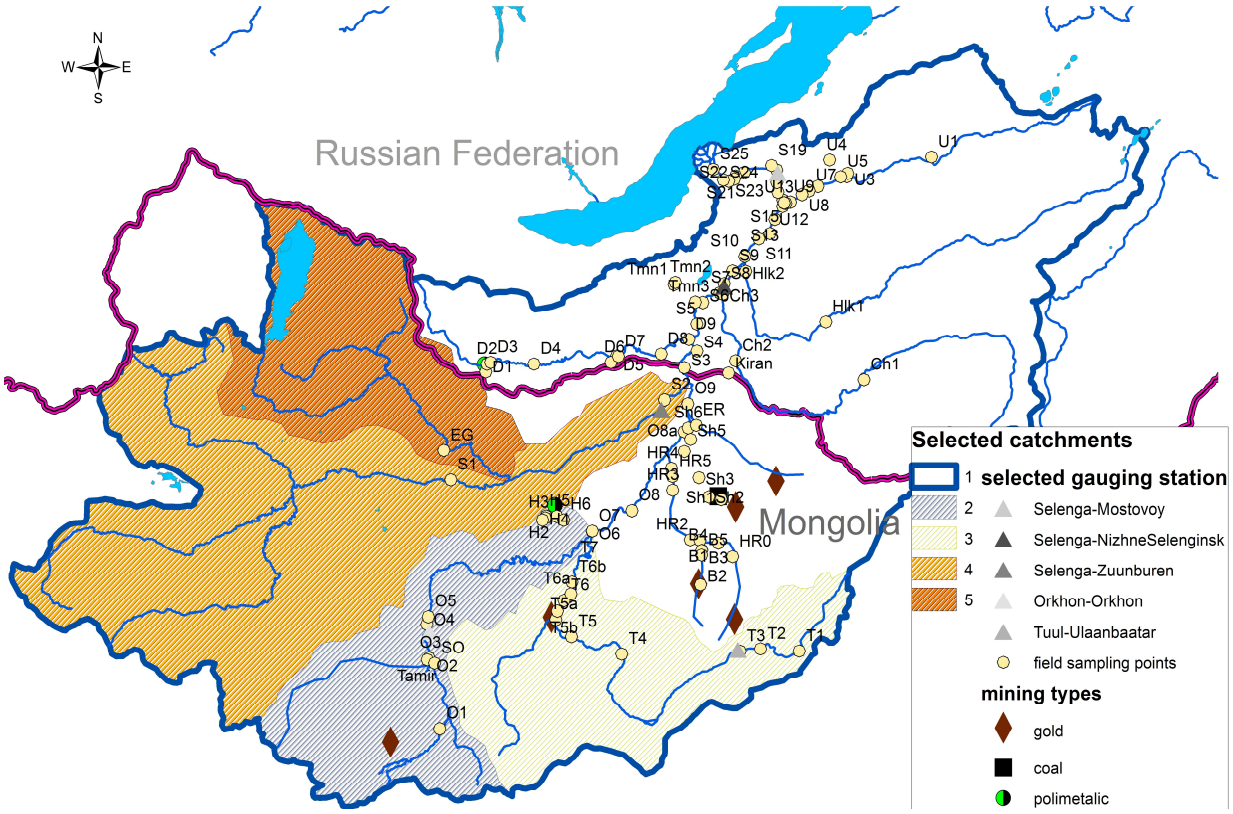

Figure 1. Selenga River Basin showing sampling sites, major mining sites and main subcatchments (1 – whole Selenga catchment. 2 – Orkhon river, upper part; 3 – Tuul river; 4,5 – upper Selenga River with Eg River and Khovsgol Lake)

DISCUSSION AND RESULTS

Climate variability and change is one major driver of hydrological trends in dry lands. In Mongolia, air temperature has increased by 1.8^{0}C since the 1940s, and precipitation decreased in some parts of the country, including the Western slopes of the Khentii mountains. The latter is regarded to be the main reason of long-lasting low water period (since around 1989) that is reported for the Selenga River. The runoff records for downstream Selenga (Mostovoy) shows statistically significant downward trend from 903 m^3/s (for the period since 1941 to 1982) to 888 m^3/s (for the period since 1983 to 2011), or even more drastic for the recent decades – from 940 m^3/s (for the period since 1975 to 1995) to 689 m^3/s (for the

period since 1995 to 2011). The mean annual discharge at some gauging stations within the Mongolian part of the basin) demonstrated even more significant decrease during the last decades, from an average of 53,3 m^3/s during the period 1975-1995 to only 18,1 for the years 1996-2011 at the upper Orkhon river (Orkhon-Orkhon) and from 35,3 m^3/s to 14,9 m^3/s for the Tuul river at UlaanBaatar respectively. The changes were caused mostly by intensive rainfall floods which determined high water period in the early 1990 and late 1970-1980. This decrease primarily caused a reduction in precipitation and an increase in evapotranspiration during that period, though intensified water use for irrigation purposes may have contributed as well.

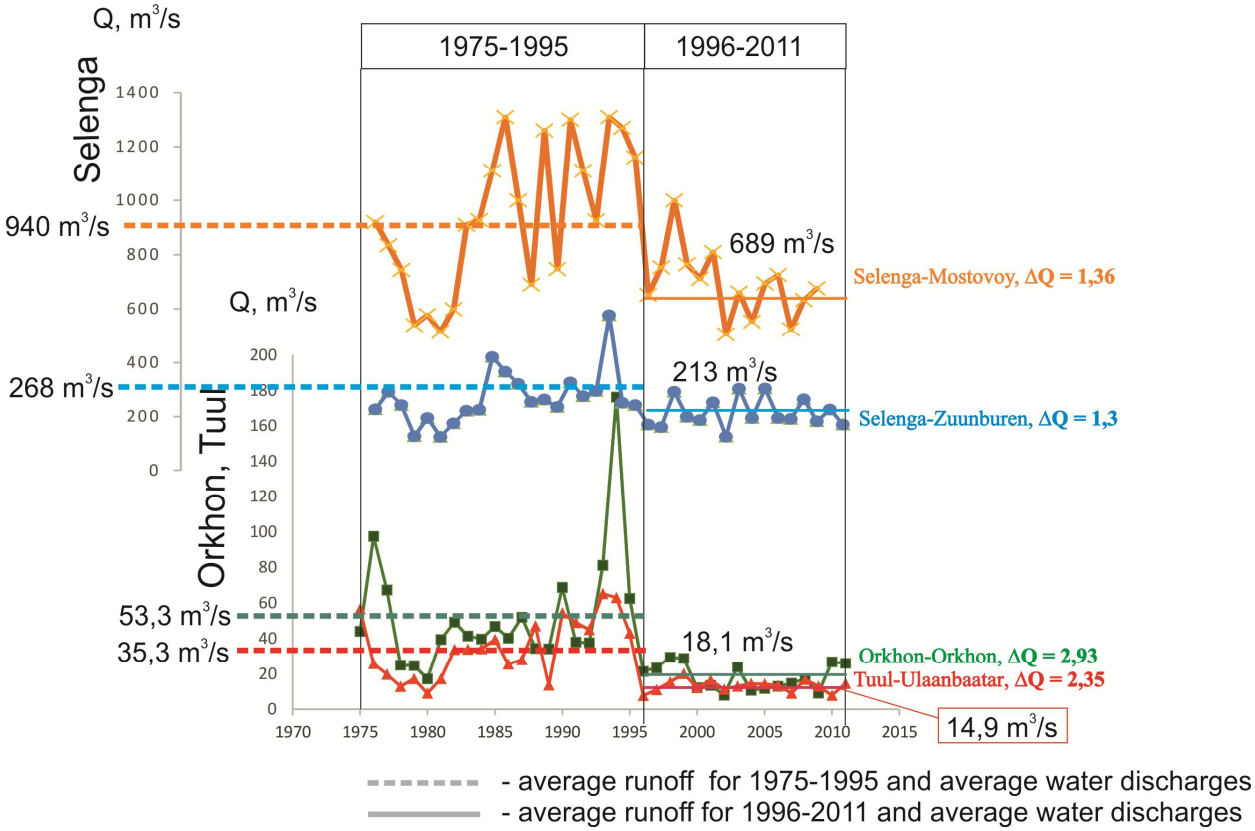

Figure 2. Changes of hydroclimatic drivers in Selenga catchment (location of the gauging station – see fig 1)

Following mentioned changes in climatic conditions, there has been a substantial decline in sediment yield of Selenga River (from 5832 t/day to 3015 t/day) and its main tributaries in the Russian part of the river basin. In the upper part of the basin where an absence of routine monitoring of sediment loads precludes statistical analyses of the sediment trends, the few evidences of the sediment yield decrease have been seen based on the comparison between SPM concentrations measured during the campaigns of 2011-2014 and historical field campaigns of 1934-1936 (Kuznetsov, 1955). At the upper part Selenga above the Eg River (S-1) SSC varied between 1.2 mg/l (20th February) to 1193 mg/l (8th August) in 1934 (Kuznetsov, 1955), whereas in 2001 it was 11.5 mg/l (18th-24th August). During our field campaigns SSC varied from 9.51 mg/l (16th June, 2012) to 114 mg/l (2nd August, 2011). At the confluence of Orkhon and Tuul, a 65-fold increase of SSC was observed during summer floods for the Tuul River (T-9) (from 11 mg/l at the 19th October, 1934 to 716 mg/l at the 26th August, 1934) and 43-fold for the Orkhon River (O-6) (from 23.3 mg/l at the 17th June, 2012 to 1000 at the 7th May, 1934).

Changes in the primary chemical composition of water of the downstream Selenga River were also related with the hydrometeorological drivers. Slight increase of total dissolved solids and twice increase of SO_4 (from 6.2-8.6 in 1950-1970 to 10.6-16.4 mg/l during 1995-2011) was caused by the lasting low-water

period. Origin of metals and sediment-associated chemical constituents could be related both to natural and anthropogenic drivers. The examples of the upper Orkhon, upper Selenga and Tuul rivers, as far as downstream Selenga river represent contrasting environmental condition (table 1). Upper Selenga is relatively undisturbed part of Selenga catchment with typical distribution of pastures as the only dominated type of land use. This is forested part of Mongolia. The upper Orkhon contains few small towns and mining sites. Tuul river drains the driest and mainly steppe part of Selenga catchment, which contains both largest mining and industrial center of Mongolia and regarded to be the mostly polluted river in the region. Half of the Mongolian population is concentrated within its capital (Ulaanbaatar). Due to poor maintenance, lack of spare parts, outdated equipment, and frequent power outages, waste water from the wastewater treatment plants in Ulaanbaatar might be released directly into the Tuul River without treatment.

№	Catchment	Precipitation (annual averaged)	ΔQ	Average elevation, m	Afforestation (%)	Population	% of mining areas
1	Selenga	321	1,46	-	-	2500 000	-
2	Selenga, upper part (within Mongolia)	248	1,3	1750	50	5000	<0,1
3	Orkhon (upper part)	242	2,93	1753	32	50 000	0,7
4	Tuul	200	2,35	1375	23	1300 000	0,7

The discharge data are according to the following stations: Selenga-Mostovoy, Selenga-Zuunburen, Orkhon-Orkhon, Tuul-Ulaanbaatar

Table 1. Key features of the Hydroclimatic Development and Anthropogenic Impacts in the selected subcatchments (fig. 1) in Selenga-Baikal region

Geochemical patterns in various parts of the catchment are determined by both natural and technogenic factors. Regional petrology causes the general enrichment of suspended matter and sediments by As, Cd, Sn, Sr, W, Pb in comparison with the lithosphere averages. The common feature of the basin consists in a prevailing transport of dissolved forms of chemical elements which a highly mobile in alkaline environment (Table 2). The share of dissolved forms of B, As, Mo, Cr, U increases (in some cases up to 98%) mostly during the low-water period (June 2012). The high water period (July 2011) is characterised by increasing turbidity of river water and the growing importance of the particulate forms of heavy metals (Fe, Mn, Ni, Co, Pb, Cu, Zn).

Concentration of chemical elements in the particulate form	Orkhon catchment		Tuul river catchment		Selenga river catchment, upstream		Selenga river catchment, downstream	
	July 2011	June 2012	July 2011	June 2012	July 2011	June 2012	July 2011	June 2012
> 75 %	V, Cr, Mn, Fe, Co, Ni, Cu, Zn, Pb	-	Mn, Fe, Co, Zn, Pb	-	V, Mn, Fe, Co, Zn, Pb	Fe		V, As
50-75 %	As, U	Fe, Cu	V, Ni, Cu	Fe	Ni, Cu	Cr, Mn, Co, Cu, Pb	Cr, Mn, Fe, Co, Ni, Cu, Zn, As, Pb	Mn, Fe, Co, Ni, Cu, Pb
25-50 %	B	V, Mn, Co, Ni, Pb	-	V, Mn, Co	B, As	V, Ni, Zn	-	B, Cr, Zn
< 25 %	Mo	B, Cr, Zn, As, Mo, U	B, Cr, As, Mo, U	B, Cr, Ni, Cu, Zn, As, Mo, Pb, U	Cr, Mo, U	B, As, Mo, U	B, Mo, U	Mo, U

Table 2. Geochemical patterns related to the hydroclimatic and anthropogenic variability

In a larger scale, there are few examples of the huge anthropogenic pressure on the geochemical patterns. Khangal River downstream of a large copper-molybdenum mine-mill complex Erdenet had sulfate concentrations that were about five times greater, and copper concentration at least 50 times greater than the background values. The similar changes in geochemical patterns of the Dzhida River and its small tributary Modonkul below Zakamensk wolfram-molybdenum mining and processing factory were related to high values of heavy metal pollution. Increase in both dissolved and suspended forms is observed. Content of heavy metals in the suspended matter of the Modonkul River increases by 1-2 orders of magnitude compared with the background values. Suspended matter of the Dzhida River is also enriched with heavy metals.

CONCLUSIONS

Results indicate that high sediment loads were reported both for altered and natural rivers. Mining impacts on sediment loads were seen mostly during relatively short hydrological events, during which an intensified slope wash near floodplain mining activities could flush large amounts of turbid water into the river. Reported multi-decadal declines in sediment loads in the downstream part of Selenga River can be attributed to the abandonment of cultivated lands and changing hydroclimatic factors, such as in particular climate-driven decrease of water flows and intensified water use for irrigation purposes.
Whereas sediment flows were connected with the hydroclimatic conditions in the catchment, elemental composition of the mass flows mostly relate to the soil/petrologic conditions. With the exception of small impacted rivers where water quality impacts associated with mining were found, the formation of elemental compositions and sediment-associated chemical constituents generally reflects catchment characteristics.

ACKNOWLEDGEMENTS

The work at Selenga River is implemented under support of Russian Scientific Foundation project (№ 14-27-00083).

REFERENCES

Chalov S., Jarsjö J., Kasimov N., Romanchenko A., Pietron J., Thorslund J., Belozerova E.. Spatio-temporal variation of sediment transport in the Selenga River Basin, Mongolia and Russia. Environmental Earth Sciences. DOI: 10.1007/s12665-014-3106-z

Kuznetsov NT (1955) Main regularities rivers regime of Mongolian People's Republic. Academy of Sciences, Moscow

Unger-Shayesteh K, Vorogushyn S, Farinotti D, Gafurov A, Duethmann D, Mandychev A, Merz B (2013) What do we know about past changes in the water cycle of Central Asian headwaters? A review. Global Planet Change 110(Part A):4–25. doi:10.1016/j.gloplacha.2013.02.004

Walling, D.E. and Fang, D. Recent trends in the suspended sediment loads of the world's rivers // Global and Planetary Change. 2003. 39. P. 111-126

GENERALIZING FLUX TOWER MEASUREMENTS WITH LIDAR-ASSISTED FOREST MAPS

T. KAURANNE[1], LI ZHANG[2]

[1] Lappeenranta University of Technology, Department of Mathematics and Physics, Lappeenranta, Finland.

[2]Institute of Geographical Sciences and Natural Resources Research, Chinese Academy of Sciences, Beijing, China.

Keywords: flux towers, greenhouse gas measurement, spatial generalization, lidar-assisted forest inventory.

INTRODUCTION

Carbon cycles in terrestrial ecosystems are controlled by many environmental factors such as solar radiation, temperature, precipitation, and carbon dioxide concentration. Any changes in these factors will cause variability in carbon sequestration and thus in the carbon sink function of terrestrial ecosystems. China's Terrestrial ecosystems absorbed carbon at a rate of 0.06-0.26 Pg C /yr. Terrestrial ecosystems in China cover a large land area and include many vegetation types including boreal forests, temperate forests, tropical forests, grassland, deserts, and cropland. Among various vegetation types, forests play a critical role in terrestrial carbon cycle in China. Forest biomass carbon stock increased significantly since 1980s. About 0.075 Pg carbon has been sequestered into forests in China per year during 1981-2000. However, the prediction of carbon cycle models remains uncertain (Liu et al, 2011), which mainly derives from driving data, model structure, model parameters, and scaling algorithms (He et al, 2010). To reduce the uncertainty in carbon cycle modeling requires a combination between carbon cycle observations from multiple sources and carbon cycle models by data assimilation techniques or model-data fusion techniques (Raupach et al, 2005).

SPATIAL GENERALIZATION OF FLUX TOWER MEASUREMENTS

Recent advances in statistical estimation methods provide several promising tools for generalizing in situ measurements to a wider geographical area using auxiliary datasets, such as satellite images. The most dramatic strides have been taken under the broad headline of Bayesian estimation methods. Bayesian estimation differs from classical regression estimation in that it allows model-based inference to be included in the estimation process. Models that describe the physical characteristics of the phenomenon under study can be taken into a unified framework, along with measurements and observations. Such model-based estimates comprise the prior of the total estimation process. This prior is then modified with a weighted average of in situ measurements to create a final - or posterior - estimate. Unlike in classical regression where the mean value of measurements is the assumed estimate, in Bayesian estimation it is the forecast from a chosen model. Measurements are included as deviations from this forecast that can be interpreted as the mode of the posterior that is used as the final estimate. In spatial generalization, such models can be constructed from the correlations obtained between in situ measurements and remote sensing data of the corresponding spatial environment. Pairs of satellite images and in situ measurements can be taken as a teaching set for a Bayesian model that generalizes e.g. carbon flux estimates based on the observed correlation between flux measurements and forest type, as inferred from satellite imagery, possibly

combined with ground observation.

LIDAR-ASSISTED CARBON FLUX MAPS

A particularly promising form of such Bayesian spatial generalization is Sparse Bayesian Regression. This estimation method was originally developed by Tipping and later on adapted to forest estimation by (Junttila, Maltamo and Kauranne, 2008). Sparse Bayesian Regression is linear regression that has been equipped with automatic variable selection and decision on the degree of the model to be automatically produced by the method. It adapts both the number and choice of variables to criteria that combine explanatory power with robustness of the estimates produced.

Sparse Bayesian Regression has been very successful when combined with Airborne Laser Scanning and optical satellite imagery. It has been used in operational forest surveys for over five years now in Finland, Sweden, Latvia, Spain, Nepal, Brazil, Laos and South Africa, among others. The total area estimated with it exceeds five million hectares. When we need to incorporate the temporal dimension in the estimation, such as is the case of calculating seasonally or diurnally varying fluxes, Bayesian estimation turns into Kalman filtering.

The linear and non-linear Kalman filters have been known to be optimal methods for Bayesian regression in the time-dependent case since the 1960s, but lack of computing power has prevented their wide-spread adoption in high-dimensional models. This is almost always the case in spatial generalization, since results with a fine spatial resolution are needed over large areas. Fortunately the latest decade has seen the emergence of efficient approximations to the Kalman filter that circumvent the problem of excessive computational complexity by approximating the most computationally heavy part of the Kalman filter, the estimation of the error covariance matrix, with a low-rank dynamic correction to a diagonal static prior covariance matrix. Some of the most promising such methods, namely the Variational Kalman Filter (VKF) and the Variational Ensemble Kalman Filter (VEnKF) have been developed at the Department of Mathematics and Physics at Lappeenranta University of Technology.

Lidar-assisted carbon change maps have been produced in Nepal using the LAMP methodology (short for Lidar-Assisted Multi-source Programme for carbon accounting) (Joshi et al, 2014). We describe the method used from lidar-capture and field calibration into computation of carbon change. The resulting carbon map has a very fine spatial resolution of 1 hectare and narrow confidence intervals. We then outline the use of such high-resolution carbon maps into high-resolution carbon flux simulations using data assimilation that generalizes local flux tower measurements into wide area high-resolution flux simulations.

LAMP ESTIMATION PROCESS

The schematic diagram on the following page describes the stages of a LAMP estimation process for carbon map production. It features the processing steps from field data measurement through lidar adata capture and model building into satellite image processing and calibration with lidar-based surrogate plots.

CONCLUSIONS

Carbon change maps are becoming vital tools not only for studying the link between terrestrial ecosystems and climate change, but also for devising measures to mitigate climate change. The latter category includes political initiatives like UN REDD+, short for Reducing Emissions from Deforestation and forest Degradation. Especially forest degradation is difficult to quantify without

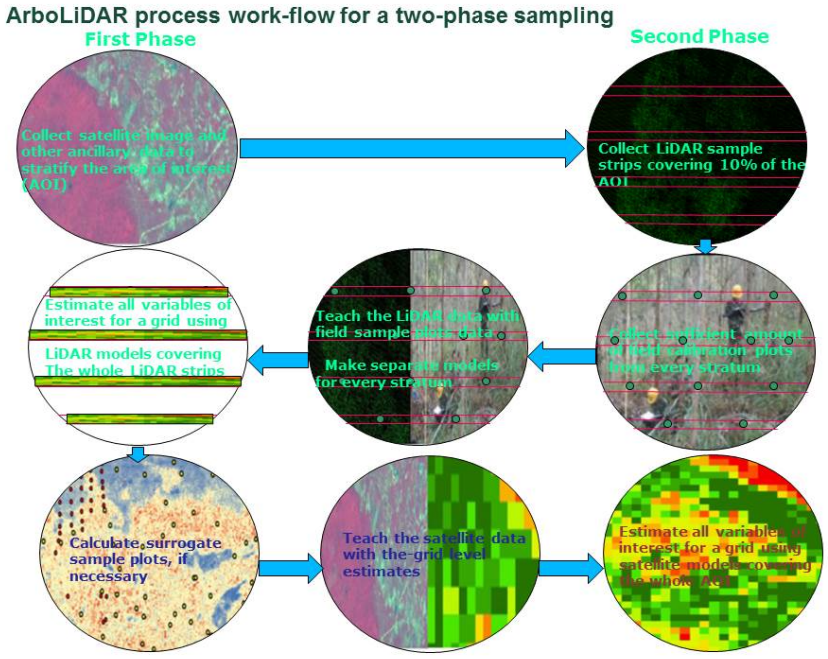

Figure 1: Flow diagram of the LAMP estimation process.

accurate forest biomass maps. And the carbon sequestration capacity of forests cannot be quantified without a combination of accurate and precise flux measurements caoupled to high resolution forest canopy and forest carbon maps. We hope Lidar-assisted Multi-source Processes will help in overcoming such bottlenecks when combined with accurate data fusion to networks of flux tower measurements.

REFERENCES

Joshi, A. R., Tegel, K., Manandhar, U., Aguilar-Amuchastegui, N., Dinerstein, E., Eivazi, A., Gamble, L., Gautam, B., Gunia, K., Gunia, M., Hall, D., Hamalainen, J., Hawkes, M., Junttila, V., Gautam, S. K., Kandel, Y., Kandel, P., Kauranne, T., Kolesnikov, A., Latva-Kayra, P., Lohani, S., Nepal, S. M., Niles, J., Peuhkurinen, J., Powell, G., Rana, P., Suihkonen, T. and Thapa, G. J. (2014). An accurate REDD+ reference level for Terai Arc Landscape, Nepal using LiDAR assisted Multi-source Programme (LAMP). *Banko Janakari*, **24(1)** 23-34.

Junttila, V., Maltamo, M., Kauranne, T. (2008). Sparse Bayesian estimation of forest stand parameters from Airborne Laser Scanning. *Forest Science*, **54(5)** 543-552.

He HL, Liu M, Sun XM, Zhang L, Luo YQ, Wang HM, Han SJ, Zhao XQ, Shi PL, Wang YF, Zhu OY, Yu GR (2010). Uncertainty analysis of eddy flux measurements in typical ecosystems of ChinaFLUX. *Ecological Informatics*, **5** 492-502.

Liu M, He HL, Yu GR, Sun XM, Zhang L, Han SJ, Wang HM, Zhou GY (2011). Uncertainty analysis in data processing on the estimation of net carbon exchanges at different forest ecosystems in China. *Journal of Forest Research* **17** 312-322.

Raupach MR, Rayner PJ, Barrett DJ, DeFries RS, Heimann M, Ojima DS, Quegan S, Schmullius CC (2005). Model-data synthesis in terrestrial carbon observation: methods, data requirements and data uncertainty specifications. *Global Change Biology* **11** 378-397.

ESTIMATING BROWN CARBON EMISSIONS USING KALMAN FILTER APPROACH

H. KOKKOLA[1], T. BERGMAN[1], A. LIPPONEN[2], A. LAAKSO[1,2], M. PITKÄNEN[1,2], A. AROLA[1], G.L. SCHUSTER[3], S. ROMAKKANIEMI[1] and T. MIELONEN[1]

[1]Finnish Meteorological Institute, Atmospheric Research Centre of Eastern Finland, Kuopio, Finland.

[2]University of Eastern Finland, Applied Physics, Kuopio, Finland.

[3]NASA, Langley Research Center, Hampton, Virginia, USA.

Keywords: CLIMATE MODELING, REMOTE SENSING, AEROSOLS, BROWN CARBON.

INTRODUCTION

One of the key aspects in climate change is the effect of atmospheric aerosol particles on solar radiation. For black carbon (BC) and brown carbon (BrC), commonly referred as light-absorbing carbonaceous aerosols (LAC), the climate effects are complex. As light-absorbing compounds they are generally thought to be climate warming compounds (Ramanathan and Carmichael, 2008). On the other hand, the aging of LAC particles increases their hygroscopicity and makes them potential cloud condensation nuclei (CCN) (e.g. Kuwata et al., 2009). While increase in CCN will have a cooling effect, LAC in cloud droplets or near the cloud tends to warm the liquid phase causing so called cloud burn-off and therefore reducing cloud lifetime. This results in a warming effect. Eventually, as LAC is deposited on snow and ice, it increases their melting and contributes to the thinning of glaciers and loss of arctic sea ice (Stroeve et al., 2011; Marks and King, 2013; Webster et al., 2014). Thus, to estimate the overall climate effect of LAC, the level of aging and the distribution of LAC in horizontal and vertical have to be known.

Current climate models have great problems in predicting BC concentrations in the Arctic especially during the spring time, which is a critical season regarding melting of sea ice and snow cover (Koch et al., 2009). It has been identified that these uncertainties come mainly from model uncertainties in removal of BC when simulating transport to the Arctic (Shindell et al., 2008, Jiao et al., 2014), although missing emission sources from e.g. gas flaring have also been proposed to affect modelled BC at the Arctic (Stohl et al., 2013). Moreover, most models do not include light-absorbing organic carbon compounds (BrC) because their importance on radiative transfer has only recently been realized. Several studies (e.g. Bond et al., 2004; Chen and Bond, 2010; Chakrabarty et al., 2010; Lack et al., 2013; Saleh et al. 2014) have shown that BrC is emitted into the atmosphere from incomplete combustion. In addition, it is formed in the atmosphere as secondary organic aerosols (e.g. Jaoui et al., 2008; Bones et al., 2010; Flores et al., 2014). Consequently, the optical properties and the emissions of atmospheric BrC aerosols are not well known and their estimates have been based on theoretical studies and laboratory measurements (Feng et al., 2013). In order to make proper estimates on the climate effects of LAC, optical properties and emissions of BrC have to be modeled adequately.

METHODS

Feng et al., (2013) estimated that 66 % of the total organic matter from biofuel and biomass burning emissions is BrC. In our model comparisons with Aerosol Robotic Network (AERONET; Holben et al., 1998) data this emission factor did not produce good agreement on atmospheric burdens of BrC. Therefore, the aim of this research is to produce new measurement based estimates for BrC emissions. We use retrievals of atmospheric BrC concentrations to estimate the fraction of BrC emissions from the total organic carbon (OC) emissions. This is done using an iteration tool based on an Extended Kalman filter (Anderson and Moore, 1979) as shown in Figure 1. With the combination of measurement data and

inverse problem methods we can optimize the BrC emission fractions for different emissions sources (biomass burning, fossil fuel, and biogenic emissions) in the ECHAM-HAMMOZ model. This optimization produces the best match between the modeled and retrieved BrC concentrations in the atmosphere.

The measurement data used in this research is from AERONET which uses Cimel sun photometers which measure columnar aerosol optical depth (AOD) at 340, 380, 440, 500, 675, 870 and 1020 nm. Measurements are provided every 15 min during daytime. AERONET also provides the angular distribution of sky radiances at four wavelengths (440, 670, 870 and 1020 nm), and aerosol properties such as aerosol size distribution, complex refractive index, and single scattering albedo (SSA), once every hour in clear sky conditions. AERONET is a global network with hundreds of active stations. The atmospheric BrC concentrations are retrieved from the complex refractive index data.

The aerosol-climate model used in this project is ECHAM-HAMMOZ which is developed by a consortium including Max Planck Institute for Meteorology and Finnish Meteorological Institute. The model describes all known relevant atmospheric aerosol processes: emissions, removal, aerosol microphysics, chemistry, radiative effects, and aerosol-cloud interactions. It includes the main atmospheric aerosol compounds: sulfate, organic/black/brown carbon, sea salt and mineral dust. ECHAM-HAMMOZ describes the aerosol size distribution using either a modal or a sectional approach. The model meteorology is nudged towards reanalysis data.

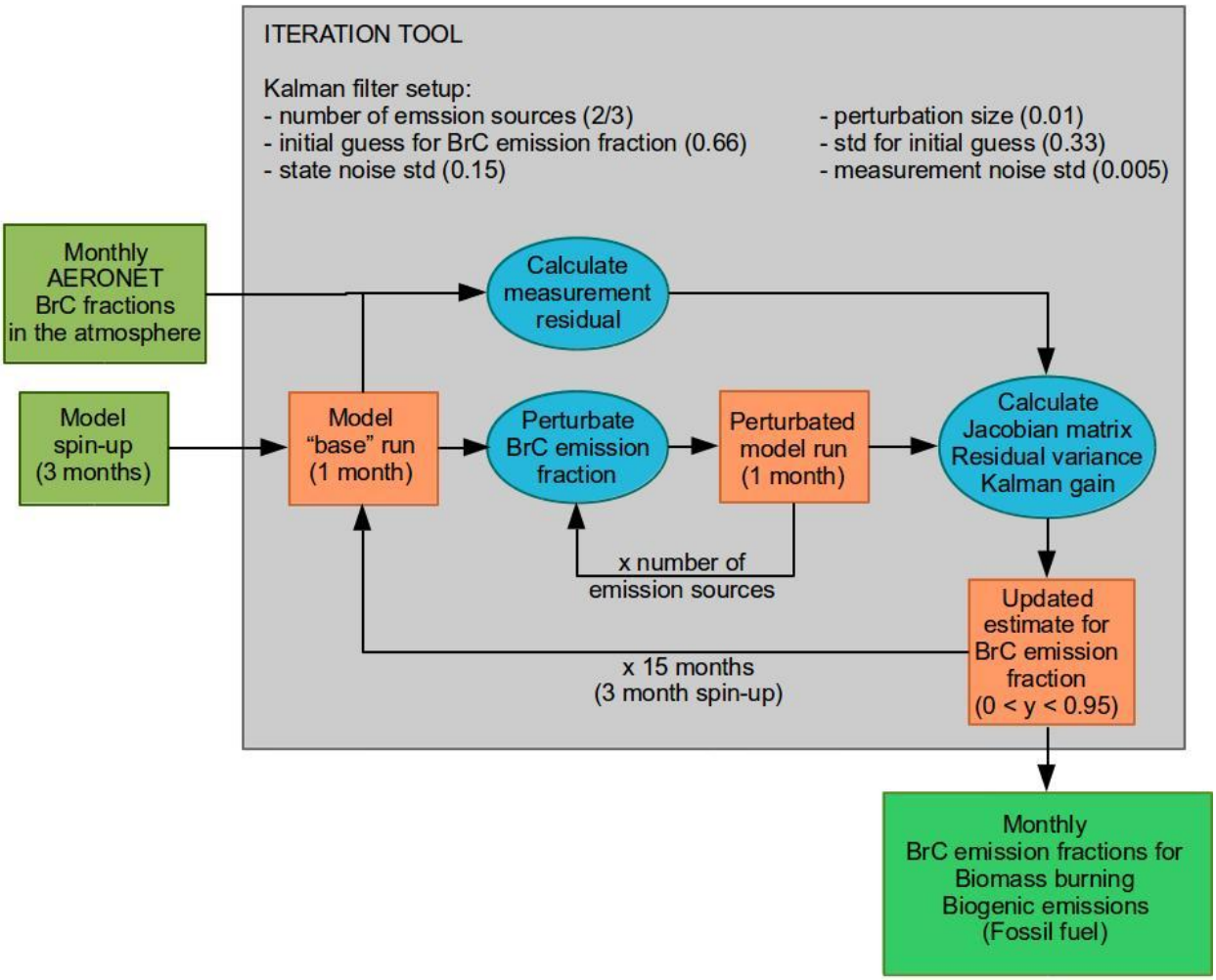

Figure 1. Schematic representation of the method for defining BrC emissions.

CONCLUSIONS

In order to quantify how much BrC is emitted to the atmosphere we have developed a tool for optimizing BrC emissions in climate models using measurement data available from AERONET. We have tested the tool with synthetic data and the optimization performed well. Furthermore, the first results with measurement data look promising. However, there are still several open questions. For example:

What emission sources (type/region) should be considered?
What are the optimal parameters for the extended Kalman filter?
How reliable are the AERONET data?
How reliable are the model OC/BC emissions?

After we have solved these questions we can provide new measurement based estimates for BrC emissions.

ACKNOWLEDGEMENTS

This work was supported by the Academy of Finland under grant no. 272041. The ECHAM-HAMMOZ model is developed by a consortium composed of ETH Zurich, Max Planck Institut für Meteorologie, Forschungszentrum Jülich, University of Oxford, and the Finnish Meteorological Institute and managed by the Center for Climate Systems Modeling (C2SM) at ETH Zurich. The authors gratefully acknowledge the AERONET Team for their effort in making the data available.

REFERENCES

Anderson B.D.O. and Moore J.B. (1979). *Optimal Filtering*, Prentice-Hall Inc., Englewood Cliffs, N.J..

Bond, T. C., et al. (2004). A technology-based global inventory of black and organic carbon emissions from combustion, *J. Geophys. Res*., **109**.

Bones, D. L., et al. (2010). Appearance of strong absorbers and fluorophores in limonene-O3 secondary organic aerosol due to NH4+-mediated chemical aging over long time scales, *J. Geophys. Res*.,**115**, D05203.

Chakrabarty, R. K., et al. (2010). Brown carbon in tar balls from smoldering biomass combustion, *Atmospheric Chemistry and Physics*, **10**(13), 6363-6370

Chen, Y. and Bond T.C. (2010). Light absorption by organic carbon from wood combustion, *Atmospheric Chemistry and Physics*, **10**(4), 1773-1787.

Feng, Y., et al. (2013). Brown carbon: a significant atmospheric absorber of solar radiation?, *Atmos. Chem. Phys*., **13**, 8607-8621.

Flores J.M., et al. (2014). Complex refractive indices in the near-ultraviolet spectral region of biogenic secondary organic aerosol aged with ammonia, *Phys Chem Chem Phys*., **16**(22):10629-42.

Holben, B. N., et al. (1998). AERONET – A federated instrument network and data archive for aerosol characterization, *Rem. Sens. Environ*., **66,** 1–16.

Jaoui, M., et al. (2008). Formation of secondary organic aerosol from irradiated a-pinene/toluene/NOx mixtures and the effect of isoprene and sulfur dioxide, *J. Geophys. Res*., **113**, D09303.

Jiao, C., et al. (2014). An AeroCom assessment of black carbon in Arctic snow and sea ice, *Atmos. Chem. Phys*., **14**, 2399-2417.

Koch, D., et al. (2009). Evaluation of black carbon estimations in global aerosol models, *Atmos. Chem. Phys*., **9**, 9001-9026.

Kuwata, M., et al. (2009). Critical condensed mass for activation of black carbon as cloud condensation nuclei in Tokyo, *J. Geophys. Res*., **114**, D20202.

Lack, D. A., et al. (2013). Brown carbon absorption linked to organic mass tracers in biomass burning particles, *Atmos. Chem. Phys*., **13**, 2415-2422.

Marks, A. A. and King, M. D. (2013). The effects of additional black carbon on the albedo of Arctic sea ice: variation with sea ice type and snow cover, *The Cryosphere*, **7**, 1193-1204.

Ramanathan, V., and Carmichael, G. (2008). Global and regional climate changes due to black carbon, *Nature Geosci*., **1**, 221 – 227.

Saleh, R, et al. (2014). Brownness of organics in aerosols from biomass burning linked to their black carbon content, *Nature Geosci*., **7**,647–650.

Shindell D.T., et al. (2008). A multi-model assessment of pollution transport to the Arctic, *Atmos. Chem. Phys*., **8**, 5353-5372.

Stohl, A., et al. (2013). Why models struggle to capture Arctic Haze: the underestimated role of gas flaring and domestic combustion emissions, *Atmos. Chem. Phys.*, **13**, 9567-9613.
Stroeve, J. C., et al. (2011). The Arctic's rapidly shrinking sea ice cover: A research synthesis. *Climatic Change*, doi:10.1007/s10584-011-0101-1.
Webster, M. A., et al. (2014). Interdecadal changes in snow depth on Arctic sea ice, *J. Geophys. Res. Oceans*, **119**.

POST-FIRE RECOVERY OF SOIL MICROBIAL BIOMASS AND ENZYMATIC ACTIVITY IN A NORTHERN BOREAL FIRE CHRONOSEQUENCE

K. KÖSTER[1,2], F. BERNINGER[1], J. HEINONSALO[3], E. KÖSTER[1] and J. PUMPANEN[1]

[1]Department of Forest Sciences, University of Helsinki, Finland.

[2]Institute of Forestry and Rural Engineering, Estonian University of Life Sciences, Tartu, Estonia.

[1]Department of Food and Environmental Sciences, University of Helsinki, Finland.

Keywords: FIRE DISTURBANCE, FUNGAL BIOMASS, SOIL CO_2 EFFLUX.

INTRODUCTION

Boreal forests are a crucial part of the climate system and carbon (C) cycle, as they contain approximately 60% of the C bound in global forest biomes (Bond-Lamberty *et al.* 2006; Preston *et al.* 2006). Fire is the dominant natural disturbance regime in the boreal forest, and it is expected that fire frequencies in boreal forests will increase with future climate change (Bond-Lamberty *et al*. 2006; Flannigan *et al*. 2009).

Fire is the primary process which organizes the physical and biological attributes of the boreal biome and influences energy flows and biogeochemical cycles, particularly the C and nitrogen cycle. Fires can directly affect the C cycle via CO_2 emissions from biomass combustion and indirectly via long-term changes in ecosystem C dynamics through forest recovery, succession and the chemical composition of remaining organic compounds (Goulden *et al.* 2011). The biggest change to occur in forest soils during a fire is the loss of soil organic matter (SOM) (Certini 2005). Fire also reduces the biomass of soil microorganisms (Certini 2005; Holden and Treseder 2013). According to different studies the negative effect of fire on microbial biomass persists for decades.

Soil organic compounds, especially in humic substance, such as cellulose, lignin and chitin are degraded enzymatically and fire-induced changes in the soil microbial community could influence the production and activity of these enzymes (Rietl and Jackson 2012). Soil fungi are responsible for a large portion of the enzyme production in litter and soils, which break down SOM and release C, nitrogen and phosphorus (Gartner *et al.* 2012) and also degrade recalcitrant organic C (Cairney and Burke 1998). Some studies exist concerning the fire effects on soil, but they mostly focus on changes in soil enzyme activity over a short period of time. Most studies have found that fire decreases the activity of most enzymes in soil (Rietl and Jackson 2012; Holden *et al.* 2013).

We have assessed the changes occurring in soil CO_2 efflux, soil C content, soil microbial biomasses and enzymatic activity along a chronosequence of fires in sub-arctic Scots pine (*Pinus sylvestris* L.) stands in Finnish Lapland.

METHODS

We measured changes in litter enzymatic activities, soil microbial and fungal biomasses and soil carbon dynamics following fire disturbance in Scots pine stands in the northern boreal forests, of eastern Lapland, Värriö Strict Nature Reserve, Finland (67°46' N, 29°35' E). The sites are situated north of the Arctic Circle, near to the northern timberline at an average of 300 m altitude.

The soil in the area is moraine (with plenty of stones). Typical herbaceous plants (*Vaccnium myrtillus*, *Vaccinium vidis-ideae*, *Empetrum nigrum*) indicate rather poor soil conditions. Treeline is around

470 m a.s.l. Annual mean precipitation in the area is about 600 mm and average annual mean temperature at Värriö research station (altitude 380 m) is around -1 °C. The climate in the area is subcontinental and the soil has no underlying permafrost. The snow covers the ground for around 200–225 days per year, and the length of the growing season is 105–120 days. The growing season in the area (mean monthly temperature more than 5 °C) lasts for 4 months and the average temperature during that period (from June to August) in the area is around 12 °C.

We have established 8 sample areas (with two replicate plots in each) in a chronosequence of 4 age classes (2 to 152 years since the last fire). The chronosequence consisted of four types of areas: (i) fire 2 years ago, (ii) fire 42 years ago, (iii) fire around 60 years ago, (iv) fire 152years ago.

To characterize the soil carbon (C) and nitrogen (N) content, and fine root biomass at the sites, we have taken 10 soil cores (0.15 m long and 0.05 m in diameter) from every sample plot. The soil cores were divided according to morphological soil horizons to litter and humus layers and the mineral layers to eluvial and illuvial horizons and sieved. Fine roots were separated from the soil. The soil C and N content was measured with elemental analyser (varioMAX CN elemental analyser, Elementar Analysensysteme GmbH, Germany) after drying the samples in an oven at 105 °C for 24 hours. Also the soil CO_2 effluxes were measured. The soil respiration in this study was defined as the sum of autotrophic respiration from plant metabolic activity and heterotrophic respiration from the decomposition of organic material by microbes

Soil fungal biomass and microbial biomass was measured from 5 soil samples per sample plot. Soil fungal biomass was measured using ergosterol analysis (Frostegard and Bååth, 1996). Soil microbial biomass was measured using Chloroform fumigation direct extraction method (Beck et al., 1997).

Five litter bags with Scots pine needles have been installed to each plot under the humus layer together with iButton temperature sensors (Maxim Integrated Products Ltd.) for SOM decomposition and enzymatic activity measurements. We measured the potential activities of lignocellulolytic enzymes; laccase (LAC), β -glucuronidase (GLR), β -xylosidase (HYL) and cellobiohydrolase (CEL), β -glucosidase (GLS) as well as the enzymes degrading chitin (N-acetylglucosamide (NAG)) and P-, N-containing organic compounds (acid phosphatase (PHO)).

RESULTS AND CONCLUSIONS

Our results indicate that fire has long lasting multi-decadal effects on the soil respiration, soil microbial and fungal biomass, and the activities of extracellular enzymes. The values for all these measured parameters were lowest straight after the fire and seem to recover to pre-fire levels within 40 to 60 years following fire disturbance.

The highest C pools were measured on old areas from top soil horizons (consisting of decomposing litter) and the lowest C pools on area where the fire was 60 years ago. When we compared the total C pools, the newly burned areas (areas where the fire was 2 – 42 years ago) formed one group (had similar values of total C) and old areas (areas where the fire was 60-150 years ago) formed another group with similar values.

Fire effects on soil microorganisms and fungi are greatest close to the soil surface, as heating is greatest in the organic horizon and in the top few centimetres of mineral soil. Both microbial and fungal biomass had an increasing trend with the age of the forest. The lowest microbial and fungal biomass values were observed in areas where the fire was not long time ago (2 and 24 years after fire disturbance). The microbial and fungal biomasses increased along with fire chronosequence and reached a stable level around 60 years after fire occurred.

Across all enzyme types we measured fire reduced the enzymatic activity. Carbon dissolving enzymes (XYL, GLR, CEL, GLS, LAC), nitrogen dissolving (NAG) and phosphorus dissolving enzymes (PHO) showed similar responses to the time since fire. In our northern boreal study area even 42 years after fire disturbance the values for microbial biomass, fungal biomass, soil CO2 efflux were significantly lower compared to the areas where the fire was 60 and 152 years ago.

ACKNOWLEDGEMENTS

This study was supported by a grants from: the Academy of Finland (project number 218094, 1255576, 138575), European Social Fund and Estonian Science Foundation "Mobilitas" grant (MJD94).

REFERENCES

Beck, T., Joergensen, R.G., Kandeler, E., Makeschin, F., Nuss, E., Oberholzer, H.R., Scheu, S. (1997) An inter-laboratory comparison of ten different ways of measuring soil microbial biomass C. *Soil Biology and Biochemistry* **29**, 1023-1032.

Bond-Lamberty, B., Gower, S.T., Wang, C., Cyr, P., Veldhuis, H. (2006) Nitrogen dynamics of a boreal black spruce wildfire chronosequence. *Biogeochemistry* **81**, 1-16.

Cairney, J.W.G., Burke, R.M. (1998) Extracellular enzyme activities of the ericoid mycorrhizal endophyte *Hymenoscyphus* ericae (Read) Korf & Kernan: their likely roles in decomposition of dead plant tissue in soil. *Plant and Soil* **205**, 181-192.

Certini, G. (2005) Effects of fire on properties of forest soils: A review. *Oecologia* **143**, 1-10.

Flannigan, M., Stocks, B., Turetsky, M., Wotton, M. (2009) Impacts of climate change on fire activity and fire management in the circumboreal forest. *Global Change Biology* **15**, 549-560.

Frostegard, A., Bååth, E. (1996) The use of phospholipid fatty acid analysis to estimate bacterial and fungal biomass in soil. *Biology and fertility of soils* **22**, 59-65.

Gartner, T.B., Treseder, K.K., Malcolm, G.M., Sinsabaugh, R.L. (2012) Extracellular enzyme activity in the mycorrhizospheres of a boreal fire chronosequence. *Pedobiologia* **55**, 121-127.

Goulden, M.L., McMillan, A.M.S., Winston, G.C., Rocha, A.V., Manies, K.L., Harden, J.W., Bond-Lamberty, B.P. (2011) Patterns of NPP, GPP, respiration, and NEP during boreal forest succession. *Global Change Biology* **17**, 855-871.

Holden, S., Gutierrez, A., Treseder, K. (2013) Changes in Soil Fungal Communities, Extracellular Enzyme Activities, and Litter Decomposition Across a Fire Chronosequence in Alaskan Boreal Forests. *Ecosystems* **16**, 34-46.

Holden, S.R., Treseder, K.K. (2013) A meta-analysis of soil microbial biomass responses to forest disturbances. *Frontiers in Microbiology* **4**, 163.

Preston, C., Bhatti, J., Flanagan, L., Norris, C. (2006) Stocks, Chemistry, and Sensitivity to Climate Change of Dead Organic Matter Along the Canadian Boreal Forest Transect Case Study. *Climatic Change* **74**, 223-251.

Rietl, A.J., Jackson, C.R. (2012) Effects of the ecological restoration practices of prescribed burning and mechanical thinning on soil microbial enzyme activities and leaf litter decomposition. *Soil Biology and Biochemistry* **50**, 47-57.

DYNAMICS OF CO_2 FLUXES ABOVE A HEMIBOREAL MIXED FOREST

A. KRASNOVA[1], S.M. NOE[1], Ü. NIINEMETS[1] and D. KRASNOV[1]

[1]Estonian University of Life Sciences, Tartu, Estonia

Keywords: BIOGEOCHEMICAL CYCLES, EDDY COVARIANCE, HEMIBOREAL FOREST.

INTRODUCTION

Forest ecosystems are a major part of the biosphere and control land surface-atmosphere interactions. They influence atmospheric composition and climate significantly being sources and sinks of trace gases and energy.

Mixed stands of both coniferous and deciduous tree species are characterized by a greater seasonal variability of forest microclimate, canopy shape and density, length of growing season and plant activity and higher biota diversity compared to pure boreal forests (Nilsson et al, 1997; Noe et al, 2011; Hickler et al, 2012;). These factors coupled with physical environment (atmospheric and meteorological conditions, soil properties) influence CO2 exchange between forest and the atmosphere (Pita et al, 2013).

A 20 m height scaffolding tower located in Järvselja (58°16'N 27°16'E) in a forest stand dominated by Norway spruce (Picea abies (L.) Karst.) with co-domination of Silver birch (Betula pendula Roth.) and Black alder (Alnus glutinosa L.) was used for the CO2 flux measurements.

Two years of continuous eddy covariance measurements over a mixed hemiboreal forest at the SMEAR Estonia (Station for Measuring Ecosystem-Atmosphere Relations) were studied to assess annual and diurnal dynamics of CO2 fluxes and their main environmental drivers.

METHODS

The eddy covariance system was placed above the forest on the 20m height scaffolding tower for two consecutive years (from September 2010 until November 2012). The three wind components and the speed of sound were measured by three-dimensional sonic anemometer (CSAT3, Campbell Scientific, Logan, UT, USA). CO2 concentrations were measured by an enclosed infrared gas analyzer (LI-7200, Li-Cor, Lincoln, NE, USA). The system was oriented into the main wind direction to minimize flow distortion and longitudinal sensor separation to the sonic anemometer.

Eddy covariance data were calculated using EddyPro software (Version 5, 2013. Lincoln, NE. LI-COR, Inc; Infrastructure for Measurements of the European Carbon Cycle consortium.) and processed with MATLAB (Versions 2012a & 2013b, The Mathworks Inc., Natick, MA, USA) software.

Net ecosystem exchange (NEE) was calculated as a sum of measured CO2 flux and calculated storage flux. Ecosystem respiration data was gap-filled using Arrhenius equation (Carrara et al., 2004) and gross primary production was calculated from the assumption that GPP = NEE - RE.

CONCLUSIONS

Net ecosystem exchange (NEE), gross primary production (GPP) and ecosystem respiration (RE) have a clear seasonal dynamics. Hemiboreal forest is a CO2 sink with the maximum uptake in summer months and maximum CO2 release in July.

NEE is a result of opposite processes (carbon uptake and release), which are exposed to the number of factors acting simultaneously, with the major influence of PAR and air temperature.
Both RE and GPP have temperature response optimums and are suppressed when air temperature reaches higher values. Optimum GPP values are less influenced by daily PAR medians but depend on the combination of temperature and water vapour pressure deficit conditions.

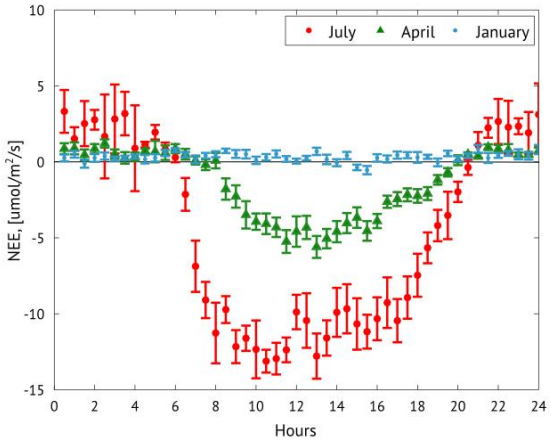

Figure 1. Diurnal cycle of net ecosystem exchange (NEE) in different months of 2011.

Diurnal cycle follows the main environmental drivers and forms an asymmetric temperature response in form of a hysteresis loop in all of the months of vegetation period.

ACKNOWLEDGEMENTS

This research is supported by the EU Regional Development Fundation, Environmental Conservation and Environmental Technology R&D Programme project BioAtmos (3.2.0802.11-0043); Internationalization of Science Programme INSMEARIN (10.1-9/13/1028); European Social Fund's Doctoral Studies and Internationalisation Programme DoRa"|

REFERENCES

Carrara, A., Janssens, I. a., Curiel Yuste, J., Ceulemans, R., (2004). Seasonal changes in photosynthesis, respiration and NEE of a mixed temperate forest. *Agric. For. Meteorol.* 126, 15–31.

Hickler, T., Vohland, K., Feehan, J., Miller, P. a., Smith, B., Costa, L., Giesecke, T., Fronzek, S., Carter, T.R., Cramer, W., Kühn, I., Sykes, M.T., (2012). Projecting the future distribution of European potential natural vegetation zones with a generalized, tree species-based dynamic vegetation model. *Glob. Ecol. Biogeogr.* 21, 50–63.

Nilsson, S. (1997) Forests in the temperate-boreal transition: natural and man-made features. *Ecol Bull* 61–71.

Noe, S.M., Kimmel, V., Hüve, K., Copolovici, L., Portillo-Estrada, M., Püttsepp, Ü., Jõgiste, K., Niinemets, Ü., Hörtnagl, L., Wohlfahrt, G., (2011). Ecosystem-scale biosphere–atmosphere interactions of a hemiboreal mixed forest stand at Järvselja, Estonia. *For. Ecol. Manage.* 262, 71–81.

Pita, G., Gielen, B., Zona, D., Rodrigues, A., Rambal, S., Janssens, I. a., Ceulemans, R., (2013). Carbon and water vapor fluxes over four forests in two contrasting climatic zones. *Agric. For. Meteorol.* 180, 211–224.

PAN-EURASIAN EXPERIMENT (PEEX) OVERVIEW

M. KULMALA[1], H.K. LAPPALAINEN[1,2], T. PETÄJÄ[1], T. KURTEN[3], V.-M. KERMINEN[1], Y. VIISANEN[2], V. KOTLYAKOV[4], N. KASIMOV[5], V. BONDUR[6] , G. MATVIENKO[7], A.BAKLANOV[8], HD. GUO[9] and S. ZILITINKEVICH[1,2,110]

[1]Dept. of Physics, P.O. Box 64, FI-00014 University of Helsinki, Finland.
[2]Finnish Meteorological Institute, P.O. Box 503, FI-00101 Helsinki, Finland
[3]Dept. of Chemistry, P.O. Box 64, FI-00014 University of Helsinki, Finland.
[4]The Institute of Geography RAS, 119017, Staromonetniy pereulok 29, Moscow, Russia
[5] Moscow State University, Moskovskij Gosudarstvennyj Universitet im. M.V. Lomonosova, Leninskie Gory, Moscow 119992, Russia
[6]AEROCOSMOS, 4, Gorokhovsky lane, Moscow, 105064, Russia
[7] Inst. of Atmospheric Optics SB RAS, Academician Zuev square, Novosibirsk, Novosibirsk reg., 634021 Russia

[8]World Meteorological Organization, Genève, Switzerland
[9]Institute of Remote Sensing and Digital Earth, Chinese Academy of Sciences, Beijing, China;
[10] Dept. of Radiophysics, Nizhny Novgorod State University, Nizhny Novgorod, 603950, Russia

Keywords: climate change, biogeochemical cycles, atmospheric aerosols, atmospheric boundary layer, research infrastructures, atmospheric and ecological measurements, Siberian ecosystems, Arctic Ocean, remote sensing, education programmes, socio-economic research

The Eurasian Pan-Eurasian Experiment (PEEX) is a multidisciplinary, multis-cale research project aimed at resolving the major uncertainties in Earth System Science and global sustainability issues concerning the arctic and boreal Pan-Eurasian regions as well as China. The vision of the PEEX is to solve interlinked global grand challenges influencing human well-being and societies in northern Eurasia and China. Such challenges include climate change, air quality, biodiversity loss, chemicalisation, food supply, and the use of natural resources by mining, industry, energy production and transport. Our approach is integrative and interdisciplinary, recognizing the important role of the arctic and boreal ecosystems in the earth system. The PEEX vision includes establishing and maintaining long-term, coherent and coordinated research activities and continuous, comprehensive research and educational infrastructures across the PEEX domain.

The PEEX initiative is motivated by the fact that the role of northern regions will increase in terms of globalization, climate change, demography and use of natural resources. Land and ocean areas located at 45◦n latitude or higher will undergo substantial changes during the next 40 years. Even the most moderate climate scenarios predict that the northern high latitudes will warm by 1.5 c -2.5 °C by the middle of the century. The Pan-Eurasian arctic-boreal natural environment will be a very important area for the global climate via the albedo change, carbon sinks and emissions, methane emissions and aerosol production via biogenic volatile organic compounds (BVOCs). In addition, the ecosystems will undergo potentially massive changes including the expansion of new species and the extinction of existing ones. These will have unpredictable consequences on food webs and the primary production of different plant ecosystems.

PEEX will develop and utilize an integrated observational and modelling framework to identify different climate forcing and feedback mechanisms in the northern parts of the earth system, and therefore enable more reliable predictions of future regional and global climate. Because of the already observable effects of climate change on society, and the specific role

of arctic and boreal regions in this context (Kulmala et al. 2011, Lappalainen et al. 2014). PEEX emphasizes the need to establish next-generation research and research infrastructures in this area. PEEX will provide fast-track assessments of global environmental change issues for climate policy-making, and for mitigation and adaptation strategies for the Northern Pan-Eurasian region.

PEEX is built on the collaboration between European, Russian and Chinese partners, and is open to a broader collaboration in the future. The PEEX community will include scientists from various disciplines, funders, policy-makers and stakeholders from industry, transport, renewable natural resources management, agricultural production and trade, and it will aim at co-designing research in the region in the spirit of the future earth initiative.

PEEX aims to be operational starting from 2015. It will start building the long-term, continuous and comprehensive research infrastructures (RI) in Northern Pan-Eurasia. These RIs will include ground-based, aircraft, marine and satellite observations, as well as multi-scale modelling platforms. The PEEX domain covers the Eurasian boreal zone and arctic regions of the hemisphere, including marine areas such as the Baltic, the North Sea and the Arctic Ocean. The PEEX area includes also China due to its crucial impact and influence. The PEEX research agenda focuses on the multidisciplinary process understanding of the earth system on all relevant spatial and temporal scales, ranging from the nano-scale to the global scale. The strategic focus is to ensure the long-term continuation of comprehensive measurements in the land-atmosphere-ocean continuum in the northern Eurasian area as well as the interactions and feedbacks related to urbanization and megacities, and to educate the next generation of multidisciplinary scientists and technical experts capable of solving the large-scale research questions with societal impact of the PEEX geographical domain.

The scientific results of PEEX will be used to understand different feedbacks mechanisms, to develop new climate scenarios on global and regional scales. PEEX aims to contribute to the earth system science agenda, to climate policy concerning topics important to the Pan-Eurasian environment, and also aims to help societies of this region in building a sustainable future.

REFERENCES

Kulmala M., Alekseychik P., Paramonov M., Laurila T., Asmi E., Arneth A., Zilitinkevich S. & Kerminen V.-M. (2011). On measurements of aerosol particles and greenhouse gases in Siberia and future research needs. Boreal Env. Res. 16: 337-362.

Lappalainen et al. 2014: Pan-Eurasian Experiment (PEEX)- a research initiative meeting the grand challenges of the changing environment of the northern Pan-Eurasian arctic-boreal areas . J. GEOGRAPHY, ENVIRONMENT, SUSTAINABILITY No 2(7) pp. 13-48.

RESPONSE OF CARBON CYCLE TO ENHANCEMENT OF CLIMATE ARIDITY IN VARIOUS ECOSYSTEMS OF CENTRAL RUSSIA

I. KURGANOVA [1], V. LOPES DE GERENYU [1], I. SAVIN [2], T. MYAKSHINA[1], D. SAPRONOV [1] and V. KUDEYAROV[1]

[1]Institute of Physicochemical and Biological Problems in Soil Science, RAS, Institutskaya Str., 2, Pushchino, Moscow region, 142290, Russia.

[2]Soil Science Institute named V.V. Docuchaev of the Russian Academy of Agricultural Sciences, Pyzhevsky pereulok, 7, Moscow, 109017, Russia.

Keywords: CARBON BIOGEOCHEMICAL CYCLES, ARIDITY ENHANCEMENT, SOIL RESPIRATION, CENTRAL RUSSIA.

INTRODUCTION

Climate changes presently observed in the large part of Russia are expressed both in general gain of air temperature and in the enhancement of climate aridity (Assessment Report…, 2008). Under some scenarios, regional climate projections show the amplification of drier conditions over most of European Russia territory and South Europe, Asian and Northern American countries (Wang *et al*., 2011; Karl *et al.*, 2012). It is suggested that the recurrence time of warm extremes will reduce from 20 yr in 1961–1990 to 1–2 yr over southern Europe and to 5 yr over Scandinavia in 2071–2100 (Nikulin *et al*., 2011). The increased frequency and area of droughts will be observed not only in regions with a forecasted decrease in precipitation, but also in areas where precipitation trends to increase due to climate changes (Zolotokrylin *et al*., 2007). The probability of this trend was more than 66% in the late 20th century and will be retained in the 21st century (Gulev *et al*., 2008).

Being the leading biogeochemical cycle in the global scale, carbon cycle and its main components interact closely with climate changes via feedbacks (Kurganova *et al.*, 2011; Reihstein *et al*., 2013). Negative effect of droughts and heat waves may reveal itself not only in a reduced net primary productivity (NPP) of cenoses (Schar et al., 2004; Ciais *et al*., 2005) and, hence, a decrease in the input of plant residues to soil, but also in possible acceleration of mineralization of soil organic matter caused by water input after droughts (Larionova *et al*., 2010; Unger *et al*., 2010). Some studies illustrate the reduction of vegetation productivity and destruction of carbon stock due to the increase of tree mortality or after fire events caused by severe droughts (Bigler *et al*., 2007).This study is aimed to assess the effect of enhancement of climate aridity on carbon cycle in various ecosystems of Central Russia based on long-term monitoring of main carbon fluxes.

MATERIALS AND METHODS

Study area. Our investigation was carried out through the period 1998-2011 in the middle part of Central Federal district of the Russian Federation which belongs to the boundary between southern taiga (mixed forest) and deciduous forest zone. Experimental sites were located on sandy Albeluvisols Umbric (forest and grassland ecosystems) on the territory of Prioksko-Terrasny State Reserve (Moscow region, Russia, 54°50'N, 37°35'E), and on loamy Phaeozems Albic (forest, grassland, and cropland), 4 km to the west Pushchino town (Moscow region, Russia, 54°50'N, 37°35'E). Thus, the long-term monitoring of main carbon fluxes was conducted in 5 various ecosystems differed in land use (forest, grassland, and cropland) and soil type (sandy Albeluvisols and loamy Phaeozems).

Meteorological data set. To assess current climatic changes in Central Russia and area studied (Moscow region), we selected thirty meteorological stations distributed over Central Federal district of Russian

Federation and four stations located in Moscow region. Long-term rows of monthly precipitation amount (P) and mean air temperature (Ta) are available on Roshydromet homepage (*http://aisori.meteo.ru/ClimateR*). The mean monthly Ta data are mostly available for the last 90-110 yrs, while rainfall data are traced from 1966. The permanent weather observations in the experimental plots (Moscow region, Danki village; 54°50'N, 37°35'E) were started in 1973 and covered the 14-yr period of CO_2 fluxes monitoring completely.

To estimate the climate aridity, the hydrothermal coefficient (HTC) of summer period was calculated according to simple formula (Zolotokrylin *et al.*, 2007):

$$HTC = \sum P/0.1 \cdot \sum T_{>10} \quad , \qquad (1)$$

where $\sum P$ is the total precipitation over the summer period (mm) and $\sum T_{>10}$ is the sum of mean daily air temperatures (>10°C) over the same period. It is suggested that severe, medium, and slight droughts corresponded to exceed of negative HTC anomalies by 2.0, 1.5 and 1.0 standard deviation (STD).

Long-term monitoring of soil CO_2 fluxes in ecosystems. Soil CO_2 flux (or soil respiration, **SR**) was measured by the closed chamber method over the period from November 1997 through October 2011 at 7-10 day intervals. Measurements were carried out between 9 and 11 a.m., when the current value of the soil respiration rate was approximately equal to the mean daily value (Kurganova *et al.*, 2003). The number of replicates was 3 during the cold period (November – April) and 5 - during the warm season (May – October). The gas samples (20 cm^3) were collected by syringe, transported to the laboratory in hermetically sealed vacuumed flasks and analysed by gas chromatography. Simultaneously, soil moisture and temperature in the upper soil layer (0-5 cm) were determined.

The CO_2 flux can be calculated according to Eq. (2) (Kurganova *et al.*, 2003):

$$C = C_0 + F_{CO2} \cdot Z_{CH}/Ds \cdot (1-\exp(-Ds/(Z_{CH} \cdot H \cdot t))), \qquad (2)$$

where F_{CO2} is CO_2-C flux, mg C m^{-2} h^{-1}; C_0 is the initial head-space concentrations of CO_2-C, mg C m^{-3}; C is the head-space concentration of CO_2-C, mg C m^{-3}, in time t (hour); H is the height of the head-space layer in the chamber, m; Ds is the CO_2 diffusion coefficient in the soil, m^2 h^{-1}; Z_{CH} is the depth (m) of the lower chamber edge below soil surface.

Monthly SR fluxes from the soils (g C m^{-2} $month^{-1}$) were calculated by using mean monthly values of CO_2 fluxes (g C m^{-2} day^{-1}). Seasonal and annual SR fluxes were obtained by summarising monthly fluxes.

Remote sensing NDVI data. The results of many researches have demonstrated a strong correlation between NPP and normalized difference vegetation index (NDVI), which leads to a common use of NDVI as a proxy of NPP (Wang *et al.*, 2005; Wessels *et al.*, 2008). The most suitable for the analysis of vegetation productivity based on NDVI are satellite data MODIS which can be obtained for any territory with a spatial resolution of 250 meters. Archive daily MODIS data are available from 2000. Purified cloudless seven-days composite images of vegetation index NDVI (Loupian et al., 2004) were constructed using daily standard data product MOD09 (*http://modis.gsfc.nasa.gov/data/dataprod/dataproducts.php?MOD_NUMBER=09*) based on technology developed by Space Research Institute of Russian Academy of Sciences (Bourtsev *et al.*, 2006). On the basis of this algorithm smoothed time-series data of seven-day composite vegetation indices were constructed. After that, for a field soil survey point smooth curves of the index for the period from 2001 to 2012 were extracted from the database using satellite service VEGA (Loupian *et al.*, 2011). Therefore, NDVI values (weekly resolution) were used as NPP predictor for the period 2000-2013. We assumed that the mean summer NDVI value may be applied as a reliable parameter for estimation of vegetation response to enhancement of climate aridity.

Data processing. Analysis of climatic data for Central Federal District and Moscow region included: (i) smoothing of meteorological data; (ii) evaluating of MAT anomalies (differences) relatively to the 1961-1990 mean which correspons to the reference period (climatic norm) for meteorological data analysis (Assessment reports, 2008), and (iii) calculation of temporal MAT and summer HTC trends for different time intervals: 39 yrs (1973-2011, medium) and 14 yrs (1998–2011, current).

Anomalies of the month, seasonal, and annual SR fluxes and summer NDVI values for the 12-14-yr data series were calculated as the deviation from the mean values SR/NDVI over the same time period. The "normal" condition means the average SR/NDVI values for the time periods when climatic anomalies did not exceed one STD interval. SR and NDVI anomalies were estimated as a percentage to the mean SR or NDVI values for "normal" years.

Temporal trends and its confidence level (P value) were calculated using least-squares linear regression with Exel program (MS office 2007). The statistical significance of the trends obtained was estimated by the determination coefficient (R^2), which shows the proportion of variance explained by the trend. The intensity (b) and sign of the trends observed were characterized by the coefficient of linear regression, which corresponds to the average rate change of the variable per 10-yr interval.

RESULTS AND DISCUSSION

Recent climate trends in the area studied. The annual and seasonal (spring, summer, and autumn) patterns of air temperature changes in Central Russia, Moscow region, and experimental area were examined over the recent medium (1973-2011) and short (1998-2011) time series (Table 1). We also estimated the corresponding total annual and seasonal sum of Ta anomalies (∑an, ^oC) relatively to the reference period 1961-1990 for the same time intervals. The significant positive linear trend ($P<0.05$) of mean air temperature for annual, summer, and autumn periods were observed for the recent 39-year time interval for all regions (Table 1). The most rapid increase in Ta (the steepest slope of linear trend) was revealed during the summer period (0.65-0.68^oC per decade), while the spring season demonstrated the most slow warming (0.28-0.30 ^oC per decade).

The absolute rates of annual and seasonal warming differed significantly during the observed time periods: the slopes of 14-year trends usually were much steeper than those for 39-years period (Table 1). This difference was the most obvious (more than 4-fold) for the autumn season: the significance of short 14-yr linear trends were much higher ($P=0.001-0.05$) than 39-years trends ($P<0.10$). Spring and summer warming for the recent 14 yrs was about 2 time higher than for 39-year period although the significance of these linear trends was low ($P>0.10$).

Region	Time interval	Annual	Spring	Summer	Autumn
Coefficient of temperature linear trend, $^oC/10$ yrs					
Central Russia	1973-2011	0.46^a	0.28^e	0.66^a	0.47^d
	1998-2011	0.60^e	0.43^{ns}	$1,15^e$	$2,02^c$
Moscow region	1973-2011	$0,47^a$	$0,30^e$	$0,68^a$	$0,44^c$
	1998-2011	$0,61^e$	$0,69^{ns}$	$1,10^e$	$2,03^b$
Experimental area	1973-2011	0.43^b	0.30^e	0.65^a	0.37^d
	1998-2011	0.73^d	1.03^e	1.40^e	1.68^c
Sum of T anomalies (∑an, ^oC) relatively to the reference period 1961-1990					
Central Russia	1973-2011	21.5	20.7	15.8	8.6
	1998-2011	17.1	13.0	18.6	12.9
Moscow region	1973-2011	24.0	25.6	17.3	8.1
	1998-2011	17.9	14.6	19.5	12.1
Experimental plots*	1973-2011	18.2	24.1	6.8	7.3
	1998-2011	15.1	14.1	14.9	10.3

Table 1. Estimates of the recent medium (1973-2011) and short (1998-2011) linear trends for regionally averaged values of mean air temperature and sum of Ta anomalies (∑an, ^oC) relation to the reference period 1961-1990 (^{a} – $P<0.001$; ^{b} – $P=0.001-0.01$; ^{c} – $P=0.01-0.05$; ^{d} – $P=0.05-0.10$; ^{e} – $P=0.10-0.30$; ^{ns} – $P>0.30$). * *Data are expressed as anomalies from 1973-1990.*

The annual and seasonal sums of Ta anomalies for 14- and 39-year periods slightly differed in Central Russia, Moscow region, and experimental area (Table 1). The sums of annual and spring Ta anomalies were significantly higher during 1973 -2011 compared to 1998-2011 while the summer and autumn sums of Ta anomalies during 1998-2011 were 1.1-2.2 times higher than those for 1973-2011.

The linear trends of summer HTC in the area studied during 1973-2011 were negative (P=0.04-0.06) and demonstrated the aridity amplification in Central Russia during last 4 decades at rate of -0.9÷(-0.12) per 10 years (Figure 2). The 14-year trends in summer HTC were also negative and steeper (-0.24÷(-0.38) per 10 years) but statistically insignificant (P=0.28-0.31). Due to more southern localization, these linear trends were more obvious in Moscow region and on experimental plots than in Central Russia. For the recent 14 years, we observed only 2 anomaly dry summers (2002 and 2010) in Central Russia and 5 anomaly dry summers (2001, 2002, 2007, 2010, 2011) both in Moscow region and on experimental plots (Figure 2). Therefore, in Moscow region (including experimental plots), every third year was found to be extremely dry: the HTC anomalies for these years were higher than standard deviation for mean HTC through 1973-2011.

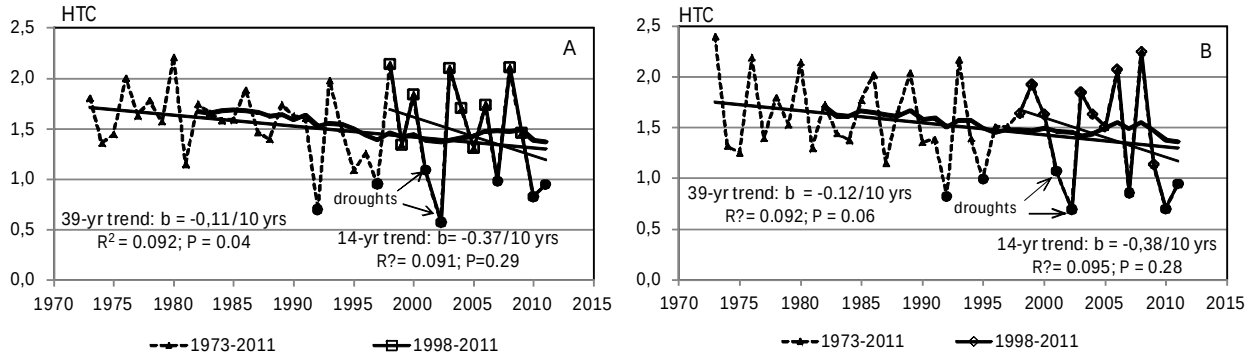

Figure 1. Trends of summer HTC for 39-year (1973-2011) and 14-year (1998-2011) data set in the Moscow region (A) and on the experimental plots (B): b – is the coefficient of linear trend; Solid black line shows the 10-year running average, black rounds denote the anomalous droughts when the negative HTC anomalies exceed of STD estimated for 39-year mean HTC.

Short-term trends and anomalies in CO_2 emission and NDVI values. Emission component of the carbon cycle (annual SR) demonstrated the negative trends in 1998–2011 for all ecosystems studied. The reduction of mean annual SR fluxes in the ecosystems on the sandy Albeluvisols (-18.1 g C m^{-2} yr^{-1}) was much significant in comparison with the ecosystems on the clay Phaeozems ((-0.33 g C m^{-2} yr^{-1}; Figure 2A).

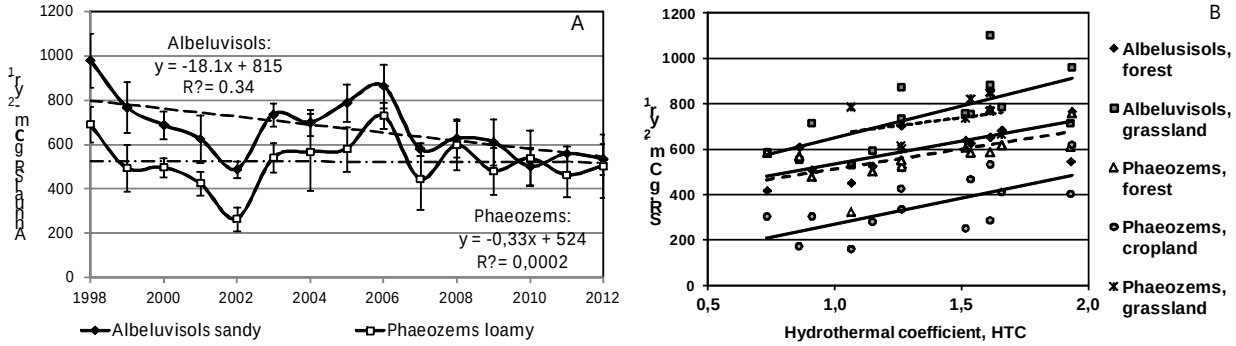

Figure 2. The trends of mean annual soil respiration in soils of different texture (A) and the relationship between annual SR flux and hydrothermal coefficient in all ecosystems studied (B).

It was found that the annual trends of SR decrease occurred mainly due to the seasonal trend of soil respiration decline during summer and autumn season. Obviously, the lack of moisture determined by the low water retaining capacity of sandy Albeluvisols resulted in appreciable inhibition of decomposition of soil organic matter and litter during the summer season and fresh litter - in autumn. The close positive correlations between annual SR fluxes from soils and hydrothermal coefficients were observed for all ecosystems studied during the observation period (R^2 = 0.37-0.48, P<0.05).

The mean summer NDVI values in natural ecosystems also demonstrated the negative tendency for the 12-yr time period (Figure 3A). Hence, the aridity enhancement caused the clear decline in plant productivity and decrease of carbon sequestration in vegetation.

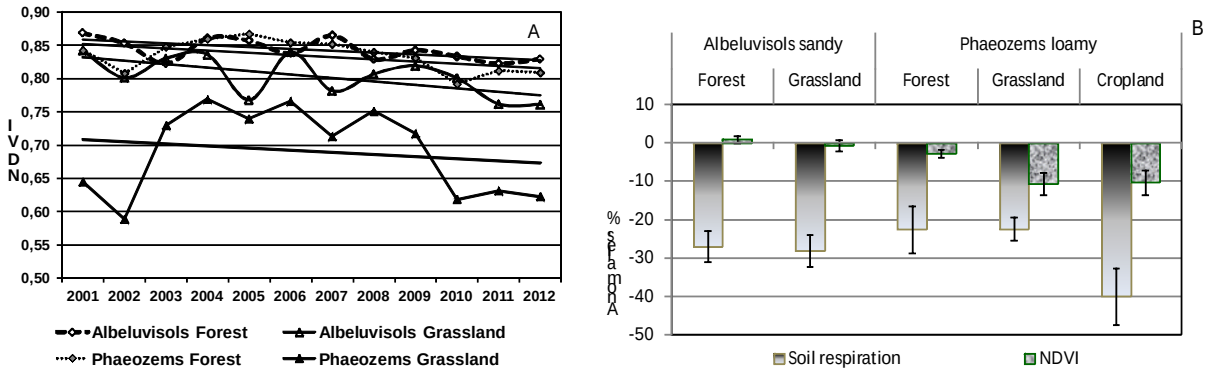

Figure 3. Trends of mean summer NDVI values in natural ecosystems (A) and mean SR/NDVI anomalies induced by summer droughts during 1998-2011 (B).

We evaluated the response of main components of the carbon cycle to extreme dry and hot conditions using the anomalies of annual SR and summer NDVI values (Figure 3B). It was found that the negative response of SR in the ecosystems studied to summer droughts was much higher than NPP (NDVI values) response. The anomalies of mean SR varied between -22 and -40% while the negative NDVI anomalies did not exceed -10%. The cropland demonstrated the highest response of annual SR as it is the most sensitive ecosystem to the enhancement of climate aridity. Negative anomalies of annual SR in forest and grassland ecosystems located on sandy Albeluvisols were higher than SR anomalies in natural ecosystems on loamy Phaeozems. The founding allowed us to suggest that the aridity enhancement in Central Russia can evoke the gain of carbon sink in ecosystems.

CONCLUSIONS

The significant enhancement of aridity was observed in Central Russia and the area studied during recent 14- and 39-yrs time intervals. This clear climatic tendency evoked negative trends of annual soil respiration flux which were more significant in sandy soils in comparison with loamy ones and in cropland versus forest or grassland. Owing to the dominance of more tolerant fungi microflora in soils, natural ecosystems are less sensitive to climate change compared to agroecosystems. Due to the higher water holding capacity, the clay soils are more persistent to extreme weather conditions than sandy soils. Hence, the soil texture and the land use are the main underlying drivers governing the vulnerability of carbon cycle in temperate ecosystems to current climate changes. We can propose that the enhancement of climate aridity observed in Central Russia may lead to increase of C sink in ecosystems due to the declining in annual soil respiration flux that is more significant than the decrease in vegetation productivity.

ACKNOWLEDGEMENTS

This study was supported by Russian Foundation for Basic Researches (grants No.12-04-00201a,12-05-00197a), ISTC (Project No. 4028), grant SciSch-6123.2014.4, Program of Presidium PAS No. 4, and Russian Scientific Foundation (grant No.14-14-00625).

REFERENCES

Assessment Report on Climate Change and its Consequences in Russian Federation (General Summary). (2008). (Moscow, RosHydromet).

Bigler, C., D.G. Gavin, C. Gunning, T.T. Veblen (2007). Drought induces lagged tree mortality in a subalpine forest in the Rocky Mountains. *Oikos* 116, 1983–1994.

Bourtsev, M.A., A. Mazur, I.A. Neustadt, A.A. Proshin (2006). Construction of satellite data archive for the analysis of vegetation dynamics. *Modern problems of remote sensing of the Earth from space* **3(1)**, 170-174 [in Russian].

Ciais P., M. Reichstein, N.Viovy, *et al.* (2005). Europe-wide reduction in primary productivity caused by the heat and drought in 2003. *Nature* **437(7058)**, 529-533,

Gulev, S.K., V.M. Kattsov, O.N. Solomina (2008). Global warming is continuing. *Vestnik RAS* **78(1)**, 20-27 [in Russian].

Karl, T.R., B.E. Gleason, M.J. Menne, *et al.* (2012). U.S. temperature and drought: Recent anomalies and trends, *Eos Trans. AGU*, 93*(47)*, 473.

Kurganova, I.N., V.O. Lopes de Gerenyu, A.S. Petrov, *et al.* (2011). Effect of the Observed Climate Changes and Extreme Weather Phenomena on the Emission Component of the Carbon Cycle in Different Ecosystems of the Southern Taiga Zone. *Doklady Biological Sciences* **441**, 412–416.

Kurganova, I., V. Lopes de Gerenyu, L. Rozanova, *et al.* (2003). Annual and seasonal CO_2 fluxes from Russian southern taiga soils. *Tellus* **55B**, 338-344.

Larionova, A.A., I.N. Kurganova, V.O. Lopes de Gerenyu, *et al.* (2010). Carbon Dioxide Emissions from Agrogray Soils under Climate Changes. *Eurasian Soil Science* **43(2)**, 168-176.

Loupian, E.A., A.A. Mazur, R.R. Nazirs, *et al.* (2004). The technology of automated systems for the collection, processing and storage of satellite data for scientific and applied problems. *Modern problems of remote sensing of the Earth from space* **1**, 81-88 [in Russian].

Loupian, E.A., I.Y. Savin, S.A. Bartalev, *et al.* (2011). Satellite service monitor vegetation ("Vega"). Modern *problems of remote sensing of the Earth from space* **8(1),** 190-198 [in Russian].

Nikulin, G., E. Kjelistro, U. Hansson *et al.* (2011). Evaluation and future projections of temperature, precipitation and wind extremes over Europe in an ensemble of regional climate simulations. *Tellus A* **63(1)**, 41-55.

Paruelo, J.M., H.E. Epstein, W.K. Lauenroth, *et al.* (1997). ANPP estimates from NDVI for the central grassland region of the United States. *Ecology* **78(3),** 953–958.

Reichstein, M., M. Bahn, P. Ciais, *et al.* (2013) Climate extremes and the carbon cycle. *Nature* **500**, 287–295.

Schär, C., P.L. Vidale, D. Lüthiet, *et al.* (2004). The role of increasing temperature variability in European summer heatwaves. *Nature* **427**, 332-336.

Unger, S., C. Maguas, J.S. Pereira, *et al.* (2010). The influence of precipitation pulses on soil respiration – Assessing the "Birch effect" by stable carbon isotopes. *Soil Biol. Biochem.* **42**, 1800–1810.

Wang, G., A.J. Dolman, A. Alessandri (2011). A summer climate regime over Europe modulated by the North Atlantic Oscillation. *Hydrol. Earth Syst. Sci.* **15,** 57-64.

Wang, Q., J. Ni, J. Tenhunen (2005). Application of a geographically-weighted regression analysis to estimate net primary production of Chinese forest ecosystems. *Global Ecology and Biogeography* **14(4)**, 379–393.

Wessels, K. J., S. Prince, I. Reshef (2008). Mapping land degradation by comparison of vegetation production to spatially derived estimates of potential production. *Journal of Arid Environments*, **72(10)**, 1940–1949.

Zolotokrylin, A.N., V.V. Vinogradova, Cherenkova, E.A. (2007). Drought dynamics over European Russia in global warming situation. *Problems of Ecological Monitoring and Ecosystem modelling* (St. Petersburg: Gidrometeoizdat) **21**, 161–182.

ENVIRO-HIRLAM BIRCH POLLEN MODELLING FOR NORTHERN EUROPE

A.R. KURGANSKIY[1,2], R.B. NUTERMAN[1,6], A.G. MAHURA[3], A. SAARTO[4], A.A. BAKLANOV[3,5], A. RASMUSSEN[3], S.P. SMYSHLYAEV[2], E. KAAS[1]

[1] Niels Bohr Institute, University of Copenhagen (NBI UC), Juliane Maries Vej 30, DK-2100, Copenhagen, Denmark.
[2] Russian State Hydrometeorological University (RSHU), Malookhtinsky prospect 98, St. Petersburg, Russia.
[3] Danish Meteorological Institute (DMI), Lyngbyvej 100, DK-2100, Copenhagen, Denmark.
[4] University of Turku, Aerobiological Unit, Vesilinnantie, 20014, Turku, Finland.
[5] World Meteorological Organization (WMO), 7 bis, Avenue de la Paix, 1211 Geneva 2, Switzerland.
[6] Tomsk State University (TSU), Lenin Ave., 36, 634050, Tomsk, Russia.

Keywords: BIRCH POLLEN, BIRCH FOREST MAP, ENVIRO-HIRLAM MODELLING.

INTRODUCTION

Recently, model studies of biological aerosols such as birch pollen have gained high interest and importance. Birch pollen is present as biological tracer in different numerical weather prediction (NWP) and atmospheric chemistry transport (ACT) models such as SILAM (Finland), COSMO-ART (Germany), WRF-CHEM (USA), CHIMERE (France), and Enviro-HIRLAM (Denmark). The main goal of birch pollen forecasting is to make a warning for population group suffering from allergic diseases. The number of allergic patients sensitive to birch pollen is assessed as 20% of European population (WHO, 2003). In particular, for Northern Europe the pollen season of 2006 was characterized by abundant birch pollen concentrations that resulted in increase of patient calls for medical assistance during spring period (Sofiev et al, 2011). Similar to 2006, the year of 2014 was defined by exceptionally high birch pollen concentrations, which was reflected in increased number of patients with asthma symptoms.
European birch forest sources are mainly located in Northern Europe Birch pollen emissions are driven not only by meteorological conditions but also depend on the amount of source pollen which varies from year-to-year; and particles can be transported for long distances if the meteorological conditions are favorable. The extreme birch pollen concentrations for Northern Europe during the season of 2006 resulted from local emissions as well as from long-range transport of pollen particles from more remote regions. Therefore, prediction of the pollen season is important from both medical and modelling points of view.

METHODS

Enviro-HIRLAM: Environment - High Resolution Limited Area Model

In our study, the Enviro-HIRLAM (Environment - High Resolution Limited Area Model) online-coupled numerical weather prediction and atmospheric chemistry transport modeling system is used (Korsholm, 2009, Baklanov *et al.,* 2008, and most recent developments are shown in Nuterman *et al.,* 2013). The model runs were performed to simulate birch pollen concentrations for Northern European domain (118 x 118 grid horizontal points; 40 vertical hybrid levels) at 0.135° horizontal resolution. This domain includes the North-West Russia, Finland, Sweden, Baltic States, and Belarus (see Fig. 1a).

Birch pollen module

Birch pollen module (Mahura *et al.*, 2007, 2009, Rasmussen, 2002) is an integral part of the Enviro-HIRLAM modeling system, and the module consists of spatial birch forest habitat map, emissions from local pollen sources, atmospheric transport, diffusion, gravitational settling and scavenging of particles in the atmosphere.

Spatial distribution of birch forest

Birch forest habitat map has been derived by GIS analysis for the selected modeling domain (shown in Fig. 1a). The map is represented by birch forest fraction in each model grid cell. Three GIS based databases were used in deriving procedure: 1) Global Land Cover (GLC), 2) European Forest Institute (EFI) and 3) Tree Species Inventory (TSI).
GLC (edc2.usgs.gov/glcc/) includes geographical distribution of land use, soil type and other various properties with 1 km horizontal resolution. Illustration of GLC database is presented in Fig. 1b. EFI (Päivinen *et al.*, 2001) has also 1 km horizontal resolution and it contains spatial distribution of forest class with sub-classes, i.e., broadleaved forest and coniferous forest. Spatial distribution of broadleaved forest, used in the current study, is presented in Fig. 1c.

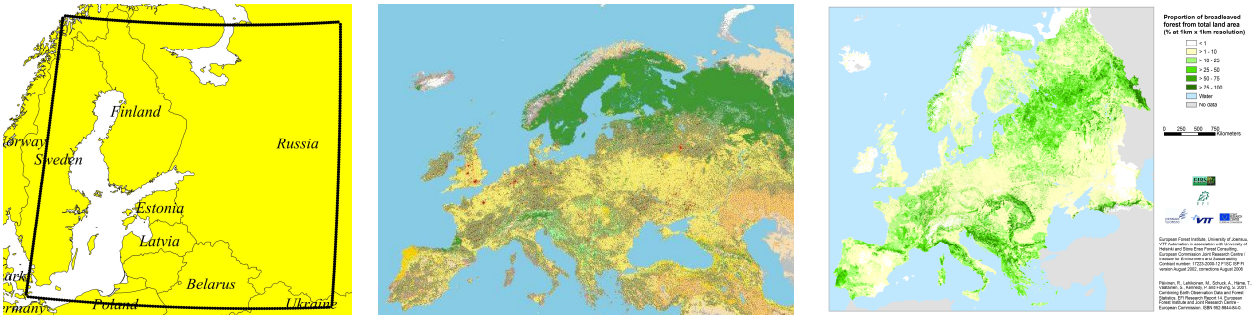

(a) (b) (c)

Figure 1*: (a): Boundaries and specifications of the modeling domain; (b): Spatial distribution of Global Land Cover classes (source: edc2.usgs.gov/glcc/eurasia_img.php); (c): European Forest Institute broadleaved forest (source: www.efi.int).*

TSI (Skjøth *et al.*, 2008) is represented by 39 types of tree species (birch, oak, alder, etc.), and it is based on national forest inventories and national statistics. Birch forest fraction within broadleaved forest layer with 50 km horizontal resolution was used for the analysis (Fig. 2a).

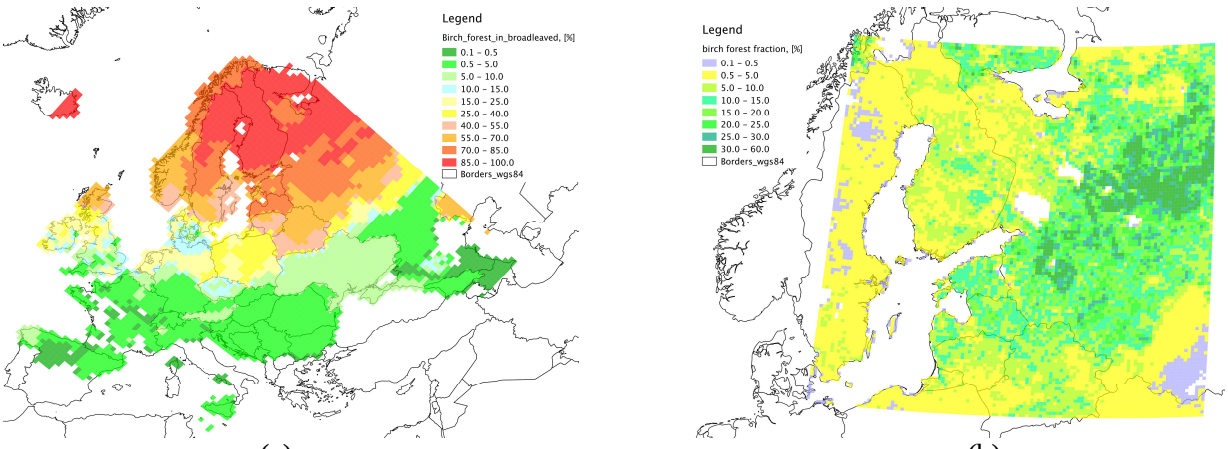

(a) (b)

Figure 2. (a): Spatial distribution of birch forest fraction within broadleaved forest (Tree Species Inventory); (b) birch forest fraction calculated for the modeling domain.

Several layers such as land-mask, forest, vegetation, urban territory (from GLC), broadleaved forest (from

EFI) and birch forest fraction in broadleaved forest (from TSI) have been extracted from these databases, recalculated for the domain as a weighted mean and combined for correct assessment of birch forest fraction in each grid cell. The calculated spatial birch forest distribution map is shown in Fig. 2b.

Birch pollen emissions

Birch pollen emission parameterization is meteorology-dependent and based on correcting dimensionless functions (Sofiev *et al.*, 2012). The main meteorological parameters influencing the birch pollen emission are air temperature at 2 meter, relative humidity at 2 meter, wind speed at 10 meter and accumulated precipitation.

Atmospheric transport, dispersion and deposition of pollen particles

Atmospheric transport of birch pollen particles is based on the Locally Mass Conserving Semi-Lagrangian (LMCSL) scheme (Kaas 2008, Sorensen *et al.*, 2013) that can be used for any aerosol and chemical species. For horizontal diffusion an implicit 4^{th} order scheme is utilized. Cuxart, Bougeault, Redelsperger (CBR) scheme is used to model vertical diffusion (Cuxart *et al.*, 2000).
Birch pollen particles are light and have a size about 20 μm. Therefore, dry deposition process is parameterized according to Stokes' law. Wet deposition of pollen particles is parameterized in a same way like for simple aerosols via scavenging coefficient. Wet deposition parameterization considers evaporation of raindrops in the atmosphere as well.

CONCLUDING REMARKS

The model results for pollen episode in 2006 were compared with observations for two Northern European sites in Finland: Helsinki and Turku (see in Fig. 3). Preliminary evaluation for both modeled and observed birch pollen concentrations showed extremely high values (daily averages more than 1000 grains/m^3), and especially during 5-12 May 2006 episode for the Northern European stations. This phenomenon can be explained by high number of birch male catkins, favorable meteorological conditions for local birch pollen emissions as well as long-range transport of birch pollen particles from remote regions during the spring period of 2006.

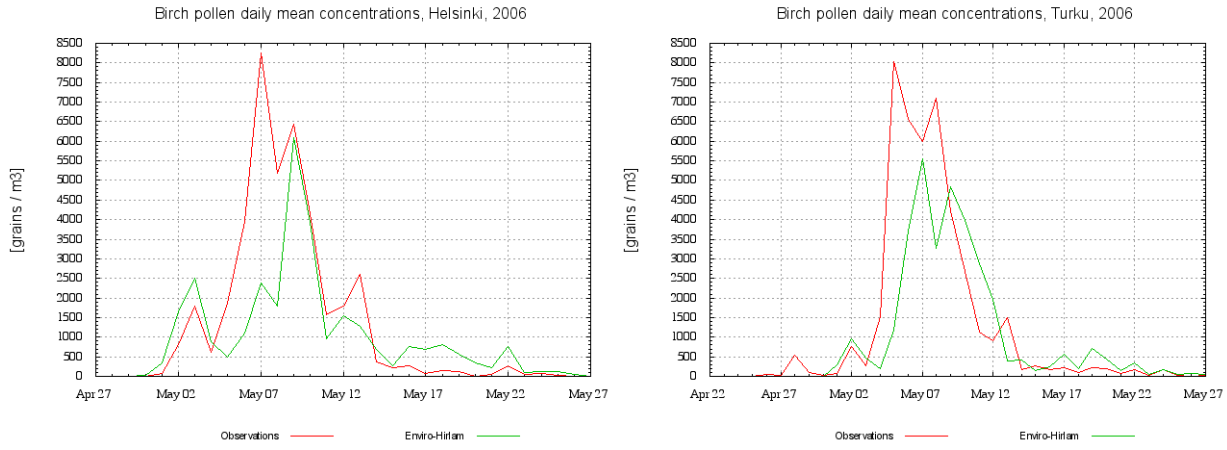

(a) (b)

Figure 3. Birch pollen concentrations observed (red) vs. modelled (green) at two Finnish sites: (a) Helsinki (60°10‘ N and 24°54‘ E), (b) Turku (60°32‘ N and 22°28‘ E).

Although the modelled results reflected the overall general shape of changes in pollen concentration during the episode studied, some underestimation of modelled concentrations is visible, especially for the occurrence of maximum concentration. It might be caused by (i) underestimated contribution due to long-range atmospheric transport of pollen from other remote regions (observed especially at the beginning of

elevated concentration episode), (ii) underestimated contribution from local pollen sources (because of low resolution /50 km/ of TSI birch forest fraction, non-accurate redistribution and assigning of pollen sources into grid cells /15x15 km/, and influence of local meteorology (observed locally vs. modeled at 15 km resolution).

ACKNOWLEDGEMENTS

The authors are thankful to Dr. Carsten Ambelas Skjøth (University of Worcester, National Pollen and Aerobiological Research Unit; UK) for providing tree species inventory data; European Forest Institute (EFI) - for broadleaved forest data; Prof. Mikhail Sofiev (Finnish Meteorological Institute, Helsinki), Aerobiological Unit at University of Turku for birch pollen observation data, Dr. Suleiman Mostamandy (RSHU, St.Petersburg) for help in getting meteorological IC/BC data.

REFERENCES

Baklanov, A., Korsholm, U., Mahura, A., Petersen, C., and Gross, A.: ENVIRO-HIRLAM: on-line coupled modelling of urban meteorology and air pollution, Adv. Sci. Res., 2, 41-46, 2008.

Cuxart, J., Bougeaults, P. and Redelsberger, J., L.: A turbulence scheme allowing for mesoscale and large-eddy simulations, Quarterly Journal of the Royal Meteorological Society, 126, 1-30, 2000.

Kaas, E.: A simple and efficient locally mass conserving semi-Lagrangian transport scheme, Tellus. Series A: Dynamic Meteorology and Oceanography, vol 60, no. 2, pp. 305-320., doi:10.1111/j.1600-0870.2007.00293.x, 2008.

Korsholm U.S.: Integrated modeling of aerosol indirect effects - development and application of a chemical weather model, PhD thesis University of Copenhagen, Niels Bohr Institute and DMI, Research Department; http://www.dmi.dk/dmi/sr09-01.pdf, 2009.

Mahura, A., Baklanov, A., and Korsholm, U.: Parameterization of the birch pollen diurnal cycle, Aerobiologia, 25, 203–208, doi:10.1007/s10453-009-9125-7, 2009.

Mahura, A., Korsholm, U., Baklanov A., and Rasmussen A.: Elevated birch pollen episodes in Denmark: contributions from remote sources, Aerobiologia, 23, 171–179. doi:10.1007/s10453-007-9061-3, 2007.

Nuterman, R., Korsholm, U., Zakey, A., Nielsen, K. P., Sørensen, B., Mahura, A., Rasmussen, A., Mažeikis, A., Gonzalez-Aparicio, I., Morozova, E., Sass, B. H., Kaas, E., and Baklanov, A.: New developments in Enviro-HIRLAM online integrated modeling system, Geophysical Research Abstracts, Vol. 15, EGU2013-12520-1, 2013.

Päivinen, R., Lehikoinen, M., Schuck, A., Häme, T., Väätäinen, S., Kennedy, P., and Folving, S.: Combining Earth Observation Data and Forest Statistics, Research Report, 14, 101 p., EFI, Joensuu and Joint Research Centre / European Commission, 2001.

Rasmussen, A.: The effects of climate change on the birch pollen season in Denmark, Aerobiologia, 18, 253–265, 2002.

Skjøth, C. A., Geels, C., Hvidberg, M., Hertel, O., Brandt, J., Frohn, L. M., Hansen, K. M., Hedegaard, G. B., Christensen, J., and Moseholm, L.: An inventory of tree species in Europe - an essential data input for air pollution modelling, Ecol. Model., 217, 292-304, 2008.

Sofiev M., Siljamo P., Ranta H., Linkosalo T., Oksanen A., Karppinen A., Kukkonen J., and Severova E.: From Russia to Iceland: an evaluation of a large-scale pollen and chemical air pollution episode during April and May, 2006, Aerobiological Monographs, Towards a Comprehensive Vision, 1, 95-114, 2011.

Sofiev, M., Siljamo, P., Ranta, H., Linkosalo, T., Jaeger, S., Rasmussen, A., Rantio-Lehtimaki, A., Severova, E., and Kukkonen, J.: A numerical model of birch pollen emission and dispersion in the atmosphere, description of the emission module, Int. J. Biometeorol.,57, 45–58, doi:10.1007/s00484-012- 0532-z, 2012.

Sørensen, B., Kaas, E., and Korsholm, U. S.: A mass-conserving and multi-tracer efficient transport scheme in the online integrated Enviro-HIRLAM model, Geosci. Model Dev., 6, 1029-1042, doi:10.5194/gmd-6-1029-2013, 2013.

WHO, Phenology and human health: allergic disorders, Copenhagen, WHO Regional Office for Europe, 55 pp, 2003.

FEEDBACK MECHANISMS MODIFYING THE AEROSOL CONCENTRATIONS IN THE CHANGING POLAR CLIMATE - NEW BIOGENIC AND ANTHROPOGOGENIC SOURCES FOR SECONDARY AEROSOLS

E.-M. KYRÖ[1], V.-M. KERMINEN[1], T. PETÄJÄ[1], A. VIRKKULA[1,2] and M. KULMALA[1]

[1] Department of Physics, University of Helsinki, Helsinki, Finland

[2] Air Quality Research, Finnish Meteorological Institute, Helsinki, Finland

Keywords: Polar regions, climate change, new particle formation, CCN.

ABSTRACT

Both northern and southern polar regions are very sensitive to the ongoing climate change. The changes in the interactions between the atmosphere, biosphere and cryosphere in these regions have inevitable consequences to global climate as well. Aerosol-cloud-climate interactions pose the largest uncertainties related to estimating our future climate (IPCC, 2013). In order to be able to quantify these, it is needed to know how the sources of aerosols will change in the future.

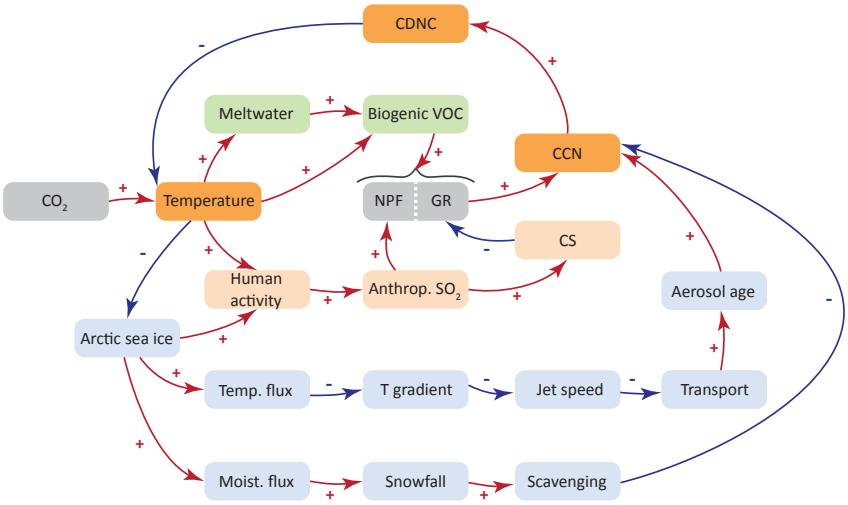

Figure 1: Feedback mechanisms related to warming Arctic. Red arrows indicate positive, blue arrows indicate negative association between two quantities.

There are several feedback mechanisms related to warming Arctic that have the potential to alter the cloud droplet number concentrations (CDNC) (Fig. 1). Here we introduce four such mechanisms, related to (i) the increase of meltwater, (ii) increase of human activity and (iii) decrease of the Arctic sea ice.

First feedback loop is related to the increase of meltwater in glaciated and snow covered areas during the summertime as the climate warms. This increases the emissions of biogenic volatile organic compounds (BVOC) which in turn may both increase the formation and growth of secondary organic aerosols and finally, cloud condensation nuclei (CCN). This has been shown to contribute significantly to the production of CCN in glaciated areas (Kyrö et al., 2013). This feedback loop also includes the increased terrestrial BVOC emissions due to increasing temperature (Paasonen et al., 2013).

On the other hand, decreasing Arctic sea ice supposedly attracts more marine activity as it opens up new, faster shipping routes and allows oil and gas drilling from new areas. The increased human activity brings more anthropogenic SO_2 emissions to the Arctic. The concentrations of CCN and CDNC can either increase or decrease depending on the balance between SO_2 increasing the formation rate but at the same time, decreasing the growth rate (GR) by increasing condensation sink (CS). Long-term study of sulphur pollution originating from Kola Peninsula shows that at least in Eastern Lapland, higher SO_2 leads to more days of active new particle formation (NPF) and increases the concentration of potential CCN (Kyrö et al., 2014).

Decreasing Arctic sea ice increases the fluxes of heat and moisture into the atmosphere. As a consequence, the atmospheric transport and snowfall rates in Siberia and Europe may change. Since snow is an efficient scavenger (Kyrö et al., 2009), this has a potential to decrease the CCN and CDNC concentrations in those areas and decrease the pollution transport into the High Arctic from lower latitudes. On the other hand, condensational growth is important in the west to east transport over Boreal forests (Väänänen et al., 2013). This, combined with increased atmospheric transport times due to slowing of the Polar jet can allow the particles to grow larger and more or them to reach CCN sizes.

ACKNOWLEDGEMENTS

The authors acknowledge the Academy of Finland Centre of Excellence program (project no. 272041), Pan-European Experiment PEEX and the Nordic Centre of Excellence CRAICC (Cryosphere-atmosphere interactions in a changing Arctic climate) for funding.

REFERENCES

Boucher, O. *et al.* (2013), Clouds and Aerosols. In: Climate Change 2013: The Physical Science Basis (IPCC). Cambridge University Press, Cambridge, United Kindom and New York, NY, USA.

Kyrö, E.-M., *et al.* (2009), Snow scavenging of ultrafine particles: field measurements and parameterization. *Boreal Environ. Res.*, **14**, 527–538.

Kyrö, E.-M, *et al.* (2013), Antarctic new particle formation from continental biogenic precursors. *Atmos. Chem. Phys*, **13**, 3527–3546.

Kyrö, E.-M, *et al.* (2014), Trends in new particle formation in eastern Lapland, Finland: effect of decreasing sulfur emissions from Kola Peninsula. *Atmos. Chem. Phys*, **14**, 4383–4396.

Paasonen, P., *et al.* (2013), Warming-induced increase in aerosol number concentration likely to moderate climate change. *Nature Geoscience*, **6**, 438–442.

Väänänen, R., *et al.* (2013), Analysis of particle size distribution changes between three measurement sites in northern Scandinavia. *Atmos. Chem. Phys.*, **13**, 11887–11903.

A NEW PEATLAND RESEARCH STATION IN THE CENTER OF WEST SIBERIA: DESCRIPTION OF INFRASTRUCTURE AND RESEARCH ACTIVITIES

LAPSHINA E.D.[1], ALEXEYCHIK P.[2], DENGEL S.[2], FILIPPOVA N.V.[1], ZAROV E.A.[1], FILIPPOV I.V.[1], TERENTYEVA I.E.[1], SABREKOV A.F.[1], SOLOMIN Y.R.[1], KARPOV D.V.[1] and MAMMARELLA I.[2]

[1]Yugra State University, Russian Federation

[2]Department of physics, University of Helsinki

Keywords: Western Siberia, middle taiga, peatland ecology, methane flux, carbon dioxide flux, eddy-covariance, chamber measurements

INTRODUCTION

The undisturbed pristine peatlands are a net sink of atmospheric CO_2, as the mire-ecosystems actively accumulate organic carbon (peat). By anoxic decomposition of the peat and of organic matter in the floodplain sediments, both areas are methane sources.

Wetlands represent an important component of the global carbon cycle, being a significant course and sink of carbonaceous compounds, which is addressed in a significant body of scientific literature. In turn, the Boreal wetland ecosystems are sensitive to the climate change.

Despite the equivocal agreement on the high importance of Boreal wetlands for the biospheric and atmospheric processes (Smith at al., 2004; Sheng et al., 2004) detailed studies involving state-of-art techniques remain scarce in this region. This is mainly due to the lack of developed measurement sites with the infrastructure suitable for continuous monitoring of the ecosystem-atmosphere exchange processes.

The international group of researchers at the Mukhrino field station aims to promote the understanding of the Siberain middle taiga wetlands ad forests. It is the only such infrastructure within approximately 1000 km radius, which makes the results obtained at the station unique for this region.

MUKHRINO FIELD STATION DESCRIPTION

Mukhrino Field Station (MFS) in the centre of Western Siberia (Khanty-Mansiysk Autonomous District, Russia, http://mukhrinostation.wordpress.com) was established as a part of the UNESCO chair “Environmental Dynamics and Global Climate Change” of Yugra State University in 2009. The location of MFS was chosen to be 30 km South-west from Khanty-Mansiysk (60°53' N; 68°42' E) on the left terrace of Irtysh River (Figure 1). It is equipped with modern facilities allowing conducting year-round long-term ecological field research, scientific excursions, summer schools, workshops, symposia and other events at regional, national and international level.

Since 2011 the Field Station “Mukhrino” became a member of the International EU-project consortium “International Network for Terrestrial Research and Monitoring in the Arctic: INTERACT” (www.eu-interact.org). The project involved 32 research institutes and universities that run arctic field stations and are active in monitoring the environment in the Arctic and Sub-arctic areas of the Northern Hemisphere (Elger et al., 2012).

Twenty research stations including MFS offered EU Transnational Access in 2011-2014. Six calls for applicants were arranged during the funding period, and access was granted to over 190 user groups from 20 countries. MFS is one of the most popular and asked-for field stations in the INTERACT network. It is the third field station after Abisko (Sweden) and Zackenberg (Greenland) in terms of the total number of visitor groups (19) and used person days (about 700 during 2012-2014).

The MFS is representative for the pristine carbon-accumulating peatland ecosystems for the West Siberian plain mires of the Middle taiga zone. These mires cover about 60 % of the land surface of this zone. Also, native old dark coniferous and mixed forests, as well as pristine wetland and meadow vegetation in vast flood plains of Irtysh and Ob rivers are presented. The site is highly representative for mire ecosystems as sources/sinks of GHG and aerosols.

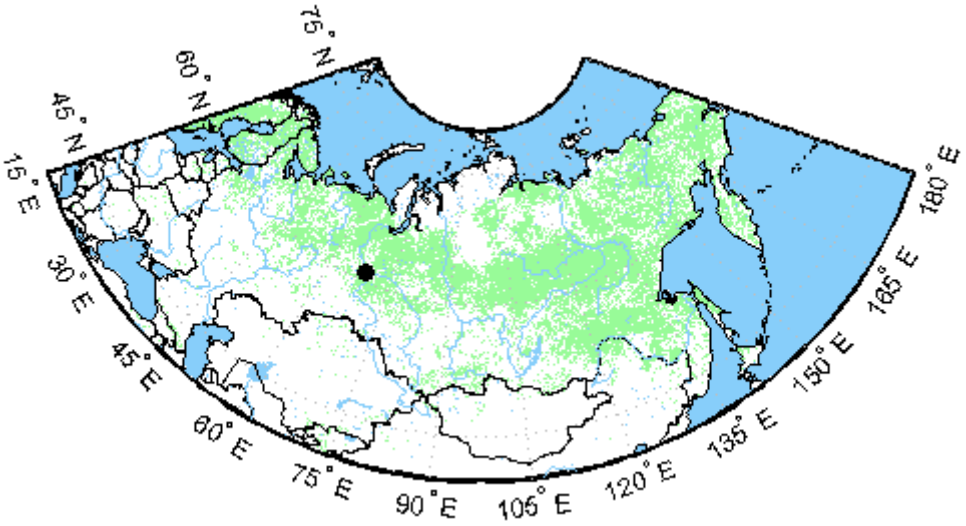

Figure 1. Location of the Mukhrino Field Station.

MATERIALS AND METHODS

1. The facility of the Field Station includes a 2-floor wooden building in a primary mixed forest, with study/laboratory rooms, simple equipped dining/kitchen room, beds for 14 persons and a (Russian) sauna.
2. The experimental field site is equipped with 1.5 km long walking boards, which crosses the main mire ecosystem types and facilitates researchers to perform experiments and measurements without disturbing the ecosystems.
3. The energy for both the accommodation and the field equipment is supplied by a wind-generator (2 kW) and solar battery (5 kW)
4. In the year 2012, a system for satellite Internet access was launched.
5. Automatic weather station measures 20 parameters both in wet hollow and in the pine-dwarf shrub-sphagnum ecosystem of oligotrophic mire, including air and soil temperature profiles, air and soil moisture, solar radiation (direct and back), wind speed and direction, precipitation, atmospheric pressure. All weather station data loggers are equipped by WiFi-antenna. In 2014, a Wi-Fi connection is scheduled for installation, which will allow for a continuous remote access to the field measurement devices.
6. Nine permanent chambers (1 m^2) have been installed in different vegetative communities to study the greenhouse gas exchange of the bog. Additionally, handheld chambers are used to study

the spatial heterogeneity in methane emissions from different type of peatlands (Kleptsova, 2010; Sabrekov, 2010; Glagolev at al., 2011; Sabrekov et al., 2012). Intensive chamber measurement campaigns were carried out at Mukhrino field station during the 2008-2014 summer-autumn periods. CH_4 exchange with the atmosphere was measured using the static opaque chamber method. Methane fluxes were measured at 6 different types of microforms that are typical for middle taiga climate zone: ridges, hollows, pine-shrub-sphagnum communities (termed *ryam* in local dialect), small wetland ponds (with area not higher than 100 m^2), wetland lakes (with area higher than 100 m^2) and peat mats. Total amount of chamber flux measurements has reached about 1000. At each site the following environmental characteristics were also measured: air and peat temperatures (at the depths of 0, 5, 15, 45 cm), pH and electrical conductivity and concentration of dissolved oxygen. Finally, botanical descriptions were made to describe the vegetation community within each chamber site.

7. Eddy-covariance (EC) measurements have been initiated in April 2014 in collaboration with the researchers from Department of Physics, University of Helsinki. Currently, the EC system consists of the LiCor-7500 gas analyzer and Gill R3 anemometer, positioned at the part of the raised bog having a sparse natural pine stand. There are plans of expanding the EC system with a methane concentration analyzer in 2015.

RESULTS

The main topics of current scientific research activities are climate change, biodiversity (fauna, vegetation, mosses, hepatics, fungi communities), carbon and water cycling of peat ecosystems, physical-chemical and biochemical properties of peat types, and paleoecology of mire landscapes in West Siberia. The station is also used for analyses of climate change effects in peatland ecosystems and carbon balance, and the spatial comparison of key areas in S-N transects (57-67° N) as an analogue for climate change over time. The station houses specialists in vegetation science, remote sensing, mycology, hydrology, and greenhouse gas emission measurements.

- Temperature and soil moisture are two the most important climatic factors influencing both biodiversity and aboveground-belowground interactions in a peatland ecosystems. The permanent microclimatic monitoring of mire micro-habitats has been carried out. For that, a large number of soil temperature loggers are installed in 6 vertical profiles down to 2.5 m below the surface. Three studied types of habitats differ in micro-climates in spite of their spatial proximity. The bog habitats have the highest daily amplitude of temperature within the 0-5 cm layer. Soil surface in pine-dwarf shrub-sphagnum bog is more subjected to frost, sphagnum lawn has lower number of frost hours at the surface and boreal forest has the intermediate position. The duration of the period with temperatures >5° at the surface is noticeable shorter in the pine-dwarf shrub-sphagnum bog compared to sphagnum hollows.
- The quantitative estimation of fungal activity and fruiting of 59 species of larger fungi and micro fungi on plant litter was performed (Filippova et al., 2014). In total, 350 mushroom species were identified at the raised bog. The communities of macromycetes and fungal communities on various substrates were described.
- Hydrological research through automated hydrological devices includes continuous monitoring of overland flow, subsurface flow and groundwater level, sampling water and snow and modeling of mire water balance, discharge response to snow melt and mass balance of C and N. A steady-state hydrological model of brook catchments has been created on a base of long-term monitoring. The model is realized in the free software ModFlow. The rain precipitation (measured by Hobo rain Gauge), snow precipitation (measured by manual volumetric method), evaporation and evapotranspiration data (measured by open-water- and mire-lysimeters equipped by Hobo-Divers) have been used as an input information in a model. Additional data about soil

properties (peat porosity, hydraulic conductivity) were measured in lab or taken from a literature. Landscape map is based on a high resolution satellite image (QuickBird) classification. All input files are prepared in PcRaster.

- Physic-chemical properties of peat (bulk density, particle density, loss on ignition, C, N content), chemical group compounds and decomposition rate of organic matter have been studied in different type of peatlands and mire ecosystems.
- One of the long-term experiments in frame of join French-Swiss-Polish-Russian project carried out at MFS engages installing of the experimental devices (Open Top Chambers and trenches for drought manipulation) and continuous *in situ* monitoring devices of climatic parameters and environmental variables (soil temperature and water table depth) in the open top chambers and the controls. The objective of the experiment is to use *Sphagnum* peatland ecosystems as a model and to analyze their vulnerability in the context of climate change (drought and warmer temperatures) using two complementary approaches: a natural climate gradient and experimental climatic manipulation along this gradient.
- Based on high resolution satellite images and a large volume of ground observations, measured gas fluxes were upscaled for the different bio-climatic zones and the whole of West Siberian lowland.
- Eddy-covariance CO_2 flux series were obtained at the raised bog in summer-2014. From the available dataset, it is apparent that the peatland had the nocturnal respiration rate of about 1-2 μmol CO_2 $m^{-2}s^{-1}$, while its maximum midday uptake rate reached -6 μmol CO_2 $m^{-2}s^{-1}$ (Figure 2).

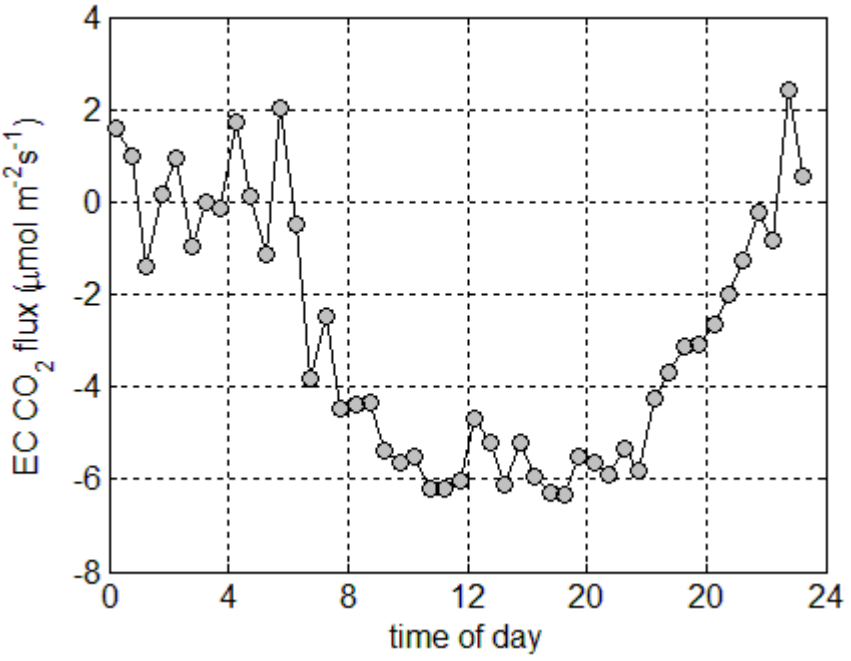

Figure 2. Mean daily course of the CO_2 flux obtained with the Eddy covariance system at the Mukhrino bog site in July-August 2014.

- The chamber data were used to derive the regional methane flux estimate for West Siberian mires (Glagolev et al., 2011). They also allowed revealing different kinds of uncertainties in the regional flux estimate caused by a limited number of potentially non-representative field observations and strong flux variability among different sites and observation periods. These uncertainties include interannual variability, seasonal variability (data cover July-September periods) and spatial variability within the mire microlandscapes (caused by local microrelief,

plant or microbial communities). This information helped estimate the regional flux uncertainty (see Sabrekov et al., 2014 for details). Average summer fluxes of CH_4 for different peatland surface types are reported in Table 1 below.

Table 1: vegetative community-specific methane effluxes at the Mukhrino bog.

Type of microlanscape	Average flux, mgCH_4 m^{-2} h^{-1}	Reference
Hollow	3,0	Sabrekov et al., 2011
Ridge	0,16	Sabrekov et al., 2011
Wetland pond	1,8	Sabrekov et al., 2012
Wetland lake	0,5	unpublished
Ryam	0,1	Sabrekov et al., 2011
Peat mat	5,3	Sabrekov et al., 2012

REFERENCES

Elger,K., Opel,T., Topp-Jørgensen, J.E., Rasch, M. 2012. *INTERACT Station Catalogue*. Aarhus University, Danish Centre for Environment and Energy (DCE).

Filippova N.V., Mourgues A., Philippe F., 2014. Notes on the phenology of fungi in ombrotrophic bog. *Environmental Dynamics and Global Climate Change*. V. 9. № 1 (9). EDCCrar0009.

Glagolev M., Kleptsova I., Filippov I., Maksyutov S. and Machida T., 2011. Regional methane emission from West Siberia mire landscapes. *Environ. Res. Lett.* V. 6. № 4. 045214. doi: 10.1088/1748-9326/6/4/045214

Kleptsova, I.E., Glagolev M.V., Filippov I.V., Maksyutov Sh.Sh., 2010. Methane emission from ryams and ridges in the Middle taiga of West Siberia. *Environmental Dynamics and Global* Sabrekov A.F. 2010. On a correlation between diurnal pattern of the methane mixing ratio above the mire surface and the diffusion coefficient. *Environmental Dynamics and Global Climate Chang*, **1**(2) (In Russian).

Sabrekov A.F., Glagolev M.V., Filippov I.V., Kazantsev V.S., Lapshina E.D., Machida T., Maksyutov S.S. 2012. Methane emissions from north and middle taiga mires of Western Siberia: Bc8 standard model. *Moscow University Soil Science Bulletin*, V. 67, № 1, 45-53. doi: 10.3103/S0147687412010061

Sabrekov A.F., Kleptsova I.E., Glagolev M.V., Maksyutov S.S. and Machida T., 2011 Methane emission from middle taiga oligotrophic hollows of Western Siberia. *Tomsk State Pedagogical University Bulletin*, № 5, 135-143

Sabrekov A.F., Runkle B.R.K., Glagolev M.V., Kleptsova I.E., Maksyutov S.S., 2014. Seasonal variability as a source of uncertainty in the West Siberian regional CH_4 flux upscaling. *Environ. Res. Lett*. V. 9. № 4. 045008. doi: 10.1088/1748-9326/9/4/045008

Smith, L.C., MacDonald, G.M., Velichko, A.A., Beilman, D.W., Borisova, O.K., Frey, K.E., Kremenetski, K.V. and Sheng, Y., 2004. Siberian peatlands a net carbon sink and global methane source since the early holocene. *Science* 303, 353–356.

Sheng Y., Laurence C. Smith, Glen M. MacDonald, Konstantine V. Kremenetski, Karen E. Frey, Andrei A. Velichko, Mary Lee, David W. Beilman, Peter Dubinin, 2004. A high-resolution GIS-based inventory of the west Siberian peat carbon pool. *Global biogeochemical cycles*, vol. 18, GB3004, doi:10.1029/2003GB002190

LONG-TERM VARIABILITY OF AEROSOL OPTICAL PROPERTIES IN NORTHERN FINLAND

HEIKKI LIHAVAINEN, ANTTI HYVÄRINEN, EIJA ASMI, JUHA HATAKKA AND YRJÖ VIISANEN

Finnish Meteorological Institute,
Erik Palmenin aukio 1, P.O.Box 503, FI-00101 Helsinki Finland

Keywords: AEROSOL, OPTICAL PROPERTIES, CLIMATE

INTRODUCTION

This work is based on measured aerosol optical properties in Northern Finland, on the gateway to Arctic areas. Aerosol optical properties and their relation to other aerosol properties are key factors when investigating the direct radiative effects by atmospheric aerosols. Because of their various sources and short life-time, the properties of these aerosols may vary significantly both temporally and spatially. In addition to the changes occurring on short time-scales, the aerosol optical properties also vary on decadal scales, especially at lower latitudes (Collaud Coen *et al.* 2013). Continuous long-term measurements on aerosol optical properties, such as the scattering and absorption coefficients in different environments, are not extensively reported. In this study analysis of ten years of scattering coefficient (2001-2010), five years of absorption coefficient (2006-2010) and a combination of scattering and absorption coefficient data and their relation are presented

METHODS

The analysed data have been measured at Pallas Global Atmosphere Watch Station Sammaltunturi measurement site located in Northern Finland (67°58'N, 24°07'E). The station is hosted by Finnish Meteorological Institute. The Sammaltunturi station lies on a top of a fjeld, round topped treeless hill, at an elevation of 565 m above sea level (a.s.l.). The vegetation on the fjeld top is sparse, consisting mainly of low vascular plants, moss and lichen. The Sammaltunturi station is about 300 m above the surrounding area and the timberline lies about 100 m below the station. The region is hilly (250–400 m a.s.l.), forested and partly swampy with some rather large lakes (ca 250 m a.s.l.). The station is located inside the Pallas-Yllästunturi National Park (total area 1020 km^2).

The scattering coefficient is measured at three wavelength by nephlelometer (model 3563, TSI, Inc., St. Paul, Minnesota), absorption coefficient at seven wavelength by Aethalometer (model AE31, Magee Scientific). Data that is affected by malfunction of the instrumentation and peaks from very local sources like snowmobile exhausts are removed. Because the station at Pallas is occasionally inside a cloud, data with hourly average visibility below 5 km was removed. Nonidealities due to nonlambertian and truncation errors in nephelometer were corrected using the method described by Anderson and Ogren (1998). The aethalometer absorption measurement is known to suffer from a filter loading artefact. These artefacts can be corrected using different methods. Here, the approach presented by Weingartner *et al.* (2003) was chosen.

Data were divided according to their air mass history into two categories: marine and continental. We used air mass back trajectories calculated with the FLEXTRA trajectory model and data from European Center for Medium-Range Weather Forecasts (ECMWF).

CONCLUSIONS

Both absorption and scattering coefficients in Pallas are the lowest measured in Finland. The scattering coefficients at Pallas GAW station are slightly lower than in an Arctic station in Alaska, Barrow. Absorption coefficient is however slightly higher than in Barrow. Higher scattering coefficient in Barrow is probably caused by sea salt and Arctic haze affecting stronger in Barrow (Delene and Ogren, 2002). Higher absorption coefficients in Pallas are probably related to winter time emissions of black carbon from continental areas.

There is a clear seasonal trend in both scattering and absorption coefficients, however their seasonal variation is different, Figure 1. Scattering coefficients are highest during summer and lowest during late fall and early winter whereas absorption is lowest during summer and highest during winter. Our results suggest the scattering coefficient in Pallas is mostly affected by natural emissions which are the highest in summer during vegetation active period. Aerosols affecting to absorption in contrast seem to be mostly from anthropogenic sources such as residential wood combustion, which is commonly used during cold winter months.

This seasonal behaviour of scattering and absorption coefficients leads to a situation where aerosols are darker in winters, i.e. single scattering albedo (SSA) is low and brighter during summers, i.e. SSA is high. These dark aerosols might have direct climate effect only in late winter and spring after the polar night. When depositing on snow, these aerosols can induce an additional effect to surface albedo and melting of snow.

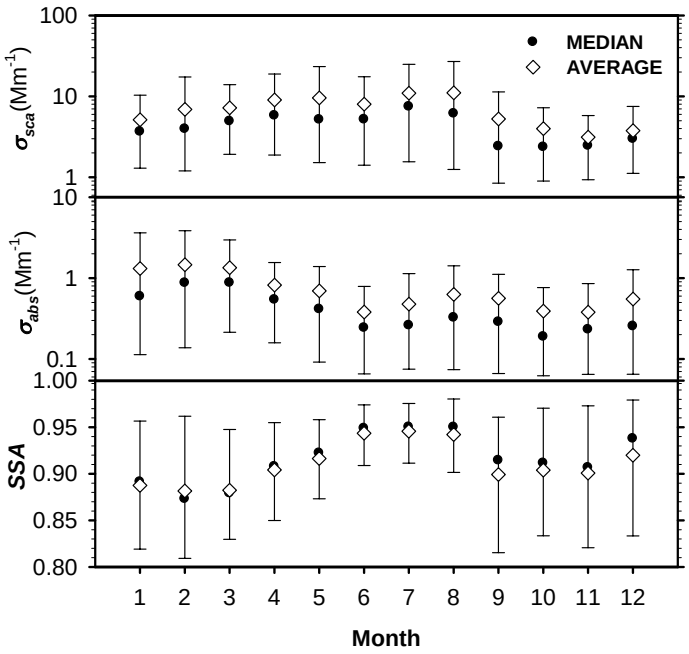

Figure 1. Seasonal cycles of scattering coefficient, σ_{sca}, absorption coefficient σ_{abs}, backscattering fraction, *b*, and single scattering albedo (SSA). All are at wavelength of 550 nm. Diamonds are average, circles are median and bars are 10 and 90 percentile range.

The Arctic haze phenomenon is observed also in Pallas during March and April which is typically Arctic haze period. Arctic haze increases absorption in marine air masses during March and April by almost 80% and scattering by about 50% compared to annual averages. The influence of Arctic haze is not visible in

total data (undivided between different source areas) because these are dominated by the clearly larger scattering coefficients of aerosols from continental sources.

We did not observe any long-term trend in scattering coefficient. However there was a decreasing trend in backscattering fraction and in scattering Ångström exponent. This supports the findings of Collaud Coen *et al.* (2013). We found that this decrease is occurring only in winters and it is stronger in marine, in comparison to continental, aerosols. The effect of decreasing backscattering fraction to direct aerosol forcing is however negligible due to the low sun elevation and a very short duration of the day, actually in few months the sun does not rise above horizon. The decrease is very substantial and in 10 years the Ångström exponent decrease about 40%, Figure 2. A part of the observed trends can be connected to a slight increase in the occurrence of marine air masses between years 2000 and 2010. However, the analysis we made separating the air mass origins confirms this cannot be the sole explanation. We hypothesised that changing emission structure is mainly causing the trends.

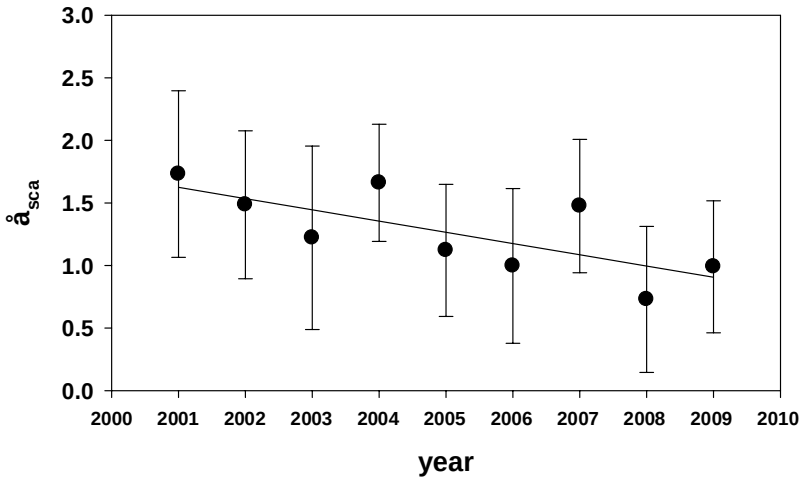

Figure 2. Trend in winter time (January-February) Ångström exponent $å_{sca}$ from 2001 to 2010. Error bars are ± STD. Linear curve fitting is also shown in the figure as a solid line.

ACKNOWLEDGEMENTS

This work was supported by the Academy of Finland as part of the Centre of Excellence program (project no. 272041), EU LIFE+ project MACEB (project no. LIFE09 ENV/FI/000572), the Academy of Finland through the Arctic Absorbing Aerosols and Albedo of Snow (project no. 3162) and Nordforsk Contractno. 26060 CRAICC-Amendement on CRAICC-PEEX Collaboration

REFERENCES

Collaud Coen M. , Andrews E., Asmi A., Baltensperger U. , Bukowieck N., Day D., Fiebig M., Fjaeraa A. M., Flentje H., Hyvärinen A., Jefferson A. , Jennings S. G., Kouvarakis G., Lihavainen H., Lund Myhre C., Malm W. C., Mihapopoulos N., Molenar J. V. , O'Dowd C., Ogren J. A., Schichtel B. A., Sheridan P., Virkkula A., Weingartner E. , Weller R. & Laj P. (2013). Aerosol decadal trends – Part 1: In-situ optical measurements at GAW and IMPROVE stations, *Atmos. Chem. Phys.* **13**, 869

Anderson T. L. & Ogren, J. A. (1998) Determining aerosol radiative properties using the TSI 3563 integrating nephelometer, *Aerosol Sci. Technol.* **29**, 57

Weingartner E., Saathoff H., Schnaiter M., Streit N., Bitnar B. & Baltensperger U.,(2003). Absorption of light by soot particles: determination of the absorptioncoefficient by means of aethalometers. *J. Aerosol Sci.* ***34,*** 1445

MEASURING PLANT AND SOIL CHARACTERISTICS TO PRODUCE LAND COVER CLASSIFICATION AND EXPLAIN CARBON FLUXES IN ARCTIC TUNDRA

M. LINKOSALMI[1], M. AURELA[1], T. VIRTANEN[2], J. NYMAN[2], J. MIKOLA[3], E. VÄHÄ[3], V. IVAKHOV[4], V. KONDRATYEV[5], A. MAKSHTAS[6] and T. LAURILA[1]

[1]Finnish Meteorological Institute, Helsinki, Finland.

[2]Department of Environmental Sciences, University of Helsinki, Helsinki, Finland.

[3]Department of Environmental Sciences, University of Helsinki, Lahti, Finland.

[4]Voeikov Main Geophysical Observatory, St. Petersburg, Russia.

[5]Tiksi Hydrometeorological Service, Tiksi, Russia.

[6]Arctic and Antarctic Research Institute, St. Petersburg, Russia.

Keywords: Arctic tundra, Vegetation and soil survey, Satellite validation

INTRODUCTION

To understand the carbon dynamics and to explain the observed methane (CH_4) and carbon dioxide (CO_2) fluxes, we have conducted a vegetation and soil characteristic survey twice, in the years 2012 and 2014, in East Siberia, Tiksi (N71°35.791', E128°53.327'). Tundra ecosystems are mosaics of different vegetation and soil types and affected by the arctic climate. Wind, snow and frost modify the soil properties and further land cover and vegetation. The study area is located close to Tiksi Hydrometeorological Observatory and the land cover is classified as tundra with permafrost. The measurement station for greenhouse gas studies was established in 2010 in cooperation between the National Science Foundation (NSF), the National Oceanic and Atmospheric Administration (NOAA), the Russian Federal Service for Hydrometeorology and Environmental Monitoring (Roshydromet), and the Finnish Meteorological Institute. The flux and concentration measurements (CH_4, CO_2, and H_2O) have been ongoing since 2010. The aim of the conducted vegetation and soil surveys was to create vegetation type and land cover maps, as well as leaf area index (LAI) and plant biomass maps, and validate the measured fluxes with vegetation type and soil properties.

METHODS

The first vegetation and soil survey was carried out in July 2012. We sampled altogether 56 plots (with three subplots, size of 50×50 cm) to different compass points in distances between 25 to 250 meters from the eddy covariance (EC) flux measurement tower. The vegetation community type and the coverage and height of different plant functional types (e.g. lichens, mosses, dwarf shrubs, graminoids, willows) were measured for all sample plots, while the soil characteristics (the depth of biologically active layer, soil organic matter (SOM) content, soil moisture, litter layer depth) and LAI were determined for 28 sample plots.

To gain more information on the seasonal change, to build more reliable vegetation type and land cover map from the area and to better cover all the vegetation types found in 2012, an extended survey was conducted during the growing season 2014. In 2014 the sample plot network consisted of altogether 92 points (with four subplots, size of 50×50 cm), including the same plots measured in 2012. The sampling lines reached up to 400 meters from the EC tower. The coverage and mean height of different plant

functional types, the phenology of ten key species, the depth of biologically active soil layer and soil temperature were monitored weekly. We also collected LAI and biomass samples at the peak of the summer to assess their maximum values. A similar soil survey as in 2012 was also executed in 2014 at the end of the growing season. To examine how well the study site represents the surrounding area, and also to upscale the flux measurements to landscape level, a number of verification points were sampled within 5 km radius of the flux tower.

In the data processing, we have utilized two high resolution satellite images of the study area: Quickbird (4 channels, pansharpened to 0.6 m pixel size, acquired on 15.7.2005, presenting the situation in the early part of the growing season) and WorldView2 (8 channels in 2 m pixel size, one channel in 0.5 m pixel size, acquired on 11.8.2012, presenting the situation in the late part of the growing season). In addition, Landsat images (30m pixel size) form the following dates: 31.7.2006, 19.9.2010, 4.7.2011 and digital elevation model (25m pixel size) from the region have been applied.

CONCLUSIONS

Based on the first vegetation survey, we classified the sample plots to following vegetation types: lichen tundra heath, shrub-moss tundra heath, tussock tundra, willow meadow, grass meadow, bog, dry fen and wet fens (Table 1). These vegetation classes were also applied and further specified in the summer of 2014. The vegetation seems to be relatively nicely distributed along the sampling lines; the drier and stony areas are located in the northern side of the study area and the terrain gets more moist and fertile in the south. The soil sampling is consistent with the vegetation types (e.g. SOM content is higher in peat soils like fen and bog types).

The preliminary results from the year 2012 suggest that the satellite image based NDVI (Normalized Difference Vegetation Index) explains well spatial variation in LAI, total plant cover and moss cover. Furthermore, SOM can be estimated by the variation in plant cover and thus satellite imagery can be used to predict the soil organic matter content. With the more thorough vegetation and soil survey executed in 2014, we hope to verify these results, to produce more reliable vegetation and land cover classification and to explain the carbon fluxes.

ACKNOWLEDGEMENTS

This work was supported by the Academy of Finland (project no 269095: Greenhouse gas, aerosol and albedo variations in the changing Arctic), European Commission (Changing permafrost in the Arctic and its Global effects in the 21st Century, PAGE 21) and Nordic Council of Ministers (DEFROST, a Top Research Initiative within NORDFORSK).

TRANSFORMATION OF HUMAN SETTLEMENTS IN ARCTIC REGIONS OF RUSSIA AND ITS RELATION TO ETHNICITY AND NATURAL RESOURCE USE

T.V. LITVINENKO and O.B. GLEZER

Institute of Geography, Russian Academy of Sciences, 109017 Moscow, Staromonetnyi pereulok, 29, Russian Federation

Keywords: socioeconomic transformation, settlements, population dynamics, indigenous population, natural resource use

INTRODUCTION

The impact of the Soviet collapse in 1991 had been felt stronger in northeast Arctic regions than in other regions of Russia, enterprises and farms were suddenly liquidated by various reasons. Political and economic reforms produced abrupt changes in the demographic situation. Unlike other demographic processes, migration responded quickly to the changes going on in society. This process was set off by the slash of the army and closure of numerous industrial enterprises based on natural resource use as these became unprofitable in the conditions of market economy. Market orientation immediately laid bare the relative overpopulation of the northern regions which the people were in a hurry to leave.

Chukotka, the most northeastern region of Russia, faced a severe economic slump and significant depopulation during the 1990s. In contrast to the gloomy past of the region in the 1990s, now Chukotka is experiencing a revival fostered by new kinds of economic activities related to natural resource use, resulting in an improvement in the living conditions of the people since 2000.

This paper investigates social conditions of Chukotka Autonomous Okrug of Russian Federation in the transition period. Post-Soviet transformation of natural resource use in Chukotka in comparison with other regions and sociodemographic features of the development of the region have been partially investigated by Russian scientists (Zaionchkovskaya, 2005; Motrich, 2006; Lomakina, 2009; Litvinenko, 2012). Our paper complements their studies by investigation of the relationship between the transformation of natural resource use, population dynamics and settlement pattern in Chukotka on variety of local areas.

METHODS

Although more information has become available since 1991, it is still difficult for academic researchers in European Russia and the West countries to get access to information about the life experience of people and social status of Arctic regions of Russia. From this viewpoint, we conducted field research trips to Magadan oblast (August 2003), Chukotka Autonomous Okrug (September 2007), the Sakha (Yakutiya) Republic (August 2005, September 2010).

A detailed study of the transformation of human settlements in relationship to ethnic breakdown and resource use were conducted in Chukotka. The reason for this was that Chukotka was geographically and politically isolated from other regions of Russia and that no much information is easily available for academic studies unless one directly visits the region. We visited the okrug's center the city of Anadyr, Iul'tin district and Anadyr district, and collected the regional and local statistical data. The main objective of the investigation was to determine the range of types of transformation of human settlements and its relation to ethnicity and natural resource use.

Our method consisted of several steps (stages):

1. Statistical analysis of regional and intra-regional differences in population dynamics and its link to ethnic breakdown of the population (the share of indigenous people in the total population).

2. Statistical analysis of the trend of natural resource production in different sectors of natural resource use (mining, and traditional natural resource management) at different stages of economic development in post-Soviet period (the years of economic crisis and years of economic growth).
3. Identification of types of transformation of natural resource use enterprises (elimination, emergence of new ones, etc.) corresponding to the different trends of natural resource production in different sectors of natural resource use at various stages of economic development.
4. Determination of the impact of different types of transformation of natural resource use enterprises on population dynamics and the appearance of settlements through interviews with local experts, analysis of local statistics, local archives, visiting various localities and visual observation of their external appearance. Identification of differences of those impact depending on the type of natural resource use (traditional based on renewable biological resources and mining-related one related to exhaustible mineral resources) and the ethnic composition of the population (predominately Russian or native people).
5. Detection of abandoned settlements and the reasons for their elimination through interviews with regional and local experts. Creation of the map of abandoned settlements by comparison of settlement patterns in Chukotka in the Soviet period and current situation.
6. Identification of new temporary workers' settlements and features of their occurrence in relation to resource management and labour migration.
7. Elaboration of a typology of transformation of human settlements in the form of a matrix indicating for each type (1) status of the settlement, (2) ethnicity, (3) population dynamics, including migration processes in the post-Soviet period, (4) relation to resource use through employment, and (5) visual representation of the type in the form of pictures.

CONCLUSIONS

The total population of Chukotka decreased more than threefold in 1990–2013 mainly due to mass migration outflow of the Russian population and other than indigenous peoples. Rate of decrease in number of people (67%) in Chukotka was the highest one in Russian Federation. While the share of the Russians, Ukrainians, and Tatars and other than indigenous peoples in total population has decreased, the share of Chukchi, Inuits, Evens increased.

Mass migration outflow of the Russian population and other than indigenous peoples, and decreasing in number of employees in excavation of mineral resources in the 1990s had been mainly the consequences of mass closing down and liquidation of production units that utilized natural resources as well as disbandment of military units following the Russia's new military doctrine and closing down of enterprises and institutions that were servicing the above mentioned spheres.

The maximum depopulation (over 75%) in 1990–2010 occurred in the north and north-east of Chukotka in the three administrative districts: Iul'tin, Chaunskii, and Shmidtovskii (Figure 1). Most of the settlements in these dictricts arose in the 1950s – 1960s in connection with the development of the mining (the mining of tin and gold). The population was predominantly Russian, the share of the indigenous population in the total population was and currently is the lowest compared to other districts. Many settlements were demolished due to migration outflow of the population after liquidation of mineral resource enterprises in 1995–1998.

The smallest depopulation (31%) occurred in Chukotskii district (Figure 1). The population is predominantly indigenous, the share of the indigenous population (81%) in the total population is the highest compared to other districts. Chukchi, Yukaghir, Koryak, Even, and Inuit have been living here for a long period of time. They are engaged in traditional natural resource management related to utilization of renewable biological resources. There are no liquidated and demolished settlements.

Spatial transformation of natural resource use caused the differentiation of settlements. Currently, five types of human settlements can be observed in the studied region. The first type are Soviet-period settlements, inhabited largely by indigenous people, whose numbers have not changed very much. An example of this is Amguema Village in Iul'tin district. Its population decreased by about 30% in 1990–2013, but it is two times less than in the whole district.

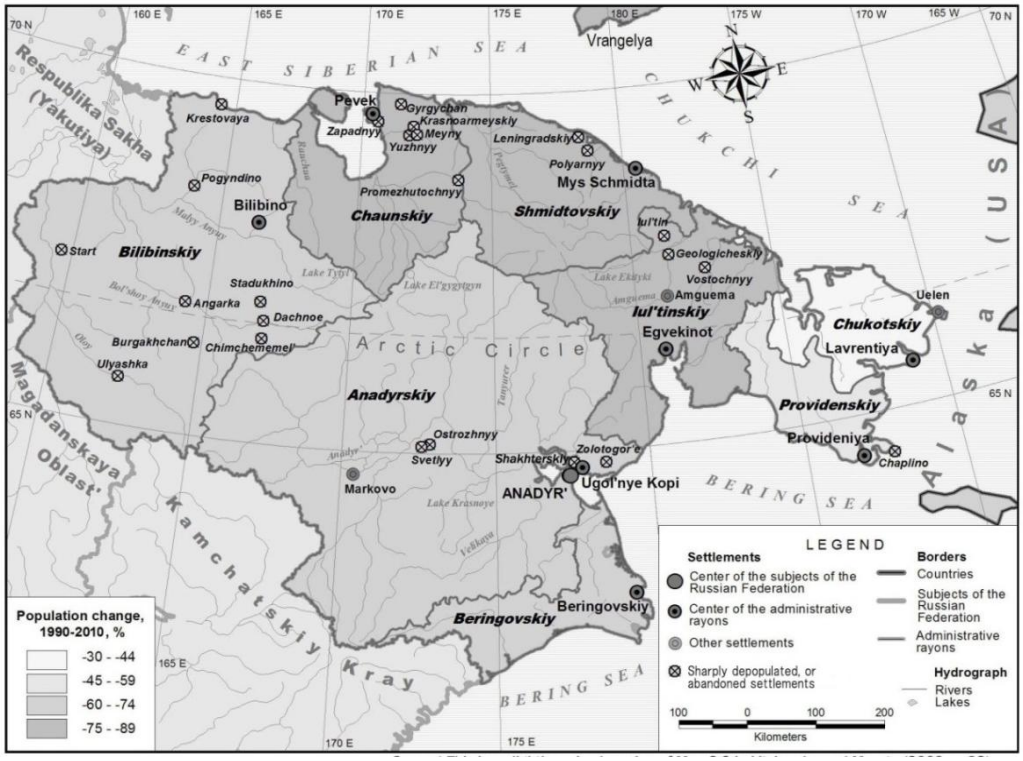

Figure 1. Population decrease and abundant human settlements in Chukotka Autonomous Okrug (1990–2010).

The second type is Soviet-period settlements, considerably depopulated and mainly enjoying the status of a district center, inhabited mostly by the Russians. For example, in 1990–2013 the population of Egvekinot, the center of Iul'tin district, decreased by 49%. Considerably depopulated settlements, with essentially Russian population, where there co-exist abandoned and preserved residential neighborhoods follow the third type. Ugolnye Kopi 'Coal Mines' settlement, where in the abandoned part there used to live military personnel until military base was closed, is an example of this type. During strong migration in the 1990s, the settlement could survive because of new employment in the budgetary organizations due to the status of the center of Anadyrskii district in 1992–2008, as well as employment in the coal mining and airport service. The fourth type are depopulated, demolished, abundant settlements that used to be inhabited by non-indigenous population employed at the enterprises that used exhaustible mineral resources or by servicemen. A large-scale analysis in Iul'tin district showed that during the post-Soviet period due to the closing down of the Iul'tinskii Mining and Dressing Plant and its servicing enterprises in 1994, Iul'tin Township and the settlements Svetlyi and Vostochnyi were demolished. We revealed 38 abundant human settlements in Bilibino, Chaunskii, Iul'tin, Anadyrskii, Shmidtovskii , and Providenskii districts (Figure 1).

The opening of new enterprises in post-Soviet time based on natural resource use and relating mainly to placer gold mining leads to the emergence of temporary workers' settlements, migrant workers' residences. Such settlements belong to the sixth type in our classification. Apparently, the number of such settlements has been increasing as a result of new natural resource use projects.

The post-Soviet period was a mosaic of the dynamic transformation of settlements from their complete elimination to the renewal of the appearance of national villages, district and regional centers. Unlike the regions with Russian population, differences in spatial transformation between settlements dominated by indigenous population (these dwellers have been preserved) and Russian population (such settlements have been either demolished or preserved and considerably depopulated if enjoyed the status of administrative centers).

The finding of different types of transformation of human settlement may be a useful tool for one to further investigate the present and future of social development in Chukotka and other Arctic regions.

REFERENCES

Litvinenko T.V. (2012). Socioecological Consequences of Transformation of Natural Resource Utilization in Russia's Eastern Part in Post-Soviet Period, *Regional Research of Russia,* vol. 2, no. 4, 284-295.

Lomakina N.V. (2009). *The Mineral Resource Sector of the Russian Far East: The Development Potential*. P.A. Minakir, Ed. Khabarovsk: RIOTIR, 240. (In Russ.).

Motrich E.L. (2006). *Population of the Russian Far East.* P.A. Minakir, Ed. Vladivostok-Khabarovsk: Russian Academy of Sciences, Far Eastern Branch, Economic Research Institute, 224. (In Russ.).

Zaionchkovskaya Zh. (2005). Migrations and demographic future of Siberia and the Far East, in *Russia and Its Regions in the 20th Century: Territory – Settlement Pattern – Migrations,* O. Glezer and P. Polyan, Eds., Moscow: OGI, 479–490. (In Russ.).

ORGANIC CARBON POOLS AND CO_2 FLUXES FROM SOILS OF FOREST ECOSYSTEMS IN THE EUROPEAN PART OF RUSSIA

LOPES DE GERENYU V.[1], KURGANOVA I.[1], KUZNETZOV M.[2], OSIPOV A.[2], MYAKSHINA T.[1], SAPRONOV D.[1], KAGANOV V.[3], BOBKOVA K.[2], KUDEYAROV V.[1]

[1]Institute of Physicochemical and Biological Problems in Soil Science, RAS, Institutskaya Str., 2, Pushchino, Moscow region, 142290, Russia

[2] Institute of Biology, Komi Scientific Centre of Ural Division RAS, Kommunisticheskaya Str., 28, Syktyvkar, 167982, Russia

[3]Centre on Problems of Ecology and Productivity of Forests, RAS, Profsoyuznaya Str., 84/32, building 14, Moscow, 117997, Russia

Keywords: biogeochemical cycles, carbon pools and fluxes, forest ecosystems, European Russia

INTRODUCTION

The global biochemical cycle of organic carbon (OC) can be viewed as series of various reservoirs, which are connected by exchange fluxes of carbon (IPCC, 2013). The third largest reservoir of organic carbon on the planet (after the lithosphere and the ocean) is the soil organic matter (SOM) which amounts for 1500-1700 Gt C (Batjes, 1996). Soil carbon is critical parameter to consider for long-term carbon storage and it forms the net biome production (NBP) in terrestrial ecosystems (Steffen *et al.*, 1998; Kudeyarov *et al.*, 2007). It has been estimated that forests contain up to 80 % of world aboveground and about 40% of terrestrial belowground (soils, litter, and roots) OC (Dixon *et al.*, 1994). Recent studies indicate that forest vegetation and soils sequester globally 359 and 787 Pg of C, respectively.

Soil carbon pool is closely associated with the emission component of the carbon cycle (or soil respiration) through the continuous decomposition processes of SOM. The amount (stock) of soil organic matter and soil respiration rate can increase or decrease depending on numerous factors including climate, vegetation type, nutrient availability, disturbance, land use, and management practices (Six, Jastrow, 2006). European Russia is characterized by the clearly defined variability (zonality) of climate, vegetation, and soils, and thus this area presents an excellent natural model to study the relationship between soil carbon pools and fluxes in ecosystems. This study was aimed to quantify the soil organic carbon stocks and emission CO_2 fluxes from soils in forest ecosystems of different bio-climatic regions of European Russia.

MATERIALS AND METHODS

This study was carried out in seven forest ecosystems, which were located in different bio-climatic regions of the European part of Russia (Table 1): (1) middle taiga (experimental stations 'Lyalsky' and '17 km', Institute of Biology, Komi Scientific Center; Syktyvkar region), (2) southern taiga (Prioksko-Terrasny Biosphere Reserve, Moscow region) and (3) deciduous forest (Experimental field station of the Institute of Physicochemical and Biological Problems in Soil Science, RAS, Moscow region). The ecosystems studied formed the meridian transect with distinct gradient of mean annual air temperature (MAT, 4.3^{o}C) and similar amounts of annual precipitation (AP, 585-646 mm). -At the same time, the forest ecosystems differed in soil taxonomy, composition, and age of vegetation. The main information about sites, vegetations, and soils are presented in Table 1.

The main climatic parameters (amount of precipitation and average air temperature) with monthly resolution are available on the Roshydromet page (*http://aisori.meteo.ru/ClimateR*). Using the open access meteorological data, we estimated the annual and season climatic norms (CliNor) for each bioclimatic region. CliNor corresponds to average value of meteorological parameter for 1961-1990 (Assessment report…, 2008). The deviations of MAT and AP from CliNor were calculated to compare the current climatic situation in the regions studied.

The soil samples were taken in each soil profile to 50 cm depth (every 10 cm, 3 replicates). The composition and storage of forest litter and litter-fall production were determined monthly during the growing season 2009 and 2010. C and N contents in soil and litter samples were determined by the CHN-analyzer (Elementar, Germany). The soil OC stock was calculated taking into account the bulk density of each horizon. To allow the comparison of selected sites, we focused on the soil OC pool of the first 0-20 cm depth, because most of the SOC is concentrated in this depth (García-Oliva *et al.*, 2006). The decomposition constant (k) was estimated according to the formula (Olson,1963):

$$k = P/L \quad (1),$$

where P is the annual litter-fall production (Mg C ha^{-1} yr^{-1}) and L is the average of standing litter necromass (Mg C ha^{-1}). The inverse of k is the mean residence time (MRT) of the litter, expressed in yrs.

Forest zone/subzone	Location	AP, mm/year	MAT Ta, °C	Forest description	Site symbol
Middle taiga; Syktyvkar region ('Lyalsky' experimental station)	61°40' N 50°52'E	622	1.5	Spruce forest with blueberry&sphagnum; 9S1B + single P, Fir; 108-200 yrs	MT-1
				Pine forest with blueberry&sphagnum; 10P + S, B, As; ~120 yrs	MT -2
Middle taiga; Syktyvkar region ('17 km' experimental station)	61°33' N 50°37' E			Spruce forest with blueberry& green moss; 8S1P1B; >100 yrs	MT -3
	61°34' N 50°38' E			Birch forest, herbaceous; 8B2S; ~100-110 yrs	MT -4
	61°34' N 50°38' E			Aspen forest, herbaceous; 5As3S2B; ~100-110 yrs	MT -5
Southern taiga; Moscow region (Prioksko-Terrasny Biosphere Reserve)	54°55' N 37°34' E	646	5.4	Mixed (coniferous-deciduous) forest; 4P3L2As1B + single Oak; 100-110 yrs	MF
Deciduous forest; Moscow region (Experimental field station of IPBPP RAS)	54°20'N, 37°37'E	585	5.8	Secondary deciduous forest; 5As3L2M + single Oak and Birch; 55-60 yrs	SDF

Table 1. General characteristics of the ecosystems studied.

In the middle taiga region, the measurements of CO_2 emission from soils were carried out on 'Lyalsky' experimental station (sites MT-1 and MT-2) through the growing season (May-October). The CO_2 fluxes were measured during the day by the open dynamic chamber method several times per month. Stationary rings (318 cm^2; 5 replicates) were installed into the forest litter till 3-5 cm depth. CO_2 concentration in the soil chamber (diameter 20 cm) was determined by infrared gas analyzer LI-COR 8100 (LI-COR Biosciences, USA). In the southern taiga and deciduous forest zones, the CO_2 emission from soils was measured trough the all year round every 7-10 days by the closed chamber method which has been modified specially for measurements during the winter (snow) period (Lopes de Gerenyu *et al.*, 2001; Kurganova *et al.*, 2003). Simultaneously, soil moisture and temperature in the upper soil layer (0-5 cm), and air temperature were determined.

Monthly soil CO_2 fluxes (g C m^{-2} $month^{-1}$) were calculated by using mean monthly values of CO_2 emissions (g C m^{-2} day^{-1}) and duration of each month (days). For soils of southern taiga and deciduous forest, the seasonal and annual CO_2 fluxes were obtained by summarizing of appropriate monthly fluxes. The annual CO_2 fluxes from forest soils of middle taiga were calculated on the basis of total summer CO_2 emission and simple linear model, which allows us the estimating of summer season contribution to the annual CO_2 flux from soils on the basis of average annual air temperature (Kudeyarov, Kurganova, 2005).

RESULTS AND DISCUSSION

Weather conditions for 2008-2010. The positive deviations of mean annual air temperatures from CliNor were registered during 2008-2010 in all bio-climatic regions (Fig. 1A). They changed from +0.6 to +2.7°C. The deviations of mean summer temperatures from CliNor were the most significant (appr. +5°C) for southern taiga and deciduous forest in 2010. In middle taiga, the surplus of precipitation occurred in 2008 while the weak deficit of precipitation was registered in 2010 (Fig. 1B). In southern taiga and deciduous forest zones, the considerable deficit of summer precipitation and extremely high mean summer temperature were observed in 2010 while the anomalously wet conditions and weak positive deviations of mean summer air temperature from CliNor occurred in 2008.

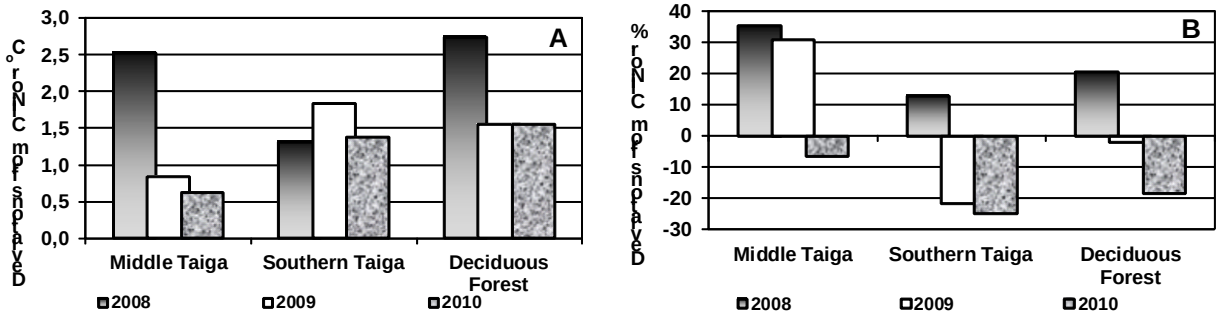

Fig.1. Deviations of mean annual air temperature (A) and annual precipitation (B) from the climatic norm (CliNor) in various climatic regions in 2008-2010.

General characteristics of soils. The soils studied differed significantly in climatic conditions of their formation. The middle taiga soils are characterized as extra wet and cold (seasonally-frozen), while soils of the southern taiga and deciduous forest zones are moderately wet and moderately cold (seasonal freezing occurs not every year). The upper (humus) horizon of forest soils showed the greatest differences in C_{org} content: from 2-4 to 36-37 g C kg^{-1} of soil (Table 2). The C/N ratio in the upper layer of soil studied ranged from 11.8 to 18.3. The wide geographical diversity of forest soils caused significant variability of pH_{KCL} values in the upper humus horizons: from 3.3 to 5.6.

Carbon stocks in soils. Stocks of C_{org} in the soils (including litter) along transect studied varied widely depending on bio-climate regions, type of forest (dominant species), soil texture, and moisture regime (hydromorphic or automorphic). The lowest stock of C_{org} (17-22 Mg ha^{-1}) was observed in the automorphic soils of middle taiga (sites MT-3, MT-4 and MT-5) while the hydromorphic soils (wetlands) of middle taiga (sites MT-1 and MT-2) and Phaeozems of deciduous forest zone (SDF) contained the highest amount of C_{org} - 66-86 C Mg ha^{-1} (Table 2). It was found that within the same bio-climatic regions, the SOC stocks in wetlands (hydromorphic soils) were 3-4 times higher than those in the automorphic positions. Total C_{org} stock in the loamy Phaeozems was more than 2.5 times higher than those in sandy Albeluvisols (Table 2). It was observed that moisture regime (degree of soil hydromorphic) is crucial factor that attributes the intensity of forest litter accumulation, the rate of its decomposition, and intensity of SOM mineralization. Among the soil studied, the share of litter in the total SOC stocks was the highest in the automorphic soils of the middle taiga (48-86%). The rate of litter turnover (MRT) varied widely in

the ecosystems studied: from 0.9 yrs in SDF of the deciduous forest zone to 21-91 yrs in wet coniferous forests of the middle taiga.

Site	Почва	C_{org}, g kg^{-1} of soil	C/N	pH_{KCl}	C stock, Mg ha^{-1}			**k**, yr^{-1}	**MRT**, yr
					Soil, 0-20 cm	Litter	Litter -fall		
MT-1	Albeluvisols Histic (loamy)	6.90	17.7	3.37	37.4	26.6	1.26	0.048	21.0
MT -2	Albeluvisols Histic (sandy)	2.00	15.4	4.35	31.9	33.5	0.37	0.011	91.0
MT -3	Podzol Haplic (loamy)	4.00	15.7	3.27	0.28	16.16	1.56	0.097	10.3
MT -4	Albeluvisols Haplic (loamy)	27.9	14.0	4.03	6.33	13.43	1.93	0.144	7.0
MT -5		33.2	15.5	*nd*	6.58	8.23	2.48	0.301	3.3
MF	Albeluvisols Umbric (sandy)	37.5	18.3	3.67	16.3	5.76	2.07	0.360	2.8
SDF	Phaeozems Luvic (loamy)	36.3	11.8	5.56	55.1	2.40	2.78	1.160	0.9

Table 2. Main chemical properties of soils studied (A1 horizon), stock of C_{org} in soil, litter, and litter-fall, the decomposition constant (k), and the mean residence time (MRT) of the litter.

CO_2 emission from the forest soils of European Russia. The average annual CO_2 fluxes from soils of forest ecosystems during the period 2008-2010 varied between 77 and 555 g C m^{-2} (Figure 2). Summer CO_2 fluxes contribute about 40-65% to the total soil respiration. The interannual variability of soil CO_2 emissions were governed mainly by weather condition during the year. For instance, in extremely hot and dry 2010 the summer CO_2 fluxes from soils of forest ecosystems were significantly lower than in 2008, which attributed the moisture surplus. The sandy Albeluvisols Histic under pine trees was an exception: the highest CO_2 emission from this soil was observed in 2010. We found that the magnitude of soil CO_2 fluxes in the middle taiga was determined mainly by the degree of soil hydromorphicity, while soil CO_2 fluxes in the southern taiga and deciduous regions were very close. Within transect studied we observed negative exponential relationship between the rate of litter turnover (MRT) and the annual CO_2 fluxes from soils (R^2 = 0.987; P = 0.006; Figure 3). In other words, the lowest CO_2 emission from soils was observed in the forest ecosystem, where the litter was characterized by the lowest turnover rate (or the longest MRT).

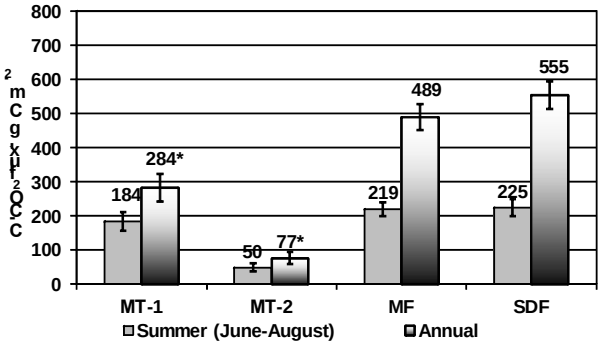

Figure 2. Annual and summer CO_2 fluxes soils in forest ecosystems in 2008-2010. (*estimated annual CO_2 emission).

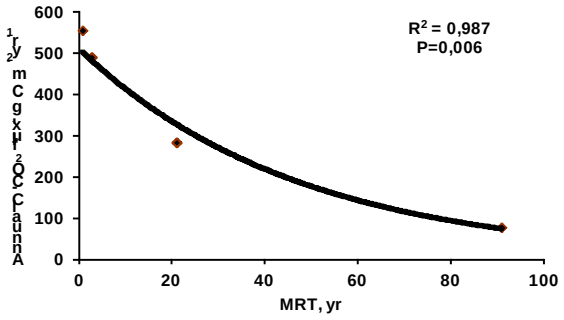

Figure 3. Relationship between annual CO_2 emissions from forest soils and MRT of litter.

CONCLUSIONS

Therefore, we have shown that SOC stocks, the intensity of litter accumulation, and its turnover rate in forest ecosystems of European Russia are determined by the wood species composition and the degree of soil hydromorphicity. Along transect studied, wetlands of the middle taiga (Albeluvisols Histic) were characterized by the highest carbon stock in litter and the lowest rate of its turnover. According to climate prognosis, the aridity enhancement is expected to be in the European Russia during next decades. Obviously, it will decrease the CO_2 emission from soils of automorphic positions, while the CO_2 losses from hydromorphic soils, in contrast, may increase. Among the forest ecosystems studied, we observed the close negative relationship between annual CO_2 fluxes from the soils and the mean residence time of the litter.

ACKNOWLEDGEMENTS

This study was supported by Russian Foundation for Basic Researches (grants No.12-04-00201a,12-05-00197a), ISTC (Project No. 4028), grant SciSch-6123.2014.4, Program of Presidium PAS No. 4, and Russian Scientific Foundation (grant No.14-14-00625).

REFERENCES

Assessment Report on Climate Change and its Consequences in Russian Federation (General Summary). (2008). (Moscow, RosHydromet).

Batjes, N.H. (1996). Total carbon and nitrogen in the soils of the world. *Eur J Soil Sci.* **47**, 151-163.

Dixon, R.K., S. Brown, R.A. Houghton, *et al.* (1994). Carbon pools and Flux of global forest ecosystems. *Science* **263**, 185-190.

García-Oliva, F., G. Hernández, J.F. Gallardo (2006). Comparison of ecosystem C pools in three forests in Spain and Latin-America. *Ann. For. Sci.* **63**, 519-223.

IPCC (2013). Working group I contribution to the IPCC fifth assessment report (AR5), Climate change: the physical science basis. (Stockholm, 23-26 September 2013).

Kudeyarov, V.N., I.N. Kurganova (2005). Respiration of Russian Soils: Database Analysis, Long-Term Monitoring, and General Estimates. *Eurasian Soil Science* **38(9),** 983-992.

Kudeyarov, V.N., G.A. Zavarzin, S.A. Blagodatsky, *et al.* (2007). *Pools and fluxes of carbon in terrestrial ecosystems of Russia.* (Moscow, Nauka) [in Russian].

Kurganova, I., V. Lopes de Gerenyu, L. Rozanova, *et al.* (2003). Annual and seasonal CO_2 fluxes from Russian southern taiga soils. *Tellus* **55B**, 338-344.

Lopes de Gerenyu, V.O., I.N. Kurganova, L.N. Rozanova *et al.* (2001). Annual emission of carbon dioxide from soils of the Southern taiga zone of Russia. *Eurasian Soil Science* **34**, 931-944.

Olson, J.S. (1963). Energy storage and balance of producers and decomposers in ecological systems. *Ecology* **44**, 322-331.

Six, J., J.D. Jastrow (2002). Encyclopedia of Soil Science (Marcel Dekker), 936-942.

Steffen, W., J. Canadell, M. Apps, *et al.* (1998). The terrestrial carbon cycle: implication for the Kyoto Protocol. *Science* **280**, 1393–1394.

UNDERSTANDING OF THE ATMOSPHERIC METHANE EVOLUTION AND CHANGE OVER THE LAST DECADES WITH FOCUS ON THE ARCTIC REGION

CATHRINE LUND MYHRE[1], STIG DALSØREN[2], OVE HERMANSEN[1], GUNNAR MYHRE[2] AND IVAR ISAKSEN[2]

[1]NILU, Norwegian Institute for Air Research, Kjeller, Norway

[2] CICERO, Center for International Climate and Environmental Research Oslo, Norway

Keywords: Permafrost, methane emissions, atmospheric composition, Arctic Ocean in the climate system

INTRODUCTION

Methane acts as a powerful greenhouse with large natural and anthropogenic sources. The concentration is increasing in the atmosphere, both globally and in the Arctic region since ~2005. The explanation to this is currently not well understood. There are huge reservoirs of CH_4 in the Arctic; both methane hydrates in seabed sediments, and organic material in land- and marine-based permafrost which can be partly converted to CH_4 after permafrost thaw. Both are vulnerable to destabilization in a warming climate. The Arctic Ocean surface waters may also represent a potentially important source of CH_4, which may be sensitive to changes in sea-ice cover. Previous studies show strong atmospheric chemistry feedback to climate warming from Arctic methane emissions (Isaksen *et al*, 2011).

Final results from the GAME project (Causes and effects of **G**lobal and **A**rctic changes in the **ME**thane budget), and first results from the MOCA project (**M**ethane Emissions from the Arctic **OC**ean to the **A**tmosphere: Present and Future Climate Effects: http://moca.nilu.no) will be presented. One goal of these studies is to improve the understanding on how emissions in different regions, transport and chemical processes contribute to observed changes in atmospheric methane distribution the last 40 years, with particular focus on the Arctic, including CH_4 emissions from the ocean like the East Siberian Arctic Shelf.

METHODS

The work is an integrated study combining new measurements at Zeppelin Observatory, Svalbard, analysis of existing and ongoing methane observations and other relevant species, and Chemical Transport Modelling (CTM). The Oslo CTM3 model (Søvde *et al*, 2012) is used to calculate distribution and changes over the last 40 years. The study include evaluation of different methane sources and source regions, and chemical processes affecting OH distribution and changes, including changes in anthropogenic and natural emissions from different sources.

RESULTS

The observed inter-annual variability at Zeppelin and numerous other sites globally, both seasonality and absolute levels, are well captured by the model, as shown in Figure 1. The model is shown to be suited to gain information the influence of various emissions on observations in the Arctic. As a part of the work we have investigated the signs and impact of emissions due to storm-induced methane release from the East Siberian Arctic Shelf, as proposed by Shakova *et al*, (2012). The first results of this focus study will be presented.

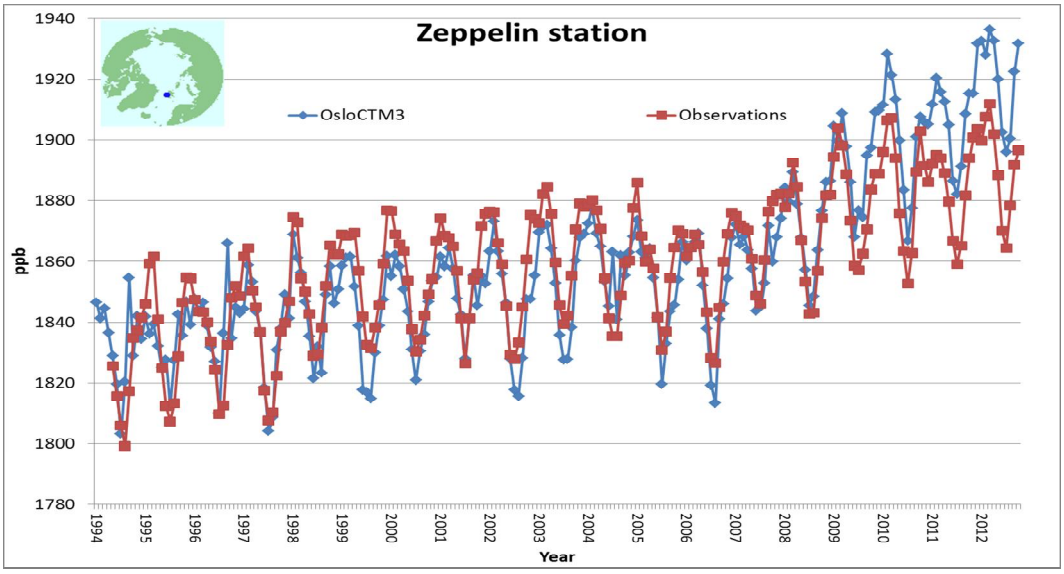

Figure 1: Comparison of monthly mean surface methane in model and observations at Zeppelin Observatory, close to Ny-Ålesund at Svalbard.

ACKNOWLEDGEMENTS

The Norwegian Research council through the project GAME (Causes and effects of **G**lobal and **A**rctic changes in the **ME**thane budget), and MOCA (**M**ethane Emissions from the Arctic **OC**ean to the **A**tmosphere:Present and Future Climate Effects: http://moca.nilu.no) is highly acknowledged for the support and funding of this activity.

REFERENCES

Isaksen, I.S.A, M. Gauss, G. Myhre K. M. Walter, A. and C. Ruppel (2011) Strong atmospheric chemistry feedback to climate warming from Arctic methane emissions. *Global Biogeochem. Cycles*, *25*, GB2002. doi:10.1029/2010GB003845.

Shakhova, N, I, Semiletov, I, Leifer,, V. Sergienko5, A. Salyuk,, D. Kosmach, D. Chernykh, C. Stubbs, D. Nicolsky, V. Tumskoy, and Ö. Gustafsson (2014), Ebullition and storm-induced methane release from the East Siberian Arctic Shelf, *Nature Geoscience* **7**,64–70, doi:10.1038/ngeo2007

Søvde, O. A.; M. J. Prather, I. S. A. Isaksen, T. K. Berntsen, F. Stordal, X. Zhu, C. D. Holmes and J. Hsu: The chemical transport model Oslo CTM3, *Geosci. Model Dev.*, 5, 1441-1469, doi:10.5194/gmd-5-1441-2012, 2012.

OBSERVATION OF ULTRAFINE PARTICLES SIZE DISTRIBUTION AT TWO DIFFERENT HEIGHTS IN AN ARCTIC SITE

A. LUPI[1], M. BUSETTO[1], M. MAZZOLA[1], C. LANCONELLI[1], F. GIARDI[2], S. BECAGLI[2], R. UDISTI[2], V. VITALE[1], J. STROM[3], P. TUNVED[3], R. KREJCI[3] and H. C. HANSSON[3]

[1]Institute of Atmospheric Sciences and Climate, ISAC-CNR, via Gobetti 143 Bologna, Italy
[2] Chemistry Department 'Ugo Schiff', University of Florence, Florence, Italy
[3] Department of Applied Environmental Science (ITM), Stockholm University, 10691 Stockholm, Sweden

Keywords: aerosol size distribution, aerosol number concentration, geometric mean diameter.

INTRODUCTION

Study of nature, properties and seasonal variability of aerosols in the arctic region is a critical point in the definition of sources, atmospheric reactions and transport processes on these region, taking also in account the peculiar characteristics of this area (characterized by high albedo values and low sun elevation angle) which exert a complex feedback mechanism which finalizes in relevant temperature increase (the so called "Arctic Amplification"). One of the basic parameter that needs to be considered is the role of aerosols, either in burden and properties. Their direct effect (scattering and absorption of solar radiation) and indirect effect (change in cloud properties and precipitation) perturb the Arctic radiative balance in many different manners (Tomasi *et al.*, 2015). Also, the relative abundance of solar radiation during the summer season reflects in a less stable atmosphere during the insulation months, which could affect the vertical distribution of aerosol particles in the lower troposphere.
In order to improve knowledge of aerosol micro-physical, chemical and optical properties of the Arctic aerosol, laboratories were settled at different heights around the village of Ny Ålesund [78°55'N, 11°56'E]: at Zeppelin, located at 470 m.a.s.l. and at Gruvebadet, 60 m.a.s.l.

DATA AND METHODS

Three years of Ultrafine Particle Size Distribution measurements have been carried out during spring/summer months (April to August 2010, 2011 and 2013) in the Ny Alesund area, at two different location: Gruvebadet, (60 m.a.s.l.) and Zeppelin, (474 m.a.s.l.). Two different instruments were adopted (SMPS TSI 3034 at Gruvebadet, ITM costum-made DMPS at Zeppelin) (Tunved *et al.*, 2013), with a diameter range fixed at Gruvebadet (range 0.0104-0.486 μm, with 54 channels and sampling time of 10 minutes), (Hogrefe *et al.*, 2006) and variable seasonally at Zeppelin (maximum extent from 0.005 to 0.819 μm, with channels varying from 22 to 31 channels, with a sampling time of 20 minutes). Aerosol Size distribution (ASD hereinafter) measurements were analyzed. Meteorological and incoming flux measurements are routinely performed at the Admunsen-Nobile Climate Change Tower (CCT), about 1 km NW off the Gruvebadet laboratory, at the same height of Gruvebadet laboratory.

AEROSOL ANALYSIS:

The homogenized (in term of time and diameter size) total number concentration (Ntot) measured at the two site were compared, as presented in figure 1, showing similar behavior during the three multi-monthly coincident datsasets. The evaluation of the linear fitting was performed using a linear relation y=mx. Together with the total number concentration, comparisons of the Geometric Mean Diameter (GMD) were also performed in order to identify a simple parameterization to represent and compare various aerosol. The Geometric Mean Diameter (GMD) illustrates the weighted mean of the size distribution, (Moorthy *et al.*, 2009), and it is defined as

$$GMD = \exp\left(\sum_j \frac{N_j \ln\left(D_j\right)}{N_{tot}}\right) \quad (1)$$

Where Nj is the concentration number for each diameter class Dj.

In this way, the above formulation is independent of the total number concentration, but it is dependent only on the modal characteristics of the ASD. The figure 2 shows the multi-monthly comparison between the two GMDs, together with their scatter plots and statistical results. Also in this case there is a good accordance between the two heights, as pointed out by correlation coefficients.
To improve knowledge and physical characterization of the ultrafine aerosol population at both sites, in term of lognormal curves, we have performed a fitting parameter estimation (slightly modifying the algorithms shown in Hussein *et al*, (2005) and using open-source software) for all data sets: as an example of the procedure, in figure 3 are shown the retrieved three mode parameters (i.e. accumulation, Aitken and eventually nuclei region), using the 24-hourly mean of the normalized monthly values of ASD, evaluated as suggested by Ström *et al.*, (2007); the figure 4 shows the statistical scatter plot of GMD in term of linear and logarithmic scale, corroborating the strong modal analogies between the two measurement site; moreover, the different seasonal ASD modal characteristics are well highlighted in figure 3.

METEOROLOGICAL CONDITIONS

In order to understand relation between vertical aerosol layering and meteorological and surface turbulent fluxes, several parameters were considered:
i) the time series of the Obukhov length L (Matvenn, 1965), defined as

$$L = -\frac{\Theta}{k \cdot g} \frac{u_*^3}{\langle w \cdot \theta \rangle} \qquad (2)$$

where Θ is a reference potential temperature, k=0.4 is the von Karman constant, g is the gravity acceleration and u_*^3 is based on the kinematic flux of momentum u_*^2, with all these quantities evaluated from the data collected at the CCTower site. The Obukhov length L is a parameter indicating the atmospheric stability/instability condition, respectively L<0/ L>0.
ii) wind properties at the two station (in term of direction and speed, utilizing 10 minutes averages for the CCTower data and 1-h data for the Zeppelin data), ,as represented in figure 6 for the considered month analyzed during the 2013, indicating different wind regimes at the two heights, with three major direction in the case of CCTower site measurements (SEE, SSW and NWW) and two major direction (SSE and NNW) for the wind direction recorded at the Zeppelin site. The data represented in figure 5 (from 10 minutes averages to 1 months average) clearly indicates more prevailing unstable condition during the "summer" months, while during the "dark" period the stable condition appears more frequently. The wind regimes depicted in figure 6 (1-h data average) clearly show different wind behaviors at the two site, indicating the strong orographic effects prevailing at the Zeppelin station.

NUCLEATION EVENTS

Together these geometrical/size distribution comparison, New Particle Formation (NPF) events are investigated, visually inspecting the daily 3-D ASD plots, following the identification suggested by Del Maso *et a.l*, 2005. As an example of coincident NPF event (type Class Ia), figure 7 shows a simultaneous NPF event recorded at both site during the 3rd August, 2013.
In order to investigate the anthropogenic influence of the Ny Alesund Village on the NPF event, figure 8 shows a wind rose reporting the starting NPF event recorded at Gruvebadet and the coincident wind direction, indicating a "non-preferred" wind direction for the NPF event, focusing in this way the importance of long range aerosol transport.

CONCLUSION

Results from this study show similar behaviour of ultrafine ASD measured at the two different heights, both in term of number concentration and geometrical mean diameter, thus remarking the same ultrafine aerosol physical characteristics; this suggest a large mixing between different height despite of contrasting averaged wind regimes recorded at the two sites and although the various turbulent flux condition recorded at the CCTower (Drofa *et al*, 2015). These similarity refers mainly to ASD physical characteristics, considering some recent studies show divergent chemical properties (Moroni *et al*, 2015) for aerosol sampled with tethered balloon at various elevation in the same region.

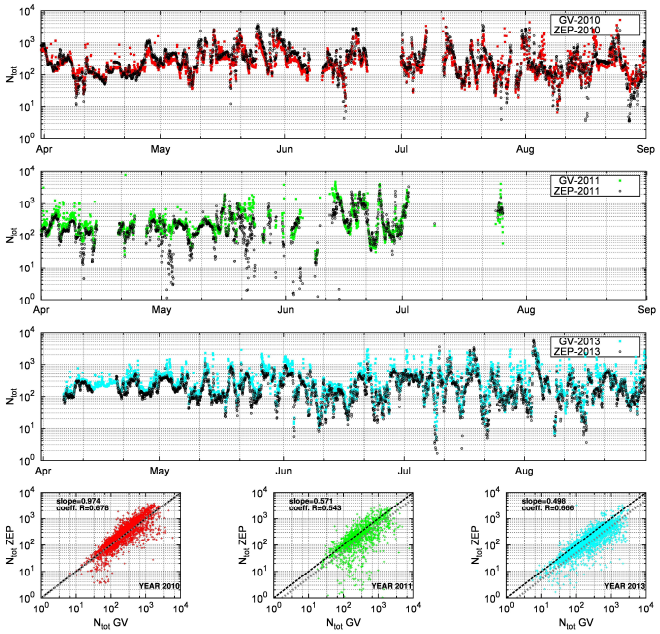

Figure 1: Time Series of the Number Concentration observed at the two sites, for the three years considered; the lower part shows the correlation between the two sites evaluated for the same time period

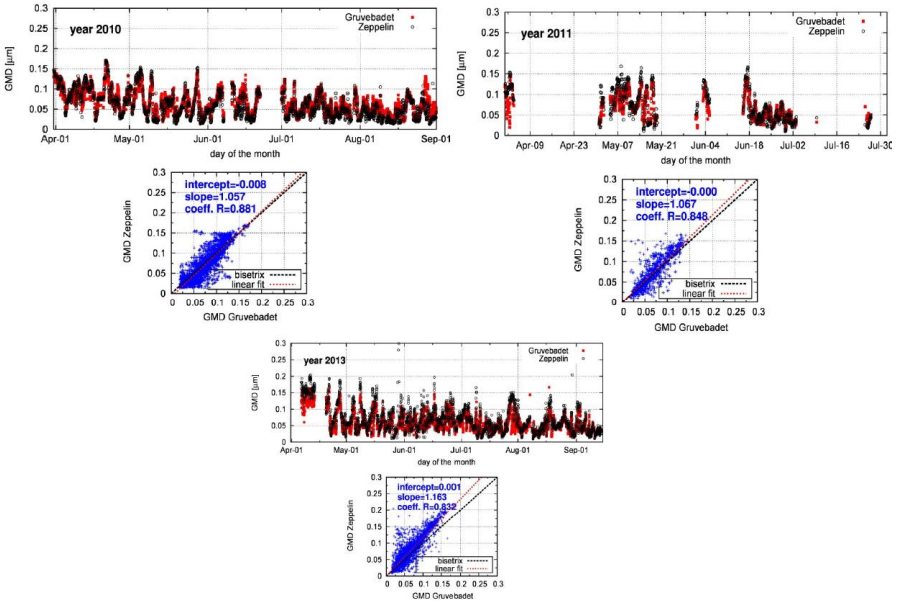

Figure 2 :The three multi-monthly GMD comparison between the two sites, together with their correlation and statistical result

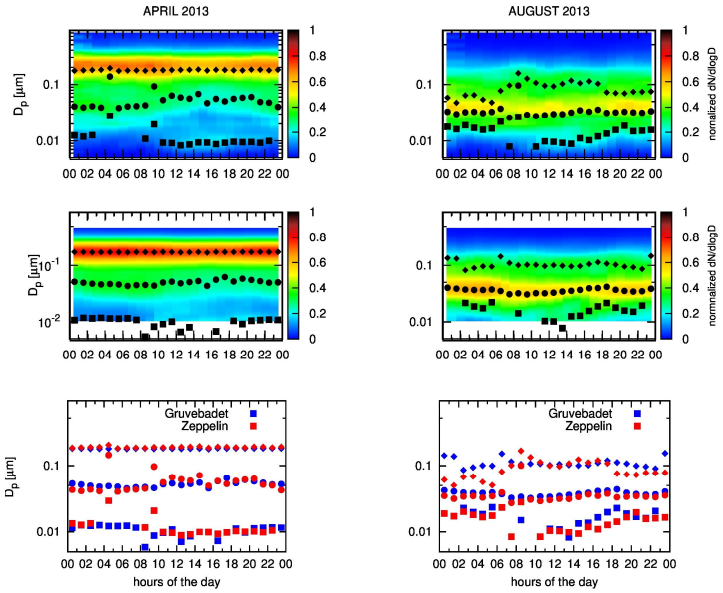

Figure 3. Examples of the 3D plots of the monthly mean 24-h averaged ASD (April and August) for the 2013 campaign: in the upper part the Zeppelin ASD, in the middle the Gruvebadet ASD; the lower part shows a direct comparison between the modal diameters retrieved from the lognormal fitting procedure.

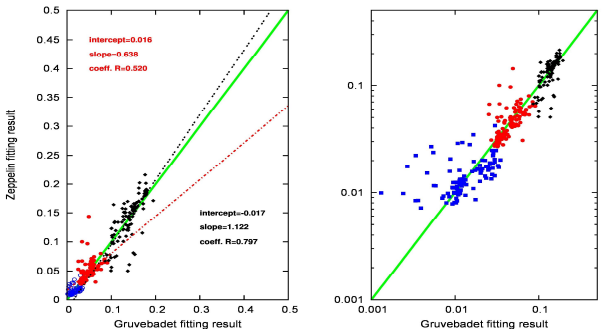

Figure 4. Scatter plot of the coincident modal diameters retrieved using the ASD observed at Zeppelin and Gruvebadet using all the monthly-mean 24-h averaged ASD (from April to August 2013): in the right part the same data are expressed using a logarithmic scale.

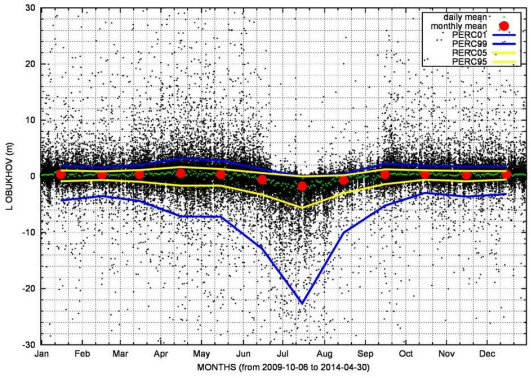

Figure 5. Yearly behaviour of the Obukhov length L, together with some statistical features (10 minutes values, daily mean, monthly mean and 5-95 and 1-99 percentiles).

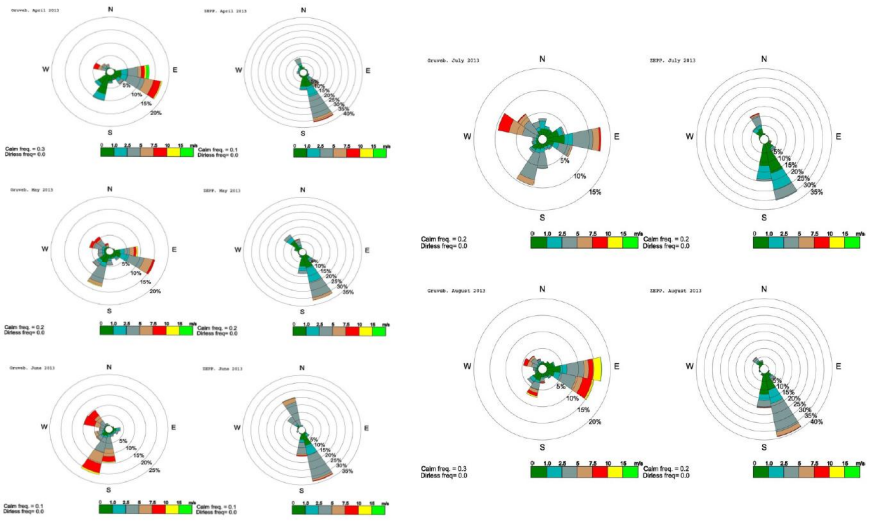

Figure 6. Monthly wind roses representing the different wind regimes frequencies (wind speed and direction) recorded at the two site (left Gruvebadet, right Zeppelin) during the April-August 2013.

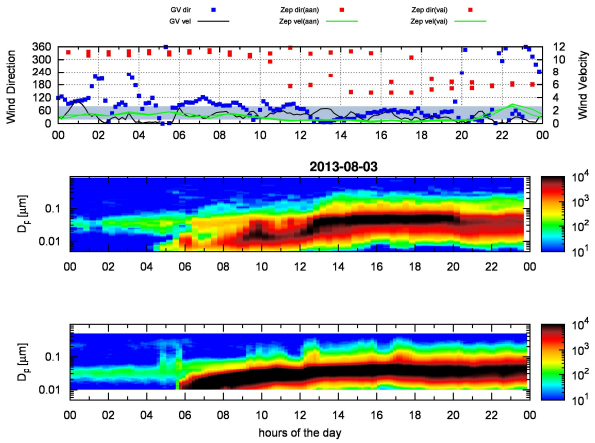

Figure 7. A NPF event registered at Zeppelin and Gruvebadet during the 3rd August 2013: the upper side shows the wind velocity and wind direction measured at the CCT tower site , while in the center the 3D-daily plot of ASD measurements performed at Zeppelin is represented: at the bottom the same plot for the ASD carried out at Gruvebadet is shown. In the wind plot, the grey zone is referred to be "likely contaminated", as wind comes the sector containing the village.

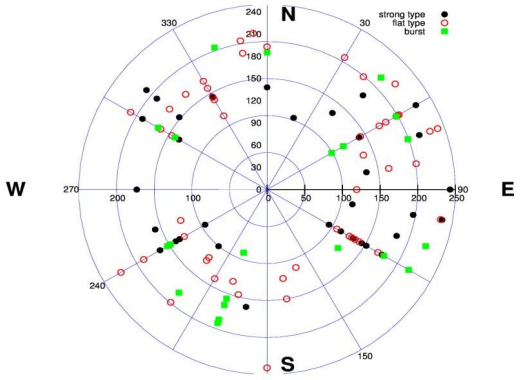

Figure 8. Wind Rose direction versus starting time of NPF event recorder at the Gruvebadet site during the three multi-monthly dataset, versus the day of the year (represented on the axis): please note the so called "contaminated area" that could be defined between 20 and 80 degree

ACKNOWLEDGEMENTS

The present study was developed as a part of the *Climate Change Tower Integrated Project* (CCT-IP), and with the supporting of the Ministero Affari Esteri (MAE) by means of research project selected within the Executive Programme of Scientific and Technological Cooperation between the Italian Republic and the Republic of Korea. The authors gratefully acknowledge the colleagues Kjetil Törseth and Mona Johnsrud of the Norwegian Institute for Air Research (NILU), for supplying the wind data recorded at the Zeppelin station, and the DTA (Dipartimento Scienze del Sistema Terra e Tecnologie per l'Ambiente, CNR) for the logistic help.

REFERENCES

Moroni B., S. Becagli, M. Busetto, D. Cappelletti, S. Crocchianti, L. Ferrero, D. Frosini, C. Lanconelli, A. Lupi, M. Maturilli, M. Mazzola, M.G. Perrone, G. Sangiorgi, R. Traversi, R. Udisti, A.P. Viola, and V. Vitale, (2015). Sources and properties of aerosol particles upon Ny-Ålesund (Svalbard Islands): results of integrated vertical profile measurements and electron microscopy analyses. Submitted to *Advances in Meteorology*.

Dal Maso, M., M. Kulmala, I. Riipinen, R. Wagner, T. Hussein, P.P. Aalto, and K. E. J Lehtinen.: (2005), Formation and growth of fresh atmospheric aerosols: eight years of aerosol size distribution data from SMEAR II, Hyytiala, Finland, *Boreal Environ. Res*., 10, 323–336, 2005.

Drofa O., Lanconelli, A. Lupi, M. Mazzola, F. Tampieri, A.P. Viola, V. Vitale, S. Becagli, F. Giardi, R. Udisti., M. Maturilli, A. Schultz, J. Ström, P. Tunved, R. Krejci and H.C. Hansson, Vertical mixing of aerosol in the planetary boundary layer at Ny Alesund, Svalbard, extended abstract submitted for the 1st Peex Science Conference, Helsinki, 10-13 February 2015

Krishna Moorthy, K., V. Sreekanth, J. Prakash Chaubey, S. S. Babu, S. Kumar Kompalli,S. P. Bagare, B. C. Bhatt, V. K. Gaur, and N. S. Singh, 2011: Fine and ultrafine particles at near free-tropospheric environment over the high altitude station Hanle, in Trans-Himalayas: new particle formation and size distribution. *Journal Of Geophysical Research*, 116, D20212.

Hogrefe, O., G. G. Lala, B. P. Frank, J. J. Schwab, and K. L. Demerjian, 2006: Field evaluation of a TSI 3034 Scanning Mobility Particle Sizer in New York City: Winter 2004 intensive campaign. *Aerosol Sci. Technol.*, 40, 753–762.

Hussein T., M. Dal Maso, T. Petäjä T., I. K Koponen, P. Paatero, P.P. Aalto, K. Hämeri K. and M. Kulmala M. 2005. Evaluation of an automatic algorithm for fitting the particle number size distributions. *Boreal Env. Res*. 10: 337–355

Matveen, L. T., 1965, *Physics of the Atmosphere*, (Leningrad, Hydrometeorological press, 876p)

Ström, J., A.C. Engvall, , F. Delbart, R. Krejci, and R. Treffeisen, R. (2009), On small particles in the Arctic summer boundary layer: observations at two different heights near Ny-Ålesund, Svalbard. *Tellus B*, 61: 473–482. doi:10.1111/j.1600-0889.2008.00412.x

Tomasi C., A. Kokhanovsky, A. Lupi. C. Ritter., A. Smirnov, N. T. O'Neill, R. S. Stone, B. N. Holben, S. N. Nyeki, C. Wehrli, A. Stohl, M. Mazzola, C. Lanconelli, V. Vitale, K. Stebel, V. Aaltonen, G. de Leeuw, E. Rodriguez, A. Herber, V. Radionov, T. Zielinski, T. Tomasz, S. Sakerin, D. Kabanov,Y. Xue, L. Mei , L. Istomina, R. Wagener, B. McArthur, P. Sobolewski, R. Kivi, Y. Courcoux, P. Larouche, S. Broccardo, S. Piketh., Aerosol remote sensing in polar regions, *Earth Science Reviews* (2015), January 2015, 108-157, doi:10.1016/j.earscirev.2014.11.001

Tunved, P., J. Ström, and R. Krejci, 2013: Arctic aerosol life cycle: linking aerosol size distributions observed between 2000 and 2010 with air mass transport and precipitation at Zeppelin station, Ny-Alesund, Svalbard. *Atmospheric Chemistry and Physics*, 13, 3643–3660.

ATLAS "RUSSIAN ARCTIC IN THE XXI CENTURY: NATURE CONDITIONS AND RISKS IN THE DEVELOPMENT"

N.I. ALEKSEEVSKY, S.A. DOBROLYUBOV, A.V. BREDIKHIN, A.V. KISLOV, V.L. BABURIN, D.V. MAGRITSKY and V.S. TIKUNOV

Moscow State University, Faculty of Geography,
PO Box 119991, Leninskie gory, GSP-1, Moscow, Russian Federation

Keywords: ARCTIC, RUSSIA, ATLAS, MAPS

INTRODUCTION

The Geography Faculty of Lomonosov Moscow State University has prepared and published in 2013-2014 an unique Atlas "Russian Arctic in the XXI century: nature conditions and risks in the development". The Atlas includes 8 main sections, in which the allocation of the Arctic region of the Russian Federation and its borders, the history of its development, the most common geographical features of the area, and (in more details) geological, geomorphological, geocryological, meteorological and climatological, hydrological, environmental and socio-economic specifics of the region are discussed. It includes 36 original, updated and adapted thematic maps of scale 1:20 000 000 and 1:30 000 000; 16 illustrative cartographic images, detailed text explanation to the maps and a variety of illustrative material (169 color and 15 black-and-white diagrams and drawings, 160 color photos).

AIMS AND OBJECTIVES OF THE CREATION OF THE ATLAS

The creation of the "Russian Arctic in the XXI century: nature conditions and risks in the development" is one of the practical steps towards creating an information framework of managing the Russian Arctic territories, which primarily needs objective scientific information. The maps showing the ocean bottom geology and topography are needed to address the international legal issues on national identification of specific areas of the Arctic Ocean waters and shelf. Spatially distributed information on the geographical environment state will be also required by government agencies of the constituents of the Russia Federation.

It is expected that the unique current Atlas materials obtained on the basis of modern data and research results will be a source or information for the people of the Arctic region, executive bodies, different organizations and agencies, business structures and enterprises, emergency services, teachers, and students. They will provide users with information on potential natural and social risks, adverse consequences of using natural resources in the region and will be of great importance for sustainable development of the Russian Arctic.

Based on the Atlas, cartographic generalization can be carried out characterizing the features of the natural environment and economy in different regions of the country to reveal the patterns of natural and socio-economic processes using specific data. These materials will make it possible to objectively study the current state of the geographical environment and also predict its future changes, form a holistic understanding of changing components of the environment, relationship between the mechanisms of natural and man-made impacts in the process of transforming the world around us and of the impact of economic activities on the Arctic ecosystems of different scales.

Such atlases in Russia have never been published. Atlas of the Arctic and Atlas of the Water Balance of the Northern Polar Area were published in 1985 and in 1996, respectively, but they have a different focus and structure.

The representatives from seven departments and a research laboratory of the Lomonosov Moscow State University's Faculty of Geography were involved in the Atlas creation.

STRUCTURE AND CONTENT OF THE ATLAS

The Atlas consists of one introductory and seven main parts. They are Borders and history of development of the Russian Arctic (the sections and maps - Geographic location and borders of the Russian Arctic, History of development of the Russian Arctic), Geological structure and relief of the Russian Arctic (the sections and maps - The topography of the Arctic land and bottom of the Arctic ocean, The tectonic structures, Geological-geomorphological resources), The Russian Arctic Climate (the sections and maps - Air temperature, Atmospheric pressure and wind, Atmospheric precipitation, Snow cover, The severity of the climate, Climate-formation factors), Permafrost and glaciers of the Russian Arctic (the sections and maps - Permafrost, Thickness of permafrost rocks, Cryogenic processes, Island and mainland glaciations), Russian Arctic seas. Waters of land (the sections and maps - Seas. The sea ice coverage, Rivers and lakes, Runoff and water regime of the rivers, Changes in water resources of the rivers, Ice and thermal regime of the rivers, The use of water resources, The quality of river waters and aquatic ecological problems, Dangerous hydrological phenomena), Flora and fauna of the Russian Arctic (the sections and maps - The animal world. The biological resources of the seas and rivers, environmental protection), The population and economy of the Russian Arctic (the sections and maps - Displacement of population, The areas of displacement of the peoples of Russia within the Arctic, Industry, Traditional agriculture and nature management in the Arctic regions of Russia, Transport) (examples on the Fig.1 - Fig. 6).

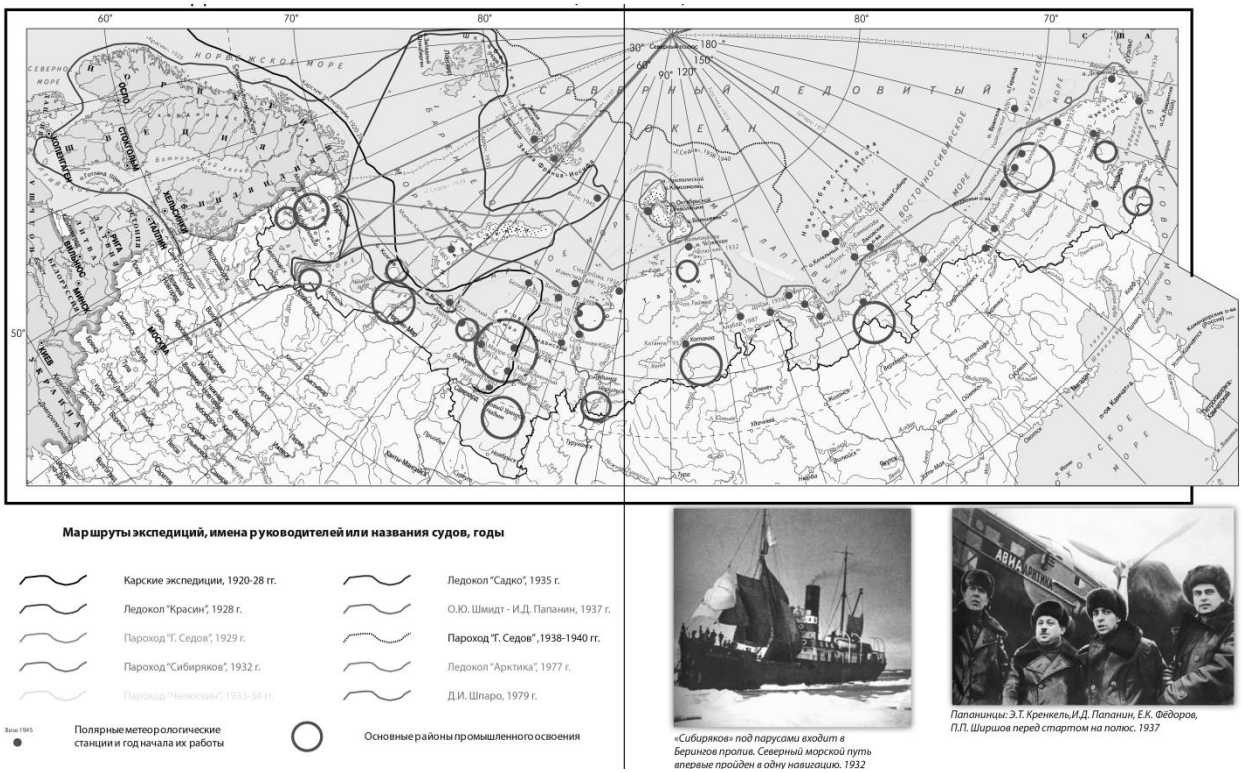

Figure 1. One of the maps on the history of exploration and discovery in the Russian Arctic

The sections of the Atlas define the notion of the Arctic Region of the Russian Federation and its boundaries, and examine the issues of its development and general geographical, geological, geomorphological, geocryological, meteorological and climatic features (Magritsky et al., 2013). Regional hydrological conditions featuring the region's sea and river water status and conditions, water resources and their annual distribution have been described in much detail. Special attention is paid to diverse (current and expected) natural hazards in the Arctic region, unique natural ecosystems and their protection. The Atias' socio-economic section describes the issues of the settlement and resource development of the Russian Arctic, the maintaining of the size and distinctive and unique culture of northern peoples.

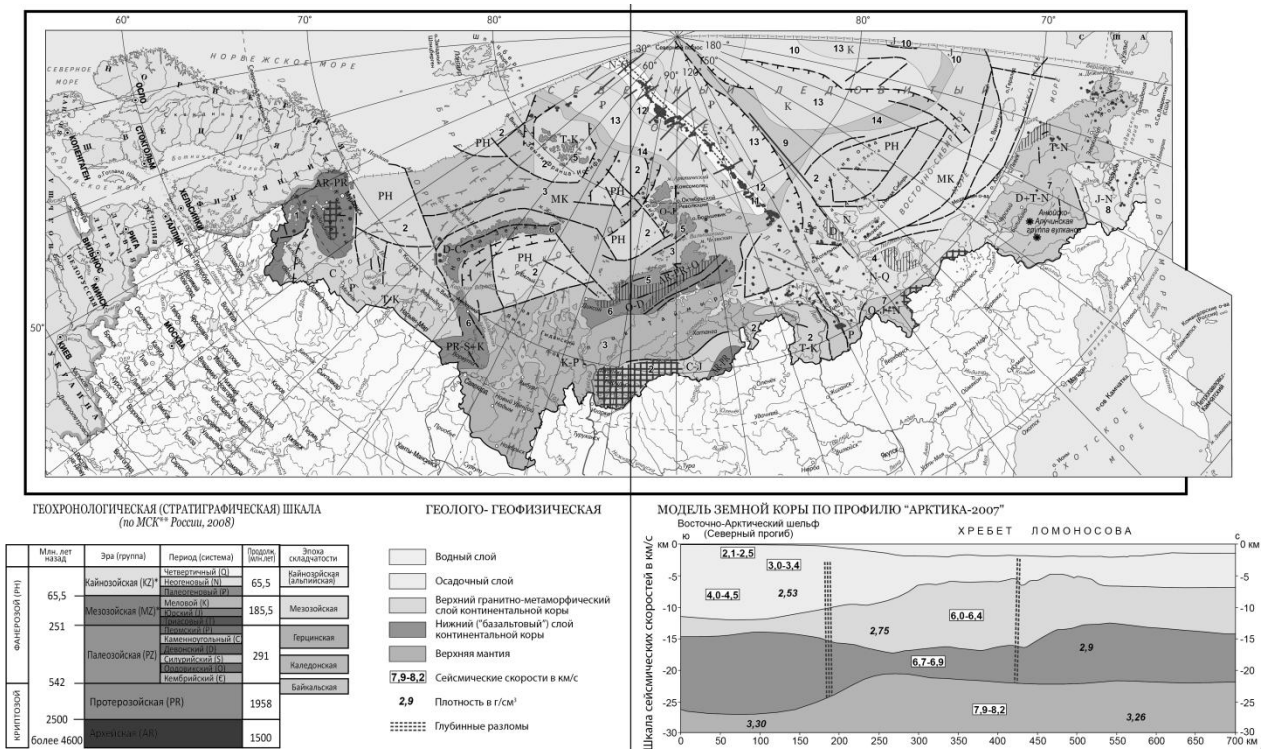

Figure 2. Map of the tectonic structure in the Russian sector of the Arctic

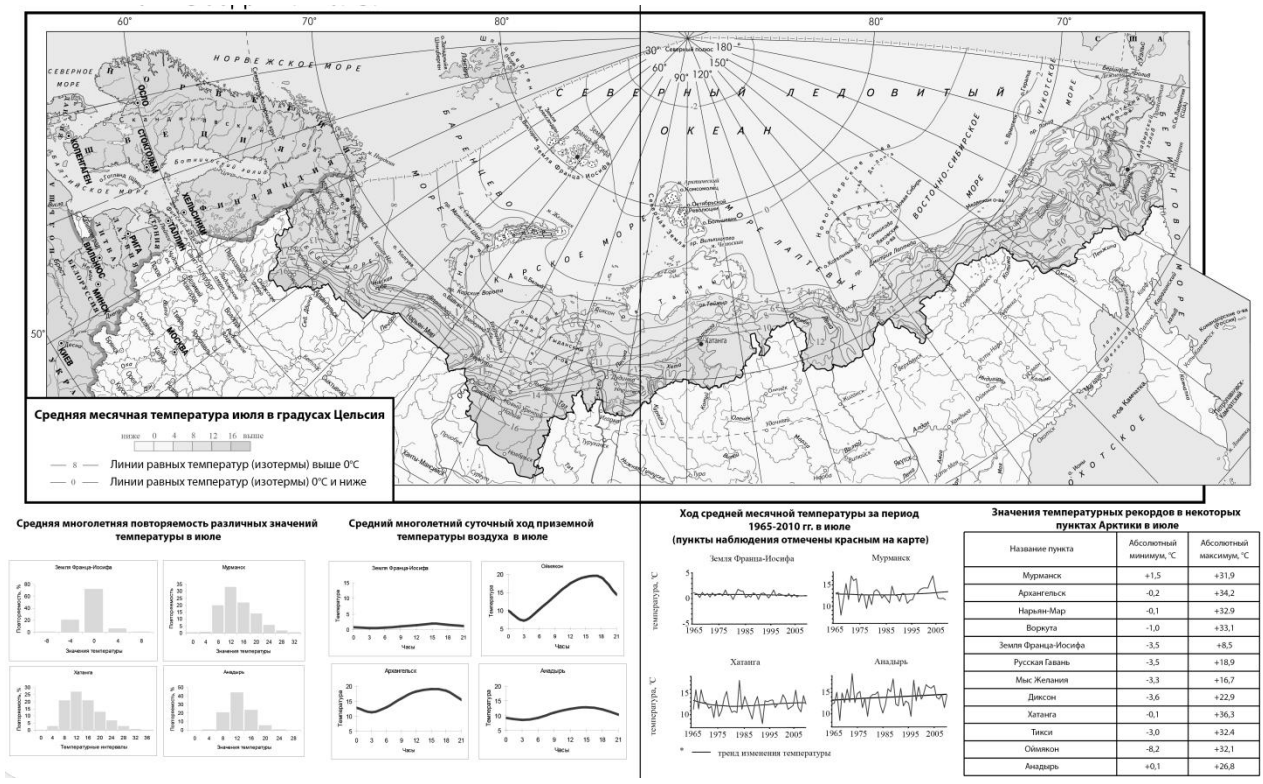

Значения температурных рекордов в некоторых пунктах Арктики в июле

Название пункта	Абсолютный минимум, °С	Абсолютный максимум, °С
Мурманск	+1,5	+31,9
Архангельск	-0,2	+34,2
Нарьян-Мар	-0,1	+32,9
Воркута	-1,0	+33,1
Земля Франца-Иосифа	-3,5	+8,5
Русская Гавань	-3,5	+18,9
Мыс Желания	-3,3	+16,7
Диксон	-3,6	+22,9
Хатанга	-0,1	+36,3
Тикси	-3,0	+32,4
Оймякон	-8,2	+32,1
Анадырь	+0,1	+26,8

Figure 3. Map of air temperature in July

The map of the Arctic Ocean geological and tectonic structure takes into account the latest concepts. Many cartographic generalizations are based on previously unavailable archival materials, synthesis of a variety of knowledge about the nature, population and economy of this Russian region. The original Arctic development maps are presented to reflect not only the areas of expeditions and their achievements, but also the milestones of the North's industrial development and history of populating these areas.

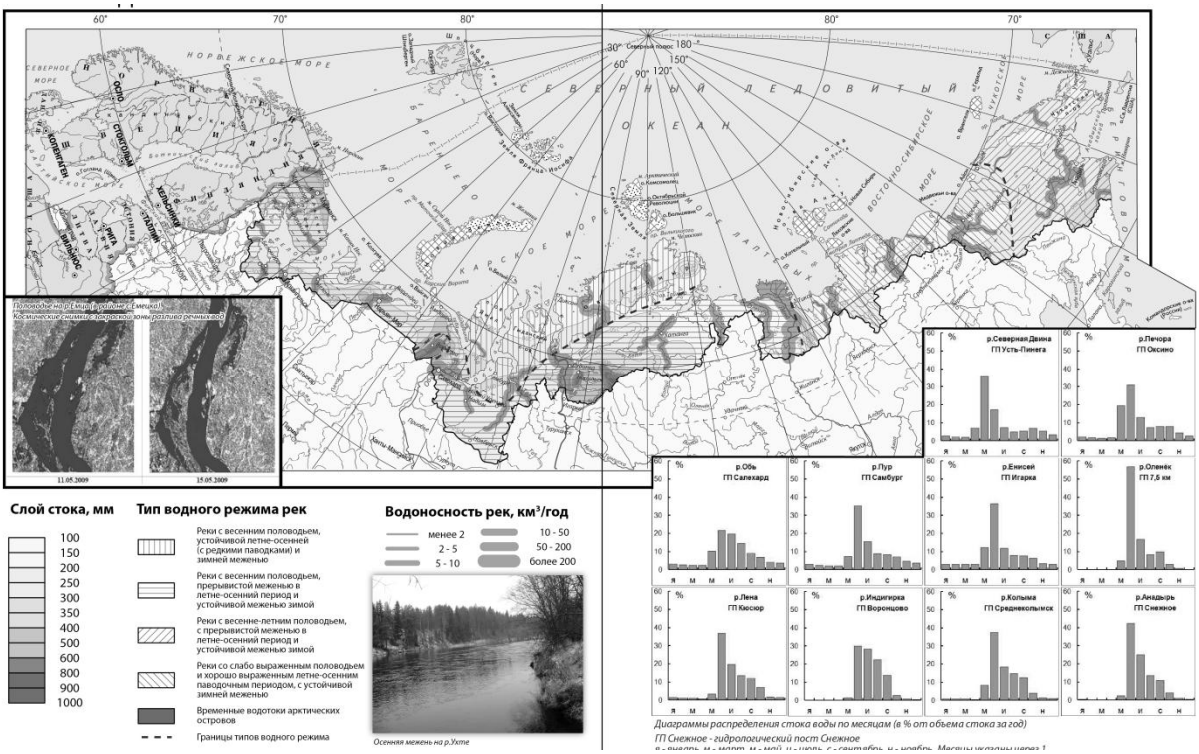

Figure 4. Map of runoff and water regime of the rivers of the Russian Arctic

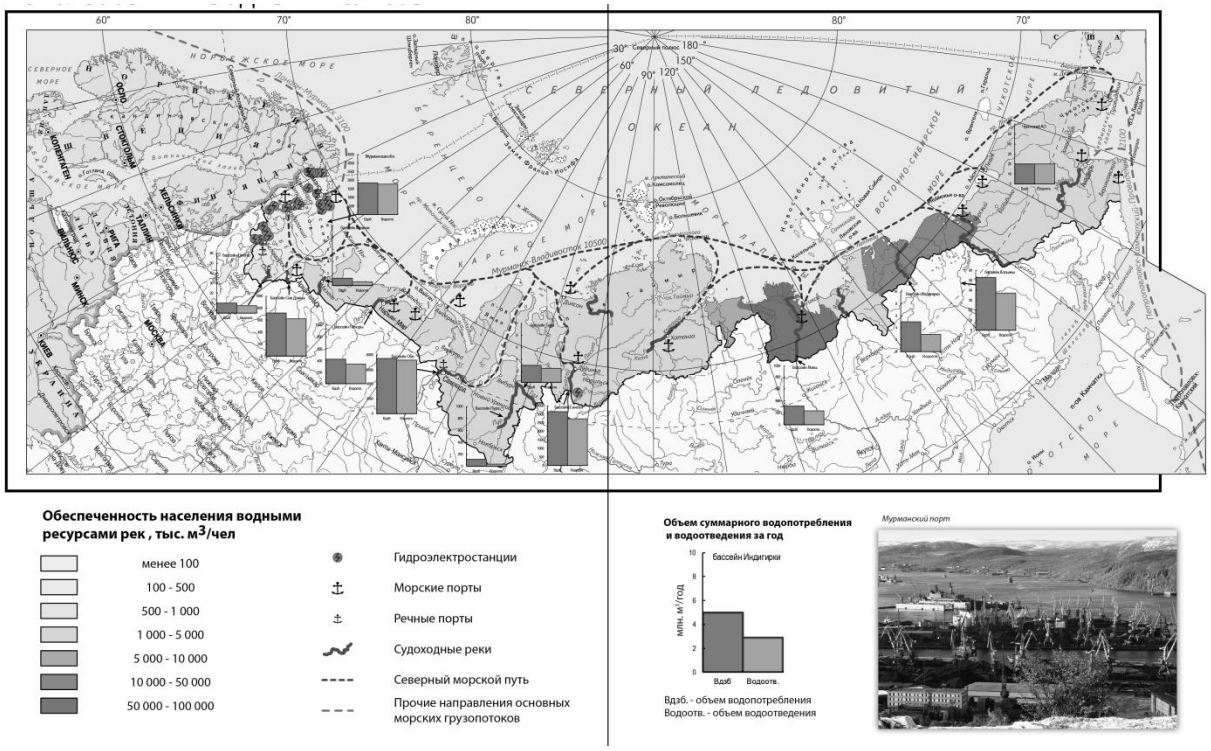

Figure 5. Map of water resource use in the Russian Arctic

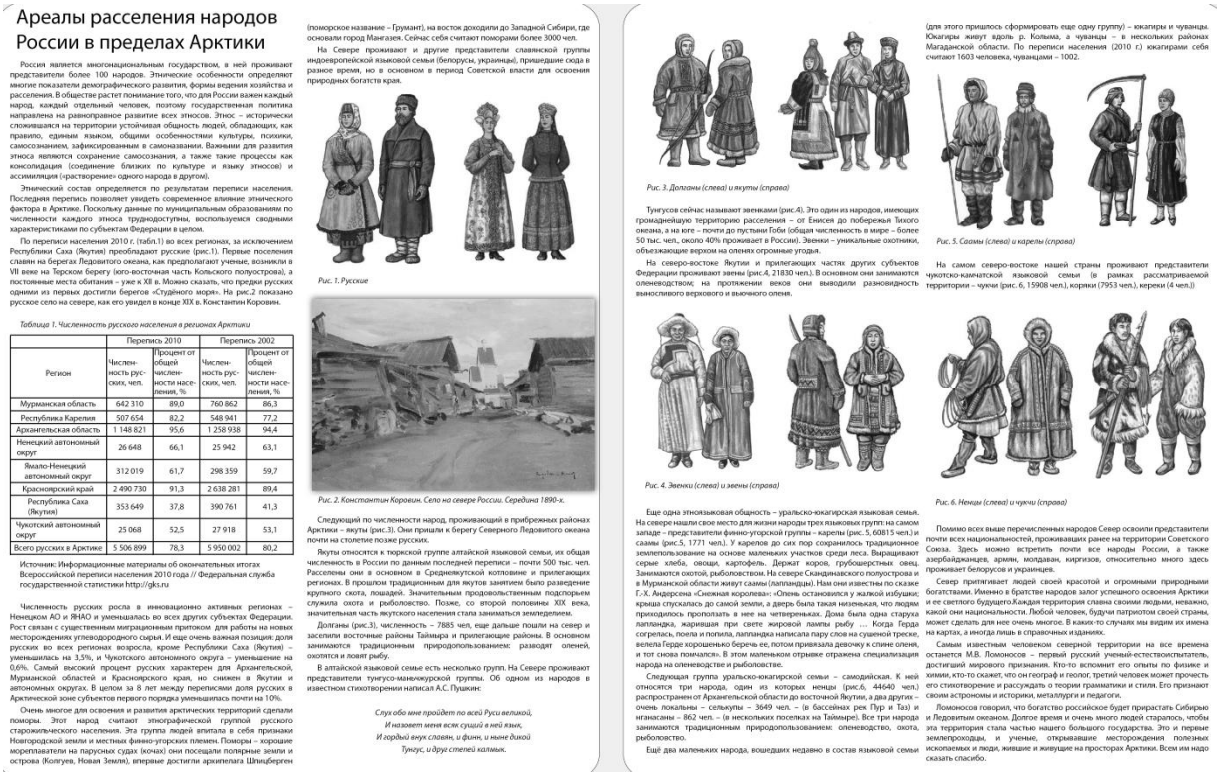

Figure 6. Section of the Atlas is devoted to the ethnic groups of the Russian Arctic

The Atlas contains the data reflecting geo-ecological conditions of the region under study in 1960-1990, at the present stage (1990-2011), and the expected changes until 2050.
The Atlas includes 36 original, updated and adapted thematic maps of scale 1:20 000 000 and 1:30 000 000; 16 illustrative cartographic images, detailed text explanation to the maps and a variety of illustrative material (169 color and 15 black-and-white diagrams and drawings, 160 color photos). The Atlas volume is 145 pages; edition - 155 copies, in Russian.

CONCLUSIONS

The creation of the Atlas "The Russian Arctic in the XXI century: nature conditions and risks in the development" is one of the practical steps towards the establishment of information bases of management of Arctic territories and marine areas.

ACKNOWLEDGEMENTS

This work was supported by the Russian Geographical Society. Continued studies of the Russian Arctic is being financed through a grant from the Russian science Foundation No. 14-37-00038

REFERENCES

Magritsky, D.V., Alekseevsky, N.I., and V.S. Tikunov (2013). Atlas "Russian Arctic in the XXI century: nature conditions and risks in the development", *The Arctic herald* **3(7)**

DOWNSCALING ENVIRO-HIRLAM MODELLING OF METEOROLOGY AND CHEMISTRY FOR LARGE URBAN AREAS

A.G. MAHURA[1], R. NUTERMAN[2,3], I. GONZALEZ-APARICIO[4] and A.A. BAKLANOV[1,5]

[1] Danish Meteorological Institute, DMI, Lyngbyvej 100, DK-2100, Copenhagen, Denmark.
[2] University of Copenhagen, Niels Bohr Institute, Juliane Maries Vej 30, DK-2100 Copenhagen, Denmark.
[3] Tomsk State University, TSU, Lenin Ave., 36, 634050, Tomsk, Russia.
[4] Institute for Energy and Transport, Westerduinweg 3, NL-1755 LE Petten, The Netherlands.
[5] World Meteorological Organization,WMO, 7 bis, Avenue de la Paix, 1211 Geneva 2, Switzerland.

Keywords: Building Effect Parameterization, Online integrated modelling, Enviro-HIRLAM.

INTRODUCTION

The most serious air pollution events occur in cities where there is a combination of high population density and air pollution. The pollutants can lead to serious human health problems. However, European-scale air quality models are not well suited for urban forecasts, as their grid-cell is typically of the order of 5-10km and they generally lack detailed representation of urban effects. Due to constantly increasing supercomputer power modern nested numerical meteorological and air pollution models realize model nesting/down-scaling from the global to urban scale and approach the necessary horizontal and vertical resolutions to provide weather and air quality forecasts for urban scales. This will bring a strong support for continuous improvement of the forecast modelling systems for weather and air quality in Europe, and underline clear perspectives for the future multi-scale air quality core-downstream services for end-users.
In recent decade, an increased resolution and improved land-use classifications for urban areas, based on existing land databases such as ECOCLIMAP, PELCOM, GLCC and others lead to further development of urban parameterization useful for Numerical Weather Prediction (NWP) models. Improved land-use classifications and models for computing in urban areas for NWP systems are based on the following. First, the increased resolution land-use surface databases (CORINE, DHM, etc.) became available. Second, different modified algorithms for estimation of roughness parameters within urban areas based on morphologic methods have been developed and tested. For that different databases on urban characteristics were analyzed for mapping morphology and aerodynamic parameters, which are characteristic for urban areas, and specifically, for different types of urban districts. Third, experimental studies of urban roughness non-homogeneity effects on the urban boundary layer development were carried out, and these results were used for model verifications.

METHODS

Rotterdam Metropolitan Area

To identify possible types of urban districts existing within a selected metropolitan area, the high resolution land-use databases are necessary. In our study, the CORINE database (of 250 m resolution) was applied (*CORINE, 2000*; http://www.eea.europa.eu/data-and-maps). The processing of its data for urban scale domain has included several steps (*González-Aparicio, 2010*): 1) extraction of original land-use-cover data, 2) integration of urban grid cells of modelling domain into GIS environment, and 3) re-classification of urban related classes within grid cells into different types of urban districts. Urban districts can be as the following: city center (CC), high buildings district (HBD; see Figure 1a), industrial commercial district (ICD), residential district (RD), and rural area (RA).
Results of reclassification for the Rotterdam area (The Netherlands) are shown in Figure 1b. The Enviro-HIRLAM-R02 modelling domain contained 27176 cells in total, where 5.64% were identified as the urban

cells (and Rotterdam metropolitan area was represented by 109 urban cells). In particular, the HBD was attributed to 1 (less than 1%), ICD - 51 (46.8%), and RD - 57 (52.3%).

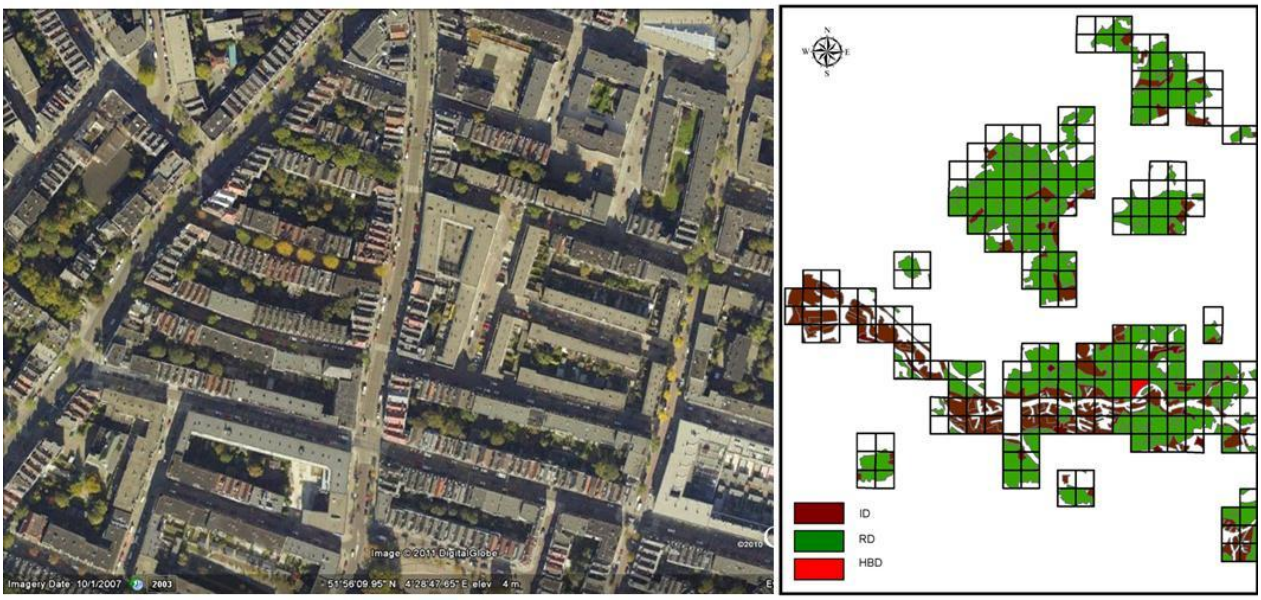

(a) *(b)*

Figure 1: Rotterdam metropolitan area: (a) Example of urban districts —high building district/extracted from Google-Earth/; and (b) Reclassification into different urban districts based on the CORINE land-use database (RD – residential district; HBD – high building district; ICD – industrial commercial district).

Building Effect Parameterization Module

In our study, the city in the urban sub-layer parameterization, so-called the Building Effects Parameterization (BEP) module (*Martilli et al., 2002*) is represented as multiple streets and buildings of constant widths, but with different heights (see Figure 2a).

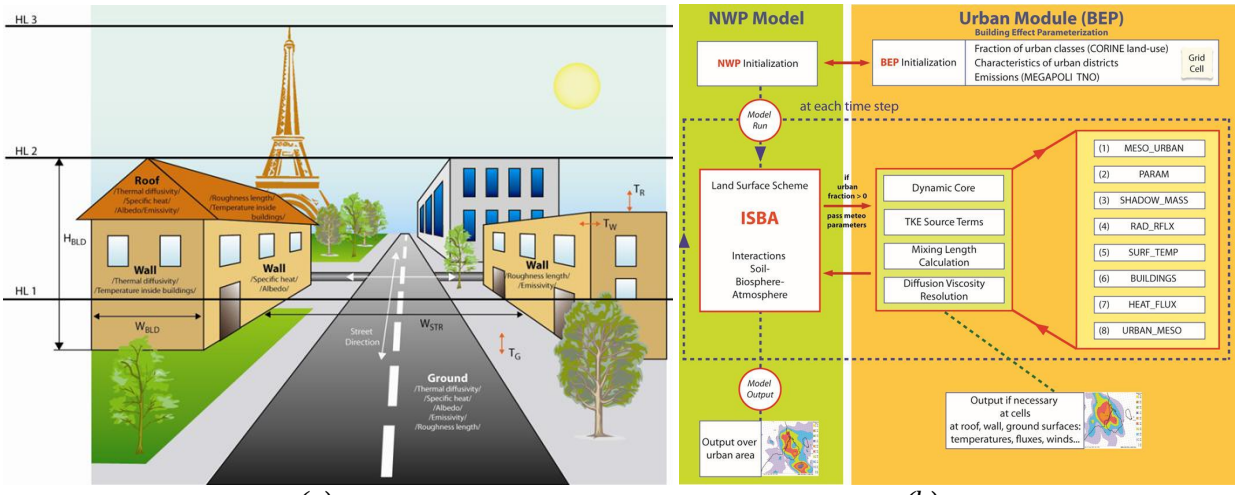

(a) *(b)*

Figure 2: (a) Schematic representation of urban features and numerical grid in the urban module / HL1, HL2 – model levels; HBLD, WBLD – height and width of the buildings; SD, WSTR – street direction and width; TG, TW, TR – temperatures of ground, wall and roof surfaces, respectively/; and (b) General scheme of the BEP module for the model urbanization with a structure of the subroutine conception.

The urban sub-layer parameterization is composed of the following blocks shown in Figure 2b. The structure of the NWP model starts generally with an initialization step. Following the initialization, the

program compute successively the pressure, the advection and the turbulent viscosity-diffusivity at each time step and cell having urban fraction. The first segment reads, computes, and initializes the urban characteristics during the initialization step of the NWP model. The second segment computes the urban effects for the diffusion-viscosity resolution within the turbulence part of the code.

Enviro- Components

Enviro-HIRLAM (Environment—HIgh Resolution Limited Area Model) an on-line coupled NWP and ACT model for research and forecasting of both meteorological and chemical weather (*Korsholm, 2008, Baklanov et al., 2008, 2014*). It is included by the European HIRLAM consortium as the baseline system in the HIRLAM Chemical Branch. Enviro-HIRLAM includes two-way feedbacks between air pollutants and meteorological processes. Components are shown in Figure 3a, and schematics of downscaling chain of runs - in Figure 3b. Different parts of Enviro-HIRLAM were evaluated versus ETEX-1 experiment, Chernobyl accident, urban case studies for selected metropolitan areas such as Paris (France), Copenhagen (Denmark), Bilbao (Spain), St. Petersburg (Russia), and Vilnius (Lithuania).

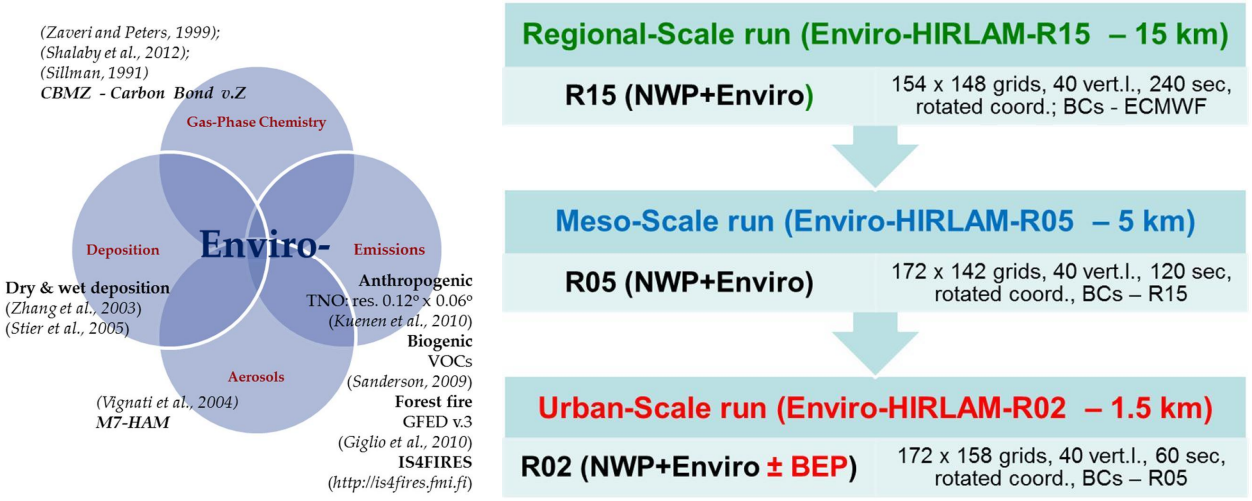

(a) *(b)*

Figure 3: (a) Enviro- Components—emissions, deposition, aerosols, and gas-phase chemistry—of the Enviro-HIRLAM modelling system; and (b) Schematics of downscaling from regional to urban scales.

CONCLUDING REMARKS

The evaluation of formation and development of meteorological and chemical/aerosol patterns due to influence of the Rotterdam metropolitan area was performed employing the urbanized version of the Enviro-HIRLAM (Environment - HIgh Resolution Limited Area Model). Anthropogenic emissions of gases and aerosols from sources (including from airplane, transport, and shipping activities) are considered (Figure 4ab). The model is urbanized based on the Building Effects Parameterization module which describes different types of urban districts such as industrial commercial, city center, high density and residential with its own characteristics. Boundary and initial conditions for the downscaling runs are taken from ECMWF and further from the inner domains of nested model runs (with 15, 5, and 1.5 km resolutions, and higher time steps of 240, 120, and 60 sec). For the studied period of Jul 2009, several specific dates with low, typical, high wind speed, precipitation, cloud free and overcast conditions were analyzed in more details (Figure 4cdef). The effects of urbanization are analyzed for atmospheric transport, dispersion, deposition, and chemical transformations.

Finer scale resolution modelling allows to simulate influence of metropolitan areas on both meteorological and chemical patterns: (i) on meteorology - these effects are more visible at low wind conditions and above/closer downwind distances to urban areas; (ii) On chemistry - higher concentrations of maxima at finer resolutions and more complex non-homogeneous structure of pollutant plumes are both observed;

Tested downscaling modelling system for regional-meso-urban scales can be applied for advanced planning safety measures, post-accidental analysis and health/environment impact assessment, and operational forecasting and emergency preparedness;
Comparative analysis between control vs. urbanized runs for several metropolitan areas – Rotterdam, Copenhagen, Paris, and Rein-Ruhr – is on-going employing GIS.

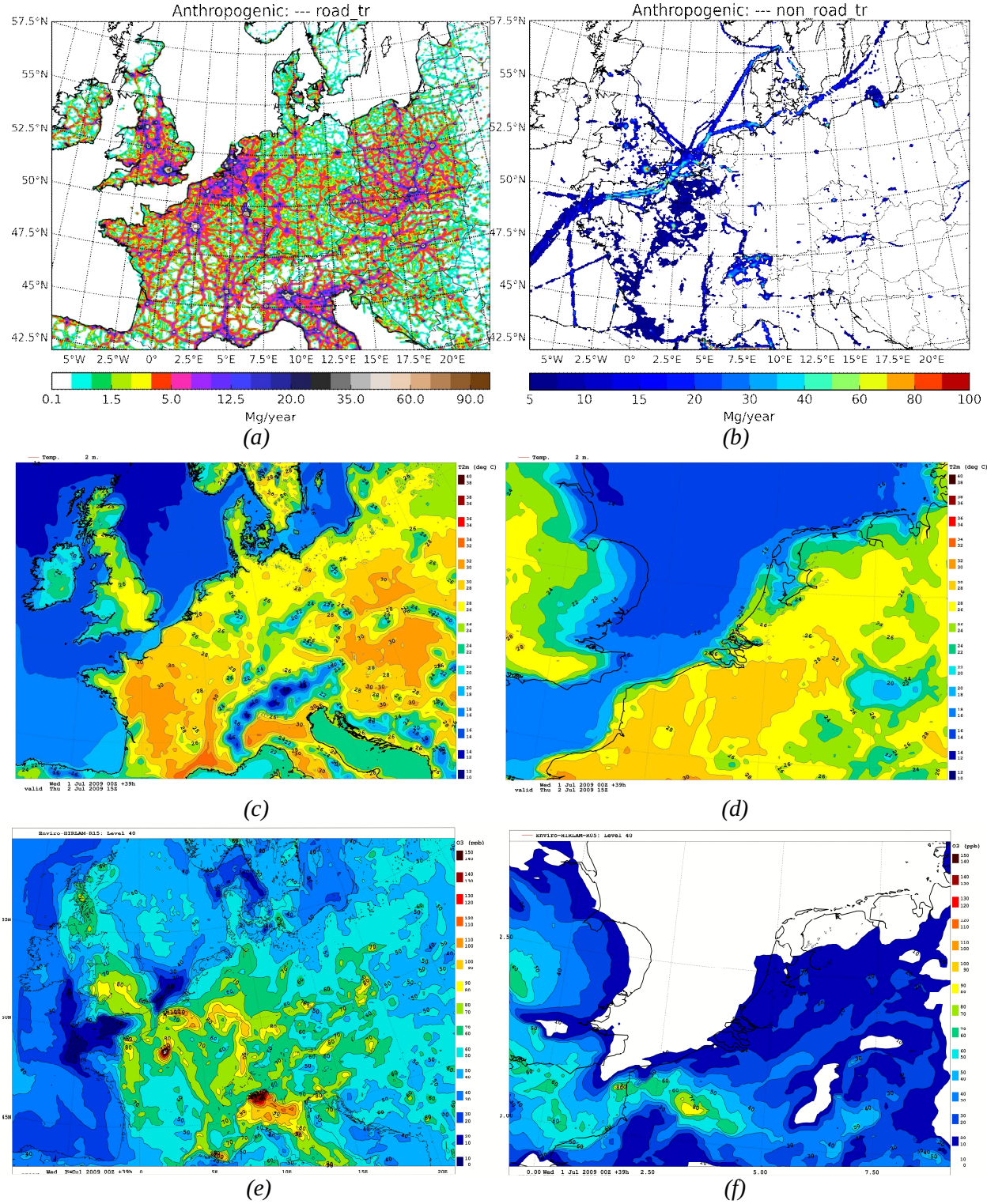

Figure 4: Annual anthropogenic (a) road transport and (b) shipping emissions (based on Kuenen et al., 2011); Simulated (by Enviro-HIRLAM) the air temperature (cd) and ozone (ef) over the low (ce) and finer (df) horizontal resolution domains on 2 Jul 2009, 15 UTC.

ACKNOWLEDGEMENTS

The financial support for this study was provided from the EU FP7 TRANSPHORM project. The CRAY-XT5 supercomputing facilities, ECMWF boundary conditions were used in this study. Thanks to DMI Computer Department for technical support and advice. Thanks to DMI colleagues for useful comments and discussions. The views expressed are purely those of the authors and may not in any circumstances be regarded as stating an official position of the European Commission.

REFERENCES

Baklanov A., U. Korsholm, A. Mahura, C. Petersen, A. Gross, (2008): Enviro-HIRLAM: on-line coupled modelling of urban meteorology and air pollution. Adv. Sci. Res., 2, 41-46.

Baklanov, A., Schlünzen, K., Suppan, P., et al. (2014): Online coupled regional meteorology chemistry models in Europe: current status and prospects, Atmos. Chem. Phys., 14, 317-398, doi:10.5194/acp-14-317-2014.

Giglio, L., Randerson, J. T., van der Werf, G. R., Kasibhatla, P. S., Collatz, G. J., Morton, D. C., and DeFries, R. S., (2010): Assessing variability and long-term trends in burned area by merging multiple satellite fire products, Biogeosciences, 7, 1171-1186, doi:10.5194/bg-7-1171-2010

González-Aparicio I., Nuterman R., Korsholm U., Mahura A., Acero J.-Á., Hidalgo J. and Baklanov A., (2010): Land-use Database Processing Approach for Meso-Scale Urban NWP Model Initialization, DMI Scientific Report ,No. 10-02, 32 p.

Korsholm U., (2009): Integrated modeling of aerosol indirect effects - develoment and application of a chemical weather model. PhD thesis University of Copenhagen, Niels Bohr Institute and DMI, Research Department.

Kuenen, J. H. Denier van der Gon, A. Visschedijk, H. van der Brugh, (2011): High resolution European emission inventory for the years 2003-2007, TNO report TNO-060-UT-2011-00588, Utrecht, 2011.

Martilli, A., Clappier, A., Rotach, M. W., (2002): An Urban Surface Exchange Parameterization for Mesoscale Models, Boundary Layer Meteorology 104, 261-304.

Sanderson M. (2002): Emission of isoprene, monoterpenes, ethane and propene by vegetation, Hadley Centre Tech.Note 40

Shalaby, A. K., Zakey, A. S., Tawfik, A. B., Solmon, F., Giorgi, F., Stordal, F., Sillman, S., Zaveri, R. A., and Steiner, A. L., (2012): Implementation and evaluation of online gas-phase chemistry within a regional climate model (RegCM-CHEM4), Geosci. Model Dev. Discuss., 5, 149-188, doi:10.5194/gmdd-5-149-2012.

Sillman, S., (1991): A numerical solution for equations of tropospheric chemistry based on an analysis of sources and sinks of odd hydrogen, J. Geophys. Res., 96, 20735–20744.

Stier, P., Feichter, J., Kinne, S., Kloster, S., Vignati, E., Wilson, J., Ganzeveld, L., Tegen, I., Werner, M., Balkanski, Y., Schulz, M., Boucher, O., Minikin, A., Petzold, A., (2005): The aerosol-climate model ECHAM5-HAM, Atmos. Chem. Phys., 5, 1125-1156, doi:10.5194/acp-5-1125-2005.

Vignati, E., Wilson, J. and Stier, P., (2004): M7: An efficient size-resolved aerosol microphysics module for large-scale aerosol transport models. Journal of Geophysical Research 109: doi: 10.1029/2003JD004485

Zaveri, R. A., and L. K. Peters, (1999): A new lumped structure photochemical mechanism for large-scale applications, J. Geophys. Res., 104(D23), 30387–30415, doi:10.1029/1999JD900876.

Zhang, L., Brook, J. R., and Vet, R., (2003): A revised parameterization for gaseous dry deposition in air-quality models, Atmos. Chem. Phys., 3, 2067-2082, doi:10.5194/acp-3-2067-2003

MODELLING AND EVALUATION OF IMPACT ON POPULATION DUE TO CONTINUOUS EMISSIONS FROM SEVERONICKEL SMELTERS (KOLA PENINSULA)

A.G. MAHURA[1], I. GONZALEZ-APARICIO[2], R. NUTERMAN[3,4] and A.A. BAKLANOV[1,5]

[1] Danish Meteorological Institute, DMI, Lyngbyvej 100, DK-2100, Copenhagen, Denmark.
[2] Institute for Energy and Transport, Westerduinweg 3, NL-1755 LE Petten, The Netherlands.
[3] University of Copenhagen, Niels Bohr Institute, Juliane Maries Vej 30, DK-2100 Copenhagen, Denmark.
[4] Tomsk State University, TSU, Lenin Ave., 36, 634050, Tomsk, Russia.
[5] World Meteorological Organization (WMO), 7 bis, Avenue de la Paix, 1211 Geneva 2, Switzerland.

Keywords: SULPHATE EMISSIONS, DISPERSION AND DEPOSITION MODELLING, GIS ANALYSIS, INDIVIDUAL AND COLLECTIVE LOADINGS.

INTRODUCTION

During last decades the enterprises of various risks (nuclear, chemical, biological, etc.) are under permanent and critical view from the society. The questions addressed are important because they are related to environmental issues and people's life. Which are the potential impacts on the and on humans? Which geographical regions, countries, population groups etc. are under the largest influence when continuous emissions or accidental releases are taken place at different risk objects? Answers on such questions are, first of all, directly linked with evaluation of atmospheric transport and deposition of pollution as well as estimation of their effects on population and environment.

Large Russian industrial major enterprises such as the Norilsk Nickel, Pechenganickel and Severonickel are sources of continuous emissions. The two latter are located on the Kola Peninsula. Many field campaigns taking meteorological and pollution measurements, soil and water samples were conducted in surroundings of the sources. In addition local and remote continuous monitoring is carried out in order to evaluate influence on various ecosystems and people.

Analyzing forest ecosystems of the Kola Peninsula, *Karaban and Gytarsky (1995*) found that within a 30-40 km radius from the emission sources the impact is the largest. Moreover, level of damage varies depending on a type of a forest (*Gutarsky et al., 1997*) and area of the forest decline is expanding (*Hagner and Rigina, 1998*). Microbial communities in polluted soils showed significant decrease in biomass and growth rate (*Blagodatskaya et al., 2008*). Following smelters production and amount of toxic loading produced, *Moiseenko et al. (2006)* found that water ecosystem (Imandra Lake near Severonickel) strongly affects human health. The higher elevation lakes in Khibiny mountains showed both contributions: from local smelters and due to transboundary pollution (*Dauvalter et al., 2003*). Modelling and estimation of concentration and deposition patterns resulted from continuous and accidental releases (radionuclides, gaseous chemical species and aerosols) from potential sources of nuclear and chemical danger/risks was performed in *Mahura et al. (2006ab; 2007; 2008).*

METHODS

Pollution from Cu-Ni Smelters

There are several major locations in the Russian Arctic associated with large amounts of sulphur dioxide (SO_2) and heavy metals emissions and known as Cu-Ni smelters having the largest environmental and health impacts. These are three Russian enterprises: Norilsk Nickel (Krasnoyarsk Krai), Pechenganickel (cities of Zapolyarny and Nikel, Murmansk region) and Severonickel (city of Monchegorsk, Murmansk region). According to the plans of Kola Mining and Metallurgical Company a reduction of emissions had been performed in recent years. For example, at the beginning of the last decade (year of 2000), the SO_2 emissions from the Severonickel and Pechenganickel enterprises reached 45300 and 151200 tonnes,

respectively (*Ekimov et al., 2001*). If assume that the emissions from Pechenganickel enterprise are uniformly distributed between two sites of smelters, so each of the sources emitted about 75600 tonnes. Thus, emission intensities of mentioned smelters are the following: in Monchegorsk - $1.433 \cdot 10^9$ μg/sec and in Zapolyarny and Nikel - $2.39 \cdot 10^9$ μg/sec. In this study, hereafter, an analysis of impact due to smelters is based on the defined above intensities and considering a "mild scenario" (i.e. about 31.6 thou. tonnes per year corresponding to about 86.4 tonnes per day). Although not the entire released amount of SO_2 can be converted following chemical transformations into sulphates (SO_4^{-2}), it has been assumed that it occurred at maximal level in order to obtain the largest/ top estimates for analysed parameters.

Long-Term Modelling of Continuous Emissions

In many studies, the modeling of atmospheric transport, dispersion and deposition of pollutants is essential input for estimation of possible consequences on different scales ranging from regional to mesoscale. Generated output is crucial for multi-level assessment of risk, vulnerability, impact, short- and long-term consequences for environment and population living near and remote from the sources of possible accidental and continuous emissions.

In our study, the long-term modeling of continuous emissions from Cu-Ni smelters was performed employing the Lagrangian-type Danish Emergency Response Model for Atmosphere (DERMA; *Sorensen, 1998; Baklanov et al., 2008*) in a long-term mode. The European Centre for Medium-Range Weather Forecast data archives were used as input meteorological 3D fields for the year 2000. The data is given at 1 x 1 degree resolution at every 6 hour interval. Only the emissions of sulphates are taken into account, although heavy metals are also linked with emissions from the Cu-Ni smelters, but these are mostly will be deposited at shorter distances from the sources, and hence, will have more influence on a local scale. For the DERMA model runs, the continuous emissions occurred daily at the constant rate, and then plume originated near the source was transported through the atmosphere during following 10 days. It should be noted that in general, levels of pollution can vary significantly depending on meteorological conditions and the highest levels of pollution are observed in vicinity of the sources.

The generated model output includes: air concentration, time integrated air concentration, dry deposition (DD) and wet deposition (WD). Note that such output - if it is summed over a long period of time (for example: month, season, year) or if it is averaged over a short period of time (for example: day, period of accidental release) - can represent possible short- and long-term effects and probabilistic characteristics of industrial pollution. In general, the geographical boundaries of potential impact due to continuous/ accidental atmospheric releases of pollutants from different sources can be evaluated.

Modeling results showed that a substantial deposition is observed not only on the regional but also the Northern Hemispheric scale, including contribution to Arctic regions (e.g. Arctic haze), regional atmospheric pollution transport between North-West Russia and Nordic countries. Partially such influence can be spread faraway on the Pacific region countries (Japan, China, and Korea). Moreover, isolated areas of wet deposition are observed even along the western seashore of Canada and USA.

GIS Integration of Dispersion Modelling Results

The results of the long-term dispersion modelling were integrated into the Geographical Information System (GIS; *ArcGIS* geospatial processing *software; http://www.gis.com/*) environment (Figure 1) in order to assess the impact on population due to continuous anthropogenic emissions from the Severonickel smelters. For that the *ArcMap* component of *ArcGIS* was applied. Note that the same coordinate system is required to work in *ArcMap* with different data-frames and layers. In particular, all data were converted into Geographical Coordinate System GCS-WGS-1984.

At first, the countries and administrative units (regions, provinces, counties) boundaries (Figure 1a) and population density of Russia and European countries were loaded. Data about administrative boundaries of Russian regions (including Murmansk region) were extracted at http://gis-lab.info/projects/osm-export.html. Data about boundaries of European countries and administrative units were downloaded from http://www.diva-gis.org/data/DataServer.htm. Data about population density were obtained from the Center for International Earth Science Information Network (CIESIN;

http://www.ciesin.org/download_data.html). At second, the header (with information on number of grid points along latitude and longitude, south-west corner of modelling domain, and attribute for missing values) has been added to the dispersion modelling output file, and it is needed for obtaining further information about spatial resolution and location. Then, the file should be converted into the same GCS-WGS-1984 coordinate system. At third, the raster centroids (centers of grid cells) are used to create the vector grid. For that, integrated raster data were converted into points and polygons. Because centroids are generated at regular grid, the *Hawth* tool (http://www.spatialecology.com/htools/tooldesc.php) was used to create a vector grid, where the resolution could be changed, in particular, increased. For a case of non-regular grid see *González-Aparicio et al., (2010).* The attribute table was used to transfer data from raster to vector grid based on spatial location. Subsequently, new layers were created for different attributes taking into account grid cells with deposition greater than zero.

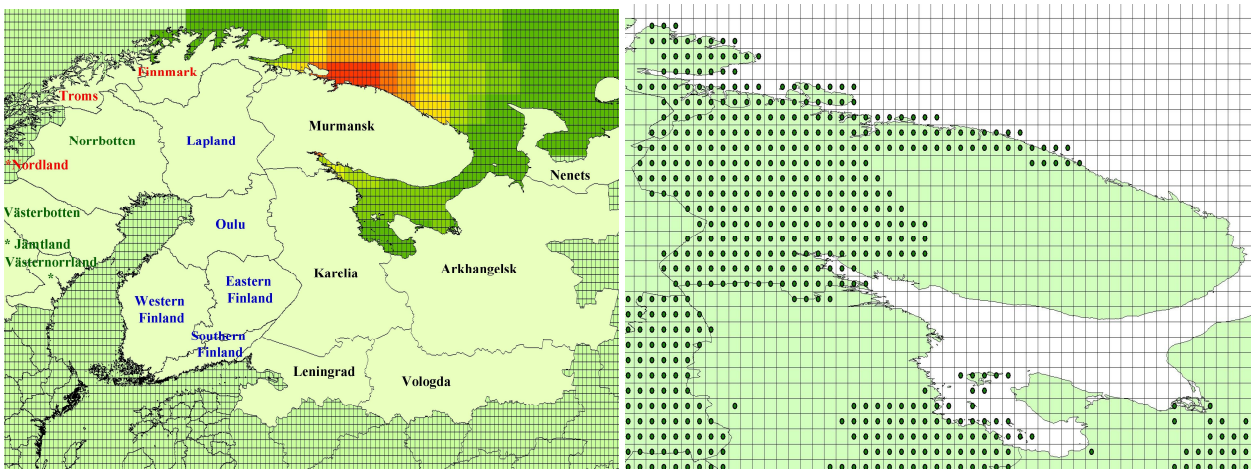

(a) *(b)*

Figure 1: (a) Geographical boundaries of administrative units (regions, provinces, counties, etc.), and (b) Example of extracted geographical region with overlapped layers of total deposition, administrative boundaries and population density in order to calculate the impact on population exposed to emissions.

Finally, the overlapping (Figure 1b) of deposition layer with administrative boundaries should be done in order to calculate total deposition for selected regions and counties. The similar procedure (but in addition using population density layer) was carried out to calculate the impact on population exposed to emissions. And then, these final results in a vector grid were converted into raster format to visualise different levels of impact.

CONCLUSIONS

In this study, the evaluation of impact on population due to continuous emissions of sulfates from the Severonickel Cu-Ni smelters (Murmansk region, Russia) was performed employing the Lagrangian long-range transport model DERMA in a long-term simulation mode and applying GIS tools for integrating and analysis of dispersion modeling results.

It was found that on annual scale, daily dry deposition is about 6 t with the highest (10 t) - in September. The wet deposition is 23 t (maximum 50 t - in February), and it is dominating in total deposition. On average, 33% of emissions could be deposited on the surface during 10 days of atmospheric transport from the smelters with the highest (65%) and lowest (14%) deposited amounts observed in February and July, respectively. The Murmansk region of Russia, where the smelters are located, is the most impacted, followed by Karelia Republic and Arkhangelsk region (with total deposition more than order of magnitude lower compared with the Murmansk region; Table 1). Among administrative units of the Scandinavian countries - Lapland (Finland), Norrbotten (Sweden) and Finnmark (Norway) - have the highest depositions. On average, it is higher in fall for all three Scandinavian countries; and lower in summer (for

Finland) and winter (for Norway). For Russian regions, on average, deposition is higher in spring (except, Arkhangelsk and Nenets regions), and it is lower in summer and winter.

The maximum deposition is observed for the northern, central, and southern territories of Finland in spring, fall and winter, respectively. For Sweden, it occurs in fall. For northernmost part of Norway it takes place in spring, and for other territories – in fall. For Russia, the largest maxima are linked with spring and fall for territories southerly and easterly of the Severonickel smelters, respectively.

Country	***Region/ County/ Province***	**Total Deposition (µg/m^2)**									
	Seasons	**Spring**		**Summer**		**Fall**		**Winter**		**Year**	
	Statistics	**Avg**	**Max**	**Avg**	**Max**	**Avg**	**Max**	**Avg**	**Max**	**Avg**	**Max**
Finland											
	Lapland	623	2263	230	571	940	2219	392	2117	2185	7170
	Oulu	282	792	61	180	802	1344	297	594	1442	2910
	Eastern Finland	70	122	21	38	316	698	160	354	567	1200
	Western Finland	30	40	8	17	131	573	37	64	205	640
	Southern Finland	42	73	9	18	48	105	85	137	183	332
Norway											
	Finnmark	826	3218	307	760	909	2242	197	889	2239	6730
	Troms	26	49	40	91	126	235	10	29	202	403
	NordLand	4	11	3	11	18	31	3	7	28	50
Russia											
	Murmansk	11228	56495	2279	7849	4369	11124	10406	46667	28282	122000
	Karelia	581	2181	198	611	542	1476	447	1677	1768	5050
	Arkhangelsk	112	578	115	1185	282	1651	42	148	551	3030
	Nenets	161	376	11	36	249	702	21	193	442	1250
	Vologda	107	391	26	216	66	243	15	47	214	864
	Leningrad	83	221	19	45	28	67	66	102	196	309
Sweden											
	Norrbotten	16	67	19	75	92	268	11	65	138	397
	Vesterbotten	2	7	1	2	15	31	12	29	30	69

Table 1: Regional distribution of total deposition (annual and seasonal) due to continuous emissions of the Severonickel smelters.

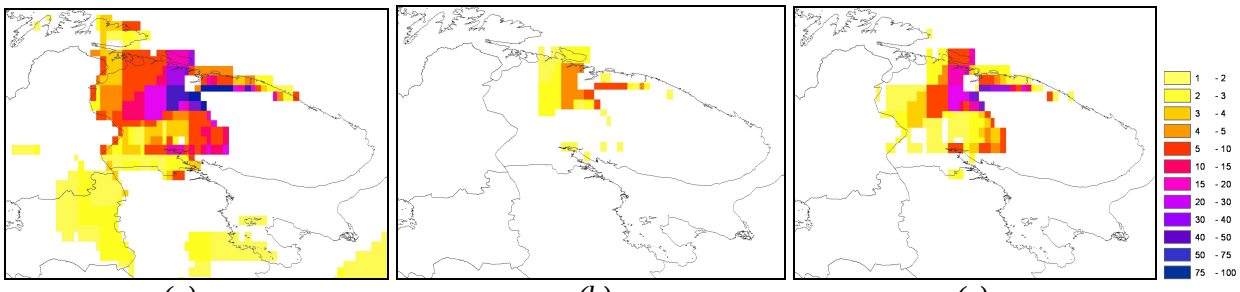

(a) *(b)* *(c)*

Figure 2: Individual loadings for population (in kg/person) from deposited sulfates resulted from the Severonickel smelters continuous emissions (mild scenario): (a) yearly, (b) summer, and (c) winter.

The smelters have the largest impact on city of Murmansk due to its proximity to the source. After Murmansk, the second largest deposition is in Arkhangelsk, and then (in descending order) in Petrozavodsk, Vologda, St.-Petersburg, Syktyvkar, and Pskov urban areas.
The yearly individual loading (Figure 2) can be up to 120 kg/person for the most populated urban areas of the Murmansk region. For bordering territories with this region such loadings are less than 5 kg/person for territories of eastern Finland, Karelia Republic, and Arkhangelsk region; and not greater than 15 kg/person – for Finnmark county of Norway. There exists seasonal variability (with lowest loadings in summer), which is less pronounced for Scandinavian countries. The percentage contribution into such loading is higher in winter-spring for Russia (in sum 85%), in spring for Norway (34%), in fall for Finland and Sweden (32 and 41%, respectively).

The yearly collective loading is the highest (2403 tonnes) for the Murmansk region. Both Karelia Republic and Arkhangelsk region have the second largest loadings (83 and 77 t). These three regions account for 97.5% of yearly value. For populated territories of bordering countries with the Murmansk region such loadings are 140.4, 13, and 10.7 t for Finland, Norway and Sweden, correspondingly.
The results of this study are applicable for (i) evaluation of risks, vulnerability, and short- and long-term consequences due to airborne pollution on population, environment, and ecosystems; (ii) complex human health impact assessments taking into account social, economic and other factors; (iii) support of decision-makers, adjustment of legislation at regional levels, control pollution exceedances; planning preventive measures, mitigation scenarios, etc.

ACKNOWLEDGEMENTS

The DMI supercomputing facilities have been used extensively in this study, as well as ECMWF meteorological data archives. Thanks to DMI Computer Department for technical support and advice. Thanks to J.H. Sorensen (Danish Meteorological Institute) and V. Koshkin, O. Rigina (Kola Science Center, Russia) for useful discussions. The views expressed are purely those of the authors and may not in any circumstances be regarded as stating an official position of the European Commission.

REFERENCES

Baklanov A, J.H. Sørensen, A. Mahura (2008): Methodology for Probabilistic Atmospheric Studies using Long-Term Dispersion Modelling. *Environ. Model Assess., 13, pp. 541-552.*

Blagodatskaya E.V., T.V. Pampura, I.N. Bogomolova, G.N. Koptsik, N.V. Lukina (2008): Effect of emissions from a Copper-Nickel Smelter on soil microbial communities in forest biogeocenoses of the Kola Peninsula. *Ecology, 35 (2), 202-210, DOI: 10.1134/S1062359008020155*

Dauvalter V., T. Moiseenko, L. Kagan (2003): Global Change in Respect to Tendency to Acidification of Subarctic Mountain Lakes. *Advances in Global Change Research, 9(2), 187-194, DOI: 10.1007/0-306-48051-4_18*

Ekimov S.V., I.V. Samodova, I.M. Petrov, V.V. Troitsky, M.A. Burstein (2001): Russian smelter emissions, http://www.infomine.ru/pages/148

González-Aparicio, I., Nuterman R., Korsholm U.S., Mahura A., Acero J.A., Hidalgo J., Baklanov A.(2010) Land-Use Database Processing Approach for Meso-Scale Urban NWP Model Initialization. *DMI Scientific Report 10-02, 34 pages. ISBN: 978-87-7478-593-4. http://www.dmi.dk/dmi/sr10-02.pdf*

Gytarsky M. L., R. T. Karaban, I. M. Nazarov (1997): On the Assessment of Sulphur Deposition on Forests Growing Over the Areas of Industrial Impact. *Environmental Monitoring and Assessment, 48(2), 125-137, DOI: 10.1023/A:1005744301889*

Hagner O., O. Rigina (1998): Detection of Forest Decline in Monchegorsk Area. *Remote Sensing of Environment, 63 (1), 1998, 11-23*

Karaban R. T., M. L. Gytarsky (1995):Studies of precipitation contamination levels over the north-western forests of Russia subject to emissions from the two nickel smelters. *Water, Air, & Soil Pollution, 85(4), 2071-2076, DOI: 10.1007/BF01186139*

Mahura A., A. Baklanov, J.H. Sørensen (2006a): Influence of long-range and long-term continuous and accidental anthropogenic emissions from Eurasian sources on Greenland environment. *Proceedings of the International Conference "The Greenlandic Environment: Pollution and Solutions", 21-23 Feb 2006, Sisimiut in Greenland, pp. 15-22.*

Mahura A., A. Baklanov, J.H. Sorensen, A. Tridvornov (2006b): Long-term modelling for estimation of man-induced environmental risks. *Abstracts of the European Geosciences Union (EGU) General Assembly,* 2-*7 April 2006,Vienna, Austria, EGU06-A-03781.*

Mahura A., Baklanov A., J.H. Sørensen, A. Svetlov, V. Koshkin (2007): Assessment of Long-Range Transport and Deposition from Cu-Ni Smelters of Russian North. *In "Air, Water and Soil Quality Modelling for Risk and Impact Assessment", Security Through Science, Series C - Environmental Security.* Eds. A. Ebel, T. Davitashvili, Springer Elsevier Publishers, pp. 115-124.

Mahura A., Baklanov A., Sorensen J.H. (2008): Enviro-RISKS: Overview of Applications for Short- and Long-Term Modelling and Assessment for Atmospheric Pollutants. *Abstracts of the International Conference on Environmental Observations, Modelling and Information Systems, ENVIROMIS-2008*, 28 June – 5 July 2008, Tomsk, Russia, p.106.

Moiseenko T.I., A.A Voinov, V.V. Megorsky, N.A. Gashkina, L.P. Kudriavtseva, O.I. Vandish, A.N. Sharov, Yu. Sharova, I.N Koroleva (2006): Ecosystem and human health assessment to define environmental management strategies: The case of long-term human impacts on an Arctic lake. *Sci. of The Total Environment, 369(1-3), 1-20*

Sorensen J.H. (1998): Sensitivity of the DERMA long-range Gaussian dispersion model to meteorological input and diffusion parameters. *Atmospheric Environment, 32 (24), 4195–4206*

MODERN CLIMATE OF THE NORTHERN YAKUTIA

A.P. MAKSHTAS, N.E. IVANOV, I.I. BOLSHAKOVA AND O.L. ZHUKOVA

Arctic and Antarctic Research Institute, St.Petersburg, Russia.

Keywords: FREE ATMOSPHERE, CLIMATE, METEOROLOGY, RADIOSOUNDINGS.

Based on the new electronic archive of standard meteorological measurements at 18 meteorological stations, located in the Northern Yakutia, the main characteristics of the regional climate are calculated for period 1978 - 2010. Among others there are trends of the meteorological parameters at the stations and maps of climate characteristics, including decadal extremes, correlations with Tiksi data, estimates of hazard repetitions, duration of the heating season, and bio – climatic indexes.

Augmented archives of radiosoundings data, based on performed at meteorological stations Tiksi Cherskii, Chokurdakh, Olenek and Verkhoyansk allowed to reveal, that the maximal positive trends in the atmosphere of the Northen Yakutia have place in the lower troposphere (from 925 to 700 hPa) during all seasons. The negative trends in the upper troposphere and lower stratosphere in the spring, summer, and autumn seasons, which are in the agreement with models, studying the role of recent carbon dioxide increase, are revealed. Same time the pronounced warming at 30 - 10 gPa is found in winter. It could be linked to factors of cosmic origin (photochemical reactions due to the recombination of oxygen atoms, changes in ozone concentration, magnetic activity) and dynamic factors (planetary, tidal, and gravity waves).

ATMOSPHERE'S SELF-CLEANING CLIMATIC POTENTIAL IN UKRAINE

L. V. Malytska and V. O. Balabukh

Ministry of Emergency of Ukraine, National Academy of Sciences of Ukraine
Ukrainian Hydrometeorological Institute UHMI, Department of Synoptic Meteorology
03028, Kiev-28, Prospekt Nauki 37,
e-mail: m_alitsk_a@i.ua, Phone: (044) 525-12-50, +380968077454

Keywords: AIR QUALITY, ATMOSPHERE'S DISSIPATION ABILITY

INTRODUCTION

Air quality is the one of the most important environmental factors affecting on people's living, activity, health and efficiency. Air quality defied by atmosphere pollution level which depends on contaminants concentration and meteorological conditions that contributes to its transportation, dissipation and removal from the atmosphere. When emissions variety is poor, pollution level depends on the meteorological conditions only. That's why temporal changes in meteorological conditions caused by climate change strongly affect air quality.

Evaluation of meteorological and climatic potential of the atmosphere's dissipation ability (ADA) and its temporal changes is an important direction in the atmospheric pollution researches. This information allows to define regions the most vulnerable to climate change and develop adaptation measures.
The main task is the study of ADA potential in Ukraine, its regional features and changes throughout 1971-2010.

METHODS

Estimation of the atmosphere ecological condition performed through analysis of the temporal variety of atmosphere self-cleaning coefficient (K). This ratio is a modification of ADA meteorological potential, calculated using Lapina method. In this method take into consideration factors both contributing to contaminants accumulation and dissipation in the atmosphere.

$$K = (P_o + P_в)/(P_ш + P_т),$$

where $P_ш$, $P_т$, P_o,$P_в$ is the frequency of calm (wind speed 0-1 mps), amount of days with fog, amount of days with total precipitation ≥0.5 mm and amount of days with wind speed ≥6 mps accordingly. This equation allows to calculate atmosphere self-cleaning ratio using the results of routine meteorological observations.

According to K value meteorological conditions divides into three categories:

- $K < 0.8$ – meteorological conditions leads to contaminants accumulation.
- $0.8 \leq K \leq 1.2$ – meteorological conditions are limitedly auspicious.
- $K > 1.2$ – meteorological conditions leads to contaminants dissipation.

So, atmosphere self-cleaning coefficient reflects the ratio between frequency of conducive and non-conducive conditions. Averaged over long time series K values describes ADA climatic potential.
Since a physiographic condition of Ukraine is pretty heterogeneous, each region demands individual approach with consideration of its features. That's why estimation of ADA climatic potential performed for whole territory of Ukraine and each region.
Data: amount of days with fog, frequency of calm, amount of days with total precipitation ≥0.5 mm and amount of days with wind speed ≥6 mps of the 187 meteorological stations across the Ukraine for 1971-2010.

RESULTS

The analysis of climatic potential of the atmosphere's dissipation ability showed that in Ukraine conditions are mostly favorable for atmosphere's self-cleaning. During the studied period meteorological conditions has been adverse to contaminants accumulation. Annual average value of the self-cleaning coefficient varied in interval 0.95 - 1.67 and long-term average value of *K* was 1.3.

The ADA climatic potential has specific spatial distribution. Top meteorological conditions for dissipation of pollutants in the atmosphere have southern and western regions (*K* is 2.8 and 1.8 accordingly). In the northern, central and eastern region K values are 200% lower than in the rest of Ukraine (Fig. 1). But in the western region Carpathian Mountains stand out with a highly conductive conditions and Zakarpatska district – with the worst conditions in Ukraine.

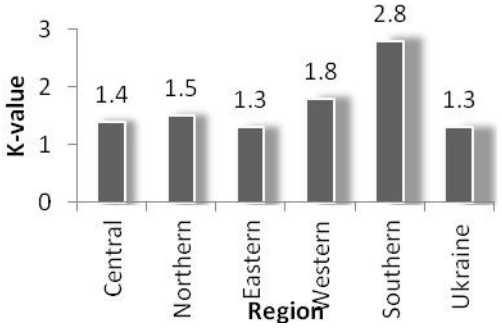

Figure 1. This is the spatial distribution of K.

Meteorological conditions are conducive for atmosphere self-cleaning from the end of winter to the middle of summer. From July to January meteorological conditions in Ukraine are limitedly auspicious. August and October stand out with the worth atmosphere self-cleaning potential (Fig.2).

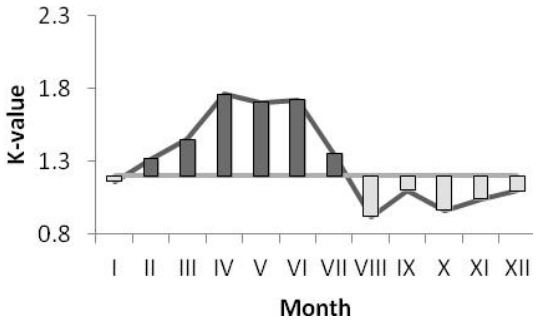

Figure 2. Annual variation of atmosphere's self-clining coefficient.

It's virtually certain that self-cleaning coefficient has tendency to decrease (p-value less than 0.01). During the 1971-2010 the rate of change was 0.1 points per 10 years. The average value of K has decreased from 1.35 in 1971-1990's to 1.15 in 1991-2010. The observed decline is due to changes in the components of atmosphere's self-cleaning climatic potential, but relative contributions from each component are not well determined.

The components of K are number of days with meteorological conditions, which leads to contaminants dissipation: amount of days with total precipitation ≥0.5 mm and amount of days with wind speed ≥6 mps and number of days with meteorological conditions, which leads to contaminants accumulation: frequency of calm and fog.

It's virtually certain that number of days with meteorological conditions, which leads to contaminants dissipation has tendency to decrease. This change is 6 days per 10 years (Fig.3). Also, it's very likely that amount of days with meteorological conditions, which leads to contaminants accumulation are increased.

The rate of change is 2 days per 10 years. So, the rates of change of the K components are not the same: the first is three times greater than second. The impact of each component of K is applied and amplified. Consequently atmosphere self-cleaning ability is getting worthier due to decrease of frequency of conducive for contaminants removal conditions and upward trend in amount of days with non-conducive conditions.

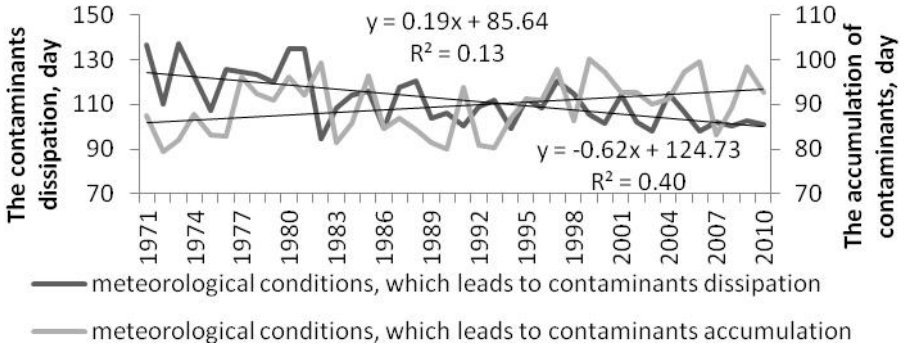

Figure 3. This is the number of days with favorable/unfavorable to the atmosphere's self-cleaning meteorological conditions.

CONCLUSIONS

According to the results of performed analysis meteorological conditions in Ukraine are principally conductive for atmosphere self-cleaning. Spatial distribution of ADA climatic potential is uneven. Western and southern regions have the most conductive conditions. In the western region Carpathian Mountains stand out with a highly conductive conditions and Zakarpatska district – with the worst conditions in Ukraine. In the northern, central and eastern region K values are 200% lower than in the rest of Ukraine.

Meteorological conditions are conducive for atmosphere self-cleaning from the end of winter to the middle of summer. From July to January meteorological conditions in Ukraine are limitedly auspicious. August and October stand out with the worth atmosphere self-cleaning potential.

Undoubtedly that atmosphere self-cleaning potential in Ukraine shows a decreasing tendency throughout 1971-2010. Atmosphere self-cleaning ability is getting worthier due to decrease of frequency of conducive for contaminants removal conditions and upward trend in amount of days with non-conducive conditions.

REFERENCES

Christopher B. Field, Visente R Barros, Michael D. Mastrandrea et al. Summary for Policymakers. Climate Change 2013 : The Physical Science Basis : Working Group I Contribution to the Fifth Assessment Report of the Intergovernmental Panel on Climate Change. ed.: Thomas F. Stocker, Dahe Qin, Gian-Kasper Plattner [and other]. – Electronic text data. – 2013. Available at http://www.ipcc.ch/report/ar5/wg1/docs/WGIAR5_SPM_brochure_en.pdf.

Лапина С. Н., Е. А. Полянская, Л. М. Фетисова, Н. А. Фетисова (2008). Способность атмосферы различных районов Саратовской области к самоочищению. Известия Саратов. ун-та. Новая сер. Сер.: Науки о Земле. Т. 8, вып. 2. – С. 8–11.

Малицька Л. В. (2013). Зміна здатності атмосфери до самоочищення як прояв зміни клімату. Наук. часоп. Нац. пед. ун-ту ім. М. П. Драгоманова. Сер. 4, Географія і сучасність / Нац. пед. ун-т ім. М. П. Драгоманова. Вип. 30. – С. 35–44.

Селегей Т. С. (1990) Потенциал рассеивающей способности атмосферы, География и природ. ресурсы, **№ 2**, 132–137.

STUDIES OF ATMOSPHERIC AEROSOL PARTICLES AND IONS FROM MOLECULAR CLUSTERS TO CLOUD DROPLETS

H.E. MANNINEN, K. LEHTIPALO, L.R. AHONEN, J. BACKMAN, S. BUENOSTRO MAZON, X. CHEN, J. DUPLISSY, J. ENROTH, A. FRANCHIN, J. HONG, N. KALIVITIS, J. KANGASLUOMA, J. KONTKANEN, K. LUOMA, J. MIKKILÄ, G. STEINER, R. VÄÄNÄNEN, R. WAGNER, D. WIMMER, T. PETÄJÄ, AND M. KULMALA

Aerosol and Ion Group, Division of Atmospheric Sciences, Department of Physics, University of Helsinki, P.O. Box 64, 00014, Helsinki, Finland.

Keywords: Atmospheric aerosol particles, new particle formation, long-term measurements, continental boundary later.

INTRODUCTION

Aerosols and Ions group at University of Helsinki has a comprehensive long-term experience of ground-level aerosol measurements (https://wiki.helsinki.fi/display/aerosolsions/Aerosols+and+Ions+group). Measurements of ambient aerosol size distributions were started at the SMEAR II station at Hyytiälä, Finland, in January 1996, and have been on-going since then. We are especially interested in these size distribution data to characterize and parameterize periods of new particle formation and growth (Kulmala et al., 2013). The 16 years of observations in a boreal-forest environment have allowed e.g. a trend analysis in atmospheric new particle formation (Nieminen et al. 2014) and a study on terrestrial climate feedback mechanisms (Kulmala et al. 2014).

Secondary formation of atmospheric aerosol particles, so-called new particle formation (NPF), is believed to be the dominant source of aerosol particles in the atmosphere. Recent research has shown that secondary organic aerosols are major contributors to ultrafine particle growth to climatically relevant sizes, increasing global cloud condensation nuclei (CCN) concentrations within the continental boundary layer (CBL). Nucleation is a process of gas-to-particle conversion, beginning with a few gas molecules colliding to form a cluster of 1-2 nm in diameter (Kulmala et al., 2013). This first step of NPF is followed by the growth of the newly formed particles. NPF is a frequent phenomenon in the lower atmosphere. Recent development in the aerosol instrumentation to measure the critical particle size below 3 nm in size has enabled the direct detection of the newly formed particles connecting the gas and particle phases (Kulmala *et al.*, 2012).

At this moment, the mechanisms of particle formation and the vapours participating in this process are not truly understood. Especially, in which part of the atmosphere the NPF takes place and which are the triggering chemical compounds, is still an open question. Until now, there exists only a few atmospheric dataset measured in lower troposphere over the Northern boreal forests. Our aim is to supplement the on-ground measurements with airborne measurements to cover the cryosphere-aerosol-cloud-climate interactions within the planetary boundary layer (PBL). The PBL is chemically and physically the most dynamic part of the atmosphere as it has high loading of aerosol particles and their gaseous precursors.

IMPORTANCE OF THE MEASUREMENT NETWORKS, INFRASTRUCTURE AND PROTOCOL DEVELOPMENT

Atmospheric NPF happens frequently in many kinds of environments (Kulmala et al., 2004; Manninen et al, 2011). In addition to our long-term measurements at the SMEARII field site at Hyytiälä, Finland. We

have field measurements in different locations (Hirsikko et al., 2009). The participation into measurement networks improve the data quality and inter-comparison, and also makes it possible to investigate e.g. atmospheric aerosol particle dynamics in a boreal forest zone in northern Scandinavia. Väänenen et al. (2013) used aerosol number size distribution data measured at three stations (Värriö, Pallas and Abisko), and combined these data with the HYSPLIT (Hybrid Single Particle Lagrangian Integrated Trajectory) air mass trajectory analysis. They aimed to answer scientific questions: i) Are there fundamental aerosol dynamical differences (sources and sinks) between air masses entering the different stations, or in air transported between the different station pairs? and ii) Does the west-to-east air mass transport differ from the east-to-west transport in any observable way?

During last 12 months, our abroad field measurement campaigns have been performed e.g. at Jungfraujoch High Alpine Research station, Switzerland, at Amazon rainforest within the GoAmazon project (T3, Manaus, Brazil), at Aboa site in Antarctica, and at High Mountain site in Nepal. In Finland, at Hyytiälä in connection with the BAECC campaign we have added to ground level (inside canopy) measurements a new 35-meter high tower (above canopy), and we had flight campaign above Southern Finland with a CESSNA measurement airplane to study the vertical and horizontal extent of new particle formation. We are also actively participating into infrastructure and protocol development (e.g. ACTRIS FP7-project).

ADVANCES IN UNDERSTANDING ATMOSPHERIC FORMATION AND GROWTH IN THE LOWER ATMOSPHERE

Within PEGASOS FP7-project, we measured the chemical and physical processes within the PBL to detect directly the very first steps of NPF in the atmosphere. These measurements of the vertical and the horizontal extension of NPF events were performed using an instrumented airship, Zeppelin. The vertical profile measurements (altitudes up to 1 km) represent the particle and gas concentrations in the lower parts of the atmosphere: the residual layer, the nocturnal boundary layer, and the PBL. At the same time, the ground based measurements records present conditions in the surface layer. Horizontal, almost Lagrangian, experiments are possible as the airship drifts with the air mass. The main nucleation campaigns were performed in Po Valley, Northern Italy (Summer 2012), and Hyytiälä, Southern Finland (Spring 2013).

The key instruments on-board Zeppelin to measure the onset of NPF were Atmospheric Pressure interface Time-Of-Flight mass spectrometer (APi-TOF), a Particle Size Magnifier (PSM), and a Neutral cluster and Air Ion Spectrometer (NAIS). Instruments are described in more detailed in Kulmala *et al*. (2013) and reference therein. These instruments are able to measure particles at the size range ~1-2 nm where atmospheric nucleation and cluster activation takes place. The high time resolution of the instruments allowed us to observe the starting time, location and altitude of the NPF. These measurements are part of the PEGASOS project, an European collaboration project, which aims to quantify the magnitude of regional to global feedbacks between the atmospheric chemistry and physics, and thus quantify the changing climate. The Zeppelin flights are observing radicals, trace gases, and aerosols inside the lower troposphere over Europe.

We have used also a small Cessna 172 one-engine aircraft with slow velocity (air velocity around 130 km/h) operating between altitudes of 300 m and 3.5 km (Schobesberger *et al*., 2013). The Cessna flight campaigns have been on-going since spring 2010 (Leino et al., 2014; Virkkula et al., 2014). We measured vertical profiles up to 3.5 km above the countryside of Southern Finland which is patched with boreal forests of different ages, mires, small lakes, and cultivated land. The aircraft carries comprehensive instrumentation to measure aerosol particle and trace gas properties, and meteorological parameters. The Cessna can easily reach the free troposphere conditions even when the PBL is fully thermally mixed and fly close to cloud deck to study aerosol-cloud interactions.

ADVANCES IN INTRUMENTAL DEVEPLOMENT AND LABORATORY STUDIES

In the atmosphere, the mechanisms and vapours contributing to the initial aerosol growth after the cluster formation are not completely understood, which is partly because of the lack of instruments capable of measuring atmospheric clusters and particles between 1 and 3 nm. The break-through to measure neutral particles in sub-3 nm size range was made with the PSM (Airmodus A09, Vanhanen *et al.* 2011) which measures particles down to the mobility diameter of about 1 nm. The PSM is a mixing-type CPC, in which the aerosol is turbulently mixed with air saturated with diethylene glycol. The 50% activation diameter of the instrument can be varied between about 1–2 nm in mobility diameter by changing the mixing ratio of the saturator and sample flows.

In addition to the PSM's capabilities, to measure the sub-7 nm growth rates and get the first indirect measurements of the particle chemical composition between 2 and 3 nm, we built a nano Condensation Particle Counter Battery (nano-CPCB, Kangasluoma *et al.*, 2013) which consists of four CPCs optimized for the detection of sub-3 nm particles, using diethylene glycol, water, and butanol as the CPC working fluids. The nano-CPCB was calibrated with seven different test aerosols, and the size, charge and composition dependent response was obtained for each CPC. From the ambient relevant test aerosols, ammonium sulphate and sodium chloride showed a clear preference to water activation, whereas organics showed preference to butanol activation, which is the foundation of obtaining indirect information from atmospheric aerosols. After the calibration, a TSI nano-DMA was integrated to the nano-CPCB, which was then deployed in an intensive field campaign in Hyytiälä in spring 2013.

On the other hand, laboratory experiments in the CLOUD-chamber (Kirkby et al., 2011) can be also used to study the cryosphere-aerosol-cloud interactions. In the forthcoming CLOUD10 (September-December 2015), 46 instruments from 14 institutes will be deployed around the CLOUD-chamber at CERN to study the NPF in controlled conditions; in the CLOUD experiments great efforts have been made to control the chamber conditions including the introduced gases.

ADVANCES IN CONNECTING ATMOSPHERIC ELECTRICITY AND AEROSOL-CLOUD INTERACTIONS

Small ions are part of the atmospheric aerosol spectrum, and in atmospheric sciences study of ion-aerosol interactions is essential. Small ions are small molecular clusters carrying a net electric charge. They are produced by ionisation of molecules in the air. Ion-induced NPF is limited by the ion production rate. The results indicate that particle formation seems to dominate over ion-mediated mechanisms, at least in the boreal forest conditions.

Atmospheric ions play an important role in the fair weather electricity. Atmosphere's fair weather condition concerns the electric field and the electric current in the air as well as the air conductivity. On the other hand, atmospheric ions are important for Earth's climate, due to their potential role in secondary aerosol formation. This can lead to increased number of cloud condensation nuclei (CCN), which in turn can change the cloud properties. Our aim is to quantify the connections between these two important roles of air ions based on field observations and existing data archives. We studied the interactions between atmospheric electricity (air conductivity, electric field, and ambient concentration of small ions), aerosol particles, and cloud properties. In other words, the correlations and trends in atmospheric ionization, electricity, aerosols, and CCN properties were studied.

OUTLOOK

Within our group, the recent advances have been obtained after collaborative research efforts between laboratory experiments and comprehensive field observations. Thus, the long-term field observations and detailed laboratory and field campaigns are both needed in the future to characterize the cryosphere-aerosol-cloud-climate interactions. The air quality and climate interactions are not neglected. And our measurements are part of international measurement networks e.g. SMEAR, WMO-GAW, NOAA and ACTRIS.

ACKNOWLEDGEMENTS

This research is supported by European Commission under the Framework Programme 7 (PEGASOS, FP7-ENV-2010-265148), the European Union Seventh Framework Programme (ACTRIS, FP7/2007-2013) under grant agreement n° 262254, the Academy of Finland Centre of Excellence program (project no. 1118615 and 272041), Academy of Finland Project (139656), the Nordic Centers of Excellence CRAICC, Maj and Tor Nessling Foundation, the Eurostars Programme under contract no. E!6911, and Nordic Centre of Excellence CRAICC (CRyosphere–Atmosphere Interactions in Changing Climate). International team of scientists and technicians working with Zeppelin are all acknowledged. The support by the Finnish Cultural Foundation is gratefully acknowledged. In addition, we acknowledge the CLOUD collaboration (FP7 215072), and the ERC-Advanced "ATMNUCLE" grant no. 227463.

REFERENCES

Hirsikko, A.et al. (2011) Atmospheric ions and nucleation: a review of observations, Atmos. Chem. Phys., 11, 767-798.

Leino, K. et al. (2014) Biomass-burning smoke episodes in Finland from eastern European wildfires. Boreal Env. Res. 19 (suppl. B): 275–292.

Kangasluoma, J. et al. (2013) Sub 3 nm Particle Size and Composition Dependent Response of a Nano-CPC Battery, submitted to Atmos. Meas. Tech.

Kirkby, J.et al. (2011) Role of sulphuric acid, ammonia and galactic cosmic rays in atmospheric aerosol nucleation, Nature, 476, 429-U477, 10.1038/nature10343.

Kulmala et al. (2004). Formation and growth rates of ultrafine atmospheric particles: a review of observations. J. Aerosol Sci. 35, 143-176.

Kulmala, M.et al. (2012) Measurement of the nucleation of atmospheric aerosol particles, Nature Protocols 7, 1651-1667, doi:10.1038/nprot.2012.091.

Kulmala M. et al. (2013) Direct observations of atmospheric aerosol nucleation, Science 339, 943–946.

Kulmala M. et al. (2014) CO2-induced terrestrial climate feedback mechanism: From carbon sink to aerosol source and back. Boreal Env. Res. 19 (suppl. B): 122–131.

Manninen H. E. et al. (2010) EUCAARI ion spectrometer measurements at 12 European sites – analysis of new particle formation events, Atmos. Chem. Phys., 10, 7907-7927.

Nieminen, T. et al. (2014): Trends in atmospheric new-particle formation: 16 years of observations in a boreal-forest environment. Boreal Env. Res. 19 (suppl. B): 191–214.

Schobesberger, S.et al. (2013): Airborne measurements over the boreal forest of southern Finland during new particle formation events in 2009 and 2010. Boreal Env. Res. 18: 145–163.

Vanhanen et al. (2011) Particle size magnifier for nano-CN detection. Aerosol Sci. Technol. 45, 533.

Virkkula, A. et al. (2014) Airborne measurements of aerosols and carbon dioxide during a prescribed fire experiment at a boreal forest site. Boreal Env. Res. 19 (suppl. B): 153–181.

Väänänen, R. et al (2013) Analysis of particle size distribution changes between three measurement sites in northern Scandinavia, Atmos. Chem. Phys., 13, 11887-11903.

PATTERNS OF PRIMARY BIOLOGICAL AEROSOL PARTICLES IN BOREAL FOREST

H.E. MANNINEN[1], J. BÄCK[2], S.-L. SIHTO-NISSILÄ[1], J.A. HUFFMANN[3,4], A.-M. PESSI[5], V. HILTUNEN[1], P.P. AALTO[1], P. HARI[2], A. SAARTO[5], M. KULMALA[1] and T. PETÄJÄ[1]

[1]Department of Physics, University of Helsinki, Finland
[2]Department of Forest Ecology, University of Helsinki, Finland
[3]Department of Chemistry and Biochemistry, University of Denver, Colorado, USA
[4]Max Planck Institute for Chemistry, Mainz, Germany
[5]Department of Biology, University of Turku, Finland

Keywords: PRIMARY BIOLOGICAL AEROSOL PARTICLES, BOREAL FOREST.

INTRODUCTION

Pollen and fungal spores are two main classes of primary biological aerosol particles (PBAP) in the atmosphere. They have been observed to be efficient ice nuclei, thus having possible effects on weather and climate. We studied annual variation of airborne pollen and fungal spore concentrations in a boreal forest in Southern Finland during 2003-2004 (Manninen et al., 2014). The pollen grains were categorized into 15 genera and fungal spores into 26 genera, in total representing a majority of higher plant pollen and fungi genera observed in the boreal environment. The highest concentrations of pollen were observed in late spring and early summer, while first pollen observations in February-March were long-range transported from central Europe or Baltic countries. Airborne fungal spores were present during the whole growing season (number concentration in the range 10^4-10^5 m-3), with the highest peak occurring in August-September. The observed annual pattern of fungal spores was similar to that of fluorescent aerosol particles measured in 2010 at the same location with alternative method for the PBAP. Although the annual pattern was similar in both years studied, the concentration levels were significantly different between 2003 and 2004.

Fungal spores constituted the largest fraction of observed PBAP numbers (~99%), whereas pollen showed a higher relative mass fraction (~97%) of PBAP. We estimated the contribution of pollen and spores to be about 65% of the observed total particle mass during the growing season (average pollen and spore mass 5.9 and 0.4 μg m-3, respectively, in respect to total PM mass 9.9 μg m-3), but the effect on total particle number was negligible. In addition, the correlations with meteorological parameters were studied. These results provide species-specific information on pollen and fungal spore concentrations in boreal forest on an annual scale and show the high relative importance of PBAP to coarse atmospheric particles (appox. 65% by mass). Atmospheric quantities of PBAP have been poorly constrained, and the high fraction of biological particles discussed here suggests that biological material may be important for complex atmospheric processes such as the formation and evolution of ice clouds and precipitation.

METHODS

Pollen and fungal spores were collected throughout the pollen season from March to September (October) using a Hirst-type volumetric spore trap (Burkard Manufacturing Co. Ltd.), which is the European standard sampling method for airborne pollen and spores (EAN, European Aeroallergen Network). The Burkard samples were examined by light microscopy, where the pollen counting method was a random sampling of microscopic fields (longitudinal and latitudinal transects). The pollen and spore count was normalised for the counted surface area and the number was reported as pollen grains per volume of air (m-3). The measurements were performed at SMEAR II (Station for Measuring Forest Ecosystem-

Atmosphere Relations II) station located in Hyytiälä, Southern Finland (61°51'N, 24°17'E, 181 asl). Coniferous and mixed coniferous-deciduous forests account for over 65% of the region surrounding Hyytiälä within a 50-km scale radius. Previously, Schumacher et al. (2013) reported year-round measurements of PBAP at Hyytiälä, using a laser-induced-fluorescence (LIF) method and a portion of these data will be shown for comparison here (Fig. 1).

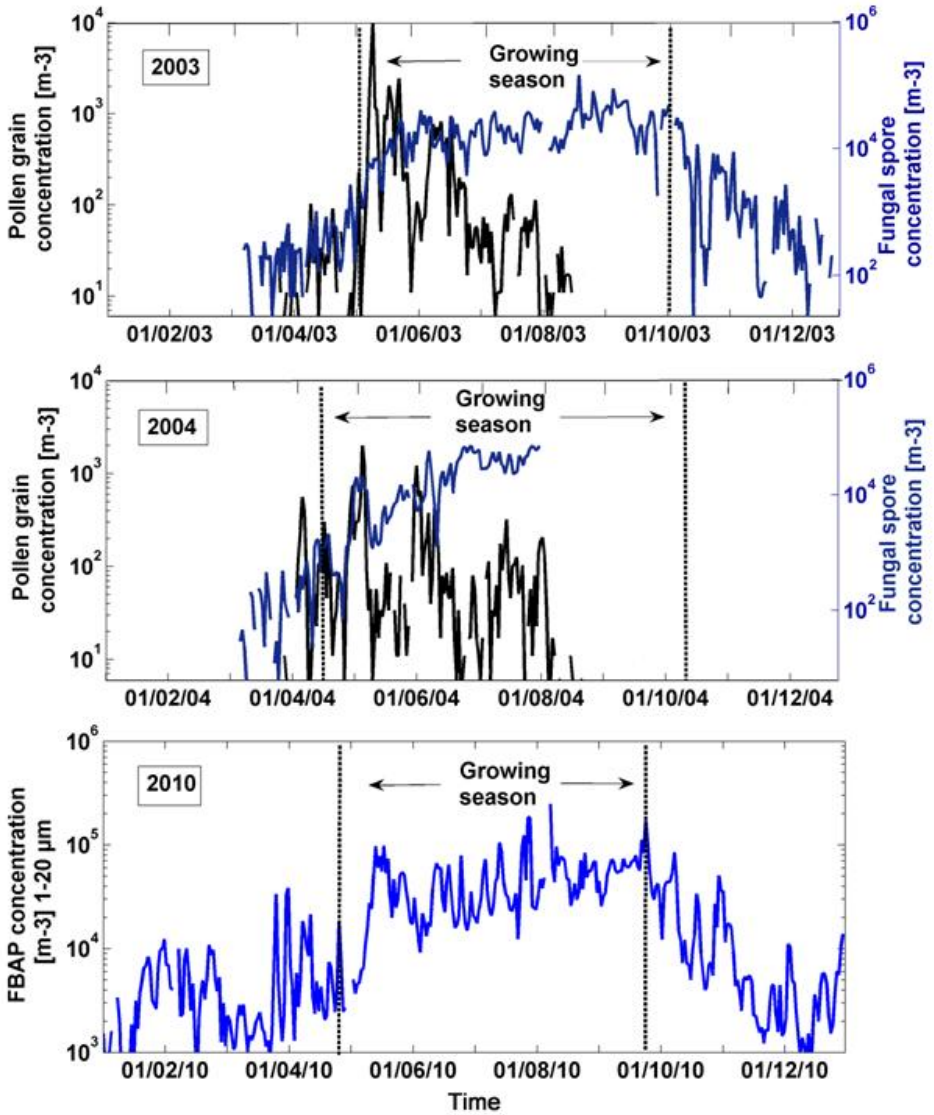

Figure 1. Annual pattern of airborne pollen and fungal spores (daily sum, number of grains in m^3, log scale) in Hyytiälä 2003-2004 measured with Burkard spore trap and 2010 with LIF method.

Further, the relationships between pollen and spore concentrations and basic meteorological parameters were characterized.

RESULTS AND CONCLUSIONS

The presence of wind-pollinated pollen follows a clear seasonal pattern in response to the flowering seasons of the source plant. Although, the pattern on different years is the same, pollen concentration levels can vary greatly (Fig. 1). In boreal forest the highest atmospheric concentrations of pollen are observed on May and June (~10^3-10^4 m-3). The highest peak in airborne spore concentrations is later in August and September (~10^4-10^5 m-3). Meteorological variables, especially air temperature, were observed to correlate with fungal spore number concentrations. Fungal spores are an "ever-present"

component of the air, while pollen is observed only on spring-summer. The pollen season for each individual species can shift slightly depending on meteorological variables. The boreal forest surrounding Hyytiälä site is typical for Southern Finland, still it should be noted that seasonal variations of airborne pollen and fungal spores in different parts of boreal forest area can be significant. The characteristics of pollen and spore season are shown in Table 1. On the peak PBAP concentration days the concentrations can be extremely high.

		Pollen grain		Fungal spores	
		2003	2004	2003	2004*
Season duration					
	Growing season	4.5.-2.10.	4.5.-2.10.	4.5.-2.10.	4.5.-2.10.
	Pollunation season	23.3.-26.8.	10.3.-28.9.	9.3.-21.10.	3.3.->*
PBAP peaks and cumulative concs					
	Maximum total count (grains m^{-3})	9741	2013	145612	72074
	Day of highest peak	13.5.	8.5.	23.8.	1.7.
	Cumulative annual sum (Σ grains m^{-3})	40870	18025	3713792	>2572449
	Season length days	156	200	266	>154

*Pollen was examined for 7.3.-29.8.2003 and 2.3.-30.9.2004 including the complete pollination season for both years, whereas the spores were analysed 6.3.-31.12.2003 and 3.3.-4.8.2004.

Table 1. Characterization of wind-dispersed pollen grain and fungal spore seasons in 2003-2004 with respect to growing season duration.

Among PBAP classes observed at Hyytiälä, fungal spores dominated the PBAP particle number, but the pollen was more pronounced in particle mass. Using the cumulative annual pollen and fungal spore number concentrations presented by Manninen et al. (2014), fungal spores represent ~99% and pollen ~1% of total PBAP number. On the other hand, the cumulative annual pollen and fungal spore mass concentrations show that pollen represents ~93% and fungal spores ~7% of total PBAP mass. Assuming pollen grain size according to Pöhlker et al. (2013) and http://www.polleninfo.org, spore size of 3.0 µm (aerodynamic diameter e.g. Jacobson and Streets 2009, Hussein et al. 2013, Schumacher et al. 2013), and a pollen and spore particles spherical with density of 1.4 and 1.2 g cm-3 (Reponen et al. 1995, Jacobson and Streets 2009), respectively, one can calculate an order-of-magnitude cumulative particle mass contribution from PBAP in 2003. Doing this shows a daily mean 6.3 µg m-3 mass of these PBAP classes during the pollen season (5.9 and 0.4 µg m-3 for pollen and spores, respectively). This corresponds to an average mass fraction of 65% with respect to the total PM mass (again 60% and 5% for pollen and spores, respectively). Thus, numbers reported here are in good agreement with previous reports, but detailed numbers from the Boreal region had not been previously reported.

Most of the spore plume observations were observed on rainless days with only moderate temperature and wind speeds, but during intense rain episodes increased number concentration of spores was detected. The relationship between pollen grains and meteorological variables showed no clear dependence when looking at daily means.

DISCUSSION

Pollen and fungal spores can be transported over long distances due to their ability to remain aerodynamically buoyant, forestalling their deposition either due to gravity, wash out by rain, or impaction on terrestrial surfaces. Bioaerosols have been observed to be transported several kilometres vertically up

in the troposphere, where they can influence the cloud formation. The changing climate enhances the strong air currents, which might lead to more significant long-range transport of the biological particles. Recently, classes of biological particles, including fungal spores and pollen, have been studied in great detail due to their enhanced activity as ice nuclei. Airborne PBAP may contribute significantly to atmospheric processes of the formation and evolution of ice clouds and precipitation. The high fraction of PBAP in the coarse mode presented here suggests that PBAP is an important component of natural aerosol in the Boreal region that should be considered when modelling cloud and precipitation effects.

ACKNOWLEDGEMENTS

This research is supported by the Academy of Finland Centre of Excellence program FCoE (project no. 272041 and 1118615), the EU FP7 project PEGASOS (project no. 265148), the EU FP7 project BACCHUS (project no. 603445), the EU FP7 ERC-Advanced 'ATMNUCLE' grant no. 227463, the BAECC project funded by U.S. Department of Energy.

REFERENCES

Hussein, T., Norros, V., Hakala, J., Petaja, T., Aalto, P. P., Rannik, U., Vesala, T. & Ovaskainen, O. 2013. Species traits and inertial deposition of fungal spores. *J. Aerosol. Sci.* 61: 81-98.

Jacobson, M. Z. and Streets, D. G. 2009. Influence of future anthropogenic emissions on climate, natural emissions, and air quality. *J. Geophys. Res. Atmos.* 114: D08118.

Manninen, H. E., Bäck, J., Sihto-Nissilä, S.-L., Huffman, J. A., Pessi, A.-M., Hiltunen, V., Aalto, P. P., Hidalgo, P. J., Hari, P., Saarto, A., Kulmala, M. & Petäjä, T.: Patterns in airborne pollen and other primary biological aerosol particles (PBAP), and their contribution to aerosol mass and number in a boreal forest. *Boreal Env. Res.* 19 (suppl. B): 383–405, 2014.

Reponen, T. 1995. Aerodynamic diameters and respiratory deposition estimates of viable fungal particles in mold problem dwellings. *Aerosol Sci. Technol.* 22: 11-23.

Schumacher, C. J., Pöhlker, C., Aalto, P., Hiltunen, V., Petäjä, T., Kulmala, M., Pöschl, U., & Huffman, J. A. 2013. Seasonal cycles of fluorescent biological aerosol particles in boreal and semi-arid forests of Finland and Colorado. *Atmos. Chem. Phys.* 13: 11987-12001.

LIGHTNING ACTIVITY IN THE CHANGING CLIMATE: AEROSOL SIGNIFICANCE

E.A. MAREEV[1,2], E.M. VOLODIN[3], N.V. ILIN[1] and S.O. DEMENTYEVA[1]

[1]Institute of Applied Physics, Russian Academy of Science, 46 Ulyanov str., 603 950 Nizhny Novgorod, Russian Federation.

[2]Lobachevsky State University of Nizhny Novgorod, 23 Gagarin av., 603950 Russian Federation.

[3]Institute of Numerical Mathematics, Russian Academy of Science, 8 Gubkin str., 119991 Moscow, Russian Federation.

Keywords: LIGHTNING, AEROSOL, THUNDERSTORM, GCM, WRF, GLOBAL CHANGE.

INTRODUCTION

It is well known that lightning plays an important role in atmospheric chemistry and in the initiation of wildfires. Moreover, the mean global flash rate and the ionospheric potential can serve as global indices relating the state of the global electric circuit to the planetary climate (e.g., Williams and Mareev, 2014). But the impact of global warming on lightning rates is still poorly constrained (e.g., Romps et al., 2014). One of the main problems in this connection is related to the role of different factors on the lightning activity and thunderstorm electrification. There is a great interest particularly to the aerosol influence onto the development of thunderstorm clouds and its significance as compared to the thermodynamic conditions, such as CAPE variation (e.g., Kalina et al., 2014; Mansell and Ziegler, 2013; Yair et al., 2010). These questions are closely related also to the fundamental problems of a big difference in lightning flash rate between the land and ocean, impact of aerosols on precipitation, possible urban effects on lightning activity, and possible mechanisms of Solar activity impact on weather and climate.

METHODS

Our strategy is to use mesoscale models for the study of different mechanisms of a possible influence on electrical processes in deep convection and clouds and derive their respective parameterizations (Dementyeva et al., 2015), and on the other hand, to use these parameterizations in global climate models to estimate future trends of lightning activity (Mareev and Volodin, 2015). We use WRF model for the analysis of the lightning activity indices and electric field. Parameterizations of cloud mycrophysics available in WRF allowed us to study several hypothesis on the aerosol influence on thunderstorm electrification. On the other hand, we use a high-resolution GCM of the atmosphere and ocean INMCM4.0 for modeling the GEC evolution and lightning flash rate. The main characteristics of this model are as follows: the atmosphere is divided into 2°×1.5° cells in longitude and latitude with 21 levels; the ocean is divided into 1° ×0.5° cells in longitude and latitude with 40 levels; the coupling without flux adjustment is assumed.

CONCLUSIONS

The modern distribution of lightning over the globe has been reproduced by the climate model INMCM4.0. In the model the simulation of lightning activity has been carried out using the well-known parameterization by Price and Rind (Price and Rind, 1992). In general, the flash rate obtained in the model for the modern climate as the mean over 2001–2010 is close to that presently observed on satellites, while in Africa it is slightly underestimated whereas in Indonesia, slightly overestimated. The mean flash rate over the globe in the model equals about 60 fl/s, which corresponds rather well to modern estimates based

on satellite data. Using the same parameterizations for the lightning flash rate in the 21st century, it was found that the mean flash rate is increasing by about 20% during the century (from 60 to 72 fl/s) while the global warming is about 2.5 degrees for the scenario RCP 8.5 (Representative Concentration Pathway 8.5 Wm^{-2}). It is interesting that at the same time numerical simulations suggest the ionospheric potential decrease with the global warming by about 10% during the 21st century if the RCP 8.5 scenario is assumed. Inter-annual variability of the ionospheric potential is low and does not exceed 1% of the mean value. It should be emphasized, however, that it is tightly correlated with the mean sea surface temperature in the Pacific ocean (El Niño area). Significant differences in the lightning flash rates over the land and the ocean may be explained at least partially by the strong difference of aerosol concentrations over these areas.

Test example simulations with the WRF model have demonstrated substantial influence of aerosol on a test cell development including updraft invigoration and delay of precipitation, whereby affecting the electric field rate and lightning activity. Possible implications of these effects in GCM simulations and respective parameterizations are discussed.

ACKNOWLEDGEMENTS

This work was supported by grants from the Russian Government (contract No. 14.B25.31.0023 and contract No. 11.G34.31.0048).

REFERENCES

Dementyeva, S.O., N.V. Ilin, and E.A. Mareev (2015). Calculation of the lightning potential index and electric field in the numerical weather prediction models, *Izv. Atmos. Ocean. Phys.* **55** (1) (accepted).

Kalina, E.A., K. Friedrich, H. Morrison, and G. H. Bryan (2014). Aerosol Effects on Idealized Supercell Thunderstorms in Different Environments, *J. Atmos. Sci*. **71**, 4558–4580.

Mansell, E. R. and C. L. Ziegler (2013). Aerosol Effects on Simulated Storm Electrification and Precipitation in a Two-Moment Bulk Microphysics Model, *J. Atmos. Sci*. **70**, 2032–2050.

Mareev, E.A. and E.M. Volodin (2015). Variation of the Global Electric Circuit and Ionospheric Potential in a General Circulation Model, *Geophys. Res. Lett.* (accepted).

Price, C. and D. Rind (1992). A simple lightning parameterization for calculating global lightning distributions, *J. Geophys. Res*. **97** (D9), 9919–9933, doi:10.1029/92JD00719.

Romps, D. M., J. T. Seeley, D. Vollaro, and J. Molinary (2014). Projected increase in lightning strikes in the United States due to global warming, *Science*, **346** (6211), 851–854, doi:10.1126/science.1259100.

Williams, E. and E. Mareev (2014). Recent progress on the global electrical circuit, *Atmospheric Research* **135–136**, 208–227, doi:10.1016/j.atmosres.2013.05.015.

Yair, Y., B. Lynn, C. Price, V. Kotroni, K. Lagouvardos, E. Morin, A. Mugnai and M. del Carmen Llasat (2010). Predicting the potential for lightning activity in mediterranean storms based on the weather research and forecasting (WRF) model dynamic and microphysical fields, *J. Geophys. Res*. **115** (D4), D04205.

ENVIRONMENTAL AND CLIMATIC CHANGES IN EURASIA (EUROPEAN RUSSIA BEING EXEMPLIFIED) AND INTERNATIONAL ECOLOGICAL CO-OPERATION

G.G. MATISHOV

Southern Scientific Centre, Russian Academy of Sciences, Rostov-on-Don, Russia

Keywords: climate, ecosystem, Holocene, periglacial

The Earth's climate changes continuously in time. The character of climate's evolution is partially determined by natural reasons and conditions, such as variations of the Earth's orbit parameters, as well as there are changes of the components of meteorological regime and long-term changes, which characterize the fluctuations of climate. Of certain impact is human activity.

The ecosystems of seas of the Northern Hemisphere are rather young in geological relation and are in the process of constant development in conformity with the global variability of climate and anthropogenic impact. To understand paleoclimate it is important to possess the knowledge about the development of the global climatic zones. The outlines, sizes, and conditions of the tropic and bipolar belts changed under the influence of the global climatic fluctuations. During the warming period, the latitudinal gradients of temperatures decreased, the width of tropic belt increased, and during the cooling periods the reversible situation was observed. The belt of oceanic periglacial existed outside the limits of continental glaciations. Mud-streams, originated during the melting of ice-shields of Scandinavia, Iceland, Greenland, Canada, flowed through the continental slope, covering it with a dense net, to the abyssal plains. Vast Scandinavian glacier started to melt 14 thousand years ago. Part of the runoff of thawed water entered the Caspian Sea and the Azov-Black Sea basin along the Volga, Don, and the Dnieper. The Late Holocene had a complex rhythmic pattern of natural processes and included the periods of both warming and cooling. This is especially true for the last millennium, within which the Little Ice Age (AD 1400-1700) and the Medieval Climate Optimum (AD 950-1250) may be distinguished in different regions of the Northern Hemisphere.

A certain series of paleontological methods is applied to reconstruct the climate of various chronological slices of the Pleistocene and Holocene. The Sea of Azov, being a large estuarine water body, is a perfect object to study paleoclimate. In the beginning of the Holocene, the Sea of Azov started to form as an independent sea basin, in which the Old Azov and Novoazov (New Azov) layers are distinguished. A vast amount of research data has been accumulated by the institutes of the Russian Academy of Sciences, allowing studying the specific geomorphologic features and stratigraphy of the Novoazov sediments in detail, determining the mean Novoazov sedimentation rates, distinguishing the main regularities of distribution of pollen and diatom algae. Marine sediments, accumulated within the Sea of Azov, contain information both about the changes in the physical-geographical conditions of the coast and overall the South of the East European Plain. And the study of paleo-soils is significant for the restoration of fertility of the current steppe Chernozem (black dirt). As a result, it is possible to conclude that the general trend towards aridization of climate, covering the entire South of the East European Plain, during the Subboreal and Subatlantic periods of the Holocene was not continuous. Minimum three periods with much more humid conditions were identified in the spore-pollen spectra of marine sediments, each of them lasted for several hundred years: during the Late Subboreal, Mid Subatlantic, and during the Little Ice Age.

The intercommunication of an organism and the environment is a complicated complex of interrelations, that is why the progress in ecological studies and current research may be achieved only on condition there is a synthesis of several research directions and efforts of researchers from various countries.

ACKNOWLEDGEMENTS

The abstract was translated from Russian into English by R.G. Mikhalyuk.

REFERENCES

Levitus, S., G. Matishov, D. Seidov and I. Smolyar (2009). Barents Sea multi-decadal variability. *Geophysical Research Letters* **36**, 19

Matishov, G.G. (1984). *Dno okeana v lednikovyi period (The Ocean Bed during the Ice Period)* (Nauka, Leningrad, USSR) (in Russian)

Matishov, G.G. (1987). *Mirovoi okean i oledenenie Zemli (The World Ocean and the Glaciation of the Earth)* (Mysl, Moscow, USSR) (in Russian)

SPATIAL AND TEMPORAL VARIABILITY OF CO_2 AND CH_4 MIXING RATIOS IN THE ATMOSPHERIC SURFACE LAYER OVER WEST SIBERIA

B. D. BELAN[1], D. K. DAVYDOV[1], A. V. FOFONOV[1], G. INOUE[2], O. A. KRASNOV[1], T. MACHIDA[2], SH. MAKSYUTOV[2], G.G.MATVIENKO[1], M. SASAKAWA[2] and M.YU. ARSHINOV[1]

[1]V.E. Zuev Institute of Atmospheric Optics, Siberian Branch, Russian Academy of Sciences, Tomsk, Russia.

[2]National Institute for Environmental Studies, Tsukuba, Japan.

Keywords: GREENHOUSE GAS, CARBON DIOXIDE, METHANE

INTRODUCTION

The investigation of greenhouse gas variability in the atmosphere plays one of the key roles when estimating global climate changes. In this connection, of particular importance is the study of trace gas source and sink distribution in the atmospheric surface layer over different locations of the globe (Apadula et al., 2003). About 65% of Russia's territory consists of vast areas with undisturbed or weakly disturbed ecological systems. At the same time, there is a huge lack in any data on the chemical composition of its air shed.

As is well known that apart from the long-term trend, the atmospheric CO_2 and CH_4 mixing ratios have seasonal cycles. Short-term fluctuations, which reflect the influence of regional sources and sinks, can contribute to the global GHG content (Kowalski and Serrano-Ortiz, 2007; Nilsson et al., 2007; Saeki et al., 2013; Sasakawa et al., 2013). Analysis of the GHG spatial distributions makes it possible to determine such fluctuations and evaluate the contribution made by individual regions to the global carbon cycle.

In order to fill up the gap in data on GHG distribution over West Siberia, the JR-STATION (Japan-Russia Siberian Tall Tower Inland Observation Network) network has been established in recent years under rhe Joint Japanese-Russian Project in the framework of the International Geosphere-Biosphere Programme (IGBP). Stations are equipped with instrumentation to measure continuously CO_2 and CH_4 concentrations and meteorological parameters as well. A description of this network can be found in Sasakawa et al. (2010).

The first station of the network was put into operation in 2002, and the last one in June 2008. So, measurement periods at each site differ. In this paper we present the greenhouse gas monitoring data obtained to date that enabled a spatial and temporal distribution of CO_2 and CH_4 in the West Siberian atmospheric surface layer to be derived.

MEASUREMENT RESULTS AND DISCUSSION

Since the measurement series differ, here we will present only analysis of the long-term variations of the CO_2 and CH_4 concentrations, and spatial distributions will be given in monthly mean values calculated for the major seasons of the year.

The 10-day moving mean values of the carbon dioxide and methane concentrations for the entire period of measurements are shown in Figures 1 and 2. Analysis of the obtained data shows that the average increase of CO_2 mixing ratio ranged between 1.95 and 2.53 ppm per year, depending on the site location.

The analysis of long-term data revealed an increase of CH_4 concentration within 3.2 – 7.2 ppb per year.

The network distributed in the large area makes it possible to study not only the temporal variability of CO_2 and CH_4 at each site and determine the spatial differences between the concentrations by comparing the data, but also enables to plot the distribution charts for different time periods. The examples of these charts are presented in Fig. 3.

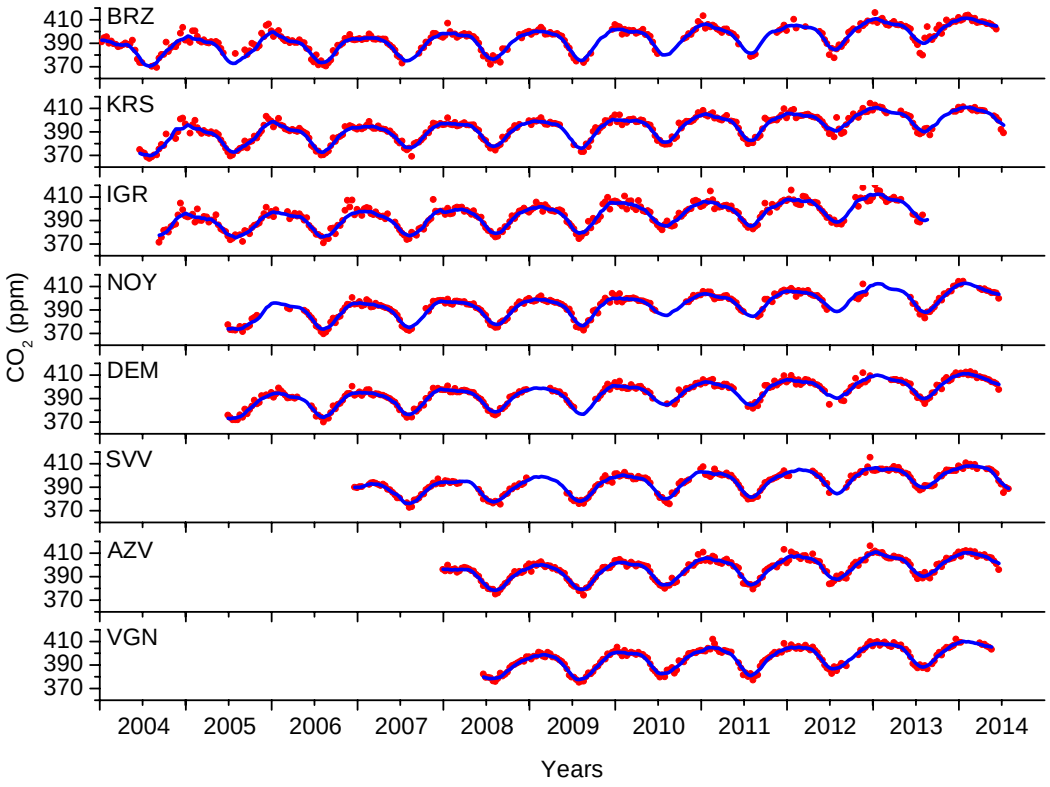

Figure 1. Long-term 10-day means of CO_2 mixing ratio observed at different sites of West Siberia..

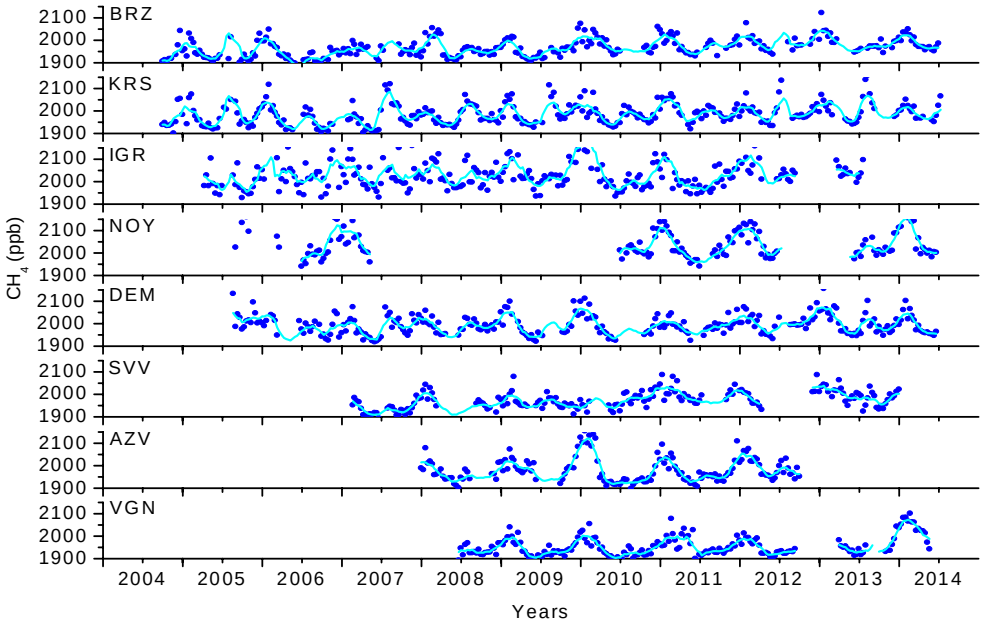

Figure 2. Long-term 10-day means of CH_4 mixing ratio observed at different sites of West Siberia.

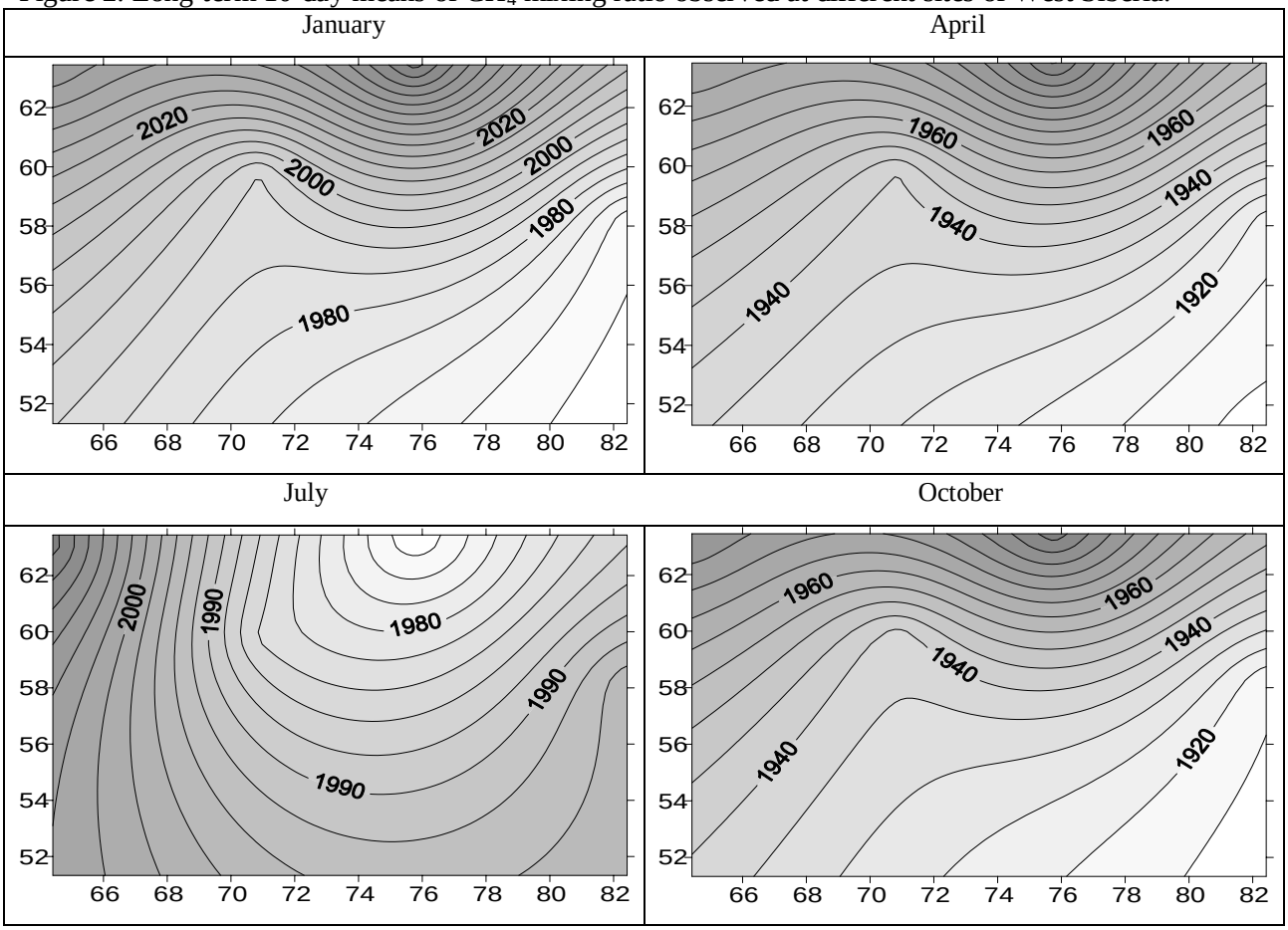

Figure 3. Average space distribution of CH_4 in the atmospheric surface layer over West Siberia observed during different seasons.

ACKNOWLEDGEMENTS

This work was supported by Presidium of the Russian Academy of Sciences (Program No. 4), the Branch of Geology, Geophysics and Mining Sciences of RAS (Program No. 5); interdisciplinary integration projects of the Siberian Branch of the Russian Academy of Science No. 35, No. 70 and No. 131; State contracts of the Ministry of Education and Science of Russia No. 14.604.21.0100, (RFMTFIBBB210290) and No. 14.613.21.0013 (RFMEFI61314X0013); and Russian Foundation for Basic Research (grants No. 14-05-00526, No. 14-05-00590, No. 14-05-93108).

REFERENCES

Apadula, F., Gotti, A., Pigini, A., Longhetto, A., Rocchetti, F., Cassardo, C., Ferrarese, S., Forza, R. (2003). Localization of source and sink regions of carbon dioxide through the method of the synoptic air trajectory statistics, *Atmos. Environ.* **37**, 3757–3770.

Kowalski, A. S. and Serrano-Ortiz P. (2007). On the Relationship between the Eddy Covariance, the Turbulent Flux, and Surface Exchange for a Trace Gas Such as CO_2, *Boundary-Layer Meteorol*. **127**, 129–141.

Nilsson, S., Shvidenko, A., Jonas, M., McCallum, I., Thomson, A., Balzter, H. (2007) Uncertainties of a Regional Terrestrial Biota Full Carbon Account: A Systems Analysis, *Water Air Soil Pollut: Focus* **7**, 425-441.

Saeki, T., Maksyutov, S., Sasakawa, M., Machida, T., Arshinov, M., Tans, P., Conway, T. J., Saito, M., Valsala, V., Oda, T., Andres, R. J., Belikov, D. (2013), Carbon flux estimation for Siberia by inverse modeling constrained by aircraft and tower CO_2 measurements, *J. Geophys. Res.* **D 118**, doi:10.1002/jgrd.50127.

Sasakawa, M., Shimoyama, K., Machida, T., Tsuda, N., Suto, H., Arshinov, M., Davidov, D., Fofonov, A., Krasnov, O., Saeki, T., Koyama, Y., Maksyutov, S. (2010) Continuous Measurement of Methane Concentration using 9-tower Network over Siberia, *Tellus B*. 2010. **62**, 403-416.

Sasakawa, M., Machida, T., Tsuda, N., Arshinov, M., Davydov, D., Fofonov, A. and Krasnov, O. (2013). Aircraft and tower measurements of CO_2 concentration in the planetary boundary layer and the lower free troposphere over southern taiga in West Siberia: Long-term records from 2002 to 2011, *J. Geophys. Res.* **D 118**, doi:10.1002/jgrd.50755.

NOCTURNAL ION-CLUSTER EVENTS: 11 YEARS OF NIGHTIME ION CLUSTERS ACTIVITY IN HYYTIÄLÄ, FINLAND

S. B. MAZON[1], H. MANNINEN[1], T. NIEMINEN[1], J. KONTKANEN[1], X. CHEN[1], V.-M. KERMINEN[1] and M. KULMALA[1]

[1]Department of Physics, University of Helsinki, Finland.

Keywords: NIGHTTIME EVENTS, NEW PARTICLE FORMATION, ATMOSPHERIC IONS, AEROSOLS.

INTRODUCTION

New particle formation (NPF) contributes significantly to the total atmospheric particle loading, which in turn has significant health and climatic implications. The common practise when identifying NPF events is by analysing a 1-day size distribution (Kulmala et al. 2012), which means the focus is normally given to the morning hours and early afternoon, when photochemical oxidation takes place. However, there are indications of night-time particle formation, such as the study by Wiedensohler et al. (1997) where an ultrafine mode of 5 to 15 nm was observed during midnight–early morning hours downhill to an orographic cloud. Suni et al. (2008) reported 'nocturnal aerosol formation' in the Eucalyptus forest of Tumbarumba, Australia, with 32% of their analysed nights presenting cluster (0.8–1.8 nm), intermediate (1.8–7.5 nm) and large (15–40 nm) ions activity. Kalivits et al. (2012) found 'nightime enhanced ion concentrations' at Finokalia, Crete. Junninen et al. (2008) presented a 4 year study (2003–2006) for SMEAR II Station, Hyytiälä, Finland, of the observation and analysis of nocturnal cluster events. Lehtipalo et al. (2011) continued with a deeper analysis of the boreal nocturnal cluster events in Hyytiälä, including neutral (nanometer condensation nuclei, or nano-CN) versus ion cluster comparison, and laboratory flow-tube experiments replicating the condensation of precursor monoterpene vapours as potential sources for the nano-CN. This study investigates 11 year time series (2003–2013) of negative and positive cluster ions (09–3nm) for indication nocturnal cluster activity.

METHODS

Positive and negative ion clusters data from the Balancing Scanning Mobility Analyser (BSMA; Tammet 2014) where analysed visually using 2-day plots, with midnight between Day 1 and Day 2 as the centre of a number size surface plot from ~0.9–7 nm, the positive and negative ion diurnal concentrations for the 0.9–3 nm range, and a corresponding Differential Mobility Particle Sizer (DMPS) surface plot with a cut off size of ~3 nm to, for example compare/identify nucleation mode day time activity (event/nonevent/undefined), possible change in air mass, and mainly, to investigate a possible relation of nocturnal ion cluster activity to NPF. The classification of nocturnal ion events (or 'NIE'), was based on Junninen et al. (2008) classification, although this study uses a higher upper range of cluster size (3nm) in an attempt to differentiate from the continuous smaller ion cluster pool, and accommodate any possible initial growth. Furthermore, the classification focused on a class I, where a NIE was observed <2.5 nm, and class II, where the NIE activity included ions >2.5nm. A night between Day 1 and Day 2 was considered a NIE if the concentration of the selected ion cluster range showed a clear increase, and/or if a 'bump' in cluster size was present in the surface plot. Each polarity was plotted simultaneously but classified independently (ie. a negative NIE could be present simultaneously to a 'nonevent' positive ion night). Additionally, start times where manually selected for each polarity from their respective number concentration plots, which during the classification process served to discriminate from too early ion cluster activity (ie. <~5pm). A nocturnal event date is recorded as the night between Day 1 and 2, even if the event began after midnight (ie. the start day was considered Day 1 + hours after midnight).

RESULTS AND CONCLUSION

A total of 33% of analysed nights where classified as NICE, with the minimum annual frequency during 2008 (~28%) (Fig. 1A). A comparable season variability to Junninen et al. (2008) was observed for both polarities with a peak frequency during April to June, with a peak in May with ~50% of days exhibiting both positive and negative NIE (Fig. 1B). The start, peak, and end times of NIE where investigated; Start times prevailed between 18–21 hours, with an end time spread out throughout the night until the morning of Day 2, in some cases overlapping and blending with a NPF in Day 2.

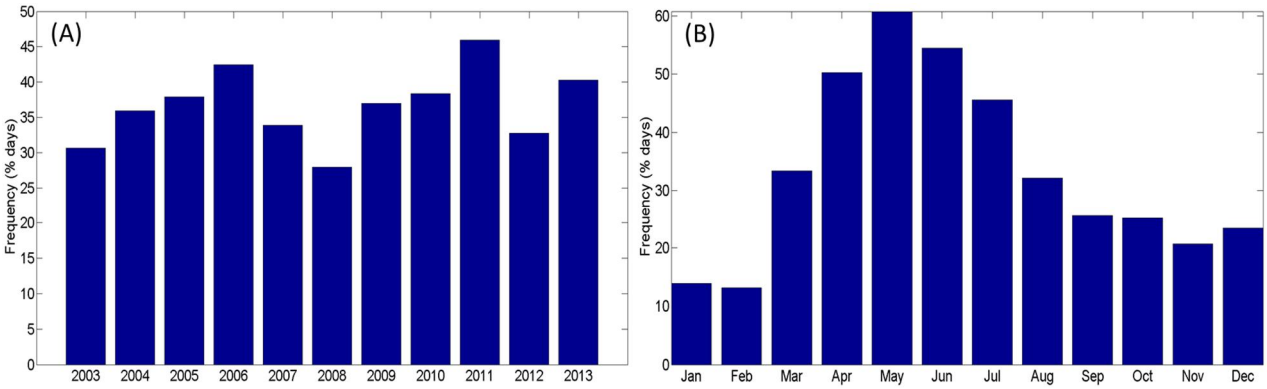

Figure 1. (A) Annual and (B) seasonal distribution of negative nocturnal ion clusters events for 2003–2013 Hyytiälä, Finland.

Median ion concentrations (0.9–3 nm) for both start and end times went from ~700 ions/cm3, rising to a peak median of 1150 ion/cm3 (Fig. 2). An additional observation is an 'M' shape in the ion concentration of NIE days, where the concentration increases during the late evening, decreases around midnight, and increases once again during early morning (4–6 am). A preliminary look at BSMA median concentrations for 2–3 nm ion sizes for NPF event days shows, in addition to the day-time NPF peak, an evening peak around 18–19 hours, suggesting a possible relation of NIE to NPF. Furthermore, out of a total of 930 NPF event days classified within this 11 year period, ~40% of those days presented a NIE during the previous or following night. In some cases, the NIE increased in concentration until overlapping with the NPF in the morning, making it indistinguishable and hinting to a possible participation of those cluster ions in the morning NPF event. It could also hint that both night- and day-time activity have parallel initial process, but night-time faces limiting conditions and is thus supressed.

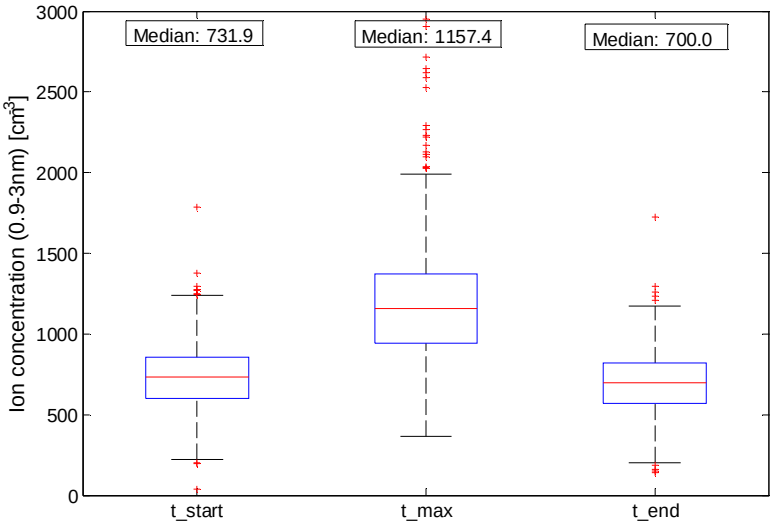

Figure 2. Start-, peak-, and end-time concentrations for negative nocturnal ion clusters events (0.9-3nm), 2003-2013, Hyytiälä, Finland.

Following Peräkylä et al. (2014) findings that night-time monoterpenes concentration and their oxidation rate from ozone correlated significantly to the following day's NPF growth, an analysis needs to be made to identify the multiple possible sources contribution to NIE, including VOC oxidation, in addition to the diurnal radon concentration and nocturnal boundary layer dynamics, to explain the observed night time cluster activity, the evening/morning (~7pm/5am) time bins, and an apparent connection to NPF.

ACKNOWLEDGEMENTS

This study was supported by Academy of Finland Centre of Excellence program (project no. 272041).

REFERENCES

Junninen, H. et al. (2008) Observations on nocturnal growth of atmospheric clusters. *Tellus* **60B**, 365–371

Kalivitis, N. et al. (2012) Night-time enhanced atmospheric ion concentrations in the marine boundary layer. *Atmos. Chem. Phys* 12, 3627–3638

Kulmala, M. et al. (2012) Measurement of the nucleation of atmospheric aerosol particles. *Nat Protoc* **7**, 1651–1667, doi:10.1038/nprot.2012091

Lee, S. et al. (2008) Observations of nighttime new particle formation in the troposphere. *J Geophys Res: Atmos* **113**, D10210

Lehtipalo, K. et al. (2011) Observations of nano-CN in the nocturnal boreal forest. *Aerosol Sci Technol* **45**, 499–509

Peräkylä, O. et al. (2014) Monoterpenes' oxidation capacity and rate over a boreal forest: temporal variation and connection to growth of newly formed particles. *Boreal Environment Research* **19B**, 293–310

Suni, T. et al. (2008) Formation and characteristics of ions and charged aerosol particles in a native Australian Eucalypt forest. *Atmos Chem Phys* **8**, 129–139, doi:10.5194/acp-8-129-2008

Tammet, H. (2006) Continuous scanning of the mobility and size distribution of charged clusters and nanometer particles in atmospheric air and the Balanced Scanning Mobility Analyzer BSMA. *Atmos Res* **82**, 523–535.

Wiedensohler, A (1997) Night-time formation and occurrence of new particles associated with orographic clouds. *Atmos Environ* **31**, 2545–2559

SNOW-ALBEDO FEEDBACK AFFECTED BY BC AND CONNECTED TO VEGETATION PHOTOSYNTHESIS AND FLUORESCENCE IN POLAR REGIONS

O. MEINANDER[1] and G. DE LEEUW[1,2]

[1]Finnish Meteorological Institute (FMI), Helsinki, Finland, outi.meinander@fmi.fi

[2] University of Helsinki, Department of Physics, Finland

Keywords: Arctic, Snow, Albedo, BC, Photosynthesis, Fluorescence, Polar

INTRODUCTION

For clean snow, the reflectance (albedo) at UV and VIS wavelengths is high, close to 90-100%. The albedo of melting snow is low, 50-70 %, and may be even lower when melt-water surrounds the snow grains (e.g., Meinander et al. 2013). In the polar region, the natural (seasonal) snow melt can be affected by, e.g., warming (climate change) or the deposition of light-absorbing impurities on snow. Such impurities may be either of natural origin (e.g., forest fires, volcanic ash, silt and dust) or anthropogenic (soot from power plants, wood burning etc.). The effect of anthropogenic soot (BC) on snow albedo is called *"BC albedo effect"*. Also, the decrease in albedo further increases the melt, which in turn decreases albedo, etc. This positive feedback mechanism is called *"snow-albedo feedback*". In addition, our findings suggest that the impurities in snow may increase snow melt via the decreased snow water holding capacity, which we name *"BC density effect"* (Meinander et al. 2014).

PHOTOSYNTHESIS UNDER SNOW

As the albedo of melting snow decreases, the light transmittance increases. Vegetation, on the other hand, absorbs radiation at UV and VIS wavelengths, and this solar energy is used for photosynthesis. Plant fluorescence tells about the part of the absorbed radiation that could not be used for photosynthesis. Some plants are capable to photosynthesize during winter, and even under snow, when sufficient amount of radiation for photosynthesis to occur, is penetrated through snow. For example, Starr & Oberbauer (2003) have investigated the photosynthesis of Arctic evergreens under snow and its implications for tundra ecosystem carbon balance. In turn, the findings by Lange&Kappen (1972) indicate that Antarctic lichens can achieve a photosynthetic gain during the long periods in which they are frozen.

MATERIALS AND METHODS

To investigate the polar snow albedo, we have several datasets (Table 1). These consist both Arctic (Sodankylä) and Antarctic (Marambio) albedo data and various types of ancillary data, e.g., meteorological and other environmental parameters. The albedo is calculated from the incoming and reflected irradiance measurements. In this work the irradiance data is also used for other purposes. Instrumentation consists of broadband (BB), multiband (MBFR) and spectral.radiometers, from UV to NIR wavelengths. Photosynthetically active radiation (PAR) is measured using a dedicated channel channel of the NILU-UV MBFR instrument. The vegetation fluorescence can be detected, e.g., from the vegetation reflectance spectra. For the snow impurities, we have both continuous data and campaign data for black carbon, organic carbon, volcanic ash, volcanic silt and volcanic dust (see Dagsson-Waldhauserova et al. 2014) in snow. In addition, atmospheric BC is continuously measured by FMI at six stations in Finland and in Marambio, Antarctica.

Place	Years	Data set
Sodankylä (Arctic)	2009-2014, ongoing	Continuous operational Sodankylä incoming solar UV radiation and reflected radiation, 1-min UV data with SL-501 during snow time
Marambio (Antarctica)	2013-2014, ongoing	Continuous operational Marambio incoming solar UV radiation and reflected radiation, 1-min UV data with SL-501, around year
Sodankylä (Arctic)	SNORTEX-campaigns (several)	SNORTEX airborne flight campaign snow UV and VIS albedo data; note: flights also over one lake with snow and over forested areas with snow cover, open snow fields, etc. including ancillary snow data; Bentham spectral data.
Sodankylä (Arctic)	SoS-2013	Sodankylä SoS-2013 experiment UV data: ASD spectral, SL-501 broadband UV, pyranometer

Table 1. Our polar snow albedo data sets.

SNOW-VEGETATION-SOLAR IRRADIANCE INTERACTION

Solar irradiance reaching the ground varies by the geographical location (latitude, longitude and altitude), time (i.e., solar zenith angle SZA), and atmospheric conditions (e.g., cloudiness, aerosols, total ozone, etc.). The life supporting photosynthesis produces stored energy (e.g., sugars) from carbon dioxide and water using energy from the available light, also under snow and below zero temperatures. In turn, snow and its properties depend especially on temperature and precipitation, i.e., climate (see Peel et al. 2007), and also on atmospheric natural and anthropogenic particles deposited in snow. In polar regions, snow, vegetation, and solar irradiance therefore form an interactive system, as illustrated in Fig. 1.

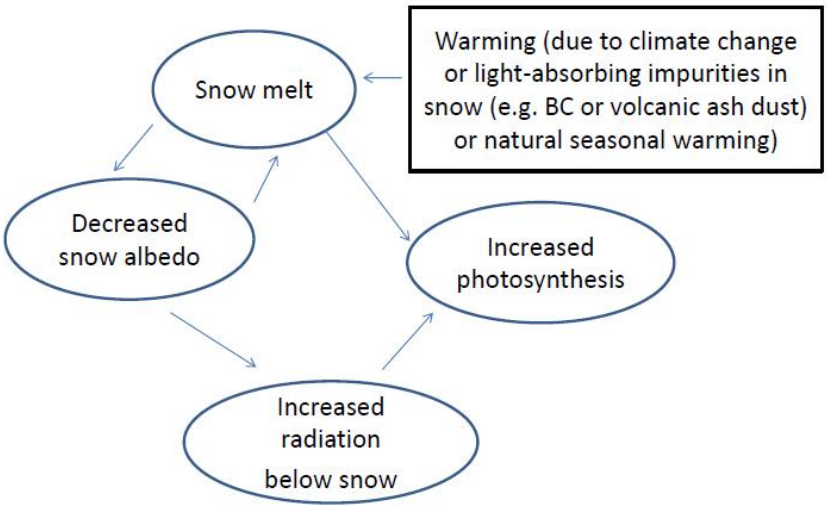

Figure 1. The snow-albedo feedback affected by light-absorbing impurities in snow (e.g., BC) and connected to photosynthesis in polar region vegetation capable to photosynthesis even under snow.

ACKNOWLEDGEMENTS

This work is supported by the Academy of Finland project Arctic Absorbing Aerosols and Albedo of Snow (A^4) (decision 254195), the Top-level Research Initiative (TRI) project CRAICC (Cryosphere-atmosphere interactions in a changing Arctic climate), and the Centre on Excellence

in Atmospheric Science funded by the Finnish Academy of Sciences Excellence (project no. 272041).

REFERENCES

Dagsson-Waldhauserova P, Olafur Arnalds, Haraldur Olafsson, Jindrich Hladil, Roman Skala, Tomas Navratil, Leona Chadimova, Outi Meinander, Snow–Dust Storm: Unique case study from Iceland, March 6–7, 2013, *Aeolian Research*, Volume 16, March 2015, Pages 69-74, ISSN 1875-9637, appeared on-line, 2014.

Lange, O. L. and Kappen, L (1972), Photosynthesis of Lichens from Antarctica, in *Antarctic Terrestrial Biology* (ed G. A. Llano), American Geophysical Union, Washington, D. C.. doi: 10.1002/9781118664667.ch4.

Meinander, O., Kazadzis, S., Arola, A., Riihelä, A., Räisänen, P., Kivi, R., Kontu, A., Kouznetsov, R., Sofiev, M., Svensson, J., Suokanerva, H., Aaltonen, V., Manninen, T., Roujean, J.-L., and Hautecoeur, O. (2013) Spectral albedo of seasonal snow during intensive melt period at Sodankylä, beyond the Arctic Circle, *Atmos. Chem. Phys*., 13, 3793-3810, doi:10.5194/acp-13-3793-2013.

Meinander, O., A. Kontu, A. Virkkula, A. Arola, L. Backman, P. Dagsson-Waldhauserová, O. Järvinen, T. Manninen, J. Svensson, G. de Leeuw, and M. Leppäranta (2014). Brief communication: Light-absorbing impurities can reduce the density of melting snow, *The Cryosphere*, 8, 991-995, doi:10.5194/tc-8-991-2014.

Peel MC, Finlayson BI and McMahon TA. (2007). Updated world map of the Köppen-Geiger climate classification. *Hydrol.Earth Syst. Sci.* 11, 1633-1644.

Starr G and Oberbauer SF, (2003). Photosynthesis of Arctic evergreens under snow: implications for tundra ecosystem carbon balance. *Ecology* 84:1415–1420.

HYGROSCOPIC PROPERTIES OF BACKGROUND AEROSOLS IN SIBERIAN BOREAL FORESTS: ZOTTO SUMMER CAMPAIGN 2013

E. F. MIKHAILOV[1,2], G. N MIRONOV[2], S.Yu. MIRONOVA[2], C. PÖHLKER[1], M. L. KRÜGER[1], J.-D. FÖRSTER[1], X. CHI[1], U. PÖSCHL[1], S.S. VLASENKO[2], T.I., RYSHKEVICH[2], M. WEIGAND[3], A. L. D. KILCOYNE[4] and M.O. ANDREAE[1]

[1] Biogeochemisty Department, Max Planck Institute for Chemistry, Mainz, Germany

[2]Atmospheric Physics Department, Institute of Physics, St. Petersburg State University, St. Petersburg, Russia

[3]Modern Magnetic Systems Department, Max Planck Institute for Intelligent Systems, Stuttgart, Germany.

[4]Lawrence Berkeley National Laboratory, Berkeley, CA, United States.

Keywords: boreal forest aerosol, hygroscopic properties, mixing state, water uptake kinetics

ABSTRACT

Aerosols influence the radiative budget of the Earth atmosphere in two different ways. The first is the direct effect, whereby aerosols scatter and absorb solar and thermal infrared radiation, thereby altering the radiative balance of the Earth-atmosphere system (Scott et al., 2014). The second is the indirect effect, whereby aerosols modify the microphysical and hence the radiative properties and lifetime of clouds (Andreae and Rosenfeld, 2008). The hygroscopic properties of atmospheric aerosol particles are vital for a proper description of these effects, since they describe how the particles interact with water vapor both at sub and supersaturated conditions (Swietlicki et al, 2008; Rastak et al., 2014). They are thus of major importance in describing the life cycle of the aerosol and the related direct and indirect effects on climate. To our knowledge no experimental data for hygroscopic properties of the accumulation mode in the size range 0.3-1.0 µm and of the coarse (>1 µm) mode in the boreal environment have been presented up to now. Therefore, we have set out to investigate and characterize the hygroscopic properties of boreal aerosol particles in the growing season, covering the sub- and supermicron size range.

Aerosol particles were sampled at the Zotino Tall Tower Observatory (ZOTTO) in Central Siberia (61º N; 89º E) from 16 to 21 June 2013. The hygroscopic growth measurements were supplemented with chemical analysis of the samples including inorganic ions and organic/elemental carbon. In addition, the microstructure and chemical composition of aerosol particles have been analysed by X-ray micro-spectroscopy (STXM-NEXAFS) (Moffet et al., 2010) and transmission electron microscopy (TEM). The mass closure study indicates that organic carbon accounted for 60% and 38% of PM in the accumulation mode and coarse mode, respectively. Accordingly, the water soluble fraction of organic matter was estimated to be 33% and 7%. Sulfate, predominantly in the form of ammoniated sulfate, was the dominant inorganic component in both size modes: ~34% in the accumulation mode vs. ~ 47% in the coarse mode.

The hygroscopic growth measurements were conducted with a filter-based differential hygroscopicity analyzer (FDHA) (Mikhailov et al., 2011) over the 5 - 99.4% RH range in the hydration and dehydration

operation modes. The FDHA study indicate that both accumulation and coarse modes exhibit pronounced water uptake approximately at the same RH, starting at ~70%, while efflorescence occurred at different humidities, i.e., at ~35% RH for submicron particles versus ~50% RH for supermicron particles . This ~15% RH difference was attributed to a higher content of organic material in the submicron particles, which suppresses water release in the dehydration experiments. The kappa mass interaction model (KIM) has been applied to characterize and parameterize non-ideal solution behavior and concentration-dependent water uptake by atmospheric aerosol samples in the 5-99.4% RH range. Based on KIM, the volume-based hygroscopicity parameter κ_v has been calculated. The $\kappa_{v,ws}$ value related to the water soluble (*ws*) fraction was estimated to be ~0.14 for the accumulation mode and ~0.36 for the coarse mode, respectively. The obtained $\kappa_{v,ws}$ for the accumulation mode is in a good agreement with earlier data reported for remote sites in the Amazonian rain forests ($\kappa_v \approx 0.15$) and a Colorado boreal forests ($\kappa_v \approx 0.16$).

The Zdanovskii–Stokes–Robinson (ZSR) mixing rule has been used to predict the chemical-composition-dependent hygroscopicity $\kappa_{v,p}$. The obtained $\kappa_{v,p}$ values overestimate the experimental FDHA-KIM derived $\kappa_{v,ws}$ by factors of 2.3 and 1.5 for the accumulation and coarse modes, respectively. The observed divergence can be explained by incomplete dissolution of the hygroscopic inorganic compounds due to kinetic limitations caused by a sparingly soluble organic coating. The TEM and STXM-NEXAFS (scanning transmission x-ray microscopy with near-edge x-ray absorption fine structure analysis) results indicate that aged submicron (>200 nm) and supermicron aerosol particles possess core-shell structures with an inorganic core and organic carbon enriched at the mixed particles surface. The direct FDHA kinetic studies provide a bulk diffusion coefficient of water of $\sim 1.3\times10^{-12}$ cm^2/s and a viscosity of $\sim 1.1\times10^{3}$ Pa s, indicating a semi-solid state of the organic-rich phase at low RH (~60%) leading to kinetic limitations of water release upon particles dehydration.

Overall the present ZOTTO data set obtained in the growing season revealed a strong influence of organic carbon on the hygroscopic properties of the ambient aerosols. The sparingly soluble organic coating controls hygroscopic growth, phase transitions, and microstructural rearrangement processes. The observed kinetic limitations can strongly influence the outcome of experiments performed on multi-second time scales, such as the commonly used HTDMA (Hygroscopicity Tandem Differential Mobility Analyzer) and CCN (Cloud Condensation Nuclei) instruments.

REFERENCES

Andreae, M. O., and Rosenfeld, D. (2008): Aerosol–cloud–precipitation interactions. Part 1. The nature and sources of cloud-active aerosols, *Earth-Science Reviews*., **89**, 13-41.

Mikhailov, E., Vlasenko, S., Rose, D., and Pöschl U.(2013): Mass-based hygroscopicity parameter interaction model and measurement of atmospheric aerosol water uptake, *Atmos. Chem. Phys*., **13**, 717–740.

Mikhailov, E. F., Merkulov, V. V., Vlasenko, S. S., Ryshkevich, T. I., and Pöschl U. J. (2011): Filter-based differential hygroscopicity analyzer of aerosol particles, Izvestiya, *Atmospheric and Oceanic Physics*, **47(6)**, 747–759.

Rastak, N., Silvergren, S., Zieger, P., Wideqvist, U., Ström, J., Svenningsson, B., Maturilli, M., Tesche, M., Ekman, A. M. L., Tunved, P., and Riipinen, I (2014).: Seasonal variation of aerosol water uptake and its impact on the direct radiative effect at Ny-Ålesund, Svalbard, *Atmos. Chem. Phys*., **14**, 7445–7460.

Scott, C. E. Rap, A., Spracklen, D. V., Forster, P. M., Carslaw, K. S., Mann, G. W., Pringle, K. J,. Kivekäs, N., Kulmala, M., Lihavainen, H., and Tunved, P.(2014): The direct and indirect radiative effects of biogenic secondary organic aerosol, *Atmos. Chem. Phys*., **14**, 447–470.

Swietlicki, E., Hansson, H. -C., Hämeri, K., Svenningsson, B., Massling, A., McFiggans, G., McMurry, P. H., Petäjä, T., Tunved, P., Gysel, M., Topping, D., Weingartner, E., Baltensperger, U., Rissler, J., Wiedensohler, A. and Kulmala M. (2008): Hygroscopic properties of submicrometer atmospheric aerosol particles measured with H-TDMA instruments in various environments - a review, *Tellus*, **60B**, 432–469.

FIRST PARAMETERISATION OF HEMITERPENOID AND ISOPRENOID EMISSIONS FROM THE BOREAL FOREST FLOOR: IMPLEMENTATION INTO SOSAA AND INVESTIGATION OF THE INFLUENCE ON ATMOSPHERIC CHEMISTRY

D. MOGENSEN[1], H. AALTONEN[2], J. AALTO[3], J. BÄCK[3], R. GIERENS[1], M. KULMALA[1] AND M. BOY[1]

[1]Department of Physics, P.O. Box 48, University of Helsinki, 00014, Finland.

[2]Fnnish Meteorological Institute, P.O. Box 503, 00101, Finland

[3]Department of Forest Sciences, P.O. Box 27, University of Helsinki, 00014, Finland.

Keywords: FOREST FLOOR, BVOCs, 1D MODELLING, ATMOSPHERIC CHEMISTRY.

INTRODUCTION

With its definite potential for influencing everyone's life, global warming has drawn the World's attention and so has boreal forest, since it is the area, together with the Arctic, that is expected to heat most in the future (as much as ~ 8.5 K by year 2100 predicted by IPCC 2013). Boreal forests are a great source of a vast amount of different biogenic volatile organic compounds (BVOCs) – emitted both from the forest soil and litter, tree trunks and branches, but mostly from the tree crown through needles and leaves (Goldstein and Galbally, 2007; Aaltonen *et al.*, 2011; Hakola *et al.*, 2003; Hakola *et al.*, 2006). These VOCs are various in their formation, chemical and physical properties, in their ability to alter the atmospheric oxidation budget and in their potential to participate in aerosol growth, production of cloud condensation nuclei (CCN) and thereby in their potential to affect climate (Makkonen *et al.*, 2012). In order to predict climate change, we need to simulate the globe, including the boreal forests, in a perturbed environment. However, in order to do that with less uncertainty, we firstly need to understand the processes that occur in the current climatic state of the boreal forests.

Considering that needles and leaves are thought to account for the majority of the isoprenoid concentration in boreal forests and since below–canopy emissions are rarely measured, emissions from the forest floor have, to our knowledge, never been included in models. However, Aaltonen *et al.* (2011) and Hellén *et al.* (2006) have shown that hydrocarbon emissions from the forest floor can contribute with up to some tens of percents of the total forest ecosystem hydrocarbon emissions especially during spring and autumn. Also, more than 70 different VOCs have been measured from soil (McNeal and Herbert, 2009) with terpenoids, acetone and methanol being the most commonly observed in field (Aaltonen *et al.*, 2011; Aaltonen *et al.*, 2013; Hellén *et al.*, 2006; Isidorov and Jdanova, 2002). Forest floor emissions may originate from several processes and sources; ground vegetation (e.g. dwarf shrubs and mosses), plant roots, decomposing litter, or soil microbes (Isidorov and Jdanova, 2002; Aaltonen *et al.*, 2011; Bäck et al., 2010; Asensio *et al.*, 2008). The relative importance of these may vary in time. Since most gas concentration measurements are done at ground level, it is important to consider the forest floor source area – especially when measuring compounds with short life time (Rinne *et al.*, 2007).

METHODS

In this study we developed parameterisations for biogenic forest floor emission of isoprene and monoterpenes and implemented these parameterisations into the 1D column model SOSAA (model to Simulate Organic vapours, Sulphuric Acid and Aerosols). We then tested the effect of the forest floor emissions on the atmospheric chemistry environment.

Forestry land covers 86% of the land area of Finland. In this study we are investigating a Scots pine (*Pinus sylvestris*) forest, since pine is the dominant tree species in the Finnish boreal forest with $\sim 50\%$ of the total forest volume (Finnish Forest Research Institute, 2012). Our location of choice was the SMEAR II station (Station for Measuring Ecosystem-Atmosphere Relations), Hyytiälä, Southern Finland (Hari and Kulmala, 2005), which is very well characterised and located in the boreal forest zone.

For parameterisation development of the forest floor emission of isoprene and monoterpenes, we considered the entire snow free periods during 2010 (May – November) (Aaltonen *et al.*, 2013) and 2011 (May – December), together with data obtained during April – June, 2012.

The forest floor fluxes of isoprene and monoterpenes were measured using (1) a dynamic method with three automated chambers analysed by PTR–MS (Proton Transfer Reaction – Mass Spectrometer) (Aaltonen *et al.*, 2013) and (2) a steady-state method with five manual chambers analysed by GC–MS (Gas Chromatograph – Mass Spectrometer) (Aaltonen *et al.*, 2011). The PTR–MS measured emission was used for parameterisation development together with simultaneously obtained chamber temperature, photosynthetically active radiation (PAR), relative humidity (RH), CO_2 flux (Aaltonen *et al.*, 2013) and soil temperature and moisture in three layers (humus, A- and B-horizon).

For investigation of the impact of forest floor emission of VOCs on atmospheric chemistry, we regard only the snow free season during 2010. This was done using the 1D chemical–transport model SOSAA (Boy *et al.*, 2011). Since the nature of the model is to describe the vertical dimension of the atmospheric boundary layer, we are also able to investigate the vertical importance of the included BVOCs. SOSAA includes modules for boundary layer meteorology (SCADIS), biogenic canopy emissions (MEGAN), gas phase chemical mechanistics (MCM) and aerosol dynamics (UHMA). The aerosol dynamics modules was disabled during this study.

CONCLUSIONS

We have developed parameterisations for snow–free forest floor emission of isoprene and monoterpenes based on PTR–MS measurements. Both parameterisations are of a quadratic nature and considers ambient temperature close to the soil and humus soil moisture as parameters.

We have investigated the fraction of the total canopy emission and concentration that is due to the forest floor source area as a function of season. We find, that though the total forest floor emission is mostly significantly less than the needle emission, there are no other sources near ground (at least when pine is considered), thus the importance of the forest floor emission depends highly on the meteorological mixing. The fraction of isoprene from the forest floor to the total canopy emission is found to be highest during autumn, while the fraction of monoterpenes from the forest floor to the total canopy emission is found to be highest during spring and autumn. The forest floor emission of isoprene has at all times a negligible influence on the isoprene concentration near ground, while the monoterpenes emitted from the forest floor always makes up some percentages of the total concentration near ground.

Further, we have investigated the impact on OH-reactivity (loss rate of OH in the atmosphere) due to the included forest floor emission. The emission due to isoprene impacts the OH-reactivity

insignificantly, which is excepted, since the isoprene concentration at the measurement station is generally low and the canopy crown emitted isoprene therefore also only makes up a very small fraction of the total OH-reactivity. By including the forest floor emission of monoterpenes, the missing OH-reactivity (difference between measured and modelled OH-reactivity) becomes smaller, however only by a few percentages, why the forest floor BVOC emission cannot account for the commonly observed missing OH-reactivity.

Finally we conclude that the processes related to forest floor emissions are currently not resolved and that more research on this is needed.

ACKNOWLEDGEMENTS

This work was financially supported by the Finnish Center of Excellence grant no. 272041. Further, we thank the CSC – IT Center for Science Ltd for computational resources.

REFERENCES

Aaltonen, H., J. Pumpanen, M. Pihlatie, H. Hakola, H. Hellén, L. Kulmala, T. Vesala and J. Bäck, (2011). Boreal pine forest floor biogenic volatile organic compound emissions peak in early summer and autumn, *Agr. Forest Meteorol.*, **151**, 682.

Aaltonen, H., J. Aalto, P. Kolari, M. Pihlatie, J. Pumpanen, M. Kulmala, E. Nikinmaa, T. Vesala, and J. Bäck, (2013). Continuous VOC flux measurements on boreal forest floor, *Plant Soil*, **369**, 241.

Asensio, D., S. M., Owen, J., Lusiá, and J. Peñuelas, (2008). The distribution of volatile isoprenoids in the soil horizons around Pinus halepensis trees, *Soil Biol. Biochem.*, **40**, 2937.

Boy, M., A. Sogachev, J. Lauros, L. Zhou, A. Guenther and S. Smolander, (2011). SOSA – a new model to simulate the concentrations of organic vapours and sulphuric acid inside the ABL – Part I: Model description and initial evaluation, *Atmos. Chem. Phys.*, **11**, 43.

Bäck, J., H., Aaltonen, H., Hellén, M. K., Kajos, J., Patokoski, R., Taipale, J., Pumpanen, and J. Heinonsalo, (2010). Variable emissions of microbial volatile organic compounds (MVOCs) from root–associated fungi isolated from Scots pine, *Atmos. Environ.*, **44**, 3651.

Finnish Forest Research Institute, Statistical Yearbook of Forestry 2012.

Goldstein, A. H. and I. E., Galbally, (2007). Known and Unexplored Organic Constituents in the Earth's Atmosphere, *Environ. Sci. Tech.*, **41**, 1514.

Hakola, H., V. Tarvainen, T. Laurila, V. Hiltunen, H. Hellén and P. Keronen, (2003). Seasonal variation of VOC concentrations above a boreal coniferous forest, *Atmos. Environ.*, **37**, 1623.

Hakola, H., V. Tarvainen, J. Bäck, H. Ranta, B. Bonn, J. Rinne and M. Kulmala, (2006). Seasonal variation of mono- and sesquiterpene emission rates of Scots pine, *Biogeosciences*, **3**, 93.

Hari, P. and M. Kulmala, (2005). Station for measuring ecosystem-atmosphere relations (SMEAR II), *Boreal Env. Res.*, **10**, 315.

Hellén, H., H. Hakola, K.-H. Pystynen, J, Rinne and S. Haapanala, (2006). C2–C10 hydrocarbon emissions from a boreal wetland and forest floor, *Biogeosciences*, **3**, 167.

Isidorov, V. and M. Jdanova, M, 2002. Volatile organic compounds from leaves litter, *Chemosphere*, **48**, 975.

Makkonen, R., A. Asmi, V.-M. Kerminen, M. Boy, A. Arneth, A., Guenther and M. Kulmala, (2012). BVOC–aerosol–climate interactions in the global aerosol–climate model ECHAM5.5–HAM2, *Atmos. Chem. Phys.*, **12**, 10077.

McNeal, K.S. and B. E. Herbert, (2009). Volatile organic metabolites as indicators of soil microbial activity and community composition shifts, *Soil Sci. Soc. Am. J.*, **73**, 579.

Rinne, J., R. Taipale, T. Markkanen, T. M. Ruuskanen, H. Hellén, M. K. Kajos, T. Vesala, T. and M. Kulmala, (2007). Hydrocarbon fluxes above a Scots pine forest canopy: measurements and modeling, *Atmos. Chem. Phys.*, **7**, 3361.

THE STORMINESS AND THE WIND WAVE CLIMATE IN THE BALTIC SEA PRODUCED BY THE SWAN MODEL

A.YU. MEDVEDEVA[1, 2], S.A. MYSLENKOV[1, 3], V.S. ARKHIPKIN[1]

[1] Department of Oceanology, Faculty of Geography, MSU, Moscow, Russian Federation.

[2] Tsunami Laboratory, P.P. Shirshov Institute of Oceanology, RAS, Moscow, Russian Federation.

[3]Hydrometeorological Research Centre of the Russian Federation, Marine forecast division

KEYWORDS: NUMERICAL MODELLING, SWAN, STORM, WIND WAVE CLIMATE

INTRODUCTION

Nowadays the study of natural hazards such as storm waves is one of the most essential problems of oceanology. The analyze of wind wave climate helps to forecast the impact of future climate changes. Wind waves have great importance for shipping, constructing on coasts and shelf, developping oil and gas fields. The Baltic Sea is a challenging area for wave scientists. A combination of its relatively small size (that virtually excludes the presence of long-period remote swells), extremely complex geometry and high variability in the wind fields naturally leads to widespread variability in the wave fields in both time and space. In present study to estimate decadal and interannual changes of the wave fields for the entire Baltic Sea the wave parameters, such as significant wave heights and periods, were simulated for the period 1948–2011 years using model SWAN (Simulating WAves Nearshore). To estimate the accuracy of the model the statistical characteristics, such as correlation coefficient, bias, scatter index and RMSE were calculated. Such extreme characteristics as wave height possible once in 100 years and significant wave heights with 0.1, 1, and 5-% probability were obtained. It was revealed that the storminess of the Baltic Sea tends to increase and the twenty-year periodicity with the increase in the 70-s and 90-s years of XX century.

METHODS

In this study to estimate decadal and interannual changes of the wave fields for the entire Baltic Sea the third generation spectral wind-wave model SWAN and the data fields of wind reanalysis NCEP/NCAR were used (http://www.esrl.noaa.gov/psd/data/reanalysis/reanalysis.shtml). The parameters of the wave fields, such as significant wave heights and periods, were simulated for the period 1948 – 2011 years. Time step of wind forcing is 6 hours and computations of wave generation were done for every hour. Space resolution of reanalysis is ~1.9×1.9° and the final computational grid for the Baltic Sea is 0.05×0.05°.

The simulated data were compared with instrumental data of the Sweden buoys (http://www.smhi.se/ecds), with the results of operational regional models and with the results of other similar numerical experiments (Blomgren *et al*., 2001; Kriezi, Broman, 2008; Saremi, 2010; Soomere *et al*., 2008). To compare obtained NCAR results a few numerical experiments were realized using another reanalysis NCEP/CFSR (http://cfs.ncep.noaa.gov/cfsr/) with time resolution 1 hour and space resolution ~0.3125×0.3125° and using different mechanisms of wave generation from SWAN model (http://swanmodel.sourceforge.net).

CONCLUSIONS

The SWAN model usually underestimates the significant wave heights and peak periods. The statistical characteristics were calculated to estimate the accuracy of the model. The correlation coefficient between simulated and instrumental data was high enough (tab. 1). The calculated values belong to the average range of the statistical characteristics according to previous studies of different authors (Blomgren *et al*., 2001; Kriezi, Broman, 2008; Saremi, 2010; Soomere *et al*., 2008). It allowed us to use SWAN with NCEP/NCAR Reanalysis wind forcing for research of the climatic variability of wind waves of the Baltic Sea. But numerical simulations using CFSR reanalysis shows evidently better results (fig. 1). The question, which generation mechanism is better for the Baltic Sea is debatable. For example in the deep ocean mechanism GEN3 (http://swanmodel.sourceforge.net) is more adequate, but in the shallow water errors are more negligible for the mechanism GEN1.

Regime average and extreme maximum and minimum characteristics of wind waves for the Baltic Sea were calculated and analyzed. Such extreme characteristics as the significant wave height possible once in 100 years exceeded 13 m in the Baltic Proper, in the East Gotland Basin. This region of the Baltic Sea is characterized by the most intensive storm activity due to the trajectories of cyclones crossing this area. The significant wave heights with 0.1, 1, and 5-% probability for the Baltic Proper were identified as 5-5.4 m, 3.2-3.6 m and 2.2-2.4 m respectively.

The wave climate of the Baltic Sea is characterized by specific features, such as: very instable character, localization of the period of strong storms in autumn and winter months, significant spatial and temporal variability of the wave properties, predominance of relatively short and steep waves, existence of waves with such heights as in much larger Mediterranean Sea (Soomere, 2008). The storm situations, when the significant wave height exceeded 2 meters, were identified for the 64-year period. In total the quantity of the storm situations was more, then 2900 cases, of about 50 storms per year happened in the Baltic Sea in this time period (fig. 2). The storminess of the Baltic Sea tends to increase (according to the linear trend). The typical time interval periods of the wave activity increase is 10–12 years. In the 1970s and 1990s, the activity was quite intensive, and in the end of 1980s and in the middle of 2000s it was low. In this work twenty-year-periodicity was revealed, which includes a ten-year increase and a ten-year decrease of the storminess. The average yearly significant wave height rises in the second part of the century too and varies from 2.4 to 3.3 m, but there is no such clear periodicity as for the quantity of the storm situations.

Storm cyclones are connected with the global atmosphere circulation patterns. According to similar research of the other west seas .of Russia, which were done in the Natural Risk Assessment Laboratory (Arkhipkin *et al*., 2014; http://www.nral.org/ru/) by the same methods, such kind of twenty-year periodicity was revealed for the Caspian Sea and the Sea of Azov. For the Black Sea there is no such clear correlation, but the connection with the NAO index (November–March) shows that periods with the lowest NAO index are accompanied by higher storminess. Such task for the Baltic Sea will be solved in future study. In contrast to the Baltic Sea the storminess of the Caspian Sea and the Sea of Azov tends to decrease, and for the Black Sea – there is no evident trend. To understand mechanisms connections between the storm features and the global atmospheric circulation is planned in future researches.

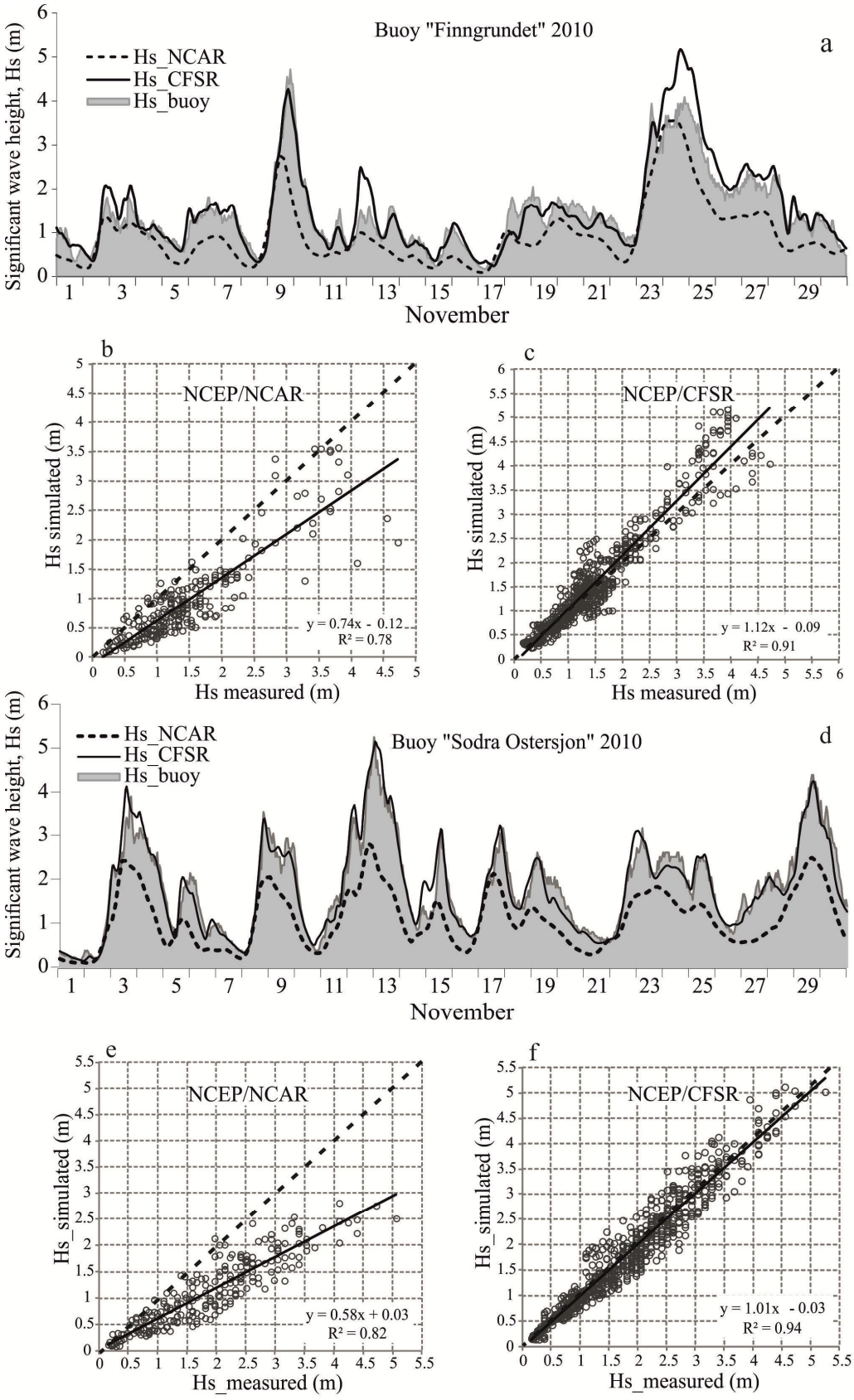

Figure 1. Comparison of measured and simulated data for November 2010 for Finngrundet buoy (a), scatter diagrams (b, c), where *y* is linear equation, R^2 is the coefficient of determination; and for Sodra Ostersjon buoy (d, e, f)

Reanalysis	Mechanism of wave generation	R	Bias	RMSE	SI
Finngrundet buoy (30.6 m) 18.67° N, 61.00° E - November 2010					
NCAR	GEN3/ 1 hour	0.884	-0.498	0.645	0.447
	GEN3/ 15 min	**0.953**	0.083	0.335	0.232
	GEN3/ 30 min	0.944	0.047	0.344	0.239
	GEN3/1 hour	0.878	-0.047	0.459	0.318
	GEN2/ 1 hour	0.950	0.069	0.291	0.202
CFSR	GEN1/1 hour	0.949	**-0.025**	**0.274**	**0.189**
Sodra Ostersjon buoy (111.7 m) 18.78° N, 55.92° E - November 2010					
NCAR	GEN3/ 1 hour	0.908	-0.730	0.889	0.487
	GEN3/ 15 min	**0.967**	**-0.003**	**0.272**	**0.149**
	GEN3/ 30 min	0.959	-0.060	0.303	0.166
	GEN3/1 hour	0.920	-0.180	0.443	0.243
	GEN2/ 1 hour	0.943	-0.041	0.354	0.194
CFSR	GEN1/1 hour	0.946	-0.157	0.367	0.201

Table 1. Comparison between measurements and modeled data

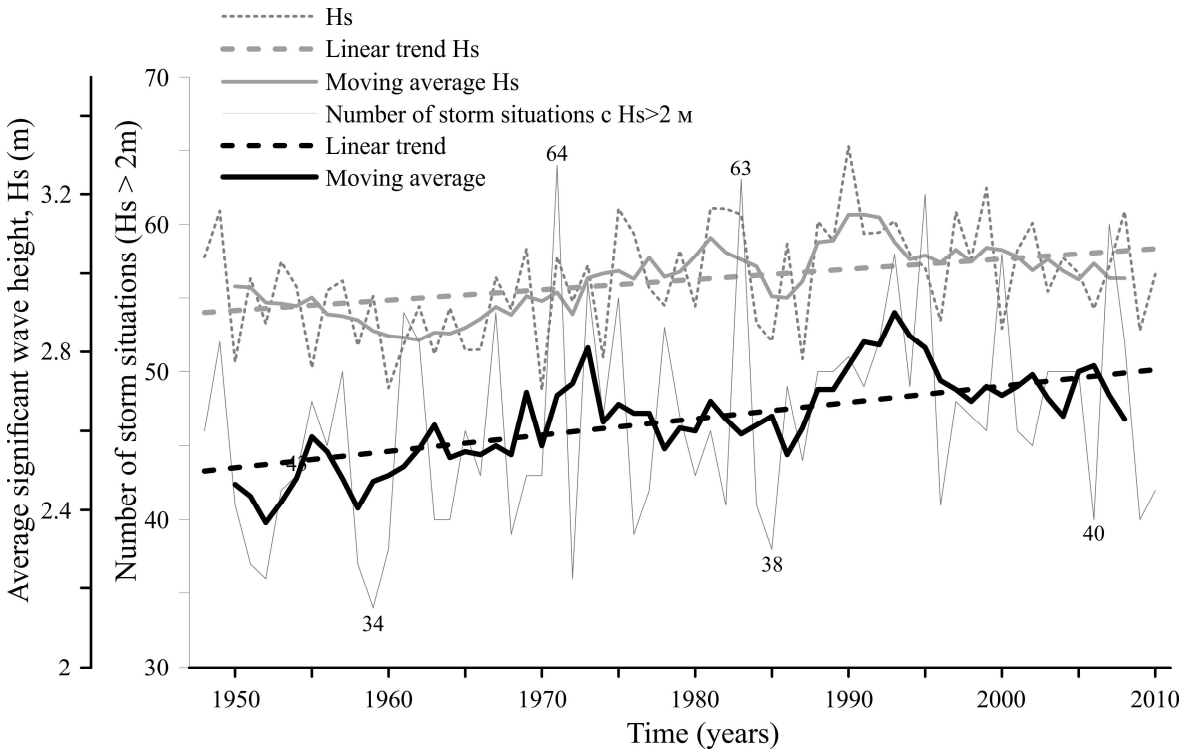

Figure 2. Number of storm situations and the average Hs from 1948 to 2010

ACKNOWLEDGEMENTS

This work was supported by the Ministry of Education and Science of Russian Federation under grant № 11.G34.31.0007 A1/001, by the Russian Foundation for Basic Research under grant 14-05-91769 and by the Russian Scientific Foundation under the grant №14-37-0 38.

REFERENCES

Arkhipkin V.S., Gippius F.N., Koltermann K.P. and Surkova G.V. (2014). Wind waves in the Black Sea: results of a hindcast study. *Natural Hazards and Earth System Sciences Discussions* 14. P. 2883–2897

Blomgren S., Larson M., Hanson H. (2001). Numerical Modeling of the Wave Climate in the Southern Baltic Sea. *Journal of Coastal Research*. V. 17. № 2. P. 342-352.

Kriezi E.E., Broman B. (2008). Past and future wave climate in the Baltic Sea produced by the SWAN model with forcing from the regional climate model RCA of the Rossby Centre. US/EU-Baltic International Symposium, 2008 IEEE/OES. IEEE (Tallin, Estonia). P. 1-7.

Saremi S. (2010). *Development of a wave database in coastal areas around Sweden using the SWAN wave model: evaluation of the influence of grid resolutions and bathymetric data*, (Chalmers University of Technology, Gothenburg, Sweden).

Soomere T., Behrens A., Tuomi L., Nielsen J. W. (2008).Wave conditions in the Baltic Proper and in the Gulf of Finland during windstorm Gudrun. *J. Natural Hazards & Earth System Sciences*. V. 8. № . P. 37–46.

http://cfs.ncep.noaa.gov/cfsr/

http://swanmodel.sourceforge.net

http://www.esrl.noaa.gov/psd/data/reanalysis/reanalysis.shtml

http://www.smhi.se/ecds

INFLUENCE OF BIOMASS BURNING PLUMES ON HONO CHEMISTRY IN EASTERN CHINA

W. NIE[1,2], A. J. DING[1,2], Y. N. XIE[1,2], Z. XU[3], H. MAO[1,2,5], V. KERMINEN[4], L. F. ZHENG[3,1], X. M. QI[1,2], X. HUANG[1], X. Q. YANG[1,2], J. N. SUN[1,2], E. HERRMANN[1], T. PETÄJÄ[4], M. KULMALA[4] and C. B. FU[1,2]

[1]Institute for Climate and Global Change Research & School of Atmospheric Sciences, Nanjing University, Nanjing, 210093, China

[2]Colaborative Innovation Center of Climate Change, Jiangsu Province, China

[3] Environment Research Institute, Shandong University, Jinan, China

[4]Division of Atmospheric Sciences, Department of Physics, University of Helsinki, Helsinki, Finland

[5]Department of Chemistry, State University of New York College of Environmental Science and Forestry, Syracuse, New York, USA

Nitrous acid (HONO) plays a key role in atmospheric chemistry via influencing the budget of hydroxyl radical (OH). In this study, we analyzed a two-month measurement of atmospheric HONO during the BB season of 2012 (May and June) at the SORPES central site in western YRD of eastern China, and demonstrated an important role of BB in the HONO chemistry in the ambient atmosphere. HONO formation was detected to be significantly elevated during the BB periods due to the combined effect of enhanced particle loadings, larger specific surface areas of particles and higher NO_2 conversion efficiency on BB aerosols. An episode of mixed plumes of intense BB and anthropogenic FF emissions was observed on 10 June, during which the HONO production potentials from the conversion of NO_2 was further promoted by the formation of secondary particulate matter on BB particles. The reaction of SO_2 and NO_2 in the aqueous phase was indicated as an important pathway to produce the observed additional HONO.

Given that BB plumes are easily mixed with other anthropogenic pollutants in eastern China, their influences on the atmospheric chemistry is expected to be important via affecting the HONO budget and thus the radical pool. Furthermore, considering the potential re-activation of BB particles (e.g. soot) during their atmospheric transport, the HONO chemistry associated with BB plumes may affect atmospheric chemistry long distances downwind BB areas, even in the marine boundary layer. Therefore, more studies are encouraged on BB related chemistry in eastern China, which is a unique “laboratory” with frequent mixed plumes of BB and anthropogenic pollutions.

OVERVIEW AND FIRST RESULTS FROM SMEAR ESTONIA

S.M. NOE[1], A. KANGUR[2], U. HÕRRAK[3], A. KRASNOVA[1], D. KRASNOV[1] and H.P.E. CORDEY[1]

[1]Institute of Agricultural and Environmental Sciences, Estonian University of Life Sciences, Kreutzwaldi 1, 51014 Tartu, Estonia.

[2]Institute of Forestry and Rural Development, Estonian University of Life Sciences, Kreutzwaldi 1, 51014 Tartu, Estonia.

[3]Institute of Physics, University of Tartu, Ülikooli xx, 5xxxx Tartu, Estonia.

Keywords: SMEAR, measurement station, hemiboreal.

INTRODUCTION

Since 2008 when the first integrated biosphere-atmosphere measurements have been conducted in Järvselja, Estonia (Noe *et al.*, 2011) a leap from short termed measurement campaigns to year-round comprehensive measurements has been done. Until 2013, most measurements where carried out at a 24 m high scaffolding tower. In 2010, the buildup of a new Station for Measuring Ecosystem-Atmosphere Relations (SMEAR) (Hari and Kulmala, 2005) in Estonia was started. From October 2013 on, the major part of ecosystem fluxes, atmospheric composition, soil structural and meteorological measurements where moved to the 130 m high atmospheric tower of the new SMEAR Estonia site.

Located in the southern edge of the boreal forest biome, the SMEAR Estonia station represent a hemiboreal mixed forest ecosystem that consist of both, coniferous and deciduous tree species. The typical share at Järvselja accounts approximately 50% coniferous species whereof the major species are Scots Pine (*Pinus sylvestris*) and Norway Spruce (*Picea abies*) and 50% deciduous tree species whereof the majority are birches (*Betula pubescens* and *B. pendula*) and a smaller share of hybrid Aspen (*Populus termula* x *tremuloides*) and Alder (*Alnus glutinosa*). A typical feature at the site are canopies with two ore more distinctive tree layers that lead to partly uncoupling of processes within and above the canopy (Noe *et al.*, 2012).

METHODS

The new build atmospheric tower measures currently at 5 height levels (30, 50, 70, 90 and 110 m) turbulent windspeed and a set of meteorological parameters. On two heights, 30 and 70 m, additionally Eddy covariance fluxes of carbon dioxide (CO2) and water vapor (H2O) are measured. Air is drawn down from the tower and analysed for greenhouse gases, ozone, nitrogen oxides (NOx) and sulfuric dioxide (SO2). At the small 24 m tower site, Eddy covariance is measured at 25 m above the canopy while air ion and aerosol measurements are conducted on 2 m height inside the canopy.

At both places, a set of more than 20 permanent sample plots were established throughout the last years that characterize the species composition and forest stand parameters, biomass, leaf litter and soil parameters above and below ground. Within and around some of the sample plots, soil flux chamber systems to assess fluxes of CO2, H2O and methane have been established.

We employ several model approaches to assess the dynamics of processes within the biosphere-

atmosphere system utilizing the SMEAR stations data. Modeling is used as tool to dynamically estimate the tower footprint area over given time intervals, to assess the emissions of volatile organic compounds from plant and soil surfaces or to assess the seasonal dynamics of mass fluxes like leaf litter.

CONCLUSIONS

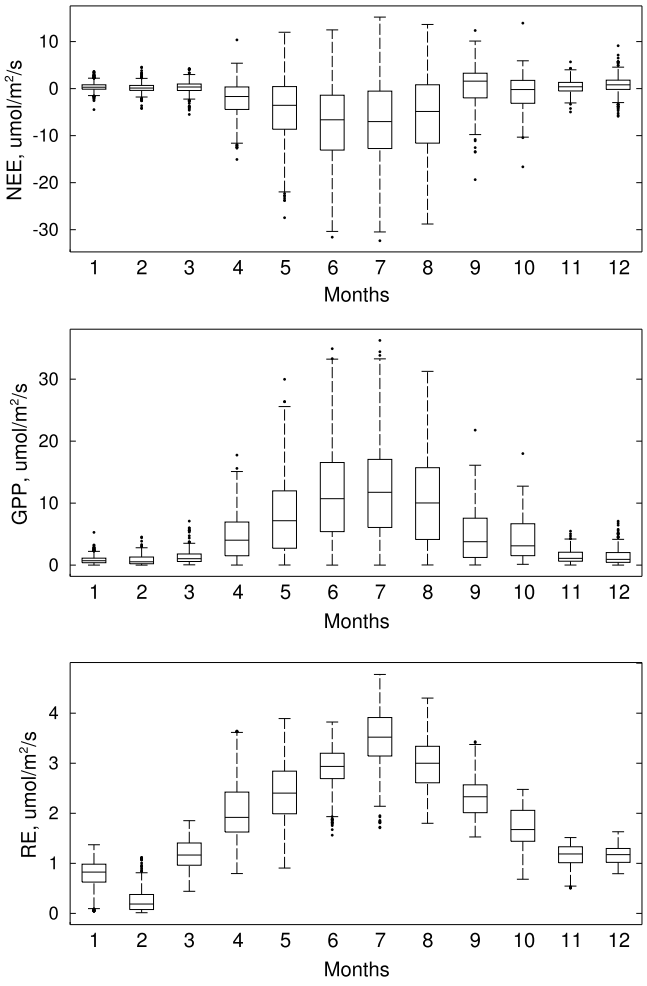

Figure 1: Example of the application of flux data at the SMEAR Estonia site to characterize general forest ecosystem parameters. NEE, Net Ecosystem Exchange (top panel), Gross Primary Production (mid panel) and Ecosystem Respiration (bottom panel).

Utilising the SMEAR Estonia station data allows to give insight into the processes of the hemiboreal forest ecosystem and it's link to the atmosphere. It allows as well comparison studies with the other sites of the SMEAR and PEEX network. The use of the data allows further to implement multidisciplinary data driven educational events. Contributing to policy and decision making bodies on European and national level.

Developing model systems that allow to utilize that data obtained from a station or a station networks enables predictions to future scenario but can be used as well to plan and prepare experiments. That proves especially useful if the experimental setup is includes a larger spatial and

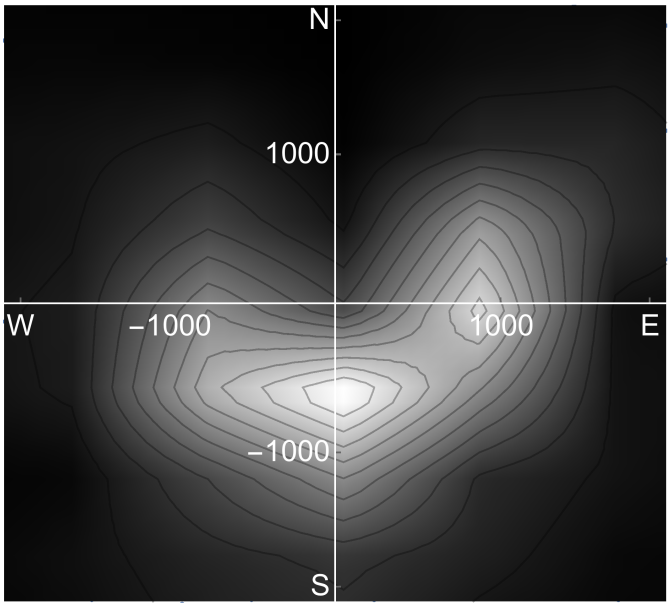

Figure 2: Example for the application of a dynamic footprint model to assess the 130 m tower's fetch area. The data shown are measured at 70 m height during July-September 2014. The density histogram shows the distance in meters and the direction where 80% of the signal arriving to the sensor where originated.

temporal range.

ACKNOWLEDGEMENTS

This work was supported by the EU Regional Development Foundation, Estonian Scientific Infrastructure Roadmap project Estonian Environmental Observatory (3.2.0304.11-0395), the Environmental Conservation and Environmental Technology R&D Programme project BioAtmos (3.2.0802.11-0043), the Internationalization of Science Programme project INSMEARIN (10.1-6/13/1028) and the Estonian Science Foundation (Grant 8110).

REFERENCES

Hari P. and Kulmala M., (2005). Station for measuring ecosystem–atmosphere relations (SMEAR II). *Boreal Env. Res.*, **10**, 315–322.

Noe S.M., Hüve K., Niinemets U. and Copolovici L., (2012). Seasonal variation in vertical volatile compounds air concentrations within a remote hemiboreal mixed forest. *Atmospheric Chemistry and Physics*, **12(9)**, 3909–3926.

Noe S.M., Kimmel V., Hüve K., Copolovici L., Portillo-Estrada M., Püttsepp Ü., Jõgiste K., Niinemets Ü., Hörtnagl L. and Wohlfahrt G., (2011). Ecosystem-scale biosphere-atmosphere interactions of a hemiboreal mixed forest stand at Järvselja, Estonia. *Forest Ecology and Management*, **262(2)**, 71–81.

Figure 3: Example for a 3D reconstruction based on photography to assess microsite specific features of soil surface parameters in permanent sample plots. This technique can be used to assess differences in the soil surface heights (pits and mounds) or to measure distances or integrate aerial information.

PARAMETRIZATION OF TURBULENT FLUXES OVER INHOMOGENEOUS LANDSCAPES

G.N. PANIN

Institute of Water Problems, Russian Academy of Sciences, ul. Gubkina 3, Moscow, 117299 Russia

Keywords: HEAT AND MASS EXCHANGE, HEAT BALANCE, STATIONARITY, HORIZONTAL HOMOGENEITY.

INTRODUCTION

In the last 10–15 years, investigation of the heat and mass exchange processes between different types of natural land surfaces and the atmosphere has received further development. This is due to the fact that results have been published on new experiments on the interaction between an inhomogeneous land surface and the atmosphere that differed substantially from the already known data. It appeared that the widely used parametrizations (e.g., of the Monin– Obukhov type) in these cases provided no satisfactory agreement with the experimental data.
Reasons for the nonclosure of the heat balance in the atmospheric boundary layers over natural land surfaces are analyzed. Results of measuring the heat-balance components over different land surfaces are used.

METHODS

The experiments FIFE, KUREX, TARTEX, CABAUW, SADE, WALDSTEIN etc are analyzed.
The data have shown that the heat balance is not closed and the imbalance is 50–250 W/m^2. It is shown that the main cause of a systematic heat imbalance in the atmospheric boundary layers over inhomogeneous land surfaces is that the methods of surface-flux measurement and estimation are based on the theory that requires the hypothesis of stationarity and horizontal homogeneity. Direct data analysis has shown that the heat imbalance increases with landscape inhomogeneity.
In the paper, have made a parametrization of the heat imbalance.

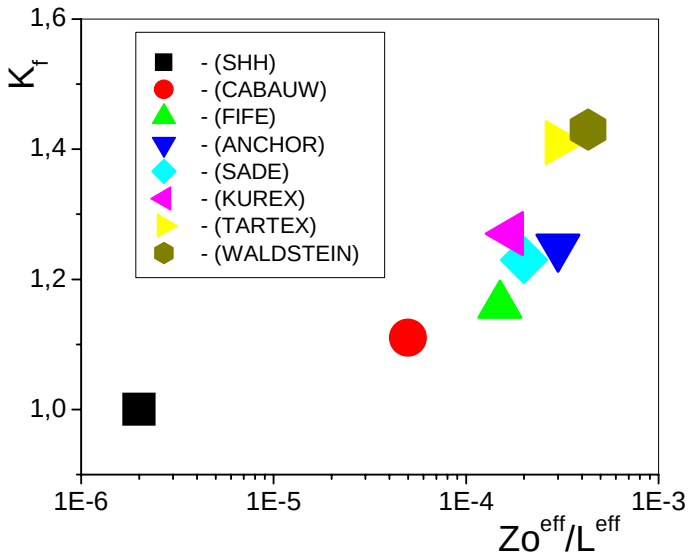

Figure 1. Dependence of the heat imbalance coefficient *kf* on the measure of inhomogeneity of the land surface from the FIFE, KUREX, TARTEX, SADE, CABAUW, and Anchor field measurements.

CONCLUSIONS

The investigations performed here show that the approach proposed in the paper may be helpful in improving the existing methods of parametrization of the turbulent heat and mass exchange. The implementation of the approach depends directly on the available digital information on characteristics of the underlying surface. Clearly the results can also be used for refining surface fluxes over inhomogeneous underlying land surfaces in order to take into account subgrid-scale effects in constructing prediction models.

Empirical formulas are presented to refine the results of direct measurements and calculations of surface fluxes over natural (inhomogeneous) land surfaces from profile and standard (using bulk parametrizations) data. These formulas can also be used to determine surface fluxes over inhomogeneous underlying land surfaces in order to take into account so-called subgrid-scale effects in constructing prediction models.

DYNAMICS OF ATMOSPHERIC MERCURY IN THE RUSSIAN ARCTIC DEPENDING ON THE MEASUREMENT POSITION VERSUS COASTLINE

F.F. PANKRATOV[1], A.G. MAHURA[2], J.V. KORPUSOVA[3] and O.V. KATZ[4]

[1] Research and Production Association (RPA) "Typhoon", Pobeda Str. 4, Obninsk, Russia.

[2] Danish Meteorological Institute, DMI, Lyngbyvej 100, DK-2100, Copenhagen, Denmark.

[3] Federal Budgetary Health Care Institution Center of Hygiene and Epidemiology, Federal Medical-Biological Agency, Lenin Str. 85, Obninsk, Russia.

[4]B-Service Ltd, Lenin Str. 82, 249038, Obninsk, Russia.

Keywords: gaseous elemental mercury (GEM), long-term monitoring, polar station Amderma, Kara Sea, Atmospheric Mercury Depletion Events (AMDEs).

INTRODUCTION

Mercury is one of the most toxic heavy metals, which poses a serious threat to the Arctic environment. Atmospheric transport in high-altitude area of Polar regions is the main channel of mercury from the middle and southern latitudes, where the sources of mercury can be of both anthropogenic and natural origins. Rivers of the Arctic Ocean basin is the second largest channel of mercury pollution in Arctic. With its unique properties mercury is capable to be transported over long distances depositing on the underlying surface and transforming into more toxic compounds. This leads to the accumulation of mercury in Arctic ecosystems. The monitoring has demonstrated that the background concentrations of elemental mercury in the surface layer in the Russian Arctic (1.5 ± 0.4 ng m^{-3}) are similar to the global background - 1.5 – 1.7 ng m^{-3} in the Northern Hemisphere (*Steffen, et al., 2008*). In 1998 the "depletion" of atmospheric mercury in the air (AMDE - Atmospheric Mercury Depletion Event) had been recorded on the polar Canadian station "Alert" (*Schroeder at al., 1998*). Since 2001, at the polar station "Amderma" (69,45°N, 61,39°E, Ugor Peninsula, Nenets Autonomous Region, Russia) the mercury analyzer was installed and AMDEs events were registered there as well (*Pankratov et al., 2008*). Such event means an abrupt decrease in the concentration of gaseous elemental mercury (GEM) in the atmospheric boundary layer during spring time. If we consider the variability of mercury concentrations within the coastal zone, than it was mostly all cases depletion of mercury were recorded within a 10 km zone from the coast (ice Chorus) at a depth of land and no more than 100 meters into the ocean (*Huiting Mao, et al., 2011*). Studies conducted for measured values of mercury concentrations in the troposphere, using air probes shown that GEM is presented in the troposphere to a height of no more than 8 km. However, even at these altitudes, there were cases of mercury depletion (*Radke et al., 2007; Swartzendruber et al., 2008*). This process is the main factor of mercury flow from the atmosphere resulting in the intensive deposition of mercury on the surfaces of snow and ice in coastal zone of the Arctic seas. In the soil, microorganisms transform deposited elemental mercury into more toxic organic forms, for example, methyl-mercury (*Sillman et al., 2007; Selin et al., 2007; Weiss-Penzias et al., 2009*). Organic forms of mercury further accumulate through food chains in fish, marine mammals and higher predators, and finally - in bodies of native population. Over the past 100 years, emissions from anthropogenic sources have led to a doubling of mercury in the upper 100 m of the world ocean, leading to intense pollution of various biological objects.

METHODS

During the 12 year observational period the analyzer "Tekran 2537A" (*Toronto, Canada, http://www.tekran.com*) was installed at three different locations. Continuous measurements of GEM in the surface layer of the atmosphere with high temporal resolution of 5 minutes at detection limit of 0.1 ng m^{-3} are conducted using this instrumental complex. The device has the following characteristics: high temporal resolution (5 minutes, up to 200 hours); the volume of the pumped air ranges from 0.7 to 1.5 dm^3 min^{-1}; the trap of triple nine gold is used for the sorption of mercury; there is an automatic internal calibration during the mercury measurement; performs continuous long-term, unattended analysis of gaseous elemental mercury and data processing. After an accumulation period, the amalgamated mercury thermally desorbs and quantifies using cold vapor atomic fluorescence spectroscopy. Measurements of mercury in the air are taken every 30 minutes for one of the two channels.

Relationship between the mercury concentration in the atmosphere and the location of the analyzer.

Since 2001, the analyzer was placed at different distances (ranging from 8.9 to 0.2 km) from the coast of the Kara Sea (see Figure 1). It is necessary to note that such experiment was carried out for the first time during the monitoring of heavy metals in surface layer of the atmosphere at the Russian polar station. The dominating surface and land-cover are mostly tundra in the area of monitoring homogeneously hilly lowland with similar climatic conditions (note, at each point of mercury measurements the meteorological parameters were also recorded). Therefore, we may assume that the observations were made under the same conditions of the coastal zone of the Kara Sea (sunny/cloudy conditions), and it cannot greatly affect a change in dynamics of atmospheric mercury (e.g. maximum distance between two subsequent relocation points does not exceed 6 km), and especially during winter seasons (*Fig. 1*).

Climatic characteristics of the Yugra Peninsula, where the analyzer was installed and long-term monitoring was carried out, have significant effect on the measured concentrations of GEM. The move sequence analyzer during the experiment at the polar station "Amderma" is shown in Figure 1. Analysis of the data measured at the Site № 1 showed that during 2001-2004 the average GEM concentration was 1.65 ±1.91 ng m^{-3} (with maximum and minimum values as 75.5 and 0.1 ng m^{-3}, correspondently).It should be noted that during this period there was no observed a decreasing trend for the average concentration of GEM. The number of events with increased mercury concentrations (e.g. > 1.8 ng m^{-3}) remained the same for all seasons. This does not correspond to the general trend of reducing the mercury concentration in the Arctic region.

Fig. 1. Geographical locations of the Tekran analyzer for observation period from 2001 to 2013.

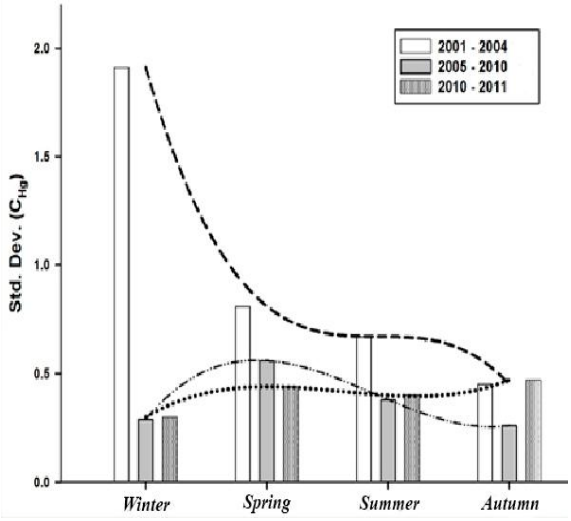

Fig. 2. Season std. deviations, for observation period 2001-2011.

At the same time, the maximum variability of the GEM concentration in the surface layer of the atmosphere was registered for this period, and the estimated value of the standard deviation (σ) for the whole period of monitoring was ± 1.91 ng m^{-3} (see seasonal variability of σ in Fig. 2). On the basis of these results the Site № 1 can be assumed to be situated on a boundary of a region (about 9 km from the coast of the Kara Sea (Fig. 1), where AMDEs are not so frequent as for the coastal zone of the Arctic seas, Site № 2 and Site № 3.

Analysis of the data measured at the Site № 2 showed that for 2005-2010 period the average and maximum GEM concentrations were 1.48 ± 0.4 ng m^{-3} and 14.53 ng m^{-3}, correspondently, and the estimated value of $\boldsymbol{\sigma}$ ranged from ± 0.4 to ± 0.6 ng m^{-3} (Fig. 2). For this period a decreasing trend of GEM concentration was identified (-0.04 ng m^{-3}/year). The standard deviation for the same period of monitoring at the Site № 2 was ± 0.4 ng m^{-3}. However, the long-term AMDEs were registered for the first time during the polar night in 2006-2007 in the total absence of solar radiation. At the same time, in the spring-summer season of 2010 the high GEM concentrations were registered, which is not typical taking into account the decreasing dynamics of its concentration in the Northern Hemisphere.

In June 2010, the analyzer was installed at the Site № 3 (about 200 m away from the coastline of the Kara Sea). Data analysis showed that from June 2010 till October 2013 the average GEM concentration was 1.38 ± 0.84 ng m^{-3}, and the maximum - 94.35 ng m^{-3}. The decreasing trend of the mercury concentration for this period was about 0.04 ng m^{-3}/year. Such dynamics is a continuation of the general decreasing trend that had started in 2005. It should be noted that the lowest GEM concentration (1.23 ng m^{-3}) was recorded in 2013 and the value of σ was gradually increasing from ± 0.42 ng m^{-3} in 2010 to ± 1.32 ng m^{-3} in 2013. In 2012 the largest the number of episodes with enhanced GEM concentrations (≥ 1.8 ng m^{-3}) (1197) and the largest number of AMDEs (84 cases) were recorded. Such dynamics of mercury in the surface layer of the atmosphere is influenced by proximity to the Kara Sea and the variability of meteorological parameters, in particular, air temperature and relative humidity (*Pankratov et al., 2013*).

Dynamics of mercury depletion and enhancement events.

Using the long-term monitoring data, it is possible to get a conception of the complex physical and chemical processes occurring in the surface layer of the atmosphere, which are significantly affected by the warming in the Arctic region. To indicate the cases when elevated concentrations of GEM (> 1.8 ng m^{-3}) are recorded in the surface layer of the atmosphere for a long time (at least 2 hours) the term "enhancement" of mercury concentration (e.g. AMEEs - Atmospheric Mercury Enhancement Events) is used as an analog of the term "depletion". From 2001 till 2004 the number of these cases was similar (58 in 2001, 56 in 2002, and 54 events in 2003) indicating the absence of decreasing trend of GEM concentration in the surface layer of the atmosphere in the Arctic region. At the same time, in summer seasons (2001-2003) the moderate upward trend (13 hours/year) was registered when calculating the duration of the enhanced GEM concentrations events. For other seasons (spring, fall and winter), there observed a decreasing trend of AMEEs duration (-51, -34 and -14 hours per year, for 2001, 2002 and 2003 years, respectively). The maximum duration of periods of increased GEM was registered for spring 2002 (110 hours). In the spring there observed a slight tendency of decreasing the number of AMDEs (16 cases/year). However, for the duration of these events in the winter (2002-2003 years) a reverse trend (+ 60 hours/year) has been recorded.

For the period 2005-2010, the processes of AMDEs were more intensive at the Site № 2 than at the Site № 3. For spring seasons from 2005 till 2008 the number of AMEEs was increasing (18 events/year). At the same time, in the spring of 2008-2010 the reverse trend to a sharp decrease of AMEEs number was registered. In the spring of 2008 the maximum number of AMEEs was recorded (80 events), which is 1.5 times more than the one recorded for the same season in 2001. At the same time considering the winter period of 2005-2008 there is a tendency of intensive increasing of the duration (60 hours/year) of these events with the maximum duration (213 hours) of the AMEEs being recorded in 2008. The maximum

duration of AMEEs, for the period was more than 4 time higher than the duration recorded during the period of 2001-2004. For the mercury, depletion there is a weak increasing trend of the annual events number for the springs during 2005-2010 (3 events/year). The maximum number of AMDEs (30 events) was reported in the spring period of 2006, and the maximum duration (70 hours) of these events was reported in winter of 2008-2009. It should be also mentioned a significant increase of duration (32 h/year) of these events in the autumn season of 2008-2010. There is a trend toward the most intensive growth of AMEEs (45 events/year) in the summer seasons during June 2010 to July 2013. The maximum number of AMEEs (75 events) was recorded in summer of 2013, but the maximum duration (112 hours) the events was obtained for summer of 2011. At the same time for AMDEs, there is a tendency to the moderate growth in spring (7 events/year) and autumn (5 events/year). For 2010-2013, the maximum number of AMDEs (62) was recorded in spring of 2011.

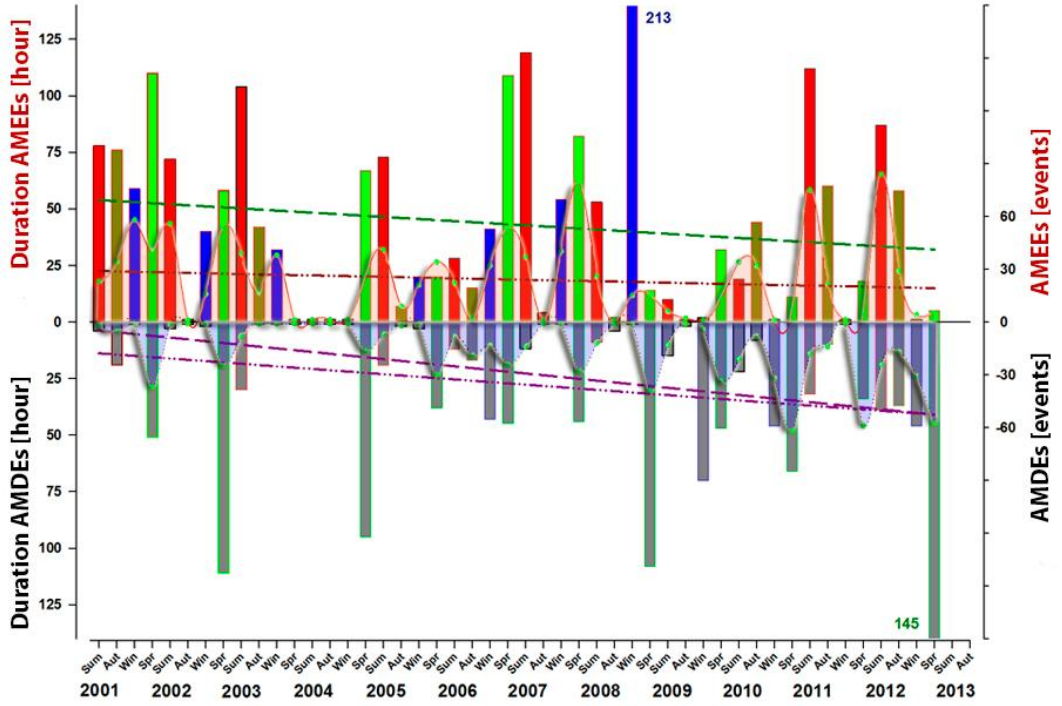

Fig. 3. Seasonal dynamics of AMDEs and AMEEs events during the monitoring period from 2001 to 2013 (sinusoidal area). Duration of AMDEs and AMEEs (bar chart, the red colour - summer, green - spring, dark yellow - autumn, blue - winter). Linear approximation for the AMEEs duration for spring (green dashed line), and AMDEs duration for winter (purple dashed line); for total AMEEs duration (brown dash with two dots) and for total AMDEs duration (purple dash with two dots).

However, the lowest average seasonal GEM concentration (0.84 ng m^{-3}) for the entire 12 year period of observations was obtained for spring 2013. It should be noted that for winter (December-February 2012-2013) an increase of AMDEs has been registered for the first time with maximum number of 31 events. For spring 2013 a sharp increase of AMDEs duration (up to 145 hours) should be noted. It is 5 times more than for a similar period in 2006 (31 h) and 10 times more than was registered for the monitoring period of 2001-2004 at the Site № 1. Data for 2010-2013 confirm a trend to a shift of the processes of mercury depletion to winter seasons. This leads to an additional mercury deposition in different ecosystems in the Arctic. However, the maximum of AMEEs has been registered to be shifted from spring to summer season. Also, the number of AMDEs was increasing in winter of 2010-2013 (maximum up to 8 times as compared to previous years) (*Pankratov et al., 2014*). Tendency of increasing of mercury depletion events in the summer and autumn seasons of 2010-2013 should also be noted relative to the entire monitoring period (2001-2013). Such dynamics of mercury can cause additional, at least, a two-fold increase of mercury deposition into ecosystems of the Russian Arctic.

The third period (from June 2010 to July 2013) can be described as the most dynamic one in relation to the entire period of monitoring. The analyzer was installed at a distance of about 200 m from the coast of the Kara Sea. The main feature of 2010-2012 was connected with the registration of a large number (475 events/year) of AMEEs in summers. In 2012 there observed the maximum the number of such events (1197) for the whole period of the monitoring (Fig. 3). Such rapid growth is related to the fact that over the site of the measurement the volcanic clouds originated from active at this period of time volcanoes Eyjafjallajökull and Grímsvötn (Iceland) have been passed over the Yugor Peninsula (Amderma station). Assessments using method of backward trajectory modelling showed that the atmospheric fronts from the north-west could bring to the area of monitoring the aerosols and volcanic ash from the active volcano Eyjafjallajökull. Determination of air parcels spatial positions in the atmosphere during such movements may allow the identification of potential paths and regions (*Pankratov et al., 2012*).The decreasing trend of AMEEs number was registered for spring and autumn (-5 and -61 events, correspondently). There were no AMEEs recorded in winter months. However, during 2010-2013 the number of decreased values of GEM concentration was considerably increasing reaching 179 events/year in spring, 58 events/year in autumn and 23 events/year in winter. The number of the low values of mercury concentration registered in spring of 2013, with 1155 being the absolute maximum for the entire monitoring period.

CONCLUSIONS

Mercury concentration in the surface layer of the atmosphere in the Russian Arctic (Amderma station) was shown to steadily decrease from 1.67±0.3 ng m^{-3} in 2001 to 1.23±1.3 ng m^{-3} in 2013. The similar mercury behavior was reported previously for the international polar stations in the Northern Hemisphere. Decrease of combustion of fossil fuels and climate change in the Arctic are supposed to be the main reasons for such trend of atmospheric mercury concentration. Atmospheric mercury depletion events (AMDEs) were reported at the polar station "Amderma" during the long-term monitoring from 2001 to 2013. This observations are simultaneously conducted with international Arctic stations "Alert" (Canada) and "New Ålesund" (Norway). The number of AMDEs in the period from 2010 to 2013 increased 2 times in spring, 3 times - in summer, and 8 times - in winter, compared with the reason period from 2010 to 2013. At the same time there observed a seasonal shift of AMDEs frequency from spring to winter season, and AMEEs - from spring to summer season. These both processes could be the result of climatic changes taking place in the Russian Arctic.

Mercury concentration and frequency of depletion events wire changing, when location of the monitoring station was positioned at different distances from the coastline of the Kara Sea. Mercury depletion was shown to proceed actively only in a narrow region along the coast of the Arctic seas with a slight extension of the zone (about 9 km) both towards the land, and towards the far sea. Meteorological parameters such as air temperature, relative humidity and wind speed have been shown to significantly influence processes of mercury depletion in the atmospheric boundary layer in spring and summer during solar maximum and during polar night in an absence of solar radiation and photochemical reactions.

For the first time the impact of the natural sources on the mercury dynamics due to the long-range atmospheric transport has been registered in the Russian Arctic. Modeling of backward trajectories underling that the increase of the mercury concentration in the surface layer of the atmosphere in 2010 and 2011 at the “Amderma” monitoring station was caused by the volcanic cloud passing over the Yugor Peninsula during the eruptions of Eyjafjallajökull and Grímsvötn volcanoes (Iceland).

ACKNOWLEDGEMENTS

The authors gratefully acknowledge colleagues Strelnikov I., Kozulin S., and Morozov V. for continuous maintaining the mercury analyzer during 2001-2010. Authors appreciate invaluable assistance from personal working at the Russian polar station “Amderma”. Thanks to Mikushin A., and Guskov V. for continuous maintaining the mercury analyzer, as well as staff of the “Amderma” hydrometeorological

service engaged in monitoring and technicians for their permanent support in performing measurements during 2010-2013. Thanks A.A. Vinogradova for comment and remark when writing this article.
Financial support for the monitoring program was provided by Environment Canada, AMAP Secretariate and Russian Federal Service for Hydrometeorology and Environmental Monitoring.

REFERENCES

Pankratov F., Konoplev A. Effect of the elemental mercury decreases in atmosphere of the Russian Arctic. Synopsis and Poster, International Conference on Environmental Observations, Modeling and Information Systems ENVIROMIS-2008, 28 June -6 July, Tomsk, Russia, 2008.

Pankratov F., Konoplev A. The dependence of atmospheric mercury depletion events at polar stations Amderma on seasonal changes of meteorological parameters. Materials of International Symposium Mercury in the biosphere: Ecological and geochemical aspects. Moscow. Russia, Vernadsky Institute of Geochemistry and Analytical Chemistry, 7 – 9 September 2010, 61 – 66.

Pankratov F., Mahura A., Katz O., Konoplev A. Long-term continuous monitoring of GEM in the ambient air on the Russian Arctic. Impact of the Eyjafjallajökull and Grimsvötn volcanic eruptions in Iceland. // Synopsis and Poster, Boundary Layers in High Latitudes: Physical and Chemical Processes Including Atmosphere-Ice Chemical Interactions (AICI). European Geosciences Union General Assembly 2012. April 22-27, 2012, Vienna, Austria: Abstract. http://meetingorganizer.copernicus.org/EGU2012/poster_programme/9022/XY130/EGU2012-10377

Pankratov F.F., Mahura A., Konoplev A.V., Katz O.V. Analysis of the data of long-term monitoring of atmospheric mercury content and meteorological parameters at Amderma polar station. Russian Meteorology and Hydrology June 2013, Volume 38, Issue 6, pp 405-413. doi: 10.3103/S1068373913060058 (2013).

Pankratov F., Mahura A., Popov V., Katz O. Long-term continuous monitoring of mercury in the Russian arctic: winter increase of atmospheric mercury depletion events. // Synopsis and Poster, Atmospheric Sciences, Pan Eurasian Experiment (PEEX). European Geosciences Union, General Assembly 2014. April 27 – 02 May, 2014, Vienna, Austria: Abstract. http://meetingorganizer.copernicus.org/EGU2014/EGU2014-16608.pdf

Radke L.F., Friedli H.R., Heikes B.G.: Atmospheric mercury over the NE Pacific during spring 2002: Gradients, residence time, stratosphere-troposphere exchange, and long-range transport. J. Geophys. Res. 112, D19305 (2007). doi:10.1029/2005JD005828.

Schroeder, W. H., K. G. Anlauf, L. A. Barrie, J. Y. Lu, A. Steen, D. R. Schneeberger, and T. Berg. Arctic springtime depletion of mercury, Nature, 1998, 394, 331-332.

Selin N.E., D.J. Jacob, R.J. Park, R.M. Yantosca, S. Strode, L. Jaegle and D. Jaffe. Chemical cycling and deposition of atmospheric mercury: Global constraints from observations. 2007, Journal of Geophysical Research, 112:D02308.

Sillman S., F. J. Marsik, K. I. Al-Wali, G J. Keeler, and M. S. Landis, Reactive mercury in the troposphere: Model formation and results for Florida, the northeastern United States, and the Atlantic Ocean, 2007, J. Geophys. Res., 112, D23305, doi:10.1029/2006JD008227.

Steffen A., Douglas T., Amyot M., Ariya P., Aspmo K., Berg T., Bottenheim J., Brooks S., Cobbett F., Dastoor A., Dommergue A., Ebinghaus R., Ferrari C., Gardfeldt K., Goodsite M. E., Lean D., Poulain A., Scherz C., Skov H., Sommar J., and Temme C.. A synthesis of atmospheric mercury depletion event chemistry linking atmosphere, snow and water. Atmos. Chem. Phys., 2008, 8, 1445-1482.

Swartzendruber P.C., Chand, D., Jaffe, D.A., Smith, J., Reidmiller, D., Gratz, L., Keeler, J., Strode, S., Jaeglé, L., and Talbot, R. Vertical distribution of mercury, CO, ozone, and aerosol scattering coefficient in the Pacific Northwest during the spring 2006 INTEX-B campaign. J. Geophys. Res. 113, D10305, doi:10.1029/2007JD009579 (2008).

Weiss-Penzias P., M.S. Gustin, and S.N. Lyman. Observation of speciation atmospheric mercury at three sites in Nevada: evidence for a free tropospheric source of reactive gaseous mercury. 2009, Journal of Geophysical Research 114: D14302. doi:10.1029/2008JD011607.

MODEL ASSESSMENT FOR CHANGING TERRESTRIAL PROCESSES OVER PAN-ARCTIC REGIONS

H. PARK[1], and Y. IIJIMA[1]

[1] Research and Development Center for Global Change, Japan Agency for Marine-Earth Science and Technology
Yokosuka, Kanagawa, 237-0061, Japan.

Keywords: Land surface model, CHANGE, pan-Arctic, permafrost.

A numerical model (CHANGE) that includes hydrological, biogeochemical, and ecological processes in terrestrial areas had developed and validated to observational data at site specific and pan-Arctic scales. The model simulates heat, water, and carbon fluxes in the atmosphere–land system, soil thermal and hydrologic states, including an explicit treatment of soil freezing/thawing phase transitions up to 50.5 m in soil depth, snow hydrology, stomatal physiology and plant photosynthesis, making it possible to increase our understandings for interactions and feedbacks between processes and components associating with climate changes. Simulation applying to the period 1910–2009 indicates that permafrost temperature is certainly increasing and active layer thickness is also deepening due to the climate warming. Snow cover that shows large heterogeneous distribution works as a factor contributing to the warming of permafrost, especially at continuous permafrost regions. The sequence of permafrost warming was found in the increasing decomposition rate of soil organic matter, enhancing positive feedback to climate change. Changes were also identified at river processes; river-ice thickness tended to be shallower and the ice period had been shortened. River heat fluxes that flow into Arctic Ocean have increased. The model simulation obviously indicates that Arctic terrestrial processes are changing, which will be introduced in the workshop.

APPLICATION OF VARIATIONAL MODELING TECHNOLOGY FOR ENVIRONMENTAL STUDIES

V.V. PENENKO[1], A.A.BAKLANOV[2], E.A.TSVETOVA[1] and A.V. PENENKO[1]

[1]Institute of Computational Mathematics and Mathematical Geophysics, Novosibirsk, 630090, Russia.

[2] World Meteorological Organization, Research Department, Geneva, Switzerland

Keywords: COUPLED ATMOSPHERIC HYDRODYNAMICS AND CHEMISTRY, DIRECT AND INVERSE PROBLEMS, VARIATIONAL DATA ASSIMILATION, ENVIRONMENTAL RISK.

INTRODUCTION

Coupling of atmospheric dynamics, pollutant transport, chemical reactions and atmospheric composition for modelling environmental impacts, climate change, weather forecasts and air quality will remain one of the most challenging tasks over the next decades as they all involve strongly integrated processes. It is well accepted that weather has a profound impact on air quality and atmospheric transport of hazardous materials. It is also recognised that atmospheric composition can influence both weather and climate directly by changing the atmospheric radiation budget or indirectly by affecting cloud formation and precipitation. In recent years, researchers from different countries are developing the integrated systems of mathematical models aimed to solving this class of problems (Baklanov *et al.*, 2011). Air quality models are multifunctional complexes. Depend on study purposes they can include models of atmospheric dynamics, transport and transformation of pollutants in gas and aerosol phases; ways to specify emission factors and assessments of existing and potential sources; quantitative description of adverse effects on human health and ecosystems; valuation methodologies of social and economic assessments of anthropogenic impacts, etc. The most advanced online integrated chemistry-meteorology models simulate two-way interacting meteorology and chemistry over the same grid in one model using one main timestep for integration (Baklanov *et al.*, 2014).

METHODS

In the frames of PEEX Modelling Platform, we plan to develop a set of mathematical tools for construction of integrated models for solution of interconnected problem of atmospheric environment and climate. The central point is a variational approach for solving direct and inverse problems of atmospheric hydrodynamics and chemistry. It is important that the accurate consistency of numerical schemes should be provided in the chain of objects like: direct/adjoint problems – sensitivity relations – inverse problems for finding parameters and sources, including assimilation of all available measurement data. To solve the problems we have developed a new enhanced set of cost-effective algorithms.

We use the formulation of the variational principle with weak constraints (Penenko, 2009). This is because the various types of uncertainties and errors exist in the model formulations and in specification of sources and initial data. To consider them, we explicitly introduce some additional unknown functions (uncertainty functions) into the formulation of the problem. To solve direct and inverse problems of estimating state functions and sources, we use data assimilation techniques. In such approach, the algorithms for direct-inverse modelling are universal. In the absence of uncertainty functions, we have perfect problems and variational principles with strong constraints in the frames of the same technology.

THE ROLES OF ADJOINT PROBLEMS AND UNCERTAINTY FUNCTIONS

In the variational modeling technology for complex systems, the fundamental role of adjoint problems is in that they are a tool for creating linkages between disturbances of the objects in the space of the state functions of the processes models and those in the space of parameters and input data. They gather up all the internal degrees of freedom of the numerical models. Then the prediction is based on the sensitivity relations. This is the basic idea of the concept: when assessing the cost functional, we move the problem from the space of state functions into the space of parameters and sources. This makes it possible to use the theory of sensitivity and methods for solving inverse problems at the level of the cost functional working only with external degrees of freedom.

An important element of the proposed concept is a method of evaluation of uncertainty functions. These functions substantially contain quantitative information about the adequacy of the prediction technology for the chosen structure of models and the precision of the input data. Uncertainty functions give an additional benefit from a computational point of view. Their inclusion in the models of the processes and in the estimated functionals gives the natural regularization of the algorithms for solving inverse problems and data assimilation (Penenko, 2009) and improves the degree of conditionality of calculations. Variational formulation of the forecasting system with the assessment of uncertainty allows us to construct the efficient algorithms for sequential data assimilation in real time.

Detailed description of our methods is given in **(**Penenko *et al*, 2012). Next, we make some remarks on solving inverse problems with the assimilation of available observational data. Currently, data assimilation problems are among the most common of inverse problems, in which the solution of direct and adjoint problems are also used.

VARIATIONAL DATA ASSIMILATION

In the implementation of our concept, we use variational methods with adjoint equations for data assimilation based on strong-constraint variational principle and weak-constraint variational principle with uncertainty (Penenko, 2009, Penenko *et al*, 2012).

In the case of weak constraints, the additional terms, uncertainty functions, are included in the models of processes. From the theory of optimal control, they can be considered as control functions, which are defined by a predetermined target functional with all the available measurement data. Accordingly, the functional of the variational principle is defined based on the total measure of all uncertainties included in the modelling system. In this formulation, 4D-Var and Kalman filtering methods are equivalent to each other. However, unlike the latter, the use of variational methods with uncertainty does not require calculation of error covariance matrix and application of the technique of ensemble approach (Penenko, 2009).

Sensitivity functions and uncertainty functions expand the scope of variational methods for solving inverse problems with data assimilation. Their use leads to efficient data assimilation algorithms. Note that the length of "assimilation window" (the time interval during which we want to consider observations if received) is defined parametrically. It can be chosen arbitrarily. In particular, if the window is chosen to be one time step of the model, we obtain the variational algorithms having non-iterative implementation schemes operating in the rate of solving direct problems of the dynamics and chemistry. Methods of this class are most in demand for practical applications when we use the models along with large amounts of observational data, including those relating to atmospheric chemistry (Penenko and Tsvetova, 2013, Penenko A. and Penenko V., 2014).

NUMERICAL REALIZATION

The nature of this class of problems is different scales of processes that need to be adequately described by mathematical models. Numerical implementation of the models is essentially important in this case. We use the well-known splitting techniques (Marchuk, 1982; Samarskii, 2001) and theory of adjoint equations (Marchuk, 1995). In addition we propose a new variational method for constructing numerical schemes using the technique of discrete-analytical approximations and adjoint integrating factors (Penenko, Tsvetova, 2009, 2013; A. Penenko, 2012; Penenko *et al*., 2014). It gives us the opportunity to build unconditionally monotone approximations for convection-diffusion-reaction operators, which are the basic elements of integrated models of the dynamics and chemistry of the atmosphere.

THE SCENARIO APPROACH

In ICMMG we develop a simulation system for constructing forecast scenarios for assessment of ecological perspectives. It includes the models of different levels of complexity. One of the main objects in the system is a global model of atmospheric dynamics based on a hybrid $\sigma - p$-coordinate system. In its area of modelling the vertical dimension is conventionally divided into two subregions: the free atmosphere and the lower part of the troposphere with the boundary layers. There are also two versions of the models of meso-regional scales in the hydrostatic and nonhydrostatic versions. In the set, the models of transport and transformation of impurities are also included.

Under this system, we set and solve various problems of environmental prediction and design. According to the above concept, we associate into a single system all the target criteria of the forecast, the restrictions on the class of functions, available information, and the models describing the processes and observations. Many problems require the use of combined methods of direct and inverse modelling. This primarily relates to the problems of long-term forecasting and risk assessments in a changing climate. In our approach, the idea of dividing the processes with respect to characteristic scales is realized to these goals (Penenko and Tsvetova, 2008).

We use optimization methods of orthogonal decomposition based on singular value decomposition (SVD) of rectangular matrices of large dimension in the phase space. These matrices are composed of a set of state functions calculated with models or with observational data. The result is a set of multi-dimensional basis of orthogonal subspaces, ranked by scale disturbances. With this approach, the singular values of the studied database, arranged in descending order, represent a quantitative measure of information content of the corresponding basic subspaces. According to this criterion, we produce a set of subspaces divided on climatically significant ones and “weather noises”. These bases are the background for identifying the elements of long-term memory of the climatic and ecological system. We use them to define the opportunities to predict the processes behaviour and to study the variability of their dynamics in general, as well as for the formation of forecast scenarios. Application of SVD-decomposition techniques for analysis of spaces composed of the sensitivity functions makes it possible to identify the major operating factors in the system and to rank the effects of various sources.

Within the framework of variational technology, the major stages of forecasting using inverse modelling techniques are as follows: solution of direct and adjoint problems for the cost functionals and calculation of the sensitivity functions. Further, we assess the functions of risk and vulnerability, and then we calculate the influence of uncertainty in the models and input data. After that, we form the equations of feedbacks from the target functional to the parameters of models and sources.

From the sensitivity functions, we provide zoning for risk and vulnerability and assess the relative contribution of the share issue of impurities from each source, falling into the sensitivity domain, to the overall quality functional. Thus, the results of the forecast are the spatial-temporal configurations of risk areas to obtain a certain level of pollution, rather than a field of concentration of impurities. If there is the data on emissions, then, using the sensitivity relations, the actual contributions of emissions into the target functional can be estimated without solving the direct problem.

In this talk we will present some results of modelling scenarios on assessment of environmental risk/vulnerability for Arctic and Siberia regions.

.

CONCLUSIONS

We have presented a brief description of the set of algorithms to evaluate and predict the quality of the environment. The weak-constraint variational principle is the basis of the proposed approach. It allows us to estimate the uncertainty in the models due to data assimilation. To include the effects of climate variability, we offer a scenario approach, which takes into account the elements of long-term memory of the climate and ecological systems revealed by orthogonal decomposition. The advantage of the approach is that the variational technology ensures the consistency of all staged in solving the direct and inverse problems of environmental prediction and design and allows us to construct the cost-efficient numerical algorithms.

ACKNOWLEDGEMENTS

This work was supported by the Presidium of RAS under Program No 43 and by RFBR under grants 14-01-00125 and 14-01-31482 and the COST Action ES1004 EuMetChem.

REFERENCES

Baklanov, A., Mahura, A., Sokhi, R., (Eds) (2011). *Integrated Systems of Meso-Meteorological and Chemical Transport Models,* (Springer).

Baklanov, A., Schlünzen, K., Suppan, P., et al. (2014) Online coupled regional meteorology chemistry models in Europe: current status and prospects, Atmos. Chem. Phys., **14**, 317-398.

Marchuk, G.I. (1982). *Methods of numerical mathematics,* (Springer-Verlag, New York)

Marchuk, G.I. (1995). *Adjoint equations and analysis of complex systems, (*Kluver, Dordrecht).

Penenko V., E. Tsvetova. (2008). Orthogonal decomposition methods for inclusion of climatic data into environmental studies, *Ecol. modelling* **217,** 279.

Penenko, V., E. Tsvetova (2009). Discrete-analytical methods for the implementation of variational principles in environmental applications, *J. of computational and applied mathematics*, **226**, 319.

Penenko V. V. (2009). Variational methods of data assimilation and inverse problems for studying the atmosphere, ocean, and environment, *Numerical Analysis and Applications,* **2,** No 4, 341.

Penenko, A.V. (2012). Discrete-analytic schemes for solving an inverse coefficient heat conduction problem in a layered medium with gradient methods, *Numerical Analysis and Applications*, **5**, 326.

Penenko, V., A. Baklanov, E. Tsvetova and A. Mahura (2012). Direct and Inverse Problems in a Variational Concept of Environmental Modeling, *Pure and Applied Geoph.* **169,** 447.

Penenko, V. and E. Tsvetova (2013). Variational methods for constructing the monotone approximations for atmospheric chemistry models, *Numerical Analysis and Applications* **16,** No 3, 239.

Penenko, A.V. and Penenko V.V. (2014), Direct data assimilation method for convection-diffusion models based on splitting scheme. *Computational technologies*, **19** Issue 4, 69 (In Russian).

Penenko, V.V., E.A. Tsvetova, A.V. Penenko (2014) Variational approach and Euler's integrating factors for environmental studies, *Computers and Mathematics with Applications*, **67**, Issue 12, 2240.

Samarskii, A.A. (2001) *The theory of difference schemes.* (Marcel Dekker, New York).

THE PALEOLIMNOLOGICAL INDICATION OF DIATOMS (BACILLARIOPHYTA) FROM YAKUTIAN LAKES (EAST SIBERIA)

L.A. PESTRYAKOVA[1], U. HERZSCHUH[2,3], R.M. GORODNICHEV[1]and S. WETTERICH[2]

[1]Institute of Natural Sciences, North Eastern Federal University, Yakutsk,
Republic of Sakha (Yakutia), Russia
[2] Department of Periglacial Research, Alfred Wegener Institute Helmholtz Centre for Polar and Marine Research, Potsdam, Germany
[3]Institute of Earth and Environmental Science, Potsdam University of Potsdam, Potsdam, Germany

Keywords: YAKUTIAN LAKES (EAST SIBERIA), LIMNOLOGICAL PARAMETERS, DIATOM ANALISIS, INDICATOR SPECIES

INTRODUCTION

As north Siberia is an area with high present-day warming rates, reliable tools for environmental reconstructions to track lake-system adjustments to climate change on millennial to decadal time scales is of high importance. In addition, the use of environmental indicators that can assess past environments by analysing samples collected from remote sites where continuous monitoring is not feasible would help to decipher recent change. For that purpose, this study aims to set up a regional indicator-diatom set for selected environmental variables for Yakutia. In arctic and subarctic lake waters where low temperatures and ice cover limit other algae, diatoms often substantially contribute to or even dominate the lake primary production. Diatoms are sensitive to various environmental variables such as nutrient content and salinity. Diatoms thus have a high potential for indicating change in most environments given that regional diatom-environment relationships are known.

Typically the environmental indication of complete diatom spectra are investigated using multivariate statistical methods, while the indicator value of individual taxa is less often examined. Furthermore, existing studies only report optima and tolerances for selected environmental variables while the inference of the decisive environmental factor for the distribution of a single taxon has not been investigated. Gaining such information for Yakutia is particularly useful to allow a more reliable qualitative and semi-quantitative interpretation of the remarkable number of available fossil diatom spectra previously published without the need for taxonomic harmonisation as would be necessary when applying multivariate transfer functions to fossil data.

In particular, this study aims (1) to examine the indicator value of individual species for specific environmental variables and (2) vegetation types (arctic tundra, forest tundra, northern taiga, mountain taiga, typical taiga), and (3) to evaluate the use of such information for both past environmental reconstruction and modern environmental assessment purposes.

STUDY AREA

The study area comprises the Republic Sakha (Yakutia) situated in eastern Siberia, Russia. The investigated sites are scattered across a large area (56.35-72.83°N; 110.2-161.0°E) covering more than 3,000 km^2 (Fig. 1). Yakutia experiences an extreme climate and belongs to three climatic zones: arctic, subarctic, and temperate. The winter is long and cold whilst summer is short, often hot and quite dry. The mean annual temperature varies from −8°C in the north to −16°C in the central areas. Mean annual precipitation ranges from less than 150 mm close to the northern coast, up to 700 mm in the southern mountainous regions. Arctic and boreal vegetation dominates in Yakutia. The forest-tundra border, i.e. the treeline lies along 72°N in the West of Yakutia and gradually descends to 69°N in the East. The arctic tundra is mainly composed of mosses, *Carex*, *Dryas*, *Cassiope* and dwarf *Salix* and in its southern part of

shrubby *Betula*, *Alnus* and further Ericaceae. Trees in forest-tundra and the northern taiga are formed by *Larix gmelinii* in the east and by *Larix cajanderi* in the west. The typical taiga of central Yakutia is mainly composed of *Larix cajanderi* (on sandy sites also of *Pinus silvestris*), and various shrub taxa (*Vaccinium vitis-idaea*, *Arctostaphylos uva-ursi*), Forest-steppe occur at few dry places in central Yakutia.

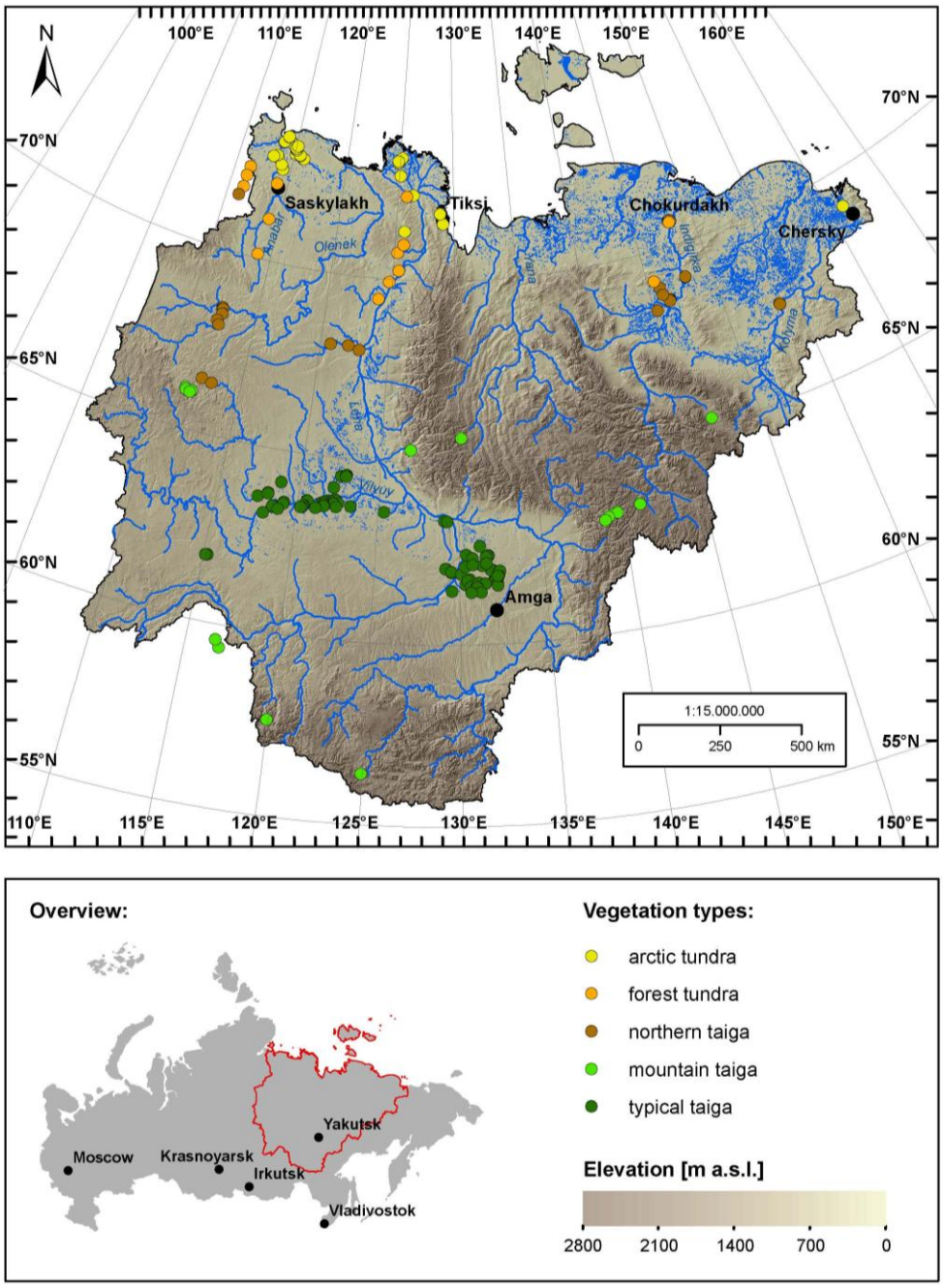

Figure 1. Map of Yakutia showing the location of all sampled lakes and the surrounding vegetation type. The vegetation type classification follows Matveev (1989).

Yakutia has a large number of lakes, (there are ~700,000 lakes with a size >1 ha; most of them of thermokarst origin. Central Yakutian lakes are usually ice-covered from late October until mid-May, whereas lakes in the northern part do not become ice-free until late June. Lake levels rise in spring due to snow melt, reach their maximum in July, and are at their lowest from November to April. Many central Yakutian lakes with closed lake basins are characterised by high ion concentrations due to strong

evapotranspiration and evaporative ion concentration (Herzschuh et al., 2013). Evidence of any anthropogenic impacts is mostly small or absent; only hay harvesting occurs in thermokarst basins in some areas of central Yakutia.

METHODS

We collected surface sediments from 206 lakes scattered throughout Yakutia in summers between 2001 and 2009 (Fig. 1). The lakes were chosen in order to cover large gradients in geography, climate, vegetation, and lake chemistry. The investigated lakes are generally shallow (median: 2.9 m) and small (median: 0.74 km^2), with small catchments. Most of them have been formed by thermokarst processes. Our selected sample set includes lakes from five vegetation zones: 40 lakes are located in the arctic tundra zone, 21 lakes in the forest-tundra zone, 25 lakes in the northern taiga zone, 16 lakes in mountain taiga, and 104 lakes are located in the typical taiga zone among them 15 in *Pinus-Larix* forests and 13 in *Betula-Larix* forests and 76 in *Larix* forests. Lakes were sampled from an inflatable rubber boat. Surface sediments were obtained from the deepest part of each lake using a sediment grab or a UWITEC® gravity corer (upper ~2 cm of sediment). The deepest part of each lake was located using a portable echo sounder. Limnological parameters such as pH, electrical conductivity, lake area, maximum lake depth, and Secchi depth, were measured in the field. Water samples were collected from 0.5 m below the surface of each lake, immediately prior to retrieval of the sediment samples. Ion analysis was performed but only silica (Si) concentration data was finally included. Mean July air-temperatures were taken from New et al. (2002) and interpolated for the geographical position of each lake. An ordination of the lake environmental variables is provided in Herzschuh et al. (2013).

Diatom analysis was conducted on about 1 g of sediment following standard procedures. The classification of diatom species is based on the latest revisions of the *Achnanthes*, *Fragilaria*, *Navicula*, and *Cymbella* genera.

Out of the 26 environmental variables which were estimated for each lake we selected the following parameters because of their known relevance for structuring diatom communities and their relatively weak inter-correlation as inferred from a PCA of environmental parameters: electrical conductivity, pH, Si concentration, water depth and mean July air temperature (T_{July}). Weighted averaging regression as well as vegetation indicator species analysis were based on environmental variables that were log(x+1) transformed (with the exception of pH and T_{July}). Diatom data are expressed as percentages of all counted valves within one sample. Species were retained for numerical analysis if they occur in at least 6 lakes with an abundance of >0.5%, or if they occur in at least one lake with an abundance of >20%. For weighted averaging regression and indicator species analysis, diatom data were Hellinger transformed in order to stabilise the variance and optimise the `signal-to-noise´ ratio in the data. (1) Boosted regression tree (BRT) analysis was used to model the relationship between individual diatom taxa and environmental variables to infer the most influential environmental variable for each taxon. We implemented boosted regression tree analysis in R version 2.9.1 extended by a further function of Elith et al. (2008). We used a default bag fraction of 0.5, a Gaussian error distribution, a very slow learning rate (0.0005), and a tree complexity of 3 to model taxa percentages along environmental gradients. (2) The weighted averaging (WA) optima and tolerances were estimated to summarize the range of variation in the taxon response to the environmental variables using the program C^2 version 1.3. (3) We *a priori* defined that taxa are reliable indicators if they have a comparatively narrow tolerance range (WA-tolerance below the 0.33-quantile of all taxa of the respective environmental variable) and are specific to a single environmental variable (i.e. when the % of split in BRT for a single environmental parameter is highest among all environmental variables). (4) Indicator species analysis was applied using the group-equalised indicator value index $IndVal^{g}_{ind}$ to detect and describe the preference of different diatom taxa for a particular vegetation type (tundra, forest-tundra, northern taiga, typical taiga) or combinations of vegetation types. Statistical significance was tested for using a randomisation procedure (9999 permutations). A p-value of 0.05 is assumed to indicate a significant relationship. Analyses were implemented using the R package indicspecies (version 1.7.0).

RESULTS

In total, 616 taxa (among them 9 subspecies, one form) were recorded in the modern diatom data-set. The class Coscinodiscophyceae includes 51 taxa representing 8.1% of the total number of taxa. The class Bacillariophyceae shows the highest diversity, comprising 513 taxa (81.9% of all taxa) in 57 genera. The class Fragilariophyceae appears with 62 taxa in 13 genera. Of the 616 taxa, the majority is fairly rare; only 157 taxa fulfil the criteria to be included in the statistical analyses. Of those taxa selected for further statistical analyses (Fig. 2), 42% prefer benthic habitats, 44% are epiphytes, and 14% are planktonic forms. Epiphytes dominate not only in the number of taxa but also in the absolute counts in most lakes, independent of vegetation type, water chemical conditions, and region.

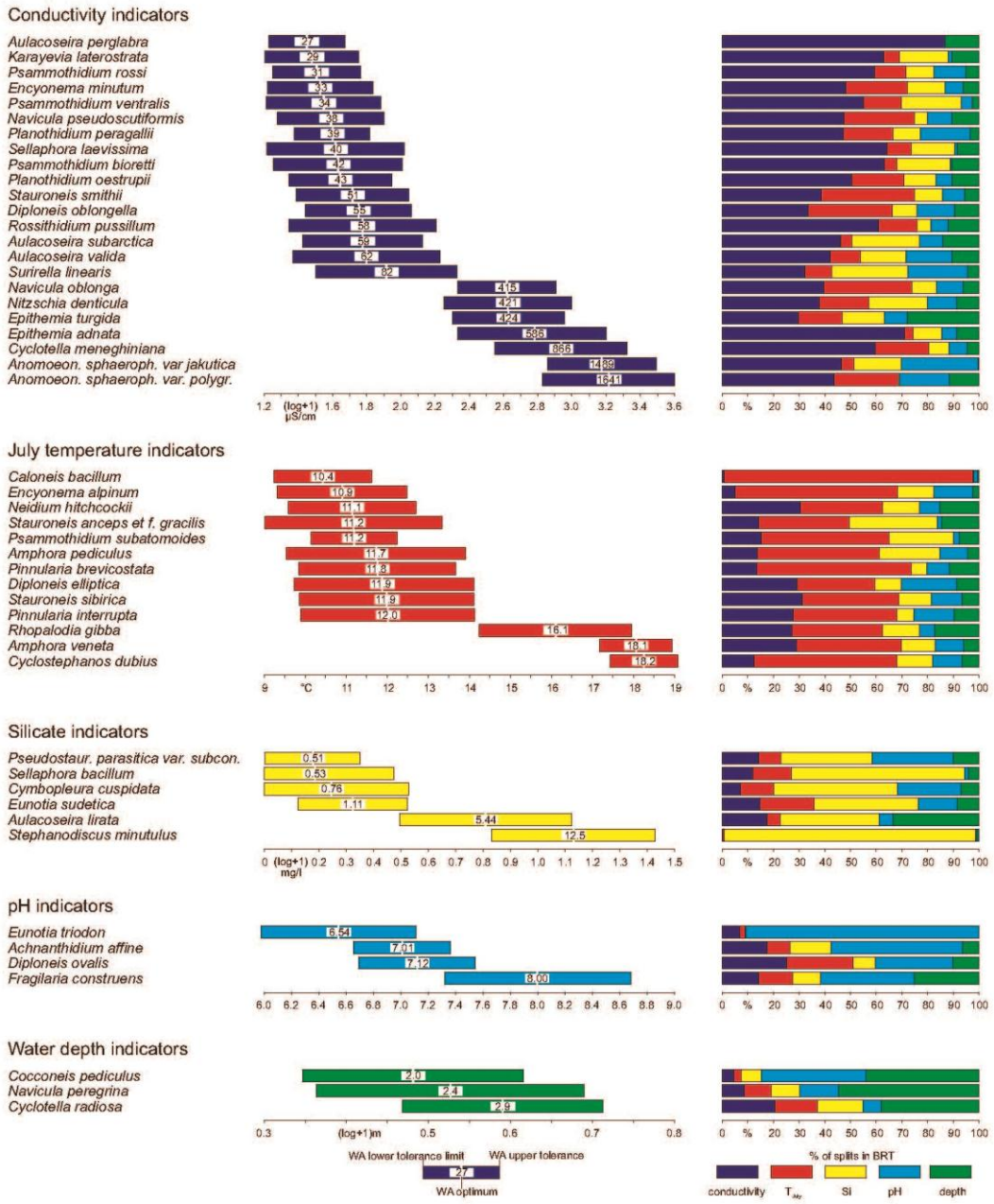

Figure 2. Tolerance and non-transformed optimum (numbers in bars) of reliable indicator taxa for the five environmental variables (left) and the relative share of each variable in splits of boosted regression tree (BRT) analysis (right) (i.e. a high percentage of BRT splits indicates a strong relationship between the respective (colour-coded) environmental variable and diatom percentage in lake surface-sediments from Yakutia).

Electrical conductivity of the lake waters ranges from 8 to 7743 µS/cm which equals an ion concentration of roughly 5 to 5000 mg/l. Lakes from tundra and forest-tundra have very low electrical conductivities mostly below 50 µS/cm. Lakes from the northern taiga and mountain lakes have moderately high electrical conductivities (100–400 µS/cm) and lakes from the typical taiga have high electrical conductivities (>400 µS/cm). Considering all taxa, electrical conductivity is most often selected as the major split variable in the BRT analysis by 45 taxa, and for 19 taxa electrical conductivity causes >50% of the splits. Reliable diatom indicator species for low, intermediate and high electrical conductivity optima are shown in Fig. 2.

The range of mean July air temperatures (T_{July}) covered by this data-set spans from 7.6 to 18.8°C. Almost all arctic tundra lakes lie between 10.1 and 12°C. In comparison to the arctic zone, lakes of the forest-tundra, the northern taiga, and the mountain zone have a much broader T_{July} range. Most of the typical taiga lakes have T_{July} above 17°C. For 35 taxa T_{July} is selected as the major or second major split variable in the BRT analysis, but for only 8 taxa did it cause >50% of the splits. In total, 54 taxa have a low T_{July} optimum (<13°C). The most common and most abundant taxon with a low T_{July} range is *Tabellaria flocculosa*, although T_{July} did not cause the majority of splits in BRT. Most of the taxa with low electrical conductivity optima have low T_{July} optima as well. The 50 taxa with intermediate T_{July} optima (13–15°C) belong to a large variety of genera. According to our definition no taxa have been selected as reliable indicators for intermediate temperatures, because of their large tolerances (median: 3.25°C). In total, 53 taxa have a high T_{July} optimum (>15°C). The more common and abundant taxa such as *Fragilaria construens*, *Staurosira venter*, *Cocconeis placentula*, *Epithemia adnata*, *Fragilaria ulna*, *Navicula radiosa*, and *Stephanodiscus hantzschii* belong to this group but either they have a large tolerance or temperature was not selected as the major split variable in BRT. *Rhopalodia gibba* (16.1°C), *Amphora veneta* (18.1°C), and *Cyclostephanos dubius* (18.2°C) are identified as reliable indicator species for high T_{July} (Fig. 2).

Silicate concentration ranges from 0 to 37.2 mg/l (median: 2.4 mg/l). Silicate concentration is the major split variable for only 17 taxa. *Pseudostaurosira parasitica* var. *subconstricta* (optimum: 0.5 mg/l), *Sellaphora bacillum* (0.5 mg/l), *Cymbopleura cuspidata* (0.8 mg/l), *Eunotia sudetica* (1.1 mg/l), *Aulacoseira lirata* (5.4 mg/l), and *Stephanodiscus minutulus* (12.5 mg/l) represent reliable silicate indicators (Fig. 2).

pH ranges from 4.9 to 10.2. Only 10.7% of the lakes are acidic (pH <6.6) most of them are located in the tundra, forest tundra, and the mountains, while lakes in northern and typical taiga cover a wider pH range. Highest pH values were found in alas lakes of the Lena-Amga interfluve. In comparison to electrical conductivity, pH is less frequently selected as the major splitting variable in BRT. No taxon had an optimum below pH 6.5. Only *Achnanthidium affine* (pH optimum 7.0), *Diploneis ovalis* (7.1), *Eunotia triodon* (6.5), and *Fragilaria construens* (8.0) are identified as reliable pH indicators (Fig. 2).

The water depth varies from 0.3 to 80 m (median: 2.9 m). Most of the central Yakutian lakes are shallow thermokarst lakes, while the deep lakes sampled are only found in the mountains. Within the data-set only three species are reliable indicators of water depth: *Cyclotella radiosa* (optimum 2.9 m), the epiphytic *Cocconeis pediculus* (2.0 m), and *Navicula peregrina* (2.4 m) (Fig. 2).

Out of the 92 taxa that have been selected as indicator taxa, only three and eight have been selected to indicate tundra and forest-tundra, respectively. In contrast, 25 taxa have been selected to indicate a combination of both vegetation types. However, individual indicator taxa always occur at low abundance rarely exceeding 5%. Nevertheless, the indicator value of these taxa for open vegetation types is very high as almost all of these taxa are completely lacking at forested sites. Similarly, 29 taxa are indicators of typical taiga lakes. In contrast, taxa that are affiliated with northern taiga or combinations of vegetation types tend to be generalists in terms of their occurrence and their indicator value reflects differing abundances in the separate vegetation types or type combinations. While *Tabellaria flocculosa*, the most abundant taxon in the northern vegetation zones, is selected as an indicator of a combination of tundra,

forest-tundra, and northern taiga, the most abundant taxa of northern forest lakes (*Staurosirella pinnata*) and typical taiga lakes (*Fragilaria construens*, *Staurosira venter*) are not selected as indicators as they occur in other vegetation types at high abundances as well.

CONCLUSIONS

Relating diatom abundances from lake surface-sediments in Yakutia to five selected environmental variables reveals many indicator taxa exist for extremes in conductivity, mean July temperature and vegetation, but only a few diatom taxa are indicative of the intermediate range of the investigated environmental variables. We did not study interactions between environmental variables on species' preferences which should be done in future to consolidate our knowledge on diatom indicators so that they can be a reliable and convenient tool for the assessment of past and present environmental conditions.

ACKNOWLEDGEMENTS

This research was performed within the joint Russian-German *Arctic Ecological Network* (*Arc-EcoNet*) supported by the Federal Ministry of Education and Research (BMBF grant № 01DJ14003), by the Russian Foundation for Basic Research (RFBR grant № 13-05-00327) and conducted in the frame of research activities defined by the Russian Ministry of Education and Science.

REFERENCES

Elith, J., J.R. Leathwick, and T.Hastie (2008). Boosted regression trees – a new technique for modelling ecological data. *Journal of Animal Ecology* **77**, 802-813.

Herzschuh, U., L.A. Pestryakova, L.A. Savelieva, L. Heinecke, T. Böhmer, B. Biskaborn, A. Andreev, A. Ramisch, A. L.C. Shinneman, and H.J.B. Birks (2013). Permafrost, larch forests, and epigenetic thaw-lake ion content are a coherent geochemical functional entity in Siberia. *Nature Communications* **4**, 2408.

Matveev, I.A. (ed.) (1989). *Agricultural Atlas of the Republic Sakha (Yakutia)*. (Nauka, Moscow).

New, M., D. Lister, M. Hulme, and I. Makin (2002). A high-resolution data set of surface climate over global land areas. *Climate Research* 21, 1-25.

PROGRESS WITHIN "BIOGENIC AEROSOLS – EFFECTS ON CLOUDS AND CLIMATE" (BAECC) IN THE CONTEXT OF PAN EURASIAN EXPERIMENT

T. PETÄJÄ[1], A. MANNINEN[1], DMITRI MOISSEEV[1], VICTORIA SINCLAIR[1], EWAN O'CONNOR[2,3] H.K. LAPPALAINEN[1,2], V.-M. KERMINEN[1] AND THE BAECC CONSORTIUM

[1]Department of Physics, University of Helsinki, Finland

[2]Finnish Meteorological Institute, Helsinki, Finland

[3]University of Reading, United Kingdom

Keywords: Atmospheric aerosol particles, aerosol vertical profiles, aerosol-cloud interactions, field experiments.

The boreal forest atmosphere provides an ideal locale to study aerosol and cloud microphysical processes in an initially clean environment that is exposed to different degrees of anthropogenic pollution (e.g. Tunved et al., 2006). Therefore, analysis of aerosol-cloud interactions in such an environment can then be used for assessing the role of anthropogenic emissions on global climate, while at the same time boreal and Arctic regions are experiencing drastic changes due to the ongoing climate change (Epstein et al., 2013; Koenig et al., 2013). This is the core area of interest within Pan Eurasian Experiment (PEEX, Lappalainen et al. 2014).

The sources of aerosol particles in the boreal environment that are large enough to act as Cloud Condensation Nuclei (CCN) include biomass burning, anthropogenic and biogenic emissions (Paramonov et al., 2013; Hong et al., 2014). There are both primary and secondary aerosol particles, emitted by the biosphere and by anthropogenic activities. At a given measurement site the aerosol budget consists of both regionally emitted particles as well as long-range transported aerosol particles. The biogenic contribution can be divided into the processes of initial formation and subsequent growth of Secondary Organic Aerosol (SOA, Tunved et al., 2006; Riipinen et al. 2012). The multi-component condensation of organic precursor vapors affects the sizes of all the particle types during their residence time in the atmosphere. Particularly the ageing of aerosol particles during long range transport increases their hygroscopicity and thereby makes them activate into cloud droplets more readily (Petäjä et al. 2005).

During "Biogenic Aerosols - Effects on Clouds and Climate" (BAECC, Petäjä, 2013), the U.S. Department of Energy's Atmospheric Radiation Measurement (ARM) Program deployed the 2nd ARM Mobile Facility (AMF2) to Hyytiälä, Finland (61° 51'N, 24°17'E) , for an 8-month intensive measurement campaign from February to September 2014. Hyytiälä hosts the Station for Measuring Ecosystem – Atmosphere Relations II (SMEAR II, Hari and Kulmala, 2005). The primary research goal of BAECC deployment is to understand how biogenic aerosols affect cloud microphysical properties.

A vast data set was collected during the BAECC campaign. One of the characteristic features of the in-situ aerosol number size distributions is shown in Figure 1 that depicts formation of aerosol particles from biogenic gas phase precursors. Such events were observed frequently during the BAECC campaign. The co-location of the AMF2 with the SMEAR2 provided benchmarking of the in-situ aerosol measurements. Overall, the measurements were in good agreement taking into account that initially the fresh aerosol particles were below the detection limit of the AMF2 instruments. The combination of the in-situ data

with Lidar derived vertical profiles enables assessment of aerosol effects on cloud properties. More detailed analysis is on-going.

The BAECC project provides a comprehensive data set of in-situ aerosol properties, aerosol and cloud vertical profiles as well as information on cloud microphysical properties and precipitation around the measurement site. The data procedures and analysis tools developed within the BAECC can be applied to other comprehensive measurement sites within Pan Eurasian Experiment (PEEX, Lappalainen et al. 2014).

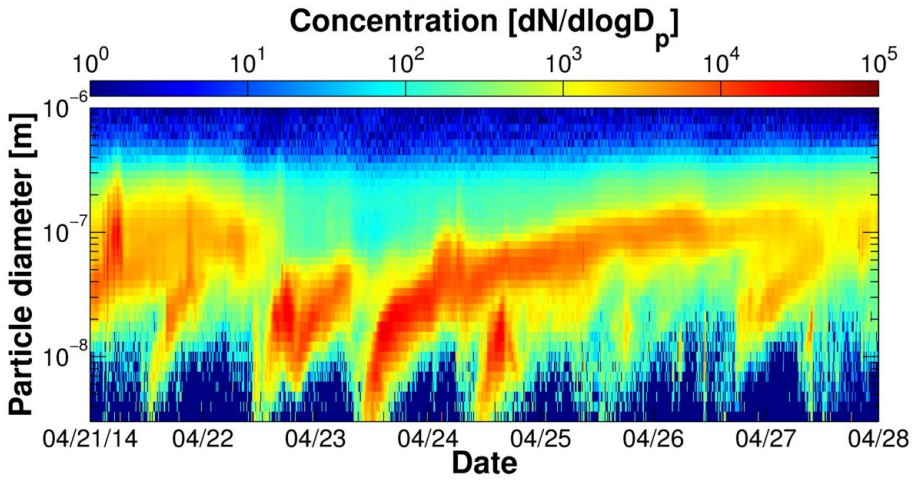

Figure 1. Sub-micron aerosol number size distribution measured with a SMEAR II DMPS at Hyytiälä, Finland between 21st -27th of April 2014 featuring the characteristic feature observed at the site: formation of secondary organic aerosol and their growth to CCN active sizes.

ACKNOWLEDGEMENTS

This research was supported by the Office of Science (BER), U.S. Department of Energy and Academy of Finland via Center of Excellence in Atmospheric Sciences.

REFERENCES

Epstein, H.E., Myers-Smith, I., and Walker, D.A. (2013). Recent dynamics of arctic and sub-arctic vegetation. *Environmental Research Letters* 8, 015040 doi:10.1088/1748-9326/8/1/015040.

Hari, P., and Kulmala, M. (2005). Station for Measuring Ecosystem–Atmosphere Relations (SMEAR II). *Boreal Environ. Res.* 10, 315–322.

Hong, J., Häkkinen, S.A.K., Paramonov, M., Äijälä, M., Hakala, J., Nieminen, T., Mikkilä, J., Prisle, N.L., Kulmala, M., Riipinen, I., Bilde, M., Kerminen, V.-M. and Petäjä, T. (2014). Hygroscopicity, CCN and volatility properties of submicron atmospheric aerosol in a boreal forest environment during the summer of 2010. *Atmos. Chem. Phys.* 14, 4733–4748.

Koenigk, T., Brodeau, L., Graversen, R.G., Karlsson, J., Svensson, G., Tjernström, M., Willén, U., and Wyser, K. (2013). Arctic climate change in 21st century CMIP5 simulations with EC-Earth. *Clim. Dyn.* 40, 2719–2743.

Lappalainen, H.,K., Petäjä, T., Kujansuu, J., Kerminen, V.-M., Shvidenko, A., Bäck, J., Vesala, T., Vihma, T., de Leeuw, G., Lauri, A., Ruuskanen, A., Lapshin, V.B., Zaitseva, N., Glezer, O., Arshinov, M., Spracklen, D.V., Arnold, S.R., Juhola, S., Lihavainen, H., Viisanen, Y., Chubarova, N., Chalov, S., Filatov, N., Skorodhod, A., Elansky, N., Dyukarev, E., Esau, I., Hari, P., Kotlyakov, V., Kasimov, N.,

Bondur, V., Matvienko, G., Baklanov, A., Mareev, E., Troitskaya, Y., Ding, A., Guo, H., Zilitinkevich, S. and Kulmala, M. (2014) Pan Eurasian Experiment (PEEX) – A research initiative meeting the grand challenges of the changing environment of the Northern Pan-Eurasian Arctic Boreal areas. *Geogr. Env. Sustain.* 2, 13-48.

Paramonov, M., Aalto, P.P., Asmi, A., Prisle, N., Kerminen, V.-M., Kulmala, M. and Petäjä, T. (2013) The analysis of size-segregated cloud condensation nuclei counter (CCNC) data and its implications for cloud droplet activation. *Atmos. Chem. Phys.* 13, 10285-10301.

Petäjä, T., Kerminen, V.-M., Hämeri, K., Vaattovaara, P., Joutsensaari, J., Junkermann, W., Laaksonen, A. and Kulmala, M. (2005) Effects of SO_2 oxidation on ambient aerosol growth in water and ethanol vapours. *Atmos. Chem. Phys*., 5, 767-779.

Petäjä, T. (2013). *Science Plan Biogenic Aerosols – Effects on Clouds and Climate (BAECC)*, US Department of Energy, Office of Science, DOE/SC-ARM-13-024.

Riipinen, I., Yli-Juuti, T., Pierce, J.R., Petäjä, T., Worsnop, D.R., Kulmala, M. and Donahue, N.M. (2012) The contribution of organics to atmospheric nanoparticle growth, *Nature Geosci.* 5, 453-458, doi: 10.1038/ngeo1499.

Tunved, P., Hansson, H.-C., Kerminen, V.-M., Ström, J., Dal Maso, M., Lihavainen, H., Viisanen, Y., Aalto, P.P., Komppula, M. and Kulmala, M. (2006). High natural aerosol loading over boreal forests. *Science* 312, 261–263.

RUSSIAN PEAT BOG FIRES: AEROSOL SOURCE CHARACTERIZATION AND CONTRIBUTION TO AIR QUALITY

O. POPOVICHEVA[1], N. PERSIANTSEVA[1], N. SHONIA[1], E. KIREEVA, N. SITNIKOV[2], I-T. KU[3] and G. ENGLING[3]

[1]Institute of Nuclear Physics, Moscow State University, Moscow, 119991, Russia

[2]Central Aerological Observatory, Moscow region, Russia

[3]National Tsing Hua University, Hsinchu, 30013, Taiwan

Keywords: peat combustion, aerosol chemical composition, megacity pollution.

INTRODUCTION

Peatland ecosystems are valued as natural archives of carbon, and the burning of soil organic matter during peat bog fires has affected Earth's terrestrial ecosystems for hundreds of millennia. Smoldering megafires in peat bogs occur frequently during the dry season in boreal ecosystems, e.g., the European part of Russia and Siberia. These fires persist for long periods of time (months) allowing the combustion to spread with time deep into the ground and over large areas. Since particles released from smoldering combustion account for nearly three-fourths of total carbonaceous aerosol mass emitted into the atmosphere globally, including peat bog smoke characterization into environmental health assessments is crucial.

Most studies on wildfires to date have focused on forest fires, while peat bog burning remains less certain in terms of the smoke emissions characteristics, although these fires are estimated to have released the equivalent of 13–40% of the mean annual global C emissions from fossil fuels (Page et al., 2002). Analysis of the extreme smoke event during August 2010 in Moscow demonstrated the strong impact of large-scale peat and forest wildfires around a megacity on aerosol chemistry and air quality, causing highly polluted environments (Popovicheva et. al., 2014). Smoldering fires present a large perturbation to atmospheric chemistry, while the contribution of peat fires to particulate air pollution such as smoke haze is of major concern because of its long-lasting adverse impact on regional air quality and the earth's radiative balance. Quantification of atmosphere pollution and impacts of peat fires in Eurasia on changes in the aerosol/climate system of boreal regions of Russia is one of the most important research priorities to be addressed.

METHODS

Intense peat bog fires occurred in spring-summer 2014 in the Tver region (north of Moscow, Russia). Regional air quality impacts and air mass transport to the Moscow megacity were analyzed using both satellite data and ground-based observations. We performed analysis of peatland fire emissions in the source region and back-trajectory simulations based on synoptic maps from the HYSPLIT model. In order to establish the characteristics of peat-emitted aerosol, a near-source sampling campaign was performed in August 2014 in the bog during intensive smoldering combustion (Fig.1 (A)). The particle and trace gas emissions were analyzed by an extensive suite of instrumentation that sampled and measured individual particles, aerosol chemistry, optical properties, and gas concentrations. Comprehensive physico-chemical characterization of peat smoke was performed, including particle morphology, elemental composition, organic/inorganic content, and organic molecular markers.

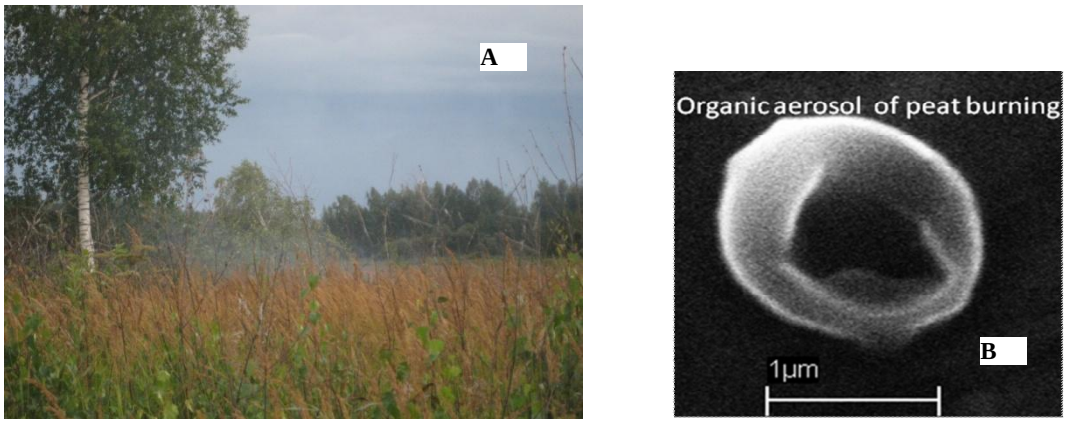

Fig.1. (A) Peat bog smoldering in Tver region, August 2014; (B) SEM image of organic aerosol.

Continuous PM10 monitoring and sampling was performed in August 2015 at a down-wind site located in the south-west of Moscow city (100 km from Tver region), 60 m above ground. Peat smoke plumes contributing to the increased mass concentration of particulate matter was observed over a period of one week from 27 July to 3 August, in agreement with the trajectories of air masses transported from the Tver region.

RESULTS

Peatland fires are dominated by smoldering combustion which is self-sustained, proceeding at low temperatures, and is a flameless form of biomass burning. Individual particle analysis of peat smoke in terms of morphology and elemental composition was performed by SEM/EDX. The cluster analyses of particles of similar morphology and composition revealed a strong relation to typical properties of aerosol produced during low-temperature combustion, as observed in the smoldering phase during small-scale studies in a large combustion chamber (Popovicheva et al., 2014). Grouping of particles revealed the dominant abundance (78.5%) of roughly spherical organic particles (Fig.1 (B)). Other groups in peat smoke, such as Ca, Fe, Si-rich are calcium oxides/carbonates and aluminosilicates with Fe and Ca inclusions.

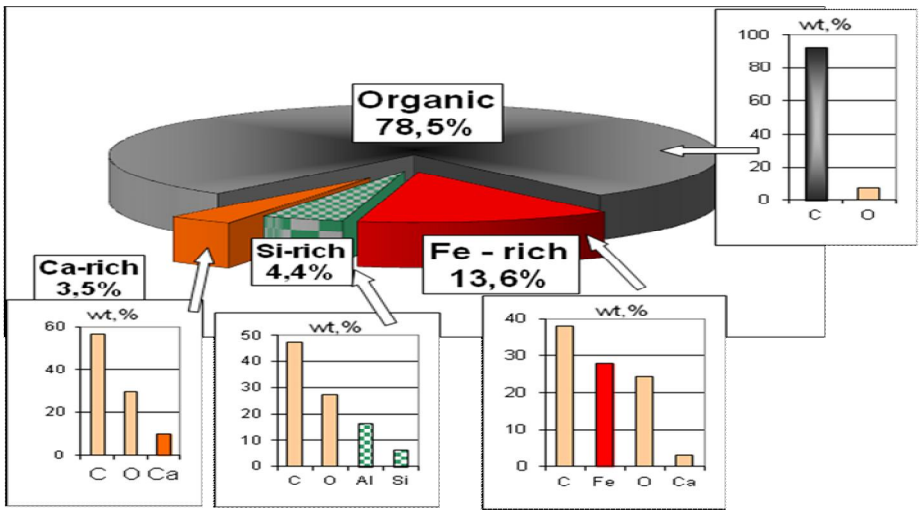

Fig.2. Microstructure of particles in smoke from Tver region peat bog fire.

Peat smoke is characterized by the strong spectral dependence of aerosol absorption obtained by a filter-based optical transmission method. The high absorption Angstrom exponent (AAE) of 4.1 confirms the presence of a large fraction of brown carbon (BrC) as the most efficient light-absorbing aerosol species in the ultraviolet spectrum, together with black carbon (BC) absorbing visible radiation. Finding of BrC

contribution to peat smoldering aerosol is well in accordance with a high ratio of organic carbon to elemental carbon (OC/EC), a specific feature of smoldering fires (Popovicheva et al., 2014). Composition of organic/inorganic compounds is revealed by prominent functionalities in FTIR spectra of peat bog smoke particles. Fig.3 shows the most intensive vibrations of aliphatic C-H (2922-2852 cm^{-1}), carbonyl C=O (1730-1668 cm^{-1}), carboxylate (1610-1550 and 1420-1300 cm^{-1}), amino NH_2 (1590-1650 cm^{-1}), aromatic NO_2^- (1300-1370 and 1500-1570 cm^{-1}), C-N (1250-1340 cm^{-1}), and CO_3 (860-890; 1410-1490 cm^{-1}) groups. The spectrum of intensive smoke evolved under grass exhibits C-O (1286, 1257, 1168 cm^{-1}), NO_3 (1350, 840 cm^{-1}), and SO_4^{2-} (1060 cm^{-1}) groups. In the spectrum of underground smoke two bands of carbonyls are prominent, corresponding to vibrations in acids, ketones, ethers, lactones (1732 cm-^{1}), and amides (1668 cm^{-1}) while smoke under grass shows a third band assigned to anhydrides (1760 cm^{-1}).

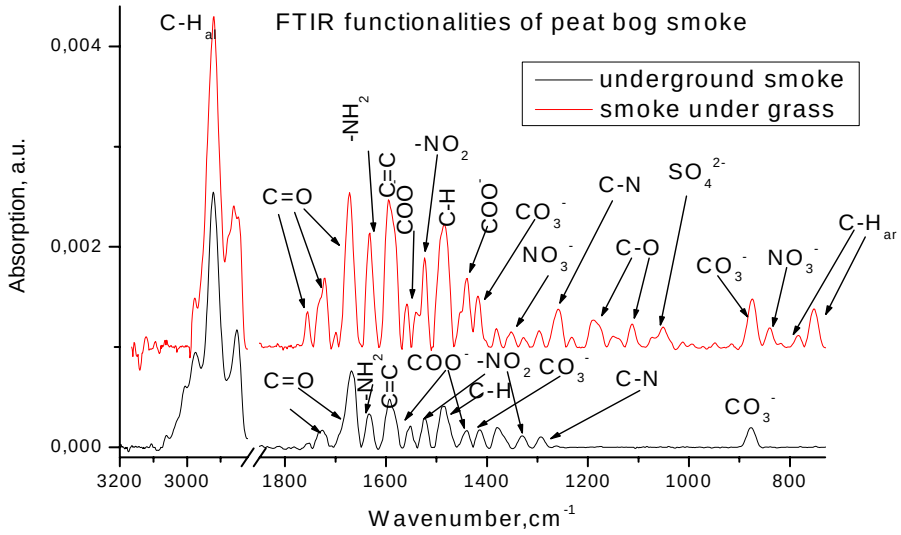

Fig.3. FTIR spectra of peat bog smoke particles. Functionalities are indicated

Calcium, sodium, and magnesium ions combined with sulfates contributed an additional mass fraction of peat smoke particles. The major finding of relevance for source apportionment studies is that peat smoldering aerosols are characterized by high levoglucosan concentrations, confirming that levoglucosan is a molecular marker for biomass burning, specifically for peat combustion.

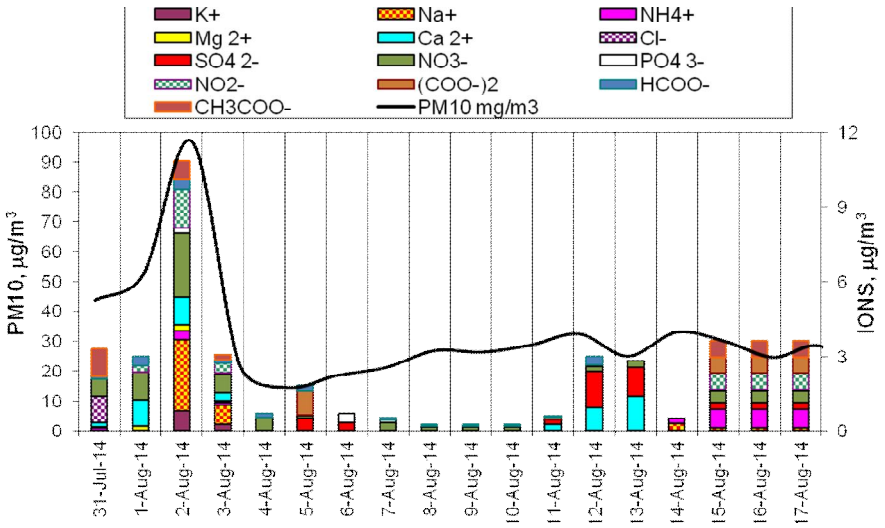

Fig.4. PM10 and ion concentrations during peat bog smoke event at a site in the south-west of Moscow city.

The elevated PM10 concentrations at the site in the south-west of Moscow city from 27 July to 3 August were related to the peat bog fire plume, according to air mass advection from the Tver region. The evolution of PM10 mass and ion concentrations during the peat bog smoke event is shown in Fig.4. We found that peat smoldering fires accounted for a significant percentage of the total enhancement of PM10 concentrations, including a significant increase in ion concentrations. Together with increased PM10 we observed elevated light absorption in form of high AAE in comparison with days not affected by smoke plumes.

Aerosol sampling and PM speciation analysis confirm the impacts of peat smoldering on aerosol chemistry by increased concentrations of biomass burning indicators, such as high OC/EC ratios and elevated molecular marker (levoglucosan) levels with peak daily concentration observed when the smoke plume reached the city. Hazardous constituents from peat smoke, such as acid and non-acid carbonyl compounds, nitrates and acetates were released together with carbonaceous particles and mineral dust. The large proportion of dust was reflected by the abundance of Ca and Fe-rich mineral compounds, which was likely evolved in form of soil dust during the long-lasting smoldering of peat bogs 100 km from Moscow city, as confirmed by peat fire source characterization.

CONCLUSIONS

The influence of Russian peat bog fire emissions is provided for the first time in form of source apportionment and air quality assessment in Pan-European boreal ecosystems. This study shows the importance of obtaining the chemical characteristics of the dominant PM components in peat bog fire emissions in order to enable the assessment of contributions from peat burning to atmospheric pollution at regional scale and transport to populated areas of a megacity. We first present the microstructural, optical, and chemical characteristics of aerosols emitted during low-temperature combustion of peat bogs in the European part of Russia. Peat smoldering fires are found to produce light-absorbing aerosols that exhibit much stronger spectral dependence than high-temperature combustion, such as diesel emissions. Levoglucosan is proposed to be a useful indicator of alterations in the atmospheric aerosol composition impacted by smoldering fires. BC, BrC, and organic pollutants constitute important fingerprints of particulates released from peat burning into the atmosphere, indicating important disturbance at the regional scale and transport pathways to urban environments from peatland fire regions.

ACKNOWLEDGEMENTS

This work was supported by the RFBR grant 12-05-92002.

REFERENCES

Page S. E., Siegert, F., Rieley, J.O., Boehm, H.V., Jaya, A. and Limin, S. (2002). The amount of carbon released from peat and forest fires in Indonesia during 1997. *Nature* 420, 61–65.

Popovicheva, O., Kistler, M., Kireeva, E., Persiantseva, N., Timofeev, M., Kopeikin, V., and Kasper-Giebl, A. (2014). Physicochemical characterization of smoke aerosol during large-scale wildfires: Extreme event of August 2010 in Moscow. *Atmos. Environ.* 96, 405–414.

Popovicheva, O.B., Kozlov, V.S., Engling, G., Diapouli, E., Persiantseva N.M., Timofeev, M.A., Fan T.-S., Saraga, D., and Eleftheriadis, K. (2015). Small-scale study of Siberian biomass burning: I. Smoke microstructure. *AAQR*, DOI: 10.4209/aaqr.2014.09.0206.

EMISSION AND TRANSPORT OF BC TO RUSSIAN ARCTIC FROM SIBERIAN WILDFIRES AND SEASON BURNINGS

O.POPOVICHEVA[1], J.E.PENNER[2], A.MAKSHTAS[3] and T.UTTAL[4]

[1]Institute of Nuclear Physics, Moscow State University, Moscow, 11999, Russia.

[2] Department of Atmospheric, Oceanic, and Space Sciences, University of Michigan, Ann Arbor, Michigan, USA.

[3]Arctic and Antarctic Research Institute, St. Petersburg, 199397, Russia.

[4]National Oceanic and Atmospheric Administration ETL, Boulder, Colorado.

Keywords: WILDFIRES, EMISSIONS, BC.

INTRODUCTION

Biomass burning produces a large amount of smoke and is responsible for a large fraction of black carbon (BC) in the atmosphere, affecting air quality, the earth's radiation budget, and aerosol/cloud interactions. Black carbon (BC) in combustion aerosols is of critical importance among other climate-active species, and may cause significant temperature changes through both their direct and indirect impacts on clouds (Yun et al, 2013). Wildland fires supply a major source of light-absorbing aerosol on a national and global scale.

Russian boreal forest occupies near 700 million ha, which is mostly dominated by Siberian coniferous forest. Satellite observations show an area of 10–14 million ha is burned annually in Siberia (Conard and Ivanova, 1997). Siberian wildfires are found to be a major source of climate-relevant species emitted at northern latitudes. Siberia shares 50% of the world emissions in the Arctic north of 60^0N which strongly pollute Europe, Canada, and China. Special concern is directed on wildfires which degrade the Arctic air quality due to long-range transport of smoke plumes which approach the Siberian Arctic coast (Paris et al., 2009). Seasonal cropland burning activities in Siberia may double BC and organic aerosol emissions (Warneke et al., 2010), and cause pronounced pollution events of "Arctic smoke" (Stock et al., 2012). BC at high latitudes has an amplifying effect on climate, decreasing Arctic snow albedo when it falls out of the atmosphere, thereby accelerating snowmelt. There is a large uncertainty in global models related to the amount of BC transported to high latitudes and deposited on snow (Zhou et al., 2012). In Russia, despite the large area covered by wildfires, information about BC emissions, long-range transport to the Arctic, and climate impacts is sparse. Observations and prescribed burns were performed in a few places in Western and North-Eastern Siberia (Paris et al.,2009; Samsonov et al., 2012), but there is a limited number of BC measurements at Russian Arctic stations. In this situation, the modeling of wildfire/seasonal burning emissions and their transport to the Arctic, is an important research priority.

METHOD AND RESULTS

Burnt area during summer wildfires and spring grass/cropland fires in Siberia is derived using burnt area remote sensing in the GFED.3 products. The spatial and temporal resolution of these inventories depends on the resolution of the underlying MODIS. Combining the burnt area information with a vegetation map allows the assessment of the amount of typical boreal forest and grass available for burning. The particulate pyrogenic emissions are then derived from emission factors that convert the vegetation burned to the amount of carbon and different constituents released by fires. Comparison of emissions from GFED.3 with those from IS4FIRES (which use different satellite products) will be undertaken. These can

also be compared to the prescribed burn data from 2000-2010 year (Samsonov et al., 2012) which produce the amount of particulate matter (PM) emitted during a typical fire in the Siberian forest (larch or pine) which, on average is 0.6 T/ha and ranged within 0.2–1.0 T/ha depending on burning conditions. The PM consists on average of 77% organic matter and 8% of Elemental carbon (EC).

We used these different fire emission products to study the transport of BC to polar regions from Siberia using the University of Michigan IMPACT aerosol model driven by two sets of meteorological fields from the NCAR CAM5 and GFDL AM3 models. The transport model also includes different wet deposition treatments, as described in Zhou et al., 2012.

Meteorological station has been operating in Tiksi (71_360N; 128_530E), northern Siberia, Laptev Sea, since 1930s but direct year-round observations of important climate forcing agents have been inadequate last decades within the Russian Arctic. International Observatory was founded in 2010 and joint the International Arctic Systems for Observing the Atmosphere network (IASOA, www.IASOA.org). BC has also been monitored since 2010, using a 7-wl Magee AE-31 aethalometer by NOAA. For the purpose of this work, 3-years database is treated to produce monthly averaged BC concentrations.

BC concentrations derived from IMPACT-CAM5 model as well as the GFDL AM3 model in polar regions north 80^0N are compared to BC observations at the ground near the Laptev sea. BC concentrations and deposition in polar regions are shown to be sensitive to both the meteorological fields, the wet deposition treatment, as well as the fire emissions products that are used. This work improve the quantification of Sibetian biomass burning impacts with final aim to reduce uncertainties in direct and indirect effects of BC on Arctic climate forcing.

REFERENCES

Yun Y., J. E. Penner, O. Popovicheva. (2013).The effects of hygroscopicity on ice nucleation of fossil fuel combustion aerosols in mixed-phase clouds. Atmos. Chem. Phys., 13, 4339–4348.

Conard S.G. and G.A. Ivanova (1997). Wildfires in Russian boreal forest –potential impacts of fire regime characteristics on emissions and global carbon balance estimates. Environ. Pollut. 98, 305–313

Paris J.-D., A. Stohl, P. Nedelec, M. Yu. Arshinov, M. V. Panchenko, V. P. Shmargunov, K. S. Law, B. D. Belan, and P. Ciais. (2009). Wildfire smoke in the Siberian Arctic in summer: source characterization and plume evolution from airborne measurements. Atmos. Chem. Phys. 9: 9315–9327.

Warneke, C., K. D. Froyd, J. Brioude , Bahreini, R., et al.(2010). An important contribution to springtime Arctic aerosol from biomass burning in Russia. Geophys. Res. Lett., 37, L01801, doi: 10.1029/2009GL041816.

Stock, M., Ritter, C., Herber, A., Von Hoyningen-Huene, W., Baibakov, K., Graser, J., Orgis, T.. Treffeisen, R., Zinoviev, N., Makshtas, A. and Dethloff, K. (2012). Springtime Arctic aerosol: Smoke versus haze, a case study for March 2008. Atmos. Environ. 52: 48-55.

Samsonov Y. N., Ivanov, V. A., McRae, D. J. and Baker, S. P. (2012). Chemical and dispersal characteristics of particulate emissions from forest fires in Siberia. Inter. J. Wildland Fire .21: 818-827.

Zhou C., J.E. Penner, M. Flanner, M. Bisiaux, R. Edwards and J. McConnell. Transport of black carbon to polar regions: Sensitivity and forcing by black carbon. Geophys. Res. Lett. 39, L22804, doi:10.1029/2012GL053388, 2012

SENSITIVITY OF CARBON FLUXES IN LAND-ATMOSPHERE-HYDROSPHERE SYSTEM OF YENISEY RIVER CATCHMENT TO CLIMATE VARIABILITY: DEVELOPMENT OF KRASFLUX NETWORK FOR THE LONG-TERM ANALYSIS

A.S. PROKUSHKIN[1,2], A.V. PANOV[1], A.V. KIRDYANOV[1], A.V. RUBTSOV[2], M.A. KORETS[1], Yu.A. KURBATOVA[3], A.V. VARLAGIN[3], N.I. TANANAEV[4], R. AMON[5], M. HEIMANN[6]

[1]V.N. Sukachev Institute of Forest, SB RAS, Akademgorodok 50/28, Krasnoyarsk 660036, Russian Federation

[2]Siberian Federal University, Svobodny 79, 660041 Krasnoyarsk, Russian Federation

[3]A.N. Severtsov Institute of Ecology and Evolution, Leninskiy pr., 33, 119071 Moscow, Russian Federation

[4]Igarka Geocryological Laboratory of P.I. Melnikov Institute of Cryolythozone SB RAS, 663200 Igarka, Russian Federation

[5]Texas A&M University at Galveston, 200 Seawolf Parkway, Galveston, Texas 77553, USA

[6]Max Planck Institute for Biogeochemistry, Hans-Knoell str. 10, 07745 Jena, Germany

Keywords: carbon dioxide, methane, net ecosystem exchange, dissolved carbon, Central Siberia

INTRODUCTION

Projected temperature increases resulting from increasing amounts of greenhouse gasses in the atmosphere (IPCC, 2013) have the potential to lead to the giant release of carbon stored over many thousands of years in Arctic and Subarctic regions (Tarnocai *et al*., 2009) and may create significant havoc in the Earth System. The annual carbon fluxes have potentially more profound and quantifiable responses to climate variation as the sizeable changes in the major carbon stores like soil organic matter or tree standing stocks occur on at least century time scales. Nevertheless, the quantification of amounts of atmospheric carbon sequestered and/or released annually on basin scale is constrained by large spatial heterogeneity in climate, vegetation, soil and geomorphology of rivers empting to the Arctic Ocean. Thus, the exchange of carbon-bearing gases (i.e. CO_2 and CH_4) between terrestrial ecosystems with atmosphere and the release of terrigenic C to aquatic systems are still of the least understood and potentially most significant carbon-climate feedbacks in current climate models (McGuire *et al.*, 2009, Dolman *et al.,* 2012). There is growing demand for accurate quantification of the carbon flows into and out of terrestrial ecosystems throughout high latitude regions representing high mosaics of vegetation, soils, geomorphology and climate. The project supported by Russian Science Foundation (2014-2016) aims to determine the magnitude and climate-driven variability of the annual carbon fluxes/gains in terrestrial ecosystems on the Yenisey River basin (above 60^{o} N) by quantifying the amount of carbon that is assimilated to tree biomass and released both into the rivers and atmosphere.

METHODS

Existing atmospheric and hydrospheric observations serve as important insights into integrated responses of monitored environments to ongoing climate changes, but alone these observations fail to identify the driving mechanisms/processes on the sub-basin scale. Vice versa, bottom up approaches are limited by the complexity of larger scale systems like river basins, comprising the variable mosaics of vegetation, soils,

geomorphology and climate. The proposed development of Krasflux network (Fig. 1, Table 1) aims to fill this gap, based on a combination of:
1. Continuous observations at “integration sites” with high precision long-term measurements of carbon-bearing gases and aerosols mixing ratios in atmosphere (ZOTTO) and hydrologic release of terrestrial C to the Arctic Ocean by Yenisey River (at Igarka);
2. Use the existing and establishment new Eddy tower sites for estimates of Net ecosystem exchange in major vegetation/bioclimatic zones of Yenisey River basin;
3. Establishment of new Arctic site in Dixon to get estimates of land-ocean exchange of GHG;
4. River cruises and stationary continuous water sampling campaigns at Eddy tower sites aiming to distinguish landscape/vegetation/climate controls over C hydrologic fluxes and to reveal hotspots of terrigenous dissolved carbon release to rivers;
5. Available remote-sensing products of different resolution providing spatial and temporal variation of GPP/NPP and climatic variables for basin scale analysis;
6. Expansion of dendrochronological network providing the magnitude and spatio-temporal variability of annual tree ring growth as a proxy of ecosystem productivity throughout the basin.

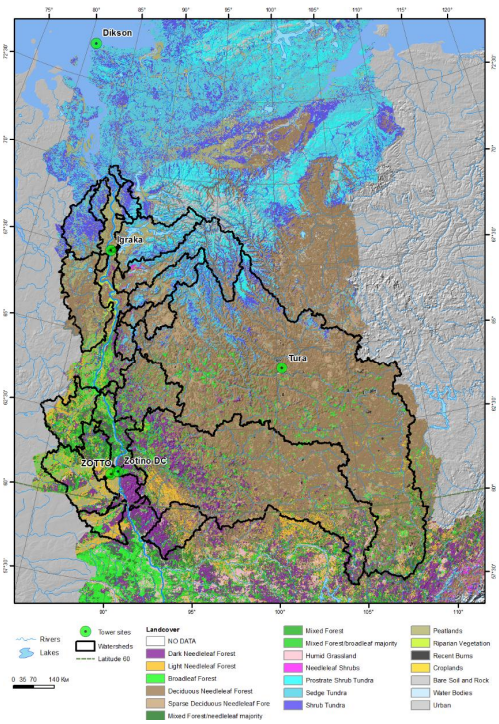

Figure 1. The vegetation map of Yenisey river basin demonstrating the main tributaries and location of existing (ZOTTO “pine” and “bog”, Tura “Larch” sites) and planned sites (ZOTTO “dark taiga”, Igarka “palsa” and Dixon “high arctic” sites) in the framework of Krasflux network.

Site	Coordinates	Status	Vegetation type / dominant tree species	Portion of vegetation type in the basin, %	MAAT, °C	MAP, mm
ZOTTO "pine" site	60° 48'N 89° 22'E	existing	Evergreen conifer/Pinus sylvestris	4.5	-3.3	558
ZOTTO "bog" site	60° 48'N 89° 22'E	existing	Olygotrophic peatbog	6.0	-3.3	558
ZOTTO "dark taiga" site	61° 01'N 89° 49'E	planned in 2015	Evergreen conifer/Abies sibirica	6.0	<-3.3	>558
Tura "larch" site	64° 12'N 100° 27'E	existing	Deciduous conifer forests/Larix	48.0	-8.5	347
Igarka "palsa" site	67° 28'N 86° 29'E	planned in 2015	Tundra-forest ecotone	~13.0	-7.8	481
Dixon "high arctic" site	73° 28'N 81° 48'E	planned in 2016	Tundra	~5.0	-11.1	344

Table 1. The list of Krasflux network sites within Yenisey River basin and their characteristics.

Additionally, we utilise novel techniques for identification of biomarkers and stable isotopes aiming to reveal biogeochemical and ecophysiological drivers and origins of atmospheric and hydrospheric C and other elements transferred from and within the basin scale.

CONCLUSIONS

The specific driving questions of the study are divided into 3 parts linked respectively to C fluxes in atmosphere, hydrosphere and assessment of terrestrial ecosystems capacity to sequester atmospheric carbon through remote sensing techniques and ground surveys.

Atmospheric C fluxes:

What is a magnitude and variation in inter-annual concentrations of trace gases and aerosols in atmosphere of Central Siberia (Fig. 2)?

What is the reason of asymmetrically higher increment of atmospheric CO_2 concentrations in growing season in comparison to winter observed in Central Siberia?

What are the major geographic and biotic sinks and sources of GHG of atmosphere in Yenisey River basin?

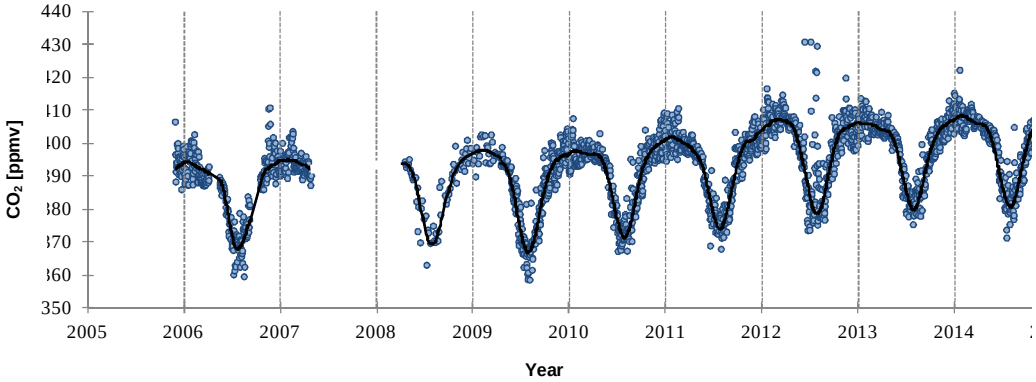

Figure 2. CO_2 mixing ratio dynamics in the atmosphere of Central Siberia (301 m height, ZOTTO data).

Hydrologic C fluxes (Fig. 3):

- What is a magnitude and variability of riverine C fluxes in the Yenisey river basin?
- What are the hotspots of terrestrial C release to aquatic systems within the Yenisey basin?

- What are terrestrial and synoptic controls over inter- and intra-annual variability of riverine C composition and concentration?

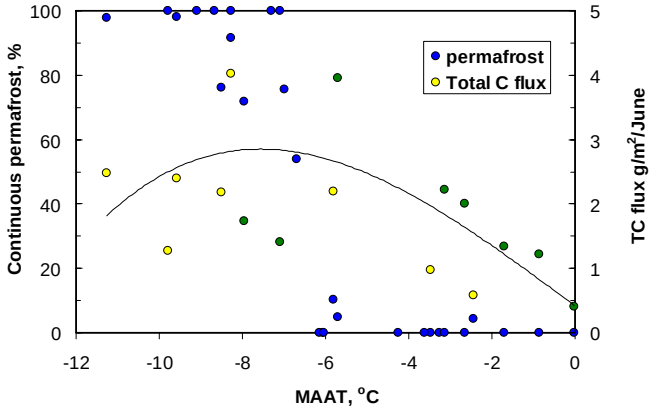

Figure 3. Relationships between mean annual temperature (MAAT) of entire river basin, continuous permafrost distribution within basin and total riverine carbon flux (as the sum of DOC, DIC, POC and dissolved GHG) for major tributaries of Yenisey River basin (see Fig. 1). Green circles – left/western tributaries, yellow circles – right/Eastern tributaries of Yenisey River.

Spatio-temporal variability of land cover and its productivity:
- What is the magnitude of regionally specific uncertainty in satellite-model-based GPP/NPP values over the main vegetation biomes of Central Siberia compared to ground-based measurements of C fluxes?
- How vegetation type mosaics and local aboveground vegetation composition contribute to NDVI trends observed from raw resolution (1 km^2) satellite data in comparison with medium (250 m) and high resolution (30 m) imagery?
- What is the inter-annual variation of tree-ring parameters at local and regional scales in Central Siberia?
- What are specific climatic factors driving tree radial growth and stem (tree) productivity in different bioclimatic zones?
- What are productivity indices derived from satellite data coherent with the radial growth parameters of trees?

ACKNOWLEDGEMENTS

This work is supported by Russian Science Foundation grant #14-24-00113.

REFERENCES

Fifth Assessment Report of the Intergovernmental Panel on Climate Change (IPCC) (2013).

Tarnocai, C., J. G. Canadell, E. A. G. Schuur, P. Kuhry, G. Mazhitova, S. Zimov (2009). Soil organic carbon pools in the northern circumpolar permafrost region. *Global Biogeochemical Cycles* **23**, .GB2023.

Dolman A.J., A. Shvidenko, D. Schepaschenko, P. Ciais, N. Tchebakova, T. Chen, M.K. van der Mole, M.L. Belelli, T.C. Maximov, S. Maksyutov, E.-D. Schulze (2012). An estimate of the terrestrial carbon budget of Russia using inventory-based, eddy covariance and inversion methods. *Biogeosciences* **9**, 5323.

McGuire A.D., L.A. Anderson (2009). Sensitivity of the carbon cycle in the Arctic to climate change. *Ecol. Monographs* **79**, 523.

PRECIPITATION AND NET ECOSYSTEM EXCHANGE ARE THE MOST SIGNIFICANT FACTORS EXPLAINING RUNOFF DOC CONCENTRATIONS AND FLUXES IN UPLAND BOREAL CATCHMENTS

J. PUMPANEN[1], A. LINDÉN[1], H. MIETTINEN[2], P. KOLARI[1], H. ILVESNIEMI[3], I. MAMMARELLA[4], P. HARI[1], E. NIKINMAA[1], J. HEINONSALO[5], J. BÄCK[1], A. OJALA[1], F. BERNINGER[1] and TIMO VESALA[4]

[1]University of Helsinki, Department of Forest Sciences, PO Box 27, FI-00014 University of Helsinki, Finland

[2]University of Helsinki, Department of Environmental Sciences, PO Box 65, FI-00014 University of Helsinki, Finland

[3]Finnish Forest Research Institute, PO Box 18, FI-01301 Vantaa, Finland

[4]Department of Physics PO Box 48, FI-00014 University of Helsinki, Finland

[5]Department of Food and Environmental Sciences PO Box 66, FI-00014 University of Helsinki, Finland

Keywords: DISSOLVED ORGANIC CARBON, NET ECOSYSTEM EXCHANGE, RUNOFF

INTRODUCTION

Part of the carbon fixed in terrestrial ecosystems is transferred through streams and rivers to lakes and the carbon is finally released as CO_2 to the atmosphere through respiration or buried into lake sediments. Recently, it has been shown that lake and stream water dissolved/total organic carbon (DOC/TOC) concentrations throughout the boreal zone are increasing (Worrall *et al*., 2004; Sarkkola *et al*., 2009; Couture *et al*., 2011). There are several theories which could explain this trend; land use changes, decrease in atmospheric acid deposition, changes in seasonal patterns in temperature and precipitation and increase in below ground C allocation due to increase in atmospheric CO_2 concentration or soil warming (Kortelainen and Saukkonen, 1998; Nieminen, 2004; Monteith *et al*., 2007; Pumpanen *et al*., 2012). Here, we tested a hypothesis that the increase in photosynthesis is reflected to soil water DOC concentrations and finally to DOC fluxes from the catchment.

METHODS

We used a 15-year-long continuous monitoring data on catchment runoff, DOC concentration in the runoff, GPP, TER and NEE of the ecosystem of two small upland boreal catchment areas in Southern Finland to explain the long-term trends in runoff DOC fluxes. We also studied the long term trends in the DOC concentration, pH of precipitation and through fall as well as the annual litter fall and soil temperature sum to study which factors are the most important drivers for runoff DOC concentration and runoff DOC fluxes. We used linear mixed effects models to estimate the effect of different factors on runoff DOC concentration and runoff DOC fluxes and conducted a sensitivity analysis for the parameters of the model to determine which factors are the most important in regulating the runoff DOC concentrations and fluxes. Finally, we studied how the short and long-term changes in precipitation, soil temperature, soil water content and net ecosystem exchange (NEE) are reflected to DOC concentrations and runoff DOC fluxes by using wavelet coherence analysis.

RESULTS

Our results indicate that the DOC concentration, especially in the spring runoff fluxes have increased over the last 15 years which seems to increase the annual DOC fluxes during wet years. The DOC flux was to a large extent determined by the amount of precipitation, but the previous year's NEE and litter production had also a small but significant effect on runoff DOC fluxes.

The annual soil temperature sum also showed an increasing trend over the study period, but in the monthly average temperatures the trend was not significant. The soil temperature was not a significantly important factor in explaining the increasing DOC trend. However, the higher temperatures in the autumn and prolonged autumn period may increase the decomposition of soil organic matter leading to increasing DOC in the soil, which is then flushed from the soil and thus from terrestrial to aquatic systems (Piao *et al*., 2008; Vesala *et al*., 2010). Increase in soil temperature may also increase the GPP of vegetation by increasing the belowground carbon sink of photoassimilates (Pumpanen *et al*., 2012). These mechanisms could accelerate the flow of easily decomposable carbon to the soil even if it was not observed in this study.

The temporal correlation between NEE and DOC concentration (and other biometeorological parameters) depends on the length of the time lag studied. In the wavelet coherence analysis, we found no temporal synchrony between the weekly average NEE and DOC concentrations whereas the sensitivity analyses of the linear mixed-effects models indicated that, when integrated on an annual scale, NEE has an important role in predicting annual runoff DOC concentrations or fluxes. The different results of these two analyses are most likely related to the time lags in biological processes, e.g. decomposition of soil organic matter.

The annual DOC fluxes were small compared to other ecosystem carbon fluxes (0.32-0.40% of the annual NEE). However, our study revealed that the DOC concentration in the runoff water is increasing which could increase the annual DOC fluxes during wet years.

ACKNOWLEDGEMENTS

This work was supported by the Academy of Finland projects 218094 and 213093 as the Academy of Finland Finnish Centre of Excellence Program. We also thank for the staff of Hyytiälä Forestry Field Station e.g. Sirkka Lietsala and Veijo Hiltunen for assisting in the field work. Academy of Finland project 218094 as well as ICOS 271878, ICOS-Finland 281255 and ICOS-ERIC 281250 funded by Academy of Finland and the Centre of Excellence programme 1118615; EU, through projects GHG-Europe and InGOS; NordForsk, through the Nordic Centre of Excellence (project DEFROST).

REFERENCES

Couture, S., D. Houle, and C. Gagnon (2011). Increase of dissolved organic carbon in temperate and boreal lakes in Quebec, Canada, *Env. Science and Pollution Research*, doi:10.1007/s11356-011-0565-6.

Kortelainen, P., and S. Saukkonen (1998). Leaching of nutrients, organic carbon and iron from Finnish forestry land. *Water, Air, Soil Poll*., **105**, 239-250.

Monteith, D.T., J.L. Stoddard, C.D. Evans, H.A. de Wit, M. Forsius, T. Høgåsen, A.Wilander, B.L. Skjelkvåle, D.S. Jeffries, J. Vuorenmaa, B. Keller, J. Kopácek, and J. Vesely (2007). Dissolved organic carbon trends resulting from changes in atmospheric deposition chemistry. *Nature*, **450**, 537-541.

Nieminen, M. (2004). Export of dissolved organic carbon, nitrogen and phosphorus following clear-cutting of three Norway spruce forests growing on drained peatlands in southern Finland. *Silva Fennica*, **38(2)**, 123-132.

Piao, S., P. Friedlingstein, P. Peylin, M. Reichstein, S. Luyssaert, H. Margolis, J. Fang, A. Barr, A. Chen, A. Grelle, D. Y. Hollinger, T. Laurila, A. Lindroth, A. D. Richardson, and T. Vesala (2008). Net

carbon dioxide losses of northern ecosystems in response to autumn warming, *Nature*, doi:10.1038/nature06444.

Pumpanen, J., J. Heinonsalo, T. Rasilo T., and H. Ilvesniemi (2012). The Effects of soil and air temperature on CO2 exchange and net biomass accumulation in Norway spruce, Scots pine and Silver birch seedlings. *Tree Phys.* **32(6)**, 724-736.

Sarkkola, S., H. Koivusalo, A. Laurén, P. Kortelainen, T. Mattsson, M. Palviainen, S. Piirainen, M. Starr, and L. Finér (2009). Trends in hydrometeorological conditions and stream water organic carbon in boreal forested catchments. *Sci. Total Env.* **408**, 92-101.

Vesala, T., S. Launiainen, P. Kolari, J. Pumpanen, S. Sevanto, P. Hari, E. Nikinmaa, P. Kaski, H. Mannila, E. Ukkonen, S.L. Piao, and P. Ciais (2010). Autumn temperature and carbon balance of a boreal Scots pine forest in Southern Finland. *Biogeosci.* **7**, 163-176.

Worrall, F., T.P. Burt, and J. Adamson (2004). Can climate change explain increases in DOC flux from upland peat catchments? *Sci. Total Environ.* **326**, 95-112.

SNOW MAPPING OVER TIBETAN PLATEAU USING EARTH OBSERVATION DATA

Y.B. QIU[1], H.D. GUO[1], D. CHU[2], J.C SHI[1], L.J. SHI[1], H. ZHANG[1], LABA ZHUOMA[2] and Z.J. ZHENG[3]

[1] Institute of Remote Sensing and Digital Earth, Chinese Academic of Sciences, Beijing, China.

[2] Tibet Center for Remote Sensing Applications, Tibet Meteorological Bureau, Lhasa, Tibet Autonomous Region, China.

[3] National Satellite Meteorological Center, China Meteorological Administration, Beijing, China

Keywords: SNOW COVER, TIBETAN PLATEAU, AMSR-E, MWRI, MODIS

INTRODUCTION

Seasonal snow has a profound impact and feedback on regional and global climate change, and plays a critical role to the water and energy balance. The recently release of IPCC AR5 (Vaughan, D.G., 2013) reported a high confidence of decreasing snow cover area in Northern Hemisphere through satellite observations, which is also strongly negative correlation with the land temperature between 40^0N~60^0N. The general decreasing trend on snow depth and snow duration of snow season was also observed by the station records in spring time, especially at the Warmer locations.

While, as the high altitude snow cover area between the lower latitudes 26^0N~40^0N in the Northern Hemisphere, in which the Tibetan Plateau locates, the snow spatial-temporal pattern and its remote relationship with the downstream precipitation and Indian monsoon are not fully understood because of the lack of the station observatories and accuracy deficiency of snow remote sensing products.

The most ever evidential result based on the station observations by Ma and Qin (2012) revealed that the snow changing pattern was not consist with the Northern Hemisphere declining trend, but present the statistically significant trends: positive in winter Snow Depth (SD) in northwest China, and negative in SD and Snow Water Equivalent (SWE) in spring for China as a whole and spring SWE for the Qinghai-Xizang (Tibet) Plateau.

The importance on the snow observations over Tibetan Plateau also lies in the irreplaceable and major role of the snow melting replenishment to rivers, such as Ganges, and Indus, and its supplementation to the mountain glaciers and inland lakes, which impact on the plateau ecosystem, such as the grassland degradation and bloom.

The spatial and temporal continuous satellite remote sensing can provide a whole view of the snow cover and SD/SWE over the Tibetan Plateau, which can fill the gaps of sparse stations observations, and provides a comparable record time from 1960s. This research firstly presents the snow changing knowledge over the research area from the literature record and analysis, then focus on the daily SWE and Snow Extent (SE) products with the adjusted algorithms by the operational passive microwave and optical remote sensing observations.

METHODS AND RESULTS

Firstly, we conducted a comparative study from the local national publications (Chinese Publications) to reveal the general/overall knowledge on the snow climatology over the Tibetan Plateau. Almost one

hundred publications were analysed, among them, we define an indicator to show the changing trend, which represents all the similar function parameters that can be derived from the observations, like maximum snow depth, annual accumulation depth, and etc. The results (see below, fig.1, several solid lines) show that the observations that can be used confidently are mostly from the station observations, while very little attenuation has been paid to the satellite remote sensing data, though it provides wider spatial coverage.

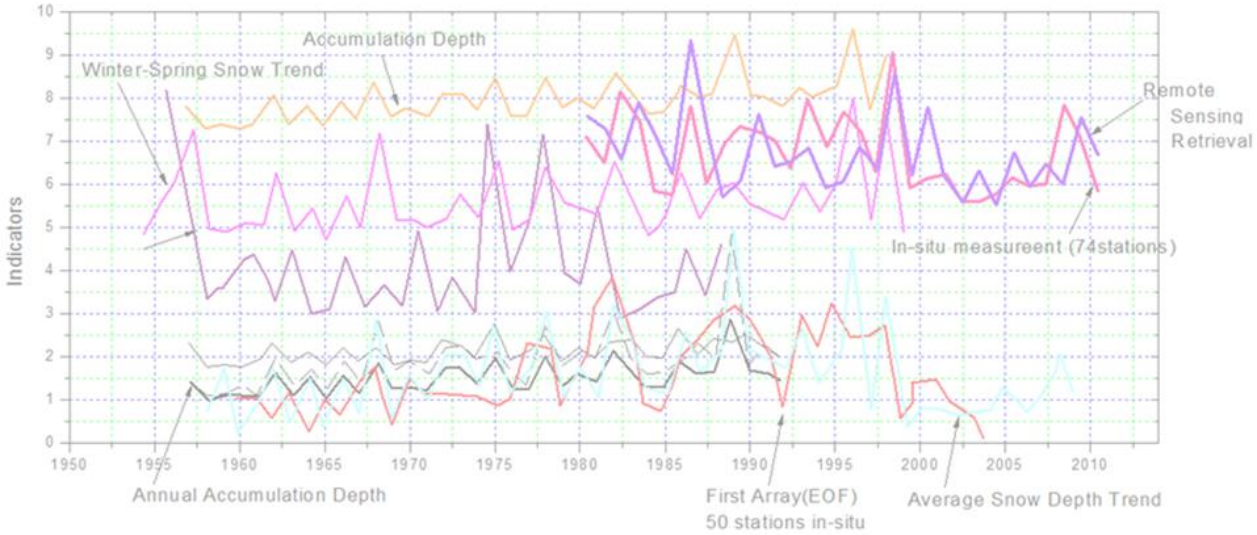

Fig. 1 An overall time series trend comparative study from the Chinese literatures, the vertical axis standard the indicators that are used to evaluated the snow climatology in the last decades.

It is also indicated generally that the snow climatology over Tibetan Plateau expressed a different increasing and decreasing trend in the past 60-years. A clear knowledge is that, before 1990, Tibetan Plateau accepted more and more snow water volume (bottom parts of fig.1), while after the 1990, an obviously declining trend was observed. There are also some controversies when the record time length is not long enough and when the representativeness are limited. The satellite-based findings are limitedly used in the study for that the desired remote sensing products don't fully expose the temporal and spatial variations there, and which are desired to provide more accuracy data to the water and energy model.

Secondly, we work on engaging the state-of-the-art satellite observations to map the snow changing and providing the validated snow products to fill the gaps, which are lack of reasonable accuracy snow mapping (SE/SWE). The operational and newly developed algorithm were evaluated over the Tibetan Plateau area (C. Bin & Y. Qiu, 2013, Y. Qiu, 2014), the accuracy was of shortage enough. From 2012, the newly investigation on the satellite mapping of snow and validation excises are under survey over Tibetan Plateau, which is one appropriate way to fulfil the gaps of the sparse station observations atop plateau.

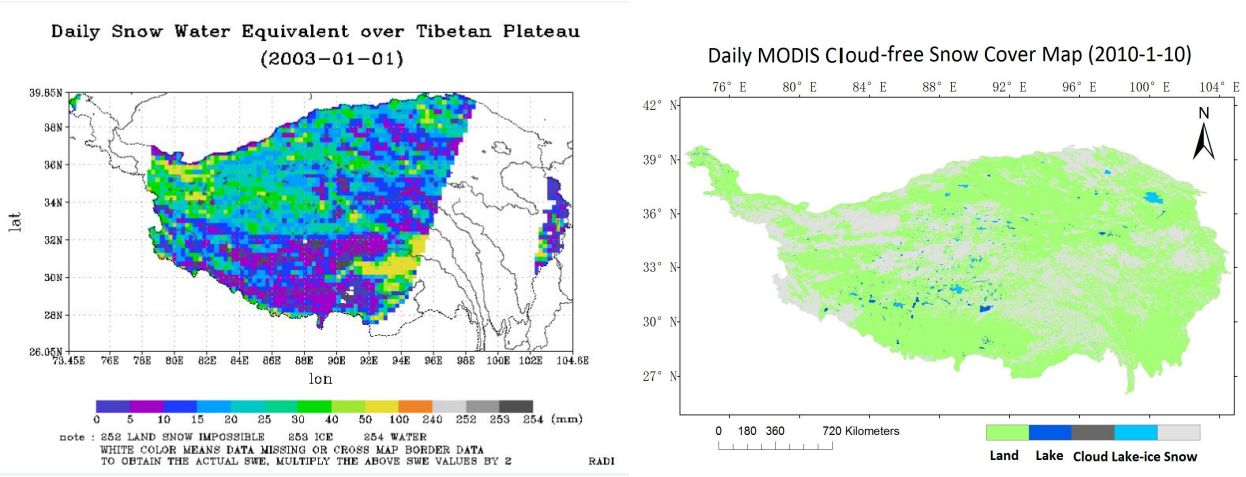

Fig. 2 the examples of snow mapping for the SWE and daily cloud-free Snow Cover over Tibetan Pleteau

The research aim is to obtain the ever higher accuracy daily snow cover (SE) and snow water equivalent (SWE) map products. The SWE products were produced by the adjusted algorithm using the observations from the Advanced Microwave Scanning Radiometer for EOS (AMSR-E) and Microwave Radiation Imager (MWRI) onboard FY-3 (see Fig.2 as the products examples). The cloud-free daily snow cover dataset was derived from the newly updated combination method by the Moderate-resolution Imaging Spectroradiometer (MODIS) observations onboard Terra and Aqua satellite. The validation testing was performed using winter months' station observations. The result indicates that the adjusted algorithm experiences a partly higher accuracy when compared with the AMSR-E operational products. The classification accuracy for the daily cloud-free snow cover products by the updated combined algorithm from MODIS (Aqua/Terra) is higher than 92.3% (when the snow depth > 3cm), while, the station records also show their representativeness problem.

As the conclusion, the station assessment was checked and classified for the validation work, the preliminary snow products was released as its first trial version online the websites of Snow Observations over Tibetan Plateau (SOTP) and the Global Environmental Resources Spatial Information Platform of Chinese Academic of Sciences.

ACKNOWLEDGEMENTS

This work was supported by the Grant of National Natural Science Foundation (Grant No.: 41371351 and 41120114001), and China Special Fund for Meteorological Research in the Public Interest (Grant No, : GYHY201206040). The MODIS snow cover products were obtained from the NASA Distributed Active Archive Center (DAAC) at the National Snow and Ice Center. The Advanced Microwave Scanning Radiometer for EOS (AMSR-E) and Fengyun - 03 Microwave Radiation Imager (FY-MWRI) was from obtained from DAAC and Data Portal at National Satellite Meteorological Center, China Meteorological Administration.

REFERENCES

Vaughan, D.G., J.C. Comiso, I. Allison, J. Carrasco, G. Kaser, R. Kwok, P. Mote, T. Murray, F. Paul, J. Ren, E. Rignot, O. Solomina, K. Steffen and T. Zhang, 2013: Observations: Cryosphere. In: Climate Change 2013: The Physical Science Basis. Contribution of Working Group I to the Fifth Assessment Report of the Intergovernmental Panel on Climate Change [Stocker, T.F., D. Qin, G.-K. Plattner, M. Tignor, S.K. Allen, J. Boschung, A. Nauels, Y. Xia, V. Bex and P.M. Midgley (eds.)]. Cambridge University Press, Cambridge, United Kingdom and New York, NY, USA.

Yubao Qiu, Huadong Guo, Jiancheng Shi, Juha Lemmetyinen, “ REMOTE SENSING OF PLANET EARTH ” ,Part1, Chapter3: Satellite-Based Snow Cover Analysis and the Snow Water Equivalent Retrieval Perspective over China, 2012.1

Ma, L., and D. Qin, 2012: Temporal-spatial characteristics of observed key parameters of snow cover in China during 1957–2009. Sci. Cold Arid Reg., 4(5), 384–393.

Yubao Qiu, Huadong Guo, Chanjia Bin, Duo Chu, Lijuan Shi, Juha Lemmetyinen:Comparasion on snow depth algorithms over China using AMSR-E passive microwave remote sensing. IGARSS 2014: 851-854

BIN Chan-jia, QIU Yu-bao, SHI Li-juan, Chu Duo, ZHU Ji, Comparative Validation of Snow Depth Algorithms Using AMSR-E Passive Microwave Data in China, Journal of Glaciology and Geocryology, 2013-04

BLACK CARBON MIXING STATE IN THE FINNISH ARTIC

T. RAATIKAINEN[1], D. BRUS[2], A.-P. HYVÄRINEN[3], J. SVENSSON[2], E. ASMI[2] and H. LIHAVAINEN[2]

[1]Climate Research, Finnish Meteorological Institute, Helsinki, Finland

[2]Atmospheric Composition Research, Finnish Meteorological Institute, Helsinki, Finland

[3]Expert Services, Finnish Meteorological Institute, Helsinki, Finland

Keywords: BLACK CARBON, AEROSOL, ABSORPTION, ARCTIC, SP2.

INTRODUCTION

Most atmospheric aerosol types scatter incoming solar radiation and therefore have a cooling effect on climate, but black carbon and soot aerosols absorb radiation which means that they have a warming effect (IPCC, 2013; Bond et al., 2013). Absorbing aerosols have the largest warming effect over reflective surfaces such as snow and ice. In addition, deposition of absorbing aerosols on snow decreases surface reflectivity which further enhances snow melt and decreases reflectivity. Detailed atmospheric absorbing aerosol composition and mixing state measurements are needed to understand their formation, aging and removal processes as well as water vapour interactions.

Absorbing material can be distributed so that a certain fraction of all particles contain absorbing material and these particles can have different volume fractions of absorbing and non-absorbing materials. Aerosol optical properties depend on the mixing state; for example, smaller absorbing aerosol size and addition of a non-absorbing coating means increased absorption due to increased effective cross sectional area. In addition, aerosol interactions with water vapour, which are important for optical properties of droplets and clouds as well as for the wet removal processes, depend on the mixing state. There are several instruments for measuring total concentrations of absorbing aerosols, but few instruments can give detailed information about the mixing state. One of such instruments is Single Particle Soot Photometer or briefly SP2 (Stephens et al., 2003), which measures the mass of refractory Black Carbon (rBC) from each particle. The detectable volume equivalent rBC diameters range from about 100 to 600 nm, which typically is the optically relevant size range.

We have measured rBC mixing state at Finnish Lapland by using a SP2 during winter 2011/2012. From the measured data we have calculated parameters such as the average rBC coating thickness and the fraction of rBC-containing particles from all particles. In addition, trajectory analysis is used to estimate the sources of rBC and the effects of different sources on rBC mixing state. Finally, rBC concentrations are compared with those from filter-based optical measurements.

METHODS

Measurements were conducted at the Pallas GAW station at Finnish Lapland (Fig. 1) during winter 2011/2012.The station is on top of a hill (Sammaltunturi) surrounded by mixed pine, spruce and birch forests (Hatakka et al., 2003). The area is sparsely populated and does not have significant local aerosol pollution sources. Elevated aerosol concentrations are typically observed when air masses are originating from densely populated and industrialized areas from south or from Kola Peninsula (e.g. Hyvärinen et al., 2011).

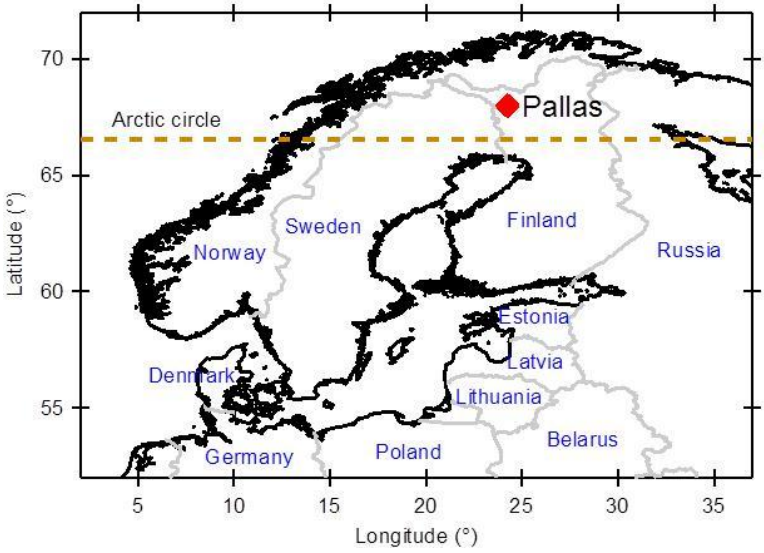

Figure 1. Location of the Pallas GAW station.

Single Particle Soot Photometer (SP2) measures mass of so-called refractory Black Carbon (rBC) by using a laser induced incandescence method (Stephens et al., 2003). The refractory Black Carbon is the fraction of absorbing material that has boiling point close to 4000 K, which typically means elemental carbon (EC). The instrument also measures particle sizes based on scattered laser light. By assuming that absorbing particles are composed of rBC core coated by a homogenous non-absorbing material, rBC mass can be converted to core diameter and the scattering size is the total particle diameter. Average particle properties can be presented by four time dependent parameters: total rBC mass concentration and mass mean diameter describe rBC core size distributions, relative coating thickness is the average particle to core diameter ratio (D_p/D_{core}), and the fraction of rBC containing particles from all particles is the fourth parameter.

The Pallas GAW station has also continuously operated instruments for measuring aerosol properties, meteorology and trace gas concentrations. The aerosol instruments include MAAP (Multiangle Absorption Photometer) and Aethalometer, which measure equivalent Black Carbon (eBC) mass concentration, and DMPS (Differential Mobility Particle Sizer) for particle number size distributions from total and gas sample lines. The difference between these two sample lines is that the total line contains all particles including those from cloud droplets, but those are not included in the gas (or PM2.5) sample line. Therefore, these two DMPS measurements can be used to identify time periods when the hilltop station is in cloud, which happens quite often during autumn and winter. These in-cloud time periods are typically removed from the data analysis, because instruments connected to the PM2.5 sample line (SP2 and MAAP) are not detecting particles that have grown to cloud droplets. Unfortunately, low coverage of the DMPS data limited our capabilities to identify in-cloud time periods (26 % no cloud, 19 % in-cloud and 55 % not known), so both no cloud and full campaign cases were considered.

RESULTS

The effects of in-cloud measurements were first estimated visually and then by comparing average values of the aerosol parameters calculated for different time periods. Figure 2 shows an example of time period where the changes in the aerosol parameters can be related to in-cloud conditions. In this example, total rBC concentration, rBC core size and relative coating thickness are smaller and the fraction of rBC particles is higher during the in-cloud conditions. This is in agreement with expectations as larger and non-absorbing or thickly coated rBC particles are more likely to from cloud droplets, which are removed at the inlet. For the longer time periods, however, in-cloud conditions have a small effect. Although

aerosol parameters depend on the averaging time period, in-cloud and no-cloud averages were not statistically distinguishable. Therefore, we will use the full data set in the further calculations.

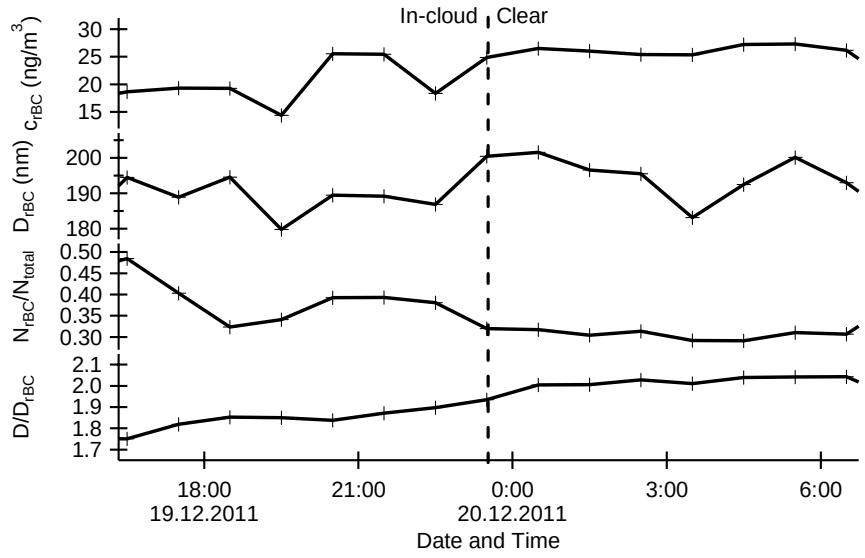

Figure 2. Example of measured aerosol parameters (concentration, rBC core diameter, fraction of rBC containing particles, and relative coating thickness) when the station is in cloud (activated particles not detected) and after that (all particles detectable). The vertical dashed line shows the transition from in-cloud to clear conditions.

The measured aerosol parameters have very weak diurnal variations, which is what can be expected during the cold Artic winter and polar nigh. Figure 3 shows diurnal cycles for rBC mass concentration and solar radiation. Although there is a weak afternoon minimum in the rBC concentration, the absolute decrease is small compared with normal concentration fluctuations (see e.g. Fig. 2). Diurnal variations increased slightly with the increasing solar radiation after the polar night.

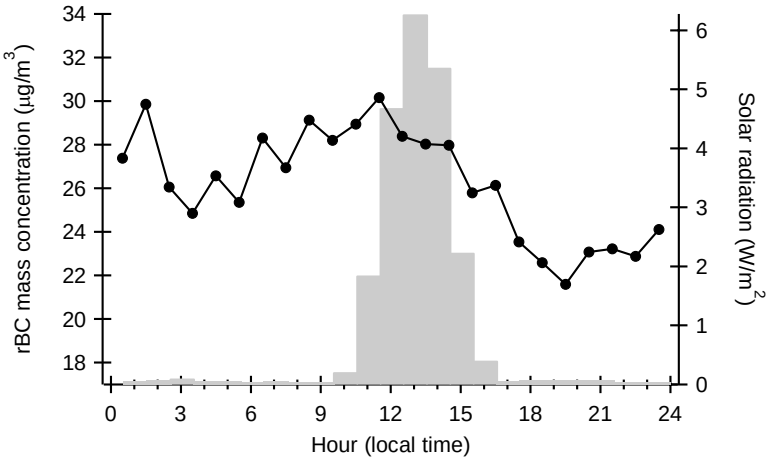

Figure 3. Diurnal cycles for rBC mass concentration (left scale; lines and markers) and solar radiation (right scale; bars).

From the three instruments measuring absorbing material, Aethalometer and MAAP detect so called equivalent Black Carbon (eBC) by measuring light attenuation from aerosols collected to a filter. Figure 4 shows correlation between the two eBC measurements and MAAP eBC and SP2 rBC. Because the Aethalometer is connected to the total sample line, which means that it detects dried cloud droplets, the

Aethalometer eBC is often larger than that from MAAP (grey dots). However, the Aethalometer eBC is about 86 % of the eBC detected by MAAP during clear time periods (open circles). The rBC is only about 20 % of the eBC. Although factors such as instrument calibration and assumed physical properties of BC can explain part of the difference, eBC and rBC concentrations are still clearly different. This difference could be interpreted as non-refractory (brown) carbon which is not detected by a SP2.

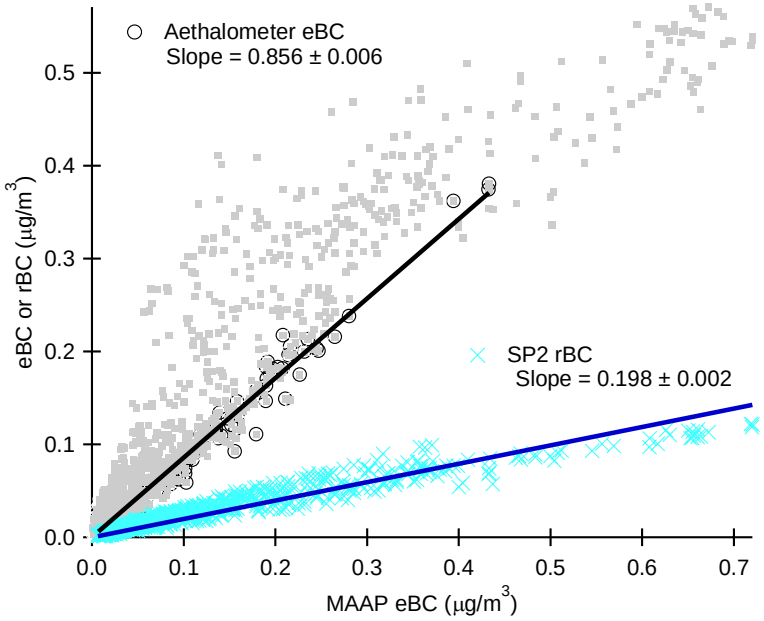

Figure 4. Correlations between the two equivalent Black Carbon (eBC from MAAP and Aethalometer) and refractory Black Carbon (rBC from SP2) concentrations. Aethalometer measurements are shown with dots which are circled for no-cloud time periods.

Backward trajectories were calculated using the HYSPLIT (Hybrid Single Particle Lagrangian Integrated Trajectory) model (Draxler and Rolph, 2003). These can give an indication of the origin of the observed particles. From the trajectories we have calculated average direction, which is the distance weighted average of the trajectory point directions. Figure 5 show that the highest rBC concentrations are observed when air masses are originating from the SE to S sector. The other aerosol parameters were less dependent on the direction.

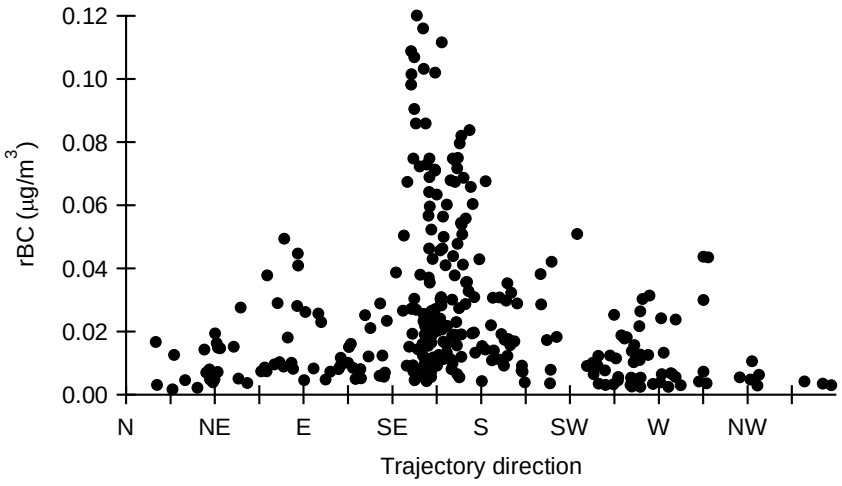

Figure 5. Observed rBC concentration as a function average trajectory direction.

CONCLUSIONS

We have measured refractory Black Carbon (rBC) mixing state at Finnish Lapland. To our knowledge, these are the first SP2 results from the area and also from northern Scandinavia. The measurements showed that the average rBC concentrations are quite often low, but moderate concentrations are also observed occasionally. Relatively high fraction of particles contains rBC (24 %), and typical rBC containing particles are large (average core size 217 nm) and thickly coated (average particle to core size ratio is 2). We have also compared equivalent and refractory BC measurements and observed a factor of five differences.

ACKNOWLEDGEMENTS

This work was supported by the EU LIFE+ project MACEB (project no. LIFE09 ENV/FI/000572), the Academy of Finland through the FCoE in Physics, Chemistry, Biology and Meteorology of Atmospheric Composition and Climate Change (program no. 1118615), black and brown carbon influence on climate and climate change in India – from local to regional scale (project no. 264242), Arctic Absorbing Aerosols and Albedo of Snow (project no. 3162), the Nordic research and innovation initiative CRAICC, and KONE foundation (project no. 46-6817).

REFERENCES

Bond, T. C., S.J. Doherty, D.W. Fahey, P.M. Forster, T. Berntsen, B.J. DeAngelo, M.G. Flanner, S. Ghan, B. Kärcher, D. Koch, S. Kinne, Y. Kondo, P.K.. Quinn, M.C. Sarofim, M.G. Schultz, M. Schulz, C. Venkataraman, H. Zhang, S. Zhang, N. Bellouin, S.K. Guttikunda, P.L. Hopke, M.Z. Jacobson, J.W. Kaiser, Z. Klimont, U. Lohmann, J.P. Schwarz, D. Shindell, T. Storelvmo, S.G. Warren and C.S. Zender (2013). Bounding the role of black carbon in the climate system: A scientific assessment, *J. Geophys. Res.* **118**, 5380.

Draxler, R. and G. Rolph (2003). HYSPLIT (HYbrid Single-Particle Lagrangian Integrated Trajectory) Model access via NOAA ARL READY Website (http://www.arl.noaa.gov/ready/hysplit4.html), NOAA Air Resources Laboratory, Silver Spring, MD.

Hatakka, J., T. Aalto, V., Aaltonen, M. Aurela, H. Hakola, M. Komppula, T. Laurila, H. Lihavainen, J. Paatero, K. Salminen and Y. Viisanen (2003). Overwiev of the atmospheric research activities and results at Pallas GAW station, *Boreal. Env. Res.* **8**, 365-383.

Hyvärinen, A.-P., P. Kolmonen, V.-M. Kerminen, A. Virkkula, A. Leskinen, M. Komppula, J. Hatakka, J. Burkhart, A. Stohl, P. Aalto, M. Kulmala, K.E.J. Lehtinen, Y. Viisanen and H. Lihavainen (2011). Aerosol black carbon at five background measurement sites over Finland, a gateway to the Arctic, *Atmos. Environ.* **45**, 4042.

IPCC (2013). *Climate Change 2013: The Physical Science Basis. Working Group I Contribution to the Fifth Assessment Report of the Intergovernmental Panel on Climate Change*, (Cambridge University Press)

Stephens, M., Turner, N. and Sandberg, J. (2003). Particle identification by laser-induced incandescence in a solid-state laser cavity, *Appl. Opt.* **42**, 3726.

COMPARISON OF SATELLITE AND GROUND BASED TOTAL CONTENTS OF METHANE AND CARBON MONOXIDE FOR BACKGROUND AND URBAN SITES

V. RAKITIN, N. ELANSKY, A. SKOROKHOD, YU. SHTABKIN, N. PANKRATOVA, A. SAFRONOV AND A. DZHOLA

Obukhov Institute of Atmospheric Physics, RAS, Moscow, Russian Federation
vadim@ifaran.ru

Results of space-borne and ground–based data validation has presented in numerous papers. However, they often operate by monthly averaged TC values of some important gases such as CH_4, CO_2 etc., or global-scale domains averaging. We often haven't representative information about relations between orbital and ground-based diurnal TC values.

We present previous validation results of IASI and AIRS CH_4 and CO, MOPITT CO satellite data for time-period 2010-2014 years with some ground-based solar spectrometers located in European Arctic region, in Europe middle altitudes, in Central Siberia and South-East Asia. Comparison was produced for different periods of averaging from diurnal data to monthly averaged means. Also the comparison of these satellite sensors data between each other has presented.

We have got enough good agreement in main ground-based and orbital AIRS TC for CH_4 (R^2~0.4-0.7), for CO (R^2~0.6-0.9) for background conditions (anthropogenic emissions and emissions from wild fires), for diurnal TC 1°x1° and 5°x5° domains averaged. Similar results were obtained for MOPITT CO TC. For "strong emissions" conditions (such as Beijing region and regions of wild fires) we found R^2~0.4-0.6 and another kind of relation between satellite and ground-based CO TC diurnal data. The reasons of some disagreements in validation results for strong pollution events are discussed.

The correlation of IASI and ground based CO TC was found (R^2~0.4-0.6). The disagreement between ground-based and IASI CH_4 TC and the same between AIRS and IASI CH_4 TC was obtained. Long-term variation characteristics of CH_4 and CO columns for different Eurasian sites for both ground-based and orbital sensors are discussed. The differences between the cases of strong pollution of Moscow and Beijing regions are discussed too. Some CH_4 and CO emission estimates for Europe and Siberia wild fires events was obtained by GFED and by independent balance model calculations.

Exchange of oxygenated VOCs between the atmosphere and a boreal forest

P. RANTALA[1], J. AALTO[2], R. TAIPALE[1], M. K. KAJOS[1], J. PATOKOSKI[1], T.M. RUUSKANEN[1], and J. RINNE[3]

[1] Division of Atmospheric Sciences, Department of Physics, University of Helsinki, Finland.
[2] Department of Forest Sciences, University of Helsinki, Finland.
[3] Department of Geosciences and Geography, P.O. Box 64, FI-00014 University of Helsinki, Finland.

Keywords: OVOC, deposition, boreal forest, PTR-MS.

INTRODUCTION

Oxygenated volatile organic compounds (OVOCs) are mostly emitted from biogenic sources and their contribution to the total biogenic VOC budget has been estimated to be ca. 20 % (Guenther *et al.*, 1995). OVOCs do not play a significant role in the boundary layer chemistry but they can be transported to the upper troposphere where e.g. methanol can possibly have a major effect on oxidant formation (Tie *et al.*, 2003).

Emissions of most important OVOCs, such as methanol, are widely studied and mostly well-known (e.g. Brunner *et al.*, 2007; Guenther *et al.*, 2012). However, it has been recently observed that OVOCs have also significant deposition that could be related to the night time dew on surfaces (Holzinger *et al.*, 2001; Seco *et al.*, 2007) but other deposition mechanisms have been suggested as well (Laffineur et al., 2012). Nevertheless, e.g. global model MEGAN 2.1 does not describe the deposition processes in detail (Guenther *et. al.* 2012).

We have measured ecosystem scale fluxes using the proton transfer reaction quadrupole mass spectrometer (PTR-MS) above boreal forest in Hyytiälä at SMEAR II (Station for Measuring Forest Ecosystem−Atmosphere Relations) since 2010. The continuous long-term measurements have given a possibility to study exchange of VOCs in various circumstances. In this abstract, we present deposition measurements of methanol, acetaldehyde, acetone and acetic acid, the common OVOCs in the atmosphere.

METHODS

The measurements were obtained in Hyytiälä at SMEAR II site (61° 51' N, 24° 17' E, 180 m a.m.s.l., UTC+2, Hari and Kulmala, 2005) in May 2010 – December 2013. The flux measurements were conducted by the PTR-MS, a fast response, high sensitivity instrument manufactured by Ionicon Analytik GmbH, Innsbruck, Austria (Lindinger *et al.*, 1998; Taipale *et al.*, 2008).

The PTR-MS was set to measure 27 different compounds from six different measurement levels of a 73 m high mast (127 m from 2013 onwards). Four of the measurement levels were above the canopy. Fluxes were derived using the surface layer profile method (Rannik, 1998; Rantala *et al.*, 2014).

RESULTS AND CONCLUSIONS

The OVOC fluxes were observed to be strongly dependent on the relative humidity (RH, Fig. 1A) and the threshold of deposition was found to be in the region of RH= 55...85 %. Therefore, the

compounds had usually deposition during early mornings when the air was typically moister (Fig. 1B). The results fit well with the earlier observations made by Altimir et al. (2006), who found that moisture typically starts gathering on the surface when RH > 60–70 %.

Negative fluxes were dominating after summer season (Fig. 2) which indicates that in the time scale of a few months the surface can be also a net sink for OVOCs. This means basically that most of the deposited OVOCs should be e.g. either used by organisms or decreased by chemical reactions without having a chance to evaporate back to the atmosphere.

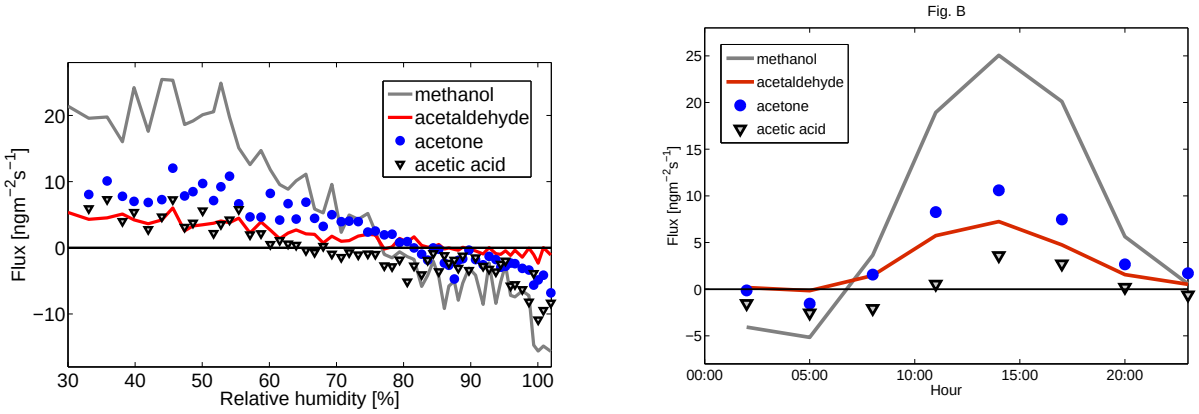

Figure 1: The left-hand side figure (A) shows bin-averaged OVOC fluxes vs. RH. Fig. B represents the median diurnal cycles of the OVOC fluxes measured in May–September.

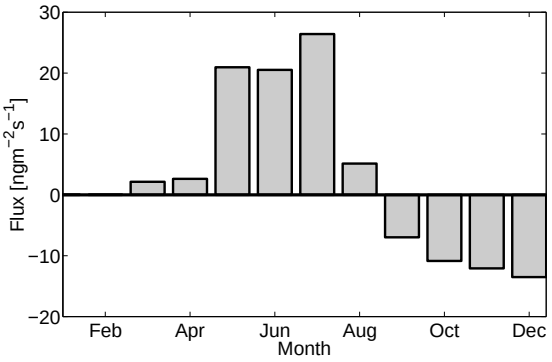

Figure 2: Monthly medians of the summed OVOC fluxes. The results from January and February did not differ statistically from zero, thus those months were disregarded from the analysis.

ACKNOWLEDGEMENTS

This research was supported by the Academy of Finland Centre of Excellence program (project number 272041).

REFERENCES

Altimir, N., P. Kolari, J.-P. Tuovinen, T. Vesala, J. Bäck, T. Suni, M. Kulmala and P. Hari (2006). Foliage surface ozone deposition: a role for surface moisture? *Biogeosciences*, **3**, 209.

Brunner, A., C. Ammann, A. Neftel and C. Spirig (2007). Methanol exchange between grassland and the atmosphere. *Biogeosciences*, **4**, 395

Guenther, A., C. N. Hewitt, D. Erickson, R. Fall, C. Geron, T. G. P. Harley, L. Klinger, M. Lerdau, W. A. McKay, T. Pierce, B. Scholes, R. S. R. Tallamraju, J. Taylor and P. Zimmerman (1995). A global model of natural volatile organic compound emissions. *Journal of Geophysical Research*, **100**, 8873.

Guenther, A. B., X. Jiang, C. L. Heald, T. Sakulyanontvittaya, T. Duhl, L. K. Emmons and X. Wang (2012). The Model of Emissions of Gases and Aerosols from Nature version 2.1 (MEGAN2.1): an extended and updated framework for modeling biogenic emissions *Geoscientific Model Development*, **5**, 1471.

Hari, P. and M. Kulmala (2005). Station for measuring ecosystem-atmosphere relations 34 (SMEAR II). *Boreal Environmental Research*, **10**, 315.

Holzinger, R., A. Jordan, A. Hansel and W. Lindinger (2001). Methanol measurements in the lower troposphere near Innsbruck (047°16'N; 011°24'E), Austria. *Atmospheric Environment*, **35**, 2525.

Laffineur, Q., M. Aubinet, N. Schoon, C. Amelynck, J.-F. Müller, J. Dewulf, H. Van Langenhove, K. Steppe and B. Heinesch (2012). Abiotic and biotic control of methanol exchanges in a temperate mixed forest. *Atmospheric Chemistry and Physics*, **12**, 577.

Lindinger, W., A. Hansel and A. Jordan (1998). On-line monitoring of volatile organic compounds at pptv levels by means of Proton-Transfer-Reaction Mass Spectrometry (PTR-MS)—Medical applications, food control and environmental research. *Int. J. Mass Spectrom.*, **173**, 191.

Rannik, Ü. (1998). On the surface layer similarity at a comples forest site. *Journal of Geophysical Research*, **103**, 8685.

Rantala, P., R. Taipale, J. Aalto, M. K. Kajos, J. Patokoski, T. M. Ruuskanen and J. Rinne (2014). Continuous flux measurements of VOCs using PTR-MS reliability and feasibility of disjunct-eddy-covariance, surface-layer-gradient, and surface-layer-profile methods. *Boreal Environment Research*, **19 B**, 87.

Seco, R., J. Peñuelas and I Filella (2007). Short-chain oxygenated VOCs: Emission and uptake by plants and atmospheric sources, sinks, and concentrations. *Atmospheric Environment*, **41(12)**, 2477.

Taipale, R., T. M. Ruuskanen, J. Rinne, M. K. Kajos, H. Hakola, T. Pohja and M. Kulmala (2008). Technical note : quantitative long-term measurements of VOC concentrations by PTR-MS - measurement, calibration, and volume mixing ratio calculation methods. *Atmospheric Chemistry and Physics*, **8**, 668.

Tie, X., A. Guenther and E. Holland (2003). Biogenic methanol and its impacts on tropospheric oxidants. *Geophysical Research Letters*, **30**, 1881.

METHANE UNDER ICE IN BOREAL LAKES

T. RASILO and P.A. DEL GIORGIO

Groupe interuniversitaire en limnologie et en environnement aquatique, Département des sciences biologiques, Université du Québec à Montréal,
C.P. 8888, succ. Centre-ville, Montréal (Québec), H3C 3P8, Canada

Keywords: greenhouse gases, winter, aquatic ecosystems, seasonality.

INTRODUCTION

Lakes are important sources of greenhouse gases (GHG) to the atmosphere, emitting both carbon dioxide (CO_2) and methane (CH_4) (Bastviken *et al.*, 2004; Tranvik *et al.*, 2009). Role of freshwater ecosystem is especially important in boreal zone, where lakes and rivers cover in average 10% of the landscape compared to 3% global average (Downing *et al.*, 2006). Boreal regions are also characterized by distinct seasons leading to lakes to be covered by ice in winter and strongly temperature saturated in summer. The winter ice cover and changes related to mixing of water column due to spring and fall overturn regulate the seasonal variation in GHG dynamics, and without considering them, the annual estimates of GHG emissions from boreal lakes will be biased. While seasonal variation of CO_2 is rather well known; highest emissions related to overturn periods when CO_2 accumulated under ice or in the hypolimnion is released, those for CH_4 are less studied and less consistent. Accumulation of both CO_2 and CH_4 has been observed in subarctic lakes (Karlsson *et al.*, 2013) but the results from boreal regions are contrasting for CH_4 (e.g. Huttunen *et al.*, 2001, 2003; Juutinen *et al.*, 2009; Demarty *et al.*, 2011). Although CH_4 in general accounts for a clearly smaller fraction of annual GHG emissions from a lake, it has much stronger warming potential that CO_2 and thus it is necessary to consider also CH_4 when estimating the role of fresh waters for climate change. Climate change can influence both the length of the ice cover and mixing periods as well as the strength of stratification and thus have remarkable effect on GHG budgets.

This study aims to investigate the seasonal variation of CH_4 concentrations and fluxes in boreal lakes and especially the inconsistency of under-ice accumulation of CH_4 in more details. For this purpose, we conducted seasonal measurements of CH_4, but also CO_2 concentrations of 13 boreal lakes in three separate regions in Québec, Canada. We explored if these boreal lakes had elevated CH_4 concentration under the ice and what characteristics of the lakes can lead to CH_4 build up. We aim to calculate the annual GHG emissions taking into account the seasonal variation of CH_4 and CO_2 dynamics and estimate what is the contribution of spring overturn releasing the possible under-ice accumulation to the annual budget.

METHODS

We sampled altogether 13 lakes around a year in three different regions in Québec, Canada (Table1). We chose six lakes from Chicoutimi (48°N, 71°W), and Abitibi (48.5°N, 79°W), and one in Laurentians (46°N, 74°W). All the lakes were visited five times a year (mid-January,mid- March, early-June, late-July, and early-October). Chicoutimi and Abitibi are both situated approximately on the same latitude and both are dominated by mixed forests (dominated by Abies balsamea (L.) Mill. and Betula papyrifera Marsh.), but while Abitibi is located on the Abitibi clay belt and thus topography is rather flat, the catchment slopes are steeper and elevation varies more in the Laurentians and Chicoutimi. Laurentians is a southern region with deciduous forests (dominated by Populus balsamifera L., Populus tremuloides Michx. and Betula papyrifera Marsh.). Lakes in the Laurentians are mainly clear water lakes, while in Chicoutimi lakes are mainly humic, and Abitibi lakes are shallow and turbid, although also kettle lakes exist.

At each measuring time, a complete depth profile (one meter interval from 0.5 m to bottom) of temperature, pH, conductivity, dissolved oxygen (YSI 600XLM, Yellow Spring Instruments Inc., Yellow Springs, OH), and CO_2 partial pressure (pCO_2, in µatm) was carried out. pCO_2 was measured by pumping lake water through a MiniModule® equilibrating module (Membrana, Wuppertal, Germany), and measuring the concentration of the equilibrated air re-circulating through an EGM-4 (PP Systems, Amesbury, MA) infrared CO_2 analyzer. The surface water CH_4 partial pressure (pCH_4) was determined using headspace method; We collected 30 ml of lake water in a 60 ml triplicate polypropylene syringes, and created a 30-ml headspace of ambient air, shook vigorously for 1 minute in order to equilibrate the gases in water and air and injected the resulting 30 ml headspace into 30-ml glass vials filled with saturated saline solution. Vials were kept inverted until analysis and the gas in the headspace was injected into a gas chromatograph (GC-8A/GC-2014, Shimadzu, Kyoto, Japan) equipped with a FID (flame ionization detector) to determine its CH_4 concentration. The original surface water pCH_4 was then calculated according Henry's law and taking into account the headspace ratio, *in situ* temperature and assuming a constant ambient air pCH_4 of 1.77 µatm.

During open water sampling, CH_4 and CO_2 fluxes were measured by the floating chamber technique. The round (darkened) plastic chamber (0.34 m diameter, 0.18 m height) was connected in a closed loop to an infrared CO_2 analyzer (EGM-4, PP-systems, Amesbury, MA) that measured the changes in pCO_2 in the chamber headspace every minute for 10 minutes. The chamber also had a sampling port that allowed the withdrawal of air samples via a syringe for CH_4 analysis, which was done every 10 minutes for 30 minutes. The collected gas was injected into 30-ml vials containing saturated saline solution, and processed as described above for ambient pCH_4 samples. Gas fluxes (fCH_4 and fCO_2, mmol m^{-2} d^{-1}) were further calculated based on the rates of change in pCO_2 and pCH_4 in the chamber with time and adjusting for *in situ* temperature.

To estimate the annual CH_4 and CO_2 fluxes, we linearly interpolated the partial pressure of the corresponding gas in between the sampling days. We expected the under ice partial pressure from March to ice off continue to change in the same rate as between January and March. The fluxes during the open water period were calculated based on these values, and using estimated k-values (based on lake area and approximated wind speed of 3 m s^{-1}, Vachon and Prairie, 2013) and assuming atmospheric concentrations of 1.8 and 390 ppm for CH_4 and CO_2, respectively. Daily fluxes were then summed for an annual estimate. We assumed that there are no emissions into the atmosphere during the ice cover period.

For background information, we also took samples of surface (0.5 m) water for total phosphorus (TP), total nitrogen (TN), dissolved organic carbon (DOC), colored dissolved organic matter (CDOM) and chlorophyll a (chlA) analysis. Water was directly collected to acid washed and and *in situ* rinsed vials and for DOC water was filtered (0.45 µm PES cartridge, Sarstedt AG & Co., Nümbrecht, Germany). Samples were kept cold during transport and stored at 4ºC until analysis. In the lab, DOC concentration was measured with a TOC analyzer (OI 1010, OI Analytical, College Station, TX) and TP and TN concentrations were analyzed spectrophotometrically after persulfate and alkaline persulfate digestions, respectively. Chl-a samples were filtered (GF/F, Whatman, Kent, UK), the filters were extracted with hot ethanol (90%) via sonication and analyzed spectrophotometrically with an acidification step to correct for phaeophytin (665 and 750 nm, Ultrospec 2100 pro, Thermo Fisher Scientific Inc., Waltham, MA). CDOM was measured as absorbance at 440 nm using an Ultrospec 3100 spectrophotometer (Thermo Fisher Scientific Inc., Waltham, MA).

Lake	Region	Area km^2	Zmax M	TP $\mu g\ L^{-1}$	TN $mg\ L^{-1}$	DOC $mg\ L^{-1}$	CDOM m^{-1}	chlA $\mu g\ L^{-1}$
Abitibi	Abitibi	9079.6	1.9	63.8	0.6	16.5	7.1	3.6
Clarence-Gagnon	Chicoutimi	2.5	13.7	5.9	0.2	11.0	1.5	0.8
Croche	Laurentians	1.8	11.8	3.6	0.1	6.7	1.3	3.7
des Fréres	Abitibi	0.2	9.4	6.3	0.1	4.4	0.6	0.8
des Îlets	Chicoutimi	19.0	5.6	9.5	0.2	6.2	2.1	1.4
Duparquet	Abitibi	467.1	5.3	25.8	0.5	13.9	5.2	3.0
Fortune	Abitibi	7.3	11.3	10.8	0.2	7.9	0.6	2.3
Hébécourt	Abitibi	77.7	3.1	25.7	0.5	10.8	2.2	4.8
Kénogami	Chicoutimi	675.1	19.3	12.6	0.3	7.7	4.1	1.4
Renaud	Abitibi	10.7	1.4	13.0	0.5	10.9	2.6	1.1
Simoncouche	Chicoutimi	8.8	7.4	8.7	0.2	6.9	2.0	1.2
St-Jean	Chicoutimi	10651.3	4.6	11.0	0.3	9.0	5.2	1.2
Tourangeau	Chicoutimi	10.0	5.5	14.9	0.3	9.7	10.0	1.1

Table 1. Basic information of studied lakes in Québec, Canada. Values are averages of all measurements. TP=total phosphorous, TN=total Nitrogen, chlA=Chlorophyl-a, CDOM=colored dissolved organic carbon, absorbance at 440 nm, Zmax=depth of the sampling point, we targeted the deepest area of a lake, DOC=dissolved organic carbon

RESULTS AND DISCUSSION

Lakes formed two distinct groups based on if they were accumulating CH_4 under ice (accumulators) or not (non-accumulators) (Fig. 1). CH_4 concentration under the ice cover increased during winter in 7 lakes (Abitibi, Clarence-Gagnon, Duparquet, Kénogami, Renaud, Simoncouche, and St-Jean), while concentration decreased or was stable in 5 lakes (Croche, des Îlets, Fortune, Hébécourt, Tourengeau). Differences were much smaller for pCO_2 (Fig 1). CH_4 concentrations in one of the lakes (des Frères) behaved in unrealistic manner and thus we excluded it from further analyses.

Lakes accumulating CH_4 under ice were in general larger than non-accumulator lakes (2985±1787 km^2 and 23±14 km^2, respectively) but there was no difference in the mean depth between the two groups of lakes. In general, lake area has been found to correlate negatively with CH_4 concentrations and fluxes (Juutinen *et al.*, 2009; Rasilo *et al.*, 2014) which seems to be contradictory to our winter accumulation results. However, as expected, the summer concentrations and fluxes were higher in smaller non-accumulator lakes. Lake size can affect the water residence time influencing the time for CH_4 accumulation under ice. Unfortunately we do not information neither of river inputs and/or outputs nor the lake volumes to be able to calculate water residence times for our study lakes. If the residence time is short, input of river water with low CH_4 concentrations can prevent the CH_4 accumulation despite the possible high production. On the other hand, if a lake is more fed by ground water with high CH_4 concentrations, CH_4 can seem to accumulate without high production in lake sediments. However, in winter the groundwater input is probably low.

In previous studies winter CH_4 accumulation has been connected to anoxic conditions (Juutinen *et al.*, 2009; Demarty *et al.*, 2011). However, most of our lakes remained oxic also in winter and thus the role of oxygen limitation seemed to be minor for winter CH_4 accumulation in these lakes. However, we measured oxygen only in water close to sediment, not in sediment itself, so we might have missed anoxic conditions in immediate proximity of sediments, which could have influenced CH4 production and accumulation.

The profile measurement showed that the bottom water temperatures tended to be lower (2.8±0.3°C) in lakes accumulating CH_4 than lakes not accumulating it (3.4°C) in winter. During open water period the

situation was opposite although the difference in bottom water temperatures was even smaller (13.1°C and 12.7°C for CH_4 accumulators and non-accumulators, respectively). As the bottom water temperatures and assumingly sediment temperatures in both groups of the lakes were close to each other, it is not likely that differences in temperature sensitive CH_4 production rates could explain the difference in winter behaviour, especially as the accumulators tended to have colder bottoms than non-accumulators.

Although temperature did not seem to affect CH_4 production rate, the nutrient status may have enhanced methanogenesis in accumulator lakes (mean TP 20.1 µg L^{-1} in CH_4 accumulator lakes compared to 12.9 µg L^{-1} in non-accumulator lakes) although the variation was large. Higher nutrient concentrations can increase primary production increasing the amount of organic matter sedimenting in the bottom and acting as a source for methanogenesis. With higher CH_4 production rate a remarkable part of CH_4 produced in sediments can be released to the water column through bubbling and as the bubbles cannot escape into the atmosphere due to the ice cover, they are likely to increase to CH_4 concentration under the ice. However, this is contradictory by looking at higher primary production of non-accumulator lakes shown by pCO_2 values below the atmospheric equilibrium in summer (Fig 1).

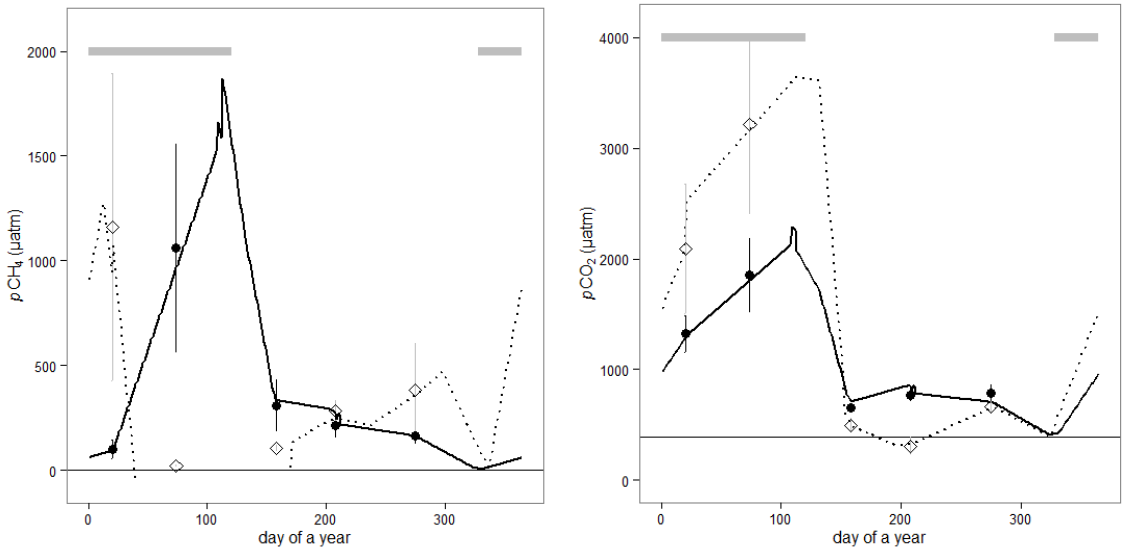

Figure 1. Annual pCH_4 and pCO_2 (ppm) in lakes in 12 lakes in Québec. Solid line is an average of the extrapolation of the lakes (n=7) where pCH_4 increased under ice from January to March and black diamonds are the means of the measurements (with error bars showing the standard error) of the same lakes. Dashed line and open diamonds are the corresponding values for the lakes (n=5) where pCH_4 was stable or decreasing. The horizontal grey bars show the length of ice cover and the vertical black line indicates the atmospheric equilibrium.

The contribution of spring overturn after ice melt to the total annual CH_4 emissions from boreal lakes has often found to be larger than the contribution of autumn overturn, although contrasting results exist also (Juutinen *et al.*, 2009; López Bellido *et al.*, 2009). Our study shows that in lakes where CH_4 was accumulating under ice, the spring overturn (10 days after ice melt) contributed 14% and autumn 12% of the annual emissions while in the lakes where we did not observe winter accumulation, the contribution of spring was minor and the autumn period contributed in average 16% of the annual CH_4 emissions as the concentrations in surface water were increasing throughout the open water period (Fig 1).

Interestingly, the contribution of spring fluxes for annual CO_2 emissions of the same group of lakes was opposite, and in CH accumulator lakes the proportion of spring CO_2 flux was smaller (13%) than in lakes not accumulating CH_4 (38%). Autumn CO_2 fluxes in the different groups were much more similar (17 and 18%, respectively).

It is interesting to note that the lakes where CH_4 concentration increased open water period where most productive, as proposed by summer CO_2 concentrations below atmospheric equilibrium (Fig 1). High production consuming CO_2 dissolved in the water may produce more material for decomposition possibly increasing the rate of methanogenesis. Nevertheless, this higher summer CH_4 concentration did not cause CH_4 accumulation under ice, *vice versa*.

The contribution CH_4 to total annual GHG emissions was in general low, but in CH_4 accumulator lakes CH_4 contributed in average almost 10% of the spring flux. At the annual scale CH_4 contribution was in average 3% in accumulator lakes and only 1% in non-accumulator lakes of total carbon flux. Considering the stronger warming potential of CH_4, the respective contribution of CH_4 fluxes are 21% and 9% of annual GHG emissions as CO_2 equivalents.

CONCLUSIONS

In some boreal lakes the under ice accumulation of CH_4 is important while less so in others. This heterogenity among lakes should be considered when estimating the annual fluxes at larger scale. Apart from possible under ice accumulation, the highest CH_4 concentrations and fluxes were measured in general in summer, contrary to CO_2 which was always highest under ice. The seasonal variation of CO_2 and CH_4 are different from each other, and thus both should be estimated separately. Variation in spring fluxes seemed to cause the most variation in annual fluxes for CH_4, while the variation of summer fluxes was more important for CO_2. Although the contribution of CH_4 fluxes is small as carbon flux, the influence is remarkable if we consider the warming potential of GHG.

ACKNOWLEDGEMENTS

This project is part of the large-scale research program of the Industrial Research Chair in Carbon Biogeochemistry in Boreal Aquatic Systems (CarBBAS), co-funded by the Natural Sciences and Engineering Research Council of Canada (NSERC) and HQ. CarBBAS members are acknowledged for field and laboratory work as well as discussion.

REFERENCES

Bastviken, D., C. Cole, M. Pace, and L. Tranvik (2004) Methane emissions from lakes: Dependence of lake characteristics, two regional assessments, and a global estimate. *Global Biogeochme. Cycles* **18**, GB4009.

Demarty, M., J. Bastien, and A. Tremblay (2011) Annual follow-up of gross diffusive carbon dioxide and methane emissions from a boreal reservoir and two nearby lakes in Québec, Canada. *Biogeosciences* **8**, 41–53.

Downing, J.A., Y.T. Prairie, J.J. Cole, C.M. Duarte, L.J. Tranvik, R.G. Striegl, W.H. McDowell, p. Kortelainen, N.F. Caraco, J.M. Melack, and J.J. Middelburg (2006) The global abundance and size distribution of lakes, ponds, and impoundments. *Limnol. Oceanogr.* **51**, 2388–2397

Huttunen, J.T., T. Hammar, J. Alm, J. Silvola, and P.J. Martikainen (2001) Greenhouse gases in non-oxygenated and artificially oxygenated eutrophied lakes during winter stratification. *J. Environ. Qual.* **30**, 387–394.

Huttunen J.T, J. Alm, A. Liikanen, S. Juutinen, T. Larmola, T. Hammar, J. Silvola, and P.J. Martikainen (2003) Fluxes of methane, carbon dioxide and nitrous oxide in boreal lakes and potential anthropogenic effects on the aquatic greenhouse gas emissions. *Chemosphere* **52**, 609–621.

Juutinen, S., M. Rantakari, P. Kortelainen, J.T. Huttunen, T. Larmola, J. Alm, J. Silvola, and P.J. Martikainen (2009) Methane dynamics in different boreal lake types. *Biogeosciences* **6**, 209–223.

Karlsson, J., R. Giesler, J. Persson, and E. Lundin (2013) High emission of carbon dioxide and methane during ice thaw in high latitude lakes. *Geophys. Res. Lett.*, **40**, 1–5.

López Bellido, J.L., T. Tulonen, P. Kankaala, and A. Ojala (2009) CO_2 and CH_4 fluxes during spring and autumn mixing periods in a boreal lake (Pääjärvi, southern Finland). *J. Geophys. Res: Biogeosci.* **114**, G04007.

Rasilo, T., Y.T. Prairie, and P.A. del Giorgio (2014) Large-scale patterns in summer diffusive CH4 fluxes across boreal lakes, and contribution to diffusive C emissions. *Global Change Biology*, doi: 10.1111/gcb.12741

Tranvik, L.J., J.A. Downing, J.B. Cotner, et al. (2009) Lakes ans reservoirs as regulators of carbon cycling and climate. *Limnol. Oceanogr.* **54**, 2298–2314.

Vachon, D., and Y.T. Prairie (2013) The ecosystem size and shape dependence of gas transfer velocity versus wind speed relationships in lakes. *Can. J. Fish. Aquat. Sci.* **70**, 1757–1764.

SEAS, LAKES AND BOUNDER WATERSHED TERRITORIES OF RUSSIA, FINLAND AND ESTONIA – INTERNATIONAL TRAINING AND EDUCATION SCHOOL-CONFERENCE FOR YOUNG SCIENTISTS

T.I. REGERAND

Northern Water Problems Institute of Karelian Research Centre Russian Academy of Sciences
Petrozavodsk, A. Nevskogo-50, Republic of Karelia, Russia

Keywords: training, education, young scientists, international co-operation

INTRODUCTION

The Northern Water Problems Institute (NWPI) is the academic research structure conducting scientific investigations of the aquatic environment in Northwest Russia for nearly 70 years already. NWPI is active in the implementation of new methods and technologies in water systems investigations. Our areas of expertise include remote monitoring, aerospace methods, geographical information systems (GIS), mathematical modeling (diagnostic, adaptation and prognostic) of water systems. A new sphere of the institute's research work is climate changes in Northwest Russia.

This active scientific position demands the new researchers with modern professional background.

Activities of NWPI in the field of environmental training and education started in the early 1990s. The most critical and actual topic is water bodies environment condition.

The challenge of harmonizing approaches towards the study, assessment, joint use and conservation of transboundary waters and their catchments in Russia and EU states (Finland, Estonia) is of high relevance. Lakes Ladoga, Onego, Pskov-Chudskoe (Peipus) and other lakes at the border in the Baltic and White Sea catchments play an essential role in the economies of the countries. It is important to work out joint approaches towards cross-calibration of the techniques for assessing the quality of surface- and groundwater, monitoring and forecasting methods, conservation of transboundary aquatic and terrestrial systems in conformance with Russian law (Water Code) and EU Water Framework Directive (FWD).

METHODS

The International School-conference "Seas, Lakes and Transboundary Catchments of Russia, Finland and Estonia" devoted to the issues stated above took place in Petrozavodsk on November 11-13, 2014, gathering representatives from scientific and educational institutions of the Republic of Karelia, such as NWPI KarRC RAS and Research and Education Centre of NWPI KarRC RAS "Waters of Karelia and Methods for Their Study", Institute of Geology KarRC RAS, Petrozavodsk State University (PetrSU), as well as leading scientific and educational organizations of Russia: Moscow State University, Russian State Hydrometeorological University, Herzen State Pedagogical University of Russia, RAS Water Problems Institute, RAS Limnology Institute, RAS Shirshov Institute of Oceanology, together with colleagues from neighbouring European countries representing the University of Helsinki, Finland and the University of Tartu, Estonia.

The International School-conference "Seas, Lakes and Transboundary Catchments of Russia, Finland and Estonia" is a continuation of long-lasting activities implemented at NWPI KarRC RAS in 2003-2013 in the frame of the Research-Educational Centre (REC) "Water resources of Karelia and methods of their investigation".

The REC was organized in NWPI in 2002 on the basis of previous wide environmental education activities of the institute using the teaching experience of its researchers and close co-operation with universities in Russia (Moscow and Saint-Petersburg) and, particularly, in Karelia within the Russian Academy of Science program "Support to young scientists". The main idea is to prepare a highly qualified professional staff for scientific research institutions. This is however a complicated process which affects not only higher educational institutions but also secondary schools and the society at large (Regerand et al., 2003; Regerand and Filatov, 2008).

The specific unique feature of NWPI REC is the continuity of the study process: school pupil - university student - postgraduate student - young scientist, with school teachers involved in the process as the basis for high-quality environmental education in schools. This closed circle of the study process gives the opportunity to monitor the results and coordinate the process to correspond to variations in the educational system and to the development of NWPI research activities. Moreover, it contributes to the formation of a new generation with an environment-friendly lifestyle and striving for sustainable development of the society.

From this point of view the main goal of NWPI REC is to conduct environmental education in co-operation with different partners preparing a highly educated young generation of scientists both for Higher Schools and Academy Scientific Institutions via the educational cycle: school – university - Higher school education/Academic scientific institution – teacher/researcher – school.

NWPI REC project aims at effective interaction between basic scientific research conducted at NWPI and the educational process at universities, taking into account the pre-university stage – schools, including teachers and final-grade students.

The goals of the REC project are:

- as applied to Universities - support to and development of basic research, enhancement of the study process quality, integration of scientific research and education, attracting talented youth to scientific research done at NWPI;
- as applied to secondary schools - earlier detection of science-gifted youth, their professional orientation to scientific research through professional development of school teachers in the field of new possibilities of scientific research work with school pupils;
- as applied to the general public (including municipalities and authorities) –wide dissemination of scientific knowledge about the environmental situation and potential anthropogenic pressure;
- as applied to NWPI – highly educated and qualified young professionals.

The NWPI REC project is very topical in a number of ways and at different levels. The activity of REC was supported at the national level by financing coming from the Russian Academy of Science for strengthening and development of professional research staff up to 2013.

In 2014 the School-conference for young scientists was organized with support from the Russian Federal Agency for Scientific Organizations (FANO) and a project under PetrSU Strategic Development Programme, as well as in the framework of the Russian Science Foundation projects "Lakes of Russia – diagnosing and predicting ecosystem condition under climatic and human impacts" and "Lake Onego and its catchment: geological development history, human interventions and present-day state".

The objective of the School-conference is to prepare talented youth for a career in science and education through close collaboration with domestic and foreign higher education and scientific institutions.

Around 100 people took part in the event, including 70 graduate and post-graduate students, early career scientists, lecturers, professors and research associates.


Figure 1. Chairs of the Organizing Committee – D.A. Subetto, DSc (on the left), Director of NWPI KarRC RAS, and N.N. Filatov, RAS Corr. Academician, Head of Geography and Geology Laboratory, NWPI KarRC RAS, Professor at Petrozavodsk State University (on the right).

International participation took the form of both personal attendance by colleagues from Estonia, and a Skype-powered virtual presentation by professor from the University of Helsinki.

Figure 2. Rosentau Alar< researcher from the University of Tartu (Estonia) with the presentation “GIS-based palaeogeographic reconstructions”


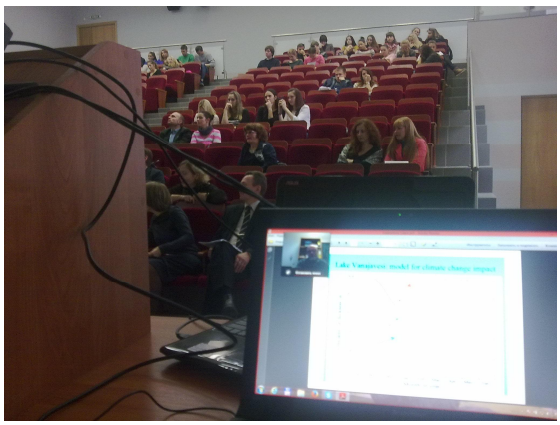

Figure 3. Matti Leppäranta, professor from the Department of Physics, University of Helsinki (Finland) with the presentation “Ice cover in polar lakes and their climate sensitivity”

The programme included two large theoretical sections: day I – PRESENT-DAY PROBLEMS IN LIMNOLOGY AND OCEANOLOGY and day II – PALAEOLIMNOLOGY, PALAEOCLIMATOLOGY, HISTORICAL GEOGRAPHY, CLIMATE, with 7-8 keynote lectures and 7-8 presentations by PhD students and young scientists in each.

The International School-conference “Seas, Lakes and Transboundary Catchments of Russia, Finland and Estonia” presented the wide opportunities for young scientists both from the research institutes and universities to recount results of their investigations.

Figure4. The young scientists on the School-conference.

There were 2 sessions of the ‘Science club’ format featuring free discussions around specific themes: session 1 “Young scientists – challenges and prospects” (defending graduation papers and PhD theses, preparation of publications) and session 2 “Friendship between science and higher education” (practical training sessions and preparation of textbooks and learning aids).

The active position of the participants of the School-conference from the both sides , science and high education systems, towards the training and education confirmed the needs and marked the possibilities for co-operation in future.

Figure 5. The ‘Science club’ “Young scientists – challenges and prospects”

The programme was completed with a day of SCIENTIFIC EXCURSIONS of choice:

- Petrozavodsk waterworks (Petrozavodsk Communal Systems)
- Weather station of the Karelian Hydrometeorology and Environmental Monitoring Centre (branch of the Northwestern Hydrometeorology and Environmental Monitoring Administration)
- Computing cluster of the Institute of Applied Mathematical Research KarRC RAS

Figure 6. Excursion to the Weather station of the Karelian Hydrometeorology and Environmental Monitoring Centre.

All the excursions produced a valuable educational effect and had career guidance implications for PetrSU graduates.

Proceedings of the School-conference “Seas, Lakes and Transboundary Catchments of Russia, Finland and Estonia” will be published as “Lectures by researchers, educators and young scientists for higher educational institutions”, which will be of use for university education, pre-application guidance for high school students, as well as for general learning.

CONCLUSIONS

The mode of the training and educational activity as the School-conference or as the “science bath” for 3 days for young scientists and especially for the university students was really successful. The university students usually expected to unfailing allegiance of the severe curriculum were dip to science atmosphere with great interest.

The colleagues, professors and researchers from Moscow and Saint-Petersburg, and also international partners from Finland and Estonia made this training and educational event more stable for development in future.

The NWPI exposes the hope for the active co-operation on the training and education platform with the colleagues from PEEX also.

ACKNOWLEDGEMENTS

NWPI KarRC RAS acknowledges the contribution of the Petrozavodsk Sate University Faculty of Mining and Geology Department of Geography and the colleguers from the Institute of Geology, KarRC RAS.

NWPI KarRC RAS acknowledges the contribution of the Petrozavodsk Communal Systems company, Karelian Hydrometeorology and Environmental Monitoring Centre and the Institute of Applied Mathematical Research KarRC RAS who helped the School-conference by organizing the excursions.

REFERENCES

Regerand T., Markkanen S.-L., Hänninen M. (2003) Environmental education across boarders. In *Environmental Education. Proceedings of the Seminar at Koli National Park in Finland 18-19.4.2002*. Lasse Loven. (eds). Joensuu Research Center. Finnish Forest Research Institute. Research Papers 887. Joensuu; 235-242.

Regerand T., Filatov N. (2008) The Educational-Scientific Centre as a New Possibility for Promoting Sustainable Development in Karelia, Russia . In *Learning for a sustainable futureinnovative solutions from the Baltic Sea region* (Ed.: Liisa Rohweder, Anne Virtanen). The Baltic University Press. Nina Printhouse, Uppsala. ISBN 978-91-976494-3-8. P. 177-190

ON THE DIRECTION OF CARBON DIOXIDE FLUXES IN THE ARCTIC OCEAN

I.A. REPINA[1], V.V. IVANOV[2,3]

[1]A.M. Obukhov Institute of Atmospheric Physics, Moscow, Russia

[2]Arctic and Antarctic Research Institute, Sankt-Petersburg, Russia

[2]Hydromrtrorological Centre of Russia, Moscow, Russia

Keywords: ARCTIC OCEAN, ACIDIFICATION, AIR SEA-ICE GAS INTERACTION.

INTRODUCTION

Global climatic changes in the Northern hemisphere have led to a remarkable environmental changes in the Arctic Ocean where there has been a noticeable shrinking of the sea-ice cover beginning from the regular satellite observations in 1970s and a rise in temperature and freshening of the Arctic surface waters associated with intensive melting of sea ice. And measurements made along the coast of the Arctic Ocean show that the concentration of carbon dioxide has increased substantially over the past several decades. Uptake of carbon dioxide (CO_2) from the atmosphere leads to decrease in the pH of the World Ocean, causing acidification of the sea water. (Sabine *et al.*, 2004) In the recent years the natural balance of CO_2 between the oceans and atmosphere is distorted because of increased import of the anthropogenic carbon. Thus, ocean acidification is driven by increased emissions of carbon dioxide in the atmosphere, and like global climate change poses a threat to the Earth ecosystems. In a business as usual CO_2 emission scenario, oceanic uptake of CO_2 will acidify the surface ocean by 0.3–0.4 pH units ([H+] increase by 100–150%) by the end of this century (Caldeira and Wickett, 2003).

Two types of forcing are driving increased ocean acidification in the Arctic Ocean and its marginal seas: loss of sea ice and high rates of primary productivity over the continental shelves coupled with increased ocean uptake of anthropogenic CO^2. Future sea ice melting may enhance the air-to-sea CO_2 flux by ~ 28% per decade (Bates *et al*., 2006). Rising atmospheric CO_2 levels combined with the opening of the central Arctic Ocean due to warming and sea ice retreat will lead to higher pCO_2 values in the surface waters of the basin. The direction and magnitude of the CO^2 flux through the air–sea interface are regulated primarily by changes in the oceanic pCO_2 (Feely et al., 2001), while the drivers of air–sea ice fluxes are under discussion (Semiletov *et al*., 2007). A number of questions remain, however, about the continental margin carbon cycle. The dominant terms affecting shelf carbon dynamics vary considerably by region, with areas of both large net positive and negative air–sea CO_2 fluxes. A global picture of the coastal carbon cycle will only emerge through a network of more intensive observations taken across the most diverse set of environments possible.

We present observational results, which demonstrate that in the Arctic Ocean the direction of carbon dioxide fluxes at the ocean/ice/air interface may vary depending on specific conditions.

METHODS

Our measurements were carried out in the Arctic Ocean in framework of NABOS (Nansen and Amundsen Basins Observations System) (2005-2009). CO_2 flux can be measured using either micrometeorological or enclosure methods. The main advantage of micrometeorological methods over the alternative enclosure methods is their ability to continuously measure the surface exchange of matter and energy. Thismakes it possible to study both the short-term variations (e.g., diurnal cycle) and the long-termbalances. The micrometeorological measurements do not disturb the surface under investigation and provide fluxes on

an ecosystem scale, thus partly avoiding the difficult upscaling problems. The markedly smaller target area of chamber measurements, however, enables a spatially detailed study on different components of the ecosystem, which could complement the micrometeorological measurements.
The most direct micrometeorological method is the eddy covariance (EC) technique (Fairal *et al.*, 2000; Baldocchi, 2003). With the EC technique the measurements are carried out using fast response instruments sampling typically at 10–20 Hz in order to cover a large proportion of the frequency range of turbulent variations. For CO_2 flux such measurements are feasible using a sonic anemometer and a fast infrared gas analyzer.

LiCor-7500 sensor coupled with sonic thermo-anemometer (USA-1,METEC) was used for those measurements. The EC technique was applied as follows. Vertical wind speed and temperature fluctuations were measured at 10 Hz using a three-dimensional sonic anemometer–thermometer (USA-1, METEK, GmbH) aligned into the mean wind. Carbon dioxide and water vapor fluctuations were measured at 10 Hz with a fast response open-path infrared Li-Cor 7500 gas analyzer. To minimize flow disturbances, the LI-7500 sensor head has a smooth, aerodynamic profile. In addition, the open path measurement eliminates the need for a pump, greatly reducing the overall power requirement of the system. The open path analyzer also eliminates time delays, pressure drops, and sorption/desorption of water vapor on the tubing employed with closed path analyzers. In our CO_2 exchange study setup, momentum and fluxes of sensible and latent heat were measured using the EC technique.

RESULTS AND DISCUSSION

Ship observations have revealed differences in intensity and direction of gas exchange, which depend on the characteristics of the underlying water masses. Coastal areas, strongly influenced by coastal erosion and the river input of terrestrial carbon (suspended and dissolved), are the sources of CO_2 into the atmosphere. Comparing distribution of CO2 fluxes with surface temperature and chlorophyll content from satellite data (Fig. 1) shows that warmer and fresher water which is probably a riverine plume acts as a source of CO_2, while relatively colder and saltier water near the ice edge is a sink.
Emission of CO_2 from the Arctic coastal zone is influenced by coastal erosion and river runoff water, which is generally low in transparency and productivity; erosion and runoff may increase as global warming continues (Fig.2).

a) b) c)

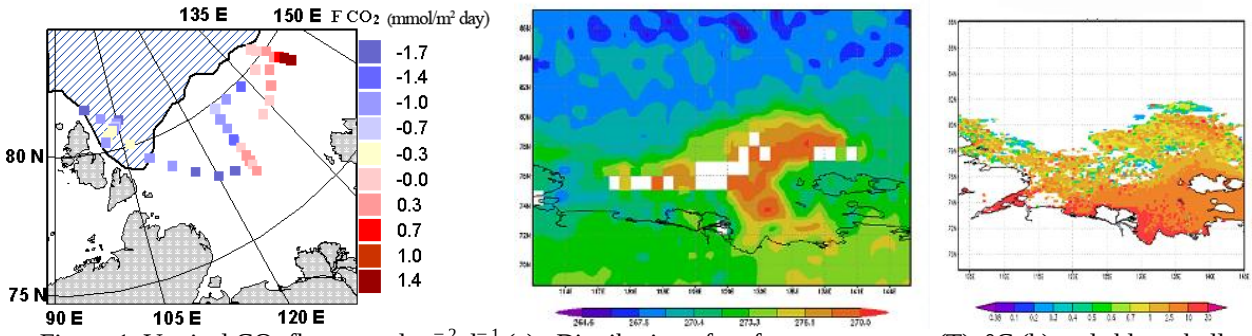

Figure 1. Vertical CO_2 flux, mmol m^{-2} d^{-1} (a), Distribution of surface temperature (T), °C (b) and chlorophyll concentration in Laptev sea, September 2005.

Eddy correlation measurements made above the open water surface of the Laptev Sea ranged between the negative (invasion) and positive (evasion) values of +1.7 mmol m^{-2} d^{-1} and −1.2 mmol m^{-2} d^{-1} Comparing the distribution of CO_2 fluxes with surface temperature and salinity shows that warmer and fresher water, which is probably a riverine plume, acts as a source of CO_2, while relatively colder and saltier water near the ice edge is a sink.

Flux measurements made on one-year ice in the Laptev Sea and fast ice provide some insights onto the influence of sea ice on CO_2 exchange between atmosphere and sea ice surface. We infer that in early summer absorption of atmospheric CO_2 by ice-covered ocean dominates; this agrees with data collected using aircraft. Our measurements also suggest the important role of melt ponds and leads in gas exchange (Fig.3).

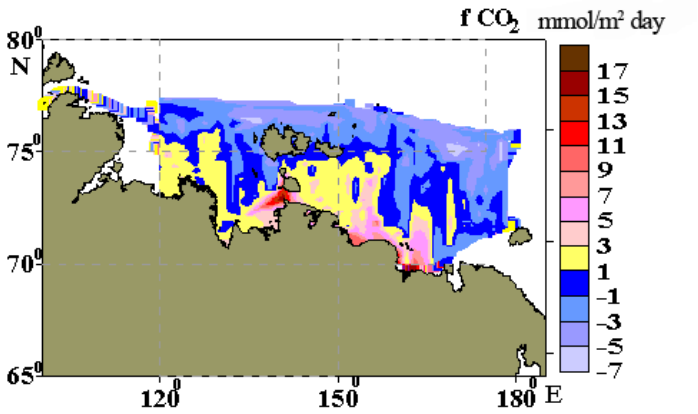

Figure 2. Vertical CO_2 flux, mmol m^{-2} d^{-1} in Arctic coastal zone.

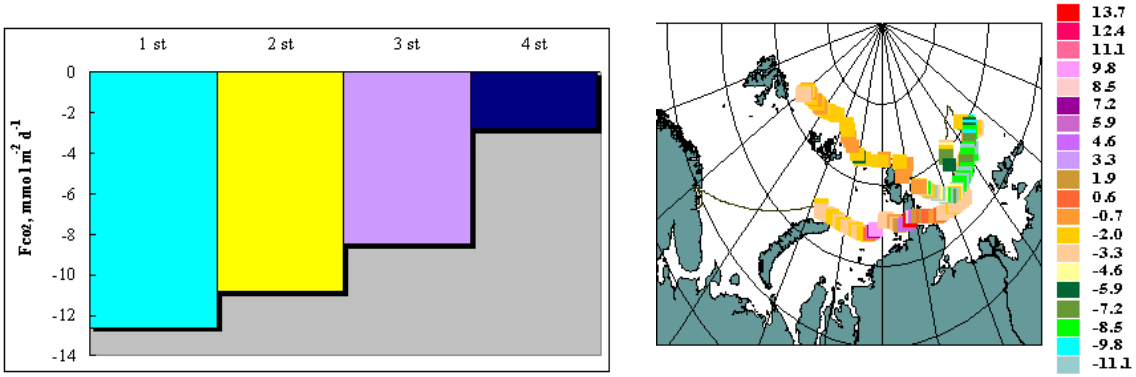

Figure 3. (a) Vertical CO_2 flux on the ice station depends on melt ponds concentration (in the first station concentration of melt ponds was most, (b) distribution of vertical CO2 flux during 2006 expedition (August). Area with melt ponds is in the Laptev sea.

The sea-ice melt ponds form an important spring/summer air CO_2 sink that also must be included in any Arctic regional CO_2 budget. Contrary to ponds, summer leads act as a source of CO_2, which is released to the atmosphere. Both: the direction and amount of CO_2 transfer between air and the sea during open water season may be different from transfer during freezing and thawing, or during winter when CO_2 accumulates beneath the Arctic sea-ice.

ACKNOWLEDGEMENTS

This work was supported by the Academy of Finland (CarLAC project) and Russian Basic Research Foundation (grant 14-05-91764).

REFERENCES

Baldocchi, D. (2003). Assessing the eddy covariance technique for evaluating carbon dioxide exchange rates of ecosystems: past, present and future, *Global Change Biology*, **9**, 479–492.

Bates, N.R., Moran, S.B., Hansell, D.A., and Mathis J.M. (2006). An increasing CO2 sink in the Arctic Ocean due to sea-ice loss? *Geophysical Research Letters*, **33**, L23609, doi:10.1029/2006GL027028.

Caldeira, K. and Wickett, M.E. (2003). Anthropogenic carbon and ocean pH, *Nature*, **425**, 365.
Feely, R.A., Sabine, C.L., Takahashi, T., Wanninkhof, R. (2001). Uptake and storage of carbon dioxide in the ocean: the Global CO2 Survey, *Oceanography*, **14**, 18–32.
Fairal, C.W., Hare, J.E., Edson, J.B., McGillis, W. (2000). Parameterization and micrometeorological measurement of air–sea gas transfer, *Boundary Layer Meteorology*, **96**, 63–105.
Sabine, C.L., Feely, R.A., Gruber, N., Key, R.M., Lee, K., Bullister, J.L.,Wanninkhof, R.,Wong, C.S.,Wallace, D.W., Tilbrook, B., Millero, F.J., Peng, T.H., Kozyr, A., Ono, T., and Rios, A.F. (2004). The oceanic sink for anthropogenic CO2, *Science*, **305**, 367–371.
Semiletov, I.P., Pipko, I.I., Repina, I.A. and Shakhova, N.E. (2007). Carbonate chemistry dynamics and carbon dioxide fluxes across the atmosphere–ice–water interfaces in the Arctic Ocean: Pacific sector of the Arctic. *Journal of Marine Systems*, **66(1)**, 204-226.

TOWARDS CONSTRAINING THE METHANE FLUX FROM THE ARCTIC OCEAN TO THE ATMOSPHERE USING ATMOSPHERIC INVERSE MODELING

F. REUM[1], M. GOECKEDE[1], C. GERBIG[1], J. V. LAVRIC[1], S. ZIMOV[2], N. ZIMOV[2] and M. HEIMANN[1]

[1] Max Planck Institute for Biogeochemistry, Department of Biogeochemical Systems, Jena, Germany.

[2] Northeast Science Station, Russian Academy of Sciences, Cherskii, Russia.

Keywords: Arctic, Methane, Atmospheric inverse modeling

INTRODUCTION

The East Siberian Arctic Shelf (ESAS) is estimated to store about 1400 PgC (Shakhova et al., 2010a). Recent results by Shakhova et al. (2013) suggest that this carbon is currently released to the atmosphere as methane at a rate of about 17±2 Tg CH4 yr^{-1}. This estimate is based on multi-year ship-based measurements, which mostly took place in the months August and September (Shakhova et al., 2010b). Due to these spatial and temporal constraints, the representativeness of Shakhova's results is still uncertain. Hence, our goal is to provide an independent, top-down estimate of the net methane emissions from the ESAS to the atmosphere based on continuous, year-round measurements of atmospheric methane mixing ratios using regional scale inverse modeling of atmospheric methane transport. Here, we present a survey on the spatiotemporal information content of the available databases for such a study, with a strong focus on the recently established Atmospheric Carbon Observation Station Ambarchik. We demonstrate how this new site, which went operational in August 2014, closes an important gap in data coverage for studies about the ESAS domain, and show patterns of footprints and observed trace gas mixing ratio variations based on the first months of data.

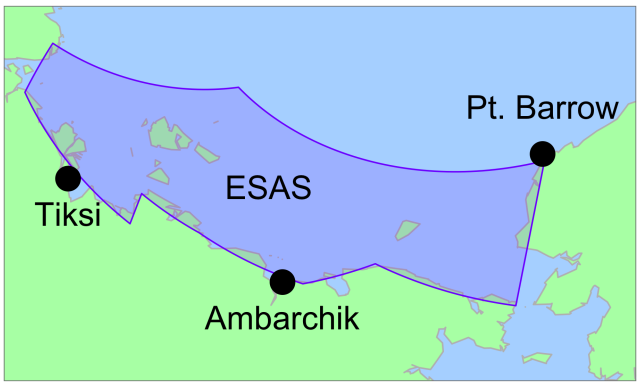

Figure 1: The East Siberian Arctic Shelf (ESAS) and the closest monitoring sites for atmospheric methane.

METHODS

In order to enhance the network of atmospheric carbon observation stations in the Arctic, we established a new site in Ambarchik, at the coast of the Arctic Ocean in northeast Siberia (69.6N, 162.3E) in August 2014. As of today, Ambarchik is uninhabited except for a manned weather station which is operated by Roshydromet, the Russian meteorological service. Its location at the border of the East Siberian Arctic Shelf makes the Ambarchik station highly suitable for inversion studies to constrain surface processes within the ESAS domain. The core of the new observation system is a Picarro G2301 analyzer for continuous monitoring of the atmospheric mixing ratios of CH_4, CO_2 and H_2O. To ensure the alignment of observations with WMO standards, the system features an automated air flow control system that allows to sample four tanks with calibrated standard air at regular intervals. Ambient air is sampled from a 27m tower, with an additional inlet at 14m used mostly for quality assessment purposes. The station is completed by meteorological instruments for monitoring environmental conditions and for comparison with meteorological model output. All instruments except the meteorology sensors reside in a temperature-controlled housing.
Other stations that border the ESAS are Pt. Barrow (Alaska, USA) and Tiksi (Russia) (Figure 1). Pt. Barrow is located at 71.3N, 156.6W, and continuous methane measurements date back as far as 1986. The continuous record of methane mixing ratios at Tiksi (located at 71.6N, 128.9E) begins in 2011.

RESULTS

Maps of backtrajectory densities of Pt. Barrow, Tiksi and Ambarchik reveal that all three stations measure air masses which are directly influenced by the East Siberian Arctic Shelf (Figure 2). However, the trajectory densities of Pt. Barrow and Tiksi are centered outside or at the edge of the shelf, respectively. In contrast, Ambarchik is influenced by a larger fraction of the center of the shelf, and therefore notably improves the data coverage needed for inverse modeling studies of the region.

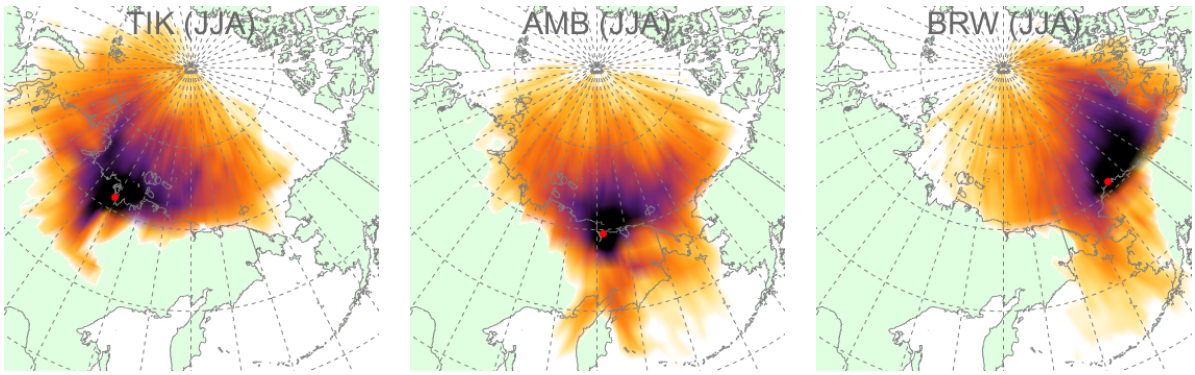

Figure 2: Backtrajectory densities for Tiksi (TIK), Ambarchik (AMB) and Pt. Barrow (BRW) for the months June, July and August of the years 2005 to 2013. HYSPLIT model, 4 trajectories per day 5 days back in time.

SUMMARY

A new site for continuous monitoring of atmospheric CO_2 and methane has been established and is operating continuously since August 2014 in Ambarchik, northeast Siberia. This is an important step towards a regional inverse modeling study that aims at quantifying the methane flux from

the Arctic Ocean to the atmosphere. A footprint analysis demonstrates that the new Ambarchik station notably improves the data coverage of the East Siberian Arctic Shelf for inverse modeling studies of the region.

ACKNOWLEDGEMENTS

This work was supported by the European Science Foundation (ESF) for the activity "Tall Tower and Surface Research Network for Verification of Climate Relevant Emissions of Human Origin"

REFERENCES

Shakhova, N. E., Semiletov, I. P., Leifer, I., Salyuk, a., Rekant, P., and Kosmach, D. (2010a). Geochemical and geophysical evidence of methane release over the East Siberian Arctic Shelf. *Journal of Geophysical Research*, 115(C8):C08007.

Shakhova, N. E., Semiletov, I. P., Leifer, I., Sergienko, V. I., Salyuk, A., Kosmach, D., Chernykh, D., Stubbs, C., Nicolsky, D., Tumskoy, V., and Gustafsson, O. (2013). Ebullition and storm-induced methane release from the East Siberian Arctic Shelf. *Nature Geoscience*, 6(12):64–70.

Shakhova, N. E., Semiletov, I. P., Salyuk, A., Yusupov, V., Kosmach, D., and Gustafsson, O. (2010b). Extensive methane venting to the atmosphere from sediments of the East Siberian Arctic Shelf. *Science (New York, N.Y.)*, 327(5970):1246–50.

CONTRIBUTION OF EXTREMELY LOW-VOLATILITY ORGANIC COMPOUNDS TO THE GROWTH AND PROPERTIES OF SECONDARY ORGANIC AEROSOLS

P. ROLDIN[1], A. RUSANEN[1], E. HERMANSSON[2], D. MOGENSEN[1], L. ZHOU[1], S. SMOLANDER[1], M. RISSANEN[1], N. KIVEKÄS[3], R. VÄÄNÄNEN[1], A. ZELENYUK[4], E. SWIETLICKI[2], M. EHN[1] AND M. BOY[1]

[1]Department of Physics, P.O. Box 48, University of Helsinki, 00014 Helsinki, Finland
[2]Division of Nuclear Physics, Lund University, P.O. Box 118, 221 00 Lund, Sweden
[3] Finnish Meteorological Institute, P.O. Box 503, 00101, Helsinki, Finland
[4]Pacific Northwest National Laboratory, P.O. Box 999, MSIN K8-88, Richland, WA 99354, USA

Keywords: ELVOC, GAS-PHASE CHEMISTRY, PARTICLE-PHASE MASS TRANSFER LIMITATIONS.

INTRODUCTION

Recent field and laboratory experiments have identified large- and rapid formation of extremely low-volatile organic compounds (ELVOC) formed in the gas-phase during ozonolysis of VOCs. In common for these VOCs is that they contain at least one endocyclic double bounds (e.g. α-pinene and limonene (Ehn *et al.*, 2014) and cyclohexene (Rissanen *et al.*, 2014)). These studies also illustrate that ELVOCs can form when peroxy radicals (RO_2) undergoing rapid intramolecular hydrogen abstraction followed by O_2 addition in several steps.

METHODS

In this work we evaluate and constrain the proposed ELVOC formation mechanism from Ehn *et al*. (2014) using the Aerosol Dynamics, gas- and particle-phase chemistry kinetic multilayer model for laboratory CHAMber studies (ADCHAM) (Roldin *et al*., 2014). We use different datasets to evaluate: (i) the ELVOC formation mechanism (Ehn *et al.*, 2014), (ii) the contribution of ELVOC to the growth of homogeneously nucleated particles (Ehn *et al*., 2014) and (iii) how ELVOC influence the phase-state and the mass-transfer limited evaporation of SOA particles (Vaden *et al*., 2011). We also use ADCHAM as a tool to test and design possible future smog chamber experiments that can contribute to more detailed picture of the ELVOC formation in the atmosphere.

The improved ELVOC mechanism has also been implemented into the process-based chemistry transport models ADCHEM (Roldin *et al*., 2011) and SOSAA (Boy *et al*., 2011). In all models the ELVOC mechanism is fully coupled to the master chemical mechanism (MCMv3.2) gas-phase chemistry (Saunders et al., 2003). ADCHEM will be run as a 1D (vertical column) trajectory model along air mass trajectories connecting three measurement stations in the Swedish and Finnish sub-arctic forest region (Abisko, Pallas and Värriö). With a combination of modelled and observed particle number size distributions we will try to constrain the contribution of ELVOC to the growth of homogeneously nucleated particles during new particle formation events, occurring simultaneously over large areas of the boreal forest. SOSAA is used as stationary 1D-column model at the SMEAR II station (Hyytiälä, in southern Finland). The SOSAA model results will be compared with measurements of ELVOCs with high-resolution chemical ionization mass spectrometers (CI-APi-TOF) (Ehn *et al.*, 2014).

RESULTS AND CONCLUSIONS

With an updated ELVOC formation mechanism (including unimolecular ELVOC peroxy radical termination as proposed by Rissanen *et al.* (2014)), ADCHAM captures the main features of the observed NO_x influence on the ELVOC composition (Fig. 1a), ELVOC SOA mass formation (Fig. 1b) and the ELVOC(g) mass spectrum at low NO_x conditions (Fig. 2), measured during the Jülich Plant Atmosphere

Chamber (JPAC) experiments by Ehn *et al.* (2014). The model results can be compared with figure 1, 2 and extended data figure 10 in Ehn *et al.* (2014), which contains analogues experimental results.

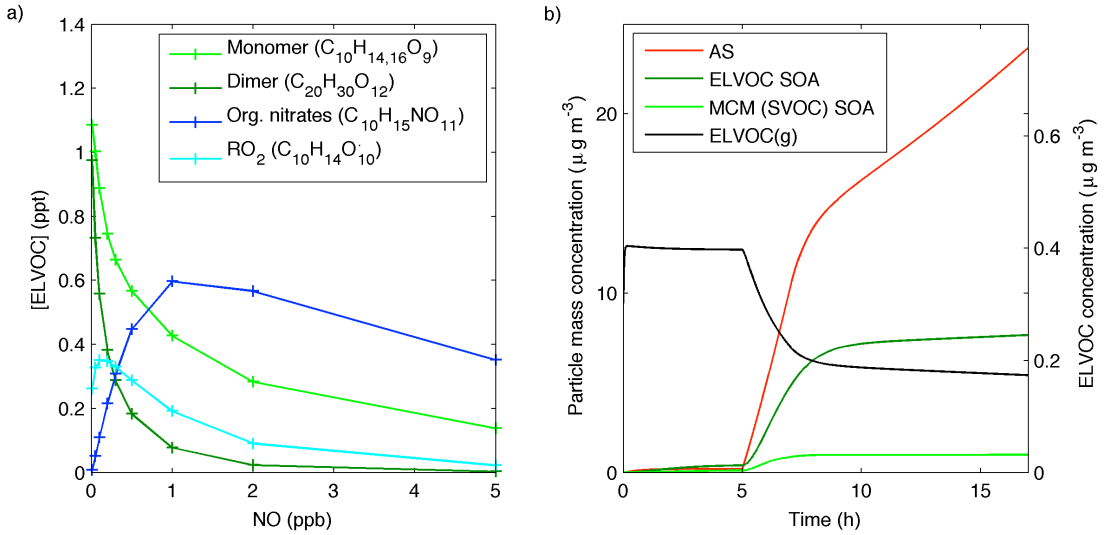

Figure 1. Modelled (**a**) effects of variable NO levels on the concentration of ELVOC monomers with 9 O atoms ($C_{10}H_xO_9$), dimers with 12 O atoms ($C_{20}H_{30}O_{12}$), organic nitrate monomers with 11 O atoms ($C_{10}H_{15}NO_{11}$) and ELVOC RO_2 containing 10 O atoms ($C_{10}H_{14}O_{10}\cdot$), and (**b**) ELVOC(g) concentration and SOA mass during an ammonium sulphate seed particle experiment in JPAC (Ehn *et al.*, 2014). Given are both the total SOA and the SOA formed exclusively from MCM oxidation products (SVOC or LVOCs).

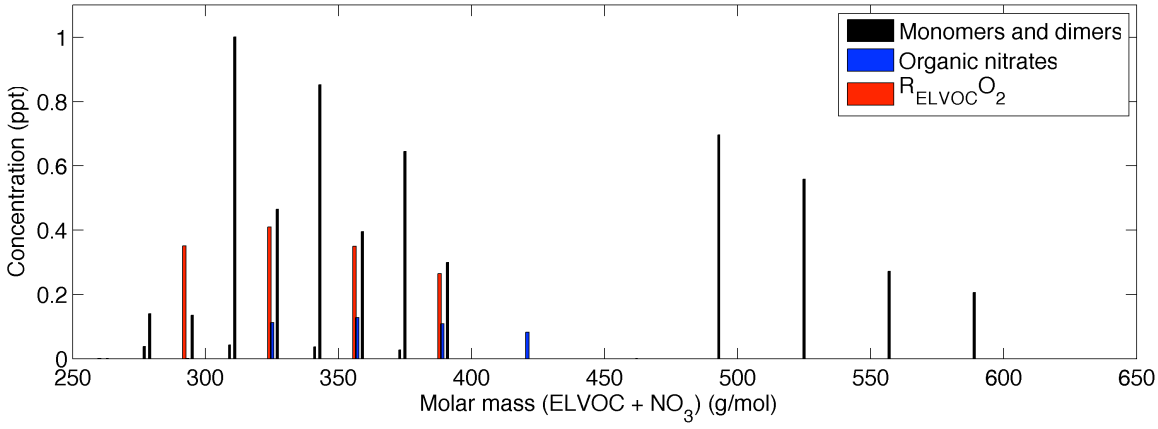

Figure 2. Modelled ELVOC mass spectrum from an JPAC experiment with 6.4 ppb α-pinene, 0.1 ppb NO, 1 ppb NO_2 and 78 ppb O_3.

Figure 3 show the modelled relative contribution of ELVOC and SVOCs to the SOA mass (Fig. 3a) and the elemental composition of the SOA (O:C-ratio and H:C-ratio) (Fig. 3b), for simulations with variable initial α-pinene concentrations from 1 to 200 ppb. Due to the large irreversible chamber wall losses of ELVOCs ($k_{ELVOC,wall}$ = 1/90 s^{-1} for JPAC (Ehn *et al.*, 2014)) the apparent ELVOC SOA mass yield never reaches the ELVOC SOA yield expected from a ideal smog chamber with no walls. Figure 4 shows how the modelled mass spectrum for simulations with an initial concentration of (**a**) 10 ppb, (**b**) 40 ppb and (**c**) 200 ppb α-pinene in the chamber. The relative contribution from MCM (SVOCs and LVOCs) α-pinene oxidation products increases with increasing SOA mass loading. Due to increasing RO_2 concentration with increasing VOC loading the relative contribution of ELVOC dimers also increases, while the ELVOC monomers decreases. This is also the reasons why the O:C-ratio of the SOA gradually decreases while the H:C-ratio increases when the VOC concentration increases (Fig. 3b).

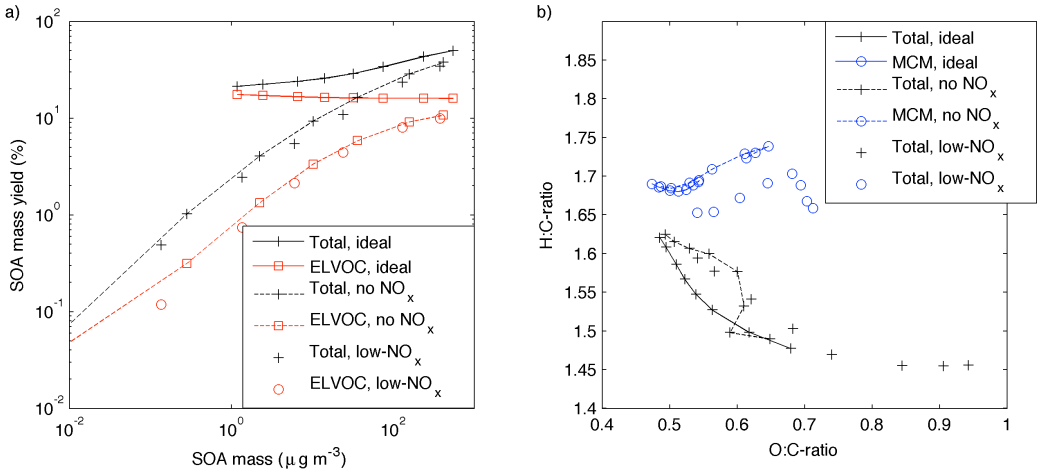

Figure 3. Modelled (a) SOA mass yield and (b) elemental composition (Van Krevelen diagram). The NO and NO_2 concentration during the low-NO_x conditions was 0.1 and 1 ppb, respectively. The other simulations were performed with no NO_x conditions and either realistic VOC chamber wall losses or no losses (ideal chamber).

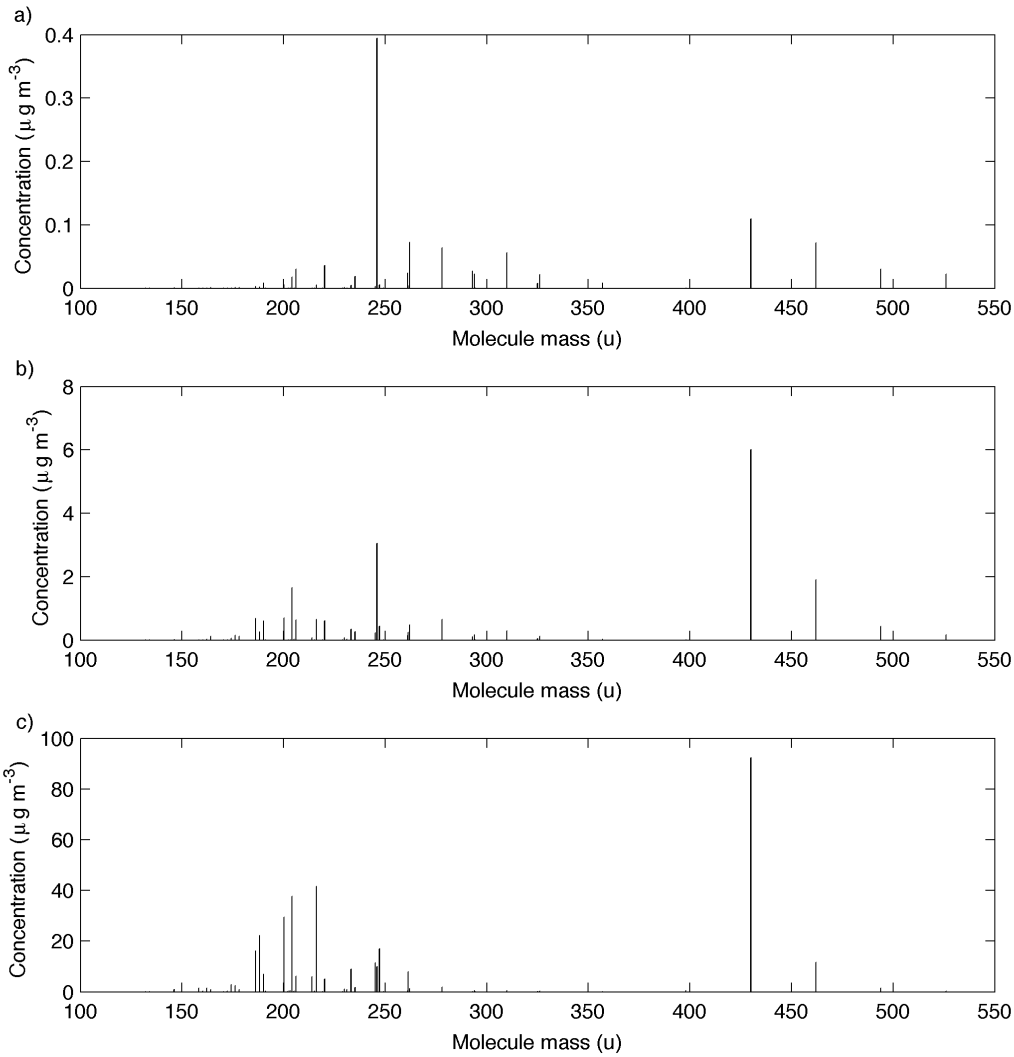

Figure 4. Modelled mass spectrum for low-NO_x conditions (0.1 ppb NO, 1 ppb NO_2), 500 ppb O_3 and an initial α-pinene concentration of (**a**) 10, (**b**) 40 and (**c**) 200 ppb, respectively.

Figure 5a shows how ELVOCs in viscous SOA particles formed during α-pinene ozonolysis at low RH conditions (Vaden *et al.*, 2011) may contributes to the observed slow evaporation, both because their extremely low vapour pressure and because they accumulate in the particle surface layer of the viscous particles (Fig. 5c). The initial growth of the homogeneously nucleated particles (starting at 2 nm in the model) is purely due to ELVOC condensation. Thus, before the molecular diffusion has mixed the ELVOC and SVOCs evenly in the particles, the ELVOC mass fraction is highest near the core of the particles (Fig. 5b). Figure 5b also illustrates that the ELVOC mass fraction near the surface of the particles start to increase already before they are introduced in the evaporation chamber. This is because some SVOCs start to evaporate from the particle surface layer already in the smog chamber.

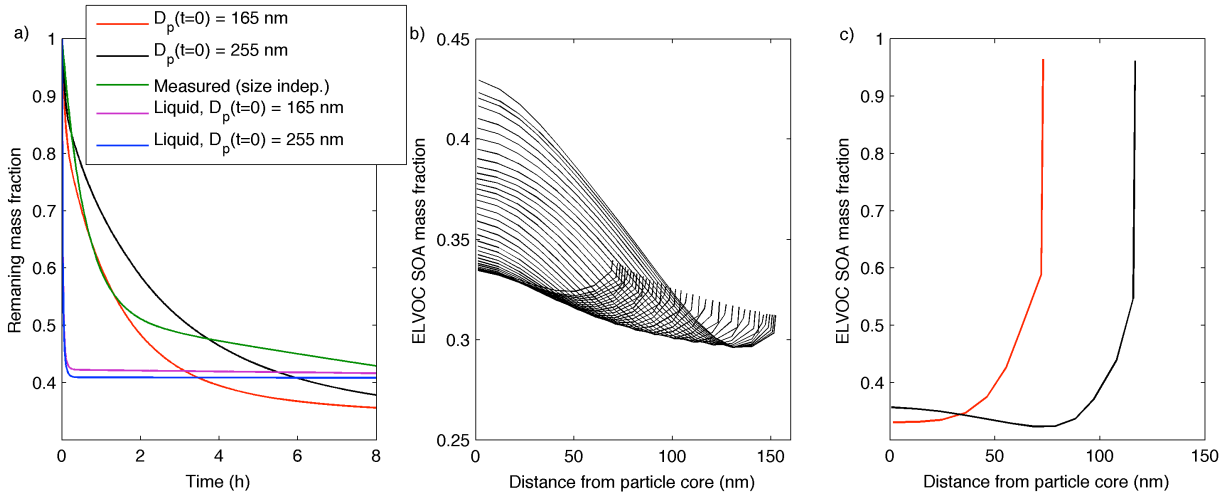

Figure 5. (**a**) Modelled and measured (Vaden *et al.*, 2011) α-pinene SOA particle mass evaporation loss in a charcoal denuder evaporation chamber. The SOA particles were formed in a smog chamber at dark conditions, with cyclohexene as OH-scavenger, 500 ppb O_3 and 200 ppb α-pinene. After 1.5 hours the particles were introduced into the evaporation chamber. (**b**) ADCHAM kinetic-multilayer model results of the ELVOC mass fraction in particles of different size (one line for each particle size), just prior to the time when the SOA particles were introduced into the charcoal denuder. (**c**) Modelled ELVOC mass fraction after 30 minutes in the charcoal denuder. Only particles with diameters equal to 165 nm and 255 nm, respectively (before evaporation), were introduced into the charcoal denuder at low concentration (100 and 50 cm^{-3}, respectively). The mass-transfer limited diffusion within the particles was modelled using obstruction theory (Stroeve, 1975) assuming that the ELVOC dimers limit (obstruct) the diffusion of the monomers. The diffusion coefficients for monomers and dimers without obstruction were assumed to be $2.5 \cdot 10^{-16}$ cm^2 s^{-1} and $2.5 \cdot 10^{-18}$ cm^2 s^{-1}, respectively. Figure (**a**) also displays the modelled mass evaporation loss if the SOA particles were assumed to be liquid like.

All model results shown in this abstract were performed with exactly the same ELVOC formation mechanism for α-pinene ozonolysis. Still, the SOA formation (SOA yields) and composition show large variability between the different model simulations. This is because the ELVOC composition is very sensitive to the VOC and NO concentration during the experiments, and the relative contribution of SVOCs, LVOCs and ELVOCs depend on the chamber wall losses, which increases with decreasing vapour pressure of the compounds. The ADCHAM model simulations illustrates that one relatively straight forward way to constrain the ELVOC formation mechanism proposed by Ehn *et al.* (2014) is to perform experiments with variable α-pinene concentrations.

ACKNOWLEDGEMENTS

This work was supported by the Cryosphere-atmosphere interactions in a changing Arctic climate – CRAICC.

REFERENCES

Boy, M., A. Sogachev, J. Lauros, L. Zhou, A., Guenther, and S., Smolander. (2011). SOSA – a new model to simulate the concentrations of organic vapours and sulphuric acid inside the ABL – Part 1: Model description and initial evaluation, *Atmos. Chem. Phys.*, 11, 43-51, doi:10.5194/acp-11-43-2011.

Ehn, M., J. A. Thornton, E. Kleist, M. Sipilä, H. Junninen, I. Pullinen, M. Springer, F. Rubach, R. Tillmann, B. Lee, F. Lopez-Hilfiker, S. Andres, I.-H. Acir, M. Rissanen, T. Jokinen, S. Schobesberger, J. Kangasluoma, J. Kontkanen, T. Nieminen, T. Kurtén, L. B. Nielsen, S. Jørgensen, H. G. Kjaergaard, M. Canagaratna, M. Dal Maso, T. Berndt, T. Petäjä, A. Wahner, V.-M. Kerminen, M. Kulmala, D. R. Worsnop, J. Wildt & T. F. Mentel. A large source of low-volatility secondary organic aerosol, *Nature*, 506, 476-479, 2014.

Rissanen, M. P., T. Kurtén, M. Sipilä, J. A. Thornton, J. Kangasluoma, N. Sarnela, H. Junninen, S. Jørgensen, S. Schallhart, M. K. Kajos, R. Taipale, M. Springer, T. F. Mentel, T. Ruuskanen, T. Petäjä, D. R. Worsnop, H. G. Kjaergaard, and M. Ehn. The Formation of Highly Oxidized Multifunctional Products in the Ozonolysis of Cyclohexene. *J. Am. Chem. Soc.* 136, 15596−15606, 2014.

Roldin, P., A. C. Eriksson, E. Z. Nordin, E. Hermansson, D. Mogensen, A. Rusanen, M. Boy, E. Swietlicki, B. Svenningsson, A. Zelenyuk, and J. Pagels. (2014). Modelling non-equilibrium secondary organic aerosol formation and evaporation with the aerosol dynamics, gas- and particle-phase chemistry kinetic multilayer model ADCHAM, *Atmos. Chem. Phys*., 14, 7953-7993, doi:10.5194/acp-14-7953-2014.

Roldin, P., E. Swietlicki, G. Schurgers, A. Arneth, K. E. J. Lehtinen, M. Boy, and M. Kulmala. (2011). Development and evaluation of the aerosol dynamics and gas phase chemistry model ADCHEM, *Atmos. Chem. Phys*., 11, 5867-5896, doi:10.5194/acp-11-5867-2011.

Saunders, S. M., M. E. Jenkin, R. G. Derwent, and M. J. Pilling. (2003). Protocol for the development of the Master Chemical Mechanism, MCM v3 (Part A): tropospheric degradation of non-aromatic volatile organic compounds, *Atmos. Chem. Phys*., 3, 161-180, doi:10.5194/acp-3-161-2003.

Stroeve, P. (1975). On the Diffusion of Gases in Protein Solutions, *Ind. Eng. Chem. Fund.*, 14, 140–141.

Vaden, T. D., D. Imreb, J. Beráneka, M. Shrivastavaa, and A. Zelenyuka. (2011). Evaporation kinetics and phase of laboratory and ambient secondary organic aerosol, *P. Natl. Acad. Sci*., 108, 2190–2195.

HOW TO MAKE AIR QUALITY EDUCATION EFFECTIVE?

T.M. RUUSKANEN[1,2], P. SIHVONEN[1,3] and L. RIUTTANEN[1]

[1]Division of Atmospheric Sciences, Department of Physics, University of Helsinki, PL64, Finland.

[2]Nature and Environment group, Palmenia Centre for Continuing Education, University of Helsinki, PL53, Finland.

[3]Heinola upper secondary school, Rajakatu 29, 18100 Heinola, Finland.

Keywords: education, multi-disciplinary, pedagogy, atmosphere.

GRAND CHALLENGES

The world is constantly changing and we are facing big challenges. Air quality is one of the Grand Challenges that EU and other authorities have listed. WHOs (2014) current estimate is that outdoor air pollution causes 3.7 million premature deaths in the world, more than a quarter of them in China.

AIR QUALITY IN A CHANGING WORLD –EDUCATION

We believe that comprehensive understanding of processes influencing air quality is the key for effective solutions. The University of Helsinki has taken action, and at the moment a research-based pilot course *Air quality in a changing world* is being developed using design research (Edelson, 2002). The basic level course, for a pilot phase, with core topics is developed with the lead of prof. Markku Kulmala. Atmospheric scientists are sharing their knowledge and taking part in this learning journey.

Air quality is a sum of complex processes and in order to make the most useful decisions it is essential to understand the governing processes and connections of different pollutants to e.g. visibility and health problems. Our education covers birth, life and death of pollutants, transport mechanisms, air quality monitoring, environmental policy solutions and health effects of pollutants. Learning during the air quality education is studied to support the formation of understanding and to improve the knowledge transfer processes.

DESIGN RESEARCH

The framework is built around learners and specialists of atmospheric science as well as education (Fig. 1) and their interaction. The research focuses not only on study of the students and their learning, but also the process of designing and making new education material as well as on the suitability of different education methods.

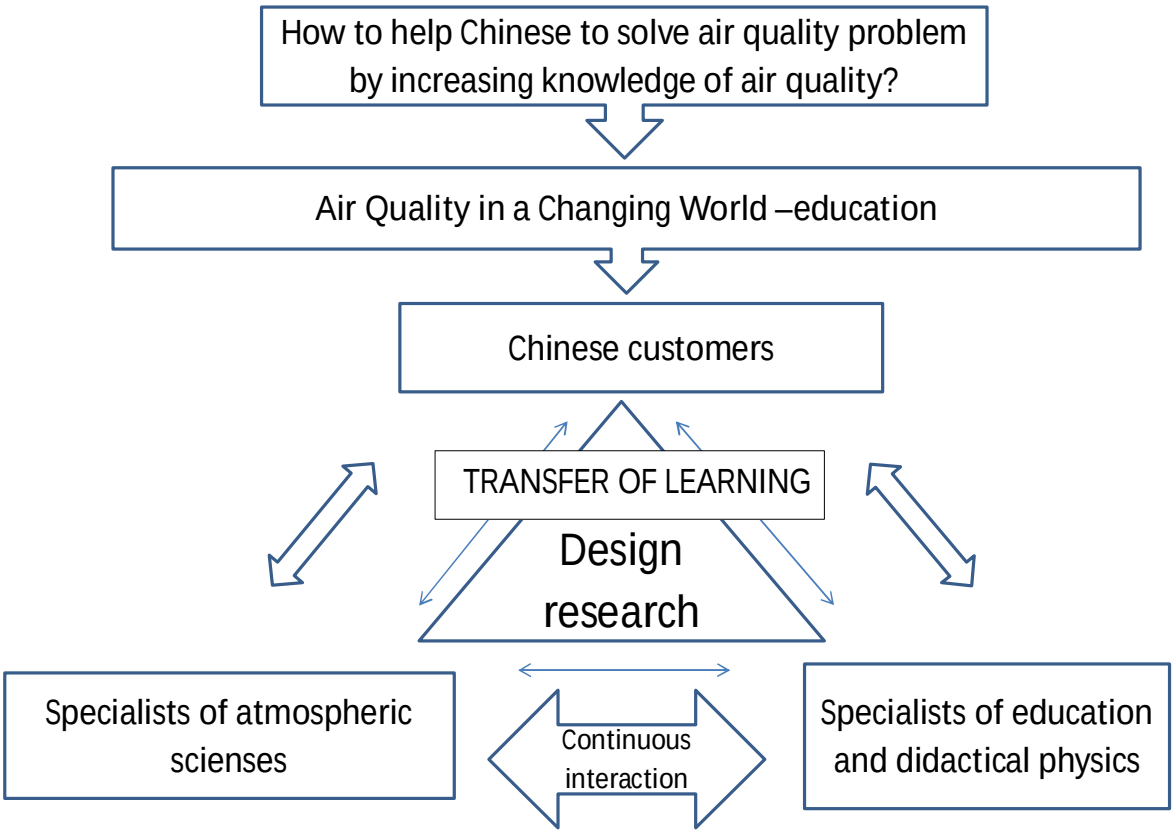

Figure 1. We use design research to develop teaching-learning strategies and materials. We develop research-based solutions to meet the needs of the customers. Our aim is to make our education as effective as possible and develop the education package systematically in cycles.

ACKNOWLEDGEMENTS

This work was supported by the University of Helsinki, Rectors strategic funding and the Finnish Centre of Excellence, Academy of Finland grant no. 272041. The Atmospheric education research team wishes to thank prof. Markku Kulmala, Dr. Kirsi Kettula, prof. Jari Lavonen and researchers contributing to education material development for constructive discussion and feedback.

REFERENCES

Edelson, D. C. (2002). Design research: What we learn when we engage in design. Journal of the Learning Sciences, 11(1), 105-121

World Health Organization WHO. (2014). Burden of disease from Ambient Air Pollution for 2012, Summary of results. [Ref. 23.5.2014]. www.who.int/phe/health_topics/outdoorair/databases/AAP_BoD_results_March2014.pdf?ua=1

A ROLE OF THE ARCTIC SEA ICE LOSS IN THE INCREASED FREQUENCY OF ANOMALOUSLY COLD WINTERS OVER THE NORTHERN EURASIA

V.A. SEMENOV[1,2,3] and M. LATIF[2]

[1]Laboratory of Climatology, Institute Geography of Russian Academy of Sciences, Moscow, Russia.

[2] Ocean Circulation and Climate Dynamics Division, GEOMAR Helmholtz Centre for Ocean Research Kiel, Kiel, Germany.

[3]Laboratory of Climate Theory, A.M. Obukhov Institute of Atnospheric Physics of Russian Academy of Sciences, Moscow, Russia.

Keywords: COLD WINTERS, ARCTIC SEA ICE, EURASIAN CLIMATE CHANGE.

INTRODUCTION

A puzzling observation during the recent years was the winter cooling over Central Eurasia with an enhanced frequency of cold events. The North Atlantic Oscillation (NAO), the most important internal mode of atmospheric variability in the North Atlantic sector, is an important driver of Eurasian climate. The anomalously warm period 1988-2002 over northern Eurasia, for example, was linked to a rather persistent high NAO index phase. However, during the recent years only the anomalously cold winter of 2010 was marked by an extremely low NAO index. This together with the global warming trend pattern during the recent decades, exhibiting in winter the strongest warming over the northern continents, made the recent anomalously cold winters over Central Eurasia so surprising. Here the role of Arctic sea ice decline in forcing such cold spells is explored.

Negative surface air temperature (SAT) anomalies over Eurasia during the recent years were accompanied by positive SAT anomalies in the Arctic with strongest warming in the Barents Sea region, suggesting a possible role of anomalous sea ice extent (Fig. 1a). The temperature anomalies were linked to a blocking anti-cyclone centered south of the Barents Sea (Fig. 1b). In fact, observational analysis previously suggested that reduced sea ice concentration (SIC) may have caused the recent cooling over Eurasia (e.g., Hopsch *et al*., 2012; Outten and Esau, 2012). However, the robustness of these results can be questioned given the short time period considered. Here, a series of dedicated experiments with a high-resolution atmospheric general circulation model (AGCM) is analyzed to obtain further insight about the possible role of Arctic SIC anomalies in driving the recent cold winters over Central Eurasia.

MODEL SIMULATIONS

The numerical simulations were conducted with the ECHAM5 AGCM (Roeckner *et al*., 2003) forced by sea ice anomalies representing the conditions during the three epochs discussed above. The model employs relatively high horizontal resolution of T106 (1.13° by 1.13°) and 31 vertical levels. High resolution may be important for capturing the atmospheric response to regionally confined sea ice extent anomalies. Sea surface temperatures (SST) and SIC were specified from HadISST1 dataset (Rayner *et al*., 2003). A reference experiment with monthly SST and SIC climatology for 1971-2000 and three sensitivity simulations were performed. The latter use the same SST but SIC averaged for 1966-1969, 1990-1995 or 2005-2012, respectively. Each run is 50 years long. Atmospheric greenhouse gases and aerosols have present-day values in all simulations, with a CO^2 concentration of 348 ppm. We present 50-yr averages of winter (DJF) anomalies from the sensitivity runs with respect to the reference experiment. Statistical significance was estimated by a double sided Student t-test.

RESULTS

A remarkable feature of the SLP response in the 2005-2012 simulation is the strong anti-cyclonic SLP anomaly over the Barents Sea region and Central Eurasia (Fig. 2a), which is very similar to what has been observed (Fig. 2b). This anomaly, exceeding 2 hPa in its center, is about half as strong as observed but statistically significant at the 95% level. Consistent with observations, the anti-cyclonic SLP anomaly is accompanied by (statistically significant) negative SLP anomalies centered over the Mediterranean region and western North Atlantic. Statistically significant cooling is simulated over Central Eurasia where strongest anomalies reach -1.5 °C (Fig. 3d). A statistically significant warming is simulated over the Arctic Ocean and northern Canada. The overall SAT response to the average sea ice change during 2005-2012 is consistent with observations and fits the "warm ocean-cold continent" pattern that has been previously linked to negative SIC anomalies (e.g., Hopsch *et al*., 2012).

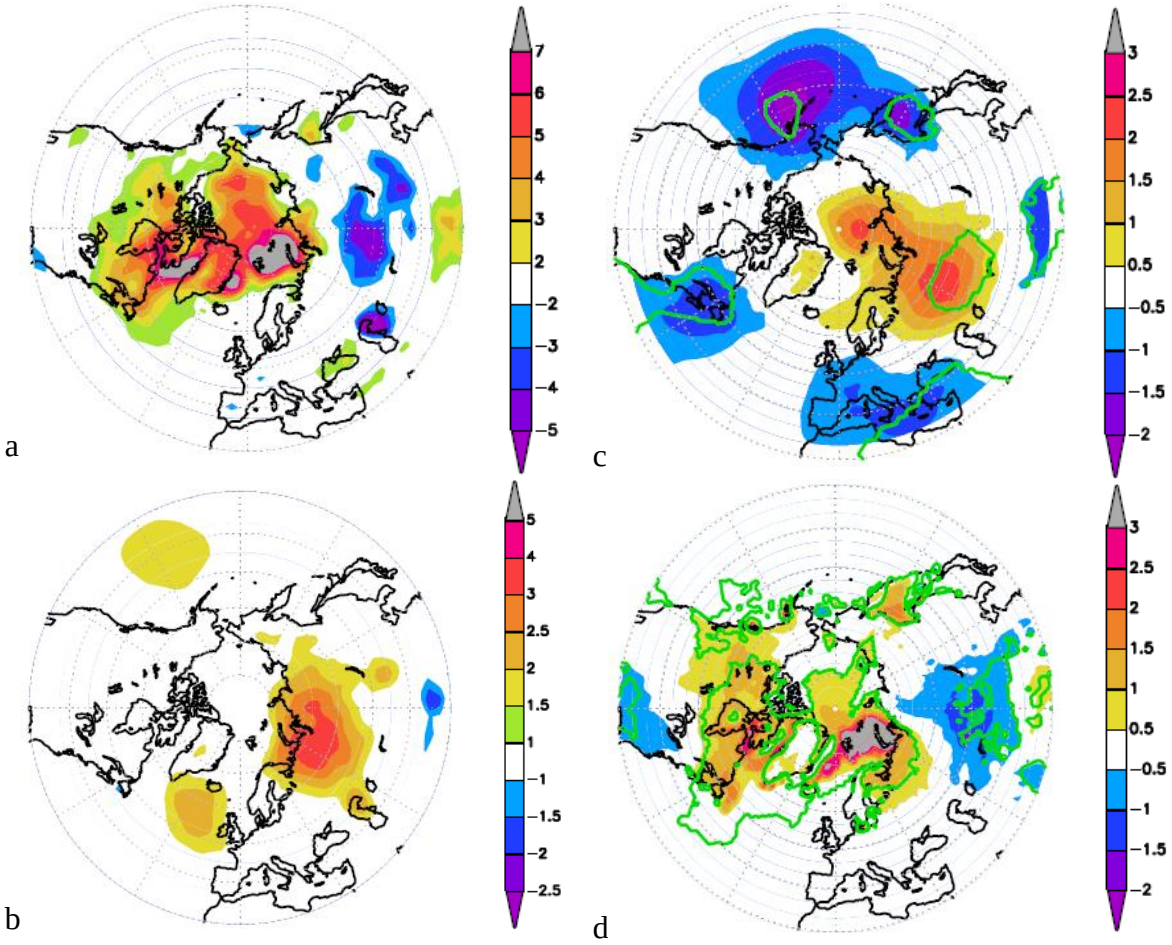

Figure 1. Observed (according to NCEP reanalysis data) (a,b) and simulated (c,d) anomalies of winter time (DJF) surface air temperature, in °C, (a,c) and sea level pressure, in hPa, (b,d) for 2005-2012 period relative to 1971-2000 period. Regions with statistically significant (at 95% confidence level) differences are marked with green contours.

The simulated 1990-1995 SLP anomalies, somewhat projecting on the negative NAO pattern, are relatively weak and in general not statistically significant. This is consistent with the picture that the SLP anomalies were largely due to internal, i.e. NAO-related variability. The corresponding SAT response exhibits statistically significant warming only over the regions of sea ice loss, where the observations also depict warming. Surprisingly, the SLP response to strongly enhanced SIC during 1966-1969 looks similar to the response to reduced SIC in 2005-2012, in the sense that they both feature an anti-cyclonic anomaly

south of the Barents Sea, which was also observed, and a cyclonic anomaly over Spain (both statistically significant) and in the northern North Pacific. This pattern projects on the negative-NAO phase, suggesting a positive feedback on the atmospheric circulation during 1966-1969.
The important new result from our simulations can be summarized as follows: while the atmospheric response to reduced SIC during 1990-1995 tends to damp the circulation pattern over the North Atlantic, the stronger amplitude SIC anomalies in 2005-2012 (and 1966-1969) tend to reinforce and thus contribute to the circulation anomalies, suggesting non-linear behavior.

CONCLUSIONS

The results suggest that wintertime Arctic sea ice anomalies during 2005-2012, which were characterized by a strong SIC decrease in the Barents Sea, may have been responsible for the observed anti-cyclonic circulation anomaly, centered south of the Barents Sea, which was associated with anomalous cooling over Central Eurasia. We also find evidence for the atmospheric circulation response to sea ice anomalies during the period of modern sea ice decline being essentially non-linear, both with respect to amplitude and pattern. The results are important for understanding the impact of diminishing Arctic sea ice cover on the atmospheric circulation. They are also relevant to understand possible feedbacks between sea ice, ocean and atmosphere in the Barents Sea region that may play a very important role in short and long-term climate variability (Bengtsson *et al*., 2004).

ACKNOWLEDGEMENTS

This work was supported by the NordForsk GREENICE project, Russian Foundation for Basic Research (14-05-00518) and Russian Ministry of Education and Science (grant no. 14.V25.31.0026).

REFERENCES

Bengtsson, L., V. A. Semenov and O. M. Johannessen (2004). The early twentieth-century warming in the Arctic - A possible mechanism, *J. Clim.* **17**, 4045-4057.

Outten, S. D., and I. Esau (2012). A link between Arctic sea ice and recent cooling trends over Eurasia, *Climatic Change* **110**, 1069–1075.

Rayner, N. A., D. E. Parker, E. B. Horton, C. K. Folland, L. V. Alexander, D. P. Rowell, E. C. Kent and A. Kaplanet (2003). Global analyses of sea surface temperature, sea ice, and night marine air temperature since the late nineteenth century, *J. Geophys. Res.* **108**(D14), 4407, doi:10.1029/2002JD002670.

Roeckner, E., *et al.* (2003). The atmospheric general circulation model ECHAM5. Part I: Model description, Rep. 349, Max Planck Inst. for Meteorol., Hamburg, Germany.

SOCIAL SYSTEMS, NEW INFRASTRUCTURE AND CLIMATE EFFECTS: YAMAL PENINSULA

A. SHCHERBININ[1,2], R. MAKKONEN[1], P. PAASONEN[1] and S. JUHOLA[2]

[1] Department of Physics, University of Helsinki, Helsinki, Finland.

[2] Department of Environmental Sciences, University of Helsinki, Helsinki, Finland.

Keywords: SOCIAL SYSTEMS, EMISSIONS, MODELING, ARCTIC, GAS FLARING.

INTRODUCTION

The process of quantification of socio-economic activities and assessment of their impacts to the environment are crucial in dealing with climate change. This process includes both the estimation of current emissions and the projection of future impacts, as the basis of understanding the interaction between society and the environment. Given the increasing impact of human activities on the environment, particularly in relation to the climate, there is a need to improve the methodologies to estimate the extent of this impact. Both the quantification of anthropogenic activities and climate science have progressed greatly in the last few years but there are still gaps that can be identified between the two.

Knowledge and information of emissions, both current and future, is the key factor in developing climate policy. However, understanding how socio-economic activities contribute emissions is a complex subject, including a great variety of processes from primary production to consumption. Currently this information is being accumulated and distributed through various channels, using different methods and by numerous statistical organizations. This results in a disharmonization of knowledge and uncertainties in the estimates of actual emissions (see for instance: Macknick, 2011). Given that this information of socio-economic activities also informs the climate modelling, it can be argued that this leads to inherent challenges in the quality of the socio-economic data. Consequently this again affects the society's forecasting and assessment capabilities with regards to environmental change and contributes to overall uncertainty in decision making process.

In this manuscript we present the application results of a multidisciplinary framework that takes into account the socio-economic activities and simulates the climate effects of those activities. This framework enables us to develop a more accurate estimation of current and future emissions and the resulting climate effects. As a case, we focus on a new infrastructural project in Yamal peninsula that has the potential to cause significant impacts to the environment. In order to do this, we estimate the future atmospheric emissions of this activity by using the GAINS model developed by IIASA and simulate pollutant transport and resulting climate effects of this contribution with aerosol-climate model ECHAM5.5-HAM2.

The response of Arctic climate to anthropogenic emissions is highly sensitive to the source location, which defines the vertical distribution of pollutants in Arctic. Sand et al. (2013) showed that the Arctic climate forcing due to black carbon is twice as sensitive (per unit mass emitted) for Arctic emissions compared to mid-latitude emissions. The Arctic surface temperature response from Arctic BC emissions was even five-fold as compared to mid-latitude sources. It is expected that large-scale anthropogenic activities in the Arctic will have significant climate impact via modification of radiative fluxes and effects on cryosphere.

METHODS

We construct a methodological framework that utilizes systemic understanding of society as well models

for estimating emissions and climate modeling.

2.1 Social systems

In previous efforts to understand the contribution of socio-economic activities to emissions, the focus has been on using aggregated economic data as a proxy to reflect the rate of emissions. Whilst this has been useful in getting an overall estimation of the rate of possible emissions, this kind of an approach does not accurately reflect the ways in which the society functions as a contributor to emissions. In order to reflect the processes of knowledge production and to emphasize the importance of communication between organizations providing crucial information we introduce here theory of social systems (TSS) (Luhmann, 2012) as a starting point in our methodological framework to better understand how socio-economic activities and social systems contribute to emissions.
Social systems, as defined by Luhmann, are our generic unit of analysis in understanding social dynamics. Society in this way is seen to comprise of organizations, the activities of which we assess and quantify. This allows us to assess the impacts that the organizations make on the environment and we are also able to project future changes based on the organization's activity. Here TSS is a descriptive tool to distinguish particular operations and justify the use of information produced by them. Organization is thus defined as a social system per se, which follows its specific logic in operations. Furthermore, it is a prerogative of an organization to both conduct an activity that impacts the environment and to create knowledge about it.

There are two specific system operations that are of importance to our framework: 1) monitoring and communication or process of auto-exo-reference, which enables system to create knowledge about itself and its environment and communicate with other systems, and to determine alternatives for future operations; and 2) decision making, which enables system to choose plausible alternatives for future operations according to knowledge produced in 1 (Luhmann, 2012). Ultimately, in climate science understanding the mechanisms of both operations is crucial: auto-exo-reference for kno2wledge production and decision making for forecasting both climatic response to socio-economic dynamics and societal response to climate change.

2.2 Emissions

The baseline emissions and emission factors were taken from the emission scenario model GAINS (Greenhouse gas and Airpollution – Interactions and Synergies; Cofala et al. , 2007), operated by IIASA (International Institute for Applied Systems Analysis, Austria). In the GAINS model the emissions of all main air pollutants and greenhouse gases are included in consistent manner for current situation and future scenarios, but in this study we focus on black carbon (BC) and sulfur dioxide (SO2) emissions. The levels of different activities are defined separately for each country or region (Russia is divided to European and Asian part), and then allocated to 0.5^{o} x 0.5^{o} grid by using the EDGAR/RCP proxy. The scenarios for activity levels and utilization of different emission abatement technologies are determined in cooperation with national (Russian Academy of Sciences, representing Russian Federation at IIASA) and international (IEA, OECD, UN) institutions and researchers.

2.3 Communication processes and production of knowledge

In order to quantify future impacts of the social system, there is a need to distinguish particular activities that organizations undertake. In this particular case, these activities are associated with the infrastructural project. In order to do this, it is necessary to acquire available information to assess and parameterize them. There are a number of examples of models that look at aggregated data of socio-economic activities. For example, the GAINS model utilizes aggregated data from various institutions to determine activity levels for specific technological processes and distribute them geographically.

Given our social systems approach and that we are interested in specific socio-economic activities; there is a need to reformulate some assumptions. More specifically, if we assume that we are dealing with vehicles

and their emissions, we are able to estimate total activity level, emissions and its spatial distribution for particular technological process (e.g. diesel engine) and energy carrier use (diesel fuel) , using the GAINS model. However, there are problems in isolating particular socio-economic activities that contribute to the activity levels of certain technological process (e.g. commercial use in particular industry). Hence, it becomes problematic to analyze a detailed scenario, e.g. infrastructural project for gas industry in particular and not macroeconomic trend for aggregated use of particular technologies.

Since we are estimating the impact of particular socio-economic activities of particular social systems, we need to know levels and proportion rate of certain industrial activities in using isolated technological processes. For that we use the GAINS model to estimate the emissions, utilizing its classification of processes associated with gas and oil industry to isolate relevant technological processes and activities. We further use available data from relevant knowledge producers and distributors (e.g. GGFR, RFSSS, OGP and RFMP) to parameterize activity levels of particular industrial sectors and their shares in the use of isolated technological processes for year 2010 and extrapolating resulted factors for the emission scenario on year 2030.

2.4 Climate system

We implemented GAINS emission inventories for years 2010 and 2030 to the ECHAM5.5-HAM2 model (Stier et al., 2005). While GAINS provides SO_2, BC and OC emission from anthropogenic sources, wildfire and natural emissions (sea salt, dust, biogenic) were incorporated as in Stier et al. (2005). The implemented emission inventories exclude any intra-annual variation. The ECHAM5.5-HAM2 model was integrated over one year for each experiment, and model meteorology was nudged towards year 2000 ERA-40 reanalysis data. Hence, climate effects of changing aerosol fields remain negligible in the simulations, and similar transport features allow detailed comparison of experiments. The aerosol-climate model analysis focuses on black carbon and cloud condensation nuclei (CCN) concentrations.

QUANTIFICATION AND PROJECTION OF EMISSIONS

Once we determined proportions and activity levels for technological processes associated with studied infrastructural project, we estimate a factor to determine the change in emissions in baseline projection in GAINS model for year 2030 with control year 2010. We have localized our research focus to Yamalo–Nenetskiy Autonomous Okrug (YNAO), regional subject of Russian Federation. However, in some cases we had to analyze information for Russian Federation as a whole, or supplement it with general information for technological processes in gas industry due to inconsistency of the aggregated data.

Key assumptions for the year 2010

- Main technological process contributing to BC emissions in respective area is NG[1] and APG[2] flaring associated almost exclusively with petroleum industry (Stohl et al., 2013).
- Proportion of SO2 emissions in petroleum industry averaged at 0.05 t for each 1000 t of hydrocarbons produced for European producers, with 67% associated with flaring and 30% with energy use (OGP, 2011).
- APG production totaled at 7.4 bcm[3] with 1.9 bcm or 12.1 % being flared (Kutepova et al., 2011)
- 47,9% of YNAO RGDP[4] belongs to Sector D (extraction of natural resources), thus being central economic activity of the region (FSSS, 2011) and associating other socio-economic activities with it

1 Natural Gas
2 Associated Petroleum Gas
3 billion cubic meters
4 Regional Gross Domestic Product

- YNAO produced 389.7 bcm of natural gas or 61% of total Russian NG production, 18.332 mt of crude oil and 7.691 mtoe[5] of gas condensate (FMP, 2014)
- 85% of gas and 62% of oil and 65% of condensate production in the region associated with activity of Gazprom corporation, making it major contributor both to economy and atmospheric emissions in the region (FMP, 2014)
- SO2 and BC emissions for baseline GAINS scenario in the domain boundary polygon corresponding to YNAO are respectively 47.42 and 12.37 kt

Key assumptions for the year 2030

- SO2 and BC emissions for baseline GAINS scenario in the domain boundary polygon corresponding to YNAO are respectively 45.94 and 10.56 kt. As we see, emissions are slightly decreased comparing to 2010. Decreasing of BC emissions could possibly be explained by recently introduced regulations forbidding flaring of APG above 5% of production level (World Bank, 2013). Trends in SO2 emissions are more complex due to variability of sources and require further research. Overall, activity levels and spatial distribution of industrial processes remain virtually the same.
- Gazprom Yamal Megaproject aims to build a comprehensive PI infrastructure on the Yamal peninsula with a maximum output capacity: 360 bcm of NG, 7 mtoe of condensate and 7 mt of crude oil (Gazprom, 2014). Total: 360*0.9+7+7 = 338 mtoe. Thus increasing activity levels in petroleum industry of the domain almost 2 times and shifting emission source further to the peninsula, even not considering other companies and industries which most likely to increase their activities as well.
- Hence, BC emissions most likely to increase at least twice from initial assumptions for year 2030 in YNAO as its primary source belong to petroleum industry.
- To calculate SO2 emissions in our first experiment we utilize emission factors proposed by OGP (2011), which will result in 338 mtoe * 0.04 = 13.52 kt.

Resulting emissions

Using information presented above, we approximated increase in emissions by factor of 2 for BC and factor 1.25 for SO2. These approximated emissions from the Yamal megaproject (12 kt for both pollutants) were spatially distributed on the peninsula, according to the projected key locations of Yamal megaproject (Gazprom, 2014). In the next series of experiments we plan to increase accuracy of our estimations by including associated activities in our analysis and especially assessing activities related to SO2 emission in further detail.

ATMOSPHERIC EMISSIONS AND CLIMATE FORCING

Fig. 1 (left panel) shows the relative change in black carbon concentration during 2010 and 2030 as simulated by the ECHAM5.5-HAM2 model. Emission reductions in Europe are reflected clearly in BC concentrations. The changes over the Russian domain remain significantly smaller than those over Europe, however, a distinct BC increase is observed over Murmansk region. The emission reductions over continents induce noticeable effects over the Arctic ocean. The baseline 2030 GAINS scenario indicates small decrease and some spatial relocation of BC emissions over the Yamal region. However, the BC concentration in 2030 (Fig. 1, right panel) shows a clear signal from the activities over the Nenetskiy region. Overall, the BC concentrations in Yamal region and over the Arctic Ocean are extremely low.

[5] million tonnes of oil equivalent

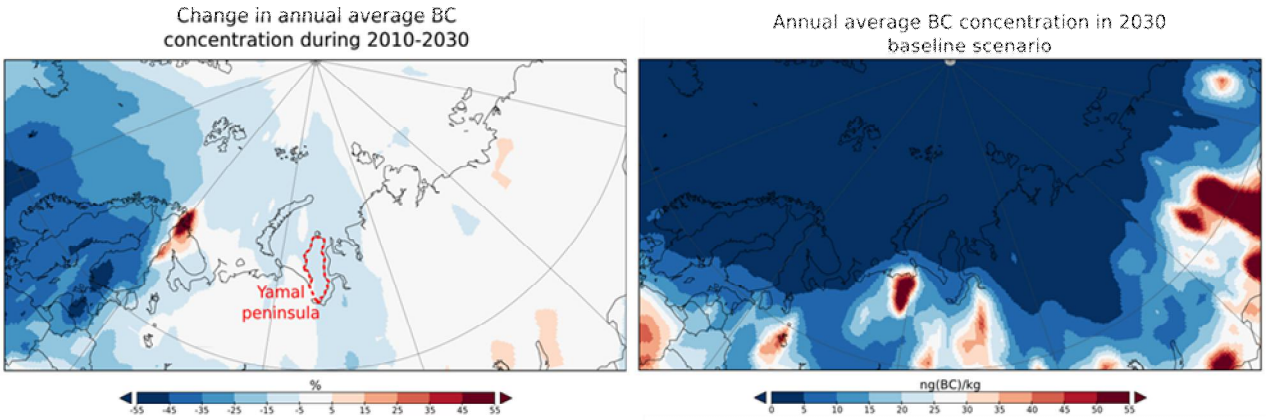

Figure 1: Change in simulated black carbon concentration between years 2010 and 2030 (left panel) and simulated black carbon concentration in year 2030 baseline scenario (right panel).

Introducing additional emissions of BC (12 kt/year) and SO_2 (12 kt/year) over the Yamal peninsula in year 2030 has significant effects over the relatively clean peninsula and Arctic regions. Annual average BC concentrations increase by several hundreds of percents over the Yamal peninsula (Figure 2). While the absolute annual-average changes in simulated BC concentrations are rather evenly spread out around the peninsula, the relative increase is intensified over the Arctic: BC increases over 100% northward from Yamal up to 87ºN and increase over 50% extends over Novaya Zemlya, Svalbard and Severnaya Zemlya. Similar to Sand et al. (2013), the Arctic emissions lead to increased concentrations mainly in the lower atmosphere: during wintertime, most of the signal from Yamal emission is confined between the surface and 1 km altitude. As seen in Figure 2, the BC concentration increase during sea-ice maximum extent is dominant over sea-ice covered regions and hence the BC is expected to affect e.g. snow properties. The co-increasing BC and SO_2 influence also cloud condensation nuclei concentrations. The CCN concentration in Yamal peninsula is increased by over 20% due to additional anthropogenic activities.

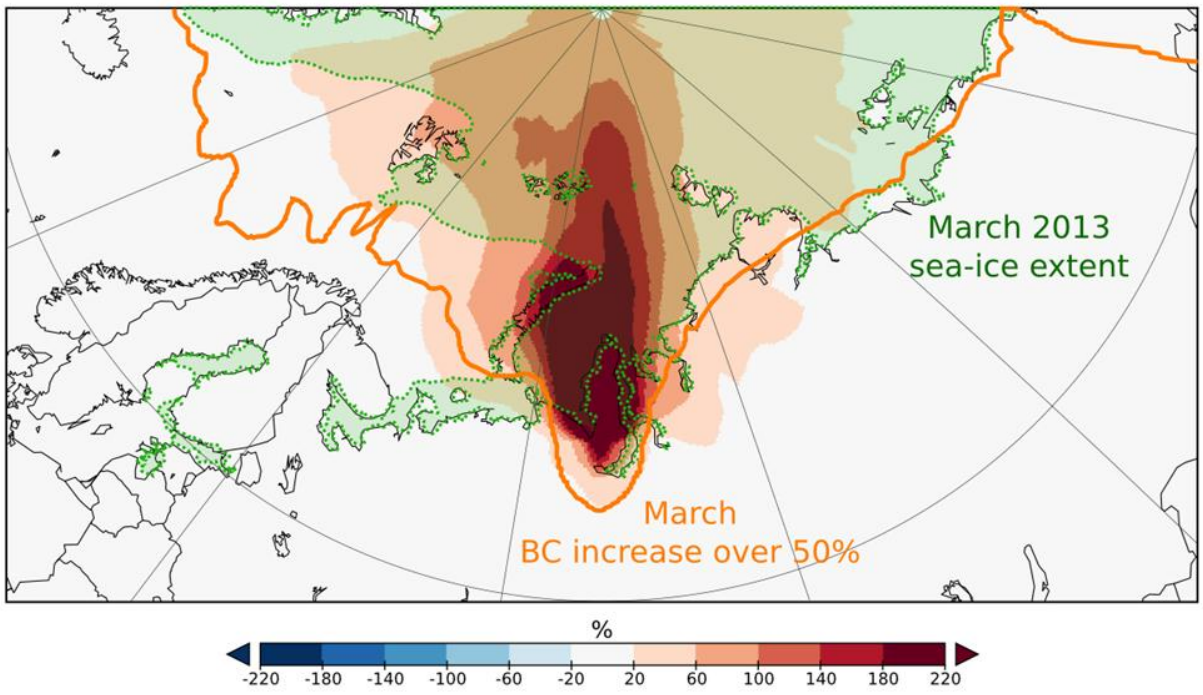

Figure 2: Relative annual-average increase of BC concentration in 2030 due to additional anthropogenic activities in Yamal (color shading), sea-ice extent in March 2013 (green line and shading) and simulated 50% BC concentration increase isoline for March.

Initial simulations indicate that projected future emissions in Yamal peninsula are efficiently transported to the Arctic, where they can influence radiative fluxes as well as cloud and snow properties. Upcoming simulations will include more detailed emission scenarios, quantification of corresponding aerosol radiative forcing and estimations of snow-albedo effects.

CONCLUSIONS

In conclusion, there are two novel contributions that this framework makes. First, this kind of approach to social systems enables us to examine the activities that organizations are engaged in, which further enables us to develop emissions data for those activities. This can, as in this case, lead to the process of localizing emissions to a geographical area, which in turn gives a more accurate picture of the impact of societies on the environment. In this way, it is possible to avoid the difficulties associated with national level statistics, the use of which may not yield results that are the most accurate.

Second, we combine the social system data to the emissions modelling and climate modeling. This enables us to examine both the drivers of emissions from socio-economic systems to study anthropogenic impacts on the environment, as well as to see what climate impacts there are to assess the environmental impacts of climate change to society. We focus on the resources extraction and in potential on energy sector, as it is one of the main contributors to global atmospheric emissions. Gas and oil sectors are in particular major producers of anthropogenic BC and associated emissions in the Arctic, highlighting the necessity of assessing their atmospheric impact in more detail.

In terms of the application of the research results, this framework makes a contribution proposing a new way of estimating the impact of socio-economic activities on the climate system. In applying this framework, it is possible to further improve our predictions of current and future emissions. This can be significant for climate policy making, in so far as better quality information can lead to better decision-making.

REFERENCES

Cofala J. et al. (2007). Scenarios of global anthropogenic emissions of air pollutants and methane until 2030 *Atmos. Environ.* **41** 8486–99

Federal Media Portal (2014). Oil and Gas of Yamal (Neft I Gas Yamala), available at: http://www.allrussia.tv/yanao/economics/ (last access: 4 December 2014).

Federal State Statistic Service of Russia (2014). Regional Gross Domestic Product for YNAO, available at:http://cbsd.gks.ru/ (last access: 4 December 2014).

Gazprom (2014) Yamal Megaproject, available at: http://www.gazprom.com/about/production/projects/mega-yamal/ (last access: 4 December 2014).

Kutepova, E.A. et al. (2011). Associated Gas Utilization in Russia: Issues and Prospects, *Annual Report KPMG Moscow* **3**.

Luhmann, N. (2012). *Theory of Society Volume 1-2*. (Stanford University Press, Stanford, USA).

Macknick, J. (2011). Energy and CO2 emission data uncertainties *J. Carbon Management* 2(2), 189–205

OGP (2011). Environmental performance in EP industry – 2010 data, *International Association of Oil and Gas Producers* **466**.

Sand, M. et al. (2013) Arctic surface temperature change to emissions of black carbon within Arctic or midlatitudes. *J. of Geophysical Research: Atmospheres* 118(14), 7788–7798.

Stier et al. (2005): The aerosol-climate model ECHAM5-HAM, *Atmos. Chem. Phys.* **5**, 1125-1156

Stohl, A. et al. Black carbon in the Arctic: the underestimated role of gas flaring and residential combustion emissions, *Atmos. Chem. Phys*. **13**, 8833-8855.

ORGANIC AND ELEMENTAL CARBON IN AEROSOLS OF THE WHITE SEA COAST

V.P. SHEVCHENKO[1], D.P. STARODYMOVA[1], A.P. LISITZIN[1], V.I. MAKAROV[2], S.A. POPOVA[2], V.V. SIVONEN[3], V.P. SIVONEN[3] and A.A. VINOGRADOVA[4]

[1]P.P. Shirshov Institute of Oceanology RAS, Moscow, Russia;

[2]V.V. Voevodsky Institute of Chemical Kinetics and Combustion Siberian Branch of RAS, Novosibirsk, Russia;

[3]White Sea Biological Station of Lomonosov Moscow State University, Karelia, Russia;

[4]A.M. Obukhov Institute of Atmospheric Physics RAS, Moscow, Russia

Keywords: organic carbon, elemental carbon, aerosols, White Sea

INTRODUCTION

Black carbon (BC), or soot is the part of carbon-containing aerosol particles which absorbs the sun light. BC is a product of incomplete combustion of various fuels (especially, coal and diesel oil), biomass (forest, grass, agricultural waste), and of biofuels. BC aerosol in snow is one of atmospheric constituents considered to be an important contributor to climate change in Arctic regions (Quinn *et al*., 2008; AMAP, 2011; Stohl *et al*., 2013). Having small diameter of particles BC is carried at large distances from natural and anthropogenic sources. Elemental carbon (EC) is principal component of soot.

MATERIALS AND METHODS

84 aerosol samples have been collected in 2010–2012 near the White Sea biological station of Moscow State University (WSBS) on the Kindo Peninsula (66.55° N, 33.1° E). This area is considered to be under the background conditions since the nearest town (Kandalaksha) is on the distance of 75 km from station (Shevchenko *et al*., 2015). There is only electric winter heating system on WSBS. Collecting of aerosols is carried out by air sampling device UAS-310 pumping air through glass fiber filters Pall A/E. PM 2.5 settled on the filter during a week. Aerosol sampling is intermitted in winter.

Elemental and organic carbon (EC and OC) contents were determined using reaction gas chromatography (Makarov *et al*., 1999). On the base of these data seasonal and interannual distribution of EC and OC was highlighted (Figure 1).

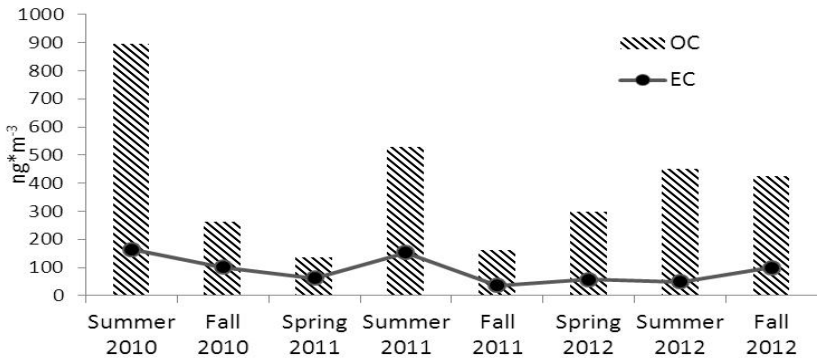

Figure 1. Seasonal and interannual variability of EC and OC concentration

Comparison of average monthly and seasonal values suggests abnormal high concentration of both OC and EC in aerosols in summer 2010. These high concentrations are related to dry weather and numerous forest fires in summer 2010 in European Russia. OC concentrations are characterized by higher variability during the year then EC concentration. Both EC and OC concentrations are highest in summer, but it may be related to incomplete annual data.

HYSPLIT model (Draxler and Rolf, 2003) was applied to reveal essential area of origin of carbon-containing aerosol. Analysis of back trajectories shows increasing of EC concentration when air masses come from oil fields of the North and Norwegian seas. Industrial areas of Kola Peninsula and Arkhangelsk Region are source region of EC and OC too. In summer 2010 there is essential increasing of OC concentration when air masses come from European Russia. It shows influence of forest fires.

CONCLUSIONS

The first continuous research of carbon-containing aerosol was carried out on the coast of the White Sea. This research reveals the main source regions of EC and OC situated in the North of the European Russia. The Western Europe is an important source of EC also. Forest fires in summer 2010 in the European Russia considerably influenced on EC and OC concentrations.

ACKNOWLEDGEMENTS

We thank A.B. Tzetlin and staff of the White Sea biological station of Moscow State University for help. This work was supported by the Russian Foundation on Basic Research (project numbers 14-05-93089, 14-05-31512, 14-05-00059), Research Council of Norway (project SLICFONIA) and Presidium of the Russian Academy of Sciences (Programm 44 of Fundamental Studies, project “Sedimentological and biogeochemical studies …”).

REFERENCES

AMAP (2011). *The Impact of Black Carbon on Arctic Climate*. By: P.K. Quinn, A. Stohl, A. Arneth, T. Berntsen, J.F. Burkhart, J. Christensen, M. Flanner, K. Kupianien, H. Lihavainen, M. Shepherd, V. Shevchenko, H. Skov and V. Vestreng. Arctic Monitoring and Assessment Programme (AMAP), Oslo.

Draxler, R.R. and G.D. Rolph (2003). HYSPLIT (HYbrid Single-Particle Lagrangian Integrated Trajectory) Model access via NOAA ARL READY Website (http://www.arl.noaa.gov/HYSPLIT.php). NOAA Air Resources Laboratory, College Park, MD.

Makarov, V.I., K.P. Koutsenogii and P.K. Koutsenogii (1999). Daily and seasonal changes of organic and inorganic carbon content in atmospheric aerosol, Novosibirsk region, *J. Aerosol Science* **30**, S255–S256.

Quinn, P.K., T.S. Bates, E. Baum, N. Doubleday, A.M. Fiore, M. Flanner, A. Fridlind, T.J. Garrett, D. Koch, S. Menon, D. Shindell, A. Stohl and S.G. Warren (2008). Short-lived pollutants in the Arctic: their climate impact and possible mitigation strategies, *Atmos. Phys. Chem*. **8**, 1723–1735.

Shevchenko, V.P., D.P. Starodymova, A.A. Vinogradova, A.P. Lisitzin, V.I. Makarov, S.A. Popova, V.V. Sivonen and V.P. Sivonen (2015). Elemental and organic carbon in atmospheric aerosols over north-western coast of the Kandalaksha Bay of the White Sea, *Doklady Earth Sciences* (in press).

Stohl, A., Z. Klimont, S. Eckhardt, K. Kupiainen, V.P. Shevchenko, V.M. Kopeikin and A.N. Novigatsky (2013). Black carbon in the Arctic: the underestimated role of gas flaring and residential combustion emissions, *Atmoc. Phys. Chem*. **13**, 8833–8855.

DYNAMICAL SCALING OF AEROELECTRICAL FIELD AND CURRENT OF ATMOSPHERIC BOUNDARY LAYER

S.V. ANISIMOV and N. M. SHIKHOVA

Borok Geophysical Observatory of IPE RAS, Borok, Yaroslavl region, RF

Keywords: STATISTICAL STRUCTURE, AEROELECTRIC FIELD SELF-SIMILARITY.

INTRODUCTION

Electrodynamics of surface atmosphere is formed by the set of physical processes of generation, separation and transfer of electric charges occurring in a wide range of spatial and temporal scales. The aim of this work was to study the fractal properties of aeroelectric field and current in a wide frequency range, including aeroelectric turbulent pulsations, diurnal and seasonal variations.

METHODS

Digital data of observation, carried out at Borok Geophysical Observatory [58°04 ' N; 38°14 ' E] of 1998 – 2013 were used for analyses. Use of 10 Hz sample-frequency of registration gave us an opportunity to form time-series of observations with duration from hour to decade. In analyses we focused on electric current density dynamics at fair-weather conditions (absence of precipitation, wind speed is not more than 2 m/s, cloudness is not more than 5 balls). Trend absence and a pronounced annual variation observed in series of average monthly values of the vertical electric current density (J_z) and electric field (E_z), presented in Fig. 1. The presented series are stationary relatively variance as well autocorrelation function.

The aeroelectric field dynamics are influenced by atmospheric boundary layer turbulence and convection, as well as by changes in the electrical air conductivity, which exposed of a direct impact of

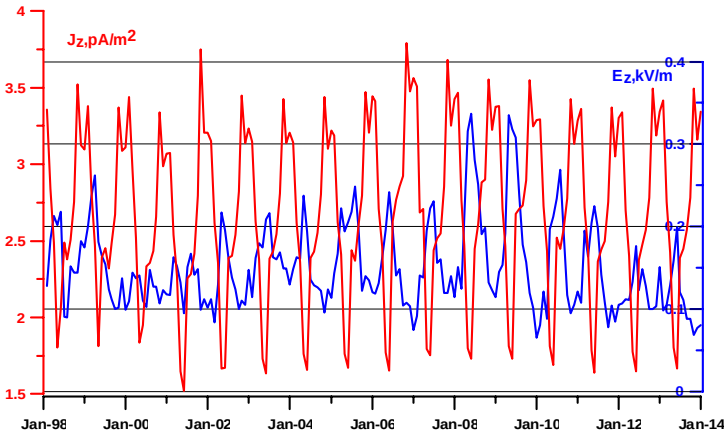

Figure 1. Dynamics of average monthly values of electric field intensity (blue) and vertical electric current density (red) of 1998 – 2013.

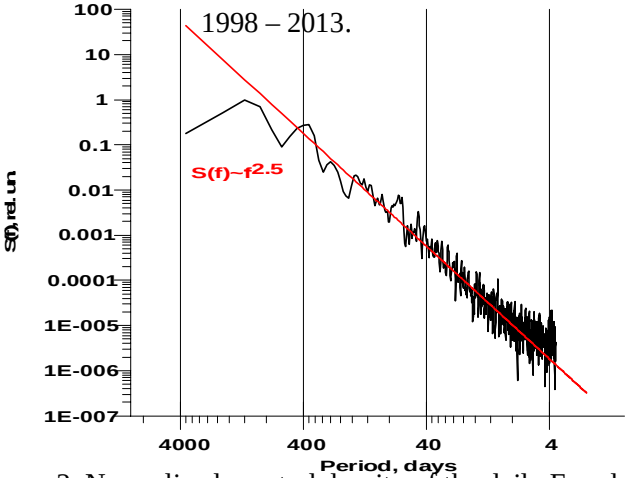

Figure 2. Normalized spectral density of the daily E_z values on 01.01.1999 - 31.07. 2012 at Borok Observatory.

radioactive emanations of the earth surface, subsurface and haze aerosols [Hoppel *et. al*, 1986; Anisimov *et.al*, 2012; Anisimov et.al, 2013; Anisimov *et.al*, 2014]. At "good weather" conditions the main factor determining the dynamics of the electrical state of the atmospheric boundary layer is turbulent mixing of air ions, charged aerosols, radon and thoron, which forms the volume space density distribution and aeroelectric field near the earth surface. The energy of E_z multiscale variations distributes on variations scales, following the common law of constant rate of dissipation. The degree of slope of the power spectral density calculated from the series of 4960 days is constant in the range of 4-400 days and is -2.5 (Fig. 2).

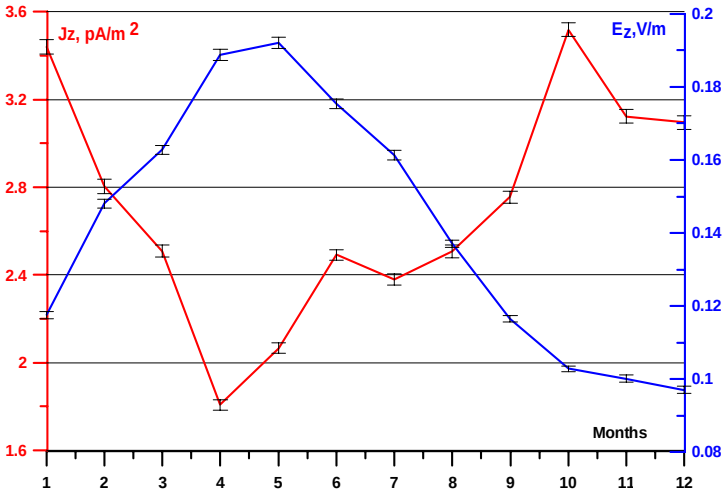

Figure 3. Annual dynamics of electric field (blue) and vertical electric current density (red) on 1999 – 2013 at Borok Observatory

A more detailed analysis of the intra-annual J_z and E_z variations, calculated using monthly average values for a period of fourteen years observations shows (Fig. 3) that significant global minimum J_z in April is accompanied by significant intra-annual maximum E_z in April-May [Anisimov *et.al*, 2013]. Presumably, this fact can be explained by a decrease in lower atmosphere conductivity of the lower atmosphere resulting from active snow and ice melting in spring.

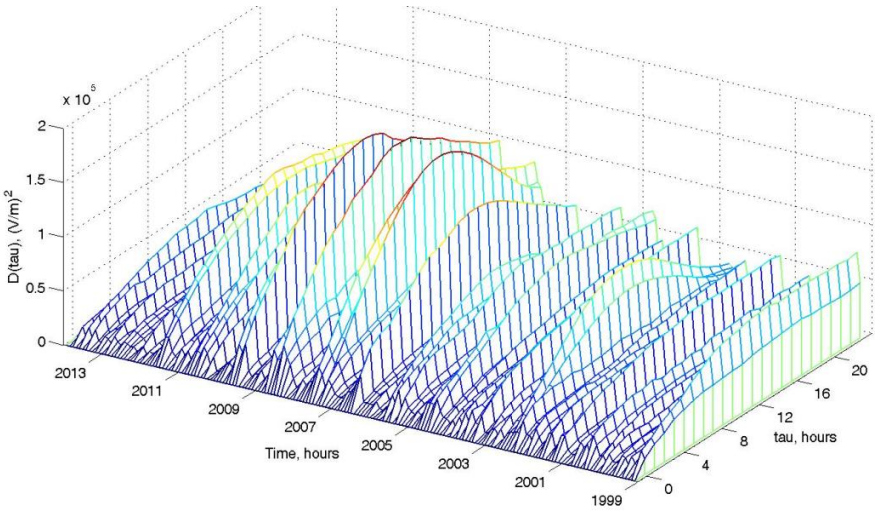

Figure 4. The second-order aeroelectric structures of E_z hour-average values on 1999 – 2013 at Borok Observatory.

Fig. 4 presents the results of structural-temporal analysis of an hourly mean E_z dynamics. Structural functions of short-period pulsations ΔE_z were calculated according to the algorithm of stationary increments: $D_E(t,\tau) = \langle|\Delta E(t+\tau) - \Delta E(t)|^2\rangle$ to research the scale τ of self-similarity of E_z [Anisimov, Shikhova, 2014].

The analysis showed that the interval of self-similarity of energy is multiple to 16-24 hours, and may be due to an influence of global thunderstorm and regional convective generators. The amplitude of the diurnal variation E_z during period of 2007-2011 was much higher than that of the average value for the whole period.

The results show that the fractal (self-similar) nature E_z variations are observed on the scales from years to tens of seconds. Figure 5 shows the dynamics of fractal regularization dimension R [Roueff and

Vehel, 1998] of aeroelectric field variations for 15 years. Each R-value was calculated for a series of 720 hours (30 days). Fractal dimension of aeroelectric field belongs to the range 1.35 - 1.8, with a mean of 1.56. This result proves fractality of atmospheric electric field, which, while R <1.5 corresponds to the physical process of superdiffusion. Presumably superdiffusion in aeroelecric field is associated with the large-scale energetic atmospheric phenomena, determined by global lightning generator (winter seasons) or regional convective generators (summer seasons).

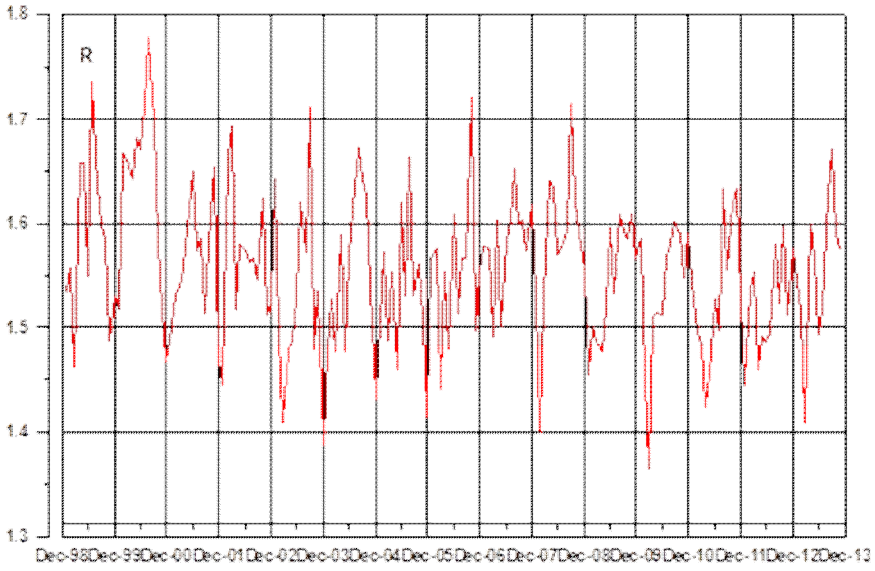

Figure 5. Fractal dimension of E_z hour-mean data calculated at every 720- hours on 1999 – 2013 at Borok Observatory.

The presence of long-term digital data of aeroelectric observations and preliminary choise of amplitude-time series with the conditions of "good weather" make it possible to detect the similarity of daily trend of aeroelectric field and unitary variation in continental mid-latitude stations [Anisimov, Mareev, 2008]. As an example, Fig. 6 (a) shows the diurnal variation of hourly mean values of aeroelectric field calculated for winter season. A characteristic of the unitary variation diurnal trend of aeroelectric field with maximum at about 19:00 UT is distinctly traced. Figure 6 (b) shows the diurnal variation of aeroelectric field with some maximums for a summer period of observations.

In order to obtain statistically significant results in the study of the form of the diurnal variation average daily E_z variation were constructed for each season of the time interval 1998-2012. Results of statistical analysis show that

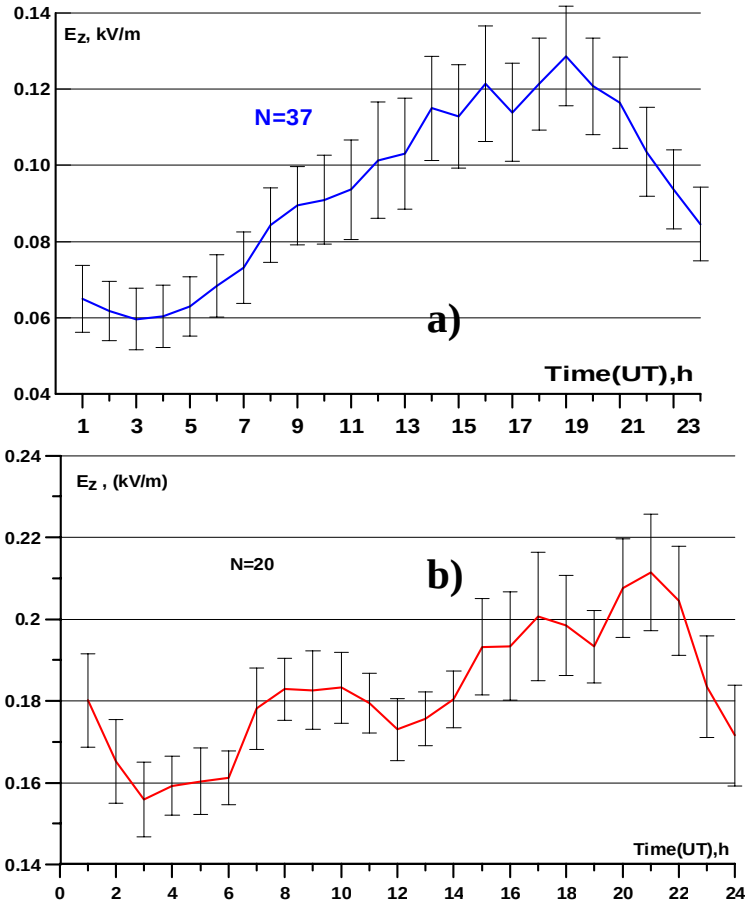

Figure 6. Daily E_z variation at Borok Observatory calculated for "good weather" conditions on January-February 2012 (a) and on July – August 2012 (b).

the unitary variation (with minimum in the morning and maximum in evening hours UT) most reliably reproduced in conditions of the unperturbed atmosphere of the northern hemisphere mid-latitudes during the winter months (December, January, February). This finding is consistent with the results have been obtained at the middle-latitude observatory Marsta [Israelsson and Tammet, 2001] , located in Sweden [59 ° 56 'N, 17 ° 35 'E].

One of the goals of investigation was to analyze the relation between atmospheric stratification [Businger et.al, 1971] and the dynamic characteristics of aeroelectric field. Figure 7(a,b) shows a typical daily aeroelectric field registrogramm at Borok Observatory in "good weather" summer conditions and dynamics of sustainability parameter $\zeta = z / L$, where L - the scale of the Monin Obukhov length scale, z-height of meteostation placement usually equals 2m. The important statistical characteristic of the dynamics aeroelectric field is skewness of field values distribution in a fixed time interval. Figure 7c shows typical changes of the skewness A_s calculated as $As = \frac{\sum_{i=1}^{360}(\Delta E_i - \overline{E})^3}{360\sigma^3}$ on series of 10-second average of field strength for each hour of summer day observations. Horizontal lines reflect the boundary of skewness significance at P> 0.9.

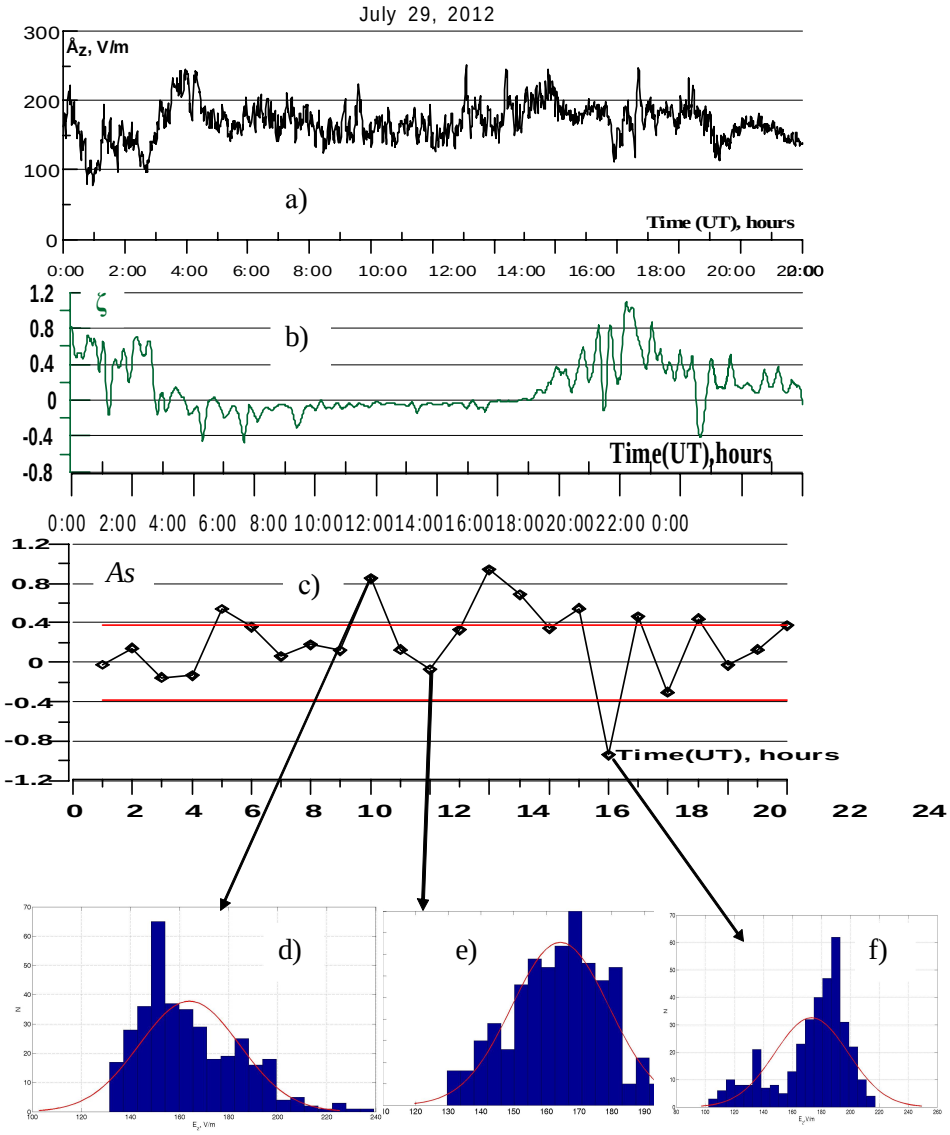

Figure 7. The daily dynamics of E_z (a), stability parameter ζ (b), mean-hours skewness A_s of aeroelectric ten-sec pulsations (c), distributions of E_z fluctuations for 09-10 UT (d), 11:30-12:30 UT (e), 17-18 UT(f) on July 29, 2012.

At time interval 04:00 - 14:00 UT stratification of the surface atmosphere is close to unstable, during the interval 09:00 - 14:00 UT there are time intervals in which the stratification is close to neutral, in time interval of 16:00 - 00:00 UT is stable stratification (Fig.7b). While significantly positive values of skewness usually

correspond to unstable, and significantly negative – to stable stratification (Fig.7c).

To obtain quantitative statistical estimates of daily aeroelectric field dynamics the distributions of aeroelectric field increments for different stratification conditions are considered. It is known that the distribution is close to normal, when the random variable is the result of the combined action of many independent factors and the influence of each factor alone is little.Distribution of aeroelectric field increments close to normal is represented on Fig.7e and corresponds to neutral stratification conditions. In time intervals of unstable stratification with a significant positive value of the skewness distribution of the field increments is non-normal (Fig.7d). Distribution of the field increments with a significant negative value of the skewness coefficient shown in Fig.7f corresponds to the conditions of stable stratification. The spectral density of aeroelectric pulsations characterizes the rate of dissipation of electrical energy (Fig. 8). Note that the dynamics of aeroelectric field in range of periods 10 – 1000 s also demonstrates the property of self-similarity with the average values of the spectral slope α_1 = -3.2 (for pulsations periods of 10-100 s) and α_2 = -1.42 (for pulsations periods of 100-2000 s).

CONCLUSION

The results of statistical analysis of long-term aeroelectric field strength observations and vertical electric current density at mid-latitude geophysical observatory are considered. The dynamics of the aeroelectric field and current demonstrates a fractal properties, fractal dimension of hourly mean series of aeroelectric field is defined. It was found that in the scale range from 10 seconds to a year aeroelectric field variations and current demonstrate self-similarity. It was revealed that the annual aeroelectric field variation during the time interval 1998 - 2013 has maximum on April-May. Corresponding seasonal variation of the vertical electric current density has minimum on April. According to middle-latitude observatory data diurnal aeroelectric field variation for summer and winter seasons of observation are detected. Exponents of slopes of the spectra in ultra-low frequency range of aeroelectric pulsations, having the property of self-similarity are calculated. It is shown that the statistical characteristics of aeroelectric field dynamics reflect changes in stratification conditions of surface atmosphere.

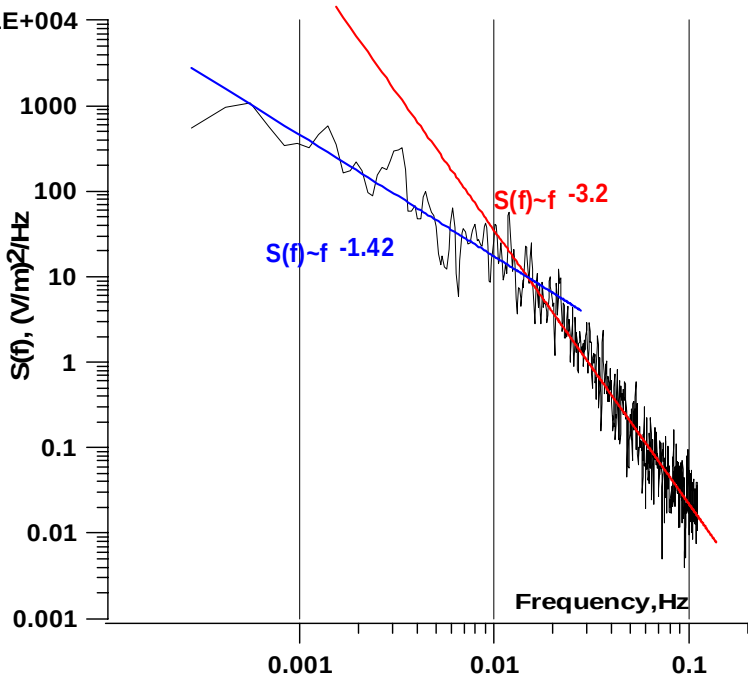

Figure 8. The spectral density of aeroelectric pulsations on 29.07.2012, 07:00-09:00 UT.

ACKNOWLEDGMENTS

The work has been supported by Russian Foundation for Basic Research (grants № 12-05-00820, №13-05-12060) and grant from the Government of the Russian Federation under contract No. 14.B25.31.0023.

REFERENCES

Anisimov S. V., Galichenko S. V., Shikhova N. M. 2012. Formation of Electrically Active Layers in the Atmosphere with Temperature Inversion. *Izvestiya, Atmospheric and Oceanic Physics*. **48**, 442-452.

Anisimov S. V., Shikhova N. M., Aphinogenov K.V. 2013.Dynamics of electricity of undisturbed mid-latitude atmosphere: from observations to scaling. *Radiophysics and Quantum Electronics.* **56**, 787-804.

Anisimov S.V., Galichenko S.V., Shikhova N.M. 2014. Space charge and aeroelectric flows in the exchange layer: An experimental and numerical study. *Atmos.Res.* **135–136**, 244–254.

Anisimov S.V., Shikhova N.M. 2014. Intermittency of Turbulent Aeroelectric Field. *Atmos. Res*., **135–136**, 255–262.

Anisimov S.V., Mareev, E.A., 2008. Geophysical Studies of the Global Electric Circuit. *Physics of the Solid Earth*. **44**, 760–769.

Businger, J. A., Wyngaard, J. C., Izumi, Y., and Bradley, E. F. 1971. Flux-Profile Relationships in the Atmospheric Surface Layer. *J. Atmos. Sci*. **28**, 181–189.

Hoppel W.A., Anderson R.V. and Willet J.C. 1986. Atmospheric Electricity in the Planetary Boundary Layer. Krider, E.P., Roble, R.G. (Eds.), *The Earth's Electrical Environment*. Natl. Acad. Press, Washington, 149-165.

Israelsson S., and H. Tammet. 2001.Variation of fair weather atmospheric electricity at Marsta Observatory, Sweden, 1993–1998. *Journal of Atmospheric and Solar-Terrestrial Physics*, **16,** 693–1703.

Roueff, F. and J. Levy Vehel, 1998. A Regularization Approach to Fractional Dimension Estimation. Novak M. M. (Ed.), *Fractals and Beyond – Complexities in the Sciences*. World Scientific, Singapore, 14.

IMPACTS OF NORTHERN EURASIAN FORESTS ON THE GLOBAL CARBON CYCLE: A SYSTEM APPROACH

A.Z. SHVIDENKO[1], D.G. SCHEPASCHENKO[1], and F. KRAXNER[1]

[1]International Institute for Applied System Analysis, Laxenburg, A-2361 Austria

Keywords: Forest ecosystems full verified carbon account, fuzzy systems, Northern Eurasian forests.

INTRODUCTION

The vast extent of Northern Eurasian forests, high level of ongoing and expected climatic change, and connecting processes in the region's forest ecosystems predetermine their substantial role in functioning the Earth system (Pan et al., 2011). There are two major generic requirements to understanding the interactions of forests with the global carbon cycle: (1) it should be a full account comprising all (forest) ecosystems, all processes, all fluxes of carbon contained substances between forest ecosystems and the atmosphere, hydrosphere and lithosphere; and (2) the approach should present the verified results keeping in mind the necessity of reliable and comprehensive assessment of uncertainties. The completeness of the account is controlled by assessments of both stock changes and account for the fluxes. The major accounted for carbon fluxes include CO_2, CO, CH_4, VOC, and aerosols. The final result of carbon account is presented in form of the Net Ecosystem Carbon Budget (NECB). It is supposed that uncertainty of NECB in limits of ± 25% (CI 0.9) would be satisfactory for policy makers (Shvidenko et al., 2010a). The uncertainties are understood as an aggregation of insufficiencies of the studied system's output, regardless of whether those uncertainties result from a lack of knowledge, the intricacies of the system, or other causes.

However, the studied system belongs to typical *fuzzy* or *underspecified* systems (Shvidenko et al., 2010a) with elements of *full complexity problem* (Schellnhuber 2003) and *wicked* system (e.g., Rittel & Weber 1973). Under some cognitive differences of the terminology, the practical consequence of studying such a class of systems is that any individually used method of carbon account is not able to assess the structural uncertainty, i.e. the "within method" uncertainty is inevitably partial. In order to assess a "full uncertainty", the methodology that is discussed in this paper suggests a complementary use of several, to a possible extent independent, methods of carbon account, assessing the uncertainties within the each individual method with following harmonizing and mutual constraints of the major intermediate and final results using the Bayesian approach.

There are other specific features of the methodology. The first one aims at a possible convergence of methods used, and mutual penetration of appropriate elements of one method into another that might substantially increase the synergism of join application of the different methods. The second supposes that the system developed for carbon account could serve as information and - to some extent - methodological background for assessing the impacts of forests on other biogeochemical cycles. The paper presents a succinct description of the methodology, indicates major results for Northern Eurasia forests (limited by the Russian territory) for recent years (2007-2009), considers the uncertainties of the results and outline the future research needs.

METHODS

The methodology is based on a joint application of four major methods of carbon account - landscape-ecosystem approach; process-based models; direct flux measurements; and inverse modelling. Multi-sensor remote sensing concept is widely used in all of these methods.

Developed by IIASA *the landscape-ecosystem approach (LEA)* presents a system integration of relevant inventory-based methods. The LEA serves for a system designing of the account and accumulates all available relevant knowledge about landscapes and ecosystems, results of different inventories and surveys (forest inventory, state land account, forest pathological monitoring etc.), diverse empirical data, semi-empirical aggregations and models. The full carbon account (FCA) within the LEA complimentary combines both pool- and flux- based approaches. Strict following the requirements of applied system analysis defines major system features of the LEA which *inter alia* include: (1) use of strict and mono-semantic definitions and classifications that are compatible with other carbon accounting methods; (2) formally explicit structuring the account, defining the inter- and intra- system boundaries; (3) consecutive estimation of uncertainties at all stages and for modules of the account; (4) presenting all accounting schemes, models and assumptions in a formal algorithmic form; (5) spatially explicit presenting the major intermediate and final results (pools and fluxes); and (6) clear identification of the temporal dimensions of the account; the overall goal is providing the results continuously in time. The simplicity of the above requirements is illusive. For instance, in definitions of forest and some of important indicators (like growing stock volume, live biomass) forest inventory uses *relative stocking*, FAO definition – *canopy cover*, and major remote sensing products are based on *canopy closure*. While these three indicators are strongly correlated, conversion one into another requires availability of ecoregion and tree species specific models. Disregarding this transition might generate uncontrolled errors up to 30% of the amount of live biomass for some widely represented forest types in high latitudes.

The uncertainties within LEA are assessed in the following order: (1) estimation of precision of intermediate and final results using error propagation theory; (2) expert assessment of completeness of the accounting scheme and (if it is recognized necessary) "transformation" precision in uncertainty; and (3) multiple harmonizing and constraint of the results. Monte-Carlo simulations serve for the analysis of sensitivity of results to variability of the parameters and structure of the account. In spite of an inevitable use of "soft" knowledge in the FCA (e.g., assessment of accuracy of initial data reported by different sources, use of "summarized errors" as a function of random and systematic errors etc.), a holistic analysis of the approach at regional and country levels showed that received in such a way "uncertainties of uncertainties" are less than initial uncertainties at least by level of magnitude. Of course, such an approach cannot find out unrecognized biases.

The information background of the LEA is presented in form of an Integrated Land Information System (ILIS) – a multi-scale and multi-layer GIS with corresponding attributive databases and cartographical part at the basic resolution of 1 km. The classification includes all classes of land cover (6 aggregated classes at the top level - agricultural land, forests, wetlands, natural grasslands and shrublands, non-vegetated lands). Forest classification consists of 9 hierarchical levels and has ~80000 of unique records presenting at the bottom level a detailed by-pixel characteristic of individual stands (forest ecosystems) including dominant species, age, average diameter and height, relative stocking, site index, growing stock volume etc.), as well as other forest land categories (sparse forests, burnt area, grassy glades, dead stands etc.). Aggregated classes of forest cover are derived from remote sensing products with following downscaling based on forest inventory and other ground data. By-pixel parametrization of the forest land cover is provided by a modified optimization algorithm described in Schepaschenko et al. (2011). The algorithm allows using the most accurate available data (including modified and updated forest inventory) in boundaries of forest enterprises (currently ~1600 for Russia) and the most probable forest parameters by each pixels. Carbon stocks are estimated by their content in live biomass (dividing in 6 components – stem, branches, foliage, roots, understory (undergrowth + shrubs) and green forest floor) based on multi-dimensional regionally distributed equations of biomass extension factors (BEF) by the components. Carbon stock in dead wood including snags, logs, stumps, dry branches of living trees is defined based on a special algorithm reconciling a number of datasets (data of forest inventory; database of biological productivity of forests of the Eurasian continent) by group of species, age, and bioclimatic zones (Shvidenko et al., 2010b). Soil organic carbon (on-ground organic layer with content more than 35% by dry matter mass and 1m top layer of mineral soils) was estimated based on the modified soil map of Russia and database of typical soil profiles (Schepachenko et al., 2013). Net Primary Production (NPP)

was assessed using a new unbiased method that yields dynamics of total production of life biomass (Shvidenko et. al., 2007). Heterotrophic soil respiration was calculated based on a system which uses available empirical data (including 780 records for the study region) and takes into account type of soils, the impacts of land cover type, dominant species, bioclimatic zones and disturbances (Mukhortova et al., 2014). The flux due to decomposition of dead wood was estimated based on its amount by tree species, components size, and zonal coefficients of decomposition (Shvidenko et al., 2010b). The fluxes to hydrosphere and lithosphere were estimated based on available publications.
The LEA results present average values of measured indicators for different periods of time. In order to take into account seasonal specifics of climate for individual years, a set of empirical regressions was developed for corrections of relevant FCA fluxes (NPP, heterotrophic respiration and flux due to decomposition of dead wood).

Disturbances include forest management (particularly harvest), fire, insect outbreaks and diseases, unfavourable weather and environment conditions. The corresponding emissions are assessed based on areal extent of disturbances (derived from remote sensing products, data of forest pathological monitoring, official statistics etc.) and their severity. For instance, fire emissions were assessed based on the areas obtained by the Institute of Forest, Siberian Branch of the RAS; amount of fuel assessed by 12 types; average long-period regional data on distribution of burnt areas by fire types; share of fuel consumption dependently on fire type, month of burning and severity of fires season. Impact of biotic factors and unfavourable weather conditions was assessed based on official data of pathological conditions of Russian forests (FFSRF, 2010) by a special algorithm (Shvidenko et al., 2010b).

Process-based models remain an only tool for understanding the mechanism of ecosystems' functioning and long term predictions. However, Dynamic Global Vegetation Models (DGVMs) suffer from grave shortcomings in their applications to such specific objects like forests of high latitudes (particularly on permafrost). Studies in the PEEX domain showed that ensembles of DGVMs might estimate well some regional indicators (e.g., NPP), but do not reflect properly others (e.g., Heterotrophic Respiration, disturbances). Additional shortcomings of DGVMs on a regional level follow from a usually small amount of plant functional types (usually 10 to 15 for the globe), consideration of only potential vegetation, and the absence of some important land classes like wetlands or croplands. Experiences show that diversity of approaches used in DGVMs might lead to substantially different results. We used for comparison an ensemble of 17 DGVMs considered in Cramer et al. (1999) and the results of 8 models from Dolman et al. (2012). Direct measurements of Net Ecosystem Exchange (NEE) by *eddy covariance* present unique information for ecosystems that constituent the footprint of towers and are extremely important for parametrization of vegetation models, but small amount of towers and lack of well understood gradients for upscaling "point measurements" limit their applicability for large territories. Finally, *inverse modelling* was used as a tool for the top-down control. We used published date of several series of inverse modelling published data for comparison (Gurney et al., 2003; Dolman et al., 2012 and others).

RESULTS AND DISCUSSION

Live biomass (LB) of Russian forest ecosystems is estimated at 37.5±1.5 Pg C, or on average 4.56±0.19 kg C m^{-2} with substantial zonal variation. Of the total amount, aboveground LB comprises 74.6% and 67.7% are in aboveground wood. The stock of dead wood is 10.3±1.0 kg C m^{-2}, or 1.3±0.11 kg C m^{-2}, i.e. 27.4% of the LB. Of the total amount, 37.8% are in dry stems and snags, 30.6% in logs and 31.6% in dead roots. Forest soils accumulated 144.5 Pg C (or 17.6 kg C m^{-2}) including 8.3 Pg C in the top-soil organic layer. The ratio of carbon stock of soil to vegetation is 3.02:1.

Major carbon fluxes (average for 2007-2009) are presented in Table 1 and spatial distribution of the NECB – in Figure 1. Due to the LEA results, Russian forests served as a net sink of ~546 Tg C yr^{-1} (or 66 g C m^{-2} yr^{-1}) during this period. In spite of this high sink, large territories of Russian forests, particularly destroyed by fire and growing on permafrost serve as a carbon source. While annual variability of the NECB for some large regions reached 25-30%, at the country level it is in limits of ± 15%. Major drivers

of this variability are specifics of seasonal weather and natural disturbances (mostly fire). There are substantial differences in the NECB and its structure by large geographical regions and bioclimatic zones; the major reasons for that is different ratio between NPP and HR. Major fluxes and their uncertainties within LEA (assuming that the used accounting schemes and models have no unrecognized biases) were defined: NPP 319±19 g C m^{-2} yr^{-1}, HR 206±17 g C m^{-2}, disturbances 20±4 g C m^{-2} (including fire emissions 45%, biotic impacts 30%, and harvest and wood products 25%), flux to the hydrosphere and lithosphere 1.1±0.33 g C m^{-2} yr^{-1}. This resulted in uncertainties of the NECB about 23% (confidential interval here and above is 0.9).

Some comparisons with previously reported results are of interest. The NPP assessed in this study differs from the estimates by DGVMs, remote sensing and methods based on chlorophyll index in limits of 5-7%. The earlier estimate of NPP given by Shvidenko and Nilsson (2003) was 224 g C m^{-2} yr^{-1}, or at ~30% less than the result of LEA in this study. The major reason of such a difference is an underestimation of NPP by using the measurements *in situ* because the latter is not able to capture some substantial parts of NPP (e.g., root exudates). The new estimate of HR is at ~20% higher that a number of previously reported results (e.g., Kurganova et al., 2003).

Table 1. Carbon budget of Russian forests (average for 2007-2009)

Zone	Carbon fluxes, Tg C yr^{-1}								
	NPP	HR	DW	FF	BD	FWP	H&L	NECB, Tg C yr^{-1}	NECB, g C m^{-2} yr^{-1}
	European part								
Tundra	12.0	7.4	0.5	0.0	0.1	0.1	0.0	3.9	96
FT, ST, NT	105.0	56.6	5.6	0.1	2.9	0.7	1.0	38.1	111
MT	229.8	128.2	20.3	0.1	7.1	5.2	2.2	66.7	117
ST	303.5	152.8	26.5	0.7	6.0	11.9	2.2	103.4	185
TF	76.7	34.1	5.6	0.0	7.1	4.4	0.7	24.8	211
Steppe	32.0	20.1	1.6	0.0	2.3	3.8	0.1	4.1	81
SD+D	1.4	0.9	0.1	0.0	0.2	0.1	0.0	0.1	34
Subtotal	**760.4**	**400.1**	**60.2**	**0.9**	**25.7**	**26.2**	**6.2**	**241.1**	**143**
	Asian part								
Tundra	36.9	30.7	1.1	0.6	0.3	0.1	0.2	3.9	24
FT, ST, NT	226.7	175.5	6.8	6.9	2.6	0.5	3.8	30.6	29
MT	1129.3	782.7	70.2	45.0	14.8	6.2	18.0	192.4	47
ST	348.4	225.5	27.3	15.7	5.4	6.3	4.3	63.9	70
TF	66.5	46.2	5.9	2.9	0.8	1.1	1.0	8.6	53
Steppe	39.4	26.1	2.9	2.6	0.9	1.8	0.3	4.8	45
SD+D	2.4	1.1	0.2	0.7	0.1	0.1	0.0	0.2	38
Subtotal	**1849.6**	**1287.8**	**114.4**	**74.4**	**24.9**	**16.1**	**27.6**	**304.4**	**47**
	Russia total								
Tundra	48.9	38.1	1.6	0.6	0.4	0.2	0.2	7.8	38
FT, ST, NT	331.7	232.1	12.4	7.0	5.5	1.2	4.8	68.7	49
MT	1359.1	910.9	90.5	45.1	21.9	18.2	20.2	259.1	55
ST	651.9	378.3	53.8	16.4	11.4	11.3	6.5	167.3	114
TF	143.2	80.3	11.5	2.9	7.9	5.5	1.7	33.4	119
Steppe	71.4	46.2	4.5	2.6	3.2	5.6	0.4	8.9	55
SD+D	3.8	2.0	0.3	0.7	0.3	0.3	0.0	0.3	37
Total	**2610.0**	**1687.9**	**174.6**	**75.3**	**50.6**	**42.3**	**33.8**	**545.5**	**66**

Abbreviation in Table 1: Fluxes-NPP-Net Primary Production, HR-soil heterotrophic respiration, DW-flux due to decomposition of dead wood, FF-forest fire, BD-biotic disturbances, FWP-forest wood products, H&L-fluxes in hydrosphere and lithosphere, NECB-Net Ecosystem Carbon Budget.

Estimates of carbon budget of Russian forests by other methods are basically compatible with results of the LEA. Using the pool-based methods and FAO definition of forest Pan et al. (2011) estimated carbon sink of Russian forests in 2000-2007 at 463±83 Tg C yr^{-1}. Recalculation for the Russian national definition resulted in 510±99 TgC yr^{-1} (Shvidenko and Schepaschenko, 2014). Average of 12 inverse modelling schemes for different period from 1998-2008 was 690±246 TgC yr^{-1}, the error means ±1 standard deviation of sink by different models (Dolman et al., 2012). Other published results reported for boreal Asia are close (e.g., Gurney et al., 2003). Dolman et al. (2012) reported results of eddy covariance upscaling for all classes of vegetation in Russian territories but a very small amount of measurement of sites do not allow any reliable estimation of uncertainties. Application of DGVMs did not give acceptable results: the results were about 2 times less that these defined by other methods. Our explanation is that the mechanism of calculation of HR in DGVMs does not correspond to the specifics of high latitude, where processes of decomposition are substantially accelerated by fire.

Russian forests are estimated as net source of methane at 1.26 Tg C-CH_4 yr^{-1}, of which 0.70 Tg C-CH_4 yr^{-1} are from forests on bogged forests and the rest is the emission due to forest fire.

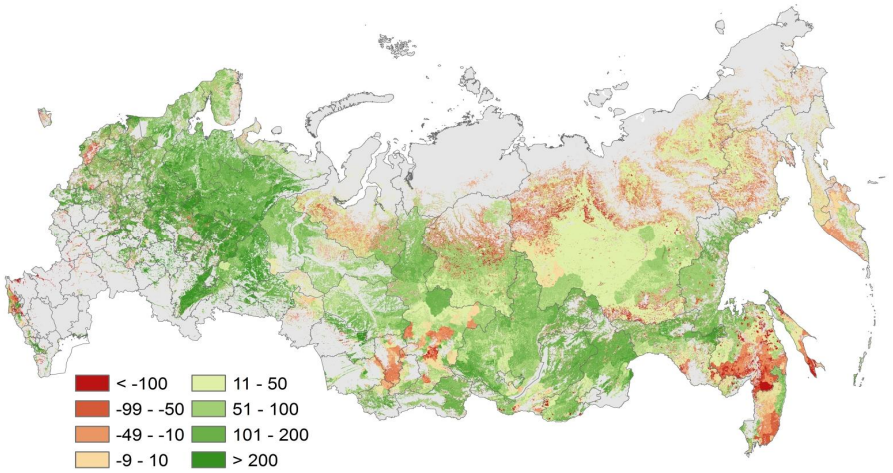

Fig. 1. Net Ecosystem Carbon Budget of Russian forests (average for 2007-2009). Pink colour denotes the source, green colour – the sink. Unit of measurements in the legend is g C m^{-2} yr^{-1}.

CONCLUSIONS

Application of the Bayesian approach to results of the LEA, pool-based method and 2 series of inverse modelling resulted in 580±107 Tg C yr^{-1}. To some extent, this result is illustrative because (1) these three methods define different indicators of carbon cycling – NECB, NBP and NEE, respectively, although the difference between these is relatively small, in range of ~10%; (2) the methods used different approaches for defining uncertainty; and (3) the results were obtained for different time periods and – in case of inverse modelling – to the all classes of vegetation cover. We did not include in the comparison upscaled results of eddy covariance and a number of "inventory based" assessments because those did not contain assessment of uncertainties. However, the conclusion that Russian forests served as a net C sink in range 550-600 Tg C yr^{-1} during 2007-2009 is clearly confirmed.

The presented methodology is currently being transformed in an automated system which would allow regular improvements based on new knowledge, incoming information and models. A new land cover (for 2010) is based on 10 remote sensing products including Landsat based forest mask 2010, 30 m (Hansen et al., 2013); PALSAR forest mask 2010, 50m; MODIS Vegetation Continuous Fields 2010, 230m (DiMiceli et al., 2011); FAO World's forest 2010, 250m (FAO, 2012), and others. All datasets were converted to 230m resolution. Synergy of different RS products was explored by geographically weighted regression, and relative reliability of the products was quantified by using the training dataset that consisted 5270 controlling points in the Geo-wiki environment. The introduction of satellite defined forest height and regionally distributed sets of models that describe interconnection of biometric characteristics of

homogeneous groups of stands (forest ecosystems) presented a possibility of more accurate by-pixel parametrization of forest cover. New modules for assessing emissions of VOC and aerosols are incorporated in the LEA approach. Preliminary estimates allow us to assume that the modified version of the FCA decreases uncertainties of the previous version by about one-third. Algorithms of modules for assessing the nitrogen cycle and major components of hydrological cycle are coupled with the carbon accounting scheme.

The high level of expected warming and increased dryness in high latitudes of Northern Eurasia necessitate a special consideration of boreal forests as a tipping element and needs of understanding the mechanisms of their possible rapid transformation. It is planned to use the new version of the ILIS as an information background for forecasting the future trajectories of dynamics and carbon budget of Russian forests using Landscape Succession and Disturbances Models Landis-II combined with physiological model PnET-II (De Bruijn et al., 2014). This model includes practically all sets of drivers – climate change, changing environment, disturbances, and forest management, and is open for modifications, which would allow representing inherent regional features of high latitudes forests.

REFERENCES

De Bruijn, A., A.J. Gustafson, B.R. Sturtevan et al. (2014). Toward more robust projections of forest landscape dynamics under novel environment conditions: embedding PnET with LANDIA-II, *Ecological Modelling* **287**, 44-57.

Cramer, W., J.G. Canadel, S. Luyssart et al. (1999). Comparing global models of terrestrial net production: overview and key results, *Glob. Change Biol.* **5**, 1-15.

Dolman, A.J., Shvidenko, A., Schepaschenko D. et al. (2012). An estimate of the terrestrial carbon budget of Russia using inventory-based, eddy covariance and inversion methods, *Biogeosciences* **9**, 5323-5340.

FFSRF (2010). Review of the forest-pathological state of forests in the RF. Federal Forest Service of the Russian Federation, Moscow, 74 pp. [in Russian].

DiMiceli, C.V. et al. (2011). Annual global automated MODIS Vegetation Continuous Fields (MOD44B) at 250 m spatial resolution for data years beginning day 65, 2000-2010, Collection 5 percent tree cover (available at http://glcf. umd.edu/data/vcf/).

Gurney, K.R., R.M. Law, A.S. Denning et al. (1999).TransCom 3 CO_2 inversion intercomparison: 1. Annual mean control results and sensitivity to transport and prior flux information, *Tellus* **B** 55, 555-579.

Hansen, M.C, et al. (2013). High-resolution global maps of 21st-century forest cover change, *Science* **342**, 850-853.

Kurganova, I.N. (2003). Carbon dioxide emissions from soils of Russian terrestrial ecosystems. Interim Report, IR-02-070, Laxenburg, IIASA, 64 pp.

Mukhortova, L., D. Schepaschenko, A. Shvidenko et al. (2015). Soil contribution to carbon budget of Russian forests, *Agricultural and Forest Meteorology* **200**, 97-108.

Pan, Y., R.A. Birdsey, J. Fang et al. (2011). A large and persistent sink in the world's forests, *Science* **333**, 988-993.

Rittel, H. and M. Weber (1973). Dilemmas in general theory of planning, *Policy Science*, **4**, 155-169.

Schellnhuber, H.J. (2003) Integration assessments of adaptation and mitigation, in Proc. World Climate Change Conf., Moscow, 94-95.

Schepaschenko, D., I.McCallum, A.Shvidenko et al. (2011). A new hybrid land cover dataset for Russia: a methodology for integrating statistics, remote sensing and in-situ information, *J. Land Use Sci.* **6(4)**, 245-259.

Schepaschenko, D.G., L.V. Mukhortova, A.Z. Shvidenko et al. (2013). The pool of organic carbon in soils of Russia, *Eurasian Soil Sci.* **46(2)**, 107-116.

Shvidenko, A. and S. Nilsson (2003). A synthesis of the impact of Russian forests on the global carbon budget, *Tellus* **55B**, 391-415.

Shvidenko, A., D. Schepaschenko, S. Nilsson et al. (2007). Semi-empirical models for assessing biological productivity of Northern Eurasia forests, *Ecol. Model.* **204**, 163-179.

Shvidenko, A., D. Schepaschenko, I. McCallum et al. (2010a). Can the uncertainty of full carbon accounting of forest ecosystems be made acceptable for policy makers? *Clim. Change* **103 (1-2)**, 137-157.

Shvidenko, A., D. Schepaschenko, and I. McCallum (2010b). Bottom-up inventory on the carbon fluxes in Northern Eurasia for comparison with GOSAT Level 4 products, Res. Report, Laxenburg, IIASA, 222 pp.

Shvidenko, A., and D. Schepaschenko (2013). Climate change and wildfires in Russia, *Contemporary Problems of Ecology*, **6(7)**, 683-692.

Shvidenko, A.Z. and D. G. Schepaschenko (2014). Carbon balance of Russian forests, *Siberian J. For. Sci.*, **1**, 69-92 [in Russian].

The FAO world's forest 2010 (2012), available at http://www.fao.org/forestry/fra/80298/en/.

UAV MONITORING TECHNOLOGY FOR OBSERVATIONS IN PAN-EURASIAN REGIONS

N.M.SITNIKOV[1], Y.A.BORISOV[1], D.V.AKMULIN[1], I.I.CHEKULAEV[1], D.I.EFREMOV[1], O.B.POPOVICHEVA[2], I.N.KUZNETZOVA[3], V.I.SITNIKOVA[1] and A.E.ULANOVSKY[1]

[1]Central Aerological Observatory, Moscow region, Russia

[2]Institute of Nuclear Physics, Moscow State University, Moscow, 119991, Russia

[3]Hydrometeorological Centre of Russia

Keywords: UAV, ENVIRONMENTAL MONITORING

Developing the new technology for assessment of air quality and environmental monitoring is of important priority, especially for Russian Pan-Eurasion regions of vast territory and huge emissions from anthropogenous sources and wildfires. Mobile laboratory based on Unmanned Aerial Vehicles (UAV) is developed for observations in Pan-Eurasion regions. It is exclusively available for using during extreme events highly dangerous for humans, in remote areas difficult for assess, in the Arctic regions. Results of development of UAV- based methods and instruments for atmospheric measurements are presented. Light weight, low power and small size of the instruments permits to use them on board of UAV [1-3]. Chemiluminescent instruments for ozone and nitrogen oxides measurements, aerosol samplers, portable black carbon monitor and other onboard equipment are presented. Some aspects of UAV applications for environment monitoring, methods and technique for using on board of UAV are discussed. Measurements of horizontal distributions and vertical profiles of atmospheric parameters (gas and aerosol species) on board of UAV have been carried out using developed instruments. Comparisons with modeling calculations have been carried out. Overview of perspectives of UAV using for atmospheric investigations and environmental monitoring is made. Possibilities of UAV application for stratospheric measurements are discussed [4]. Mobility, comparably low cost and efficiency of UAV based monitoring tools enable to use them in wide range of applications. Combination of instruments based on contact methods with UAV permits to provide high accuracy remote measurements for different purposes.

REFERENCES

Sitnikov N.M., Y.A.Borisov, D.V.Akmulin, I.I.Chekulaev, V.I.Sitnikova, A.E.Ulanovsky, I.I.Chekulaev, F.Ravegnani (2013). Application of unmanned aerial vehicles for atmospheric monitoring. *Meteorology and hydrology*, **1**, 90-99.

Sitnikov N.M., Y.A.Borisov, D.V.Akmulin, I.I.Chekulaev,, D.I.Efremov, V.I.Sitnikova, A.E.Ulanovsky, O.B.Popovicheva (2014). Unmanned aerial vehicles (UAV) in atmospheric research and satellite validation, in Proc. International conference COSPAR 2014, Moscow (Russia).

Sitnikov N.M., Y.A.Borisov, D.V.Akmulin, A.E.Ulanovsky, A.O.Sokolov, V.I.Sitnikova, I.I.Chekulaev (2014). Chemiluminescent methods and instruments for monitoring of the atmosphere and satellite validation on board of research aircrafts and unmanned aerial vehicles. in Proc. International conference COSPAR 2014, Moscow (Russia).

Sitnikov N.M., Y.A.Borisov, I.I.Chekulaev, D.I.Efremov, D.V.Akmulin, V.I.Sitnikova, A.E.Ulanovsky (2014). Returnable aerological sonde based on UAV for balloon sonding of the atmosphere. Meteorology and hydrology, 9, 90-96.

TRACE GASES IN THE ATMOSPHERE OVER RUSSIA UNDER POLLUTED AND BACKGROUND CONDITIONS

A.I. SKOROKHOD, I.B. BELIKOV, E.V.BEREZINA, A.N.BOROVSKY, E.I.GRECHKO, O.V.LAVROVA, K.B.MOISEENKO, N.V.PANKRATOVA, O.V.POSTYLYAKOV, V.S.RAKITIN, Y.A.SHTABKIN and N.F.ELANSKY

A.M.Obukhov Institute of Atmospheric Physics RAS, Department of Atmospheric Chemistry, Moscow, Russia

Keywords: ATMOSPHERIC CHEMISTRY, TRACE GASES, EMISSIONS, OBSERVATIONS

INTRODUCTION

One of the strategic objectives PEEX is a comprehensive study of closely related processes in atmospheric chemistry over Northern Eurasia against an abrupt climatic and ecosystem changes and anthropogenic pressure. Atmospheric air composition (including greenhouse gases and aerosols) and its trends for the vast and low inhabited areas of Northern Eurasia are still poorly studied because of lack of the precise direct measurements. This harms to accuracy of both global and regional models which simulate climatological and ecosystem changes in that highly important region. Partly this gap has been compensated by A.M.Obukhov Institute of Atmospheric Physics RAS (OIAP) observational program including transcontinental train-based TROICA campaigns in 1995-2010, permanent direct *in situ* measurements at ZOTTO station in the middle of Siberia (since 2007), at Zvenigorod station in Central Russia and in Moscow megacity (since 2002). This unique database gave us a possibility to study climatically relevant species (CH_4, O_3, CO, NO_x, BC, aerosols, HCHO) behavior in tropospheric air both under polluted and background conditions.

METHODS

OIAP observational program includes both surface (in situ) measurements performed by commercial analyzers and ground-based remote sensing using different kind of spectrometric equipment. Thus, CH4 total column content observations on base of original spectrometric technique have been conducted at Zvenigirod scientific station (ZSS) located at 55°41'N, 36°46'E in 38 km westward from Moscow since early 1970-ies (Fig. 1). In 1990-ies international project TROICA (TRanscontinental Observations Into the Chemistry of Atmosphere) initiated by P.Crutzen and leaded by OIAP gathered several scientific groups for performing unique set of field campaigns (totally 15) across Russia (Elansky *et al*., 2009). TROICA observations allowed OIAP to establish large database of unique observations of trace gases (including VOCs), aerosols, meteorological and solar radiation characteristics. Larger part of those data was received at first time for extended continental regions of Russia. The original datasets were obtained with 10 sec response from basic instrumentation. Additionally data were averaged by 1, 10 and 60 minutes in time, and by 1, 10 and 50 kilometers in space to make easier study of different scale atmospheric phenomena.

To separate polluted and unpolluted conditions threshold method of CO and NO concentrations was used. After defining urban territories using coordinates of cities borders background conditions were determined by choosing sections with NO≤0.4 ppbv, CO≤0.2 ppmv. These unpolluted conditions on Transsiberian railway accounted for from 35% of observational time in summer and upto 52% in winter - which suggests a weak human impact on the composition of the atmosphere over northern Eurasia in the latitudinal belt 48-58 °N. Cities were divided into three groups: large (500-1500 thousands residents, 10 cities), medium (50-500 thousands residents, 33 cities) and small ones (19-50 thousandsresidents, 67 cities).

In February 2002 most of TROICA equipment was installed and launched on the territory of Meteorological observatory of Lomonosov Moscow State University for permanent observations of

atmospheric chemistry in Moscow megacity. In March, 2007 OIAP has started permanent observations of near surface concentrations of reactive gases (O_3, NOx) at International station ZOTTO in Central Siberia. Later research program at ZOTTO was completed by sessional measurements of CO, CH_4, NO_2 TC.

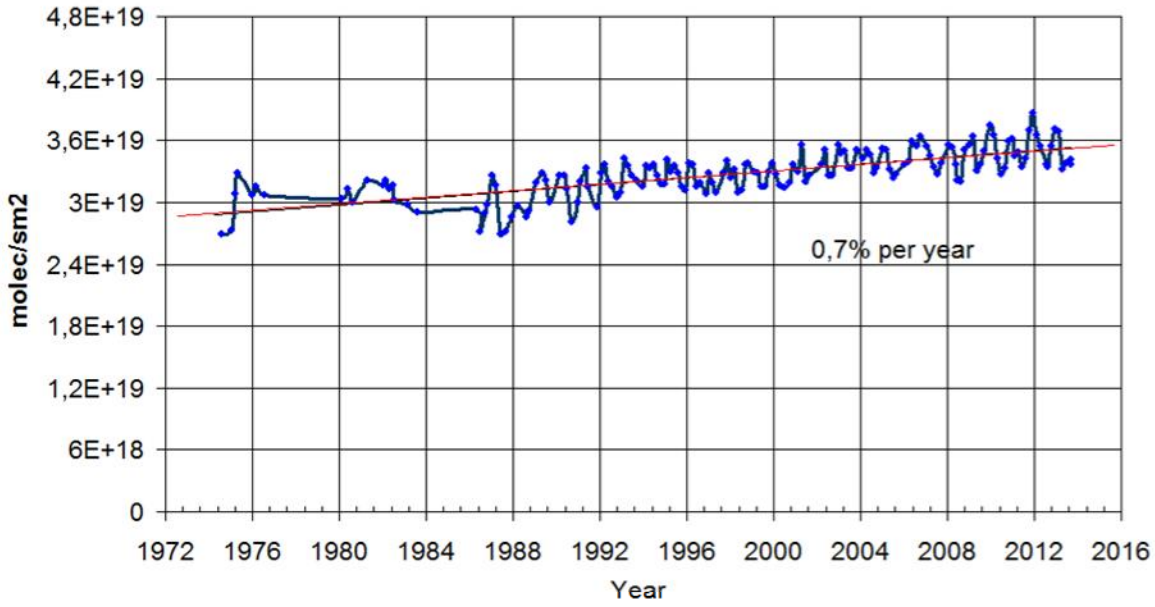

Figure 1. CH_4 total content according to measurements at Zvenigorod Scientific Station (2-monthly averaging).

Beginning from 2008 the formaldehyde (HCHO) atmospheric column is measured at ZSS using DOAS technique. Formaldehyde (HCHO) is a significant constituent of the atmospheric chemistry involved in a lot of chemical reactions which principal global source is the intermediate oxidation of volatile organic compounds (VOCs). Methane which is almost evenly mixed in the atmosphere causes global background level of HCHO of $0.2–0.8\times10^{16}$ mol cm^{-2} which is observed in remote oceanic areas. Among non-methane VOCs, photo-oxidation of isoprene contributes in HCHO production more significantly, hence, HCHO may indicate changes of isoprene emissions by plants. Taking into account that HCHO basically undergo within a few hours, isoprene and other short-lived VOCs together with direct HCHO emissions can cause local HCHO enhancement over certain areas, and, hence, indicate possible local pollution of the atmosphere by VOCs.

CONCLUSIONS

In the absence of explicit anthropogenic sources daily course of NO, NO_2, CO, SO_2, anthropogenic VOCs is an almost flat line (Figure 2). In the cities, the distribution becomes more complex with distinct morning and evening peaks corresponding to rush-hours, and (especially in the morning) reinforced by temperature inversion.

Trace gases having both biogenic and anthropogenic origin (greenhouse gases CO_2, CH_4, and biogenic VOCs (isoprene, monoterpenes)), are characterized by a distinct daily course in the background conditions during the growing season, when processes of plant metabolism, soil formation etc. are active. Under cold weather, it is almost indistinguishable. Under polluted conditions their daily course gets broken by anthropogenic impact (especially in the case of CO_2), but overall his features are preserved.
According to this study, in unpolluted conditions concentrations of NO and NO_2 decrease eastward. The highest values of longitudinal gradients occur in spring and autumn (for NO + NO_2 is about -5-10 ppb per 10 ° E, respectively). Summer gradient for both NO and NO_2 is much weaker (for NO + NO_2 is around -3 ppb per 10°E), that may be due to the combustion of biomass and pollution from China, Korea and Japan in the summer Pasific monsoon system (Pankratova *et al.*, 2011).

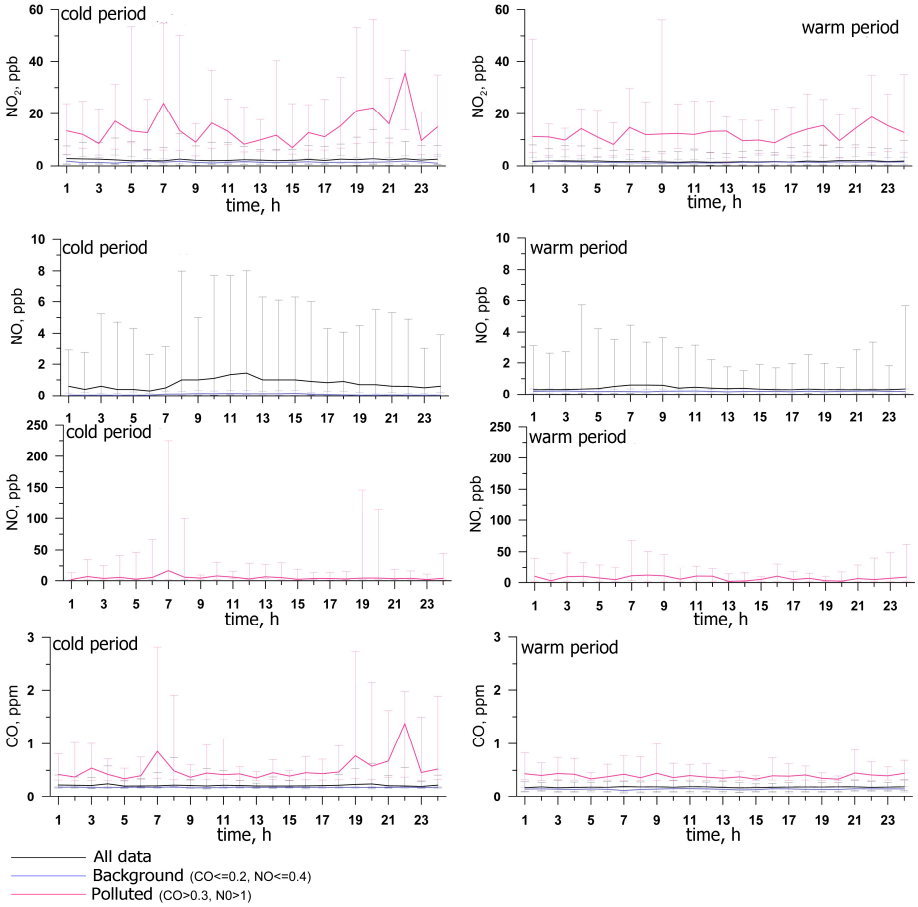

Figure 2. Average daily course of NO_2, NO and CO near surface concentrations for cold (left) and warm (right) periods under the background (blue) and polluted (pink) conditions. Vertical lines mark the 10 and 90 percentiles. Black line means results obtained from all TROICA database.

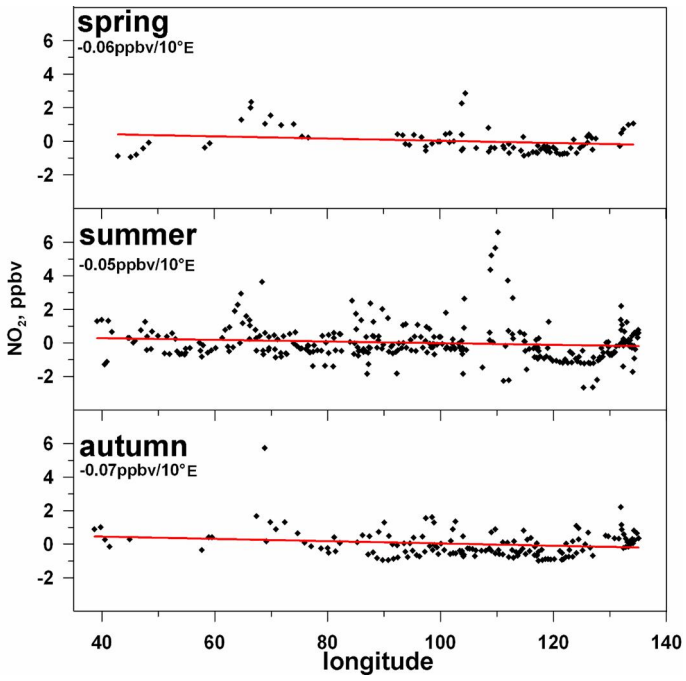

Figure 3. NO_2 spatial gradient according to TROICA data

Concentration of most trace gases in urban air (besides the ozone) is considerably higher than in unpolluted atmosphere (Table 1). Nitrogen oxide NO that is almost completely formed during combustion, but quickly transformed into a more long-lived nitrogen dioxide NO_2 by reaction with ozone is in highest extent influenced by urban sources. Background NO concentration is very low, and its content in urban air varies greatly depending on the size of cities and their infrastructure (RMS values are 1.5-2 times higher than the average value). Sulphur dioxide SO_2 is in lesser extent, but also is a product of combustion of predominantly solid (primarily coal) and liquid fuels. Due to a longer lifetime in the lower atmosphere (from several days to several weeks, depending on weather conditions) its background concentration does not significantly differ from urban values as NO and NO_2. Carbon monoxide CO is mostly of natural origin, and has a long lifetime in the atmosphere (up to several months). Its excess above the background in the cities is no more than 2-3 times. The minimum contrast of urban and background concentrations one can see for CO_2 and CH_4, the sources of which are predominantly terrestrial and aquatic ecosystems, and the lifetime is enough for relatively uniform mixing in the atmosphere.

	Season	O_3	NO_2	CO	CO_2	SO_2	CH_4
Background	s	24.5	0.6	148	373	1.1	1856
	f	27.5	0.5	132	384	2.0	1889
	w	47.1	1.0	180	391	1.5	1840
All cities	s	23.0	5.2	243	380	1.4	1947
	f	19.8	6.8	430	396	4.0	2030
	w	36.3	10.3	330	394	5.3	1900
Large cities	s	20.3	7.5	293	380	1.4	1949
	f	15.0	10.6	616	401	5.6	2118
	w	34.0	14.9	385	396	7.7	1900
Middle cities	s	23.9	4.4	223	382	1.5	1938
	f	23.9	4.2	255	391	2.9	1977
	w	36.3	8.1	292	394	3.8	1900
Small cities	s	25.8	3.0	194	380	1.2	1952
	f	23.2	3.7	320	392	2.6	1956
	w	39.3	6.6	288	394	3.8	1885

Table 1. Average concentration of trace gases in Russian cities of different size and under background conditions in different seasons (s – summer, f – fall, w – winter). All concentrations except CO_2 are in ppbv (CO_2 – in ppmv).

All gases have significant seasonal changes. Under the background conditions they are associated with natural processes, and in the cities they are mainly related to non-uniform action of local sources and the activity of photochemical processes. Dependence of trace gases concentrations on the city size is determined by the ratio of anthropogenic and natural emissions. The concentrations of NO, NO_2 and CO are to the greatest extent related to industrial and transport sources and normally grow with the city size. SO_2 concentration in the summer for almost all cities remains at a nearly background level. Some addition is given in the cities where there are metallurgical enterprises. In winter, during the active heating period the concentrations of SO_2, NO, NO_2 and CO increase with the size of the city. CO_2 and CH_4 are almost independent of the city size throughout the year. On the contrary to anthropogenic gases, the concentration of ozone is less the larger the city. It is important to note that, ozone concentration in small and middle towns often exceeds the background in the summer. This tendency of recent years is likely to strengthen that gradually brings the photochemical state of Russian cities to the cities of southern Europe, USA and Japan.

Recent observations revealed the dependence of the formaldehyde VCD on the temperature at ZSS for the east (from Moscow) and west winds (cases with the wind speed greater than 2 m/sec, airmass comes from Moscow in less than 5.3 hours) (Figure 4).

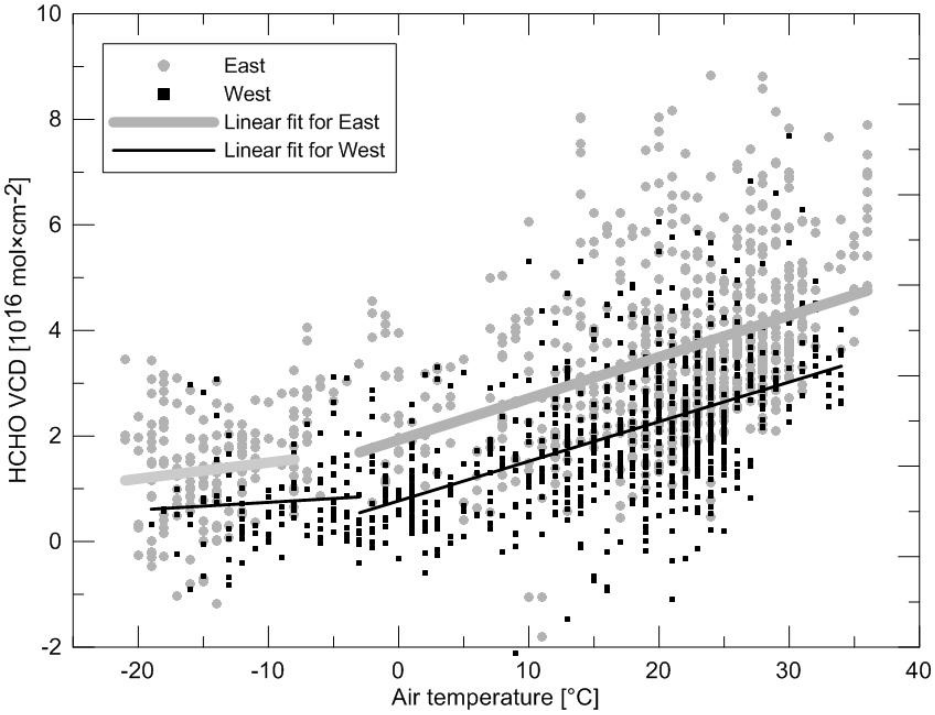

Figure 4. Dependence of HCHO VCD on air temperature at ZSS in 38 km westward from Moscow and it trend lines for different temperature ranges.

The temperature trends of the formaldehyde VCD are positive from –5 to +35°C for different wind directions with the gradient coefficients of about 7.8×10^{14} mol cm^{-2} $°C^{-1}$. The higher HCHO content at the higher air temperature is consistent with the main background HCHO source – the formation of HCHO from non-methane VOCs, presumably from isoprene. Isoprene is emitted into the atmosphere by many species of plants, and their emissions increase with growth of temperature.

Below approximately –5°C trends of formaldehyde VCD for both winds become significantly smaller. The average HCHO VCD for west winds becomes close to background levels. The effects of Moscow megacity are obvious if to compare data for western and eastern winds. The contribution of Moscow is about 1.1×10^{16} mol cm^{-2} for positive temperatures and about 0.8×10^{16} mol cm^{-2} for negative ones.

ACKNOWLEDGEMENTS

This work was supported by the Russian Scientific Fund under grant 14-47-00049.

REFERENCES

Elansky N.F. et al. (2009). *Atmospheric composition observations over Northern Eurasia using the mobile laboratory: TROICA experiments*. ISTC, Moscow, 73 p

Pankratova N.V. *et al* (2011). Ozone and nitric oxides in the surface air over Northern Eurasia according to observational data obtained in TROICA experiments. Izv. Atm. and Ocean. Phys. **47**, N 3, 313.

Postylyakov O.V., and A.N. Borovski (2014). Measurements of formaldehyde total content using DOAS technique: a new retrieval method for overcast. Proc. of SPIE**, 9259**, 925918.1-7.

INTEGRATED STUDIES OF THE ARCTIC ENVIRINMENT AT THE SCIENTIFIC STATIONARY "ICE BASE CAPE BARANOVA"

V.T. SOKOLOV and A.P. MAKSHTAS

Arctic and Antarctic Research Institute, St. Petersburg, Russia

Keywords: SCIENTIFIC STATIONARY, FIELD STUDIES

The key places for comprehensive studies in the Arctic, needed as a source of quality meteorological and oceanographic information, are the research stations, located on the Arctic Archipelagos. One of such stations had been organized in 1986 at the Cape Baranova (Archipelago Severnaya Zemlya) as a research field stationary base of AARI. The station had been closed in 1991. In the summer 2013, after complex repair - restoration works, it had been reopened as Scientific Stationary "Ice Base Cape Baranova."

The Stationary is located at a sufficiently high (30 m) shore of the Shokalski Strait separating the Bolshevik and October Revolution Islands, near the Cape Baranova. Its coordinates are $79^0$16' N, $101^0$45'E. The Shokalski Strait has 40 km wide and 350 meters depth. Area, adjacent to the location of the Stationary, is characterized by a wide range of drifting and fast sea ice, small lakes and rivers, high (up to 800 м) dome-shaped glaciers, and numerous of grounding icebergs (Figure 1).

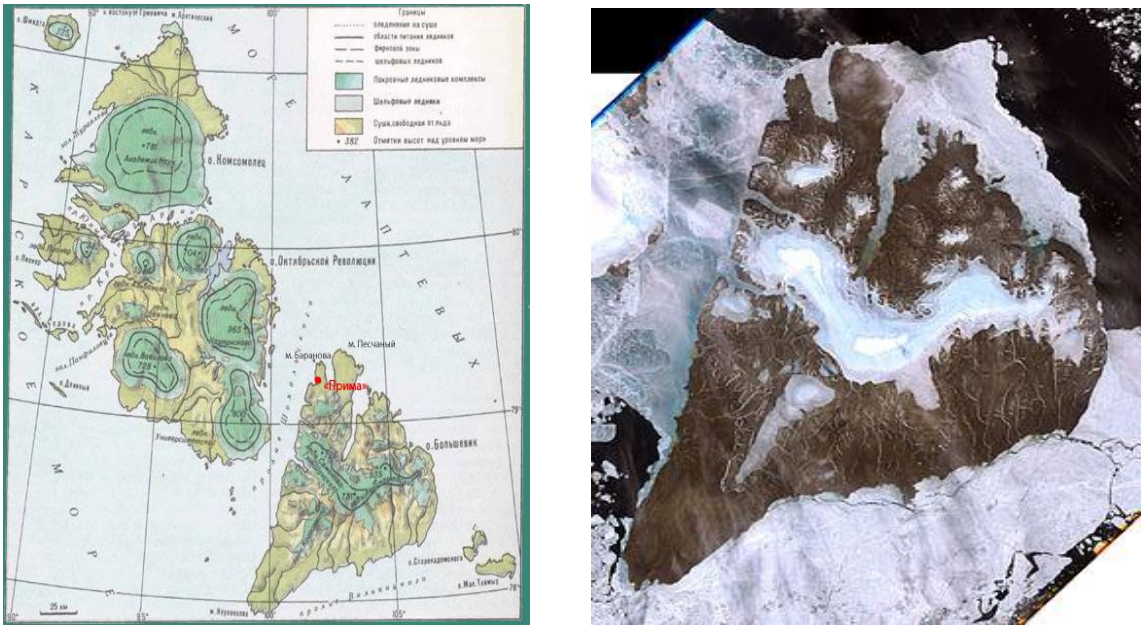

Figure 1. The map of Archipelago Severnaya Zemlya and view of the Bolshevik Island from space.

Since the opening standard meteorological, radiation and upper-air (including ozone) observations and studies of physical - mechanical characteristics of fast ice had been organized. The main investigations started in April 2014, are as follows:

- conducting of standard and special weather, solar radiation and upper-air observations, including observations of the atmospheric gas composition;
- studies of dynamic-thermodynamic processes and evolution of the physical - mechanical and morphometric characteristics of sea and lake ice cover;
- investigations of thermohaline and hydrochemical structure of the water masses, and currents in the Shokalski Strait;
- studies of the components of carbonate system in the upper mixed layer of the sea and in the atmospheric surface layer;
- execution of hydrological and hydro-biological studies;
- conducting of glaciological investigations on the Mushketov glacier;
- study of the history of the formation and current state of landscape in the vicinity of the Stationary.

The report presents the preliminary results of fieldworks carried out in September 2013 - summer 2014 and prospects of Scientific Stationary "Ice Base Cape Baranov." in future.

MODELLING CLEAR-SKY ATMOSPHERIC BOUNDARY LAYERS OVER SNOW

H.A.M. STERK, G.J. STEENEVELD and A.A.M. HOLTSLAG

Meteorology and Air Quality Department, Wageningen University, PO Box 47, 6700 AA Wageningen, The Netherlands

Keywords: STABLE BOUNDARY LAYERS, SNOW, SMALL SCALE PROCESSES, PARAMETERIZATIONS, WRF

INTRODUCTION

The evolution of the stable boundary layer (SBL) is strongly determined by turbulent mixing, the coupling between the atmosphere and the surface, and radiative effects. Additionally, the presence of clouds or fog, subsidence, geostrophic wind speed, advection, gravity waves, and drainage and katabatic flows may play a role (Holtslag et al, 2013). The reason why SBL modelling remains complex, could be related to the large amount of relatively small-scale processes which may act simultaneously and interactively, while on top of that the physical processes and their interactions are not completely understood and are represented incompletely in models.

Furthermore, a large variety of SBL types exists, e.g. there can be continuous or intermittent turbulence, or even laminar flow, which influences the SBL depth and the vertical and horizontal exchanges of quantities. A relatively coarse resolution (e.g. in operational models) can also hamper proper SBL modelling. Especially over snow-covered polar surfaces where atmospheric conditions can become very stable, modelling the SBL is challenging. For example, in the Arctic and Antarctic, many global and regional climate model outputs diverge from one another, as well as from observations. Though simplified model representation of SBL processes may not be the only cause of these model biases, we will focus on the SBL processes in this paper.

Single-column models (SCMs) are convenient to evaluate the physical processes in the boundary layer and can thus be used to improve the understanding of SBL processes (e.g., Bosveld et al., 2014). Therefore in this study the SCM version of the Weather Research and Forecasting (WRF) mesoscale meteorological model is evaluated for stable conditions over snow-covered surfaces. To evaluate the model performance against observations, the SCM needs to be driven by realistic forcings of the 3D atmospheric field. A complete observational dataset at high temporal resolutions is typically not always available, e.g. due to a low temporal data coverage, possible equipment failure with low temperatures, and measurement stations that may be limited spatially and not measure all required quantities. A full 3D model may be used to determine the SCM large-scale forcings, which is also advantageous since some aspects of the forcings are difficult to measure. As such we perform WRF-3D runs to determine the forcings (Sterk et al, 2015a).

We have evaluated the model for clear-sky stable conditions with approximately the same low wind speeds for 3 contrasting terrains with snow, i.e. for the Cabauw site in the Netherlands, the Sodankylä site in northern Finland and the Halley station on Antarctica (Sterk et al, 2015a). These sites are characterized by snow over grass/crop-land, snow in an evergreen needle-leaf forest, and snow on an ice sheet respectively. Here we focus on the results for the case selected at the Sodankylä site with relatively low wind speeds.

OBSERVATIONS AND CASE SET UP

The case study shown here is built on observations from the Arctic Research Centre of the Finnish Meteorological Institute (FMI-ARC) located at Sodankylä in northern Finland (67:36N; 26:63E). The area is fairly flat at, though the land use is rather heterogeneous with coniferous and deciduous forests (49%) alongside more open areas of peat bogs and shrub lands and a river close by.
A 48-m-high micro-meteorological mast in a Scots pine forest, having a moderate density of trees 10 -12 m tall, measured temperature and relative humidity at the heights of 3, 8, 18, 32 and 48 m, and wind speed at the heights of 18, 30, 38 and 47 m. An automatic weather station (AWS) in a more open land located some 500 m from the weather mast provided data on air temperature and relative humidity at the height of 2 m, wind speed and direction at 10 m, as well as surface pressure. Comparing data from the two sites for the study period, the air temperatures at 2 and 3 m heights typically agreed within 0.5 K, and the wind speeds at 10 and 18 m within 0.2 m/s. Furthermore, soundings were launched twice a day (0 and 12UTC) at the AWS site, and provided additional data on temperature, relative humidity, wind speed and direction in the vertical direction. Also the surface radiation fluxes (at the AWS site) and sonic anemometer based turbulent fluxes (at the mast) were measured.

The case study covered the night of 26 - 27 March 2009 when a low pressure system was located east of Finland, as well as just north of the British isles with a weak pressure gradient over Finland resulting in weak wind speeds. Cloud free conditions were observed with very low wind speeds of 0 - 1.5 m/s at the 10-m level (so somewhat intermittent), and between 0 and 2.7 m/s at 47 m at the top of the mast. The wind direction was mostly from the north to north-west. The 2 meter temperature dropped from 269 K during the day on 26 March to 243 K at the end of the night on 27 March, while for the 48 m height this was 267.5 K during the day which dropped to just over 252 K at night. Therefore during the night a temperature inversion of over 9 K was reached between 2 and 48 m.
The observed snow depth was 62 cm. The snow heat flux G was determined with $G = -\lambda \, dT/dz$ where we took the difference in temperature from the snow skin temperature determined from the long wave radiation components, and the observed temperature at 60 cm snow depth above the soil (2 cm below the snow-atmosphere interface). For the conductivity the value 0.084 W/m/K for snow with a density of 200 kg/m3 was used following Stull (1988).

MODEL DESCRIPTIONS

To evaluate the WRF single-column model , the full 3D model provided meteorological fields for the initial input files, and the time dependent advective forcings (Sterk et al, 2015a). For the 3D runs, the parameterization schemes were selected following the operational Antarctic Mesoscale Prediction System. The BL physics were represented with the Mellor-Yamada-Janjic local, 1.5 order scheme (MYJ), for which the eddy diffusivities are determined utilizing the turbulent kinetic energy equation. The MYJ-BL scheme runs in conjunction with the Eta-similarity surface-layer scheme. For the long wave and short wave radiation the Rapid Radiative Transfer Model for GCMs and Goddard scheme were used respectively. For the micro-physics, the WSM 5-class scheme was employed, while for the cumulus parameterization the Kain-Fritsch scheme was used. Finally, the 4-layer Noah land-surface model (LSM) was applied. Considering that the thermal coupling is relatively important in the SBL for calm wind regimes (e.g. Sterk et al., 2013), the surface characteristics are captured as accurately as possible.

The WRF-SCM is based on the WRF-3D model and uses the same physics and dynamics. A vertically stretched coordinate was used for the vertical levels, but now 200 levels were applied, again with the highest resolution close to the surface, up to the model top at approximately 12 km. We performed runs with similar physics as in WRF-3D, but did additional runs with different BL and long wave radiation schemes to test which scheme is more appropriate for the SBL modelling in the different case studies. In addition to the MYJ-BL scheme, we applied the YSU-BL scheme, which is a first-order scheme for which the eddy diffusivities in stable conditions are described with a profile on basis of a

diagnostic boundary layer depth. The YSU-BL scheme runs in conjunction with the MM5 surface-layer scheme. For references to the physical packages used we refer to Sterk et al (2015a).

METHODOLOGY

This study emphasizes the evaluation of the WRF-SCM over a snow-covered surface for stable conditions. To compare SCM results with observations, we needed realistic input for the SCM. Studies often use a blend of observations and 3D model output to make an independent estimate of the required forcings (Baas et al., 2010; Bosveld et al., 2014a). Complete measurements to retrieve the atmospheric state are not always available, and therefore we test whether the available set of WRF-3D fields provide reasonable forcings. Hence we will also evaluate one WRF-3D run. Regarding the SCM runs, we performed a run without lateral forcings (set A). Next, we repeated the SCM runs where first only the geostrophic wind speed (Ug) changed in time (set B), secondly where advection of momentum was added to the forcings in set B (set C), and thirdly advection of potential temperature θ and specific humidity q was included in addition to set C (set D). Furthermore, SCM runs were performed where a form of data-assimilation was applied above the BL height (set E). All time varying parameters were updated every hour.

RESULTS

The WRF-3D model was started at 0 UTC on the 26th of March, 2009. The 3D run performed very well for the first few hours (after the 12h spin-up period) regarding T_{2m} and $U_{tot\ 10m}$ (Figure 1), but it remained too warm when the sun sets. At this time also the observed 10 meter wind speed vanished which was not captured by WRF-3D, though the modelled wind speed was mostly below 1.7 m/s. Compared with sounding observations at 0UTC on the 27th of March (6h into the SCM simulation), near surface temperatures remained too high, with strongest biases close to the surface, and temperatures above 60 m were too low. This underlines that the stratification was not strong enough. The LLJ was modelled at about the correct height at 6h and with only a slightly lower magnitude, later the LLJ was located a bit too high with slightly stronger wind speeds than observed. WRF-3D followed the sounding data above 100 m nicely for wind speed and was in good agreement with the tower data, though it missed the observed vanished winds at the lowest tower level.

The warm bias during night time could be partly explained by the overestimated specific humidity q (Figures 1 and 2). Though q was also overestimated before night time, the bias increased somewhat during the night. This also resulted in an overestimation of downward long-wave radiation at the end of the SCM study period. This overestimation can also be related to low clouds that were modelled for the lowest model levels for 20 - 23 UTC, and 2 UTC the next day. For other time steps the cloud fraction was 0 or below a fraction of 0.1, but also for clear-sky conditions the downward long-wave radiation was overestimated, making it unlikely that these clouds are the main contributor for this.

The WRF-SCM results are presented for the Sodankylä case for sets A-E and the runs with different BL and radiation schemes (Figures 1 and 2). All runs are with the snow depth as observed, 200 vertical levels, - and an improved representation of the surface characteristics. The period of interest was from 18UTC on the 26th of March 2009, which was the first hour after sunset, until 3 UTC (27h) the next day which was just before sunrise. During this time stable conditions were observed along the tower.

The 2-m temperature modelled with the WRF-SCM improved compared to WRF-3D with a few K depending on the forcings, resulting in a stronger gradient. Differences between sets A-D were small close to the surface, though higher up in the temperature profile slightly lower temperatures (about 0.7 K at 60 m) were found for set D compared to sets A-C. Even better 2-m temperatures were obtained with set E, however, an artificial inversion below the threshold height of 300 m is present. For wind again differences close to the surface were small (Figure 1a), though now large differences between the sets were found at higher levels (Figure 1e, 2b).

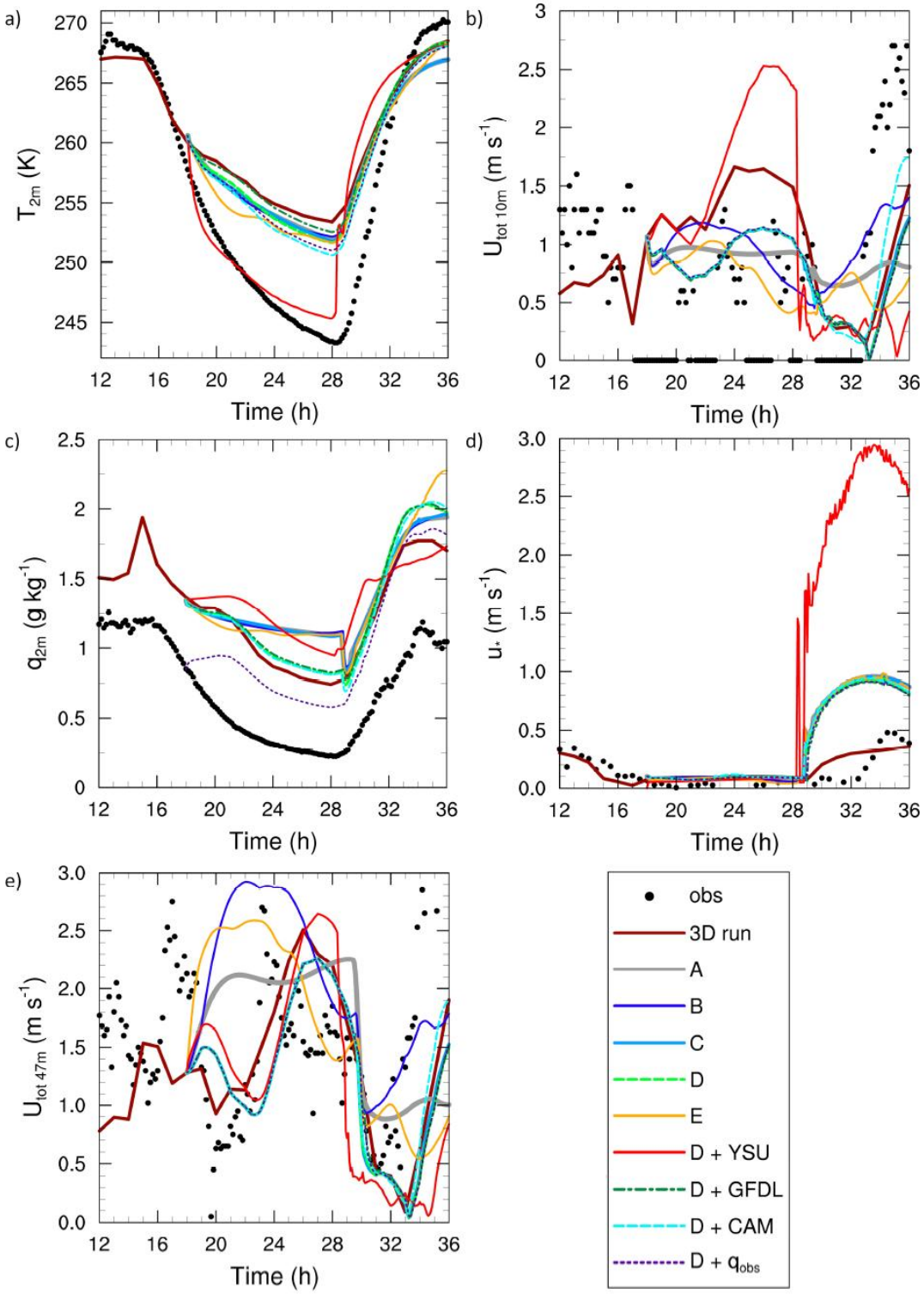

Figure 1: Time series for the Sodankylä case for a) 2 m temperature T_{2m} (K), b) 10 m wind speed $U_{tot\ 10m}$ (in m/s), c) 2 m specific humidity q_{2m} (g/kg), d) friction velocity u_* (m/s), and e) 47 m wind speed $U_{tot\ 47m}$ (m/s). Time series are given for the observations (obs), the WRF-3D run (3D run), the WRF-SCM simulations for the different forcing methods (set A-E), the WRF-SCM simulation with initial specific humidity profile based on observations (D + qobs), WRF-SCM with YSU-BL scheme (D + YSU), and with various LW radiation schemes (D + GFDL, and D + CAM).

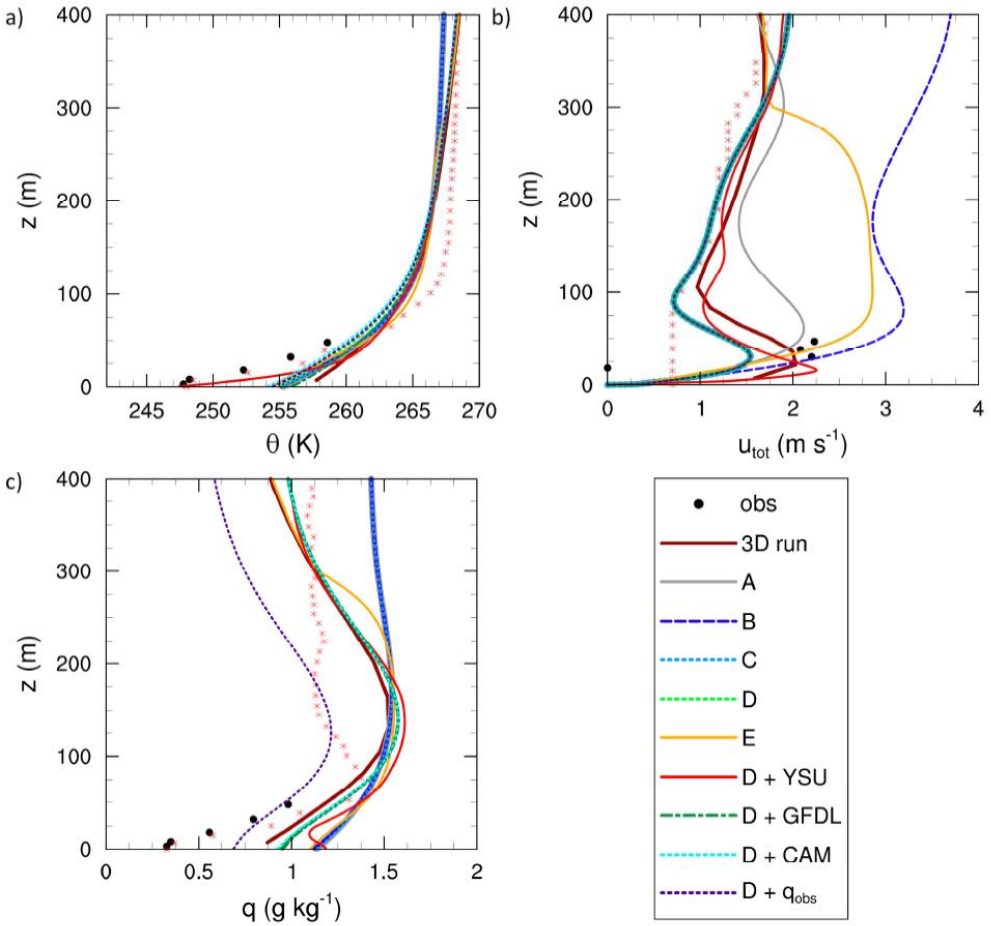

Figure 2: Vertical profiles for the Sodankylä case at 0UTC, 6h into the WRF-SCM simulation when sounding data was available, for a) the potential temperature θ (K), b) the total wind speed U_{tot} (m/s), and c) the specific humidity q (g/kg). (For an explanation of the legend, see Figure 1, sounding data is indicated with the red asterisks.)

Regarding the profiles in Figure 2b at 0UTC, results from sets C-D were in better agreement with the sounding data compared to sets A-B. At least between 100 and 400 m the biases between set C-D and observations were within 0.25 m/s, while this was up to1.2 m/s for set A, and up to even 2.5 m/s for set B, supporting that prescribing proper momentum advection was necessary. At this particular time, sets C-D underestimate the higher level tower data compared to the other sets, though the general bias over 9h at 47 m decreases somewhat and indeed a better agreement with the tower data for sets C-D is seen at other times (not shown).

To evaluate the model skills for higher level wind speeds, the 47 m wind speed ($U_{tot\ 47m}$) time series are shown in Figure 1e. This figure also indicates that prescribing momentum advection was beneficial for the WRF-SCM simulation, especially for the first hours of the simulation, which already followed from the decreased biases between model runs and observations at 47 m (not shown). Runs were repeated with the revised YSU-BL scheme with changing geostrophic wind and advection for all variables and this resulted in reduced biases for the 2-m temperature. The runs with set D were also repeated with 2 different long-wave radiation schemes (D + GFDL and D + CAM). With the latter schemes higher and lower temperatures were obtained, respectively (as compared with the RRTMG LW radiation scheme).

CONCLUSIONS

Many numerical weather prediction and climate models experience difficulties with simulating stratified conditions, especially over snow and when low wind speeds are observed (e.g. Holtslag et al., 2013). In this study, the WRF-3D and SCM, employed with the MYJ and YSU boundary-layer schemes, are evaluated for these conditions with snow over a needle-leaf forest at Sodankylä in Northern Finland. Overall the performance of 3D WRF was quite good, especially regarding the wind speed simulations. Close to the surface, wind speeds were modelled with a very small overestimation. Modelling the near surface temperature appeared to be (more) challenging. T_{2m} was strongly overestimated up to 11 K at the end of the night, while the model performed better at higher altitude. For the Single Column Model (SCM) study we found that runs without lateral forcings and constant geostrophic wind speeds, lead to a substantial bias for wind speed. Prescribing momentum advection improved the modelled wind speed substantially, while model results for temperature, stratification and specific humidity improved considerably with set D. The nudging approach provided a deterioration of the model results and is therefore not advised. Hence, we conclude that prescribing time-varying geostrophic wind speed and momentum, temperature and humidity advection provides the best results.
Though a perfect match between the model simulations and the observations has not been obtained, significant improvements were made with the right forcings. From this reference, the SCM can be used as a tool to study the small scale processes in SBL modelling to improve our understanding of the SBL processes. In Sterk et al (2015b) we perform a sensitivity analysis with the WRF-SCM, where we focus on the processes of snow-surface coupling, radiation and turbulent mixing for Sodankylä, as well as Cabauw and Halley for different surface characteristics.

ACKNOWLEDGEMENTS

This paper is a summary of one particular case study given by Sterk et al (2015). We thank the Finnish Meteorological Institute for the data that was used in this study and Timo Vihma for his contributions. This study was supported by NWO grant 829.09.005 (Quantifying contributions of surface climate feedbacks to the Arctic amplification of greenhouse warming in the Sustainable Earth program).

REFERENCES

Baas P, Bosveld FC, Lenderink G, van Meijgaard E, Holtslag AAM, 2010: How to design single column model experiments for comparison with observed nocturnal low-level jets? *Quart. J. Roy. Meteor. Soc.*, 136, 671–684

Bosveld FC, Baas P, Steeneveld GJ, Holtslag AAM, Angevine WM, Bazile E, de Bruijn EIF, Deacu D, Edwards JM, Ek M, Larson VE, Plein JE, Raschendorfer M, Svensson G. 2014. *The Third GABLS Intercomparison Case for Evaluation Studies of Boundary-Layer Models: Part B: Results and Process Understanding.* Boundary Layer Meteorol. 152, 157-187.

Holtslag AAM, Svensson G, Baas P, Basu S, Beare B, Beljaars ACM, Bosveld FC, Cuxart J, Lindvall J, Steeneveld GJ, Tjernstrom M, Van De Wiel BJH. 2013. *Stable Atmospheric Boundary Layers and Diurnal Cycles - Challenges for Weather and Climate Models.* Bull. Amer. Meteor. Soc., 94, 1691-1706.

Sterk HAM, Steeneveld GJ, Holtslag AAM. 2013. The role of snow-surface coupling, radiation, and turbulent mixing in modeling a stable boundary layer over Arctic sea ice. J. Geophys. Res. Atmos.118., 1199–1217

Sterk H.A.M, Steeneveld GJ, Vihma, T, Anderson, PS, Bosveld FC, Holtslag AAM. 2015a. *Clear sky stable boundary layers with low winds over snow covered surfaces – Part I: A WRF model evaluation.* Quart. J. Roy. Meteorol. Soc., in press. doi: 10.1002/qj.2513.

Sterk HAM, Steeneveld GJ, Vihma, T, Anderson, PS, Bosveld FC, Holtslag AAM. 2015b. *Clear sky stable boundary layers with low winds over snow covered surfaces – Part II: Process Sensitivity.* QJMRS (under review).

Stull RB, 1988: *An Introduction to Boundary-layer Meteorology*, Kluwer Academic Publishers, Dordrecht, 666 pp.

SENSITIVITY OF REGIONAL EUROPEAN BOREAL CLIMATE TO CHANGES IN SURFACE PROPERTIES RESULTING FROM STRUCTURAL VEGETATION PERTURBATIONS

J.H. RYDSAA, F. STORDAL and L.M. TALLAKSEN

Department of Geosciences, University of Oslo, Norway.

Keywords: Shifting vegetation zones; Structural changes in the ecosystems; Impacts on the atmosphere.

INTRODUCTION

Amplified warming at high latitudes over the past decades has led to changes in the boreal and Arctic climate system, such as structural changes in high latitude ecosystems and soil moisture properties. These changes trigger land-atmosphere feedbacks, through altered energy partitioning in response to changes in albedo and surface water fluxes. Local scale changes in the Arctic and boreal zone may propagate to affect large scale climatic features.

METHODS

In this study the Weather Research and Forecasting model (Skamarock and Klemp, 2008) and Noah LSM (Tewari et al., 2004) is run in a sensitivity experiment to simulate the influence of structural vegetation changes on the atmosphere over a Northern European boreal ecosystem. MODIS IGBP modified 21 class land surface data is used. This dataset is available with the standard WRF package download. The dataset is based on the original 1 km resolution MODIS IGBP vegetation map (Friedl et al., 2010), but excludes permanent wetland and has three tundra classes and lakes added by the Land Team at EMC/NCEP. To represent high latitude and altitude ecosystems more accurately, the vegetation category of open shrub land has been replaced by various tundra vegetation classes at high northern latitudes in a modified dataset. The goal of the setup of the sensitivity experiment is to represent a northward migration of boreal ecosystems based on observed and anticipated features in vegetation migration patterns. Experiments are designed to induce atmospheric response and feedback mechanisms, while keeping perturbation complexity low enough to be able to identify the respective response mechanisms. The aim has been to induce moderate and realistic scale changes, representative of actual vegetation shifts on a century long timescale. The changes which are introduced in the sensitivity experiment are shown in Figure 1 and are based on 10 years simulations of the sensitivity as well as a control experiment.

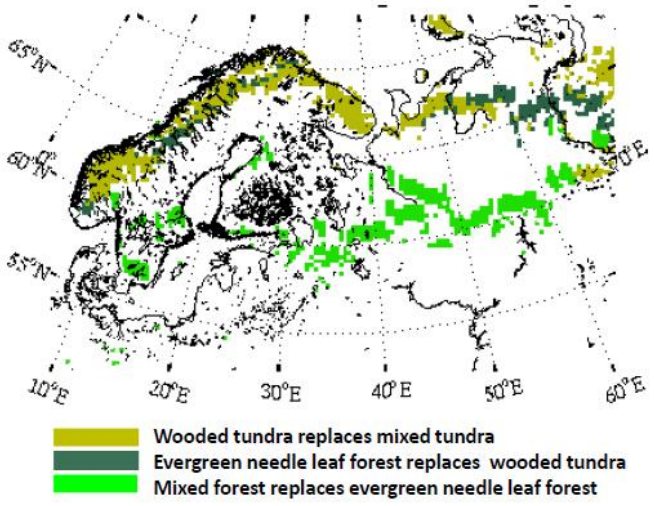

Figure 1. Changes in dominant vegetation category as compared to control simulation

RESULTS AND CONCLUSIONS

Emphasis is placed on surface energy partitioning and near surface atmospheric variables (Figure 2), in order to investigate changes in atmospheric response due to observed and anticipated structural vegetation changes.

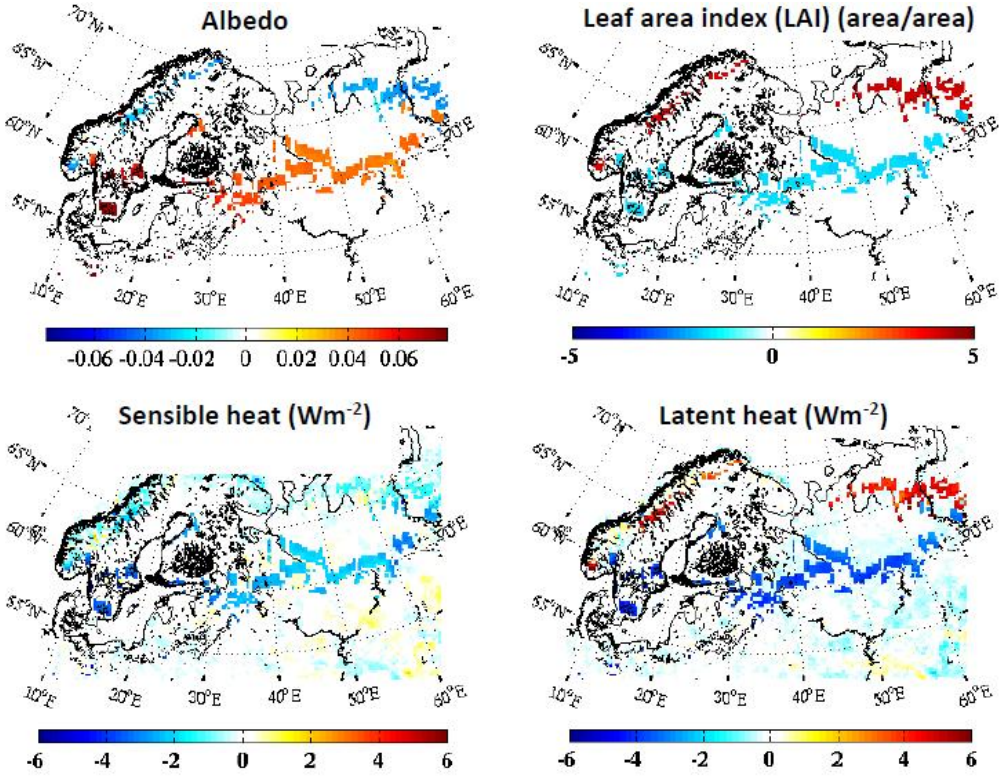

Figure 1. Changes in surface albedo, leaf area index, surface sensible heat flux (10 year average) and latent heat flux (10 year average), as compared to control simulation.

We find that a northward migration of evergreen needle leaf forest into tundra regions causes an increase in latent rather than sensible heat fluxes, increased near surface temperatures and boundary layer height. Shrub expansion in tundra areas has only small effects on surface fluxes. However, it influences near surface wind speeds and boundary layer height. Northward migration of mixed forest across the present southern border of the boreal forest has largely opposite effects on surface fluxes and the near surface atmosphere, and acts to moderate the overall mean regional effects of boreal forest migration on the near surface atmosphere.

REFERENCES

Friedl, M. A., Sulla-Menashe, D., Tan, B., Schneider, A., Ramankutty, N., Sibley, A., and 1 Huang, X. (2010). MODIS Collection global land cover: Algorithm refinements and characterization of new datasets, *Remote Sens Environ*, 114, 168-182, http://dx.doi.org/10.1016/j.rse.2009.08.016.

Skamarock, W. C., and Klemp, J. B. (2008) A time-split nonhydrostatic atmospheric model for weather research and forecasting applications, *J Comput Phys*, 227, 3465-3485, DOI 10.1016/j.jcp.2007.01.037.

Tewari, M., Chen, F., Wang, W., Dudhia, J., LeMone, M. A., Mitchell, K., Ek, M., Gayno, G., 1Wegiel, J., and Cuenca, R. H. (2004). Implementation and verification of the unified NOAH land surface model in the WRF model, 20th conference on weather analysis and forecasting/16th conference on numerical weather prediction.

SOIL HONO EMISSION AND ITS POTENTIAL IMPACT ON THE ATMOSPHERIC CHEMISTRY AND NITROGEN CYCLE

H. SU, Y. CHENG and U. PÖSCHL

Max Planck Institute for Chemistry, Multiphase Chemistry Department,
Mainz, 55128, Germany.

Keywords: HONO, NITROGEN CYCLE, OH RADICAL, SOIL.

Hydroxyl radicals (OH) are a key species in atmospheric photochemistry. In the lower atmosphere, up to ~30% of the primary OH radical production is attributed to the photolysis of nitrous acid (HONO), and field observations suggest a large missing source of HONO. The dominant sources of N(III) in soil, however, are biological nitrification and denitrification processes, which produce nitrite ions from ammonium (by nitrifying microbes) as well as from nitrate (by denitrifying microbes). We show that soil nitrite can release HONO and explain the reported strength and diurnal variation of the missing source. The HONO emissions rates are estimated to be comparable to that of nitric oxide (NO) and could be an important source of atmospheric reactive nitrogen. Fertilized soils appear to be particularly strong sources of HONO. Thus, agricultural activities and land-use changes may strongly influence the oxidizing capacity of the atmosphere. A new HONO-DNDC model was developed to simulate the evolution of HONO emissions in agriculture ecosystems. Because of the widespread occurrence of nitrite-producing microbes and increasing N and acid deposition, the release of HONO from soil may also be important in natural environments, including forests and boreal regions.

ACKNOWLEDGEMENTS

This work was supported by the Max Planck Society (MPG), the European Commission under the projects EUCAARI (No 036833-2) and PEGASOS (No 265148).

REFERENCES

Su, H., Cheng, Y., Oswald, R., Behrendt, T., Trebs, I., Meixner, F. X., Andreae, M. O., Cheng, P., Zhang, Y., and Pöschl, U. (2011). Soil Nitrite as a Source of Atmospheric HONO and OH Radicals, *Science*, 333, 1616-1618.

Oswald, R., Behrendt, T., Ermel, M., Wu, D., Su, H., Cheng, Y., Breuninger, C., Moravek, A., Mougin, E., Delon, C., Loubet, B., Pommerening-Röser, A., Sörgel, M., Pöschl, U., Hoffmann, T., Andreae, M. O., Meixner, F. X., and Trebs, I. (2013). HONO Emissions from Soil Bacteria as a Major Source of Atmospheric Reactive Nitrogen, *Science*, 341, 1233-1235.

AEROSOL CONTRIBUTION TO THE DECADAL CHANGES IN OBSERVED CLEAR-SKY SHORTWAVE RADIATIVE FLUXES OVER PAN-EURASIA

A.-M. SUNDSTRÖM[1], A. AROLA[2], E. HYER[3], G. DE LEEUW[1,4] and M. KULMALA[1]

[1]Department of physics, University of Helsinki, Helsinki, Finland.

[2] Finnish Meteorological Institute, Kuopio, Finland.

[3]Naval Research Institute, Monterrey, CA,US.

[4]Finnish Meteorological Institute, Helsinki, Finland

Keywords: Remote sensing, aerosol optical depth, shortwave radiative flux, aerosol direct radiative effect.

INTRODUCTION

Aerosols influence the radiative budget of the Earth-atmosphere system directly by scattering and absorbing solar and thermal radiation, and indirectly through various cloud microphysical and dynamical processes (Lohmann *et al*., 2005, Bister and Kulmala 2011), as well as by changing snow and ice albedo (Hansen *et al.,* 2004). In this work decadal changes in the observed shortwave (SW) clear-sky top of the atmosphere (TOA) fluxes are studied over the Pan-Eurasian area using satellite data. More specifically, the aim is to estimate aerosol particles' contribution to the observed SW TOA flux changes. To asses this, also changes in the satellite-based aerosol optical depth (AOD) are analyzed.

There are also other factors than aerosol particles that can cause changes in SW TOA fluxes. These factors could be changes in snow/ice cover and albedo, changes in snow-free surface albedo, and changes in the atmospheric precipitable water content. In fact, most probably the observed TOA flux changes are joint effects of several above-mentioned factors. In this work only snow- and ice-free areas/seasons are considered, but the changes in surface albedo and precipitable water content are analysed with the AOD.

DATA AND METHODS

Ten years (Jan. 2002- Dec. 2011) of global satellite data are used in this study from three different instruments. The shortwave radiative flux observations at TOA are obtained from the Clouds and the Earth's Radiant Energy System (CERES) onboard the EOS Terra satellite platform. The CERES instrument provides radiance measurements converted into TOA fluxes in the shortwave (0.3-5.0 μm), infrared window (8.0-12.0 μm) and total (8.0-200 μm) broadband channels. The AOD observations are obtained from Moderate Resolution Imaging Spectroradiometer (MODIS) and Multi-angle Imaging Spectroradiometer (MISR), that both are also onboard the Terra satellite. In addition, surface albedo data from MODIS and atmospheric precipitable water content from a model are used (Table 1.).

Parameter	Instrument/model	Dataset name
SW TOA flux	CERES (Terra satellite)	SSF-1 deg. month lite
AOD	MODIS & MISR (Terra satellite)	MODIS data assimilation L3 AOD, MISR L3 monthly AOD
Precip. water	GMAO (model)	G5-CERES
Surface albedo	MODIS (Terra & Aqua satellite combined)	MCD43C3

Table 1. Description of the data that have been used in this study. The study period is Jan. 2002- Dec. 2011.

To identify the areas where aerosols potentially could have an effect on changed SW TOA fluxes, AOD anomalies in a 1x1deg. grid are defined from both MODIS L3 data assimilation product and MISR L3 data. The anomalies are calculated using three-year seasonal averages (DJF, MAM, JJA, and SON) for 2009-2011 and 2002-2004, e.g. the AOD anomaly is defined as

$$\Delta AOD = AOD^{season}_{2009-2011} - AOD^{season}_{2002-2004}$$

Only those 1x1 deg. grid cells are included in the study where AOD data for each month are available from both MODIS and MISR. And further, after defining seasonal AOD anomalies from both instruments, only those grid cells are selected where both MODIS and MISR show similar (positive or negative) AOD anomaly. After selecting the grid cells based on the AOD anomalies, seasonal anomalies for the SW TOA flux, surface albedo, and precipitable water content are defined.

The changes in SW TOA fluxes are also modelled using LibRadtran radiative transfer software (Mayer and Kylling 2005) in order to see how much the observed changes in aod, surface albedo, and precipitable water could potentially affect the TOA flux anomaly. Since information about aerosol type was not available, the simulations are carried out using scattering type (single scattering albedo SSA=0.97 at 500 nm) and absorbing type (SSA=0.8) aerosols.

CONCLUSIONS

Results show that the most notable decreases in AOD within the Pan-Eurasian region are observed over Southern Europe and the Mediterranean area, as well as over South Eastern Russia and North Eastern China, including Beijing, during summer (JJA) (Figure 1.). As is seen, over the major parts of these areas the decrease in AOD is connected to weaker SW radiative cooling at TOA. A closer investigation over these areas reveals that the main contributing factor to the decreased SW cooling at TOA during summer is in fact aerosols, since there are no notable changes in the surface albedo or precipitable water content. On the other hand, an increase in AOD during summer is seen over an area extending from Middle East to Kazakhstan. Over that region also SW radiative cooling at TOA has increased. The results show, however, that the stronger cooling is not only due to aerosols, but also due to increased surface albedo.

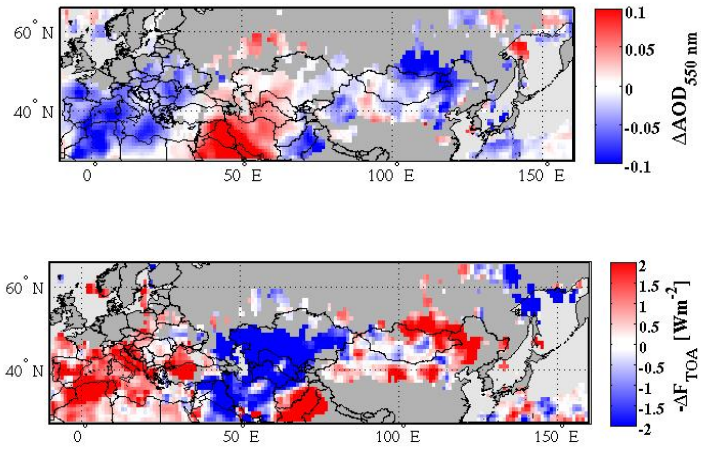

Figure 1. AOD (upper panel) and SW TOA flux (lower panel) anomalies for the summer season (JJA). The flux anomalies are coloured so that increased outgoing SW radiation at TOA is denoted with blue (more cooling), and decreased SW radiation at TOA with red (less cooling).

ACKNOWLEDGEMENTS

This research was supported by the Academy of Finland Center of Excellence program (project number 272041).

REFERENCES

Bister, M., and M. Kulmala (2011). Anthropogenic aerosols may have increased upper tropospheric humidity in the 20th century, *Atmos. Chem. Phys.*, 11, 4577-4586.

Hansen, J., and L. Nazarenko (2004). Soot climate forcing via snow and ice albedos, *Proc. Natl. Acad. Sci. USA*, 101, 423-428.

Lohmann, U., and J. Feichter (2005). Global indirect aerosol effects: a review, *Atmos. Chem. Phys*, 5, 715-737.

Mayer, B., and A. Kylling (2005).Technical note: The libRadtran software package for radiative transfer calculations- description and examples of use, *Atmos. Chem. Phys*, 5, 1855-1877.

SOOT ON SNOW EXPERIMENTS: LIGHT-ABSORBING IMPURITIES EFFECT ON THE NATURAL SNOWPACK

J. SVENSSON[1,2], A. VIRKKULA[1,3], O. MEINANDER[1], N. KIVEKÄS[1,5], H.-R. HANNULA[4], A. HEIKKILÄ[1], A. KONTU[4], A.-P. HYVÄRINEN[1], O. JÄRVINEN[3], K. NEITOLA[1], D. BRUS[1], P. DAGSSON-WALDHAUSEROVA[6,7], K. ANTILA[1,8], J. PELTONIEMI[3,8], M. GRITSEVICH[8,3], T. HAKALA[8], H. KAARTINEN[8], G. DE LEEUW[1,3], and H. LIHAVAINEN[1]

[1]Finnish Meteorological Institute, Helsinki, Finland
[2]Department of Environmental Sciences, University of Helsinki, Helsinki, Finland
[3]Department of Physics, University of Helsinki, Helsinki, Finland
[4]Arctic Research Center, Finnish Meteorological Institute, Sodankylä, Finland
[5]Department of Physics, Lund University, Lund, Sweden
[6]Faculty of Environment, Agricultural University of Iceland, Hvanneyri, Iceland
[7]Department of Physics, University of Iceland, Iceland
[8]Finnish Geodetic Institute, Masala, Finland

Keywords: Black Carbon, Snow, Albedo.

INTRODUCTION

Snow play an important part in Earth's radiative energy balance. With its high albedo (for fresh snow it is typically 0.7-0.9) it reflects much of the incoming light. The albedo of the snow is modified by many parameters, including the snow's physical properties (e.g. snow grain size and thickness) and the wavelength of incoming solar radiation. Additionally, the presence of light-absorbing impurities in the snow can also have an effect on albedo and consequent snow melt (e.g. Clarke and Noone, 1985; Warren and Wiscombe, 1980). Soot particles, containing black carbon (BC) and organics, is a light-absorbing aerosol that is produced by the incomplete combustion of fossil and bio fuels. Soot on snow has been suggested to be responsible for a much as a quarter of the observed warming in the Arctic (Hansen and Nazarenko, 2004).

With limited experimental work done on soot's effect on snow, the Finnish Meteorological Institute (FMI) in cooperation with University of Helsinki Physics department, Finnish Geodetic Institute, and Agricultural University of Iceland organized a series of experiments to study these effects. A set of experiments were conducted in different regions of Finland, on natural snowpack's, with soot deposited in a controlled way. After soot deposition our objective was to study the soot's effect on albedo and the snow physical characteristics throughout the entire melting season. Some of our measured experimental data were thereafter compared with the SNICAR model (Flanner et al., 2007).

METHODS

The first experiment (SoS2011) was conducted at a private farming field in Nurmijärvi, southern Finland, March – April 2011. The second experiment (SoS2012) was conducted at the FMI observatory in Jokioinen, southern Finland, February – March 2012. The third experiment (SoS2013) was conducted at the Sodankylä airfield near the FMI Sodankylä observatory, Finnish Lapland, April – May 2013.

Soot was deposited with different methods onto the snow surface in the experiments. In SoS2011 soot particles were produced by burning various organic materials (wood and rubber pellets from used tires) in a wood-burning stove. The smoke was lead through a pipe, cooled by snow surrounding the pipe, and lead into a rectangular chamber situated on top of the snow. A different approach to deposit the soot was taken in SoS2012 and SoS2013. Soot was acquired beforehand from a chimney-sweeping company in Helsinki, which collected the soot from residential buildings with small-scale wood burning. The soot was blown

into in-house made cylindrical chamber (diameter of 4 m) carefully installed on top of the snow. The blowing system consisted of a blower, a tube blowing air into a barrel filled with the soot, and a cyclone removing particles larger than about 3 µm.

After soot deposition to the snow, pyranometers were installed at the sites to measure incoming global radiation and reflected radiation. Snow samples were also collected and analyzed for elemental carbon (EC) with a Sunset Labs EC/OC analyzer. Further, the snow physical characteristics were measured (including thickness, hardness, grain shape and size).

RESULTS

The effects of soot on snow were visible in our experiments. The albedo of the soot contaminated snow decreased more compared to the clean reference snow. The physical characteristics of the snowpack also changed when comparing the sooted snow to the clean reference snow.

Our experimental data of albedo and EC concentration is compared to SNICAR simulations in figure 1. A general decrease in albedo with increasing EC concentration is visible, and the SoS data generally agree with the SNICAR model. In more detail, when the model is tuned to a measured effective snow grain radius of 274 µm the results agree the best. With the effective radius modified to 750 µm, which is a hypothetical upper limit of the effective grain radius observed in the experiments, the SNICAR overestimates the albedo reduction compared to our measured SoS data (with the exception of the most contaminated spot from SoS2013). A parameterization was established from the SoS-data, showing the albedo decrease with EC loading on the snow. The black dashed line in figure 1 shows this relationship.

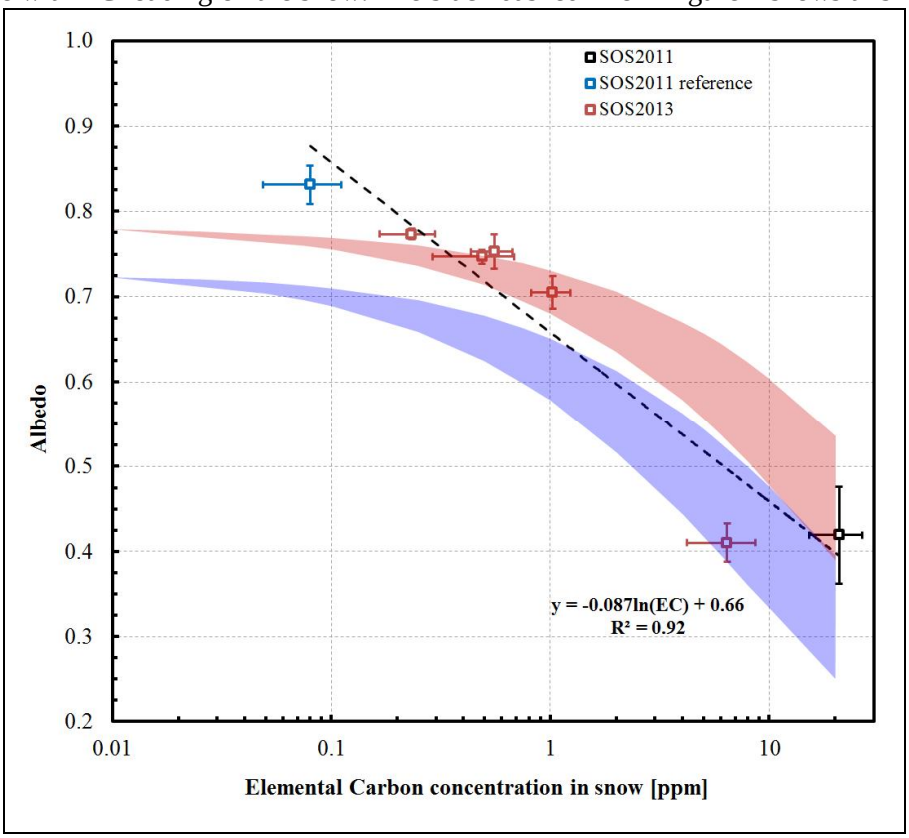

Figure 1. Albedo as a function of EC concentration. Boxes with whiskers represent measurements (Black=Nurmijärvi 2011, Blue=Natural snow Nurmijärvi 2011, Red=Sodankylä 2013. Red shaded band corresponds SNICAR model tuned to a snow grain effective radius of 274 µm, with BC mass absorption cross-section at λ=550 nm of 7.5 m^2 g^{-1} and of 2.25 m^2 g^{-1}, as lower and upper limit, respectively. Blue shaded band corresponds to a snow grain effective radius of 750 µm, with BC mass absorption cross-section at λ=550 nm of 7.5 m^2 g^{-1} and of 2.25 m^2 g^{-1}, as lower and upper limit, respectively. Black dashed line is fitted to all SoS-data points.

CONCLUSIONS

A series of experiments were conducted to further study the effects of BC on the snowpack. Combustion generated soot was deposited onto a natural snowpack, followed by monitoring the albedo and snow physical characteristic throughout spring melt. A clear effect on the albedo and snow melt was visible when soot concentrations of 1000 ppb were used, whereas it was more difficult to attribute the soot's effect when concentrations of 100 ppb were used. Our experimental data generally agreed with the SNICAR model when it was tuned to our measured specific effective snow grain radius. However, when the effective grain radius was simulated to our measured upper estimate, SNICAR seem to overestimate the albedo reduction. Similarly, the SNICAR model failed to simulate the measured high albedo in the undisturbed reference site in SOS2011 and SOS2012.

ACKNOWLEDGEMENTS

The Chimney seeping company (Consti Talotekniikka Oy) is acknowledged for supplying us with the soot. This work has been supported by the EU LIFE+ project MACEB (project no. LIFE09 ENV/FI/000572); the Academy of Finland through the Arctic Absorbing Aerosols and Albedo of Snow (project no. 3162) and the Electromagnetic Wave Scattering in a Complex Random Medium (project no. 260027); the Maj and Tor Nessling Foundation (projects 2012456 and 2013093); and the Nordic research and innovation initiative Cryosphere-Atmosphere Interactions in a Changing Arctic Climate (CRAICC).

REFERENCES

Clarke, A. D. and Noone, K. J. (1985). Soot in the Arctic snowpack: a cause for perturbations in radiative transfer, *Atmos. Environ.*, **19**, 2045–2053.

Flanner, M. G., C. S. Zender, J. T. Randerson, and P. J. Rasch (2007). Present-day climate forcing and response from black carbon in snow, *J. Geophys. Res.*, 112, D11202, doi:10.1029/2006JD008003.

Hansen, J. and Nazarenko, L. (2004). Soot climate forcing via snow and ice albedos, *Proc. Nat. Acad. Sci*., 101, 423–428, 2004.

Warren, S., and W. Wiscombe (1980). A model for the spectral albedo of snow. II: Snow containing atmospheric aerosols, *J. Atmos. Sci.*, 37, 2734– 2745.

MONITORING OF CLIMATE-INFLUENCING ATMOSPHERIC PARAMETERS IN SAINT-PETERSBURG STATE UNIVERSITY (PETERHOF, RUSSIA)

YU.M. TIMOFEYEV, A.V. POBEROVSKY, M.V. MAKAROVA, YA.A. VIROLAINEN, D.V. IONOV, A.V. POLYAKOV, KH. IMHASIN, N.A. ZAITSEV, I.A. FRANTSUSOVA, I. BERESIN, D. ARABADZHAN and S. FOKA

Saint-Petersburg State University, Department of Physics, 1 Ulyanovskaya, Saint-Petersburg-Peterhof, Russia

Keywords: ATMOSPHERIC COMPOSITION, GROUND-BASED FTIR

INTRODUCTION – PETERHOF STATION

Different devices for atmospheric monitoring are situated at the University campus, in a suburb of Saint-Petersburg (~ 35 km from the city center). Geographic coordinates of the Peterhof site are as follows: 59.88°N, 29.83°E, 20m asl. Saint-Petersburg is the 4th largest city in Europe with the population of 5.1 million people. Hence, the possibility of anthropogenic pollution influence should be borne in mind during measurement data processing and the following analysis of retrieval results (total columns (TC) and profiles of gases, aerosol characteristics and etc.). The cases of FTIR observations through polluted air could be identified using data of in situ gas analysers (NOx, O_3, CO, CH_4 and CO_2) which started in 2013. The Saint-Petersburg region suffers from cyclone activity for about 140 days in a year; therefore the number of overcast days is relatively high for the Peterhof station (~ 165 days per year). Numbers of Sun direct radiation measurement days per year for the period of 2009–2014 changed from 128 to 67.

MONITORING INSTRUMENTATION

Measurements of climate-influencing atmospheric parameters in St. Petersburg State University are carried out using various methods (local and remote) and equipments. The main measurement devices, the beginning of regular measurements and the measured parameters are given in Table 1.

Instrument	Model	Date of start	Target parameters
FTIR interferometers	Bruker IFS 125HR	2009	About total column amounts of 20 gases
FTIR interferometers	Bruker IFS 125M	2015	About total column amounts of 20 gases
Spectrometers	OceanOptics, HR4000-UV, HR4000-VIS	2007	O_3 and NO_2 total column amounts
Microwave radiometer	RPG-HATPRO	2013	Humidity and temperature profiles (0-10km), liquid water path and integrated water vapor
Ozone MWsounder		2011	Vertical profiles (25-70 km)
GPS		2013	Integrated water vapour
Sun photometer	CIMEL CE 318-2	2013	Aerosol optical and microphysical characteristics
Ceilometer	Jenoptik CH-15K	2013	Aerosol backscatter coefficient, cloud base height
Lidar		2014	Aerosol attenuation and backscatter coefficient, cloud base height
In situ	Los Gatos Research GGA-24r-EP	2013	CH_4, CO_2, H_2O volume mixing ratios
	Los Gatos Research CO-23r	2013	CO volume mixing ratios
	ThermoScientific 49i	2013	O_3 concentrations
	ThermoScientific 42i-TL	2013	NO_x, (NO, NO_2)

Table 1. Information on instruments and target atmospheric parameters for ground-based atmospheric measurements.

RESULTS

Combined ground-based spectroscopic measurements of atmospheric composition are carried out by various passive methods (using measurements of direct and scattered UV, visible and IR solar radiation, measurements of downwelling MW thermal radiation), and also by means of local sensors. The studied gases, measurement spectral intervals, interfering gases and estimates of random errors of a TC single measurement by Bruker IFS 125HR are given in Table 2.

N	Gas	Spectral interval, cm^{-1}	«Interfering gases»	Errors, %
1	H_2O	1110.00–1113.00, 1117.30–1117.90, 1120.10–1122.00, 1196.00–1200.40, 1220.50–1221.50, 1251.75–1253.00	H_2O (isotopes), N_2O, CO_2, CH_4, O_3, HNO_3	~ 1
2	CH_4	2613.70–2615.40, 2650.60–2651.30, 2835.50–2835.80, 2903.60–2904.03	O_3, CO_2, NO_2	≤ 0.5
3	N_2O	2551.435 2552.400	CH_4, HDO, O_3	~ 1
4	CO	2057.70–2058.00, 2069.56–2069.76 2157.50–2159.15	O_3, CO_2, N_2O, H_2O, OCS	≤ 0.8
5	CO_2	2626.3–2627.0	CH4, HDO	1.0
6	C_2H_6	2976.6–2977.1	CH_4, H_2O, O_3	2.0
7	CFC-11	810–880 $см^{-1}$.	H_2O, CO_2, O_3	~ 13
8	O_3	991.25–993.80, 1001.47–1003.04 1005.00–1006.90, 1007.35–1009.00 1011.15–1013.55,	H_2O, CO_2, C_2H_4, O_3 (изотопы)	– 1.5
9	HCl	2727.73–2727.83, 2775.70–2775.80, 2925.80–2926.0	CH_4, H_2O, O_3, NO_2, N_2O	~ 4
10	HF	4038.0–4039.	CH_4, H_2O	1–2
11	HNO3	867.5–870.1	H_2O, CO_2, OCS	2.0–7.0
12	$ClONO_2$	779.0–779.8, 780.0–780.3, 780.3–781.3	H_2O, CO_2, O_3, HNO_3, C_2H_2	14–24
13	NO_2	2914.6–2914.7	H_2O, CH_4, HDO	8–18

Table 2. Spectral intervals, «interfering» gases, estimates of random errors of a TC single measurement.

Data on ozone and NO_2 TCs are retrieved also from measurements of scattered UV and visible solar radiation by means of DOAS technique.

Measurements of TCs of various gases give a possibility:
- to analyse temporal variations of different scales (from daily to trends);
- to compare results with data of other observation stations including NDACC stations;
- to compare and inter-calibrate measurements performed by different devices;
- to compare measurements with modeling data;
- to validate satellite measurements.

Let us give some examples of obtained results.

TC temporal variations of various gases measured by Fourier spectrometer at Peterhof, and monthly total methane means measured by SIKS-2 and Fourier spectrometer are given in Figure 1, 2, respectively.

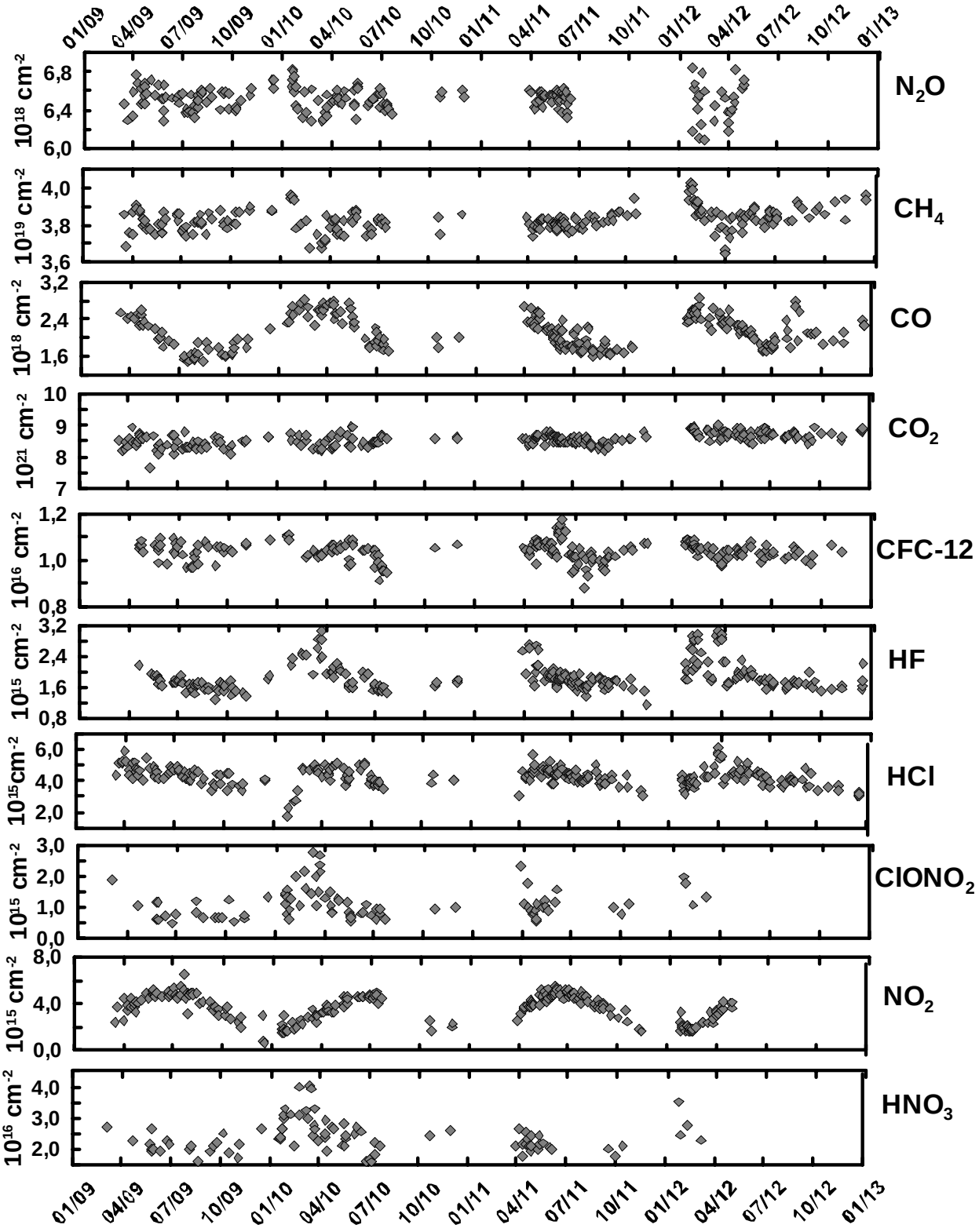

Figure 1. Temporal variations of various gases measured by Bruker IFS 125HR at Peterhof.

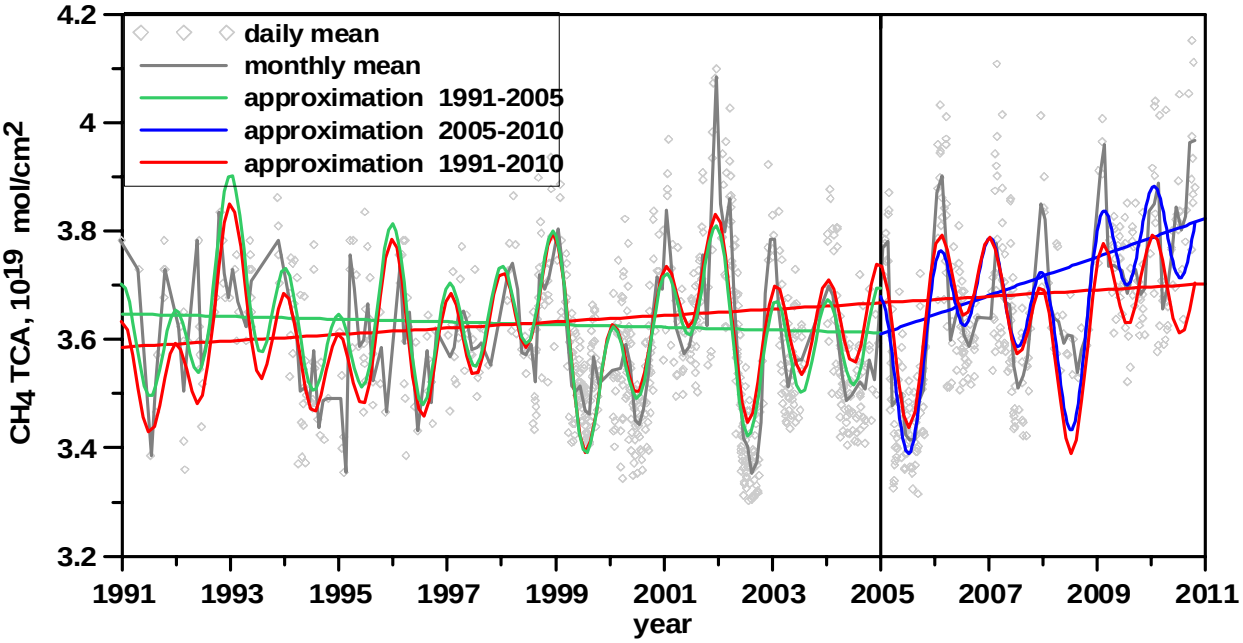

Figure 2. Daily (rhombs) and monthly total methane means measured at Peterhof using SIKS-2 (with middle spectral resolution) and Fourier spectrometer. Lines of linear trend for different observation periods are also given at the Figure.

In our studies much attention is paid to validation of satellite measurements. Examples of comparing ground-based ozone total column measurements with satellite (OMI and GOME-2) data are given in Figure 3. Table 3 demonstrates the statistics of the comparison of ground-based and satellite measurements.

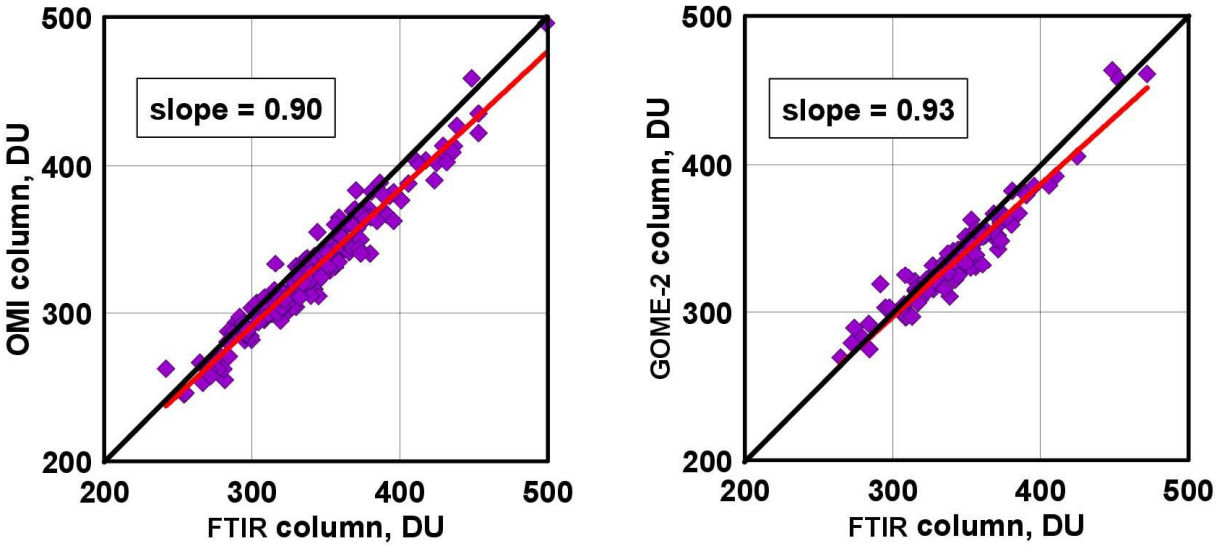

Figure 3. Scatter plot of ozone total columns measured by ground-based FTIR versus observed OMI (TOMS v.8) (left panel) and GOME-2 (DOAS) (right panel).

Devices	Number of days	RMS, %	Mean, %	Standard deviation, %	Correlation coefficient
FTIR–OMI	178	4.5	+ 3.4	2.9	0.98±0.01
FTIR– GOME-2	95	3.7	+ 2.2	3.0	0.97±0.01
FTIR–Dobson	74	3.7	+ 1.4	3.4	0.95±0.01

Table 3. Statistics of comparisons between ground-based and satellite FTIR measurements of the ozone total columns.

Ground-based measurements of direct IR solar radiation with high spectral resolution make it possible to retrieve elements of vertical distributions of different gases. Temporal variations of ozone columns in various atmospheric layers are shown in Figure 4.

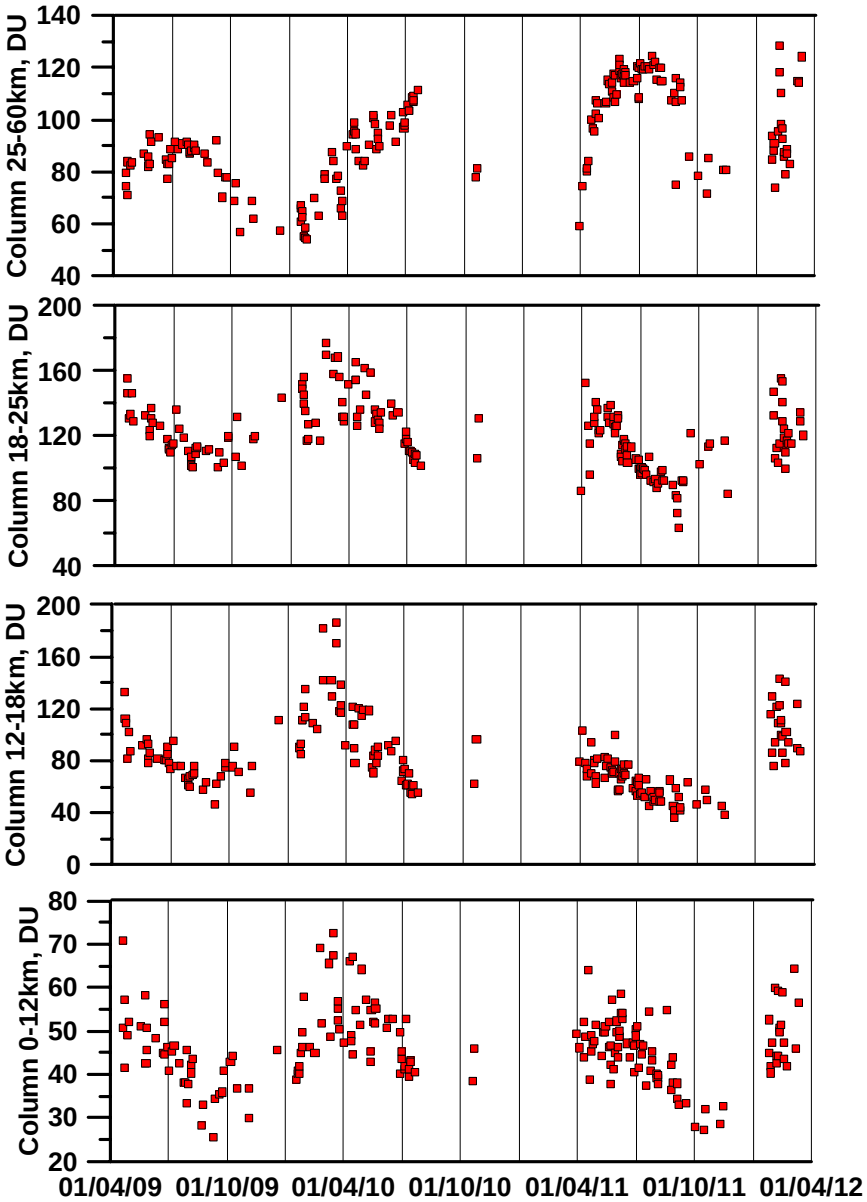

Figure 4. Seasonal behavior of total ozone column in four atmospheric layers from FTIR measurements.

In the field of MW atmospheric sounding, studies of errors of retrieving the temperature and humidity profiles, and also the developing of optimal algorithms for solving the inverse problems were carried out.

In REFERENCES we will bring the list of main publications devoted to various aspects of monitoring the atmospheric parameters in St. Petersburg State University.

ACKNOWLEDGEMENTS

The experimental part of this study was supported by SPSU (grant 11.37.28.2011), and using the devices belonging to the SPBU RC "Geomodel" for ground-based FTIR measurements. The processing and analysis of data were performed with financial support of RSF (grant 14-17-00096).

REFERENCES

Poberovskii A.V. (2010). High-resolution ground measurements of the ir spectra of solar radiation, Atmospheric and Oceanic Optics **23**, 161.

Poberovskii A.V., M.V. Makarova, A.V. Rakitin, D.V. Ionov, and Yu.M. Timofeev (2010). Variability of the total column amounts of climate influencing gases obtained from ground-based high resolution spectroscope measurements, Doklady Earth Sciences **432**, 656.

Poberovskii A.V., Polyakov A.V., Yu.M. Timofeev (2010). Measurements of the hydrogen fluoride total column amount in the atmosphere over the vicinity of St. Petersburg, Izv., Atm. Oceanic Physics **46**, 263.

Virolainen Ya. A., Yu.M. Timofeev, D.V. Ionov, A.V. Poberovskii & A.M. Shalamyanskii (2011). Ground-based measurements of total ozone content by the infrared method. Izv., Atm Oceanic Physics **47**, 480.

Polyakov A.V., Yu.M. Timofeev, A.V. Poberovskii, I.S. Yagovkina (2011). Seasonal variations in the total content of hydrogen fluoride in the atmosphere. Izv., Atm. Oceanic Physics **47**, 760.

Timofeyev Yuriy, Dmitry Ionov, Maria Makarova et al. (2013). Measurements of trace gases at Saint-Petersburg State University (SPbSU) in the vicinity of Saint-Petersburg, Russia. In Disposal of Dangerous Chemicals in Urban Areas and Mega Cities, NATO Science for Peace and Security Series C: Environmental Security 2013 **XV**, 173.

Polyakov A.V., Yu.M. Timofeev & A. V. Poberovskii (2013). Ground-based measurements of total column of hydrogen chloride in the atmosphere near St. Petersburg, Izv., Atm. Oceanic Physics **49**, 411.

Rakitin A.V., Poberovskii A.V., Yu.M. Timofeev, M.V. Makarova, and T.J. Conway (2013). Variations in the column-average dry-air mole fractions of CO_2 in the vicinity of St. Petersburg. Izv., Atm. Oceanic Physics **49**, 271.

Semakin S.G., A.V. Poberovskii, and Yu.M. Timofeev (2013). Ground-based spectroscopic measurements of the total nitric acid content in the atmosphere, Izv., Atm. Oceanic Physics **49**, 3, 294.

Gavrilov N. M., M. V. Makarova, A. V. Poberovskii, and Yu. M. Timofeyev (2014). Comparisons of CH_4 ground-based FTIR measurements near Saint- Petersburg with GOSAT observations, Atmos. Meas. Tech. **7**, 1003.

Zaitsev N. A., Yu. M. Timofeyev, V. S. Kostsov (2014). Comparison of radio sounding and ground-based remote measurements of temperature profiles in the troposphere, Atm. Oceanic Optics **27**, 386.

Gavrilov Nikolai M., Maria V. Makarova, Yury M. Timofeev, et al. (2014). Comparisons of satellite (GOSAT) and ground-based spectroscopic measurements of CH_4 content near Saint Petersburg: influence of data collocation, Int. J. Rem. Sens. **35**, 5628.

Makarova M.V., V.I. Serdyukov, M.Yu. Arshinov et al. (2014). First results of ground-based Fourier Transform Infrared measurements of the H_2O total column in the atmosphere over West Siberia, Int. J. Rem. Sens. **35**, 5637.

Virolainen Yana, Yury Timofeyev, Alexander Polyakov, et al. Intercomparison of satellite and ground-based measurements of ozone, NO_2, HF, and HCl near Saint Petersburg, Russia, Int. J. Rem. Sens. **35**, 5677.

SMALL-SCALE ATMOSPHERE-OCEAN COUPLING IN GALE-FORCE WINDS: MODELS, EXPERIMENTS, REMOTE SENSING

YU. TROITSKAYA[1,2], D. SERGEEV[1,2], A. KANDAUROV[1,2], E. EZHOVA[1,2], O.DRUZHININ[1], I.SOUSTOVA[1,2], O.ERMAKOVA[1], M.VDOVIN[1,2]

[1] Institute of Applied Physics Nizhniy Novgorod, Russia
[2] N.I. Lobachevski State University of Nizhniy Novgorod, Russia

Keywords: hurricanes, sea surface drag, spray, microwave remote sensing.

INTRODUCTION

Gale force wind at the sea represents one of the most hazardous meteorological phenomena. It is observed, first of all, under the condition of tropical cyclones. For moderate and sub-tropical parts of Europe the most dangerous storms occur due to the penetration of tropical cyclones far beyond the tropical zone. Apart from the risks for population inland, extreme storms pose a considerable threat to the safety of offshore industries, sea routes, wind technologies, oil and gas. Strong atmospheric vortices similar to tropical cyclones in genesis can be sometimes observed in mid latitudes like the quasi-tropical cyclones over the Black sea and "medicanes" over Mediterranean. In high latitudes adverse weather conditions occur during cold air advection, in Arctic fronts, and polar lows – very intensive atmospheric vortices similar to tropical cyclones in the physics of their development. The currently employed models of storms and storm surges are unsatisfactory precisely for the most severe events, where accurate modelling is the most important. One of their key shortcomings is their inability to account for the effect of the sharp drop of sea surface aerodynamic drag observed under very strong winds. Under these conditions there is no longer a well defined water surface, as air is filled by water droplets and water by air bubbles; there is a continuous transition from liquid water to air with a mean density gradually changing from the density of water to the density of air, which radically changes the processes of the air/sea momentum, heat and gas exchange. These small scale processes have to be properly understood to be incorporated into operational weather forecasting and large scale circulation climate models.

THE SEA SURFACE DRAG UNDER STRONG WINDS

Wind-wave interaction at extreme wind speed is of special interest now in connection with the problem of explanation of the sea surface drag saturation at the wind speed exceeding 30 m/s. The idea on saturation (and even reduction) of the coefficient of aerodynamic resistance of the sea surface at hurricane wind speed was first suggested in by Emanuel (1995) on the basis of theoretical analysis of sensitivity of maximum wind speed in a hurricane to the ratio of the enthalpy and momentum exchange coefficients. Both field (Powel et al (2003), Jarosz et al (2007)) and laboratory (Donelan et al, (2004)) experiments confirmed that at hurricane wind speed the sea surface drag coefficient is significantly reduced in comparison with the parameterization obtained at moderate to strong wind conditions (see Fairall et al, (2003)).

Factors determining momentum exchange under high wind speeds basing on the laboratory experiment in a well controlled environment were investigated. The experiments were carried out in the Thermo-Stratified WInd-WAve Tank (TSWIWAT) of the Institute of Applied Physics. The parameters of the facility are as follows: airflow 0 - 25 m/s (equivalent 10-m neutral wind speed U10 up to 60 m/s), dimensions 10m x 0.4m x 0.7 m, temperature stratification of the water layer. Simultaneous measurements of the airflow velocity profiles and wind waves were carried out in the wide range of wind velocities. Aerodynamic resistance of the water surface was measured by the profile method at a distance of 7 m from the inlet. Wind velocity profiles were measured by the L-shaped Pitot tube with differential pressure

transducer Baratron MKS 226A with accuracy of 0.5% of full scale range i.e. 3 cm/s. Scanning method with consecutive height increment of 3 – 5 mm and accruing time of 2 minuets at each point was used. For fixed wind parameters 5 profiles were measured for subsequent averaging.

Wind friction velocity and surface drag coefficients C_{D10} were retrieved from the measurements by the profile method, the dependence of C_{D10} on U10 are shown in Figure 1. Similar to data by Donelan et al (2004) surface drag coefficient demonstrates tendency to saturation for wind speed exceeding 30 m/s.

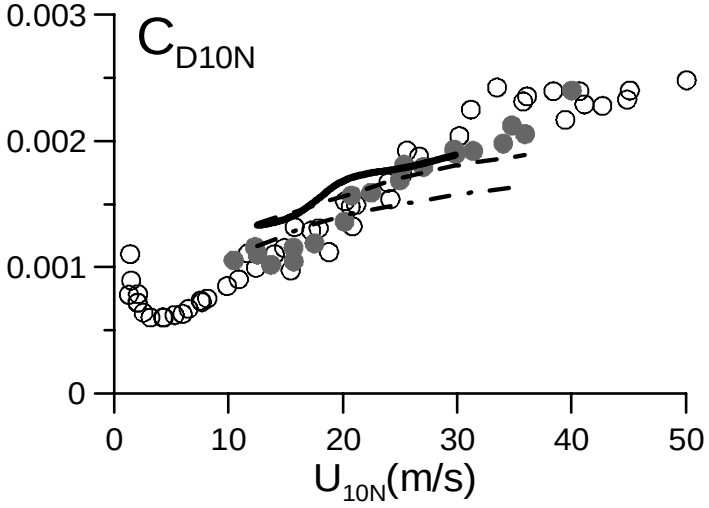

Figure 1. Surface drag coefficient via 10-m wind speed. Open circles – data from Donelan etal (2004), closed circles – data obtained at TSWIWAT, dash-dot line – theoretical calculations within quasi-linear theory (no ripples), dash line - theoretical calculations within quasi-linear theory (with ripples, model [15]), solid line - theoretical calculations within quasi-linear theory (with measured ripples)

Simultaneously with the airflow velocity measurements, the wind wave field parameters in the flume was investigated by three wire gauges positioned in corners of an equal-side triangle with 2 cm side, data sampling rate was 100 Hz. Three dimensional frequency-wave-number spectra with the wavenumbers up to 1 cm^{-1} were retrieved from this data by the algorithm similar to the wavelet directional method [12] based on window fast Fourier processing. Wave number spectra for the bandwidth 2-10cm^{-1} were measured by the optical method. The wave fields at different wind speeds are characterized by narrow wave-number spectra with the peak wave-number decreasing with the wind speed increasing. The wind-wave saturation spectra at different 10 m wind speeds U_{10} are plotted in Figure 2a. The presence of a sharp peak downshifting with the increasing wind speed and a long plato is typical for the measured spectra.

In Figure 3 we present the dependencies of the mean square slope on the wind velocity. The open circles show the mean square slope of the peak wave S_p. Other symbols present the mean square slope of the wave field calculated according to the definition:

$$Slope = \int_{k\min}^{k\max} k^2 S(k) dk, \qquad (1)$$

where $S(k)$ is the omnidirectional elevation spectrum.

Here the upper limit k_{min}=0.01 cm^{-1} was selected below the lowest wavenumber observed in the experiments. It is well known, that the integral (1) strongly depends on the upper limit k_{max}. Measurements with the array of 3 wave staffs provide $k_{max}=k_u$=1.25 cm^{-1}. The dependence $Slope(U_{10})$ for this upper limit is shown in Figure 2b by closed circles. To take into account the short wave ripples both generated near the crests of the waves due to wave breaking and excited by the wind, we continued the spectrum for $k>k_{max}$ by the model based on the ideas suggested by (Elfouhaily et al 1997). The mean square slope calculated for the composite spectrum with the upper limit k_{max}=20 cm^{-1} is shown by squares in Figure 3 as a function of U_{10}. Figure 2b clearly shows, that for both values of the upper limit k_{max} in the integral (1) the mean square slope tends to saturation when U_{10}>25 m s^{-1}. The comparison with the Figure 1 shows that

the saturation spectrum as a whole demonstrates the tendency to saturation for U_{10}>25 m s^{-1}. It means that at the wind speed about 25 m s^{-1} the regime changing of the wave field occurs. Figure 2c clearly shows linear dependence between surface drag coefficient and mean square slope. Video filming indicates onset of wave breaking with white-capping and spray generation at wind speeds approximately equal to U_{cr}.

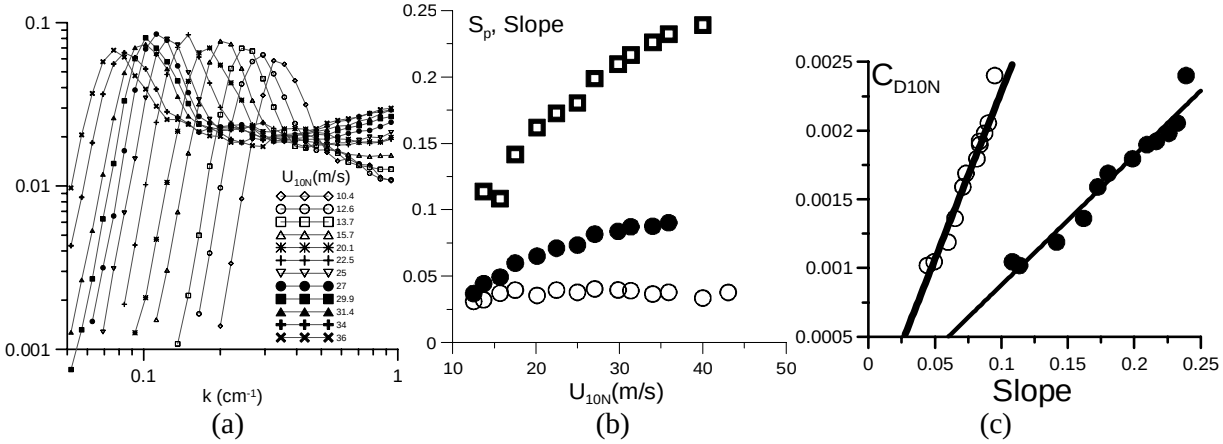

Figure 2. Saturation wave number spectrum of the waves for a definite fetch (7 m) and different wind speeds (a); dependences of the mean square slope on the wind velocity defined as (a_p k_p)/2 (open circles), the calculated accordingly integral (1) for $k_{max}=k_u$ (black circles) and k_{max}=2000 m-1 (open squares) (b); CD against mean square slope diagram. Black symbols for k_{max}=2000 m-1, open symbols for $k_{max}=k_u$ (c).

We compared the obtained experimental dependencies with the predictions of the quasi-linear model of the turbulent boundary layer over the waved water surface (Reutov, Troitskaya (1995)? Troitskaya, Rybushkina (2007)). Comparing shows that theoretical predictions give low estimates for the measured drag coefficient and wave fields (see Figure 1, dashed-dotted curve). We took into account small scale (high frequency) part of the surface roughness (k <1 см$^{-1}$). First, we add model spectrum of short from the work (Elfouhaily et al (1997)) to measured long wave part $S(k)$:

$$S_{tot}(k) = S(k) + \frac{10^{-2}}{2}\left(1+3\ln\frac{u_*}{c_m}\right)\frac{c_m}{c}e^{-\frac{1}{4}\left(\frac{k}{k_m}-1\right)^2}, c_m = 23cm/s,$$

New theoretical results are in better agreement with experiment (see. Figure 1, dashed curve). The agreement was significantly improved, when we added high-wave-number part of the wind wave spectra measured by the laser system (see Figure1, solid curve).

EFFECT OF DROPLETS ON HEAT AND MOMENTUM EXCHANGE AT STRONG WINDS

A series of experiments was carried out in the TSWIWAT IAP RAS for the study of momentum and heat exchange in a stably stratified temperature turbulent boundary layer air flow over waved surfaces. The experiments were conducted in a wide range of wind speeds and the roughness parameters (waves), including extreme with heavy wave breaking and spray.

To create a temperature stratification of the atmospheric boundary layer air entering the flume was heated to 30-40 degrees C (depending on air flow rate). The temperature of the water in all experiments was maintained constant at about 15 degrees. The studies were conducted in a wide range of wind speeds. Maximum rate on the channel axis of 8.8 m / s to 19 m / s, corresponding to an equivalent 10-m wind speed 10-35 m / s. The peculiarity of this experiment was the presence of the possibility of changing the heights of the surface waves regardless of the speed of the wind flow in the channel. For this purpose a net with thread thickness 0.25 mm and a cell of 1.6 x 1.6 mm was stretched along the channel. This net does not affect the heat exchange, but the characteristics of surface waves varied depending on the position of the grid: the waves were absent when the grid was located at the level of the undisturbed surface of the water, and the amplitude was maximal when the net was at the maximum depth 33cm.

Simultaneous measurements of velocity profiles of wind and temperature flow in the test section of the channel (at a distance of 6.5 m from the entrance to the canal) was performed using a Pitot tube with a differential pressure gauge and film hot-wire anemometer. Both sensors were mounted on the vertical scanner. The temperature and wind speed at the entrance controlled by an additional hot-wire anemometer. To measure the surface water temperature in the test section, a special temperature sensor was positioned. The average velocity and temperature profiles were obtained of the working section of the channel. By the profiling method values of friction velocity and the equivalent 10-m wind speed and the equivalent air-water temperature difference $\Delta T10$ were obtained and their errors were estimated. As a result, the drag coefficient C_D and the water surface heat transfer coefficient C_T were calculated.

Simultaneously, the presence and number of sprays in the surface layer of air were determined. We used non-standard method of indirect estimation of the amount of the volume of spray in the air stream. It is based on the effect of a sharp decline in reading of the thermoanemometer when struck by the spray. 10-min recording was conducted at several fixed heights above the water surface. After the time series smoothing to remove hardware noise, maximum temperature value has been subtracted from the current value of the effective temperature, after which the time series was integrated. The integral was used as a marker of the amount of spray in the air flow over the waves.

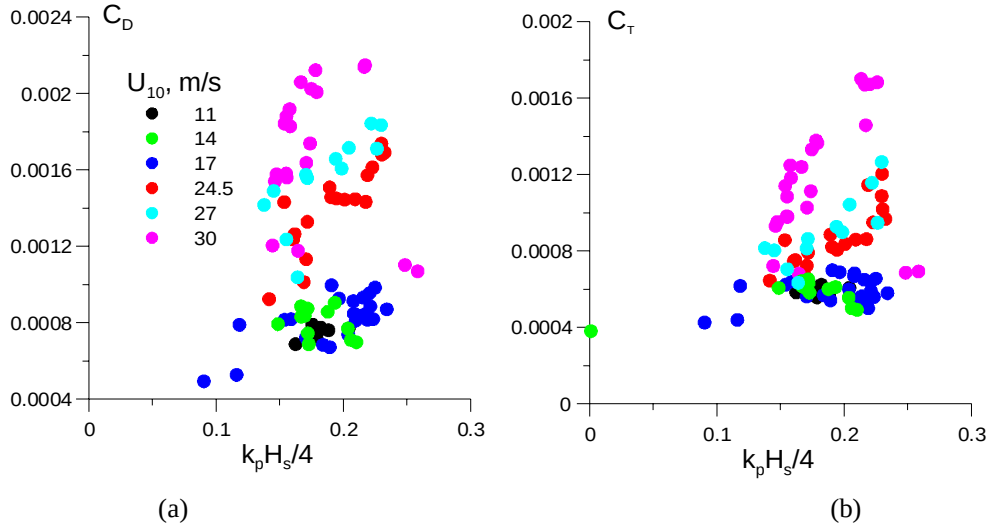

(a) (b)

Figure 3. The drag coefficient (a) and Stanton number as a function of the slope of energy-waves (b)

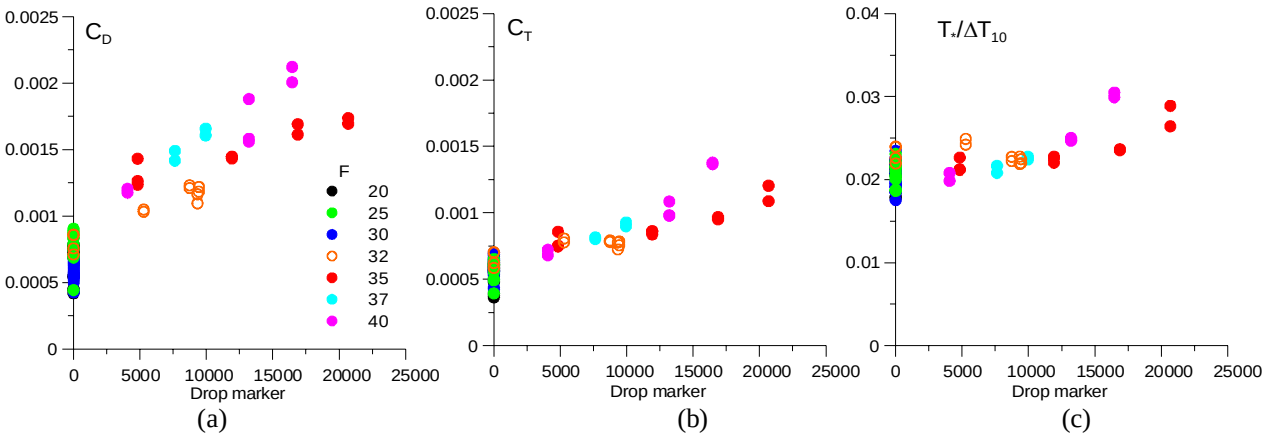

(a) (b) (c)

Figure 4 The drag coefficient (a), the number of Stanton (b) and the logarithm of the temperature roughness (c) as a function of the spray marker.

The experimental dependences of the exchange coefficients on the parameters of the air flow and wave characteristics, as well as the number of marker spray were obtained. We found that a sharp increase in the drag coefficient and Stanton numbers at wind speeds greater than 25 m / s was accompanied by the emergence and increasing concentration of the spray in the air boundary layer. (Figure 3a). The correlation coefficient between the coefficient of resistance marker and the number of sprays was close to 0.9 (Figure 4).

We suggested the hypothesis that the observed phenomenon can be explained by the phenomenon of the instability of the air and water type "bag break-up"(Villermaux, E. (2007)) (Figure 5), which was detected by the shadow method with illumination up to the light and high speed video using a high-speed camera NAC Memrecam HX-3.

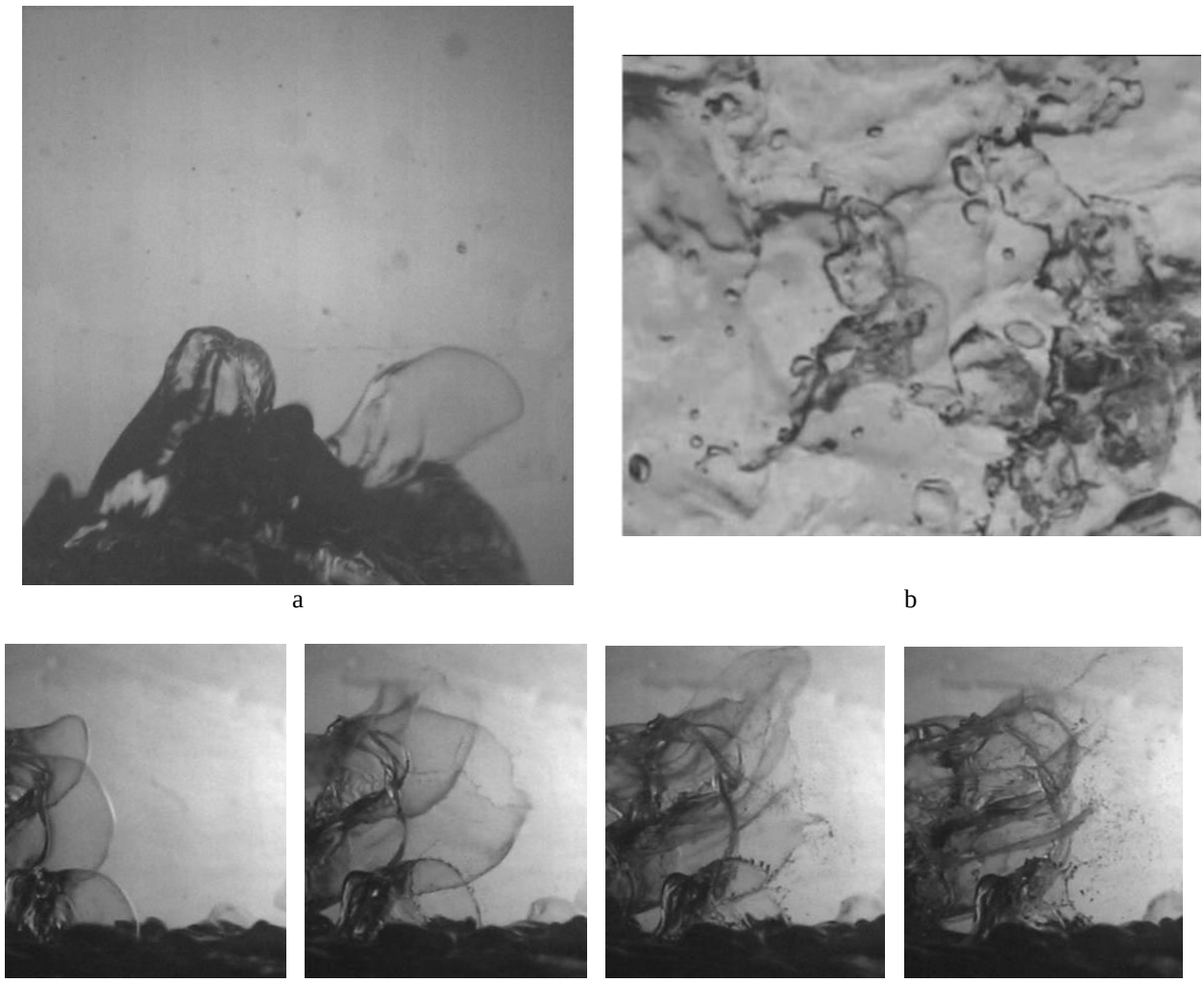

a b

Figure 5 Examples of images "membranes" side view (a) and top view (b). An example of the development of instability "membrane" to form a spray (lower panel).

CONCLUSIONS

Factors determining momentum and heat exchange under high wind speeds basing on the laboratory experiment in a well controlled environment were investigated. Basing on the experimental data a possible physical mechanism of the drag saturation at severe wind conditions is suggested. Tearing of the wave crests at severe wind conditions leads to the effective smoothing (decreasing wave slopes) of the water surface, which in turn reduces the aerodynamic roughness of the water surface. Quantitative agreement of the experimental data and theoretical estimations of the surface drag occurs if momentum flux associated with short wave part of the wind wave spectra is taken into account. A series of laboratory experiments on

modeling of wind-wave interaction in presence of stable temperature stratification surface layer of the air flow (caused by the difference between the temperature of water and air). Investigations were carried out in a wide range of wind speeds up to hurricane and wave parameters, including breaking waves. Mean velocity and temperature profiles and parameters of surface waves were measured. The dependences of the drag and heat exchange coefficients on the wind speed, wave parameters (amplitude, slope) and the values characterizing the volume of spray in the surface layer of the air flow were obtained. It was shown growth of exchange coefficients with increasing concentration of the spray. Using high-speed video revealed the dominant mechanism for the generation of spray when the wind is strong. It turned out that it is associated with the development of a special type of instability of the air and water, which is known as "bag-breakup instability" in the theory of disintegration of liquids. According to records obtained investigated the statistics of events that resulted in the spray generated in the surface layer of the atmosphere in a strong wind through the mechanism of «bag-breakup instability».

ACKNOWLEDGEMENTS

This work was supported by the Russian Foundation of Basic Research (13-05-00865, 14-05-91767, 13-05-12093, 15-05-) and Alexander Kandaurov, Maxim Vdovin and Olga Ermakova acknowledge partial support from Russian Science Foundation (Agreement No. 14-17-00667)..

REFERENCES

Emanuel, K.A. (1995) Sensitivity of tropical cyclones to surface exchange coefficients and a revised steady-state model incorporating eye dynamics. J. Atmos. Sci, Vol.52, No 22, p. 3969-3976.

Powell, M.D., Vickery P.J., Reinhold T.A. (2003) Reduced drag coefficient for high wind speeds in tropical cyclones. Nature, Vol.422, p.279-283

Jarosz E., Mitchell D. A., Wang D.W., Teague W.J. (2007) Bottom-up determination of air-sea momentum exchange under a major tropical cyclone. Science, v 315, p. 1707-1709 DOI: 10.1126/science.1136466.

Donelan M.A., Haus B.K , Reul N., Plant W.J., Stiassnie M., Graber H. C., Brown O. B., Saltzman E. S. (2004) On the limiting aerodynamic roughness of the ocean in very strong winds. *Geophys. Res. Lett.*, Vol.31, L18306.

Fairall C.W., Bradley E.F., Hare J.E., Grachev A.A., Edson J.B. (2003) Bulk parameterization of air–sea fluxes: updates and verification for the COARE algorithm . J. Climate, Vol.16, No 4, p.571–591

Rikiishi, K. (1978)A new method for measuring the directional wave spectrum. Journal Physical Oceanography. Vol. 8, p. 508 – 517

Reutov, V.P. and Yu. I. Troitskaya, (1995) On the nonlinear effects in the interaction of gravity waves with turbulent airflow. Izvestiya, Atmospheric and Oceanic Physics, Vol. 31, No 6, p. 825–834

Troitskaya, Yu. I., G. V. Rybushkina. (2008) Quasi-linear model of interaction of surface waves with strong and hurricane winds. Izvestiya, Atmospheric and Oceanic Physics Vol. 44, No 5, p. 621-645

Elfouhaily T.B., Chapron B., Katsaros K., Vandemark D. (1997) A unified directional spectrum for long and short wind-driven waves // J. Geophys. Res., , v.107, p.15781–15796.

Villermaux, E. (2007) Fragmentation. Annu. Rev. Fluid Mech. 39, 419–446.

AEROSOL EMISSION REDUCTIONS OVER THE 20TH AND 21ST CENTURY AND THEIR IMPACT ON POLAR CLIMATE.

V. VARMA[1,2], Ø. SELAND[3], A. M. L. EKMAN[1,2], T. IVERSEN[3,4], A. KIRKEVÅG[3], I. RIIPINEN[2,5] and H. C. HANSSON[2,5]

[1]Department of Meteorology, Stockholm University, Stockholm, Sweden.

[2]The Bolin Centre for Climate Research, Stockholm University, Stockholm, Sweden.

[3]Norwegian Meteorological Institute, Oslo, Norway

[4]Department of Geosciences, University of Oslo, Norway

[5]Department of Applied Environmental Science, Stockholm University, Stockholm, Sweden.

Keywords: AEROSOL, EMISSIONS, ARCTIC, EUROPE, CLIMATE.

INTRODUCTION

Large changes in the magnitude and spatial patterns of global aerosol emissions have occurred during the 20th century and are projected to continue over the coming century. It is not clear how the Arctic climate is affected by changes in global and European aerosol emissions. As more and more countries adapt different strategies to reduce air pollution, it is important to examine how this will affect not only the top-of-the-atmosphere radiative forcing, but also the surface temperature and other parameters important for society. Of particular relevance for the Arctic are the reductions in sulfate emissions from industrial activities, domestic heating, and power production that have taken place in Europe during the latest decades. These changes provide an opportunity to study in detail how regional emissions over Europe affect the radiative balance and the global and Arctic climate. Detailed estimates of the European emission reductions are readily available, in addition to temperature and radiation measurements.

METHODS

Transient climate simulations over the industrial period (1850 to present) from the Norwegian Earth system model NorESM (Kirkevåg et al., 2013) with different emission levels have be conducted and analysed. The simulated aerosol number size distribution and mass composition have been evaluated versus in-situ observations from different European measurement networks. The analysis is focused on Europe and the Arctic and how surface radiative flux and temperature changes relate to different emission scenarios. As a first step, we present results from a comparison between the actual estimated emissions 1850 to 2005 NorESM simulations with simulations using constant 1980 SOx emissions for Europe while all other are the actual emissions.

CONCLUSIONS

The simulations show a significant change in the Arctic temperature as a result of the air quality regulation giving strongly decreased SOx emissions especially during the 1990-ties. However the effect in Europe is quite smaller. Comparing with the actual temperature change in the Arctic implies that the sulphate

aerosol only contribute with a minor fraction in the climate change. These is only results from simulations with one model and have to be corroborate by other models but also by detailed studies to identify the key processes and evaluation of the models towards observations.

ACKNOWLEDGEMENTS

We thank CRAICC and the Swedish Environmental Agency for support of this project.

REFERENCES

Kirkevåg, A., T. Iversen, Ø. Seland, C. Hoose, J. E. Kristjansson, H. Struthers, A. M. L. Ekman, S. Ghan, J. Griesfeller, E. D. Nilsson, and M. Schulz (1986). Aerosol-climate interactions in the Norwegian Earth System Model – NorESM1-M. *Geophysical Model Development*, **6**, 207-244.

SIMULATION OF EMISSIONS FROM WILDFIRES IN HEILONGJIANG PROVINCE, NORTHERN CHINA USING DYNAMIC GLOBAL VEGETATION MODEL

S. VENEVSKY[1] and C. WU[1]

[1]Center for Earth System Studies, Tsinghua University, Beijing, 100084, China
*venevsky@tsinghua.edu.cn

The new global fire model SEVER-FIRE is a mechanistic model which calculates number of human-induced and lightning fires as well as area burnt and carbon and particle emissions for both cases. The model operates at a daily time step and uses climate data (daily minimum/maximum temperature, daily precipitation/convective precipitation and daily short-wave radiation) as an input. The model works in interactive mode with a dynamic global vegetation model (DGVM), which provides fuel content and moisture and receives back amount of biomass burnt. SEVER-FIRE applies at a variable spatial resolution and for regional and global scale. This model was applied for simulation of Russian wildfires in 2010.

We calculated burnt area for a case study of Heilongjiang province, Northern China and compared it with GFED satellite data products and field statistics of forest authorities in the province for 1980-2010. It was found that carbon dioxide emissions from this fire prone area are slightly decreased in three decades.

REMOTE SENSING AND FIELD DATA APPLIED TO THE REGIONAL VALIDATION OF A SNOW CLIMATE MODEL

D. VERSEGHY

Climate Research Division, Environment Canada, 4905 Dufferin St., Toronto, ON, M3H 5T4, Canada

Keywords: Snow modelling, climate models, snow processes, snow data sets

INTRODUCTION

The simulation of snow amount and extent is an important aspect of modelling the global climate, owing for example to the well-known snow-albedo feedback (e.g. Qu and Hall, 2007). Thus it is important for snow schemes used in global climate models to be well validated, both at the field scale and at regional to global scales. This study presents the results of such a validation exercise focusing on the snow portion of the Canadian Land Surface Scheme, CLASS. A regional domain centred on eastern Canada was selected, and several satellite-derived datasets for snow cover, snow melt onset date, snow disappearance date, and snow water equivalent were used, as well as a unique Canadian snow course dataset.

METHODS

Part of the Canadian participation in the International Polar Year involved the offline testing of the snow modelling capability of the Canadian Land Surface Scheme, CLASS, which is used in the Canadian Global Climate Model and Regional Climate Model. This testing was done over a domain centred on the province of Quebec in eastern Canada, at a resolution of 1/4°. The modelling time period incorporated one spin-up year (1991-1992), followed by six simulation years (1992-1998). Atmospheric forcing data were obtained from ERA-40 reanalyses, scaled down in space and time using the Environment Canada GEM model as the interpolator. Validation data were limited, and consisted of gridded climate records of monthly air temperatures, NOAA daily snow cover data, a daily snow depth and snow water equivalent (SWE) reconstruction, and bimonthly SWE observations over Quebec from snow courses.

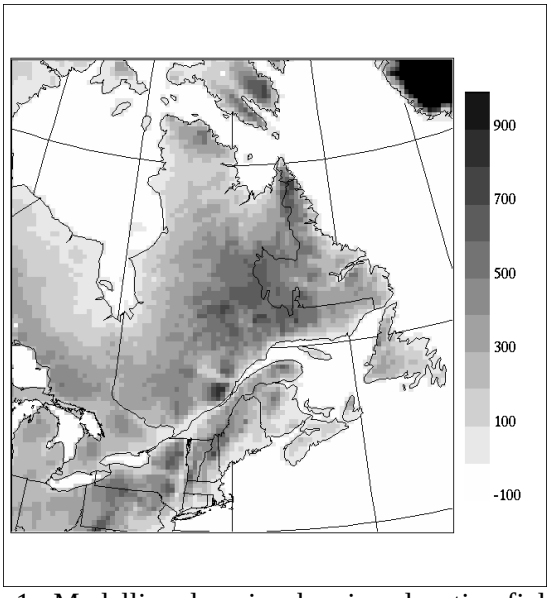

Figure 1: Modelling domain, showing elevation field (m).

This study has now been expanded into a more comprehensive validation effort, extending both the length of the simulation and the number of datasets employed. The model testing period now covers the years 1991 to 2011, and the atmospheric forcing are obtained from ERA-interim reanalyses, again scaled down in space and time using the GEM (Global Environmental Multiscale) model as the interpolator. Validation data now include several remote sensing datasets: snow cover data from the National Oceanographic and Atmospheric Administration (NOAA); snow cover derived from MODIS satellite observations; snow melt onset date obtained from QuikSCAT satellite observations: snow disappearance date from a dataset produced at the Canada Centre for Remote Sensing on the basis of AVHRR satellite observations; and snow water equivalent from the GlobSNOW dataset derived from passive microwave data and station observations. In addition, two datasets based on surface observations have been used: the CANGRD dataset maintained by Environment Canada, containing gridded monthly air temperature and precipitation over Canada; and a collection of snow depth and snow water equivalent values obtained from decades of snow course measurements carried out by Hydro-Quebec (Brown and Tapsoba, 2007).

RESULTS

The results in general show that the CLASS snow scheme produced quite a credible simulation of snow cover and snow water equivalent, after accounting for biases in the snowfall rate supplied in the forcing data. Part of the analysis of the results included test runs to investigate the sensitivity of the simulation to a variety of factors, such as canopy interception of snowfall and its sublimation; the timing and phase of precipitation; snow thermal conductivity; the treatment of snow albedo refreshment; and the effect of underlying organic soils. Of these factors, the simulation proved to be particularly sensitive to the value assigned to the snow albedo refreshment threshold (the amount of snow required to refresh the albedo to the fresh snow value). Interpretation of the results was complicated by the fact that in several instances, the validation datasets showed mutually contradictory values for snow parameters such as snow water equivalent and snow disappearance date. It was also found that in the case of one dataset (GlobSNOW), the model simulated snow water equivalent was actually more realistic at times, because the GlobSNOW values reached saturation at levels well below the observed values in central Quebec. This demonstrates that it is imprudent to base a model validation on only one type of dataset, since observational datasets, like model simulations, have their own characteristic weaknesses.

REFERENCES

Brown, R.D. and D. Tapsoba (2007). Improved mapping of snow water equivalent over Quebec, in Proc., 64th Eastern Snow Conference, St. John's, Newfoundland, Canada.

Qu, X., and A. Hall, (2007). What Controls the Strength of Snow-Albedo Feedback?. *J. Climate*, **20**, 3971–3981. doi: http://dx.doi.org/10.1175/JCLI4186.1

EFFECTS OF THE ARCTIC SEA ICE DECLINE ON EURASIAN CLIMATE

T. VIHMA and P. UOTILA

Finnish Meteorological Institute, Helsinki, Finland

INTRODUCTION

The rapid sea ice decline in the Arctic has been one of the most dramatic signs of the climate change during the latest decades. The sea ice extent in late summer and early autumn, and the ice thickness in both winter and summer have decreased by approximately 50% since 1980 (Cavalieri and Parkinson, 2012; Kwok and Rothrock, 2009). These decreases have both contributed to and been affected by the rapid warming of the Arctic. The climate warming in the Arctic has been at least twice as fast as the global mean (Blunden and Arndt 2012). Simultaneously with the strong warming in the central Arctic, several mid-latitude regions have experienced cold and snow-rich winters during the last ten years. These include winter 2005–2006 in large parts of Europe and northern Asia, winter 2009–2010 in large parts of the circumpolar mid-latitudes, winter 2010–2011 in most of Europe, and March 2013 in northern Europe.

The potential linkages between the Arctic sea ice decline and these cold winters have received a lot of public and scientific attention. This topic has been addressed by studies based on observations, atmospheric reanalyses, model experiments with prescribed sea ice conditions, coupled model experiments, and analyses of climate model output. Several studies have suggested effects of Arctic sea ice cover on mid-latitude climate, but the results scatter with respect to the magnitude, timing, region, and spatial extent of the effects, as well as on the physical mechanisms behind them (see Vihma (2014), Walsh (2014), and Cohen et al. (2014) for recent reviews).

In this paper we address the effects of Arctic sea ice decline on air temperature in Eurasia. Our objective is to better understand the regional differences in the Arctic-mid-latitude linkages, which is an issue that has received too little attention in previous studies.

METHODS

As high-quality atmospheric reanalyses are available since 1979, we focus on the period since 1979. We address the annual means and separately the autumn and winter seasons, as the strongest sea ice decline has taken place in early autumn and the thermodynamic effects of increased open water areas are strongest in winter. We recognize the fact that the remote effects of Arctic sea ice decline on Eurasia may occur with a time lag of several months. Hence, we calculate correlations between the monthly means of Arctic sea ice area and Eurasian air temperatures in the same and successive months during the same autumn/winter season.

We apply the Self-Organising Maps algorithm (SOMs; Kohonen, 2001) to extract the patterns of Earth surface temperature in the Arctic, and relate these patterns with those of 2-m air temperature in the Arctic and mid-latitudes. The SOM algorithm is applied to compact large data sets to easily interpretable forms visualised as arrays of nodes, which in our case are geographical surface maps of surface and air temperatures. For more information on the application of SOMs in climate research, see Hewitson and Crane (2002), Uotila et al. (2007), and Skific and Francis (2012).

RESULTS

Examples of the Arctic – Eurasia linkages are presented in Tables 1 and 2. In Table 1, the sea ice area in the Barents and Kara seas is correlated against central Eurasian 2-m air temperatures. We see that the September, October, November, and December sea ice areas have a significant positive correlation with

December 2-m air temperature, indicating that reduced sea ice area is related to colder temperature in December. Further, November sea ice area also has positive correlations with January and February air temperatures. These results support those of Overland et al. (2011), who suggested that the Arctic warming and sea ice decline favours a pattern of warm central Arctic surrounded by cold continents. This is partly due to the fact that the warming of the Arctic reduces the mid-tropospheric geopotential height difference between mid-latitudes and the Arctic. Via the thermal wind relation this reduces the mid-tropospheric westerly winds in mid-latitudes, typically resulting in lower winter temperatures (Overland and Wang, 2010). Later in the season, however, the opposite relationship is observed (Table 1): less sea ice in the Barents and Kara seas in January and February is related to higher air temperatures in central Eurasia in March. The physical mechanisms are not clear, but they may be related to the fact that with reduced sea ice cover the cases of northerly cold-air advection are less cold (Serreze et al., 2011).

	Sept T2m	Oct T2m	Nov T2m	Dec T2m	Jan T2m	Feb T2m	Mar T2m
Sept SIA	-0.26	-0.33	-0.18	**0.46**	0.22	0.13	-0.12
Oct SIA		-0.33	-0.21	**0.53**	0.26	0.31	-0.24
Nov SIA			-0.16	**0.53**	**0.44**	**0.39**	-0.22
Dec SIA				**0.38**	0.31	0.16	-0.15
Jan SIA					0.21	0.22	**-0.40**
Feb SIA						-0.29	**-0.40**
Mar SIA							-0.33

Table 1. Sea-ice area (SIA) in Barents/Kara Seas correlated against 2-meter air temperature (T2m) in central Eurasia (60-120°E, 45-60°N) in 1979-2012. The correlation coefficients marked in bold are statistically significant ($p < 0.05$).

In the Northern Europe, however, the situation is different and we do not observe positive correlations between the autumn sea ice area in the Barents and Kara seas and the continental 2-m air temperature (Table 2). All statistically significant correlations are negative, indicating that the reduced sea ice cover is related to warmer weather in autumn and winter. Considering March air temperatures, the situation is, however, very similar to that in the central Eurasia. This suggests that the linkages between the sea ice and temperatures in Northern Europe are basically similar in autumn and late winter, and similar to those in Central Eurasia in late winter. The lack of the warm Arctic – cold continents pattern in Northern Europe may be related to the dominating effect of the North Atlantic.

	Sept T2m	Oct T2m	Nov T2m	Dec T2m	Jan T2m	Feb T2m	Mar T2m
Sept SIA	**-0.41**	-0.33	**-0.38**	0.18	-0.09	0.23	-0.02
Oct SIA		**-0.54**	**-0.46**	0.16	-0.23	0.23	-0.11
Nov SIA			-0.26	0.15	0.07	0.19	-0.15
Dec SIA				0.00	-0.11	-0.01	-0.14
Jan SIA					-0.28	-0.07	**-0.36**
Feb SIA						-0.11	**-0.37**
Mar SIA							-0.30

Table 2. As Table 1 but for northern Europe land areas (50-72°N, 10°W-45°E).

In Figure 1 we present the SOM pattern of surface temperature calculated on the basis of monthly means of the whole year. The 2-m air temperature composites corresponding to the six surface temperature patterns are shown in Figure 2. We see that although some surface temperature patterns and 2-m air temperature composites are similar, such as (0,0) and (2,1), others, such as (2,0) and (0,1) display drastic

regional differences. For example, the surface temperature pattern (2,0) represents positive anomalies in the Arctic, but the corresponding 2-m temperature anomalies over the Eurasia are strongly negative. This discrepancy could be because of the increased snow cover related to the increased evaporation from a warmer Arctic Ocean or due to a zonally shifted atmospheric main storm track and increased high pressure blocking. We further see that the patterns of warm anomalies in the Arctic sea ice zone (2,0 and 2,1) are related to predominantly cold anomalies in central Eurasia and to either warm or cold anomalies in Northern Europe, which qualitatively resembles the results presented in Tables 1 and 2.

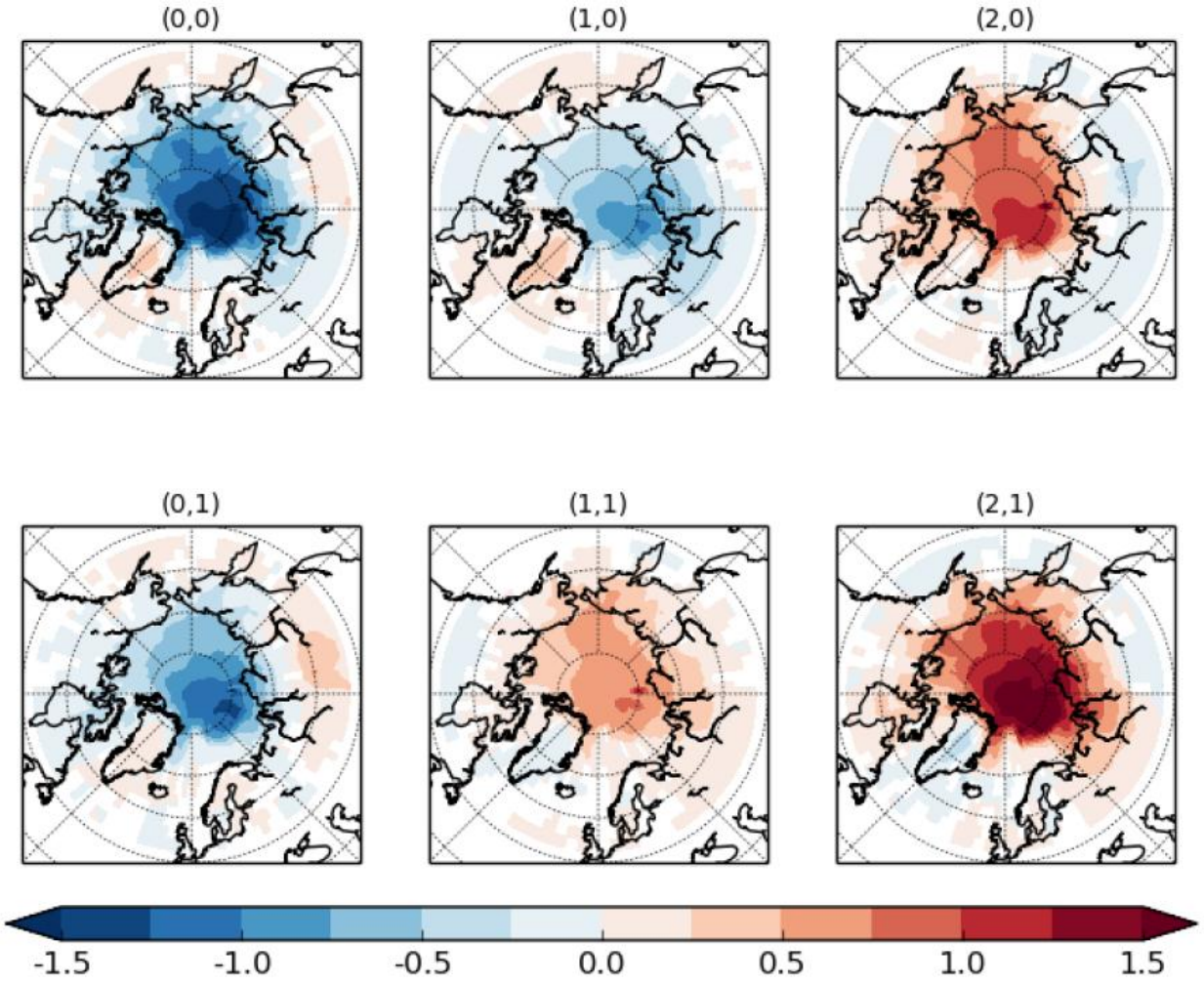

Figure 1. A six-node Self-Organising Map of the detrended Earth surface temperature anomaly during the period 1979-2013 calculated on the basis of ERA-Interim reanalysis. Units are in degrees of Celsius. The first SOM pattern (0,0) represents opposite surface temperature conditions than the last SOM pattern (2.1). The other SOM patterns represent intermediate surface temperature conditions.

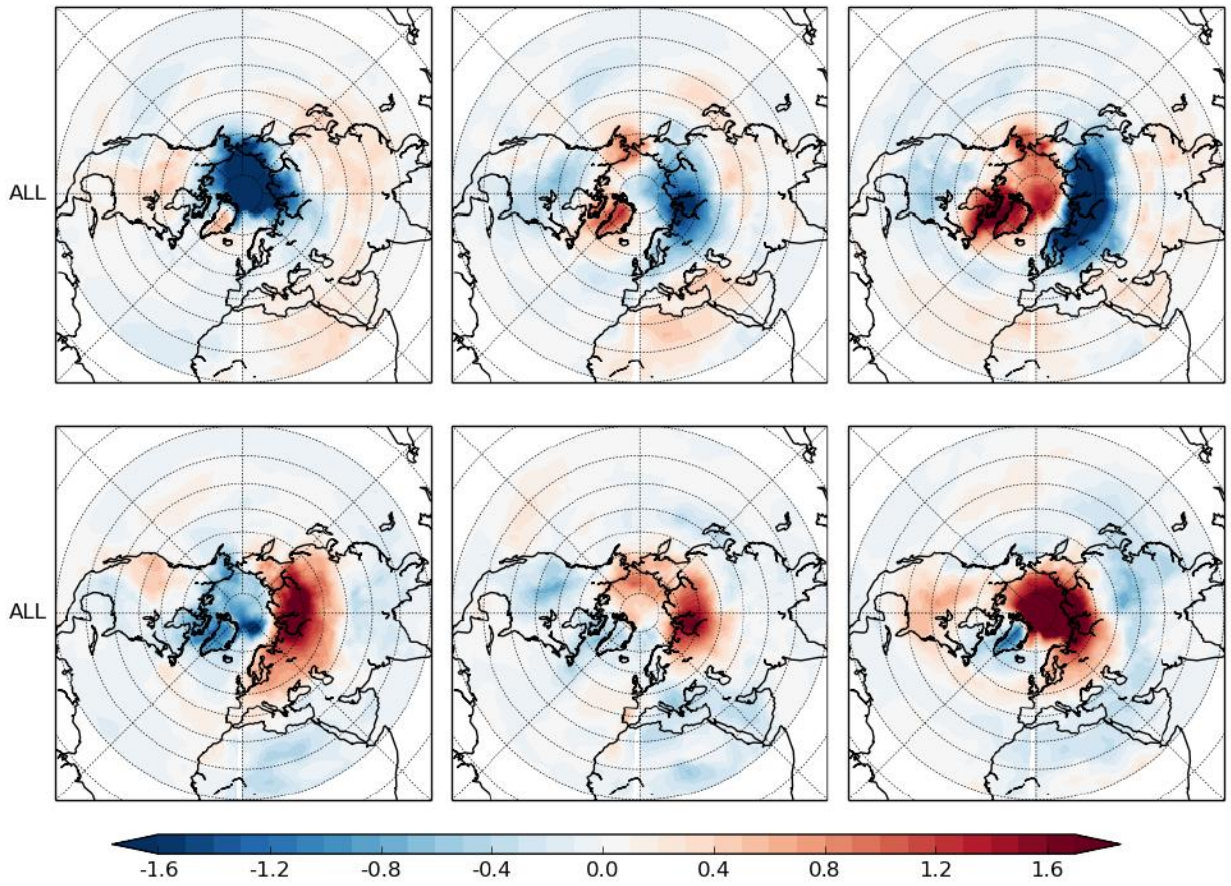

Figure 2. Detrended 2-m air temperature anomaly composites in degrees of Celsius mapped on the SOM patterns in Figure 1.

CONCLUSIONS

The linkages between the Arctic sea ice cover and mid-latitude climate are a new, very actual field of research. The detection of statistically significant signals is difficult due to the shortness of time series with a large sea ice decline. Another challenge is to physically interpret the statistically significant relationships detected. Despite these challenges, it is evident that there is a need for more regional studies. We have demonstrated this by presenting fundamental differences in the Arctic – mid-latitude linkages between the western and central parts of the Eurasian continent. To summarise, in autumn and winter, the sea ice cover and air temperatures have different statistical relationships in the western and central Eurasia, but in later winter the relationships become similar. More analyses will be carried out to refine these findings by applying the SOM technique on a range of variables related to atmospheric processes that can potentially explain the detected sea ice – air temperature relationships. These refined findings and identified physical processes will be particularly useful in enhancing our capability to predict regional changes more accurately than earlier.

ACKNOWLEDGEMENTS

This work was supported by the Academy of Finland under grant 259537.

REFERENCES

Cavalieri, D.J., and C. L. Parkinson (2012) Arctic sea ice variability and trends, 1979-2010. *The Cryosphere*, **6,** 881–889.

Cohen, J. et al. (2014). Recent Arctic amplification and extreme mid-latitude weather. *Nature Geosci.* **7**, 627–637.

Hewitson, B. C., and R. G. Crane (2002), Self-organising maps: Applications to synoptic climatology, *Clim. Res.*, **22**, 13–26.

Kohonen, T. (2001), *Self-Organizing Maps*, Springer, New York, 501 pp.

Kwok R, Rothrock DA (2009) Decline in Arctic sea ice thickness from submarine and ICESat records: 1958–2008. *Geophys Res Lett*, **36**, L15501.

Overland JE, Wang M (2010) Large-scale atmospheric circulation changes associated with the recent loss of Arctic sea ice. *Tellus.* **62A**, 1–9.

Overland, J E, K. R. Wood and M. Wang (2011). Warm Arctic cold continents: climate impacts of the newly open Arctic Sea, *Polar Res.* **30**, 15787.

Skific N., and J. Francis (2012). Self-Organizing Maps: A Powerful Tool for the Atmospheric Sciences, In: *Applications of Self-Organizing Maps*, Magnus Johnsson (Ed.), ISBN: 978-953-51-0862-7, InTech, doi:10.5772/54299, 251-268.

Serreze MC, Barrett AP, Cassano JJ (2011) Circulation and surface controls on the lower tropospheric temperature field of the Arctic. *J Geophys Res*, **116**, D07104.

Uotila, P., A. H. Lynch, J. J. Cassano, and R. I. Cullather (2007), Changes in Antarctic net precipitation in the 21st century based on Intergovernmental Panel on Climate Change (IPCC) model scenarios. *J. Geophys. Res.*, **112**, D10107. doi:10.1029/2006JD007482.

Vihma, T. (2014), Effects of Arctic sea ice decline on weather and climate: a review. *Surv. Geophys.*, **35**, 1175–1214, doi:10.1007/s10712-014-9284-0.

Walsh, J. E., 2014: Intensified warming of the Arctic: Causes and impacts on middle latitudes. *Glob. Plan. Change*, **117**, 52–63, doi:10.1016/j.gloplacha.2014.03.003.

RUSSIAN BLACK CARBON EMISSIONS FROM ANTHROPOGENIC SOURCES AND OPEN FIRES: ATMOSPHERIC TRANSPORT TO THE RUSSIAN ARCTIC

A.A. VINOGRADOVA[1], A.A. ROMANOVSKAYA[2], N.S. SMIRNOV[2] AND V.N. KOROTKOV[2]

[1] A.M. Obukhov Institute of Atmospheric Physics, Russian Academy of Sciences, Moscow, Russia.

[2] Institute of Global Climate and Ecology, Roshydromet and Russian Academy of Sciences, Moscow, Russia.

Keywords: RUSSIAN BLACK CARBON EMISSIONS, OPEN FIRES, ARCTIC, ATMOSPHERIC TRANSPORT.

INTRODUCTION

Black carbon (BC) is one of short-lived climate forcers (SLCF) in the atmosphere on the global scale (AMAP, 2011; Bond *et al*., 2013). Russia occupies about a half of the Arctic land and about one third of the water area of the Arctic Ocean, so, Russian atmospheric emissions play an important role in forming the Arctic environment composition (Vinogradova, 2000; Stohl *et al*., 2013). The main sources of atmospheric BC are domestic ovens, plant facilities, land, water and air transport, natural and anthropogenic wood and grass fires, as well as open flares attached to oil/gas extractive industry. The locations of Russian BC sources were analyzed distantly (Hirdman *et al*., 2010; Sharma *et al*., 2013; Cheng, 2014) by long-term air mass transport climatology, but with rough spatial resolution. On the other hand, the official data available on Russian anthropogenic emissions (Yearbook, 2010) are not adapted to the standards and terminology commonly used in the world. Moreover, the values represent either dotted sources or, in contrast, too large areas (from separate towns to whole administrative territorial units).

This article is aimed to overcome this gap: to calculate absent data, to extend the official emission data to the whole Russian territory, and to adapt the final results to a suitable form for wide modelling. We estimated air BC concentrations and BC fluxes onto the surface near Russian northern Nature Reserves to explore the role of those sources in the Arctic pollution.

INITIAL DATA, METHODS AND APROACHES

The initial data on anthropogenic emissions were taken from the official statistic data of the Russian Federal Service for Hydrometeorology and Environmental Monitoring (Roshydromet) (Yearbook, 2010). This issue contains information on annual atmospheric emissions for a lot of gas and aerosol pollutants, separately from land transport and stationary anthropogenic sources. Particularly, there are emissions of so called “soot”, which we used as BC emissions, taking into account that it is not fully correct. We took the data for 2010 as the last and the most complete available information item.

Concerning BC emissions, there are information (i) for some Russian large towns (only from stationary sources) and (ii) for all Russian regions (only from land transport) in (Yearbook, 2010). Our own original method gave us possibility to get over this lack by using the data on carbon monoxide (CO) emissions from the same issue. Both CO and BC are emitted to the atmosphere as a result of incomplete combustion of carbonaceous fuels. The ratio between CO and BC emissions depends on specific fuel type, industry and domestic traditions of a region. We assumed correlation between BC and CO emissions in a region, separately in transport emissions and in emissions from stationary sources. So, every region can be described by two coefficients (ratios of BC/CO emissions), one for stationary sources and the other for transport emissions. Also, we included effects from open flares of oil/gas industry in stationary sources.

As a whole, we analyzed the area (50-72)°N × (30-180)°E, which covers about 94% of the total Russian territory. The 54 administrative regions and more than 100 large towns were included in the analysis. The total square is about 16×10^6 km^2 with population more than 90×10^6 inhabitants. The final BC emissions from anthropogenic sources were presented on grid cells (1°×1°) (Vinogradova, 2014).

The fire data are from ISDM – Russian Forest Service (*http://www.aviales.ru/default.aspx?textpage=25*) and from (*www.cepl.rssi.ru*) for 2000-2013. The open fire squares were recalculated in carbon mass production, and then in BC emission using different coefficients for vegetation surfaces and fire types (high, low wood fires, grass fires, etc.) in accordance with the IPCC recommendations and (Akagi *et al*., 2011). One can see more details in (Smirnov *et al*., 2015). The main fires are localized in the Asian part of Russia. Thus, we analyzed BC fire emissions from the fire area (50-68)°N × (60-160)°E, distributed through the territory on grid cells (1°×1°).

RESULTS: BC EMISSIONS

Total annual anthropogenic BC and CO emissions from the regarded Russian territory are about (210 ± 30) kt and about 12 Mt, respectively. The reference values are 230 kt BC in 2008 (Wang Q. *et al*., 2011) and about 11 Mt CO in 2010 (http://edgar.jrc.ec.europe.eu). The rough estimate of BC emissions from oil/gas flares to the atmosphere is about 23 kt/yr. Averaged (through 2000-2013) total annual BC emission from open fires in Siberia and Far East is (27 ± 9) kt, and about 140 kt fall to the share of anthropogenic BC emission from these regions (and about 120 kt only from the regions with fires). Some features of Russian BC emissions are presented in Figs. 1 – 4.

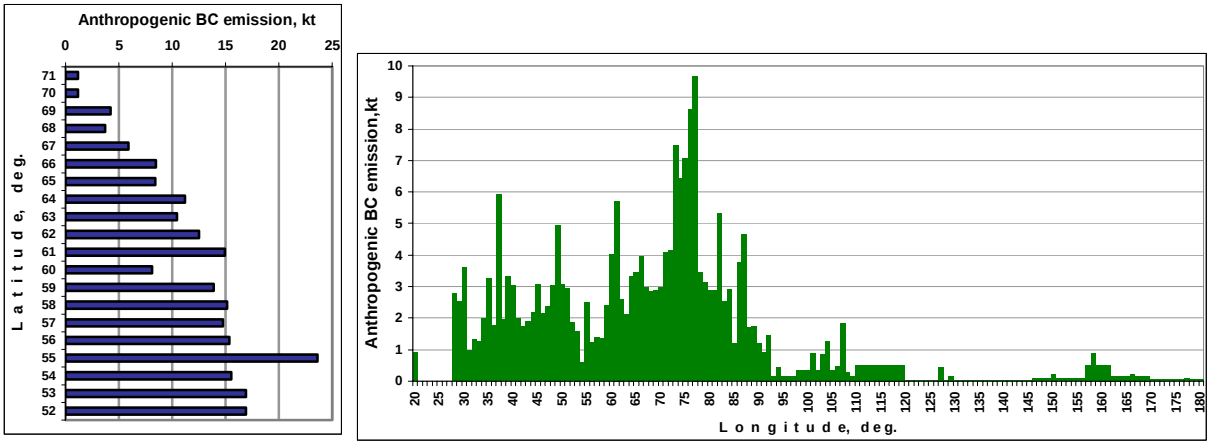

Figure 1. Spatial distributions of annual anthropogenic BC emissions.

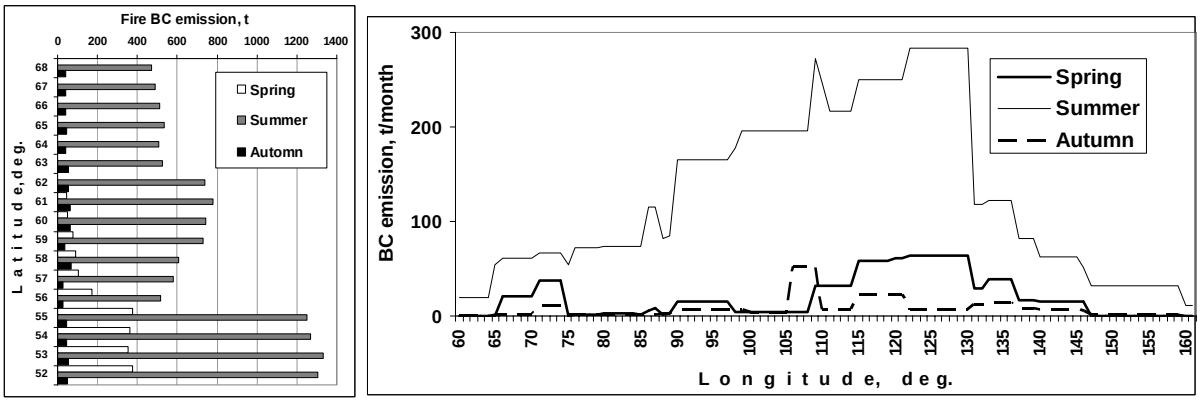

Figure 2. Spatial distributions of fire BC emissions in seasonal variations.

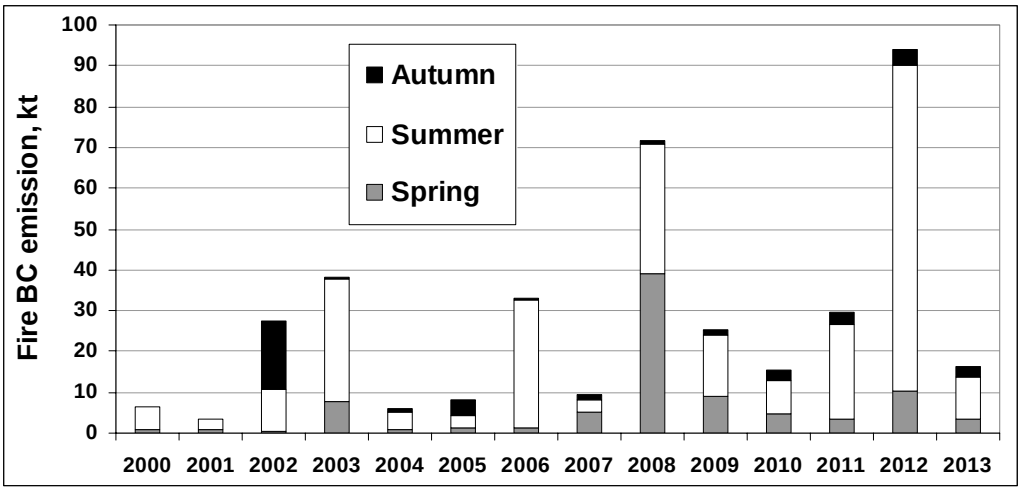

Figure 3. Temporal variations of Russian fire BC emissions.

Fire BC emission shows great seasonal (Fig. 2) and long-term (Fig. 3) variations. We have no information on temporal variations in anthropogenic BC emissions, but, most likely, they are not so high.

In Fig. 4 monthly means of BC emissions from anthropogenic and open fire sources are compared, totally from the fire area. The difference is not too high in total values, but the main variations are obvious from Figs. 1 and 2.

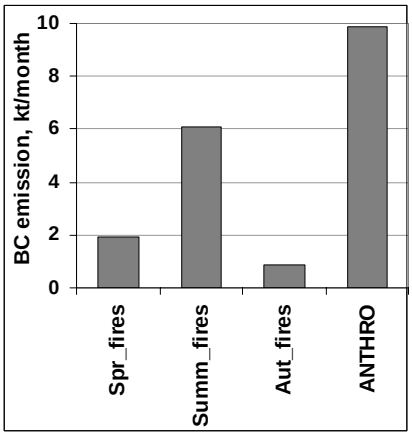

Figure 4. Monthly mean values of BC emissions from anthropogenic (ANTHRO) and fire (three seasons) sources in the fire area.

RESULTS: BC AIR MASS TRANSPORT TO THE ARCTIC

We estimated the effects from Russian BC emissions on the environment of the Russian Arctic using the approach presented in (Vinogradova and Veremeichik, 2013). Long-term climatology in atmospheric long-range air mass transport was used to calculate the special function of emission sensitivity for some points near the Russian Arctic nature Reserves. The parameters were chosen for the surface emission sources and air transport within mixing layer. The air BC concentration (C) and BC flux onto the surface (D) are analyzed for Nenetzky (the Pechora River delta), Gydansky (the Ob River delta), Ust-Lensky (the Lena River delta) nature Reserves, and Wrangel Island. The main effects from anthropogenic sources are shown in Fig. 5.

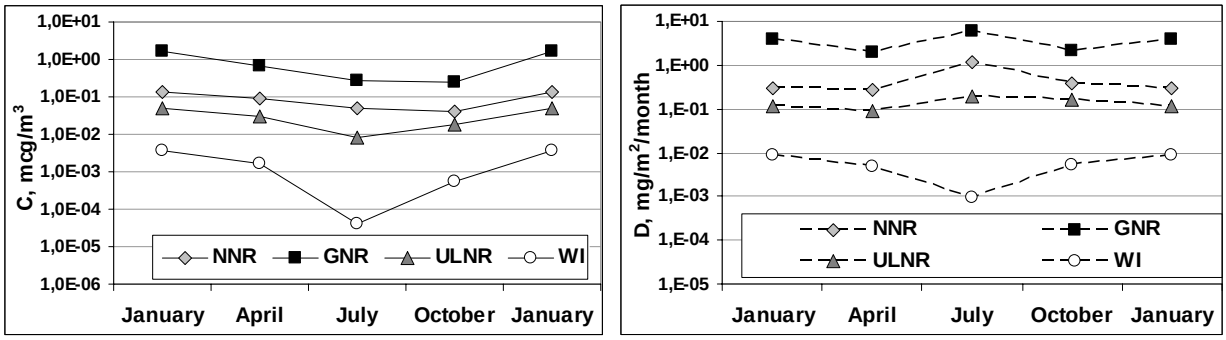

Figure 5. Monthly mean air BC concentration (C) and BC flux onto the surface (D) from anthropogenic Russian sources near four nature Reserves. Logarithmic scale.

There is maximal anthropogenic BC pollution near GNR caused by flares of oil/gas extractive industry in Western Siberia. Low values for WI are due to remoteness from the sources. Differences in C and D seasonal variations are due to high precipitation values in summer. The values are in reliable correlation with experimental data measured both in the Russian Arctic and at other arctic stations (Vinogradova, 2015).

Similar estimates of fire BC emission effects in the Russian Arctic show that anthropogenic impacts are 10 times or more higher, than fire ones at different arctic areas. This is connected with the fact that maximal fire BC emissions come principally from southern regions (Fig. 3, 4) in summer (Fig. 2), when BC deposition velocity in the air is minimal.

CONCLUSIONS

First of all, we presented the spatial distributions of anthropogenic and fire BC emissions from Russia in a suitable form for modelling. The numerical values were estimated for different territories and seasons.

The effects of those emissions were calculated for different Russian Arctic points. The area near Gydansky nature Reserve (in the Ob River delta) is more polluted by BC, than other areas under investigation.

The fire effect is significantly lower, than anthropogenic one for all Reserves all year round. The role of Russian open fires in BC pollution of the Arctic has great seasonal variations and, in general, is not so important.

ACKNOWLEDGEMENTS

This work was supported by RFBR under grants 14-05-00059-a, 14-05-93089 Norv-a.

REFERENCES

Akagi, S.K., R.J. Yokelson, C. Wiedinmyer, M.J. Alvarado, J.S. Reid, T. Karl, J.D. Crounse and P.O. Wennberg (2011) Emission factors for open and domestic biomass burning for use in atmospheric models, *Atmos. Chem. Phys.* **11**, 4039.

AMAP, 2011. The Impact of Black Carbon on Arctic Climate (2011). By: P.K. Quinn, A. Stohl, A. Arneth, T. Berntsen, J. F. Burkhart, J. Christensen, M. Flanner, K. Kupiainen, H. Lihavainen, M. Shepherd, V. Shevchenko, H. Skov, and V. Vestreng. Arctic Monitoring and Assessment Programme (AMAP), Oslo. 72 pp.

Bond, T.C., S.J. Doherty, D.W. Fahey, P.M. Forster, T. Berntsen, B.J. DeAngelo, M.G. Flanner, S. Ghan, B. Kärcher, D. Koch, S. Kinne, Y. Kondo, P.K. Quinn, M.C. Sarofim, M.G. Schultz, M. Schulz, C. Venkataraman, H. Zhang, S. Zhang, N. Bellouin, S.K. Guttikunda, P.K. Hopke, M.Z. Jacobson, J. W.

Kaiser, Z. Klimont, U. Lohmann, J.P. Schwarz, D. Shindell, T. Storelvmo, S.G. Warren and C.S. Zender (2013) Bounding the role of black carbon in the climate system: A scientific assessment, *J. Geophys. Res. Atmos.* **118**, 5380.

Cheng, M.-D. (2014) Geolocating Russian sources for Arctic black carbon, *Atmos. Environ*. **92**, 398. doi.org/10.1016/j.atmosenv.2014.04.031.

Hirdman, D., H. Sodemann, S. Eckhardt, J.F. Burkhart, A. Jefferson, T. Mefford, P.K. Quinn, S. Sharma, J. Ström and A. Stoh (2010) Source identification of short-lived air pollutants in the Arctic using statistical analysis of measurement data and particle dispersion model output, *Atmos. Chem. Phys.* **10**, 669.

Sharma, S., M. Ishizawa, D. Chan, D. Lavoue, E. Andrews, K. Eleftheriadis and S. Maksyutov (2013) 16-year simulation of Arctic black carbon: Transport, source contribution, and sensitivity analysis on deposition, *J. Geophys. Res. Atmos.* **118,** 943. doi:10.1029/2012JD017774, 2013

Smirnov, N.S., A.A. Romanovskaya and V.N. Korotkov (2015) Estimates of black carbon emissions from open fires in Russian Federation, *Meteor. and Hydrol.* in press.

Stohl, A., Z. Klimont, S. Eckhardt, K. Kupiainen, V.P. Shevchenko, V.M. Kopeikin and A.N. Novigatsky (2013) Black carbon in the Arctic: the underestimated role of gas flaring and residential combustion emissions, *Atmos. Chem. Phys.* **13,** 8833.

Vinogradova, A.A. (2000) Anthropogenic pollutants in the Russian Arctic atmosphere: sources and sinks in spring and summer, *Atmos. Environ*. **34,** 5151.

Vinogradova, A.A. (2014) Anthropogenic black carbon emissions to the atmosphere: surface distribution through Russian territory, *Atmospheric and Oceanic Optics* **27**, 1059. [in Russian]

Vinogradova, A.A. (2015) Anthropogenic pollution of the environment through the atmosphere in Russian Arctic Nature Reserves: spacial and seasonal variations, *Issledovanie Zemli iz Kosmosa*, in press. [In Russian]

Vinogradova, A.A. and A.O. Veremeichik (2013) Model estimates of anthropogenic black carbon concentration in the Russian Arctic atmosphere, *Atmospheric and Oceanic Optics* **26,** 414. [in Russian]

Wang, Q., D. J. Jacob, J. A. Fisher, J. Mao, E. M. Leibensperger, C. C. Carouge, P. Le Sager, Y. Kondo, J. L. Jimenez, M. J. Cubison and S. J. Doherty (2011) Sources of carbonaceous aerosols and deposited black carbon in the Arctic in winter-spring: implications for radiative forcing, *Atmos. Chem. Phys.* **11**, 12453.

Yearbook 2010 on Atmospheric Emissions of Pollution in Towns and Regions of Russian Federation (2011). (SRI Atmosphere, St.Petersburg), 560. [in Russian]

THE LARGE-SCALE CIRCULATION DURING AIR QUALITY HAZARDS IN BERGEN, NORWAY

T. WOLF[1], I. ESAU[1] AND J. REUDER[2]

[1]Nansen Environmental and Remote Sensing Center / Bjerknes Centre for Climate Research, Bergen, Norway

[2]Geophysical Institute, University of Bergen, Bergen, Norway

Keywords: air quality, blocking, large-scale circulation

INTRODUCTION

We present our analysis of the connection between the large-scale atmospheric circulation and winter-time air quality hazards in Bergen, Norway. We focus on days with high concentrations of Nitrogen dioxide (NO_2) defined as days with at least one hourly mean measurement of NO_2 concentrations, $\mu(NO_2) > 150$ $\mu g\ m^{-3}$.

Air quality hazards are a challenge for both the urban population and governance. The effect of air pollution by both NO_2 and particulate matter on mortality rates in the urban population has been shown both for long-term exposure [*Naess et al.*, 2007] and exposure to short-term peak pollution levels [*Madsen et al.*, 2012]. In particular the peak NO_2 pollution levels are connected to two factors: the variability in traffic, which is the main emission source for NO_2, and the variability in the dispersion conditions in the lower atmospheric boundary layer (ABL) within the city.

Bergen, Norway is located in a narrow, curved valley at the Norwegian west coast. The specific shape of the valley shelters the city from storms [*Jonassen et al.*, 2013] but is also the main reason for the frequent existence of winter-time ground-based temperature inversions leading to inefficient removal of the mostly traffic emitted NO_2. This causes exceedances of air quality thresholds especially in areas with high traffic, despite the overall low emissions [*Wolf et al.*, 2014].

In a previous study [*Wolf and Esau*, 2014] we showed that both the inter-monthly and inter-annual variability of the occurrence of these pollution events can be reasonably explained by the variability in the large-scale circulation. For this, we developed a simple proxy based on ERA-Interim wind, temperature and cloud fields directly over Bergen. We stated that a certain persistence in the large-scale circulation is necessary to reach the given threshold for high or very high pollution events ($\mu(NO_2) > 150$ $\mu g\ m^{-3}$ and $\mu(NO_2) > 200$ $\mu g\ m^{-3}$, respectively) according to Norwegian standards [http://luftkvalitet.info]. It usually takes a few days with fairly persistent ground-based temperature inversions in order to reach these threshold values. In this study we included a condition on the persistency of the circulation directly over Bergen into our proxy.

The local authorities issuing a regular air quality forecast often argue that persistent anticyclonic high-pressure systems or even blockings of the westerly jets over Bergen, Norway are necessary to reach events with hazardous air quality in the city [*Ødegaard et al.*, 2013]. These large-scale features should be easily predictable based on the ECMWF operational forecasts or the ERA-Interim reanalysis [*Dee et al.*, 2011]. However, in our prior analysis we did not find a lower cut-off pressure for the ERA-Interim sea-level pressure over Bergen, as it would be expected from this line of argumentation. In this study we identified the spatial patterns of the corresponding large-scale circulation

METHODS

The proxy in [*Wolf and Esau*, 2014] was based on the 24 h mean ERA-Interim fields of the 1000 hPa wind direction, wind speed, the deviation from the seasonal climatological mean surface temperature cycle and the cloudiness directly above Bergen. Since the 1000 hPa wind-speed varies in its distance from the ground, we now instead use surface (10 m) wind fields. We included thresholds for the meteorological fields also during the day prior to each potential high pollution day. The thresholds are given in Table 1. To account for the low emissions during typical low traffic days we used to set our proxy to 0 during Sundays and public holidays. Because of the above discussed persistence however, we now consider single days without high pollution in between two days with high pollution as polluted. This made the manual filtering of low-traffic days unnecessary.

variable	Thresholds	Thresholds (day-1)
Wind	05º < d < 175º, s < 3m/s	00º < d < 360º, s < 3m/s
	85º < d < 155º, s < 4m/s	85º < d < 165º, s < 5m/s
	85º < d < 135º, s < 5m/s	105º < d < 165º, s < 7m/s
	105º < d < 135º, s < 6m/s	105º < d < 115º, s < 8m/s
	105 º < d < 115 º, s < 7m/s	
Temperature	dT < -0.7	dT < -0.5
Cloud	Σ(clouds) < 1.75	Σ(clouds) < 2.0

Table 1.The empirically identified thresholds for the atmospheric circulation proxy: d – wind direction; s - wind speed; dT - temperature deviation from the seasonal climatological mean cycle and Σ(clouds) – cloudiness (the sum of low, middle and high cloud cover). The atmospheric circulation proxy is set to 1 if all variables are within their respective ranges.

To analyse the spatial pattern of the large-scale circulation during high pollution events we conducted a maximum covariance analysis of the NO_2 concentrations at the high traffic reference station and at an urban background station together with the 500 hPa geopotential height anomaly from the climatological monthly mean. For this we calculated the covariance matrix between a matrix consisting of the pollution measurements at the two reference stations ($\mathcal{A}$) and the 500 hPa geopotential height anomaly at each grid point ($\mathcal{B}$). After removal of the temporal means from $\mathcal{A}$ and $\mathcal{B}$ and normalisation against their standard deviations, we identified the two dominating modes of co-variability (only two modes are possible since there are only two pollutant measurement stations in Bergen, Norway) using SVD analysis

$$\mathcal{A}' * \mathcal{B} = \mathcal{U} * \mathcal{D} * \mathcal{V}'$$

with U and V the matrices of the singular vectors and D the matrix of the singular values.

Finally, we tested for the existence of atmospheric blockings during days with hazardous air quality with a simplified version of the blocking index used in [*Pelly and Hoskins*, 2003] based on the ERA-Interim 500 hPa geopotential height at a 2.5º horizontal resolution.:

$$B = \frac{2}{\Delta\varphi}\int_{\varphi_0}^{\varphi_0+\Delta\varphi/2} geop(\varphi,\lambda)\,d\varphi - \frac{2}{\Delta\varphi}\int_{\varphi_0-\Delta\varphi/2}^{\varphi_0} geop(\varphi,\lambda)\,d\varphi$$

With $\Delta\varphi = 30º$, geop(φ,λ) the 500 hPa geopotential height for each grid cell centred on latitude $\varphi_0 = \varphi_c \pm \delta$ and longitude λ. We used $\varphi_c = 57.5ºN$ as the constant centre latitude. This is in good agreement with the mean central latitude of the NH jet axis over Western Europe (personal communication Clemens Spensberger, Geophysical Institute, University of Bergen) and with the winter-time central blocking latitude in [*Pelly and Hoskins*, 2003]. The span of the centre latitude δ was between -5º and 5º. We assumed a grid-cell to be blocked if $\max_\delta(B) > 0$ as part of a longitudinal belt longer than 15º and during at least 5 consecutive days. For the SVD analysis and the comparison to the blocking pattern, we treated gap-days between two measured pollution days as not polluted.

RESULTS

The strongest improvement in the revised ERA-Interim proxy for high pollution events is visible in the falls alarm rate, changing from 0.6 to 0.5 (see Table 2). A comparison of the skill scores obtained without treatment of gap-days in the measured high pollution events resulted in a detection rate of 0.81 / 0.81 and a falls alarm rate of 0.56 / 0.53 confirming that most of the improvement in the skill-scores of our proxy resulted from invoking additional conditions from the day prior to high pollution events and not from the slightly higher number of measured high pollution days. The improvements illustrate the importance of the persistence in the local conditions leading to high pollution events. However, the small range of the improvements also indicates that the necessary combination of the local atmospheric variables to a large degree only occurs during persistent larger-scale circulation features – persistent enough to reach the high pollutant concentrations within the Bergen valley. Therefore, there is also only little change between the overview over the monthly and seasonal number of high pollution days in Fig.1 and in the correlation indices between the measurements and our proxy on a monthly (0.88, before 0.85) and seasonal (0.93, before 0.93) basis, when compared to [*Wolf and Esau*, 2014].

	Skill scores
Detection rate	0.82 / 0.82
False alarm rate	0.53 / 0.50
Correct null prediction rate	0.88 / 0.89
Critical success index	0.43 / 0.45
True skill score	0.69 / 0.70
Heidke skill score	0.53 / 0.55

Table 2: Skill score measures after [*Ryan et al.*, 2000]. The first/second numbers are the skill scores without/with constraint on cloudiness.

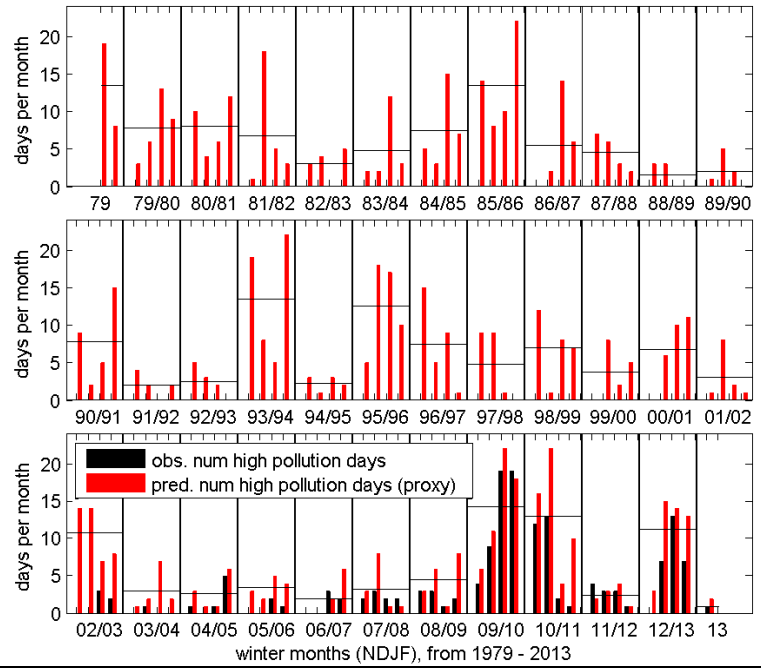

Fig. 1: Monthly sum of observed and predicted days with high NO2 air pollution based on our proxy in ERA-Interim for the extended winter seasons 1979 – 2013. The horizontal lines show the seasonal mean of the monthly sum of predicted high pollution days.

These larger scale circulation features are visible as the two possible modes of variability. The results confirm the assumption that high pressure systems are not the main steering parameter of the high pollution events in Bergen, Norway. The high pressure pattern is only the second mode of co-variability, explaining only 11% of the explained co-variance between the climatologic monthly mean 500 hPa geopotential height anomaly and the pollution.

The first and dominant mode is characterized by a low pressure system centred over Southwest-France and a high pressure system centred over Iceland. There is some resemblance to a strongly negative NAO-like pattern but the centres of activity are shifted. This pattern also agrees well with the characteristic easterly winds used for our atmospheric circulation proxy and explains the negative correlation between the monthly number of high pollution events and the monthly mean NAO index - characterizing the strength of the westerlies over Bergen - that we found in our previous analysis. The long sequence of highly polluted days in January 2010 resulted in extreme NO_2 concentrations both at the high traffic and the urban background reference stations. The length of this sequence can be attributed to the specific behaviour of the large-scale circulation pattern. The decreasing first and increasing second principle components suggest that the sequence started off with a pattern characteristic for the first mode of variability while later becoming more similar to the second mode.

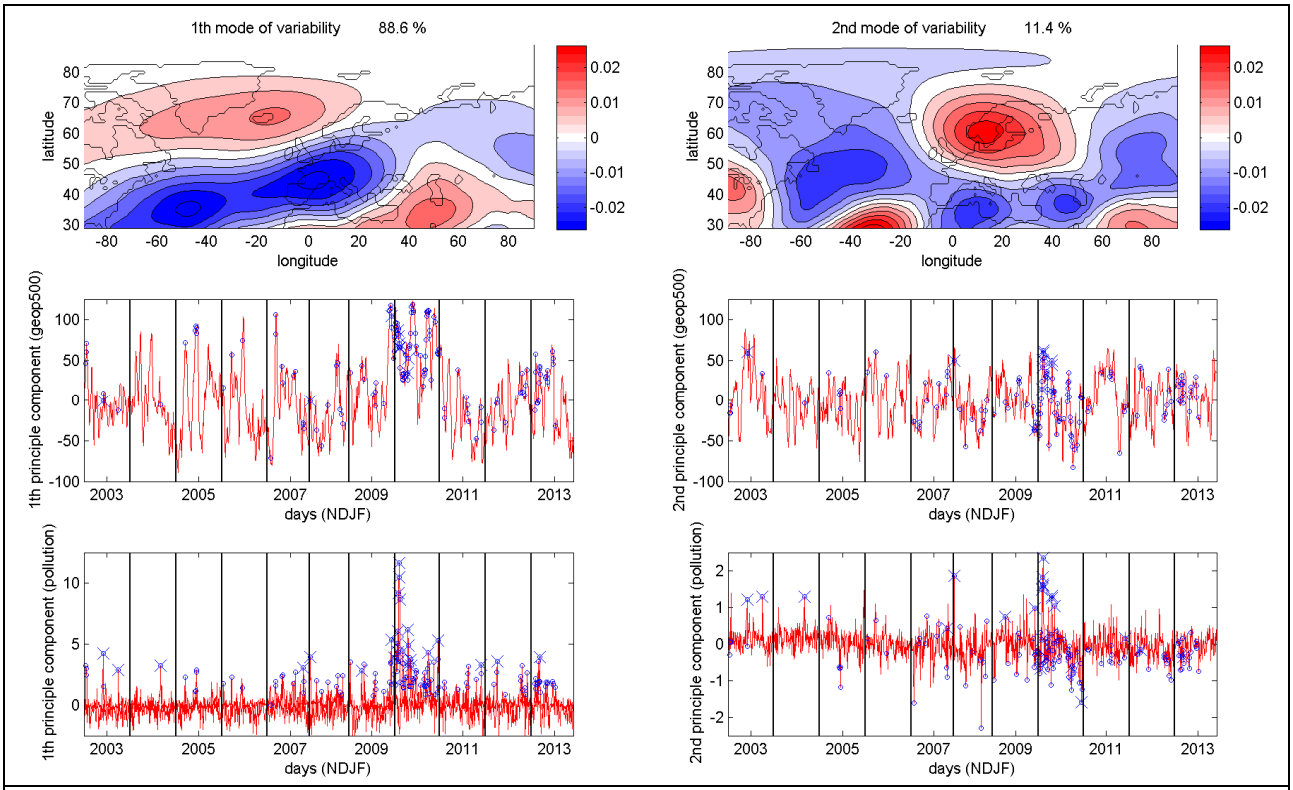

Fig. 2: SVD analysis of the climatologic monthly mean 500 hPa geopotential height anomaly and the daily maximum NO_2 concentration at the high traffic and urban background reference stations in Bergen, Norway. The top-row shows the pressure distribution characteristic for the 1th and 2nd mode of variability. The numbers above the panels state the explained co-variability by each mode. The 2nd and third row show the principle components connected to each mode of variability for the 500 hPa geopotential height anomaly and NO_2 concentrations. The blue circles and crosses mark measurements with NO_2 concentrations above the 150 µg m^{-3} and 200 µg m^{-3} thresholds at the high traffic and urban background reference stations, respectively.

The comparison of the blocking index to the measured high pollution events confirms the results from the EOF-analysis (see Table 3). There is only little overlap between a blocking pattern directly above Bergen and high pollution cases. There was however a much higher correlation to blockings west of 0º longitude (between 0.55 on a monthly and 0.83 on a seasonal basis) consistent with the first mode of

variability that resembles a blocking-like pattern. The overlap between the blockings and the high pollution cases however was still only 48 and 20 for the 150 μg m^{-3} and 200 μg m^{-3} thresholds, respectively. When drastically reducing the conditions on the zonal and temporal extent of the blockings to only 5º in the zonal direction and a minimum duration of 2 days, the overlap was higher for both the blockings directly above Bergen and for blockings west of 0ºW. The correlations for the blockings above Bergen increased, whereas the correlations west of 0ºW even slightly decreased. A test with the central latitude 50ºN that is more resembling our first mode of variability resulted in a lower overlap between the blockings west of 0ºW but in slightly higher correlation indices. This is also the central latitude that was originally proposed by *Tibaldi and Molteni* [1990].

		comparison pollution and blockings		
	number of events	coinciding	correlation (monthly)	correlation (seasonally)
$\mu(NO_2) > 150$ μg m^{-3}	149	28 (51)	0.29 (0.45)	0.41 (0.59)
$\mu(NO_2) > 200$ μg m^{-3}	45	14 (17)	0.16 (0.28)	0.36 (0.50)

Table 3: Comparison between high pollution events and atmospheric blockings. The number in the parenthesis denote the results for a proxy index based on strongly reduced conditions on the zonal and temporal extend of the blockings (see text for details).

CONCLUSIONS

For the analysis of high pollution events and the prediction of their future occurrence under a changing climate, it is important to use a bottom-up approach basing the identification of conditions with weak pollutant dispersion on actual local measurements. The analysis of the large-scale circulation during the high pollution events together with the results from [*Wolf et al.*, 2014] also suggests that any forecast of the pollution levels within the valley will suffer from large biases if the valley topography is not properly resolved or the applied models are unable to simulate turbulence in the stably stratified ABL.
Through the strong steering of the circulation at the Norwegian west coast by the Norwegian topographic features [*Barstad et al.*, 2008] and of the circulation within the Bergen valley by the specific shape of the surrounding mountains [*Wolf et al.*, 2014], there is a distinct pattern of wind-speeds and directions, during which high pollution events can occur in Bergen, Norway. Our simple atmospheric circulation proxy was able to reasonably reproduce the variability in the occurrence of such events on both monthly and seasonal time scales.

ACKNOWLEDGMENTS

This study was supported by the Ph.D. studentship funding from the GC Rieber Foundation, the FinKlima project of the Regional research foundation for Western Norway and the REGSCEN internal project of the Bjerknes Centre for Climate Research. The pollution measurements have been provided by the Norwegian Institute for Air Research (NILU).

REFERENCES

Barstad, I., A. Sorteberg, F. Flatøy, and M. Déqué (2008), Precipitation, temperature and wind in Norway: dynamical downscaling of ERA40, *Clim. Dyn.*, *33*(6), 769–776, doi:10.1007/s00382-008-0476-5.

Dee, D. P. et al. (2011), The ERA-Interim reanalysis: configuration and performance of the data assimilation system, *Q. J. R. Meteorol. Soc.*, *137*(656), 553–597, doi:10.1002/qj.828.

Jonassen, M. O., H. Olafsson, A. S. Valved, J. Reuder, and J. A. Olseth (2013), Simulations of the Bergen orographic wind shelter, *Tellus A*, *65*, 19206, doi:10.3402/tellusa.v65i0.19206.

Madsen, C., P. Rosland, D. A. Hoff, W. Nystad, P. Nafstad, and O. E. Naess (2012), The short-term effect of 24-h average and peak air pollution on mortality in Oslo, Norway., *Eur. J. Epidemiol.*, *27*(9), 717–27, doi:10.1007/s10654-012-9719-1.

Naess, Ø., P. Nafstad, G. Aamodt, B. Claussen, and P. Rosland (2007), Relation between concentration of air pollution and cause-specific mortality: four-year exposures to nitrogen dioxide and particulate matter pollutants in 470 neighborhoods in Oslo, Norway., *Am. J. Epidemiol.*, *165*(4), 435–43, doi:10.1093/aje/kwk016.

Pelly, J. L., and B. J. Hoskins (2003), A New Perspective on Blocking, *J. Atmos. Sci.*, *60*(5), 743–755, doi:10.1175/1520-0469(2003)060<0743:ANPOB>2.0.CO;2.

Ryan, W. F., C. A. Piety, and E. D. Luebehusen (2000), Air Quality Forecasts in the Mid-Atlantic Region: Current Practice and Benchmark Skill, *Weather Forecast.*, *15*(1), 46–60, doi:10.1175/1520-0434(2000)015<0046:AQFITM>2.0.CO;2.

Tibaldi, S., and F. Molteni (1990), On the operational predictability of blocking, *Tellus A*, *42*(3), 343–365, doi:10.1034/j.1600-0870.1990.t01-2-00003.x.

Wolf, T., and I. Esau (2014), A proxy for air quality hazards under present and future climate conditions in Bergen, Norway (in production), *Urban Clim.*, doi:10.1016/j.uclim.2014.10.006.

Wolf, T., I. Esau, and J. Reuder (2014), Analysis of the vertical temperature structure in the Bergen valley, Norway, and its connection to pollution episodes, *J. Geophys. Res. Atmos.*, *119*(18), 10,645–10,662, doi:10.1002/2014JD022085.

Ødegaard, V., K. I. Gjerstad, L. H. Slørdal, H. Abildsnes, and T. Olsen (2013), *Bedre byluft Prognoser for meteorologi og luftkvalitet i norske byer*, Norwegian Meteorological Institute.

COMPOSITION OF NORMAL ALKANES CONTAINED IN THE ORGANIC PARTICULATE MATTER SAMPLED IN THE TROPOSPHERE OVER WEST SIBERIA: RESULTS OF AIRCRAFT OBSERVATIONS CARRIED OUT IN 2012-2013

N.G. VORONETSKAYA[1], G.S. PEVNEVA[1], A.K. GOLOVKO[1], A.S. KOZLOV[2], M.YU. ARSHINOV[3], B.D. BELAN[3], D.V. SIMONENKOV[3] and G.N. TOLMACHEV[3]

[1]Institute of Petroleum Chemistry, Siberian Branch of the Russian Academy of Sciences, Tomsk, Russia.

[2]Institute of Chemical Kinetics and Combustion, Siberian Branch of the Russian Academy of Sciences, Novosibirsk, Russia.

[3]V.E. Zuev Institute of Atmospheric Optics, Siberian Branch of the Russian Academy of Sciences, Tomsk, Russia.

Keywords: ATMOSPHERIC AEROSOL, NORMAL ALKANES, COMPOSITION

INTRODUCTION

In the composition of the aerosol particles in addition to the inorganic component of the important role, as it turned out, plays an organic component (Bialek *et al.*, 2012; Elsasser *et al.*, 2012; Ge *et al.*, 2011; Wang *et al.*, 2012; Shakya *et al.*, 2012; Kim *et al.*, 2013). The composition of the organic aerosol is varied: 150 amines only had been identified in the aerosol composition in work (Lee and Wexler, 2013); another authors (Park *et al.*, 2013) detected from 186 organic ions to 494 radicals in different samples. Furthermore, in the aerosol material there are many such organic compounds as aromatic hydrocarbons and chlorine-, sulfur-, and nitrogen-containing species (Isidorov, 1985; Ravindra *et al.*, 2008). At present, organic aerosols are intensely studied around the world. An exception is the territory of Russia, for which information on the amount, composition, and spatiotemporal variations in the organic component of the atmospheric aerosol is totally absent. For this reason, the authors of the present paper initiated in 2012 the interdisciplinary project of the Siberian Branch of the Russian Academy of Sciences aimed at studying the conditions for the formation and behavior of the organic component of aerosols in the atmosphere over the Siberian region. Some part of this research related to the study of the organic component of the atmospheric aerosol is presented here.

METHODS

Studies are performed on board the research aircraft laboratory “Optik” (Antokhin et al., 2012) based on Tupolev-134 since 2011. In the 2012 - 2013, atmospheric aerosol samples were taken on board the research aircraft TU-134 “Optik” in the region of the Karakan Pine Forest on the right-hand coast of the southern part of the Novosibirsk Reservoir. The samples were collected in the tropospheric layer of 500–7000 m on reinforced Teflon filtering membranes Grimm 1.113A with a mean pore diameter of 0.8-1.2 μm.

The collected aerosol samples were treated as follows: the organic part was extracted from the filter, using chromatographic acetone in an ultrasonic bath; then, it was concentrated in vacuum up to 50 μL, with the subsequent analysis using a chromatography mass spectrometer Agilent 6890N (50 - 250 °C with velocity 5 °C/min., isotherm at the initial and final temperature – 3 and 45 min, respectively). Hydrocarbons were identified using mass spectral library databases NIST, Wiley, as well as by comparing retention times of reference compounds in model mixtures (Alkane Standard Solutions $C_8 – C_{20}$ and $C_{21} – C_{40}$ by SIGMA –

ALDRICH). Detailed description of the selection of aerosol sampling and analysis are described in (Voronetskaya *et al.*, 2014)
Aerosol sampled in the winter of 2012, differ significantly in the total content of n-alkanes. In the sample of the January content of alkanes is 15.4 ng/m^3, in December - 0.4 ng/m^3. The molecular weight distribution (MWD) of n-alkanes of samples taken in January and December 2012, also have differences: homologous series of n-alkanes in the sample aerosol January comprise compounds with a carbon number of 12 - 26; in the December sample, this series presents the compounds C_{13} - C_{19} (fig.1a). Among the n-alkanes in the sample January predominate hexa- ($C_{16}H_{34}$) and heptadecane ($C_{17}H_{36}$), whereas in the December aerosol sample contained in a maximum amount pentacozane ($C_{25}H_{52}$). Index value CPI, used to determine the type of source of n-alkanes in the atmosphere, January sample is 2 or more than 2 times the value of the same index in December sample aerosol (0.9). These differences are probably due to a significant period of time (actually 11 months) between sampling.
At the same time, the total content of n-alkanes in aerosol sampled in December 2012 (0.4 ng/m^3), is comparable to their content in January 2013 (1.6 ng/m^3). Also MWD of n-alkanes of the two samples are similar character. Maximum of MWD in the December samples (2012) accounted for hexadecane ($C_{16}H_{34}$) and in January (2013) - on heptadecane ($C_{17}H_{36}$) (fig. 1d).
Comparison of n-alkanes sampling aerosols January 2012 and January 2013 showed their considerable similarity: homologous series of n-alkanes are compounds C_{12} - C_{26} and C_{14} - C_{23}, respectively; the values of the CPI was 2.0, and a year later - 2.8

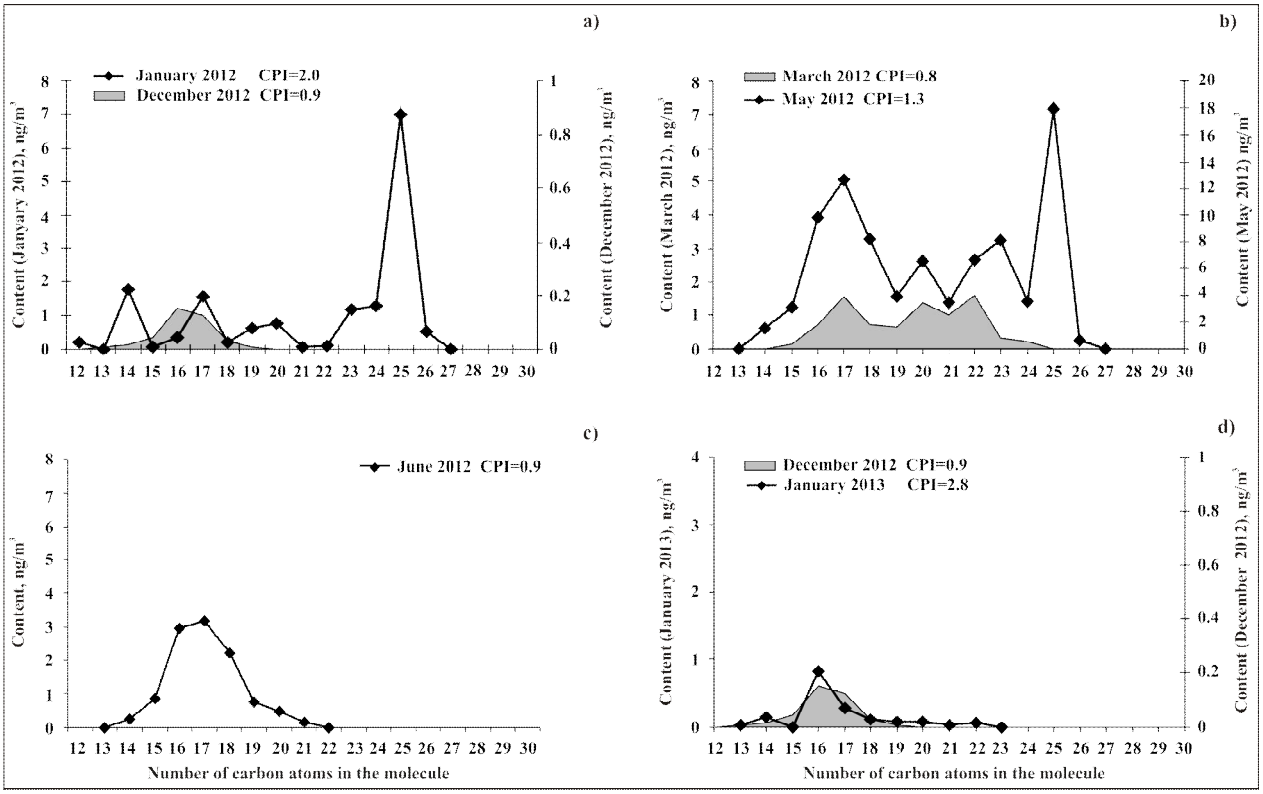

Figure 1. Molecular weight distributions of normal alkanes in aerosol samples of regular flights in 2012 year

The total content of n-alkanes of aerosol samples collected in the spring of 2012, was 8.3 ng/m^3 in March and 86.0 ng/m^3 in May.
Despite the large difference in the amount of n-alkanes in the samples collected in spring, their MWD have similar character - they are bimodal with peaks attributable to heptadecane (C_{17} H_{36}), eicosane ($C_{20}H_{42}$) and docozane (C_{22} H_{46}) in the March sample; heptadecane (C_{17} H_{36}) and pentacozane (C_{25} H_{52}) - in the May sample (fig.1b). The length of the homologous series of n-alkanes in the spring aerosol

samples is virtually identical and includes compounds with 14, 15 – 24, 26 carbon atoms in the molecule. The value of the CPI is higher in aerosol sample in May 2012 (1.3), compared with the March sample (0.8).

In the summer, in June 2012, the total content of n-alkanes is 10.9 ng/m^3, which is close to the content of n-alkanes in the sample taken in March of the same year. The molecular weight distribution of n-alkanes of June sample has unimodal peak attributable to heptadecane ($C_{17}H_{36}$) (fig. 1c). The length of the homologous series comprises compounds having 14 - 21 carbon atoms in the molecule. The value of the CPI is low (0.9).

In winter 2013 the total amount of n-alkanes in the January sample is 1.6 ng/m^3, whereas in the sample of February their content increases to 9.8 ng/m^3. Among the identified n-alkanes in both samples shows a maximum concentration for heptadecane ($C_{17}H_{36}$) (fig. 2a). The value of the CPI is reduced from 2.8 in January to 1.7 in February. Homologous series of n-alkanes in the January aerosol sample comprises compounds having 14 - 23 carbon atoms in the molecule; in the February sample the number of the series is much broader and includes compounds of C_{12} - C_{30} (fig. 2a).

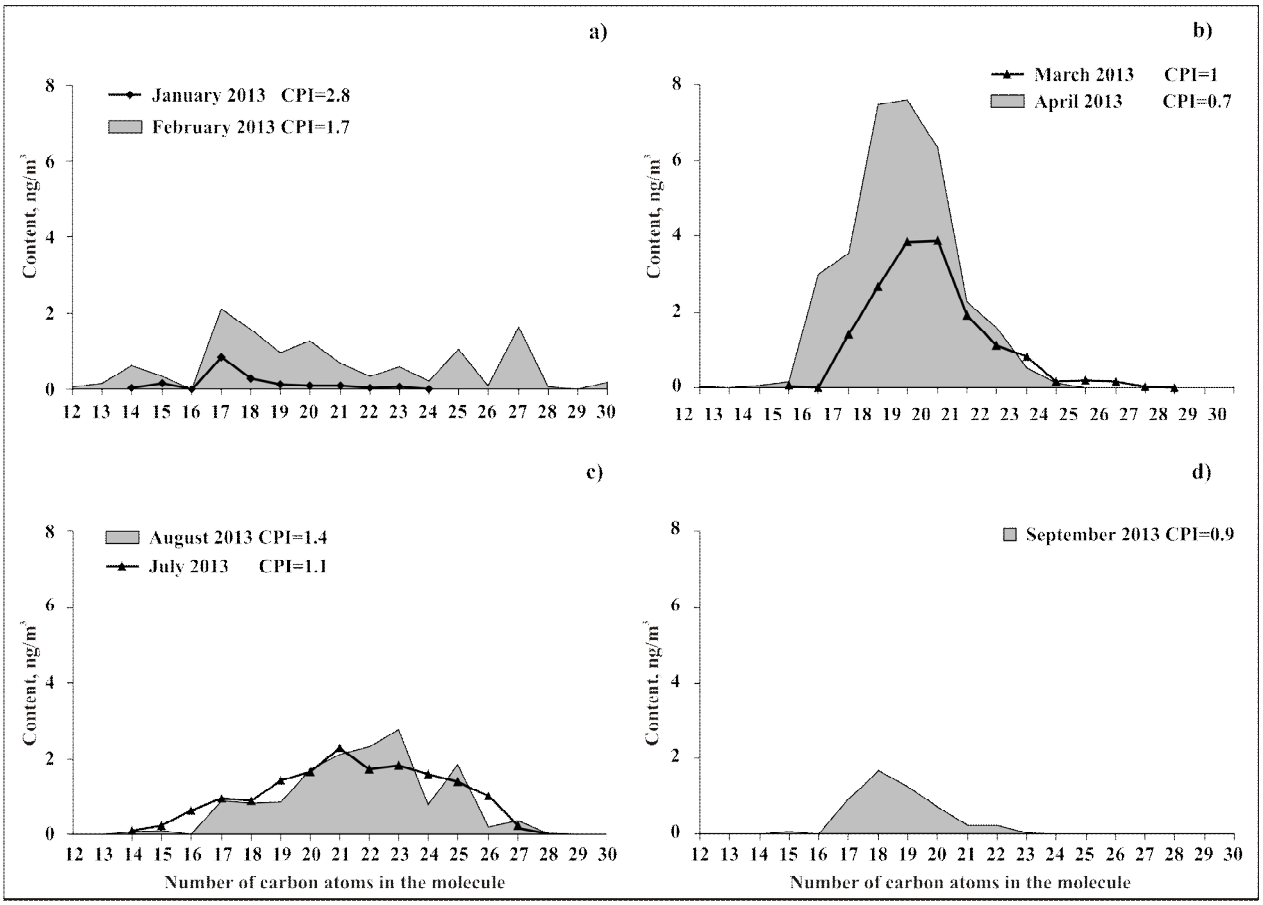

Figure 2. Molecular weight distributions of normal alkanes in aerosol samples of regular flights in 2013

In spring 2013 the content of n-alkanes in aerosols is 16.2 ng/m^3 in March and 32.7 ng/m^3 in April, which is higher than the content of n-alkanes in the winter samples of aerosols. In March aerosol identified compounds 15 - 27 carbon atoms in the molecule, in the April sample - 12 - 24 carbon atoms. The character of the molecular weight distributions of n-alkanes in spring aerosol samples is similar (fig. 2b). At the highest concentration in the March sample contains nonadecane ($C_{19}H_{40}$) and eicosane ($C_{20}H_{42}$), in the April sample - octodecane ($C_{18}H_{38}$) and nonadecane ($C_{19}H_{40}$). Value of the index CPI = 1 in the March aerosol sample and 0.7 in the April sample, which is below the value of the index in the aerosol samples taken during the winter.

In summer 2013 the total amount of n-alkanes is 15.7 ng/m^3 in the July aerosol sample and 14.5 ng/m^3 in the August sample, which is lower than the total content of n-alkanes in aerosols sampled in the spring. The length of the homologous series of n-alkanes aerosol samples taken in the summer, almost the same and includes compounds with 14 - 27, 28 carbon atoms in the molecule (fig. 1c). Among n-alkanes in aerosol sample of July the heneicozane ($C_{21}H_{44}$) contained in a maximum concentration; in the August sample prevails tricozane ($C_{23}H_{48}$).
The values of the CPI are 1.1 in the July aerosol sample and 1.4 in the August one, which is higher than the CPI spring aerosol samples, but lower than the same index in winter aerosol samples.
The aerosol sampled in September 2013 contain 5 ng/m^3 n-alkanes. Homologous series of n-alkanes are compounds having a carbon number in a molecule of 15 to 23 (fig. 2d). At the maximum concentration found octodecane ($C_{18}H_{38}$). Value of the index CPI = 0.9, which is close to the values of the same index in the spring aerosol samples.

CONCLUSIONS

Analyzed the composition of aerosol samples on alkanes for two years, we can conclude that:
- the total content of n-alkanes in the spring increases and decreases in the winter.
- the length of the homologous series of n-alkanes has no seasonal dependence.
- a maximum in the molecular weight distribution of n-alkanes varies depending on the season. In 2012, during the winter and spring seasons predominate compounds of C_{17}, C_{22} and C_{25}, whereas in the summer - the connection of C_{17}. In 2013, the winter is dominated by compounds of C_{17}, in the spring - a compound of C_{18} - C_{20}, and in the summer - the connection of C_{21} and C_{23}.
- CPI index value for a given length of the homologous series (mean, C_{12} to C_{28}) does not reflect the contribution of sources of n-alkanes in the atmosphere.

ACKNOWLEDGEMENTS

This work was supported by Presidium of the Russian Academy of Sciences (Program No. 4), the Branch of Geology, Geophysics and Mining Sciences of RAS (Program No. 5); interdisciplinary integration projects of the Siberian Branch of the Russian Academy of Science No. 35, No. 70 and No. 131; State contracts of the Ministry of Education and Science of Russia No. 14.604.21.0100 (RFMTFIBBB210290) and No. 14.613.21.0013 (RFMEFI61314X0013); and Russian Foundation for Basic Research (grants No. 14-05-00526, No. 14-05-00590, No. 14-05-93108).

REFERENCES

Antokhin, P.N., Arshinov, M.Yu., Belan, B.D., Davydov, D.K., Zhidovkin, E.V., Ivlev, G.A., Kozlov, A.V., Kozlov, V.S., Panchenko, M.V., Penner, I.E., Pestunov, D.A., Simonenkov, D.V., Tolmachev, G.N., Fofonov, A.V., Shamanaev, V.S. and Shmargunov, V.P. **(**2012) Optik-É AN-30 aircraft laboratory: 20 years of environmental research, *J Atmos. Ocean. Tech.*, **29**, 64.

Bialek, J., Dall'Osto, M., Monahan, C., Beddows, D. and O'Dowd, C. (2012) On the contribution of organics to the North East Atlantic aerosol number concentration, *Environ. Res. Lett.*, **7**, 7.

Elsasser, M., Crippa, M., Orasche, J., DeCarlo, P.F., Oster, M., Pitz, M., Cyrys, J., Gustafson, T.L., Pettersson, J.B.C., Schnelle Kreis, J., Prevot, A.S.H. and Zimmermann, R. (2012) Organic molecular markers and signature from wood combustion particles in winter ambient aerosols: Aerosol mass spectrometer (AMS) and high time-resolved GC-MS measurements in Augsburg, Germany, *Atmos. Chem. Phys.*, **12**, 6113.

Ge, X., Wexler, A.S., and Clegg, S.L. (2011) Atmospheric amines – Part 1. A review, *Atmos. Environ.* **45**, 524.

Isidorov, V.A.(1985) *Organic Chemistry of the Atmosphere* (Khimiya, Leningrad, U.S.S.R.) [in Russian].

Kim, K.H., Sekiguchi, K., Kudo, S., Kinoshita, M. and Sakamoto, K. (2013) Carbonaceous and

ionic components in ultrafine and fine particles at four sampling sites in the vicinity of roadway intersection, *Atmos. Environ.* **74**, 83.
Lee, D.Y. and A.S. Wexler (2013) Atmospheric amines – Part III: Photochemistry and toxicity, *Atmos.Environ.* **71**, 95.
Park, J.H., Goldstein, A.H., Timkovsky, J., Fares, S., Weber, R., Karlik, J. and Holzinger, R. (2013) Active atmosphere-ecosystem exchange of the vast majority of detected volatile organic compounds, *Science* **341**, 643.
Ravindra, K., Sokhi, R. and Van Grieken, R (2008) Atmospheric polycyclic aromatic hydrocarbons: Source attribution, emission factors and regulation, *Atmos.Environ.* **42**, 2895.
Shakya, K.M., Place Jr., P.F., Griffin, R.J. and Talbot, R.W. (2012) Carbonaceous content and water-soluble organic functionality of atmospheric aerosols at a semirural New England location, *J Geophys. Res.* **117**, doi: 10.1029/2011JD016113
Voronetskaya, N.G., Pevneva, G.S., Golovko, A.K., Kozlov, A.S., Arshinov, M.Yu., Belan, B.D., Simonenkov, D.V. and Tolmachev, G.N. (2014) Hydrocarbon Composition of Tropospheric Aerosol in the South of Western Siberia, *Atmos. Ocean. Opt.*, **27**, 547.
Wang, Z., Wang, T., Guo, J., Gao, R., Xue, L., Zhang, J., Zhou, Y., Zhou, X., Zhang, Q., and Wang, W. (2012) Formation of secondary organic carbon and cloud impact on carbonaceous aerosols at Mount Tai, North China, *Atmos. Environ.* **46**, 516.

CITY AND MODERN CLIMATE CHANGE

N.N.VOROPAY[1,2]

[1]V.B.Sochava Institute of Geography SB RAS, Irkutsk, Russia.

[2]Institute of Monitoring of Climatic and Ecological Systems SB RAS, Tomsk, Russia.

Keywords: heat island, climate change, solar radiation, air temperature, precipitation.

Climatic conditions in the cities are considerably differed from the surrounding rural areas, and these changes are higher in cities with large area. Evidences of climate changes were registered in large cities hundreds years ago. For example, H.E.Landsberg (1956) shows testimony on a severe air pollution in London in the XVII century. The pollution greatly weakened the solar radiation in the city.

City heat island is one of the main features of the urban climate. Heat island is characterized by elevated air temperatures compared to the countryside. This effect has been studied in many experimental works, including direct temperature measurements, remote sensing of radiation temperature of the underlying surface and numerical simulation. Many authors (Landsberg, 1970; Berlyand, Kondratyev 1972; Unintended effects ..., 1974; Marchuk, Penenko *et al.*, 1979; Trofimova, Konovalova, 1988; Kislov, Konstantinov 2011) claims that usually the heat island is a complex structure. Each quarter of the urban area is a heat source for the surrounding open spaces. The average temperature in the big city often higher than the temperature of the surrounding areas by 1-2^{o}C. The temperature difference can reach 6-8^{o}C at night with weak winds. The difference is usually reduced at strong winds. The effect of urban heat island is seasonal.

Some authors (Kato, 1996, Hansesn, 2010) attempts to separate the impact of the heat island from the actual warming. Revealed that in cities with a population of over 100 thousands for the period 1920-1992 the effect of heat island is about 1.0-2.5^{o}C/100 years. This value is comparable to the magnitude of global warming.

Great influence on the urban climate has an air pollution with various contaminants. The source of anthropogenic aerosol are industrial emissions of solid and liquid particles, heating system and transport.

Increase of aerosol concentration over cities dramatically reduces incoming solar radiation. According to Landsberg (1970) direct solar radiation in the big cities reduced by about 15%, ultraviolet radiation decreases by 30%, and in the winter months, it can disappear completely. The sunshine duration contracts by 5-15%. Major role in reducing of the solar radiation in urban areas plays a thin bottom layer of air containing the largest number of aerosol particles. Within this layer, horizontal visibility sharply reduced up to 10-20% in comparison with its value in suburban areas.

Raised amount of condensation nuclei in the air over cities and strengthening of upward air movements lead to an increase in cloud cover and local precipitation. There is evidence that in some industrial cities there is a weekly cycle in the amount of precipitation. Precipitations decreases over the weekend when the industrial enterprises do not work (Budyko, 1971).

Some features of urban climate cover vast areas reaching hundreds of kilometers with the development of urbanization in areas of high population density. Summing climate impact of numerous closely located cities each of them acts as a source of heat and air pollution.

Placement of industrial plants in the Predbaikalie region is not uniform. Almost two-thirds of factories is located in the Irkutsk-Cheremhovo industrial area - a narrow strip stretched 150 km from Cheremhovo to Shelekhov. It is limited agricultural areas of the Ust-Orda Buryat Ocrug in the North, and sparsely populated taiga areas in the south.

The Irkutsk-Cheremhovo industrial area have extremely unfavorable weather conditions for the purification of the atmosphere (Linevich, Sorokin, 1992). The area is influenced by Siberian anticyclone developed during the winter months. A large number of windless days and deep temperature inversions characterizes winter. For example, in Irkutsk repeatability of weak winds is 70%, surface temperature inversions - 80%, periods with air stagnation - 44% during winter. The lowest temperature at the same time related with maximum fuel consumption, and heat and the highest pollution from combustion products.

To determine the effect of the city on the direct solar radiation we analyzed the long-term distribution of its intensity at weather stations Irkutsk and Ilchir during 1961-1986. It is known, the solar radiation determined by the height of the sun and the transparency of the atmosphere at cloudless sky. Studied weather stations located almost on the same latitude (about 52N). The sun height throughout the year is the same. The atmosphere transparency in Irkutsk should be much lower because it is one of the largest industrial centers in Eastern Siberia. We have found that, the intensity of direct solar radiation at noon on a perpendicular surface with cloudless sky (with optic atmosphere mass m = 2) in Ilchir is higher by 0.14 kW/m^2 in average during the year. This difference varies from 0.1 kW/m^2 (May) to 0.19 kW/m^2 (January). Thus, local changes of atmospheric transparency occurring in Irkutsk due to industrial air pollution may reduce the influx of solar radiation by 10-20%.

Long-term data on the global mean annual temperatures indicate a warming over the past 100 years, and much of this warming accounts for the last 30-40 years (IPCC, 2013). Partly it is due to the growth of cities. Weather station Irkutsk has a period of measurements of air temperature from 1882 to the present time. In the XIX century station was located away from the city. During the XX century in the period of industrialization Irkutsk become the regional center and has grown significantly. The area of the city has increased tenfold. Now the site of the weather station is located in the city center. One of the factors of climate change is the city itself.

The Irkutsk city heat island effect is visible at comparison of long-term observations at weather stations Irkutsk and Homutovo, located 25 km from the city. The maximal effect occurs in winter months when differences between urban and rural areas exist even at mean monthly air temperature (up to 5^{o}C) (Table. 1). The temperature contrasts in summer months are smoothed and the difference in temperature rarely exceeds 0.5^{o}C. At the same time in June in most cases the average monthly temperature in Homutovo by 0.6-1.1 ^{o}C higher than in Irkutsk. The long-term fluctuations in air temperature at both stations occur synchronously with regional and global variations. Trends in the monthly average and annual air temperature over the past 50 years in urban and rural areas do not differ from each other (Table. 2). Annual temperature trends are 0.46-0.47 ^{o}C / 10 years.

	I	II	III	IV	V	VI	VII	VIII	IX	X	XI	XII	Year
Mean	4.25	4.15	2.73	0.46	0.17	-0.2	0.04	0.23	0.51	1.37	2.96	3.67	1.69
Min	3.3	3	1.6	0	-0.3	-0.9	-0.3	-0.2	0.2	0.9	2.1	2.5	1.33
Max	5.0	5.3	3.9	1.2	0.7	0.3	0.7	0.7	1.0	1.9	3.9	4.6	2.08

Table 1. Difference in monthly and annual air temperatures at weather station Irkutsk and Homutovo for 1960-2008, ^{o}C.

	I	II	III	IV	V	VI	VII	VIII	IX	X	XI	XII	Year
Homutovo	0.38	1.09	0.47	0.41	0.39	0.36	0.40	0.34	0.36	0.41	0.56	0.49	0.47
Irkutsk	0.41	1.09	0.52	0.46	0.39	0.30	0.36	0.31	0.33	0.46	0.47	0.51	0.46

Table 2. Trends in monthly and annual air temperature (^{o}C/10 yr) for 1961-2008.

Factors modifying and increasing precipitation in the cities includes (Landsberg 1983) the presence of heat island, which leads to more intense vertical air movement, which is the main condition for the formation of precipitation. The second factor is the effect of obstacles that is slowing the movement of synoptic systems, in which rain forming. In many cases, both factors act simultaneously and therefore it is very difficult to distinguish the contribution of each factor in the total perturbation introduced by the city

into precipitations. The third factor affecting the formation of precipitatio0ns is an air pollution.

The highest repeatability in the study area have north-west winds. Impact of industrial centers should be most noticeable in the settlements located in the direction of the prevailing wind – at the south spurs of the Lena-Angara plateau. On the background of general decrease in annual precipitation, some increase occurs at weather stations Bohan, Ust-Orda, Homutovo (with rate 0.2-1.3 mm / yr). Analysis of the seasonal changes in precipitation shows that in winter increase of precipitations occurs also at northern and mountain areas, which is likely due to the influence of local physiographic conditions.

ACKNOWLEDGEMENTS

The work was supported by Russian Fund for Basic Research grant №14-05-00502

REFERENCES

Berlyand M.E., Kondratev K.Ya. (1972) *Cities and climate of the planet*. (L.: Gidrometeoizdat). 40 p. (in Russian)

Budyko M.I. (1971) *Climate and life*. (L. Gidrometeoizdat). 472 p. (in Russian)

IPCC, 2013: Climate Chang 2013: *The Physical Science Basis. Contribution of Working Group I to the Fifth Assessment Report of the Intergovernmental Panel on Climate Change* [Stocker, T.F., D/ Qin, G.-K. Plattner, M.Tignor, S.K. Allen, J. Boschung, A.Nauels, Y. Xia, V. Bex and P.M. Midgley (eds.)]. (Cambridge University Press, Cambridge, United Kingdom and New York, NY, USA), 1535 p.

Hansen, J., R. Ruedy, M. Sato, and K. Lo (2010) Global surface temperature change, *Rev. Geophys*., **48**, RG4004.

Kato H. (1996) A statistical method for separating urban effect trends from observed temperature data and its application to Japanese temperature records, *J. Meteorol. Soc. Jap*. **74(5)**. p.639-653.

Kislov A.V. Konstantinov P.I. (2011) Detailed spatial modeling of the temperature of the Moscow metropolis, *Meteorology and Hydrology* **5**. P 25-32. (in Russian)

Landsberg H.E. (1970) Man-made climatic changes, *Science*. **170**. P.1264-1265.

Landsberg H.E. (1956) *The climate of towns. Man`s role in changing the face of the Earth* (University of Chicago Press). P.584-606.

Linevich N.L., Sorokina L.P. (1992) Climatic potential of self-purification of the atmosphere: the experience of multiscale assessment, *Geography and natural resources*. **4**. P.160-165. (in Russian)

Marchuk G.I., Penenko V.V., Aloyan A.E., Lazriev G.L. (1979) Numerical simulation of climate of the city, *Meteorology and Hydrology*. **8**. P.5-15. (in Russian)

Trofimova I.E., Konovalova T.I. (1988) Climatic and ecological state of the city and its surroundings // *Ecological problems of urban areas*. – Irkutsk. P.72-81. (in Russian)

Unintended effects on climate (1974) / Ed. M.I. Budyko. (L .: Gidrometeoizdat) 260 p. (in Russian)

MUD VOLCANOES AND THEIR IMPACT TO LAND AND ATMOSPHERE (EXAMPLE OF TAMAN PENNINSULA, RUSSIA)

G. WOSKOBOINIKOVA[1] and S. VENEVSKY[2]

[1]Institute of Computational Mathematics and Geophysics, Novosibirsk, Russia

[2]Centre for Earth System Studies, Tsinghua University, Beijing, China
E-mail: venevsky@tsinghua.edu.cn

Mud volcanoes are well known example of natural release of greenhouse gases. However, direct measurements of methane emissions and land and pollution by debris from these volcanoes are scarce and highly depend on inner dynamics of volcanoes which is hard to study. The structure of mud volcanoes is complicated: they are non-homgenous, often include angular or rock clasts of various lithological types derived from walls of conduits (conduits may be deep up to 15 km) trough which gas-liquid mixture flows. Eruptions may be violent or slow, which is determined by their inner structure.. So study of recent and potential dynamics of inner structure, related eruptions and ecological consequences of eruptions can be rather challenging and complicated. Network of seismic vibrators (seismic vibrators CB -10/100 and registering complexes RefTek -125) was used for study of mud volcanoes at Taman Peninsula, Russia (one of the world largest mud volcanoes field) with case studies Karabetova Gora and Shuro. Mathematical and software tools for interpretation of waves dynamics recorded during vibration experiments at mud volcanoes was developed. 3-D structure of mud volcanoes was simulated and estimates of methane emissions to the atmosphere and fluxes of debris to land and sea were obtained.

A CONSISTENT AEROSOL OPTICAL DEPTH (AOD) DATASET OVER CHINA BY INTEGRATING OF VARIOUS AOD PRODUCTS

Y. XUE[1, 2], Y. H. CHE[1, 3], H. XU[1, 3], J. GUANG[1] and X. HE[1, 3]

[1]Key Laboratory of Digital Earth Sciences, Institute of Remote Sensing and Digital Earth, Chinese Academy of Sciences, No. 9 Dengzhuang South Road, Haidian District, Beijing 100094, China

[2]Faculty of Life Sciences and Computing, London Metropolitan University, 166–220 Holloway Road, London N78 DB, UK

[3]University of Chinese Academy of Sciences, Beijing 100049, China

Keywords: Merging, Aerosol Optical Depth, MODIS, MISR, SeaWiFS, Albedo

The Moderate Resolution Imaging Spectroradiometer (MODIS), the Multiangle Imaging Spectroradiometer (MISR) and the Sea-viewing Wide Field-of-view Sensor (SeaWiFS) provide validated aerosol optical depth (AOD) products over both land and ocean. However, the values of the AOD provided by each of these satellites may show spatial and temporal differences due to the instrument characteristics and aerosol retrieval algorithms used for each instrument. In this article we present a method to produce an AOD data set over Asia for the year 2007 based on fusion of the data provided by different instruments and/or algorithms. First, the bias of each satellite-derived AOD product was calculated by comparison with ground-based AOD data derived from the AErosol RObotic NETwork (AERONET) for different values of the surface albedo and the AOD. Then, these multiple AOD products were combined using the maximum likelihood estimate (MLE) method using weights derived from the root mean square associated with the accuracies of the original AOD products. The merged AOD dataset has been validated by comparison with AOD data from the China Aerosol Remote Sensing NETwork (CARSNET). Results show that the merged AOD dataset has high overall accuracy (RMSE (root mean square error) = 0.19). By only considering the common AOD estimates with MODIS-DT, MODIS-DB and MODIS SRAP AOD data, the merged AOD estimates are closer to the reference field than any of these individual data sets in terms of correlation coefficient, root-mean-square (RMS) and the ratio of the standard deviation.

ASSESSMENT OF CLIMATE DRIVEN DYNAMICS OF ACTIVE LAYER, HYDROLOGICAL AND VEGETATION STATUS IN HEILONGJIANG PROVINCE, NORTHERN CHINA USING DYNAMIC GLOBAL VEGETATION MODEL

Y. YANG and S. VENEVSKY

Tsinghua University, China
862253013@qq.com
venevsky@tsinghua.edu.cn

Extensive permafrost degradation starting from 1970s is observed near Heilongjiang (Amur) River, Northern China. Degradation is attributed to an increase in mean annual ground temperature 0.1◦-0.5◦ C with mainly winter warming. Permafrost degradation caused negative environmental consequences in the area for infrastructure. The general pathway of future joint dynamics of permafrost, vegetation and hydrological status in Northern China is still poorly understood and foreseeable. Hydrology in the area is determined by heat-moisture dynamics of active layer. This dynamics is highly non-linear and depends as on external climatic variables temperature and precipitation, so on soil and rock properties (amount of sand against aeolian deposits in the Plateau) as well as vegetation cover, which determine thaw and freeze processes in the active layer and evaporation and run-off.

Global vegetation model SEVER DGVM was modified to include heat-moisture dynamics of active layer in the Heilongjiang province. SEVER DGVM is state of the art process oriented global vegetation model that imitates processes in 10 plant functional types (which represents plants from tropical to boreal area) in grid cells at coarse resolution of 0.5 degrees. This model imitates behavior of average individual of each plant type in each grid cell through simulation years. Each of those grid cells processed independently and not influences each other. First this model start from “bare soil”, place a bit of each plant type and gives them some time to grow and achieve equilibrium (of plant parameters and vegetation distribution), after this main simulation performed.

Inclusion of active layer thickness and soil moisture dynamics in this layer allowed assessment of potential environmental dynamics in Heilongjiang province.

THE SOUTH TUNDRA LANDSCAPE STRUCTURE MAP BASED ON REMOTE SENSING DATA AND FIELD SURVEY

E.A. Zarov

UNESCO chair "Environmental dynamics and global climate change", Yugra state university
Khanty-Mansiysk, KhMAO-Yugra, Russia.

Keywords: tundra, landscape structure, permafrost.

INTRODUCTION

It is well-known about high peatland abundance in Western Siberia. Dozens of papers have been devoted to issue of peat recourses assessment by Geoltorfrazvedka (Soviet peat-research department). Peatlands play an important ecosystem role and participate to substances cycle.
Around 29 % of tundra zone of Western Siberia are peatland occupied [Romanova, 1985]. A lot of scientific works exist in a field of carbon storage in the West Siberian peatland including a south tundra zone [Kremenetski et al, 2003; Sheng et al, 2004; Zimov et al, 2006; Peregon et al, 2008]. There are several works about greenhouse gases emission from tundra landscapes [Sabrekov et al, 2011; Sabrekov et al, 2011]. There are the works about a vegetation and soil interactions [Peteel, 1998; Tedrow, 1960] and general article about a tundra knowledegs [Karen, 2007]. In spit on high scientific interest to this biom there is almost nothing about tundra landscape structure.

METHODS

The study area is located in the south tundra (67.43457 N, 78.6146 E), around 35 km south-east from Tazovskiy, on the Pur-Taz watershed (right Lukyiaha-river terrace). The territory is characterized by extension of polygonal mires combined with grass and grass-mosses mires [Romanova, 1977]. It is a zone of continuous permafrost [Tedrow, 1960] and all landscapes are caused to this factor. There are average temperatures of July is 13-14°C, of January - 26 to – -28°C. Annual temperature is 8.5°C. The frost-free period is about 75 days. Annual precipitation is till 500 mm, and combination with low temperatures resulting to relatively humid climate which cause the wide wetland extension and permafrost appearance [Peteel, 1998].

The aim of this study is to investigate the south-tundra zone key area and describe the landscape structure on a base of remote sensing data and fieldwork survey. It has been organized 2 expeditions to a key area to collect landscape descriptions and provide a verification of prepared map in June 2013 and July 2014.
For preliminary assessment the territory was used a LandSat-5 image. It was accepted a 4-5-3 band combination to distinguish the different classes. It gave the possibility to divide all area for 9 general classes by expert assessment (Table 1).

Afterward a supervised classification in module GRASS (smap method, accuracy by Kappa-statistic=81.11 %) integrated into QGIS software was produced (Figure 1). For classification was used a smap method [Bouman, 1992; McCauley, 1995]. For accuracy assessment was chosen a Kappa-statistic method [Congalton, 1983] and observed correctness was 81.11 (based on 180 control points).
It was decided 5 visiting points for each class to clarify the real landscape elements. There were measured the pH and mineralization (expressed by electroconductivity (EC), μSm), ground water and thawed layer depths, soil description and location of class in a general landscape structure.
On a base of filed work it was prepared a description of all classes. And on a base of classified map it was calculated a coverage of key area for each class (Table 1).

№	Class	Colour on LandSat-5 (4-5-3 band combination)	Coverage of key area, %
1	Water	deep-black	4.79
2	Hasyrey* (1st type)	deep-orange	3.77
3	Hasyrey* (2nd type)	pink-white	4.67
4	Yernik**	orange	21.14
5	Dry- lichen land	green	44.83
6	Polygon-patterned wetland	faded green	13.27
7	Wet-sedge	light-green	1.82
8	Thaw (1st type)	white	2.00
9	Thaw (2nd type)	faded blue	3.72

Table 1. Detected classes on the LandSat-5 satellite image

* - pour out lake by thermokarst processes

** - dwarf shrubs thicket

Class 1 – Water

This class is usually presented by thermokarst-created lakes. Sometimes it is the flooded site at the beginning of brooks. Water has the lowest for the key area acidity and low mineralization (pH=5.391, EC=17 μSm).

Class 2 - Hasyrey* (1st type)

Pour out lake with developed permafrost landscape. Relief depressions are occupied by small ponds (till 15 %). There are the hypnum and brown mosses, sedge, cotton-grass and dwarf birch growing on palsas. Upper soil layer is composed by thin peat deposits (usually till permafrost layer). Seasonally thawed layer extends to a depth of 38 cm. Ground water is weak acidic and medium mineralized (pH=5.360, EC=58 μSm), and lies on a depth 13-20 cm. Sometimes similar structure appears in a middle of brook stream. This is due to a water access and active permafrost processes.

Class 3 - Hasyrey* (2nd type)

Newly created pour out lake. It is formed in a lake basin. Active permafrost processes has only initial stage that expressed in appearing of small (till 30-40 cm) palsas. Palsas are occupied by brown and hypnum mosses and sedges. In hollows are dominated the hollow brown mosses. Thin peat deposit (30-35 cm) is formed on a mineral ground. Area has a high humidity level with weak acidic and low mineralized (pH=4.1, EC=22.5 μSm) water.

Class 4 - Yernik

This is the shrubby areas presented by tall (till 1.2 m height) *Duschekia* and *Betula nana* (90 %) with green mosses and lichens. Usually it occurs on the mineral slopes with good derange and thin peat layer (15 cm). Water doesn't appear on a surface. The thawed layer is 45 cm.

Class 5 - Dry-lichen land

This is lichen tundra on mineral soils. This class is timed to well-drained elevation in relief. Soils are the gley loam and thixotropic clay. There are often occurring the swelling clays. Seasonally thawed layer extends more 60 cm. Ground water doesn't appear on surface and all soil moisture is in capillary state. The lichens are dominated in a surface cover (till 95 %). The hillocks occupy 15-20 % with hypnum, brown mosses, *Salix, B. nana, Vaccínium myrtíllus* and sedges growing on it.

Class 6 - Polygon-patterned wetland

This class is presented by typical for region polygon-patterned wetlands. Usually it occurs in a water flow zone and beginning of brooks. It gives a good water inflow and lets to form this type of relief. Polygons have a length since 8 to 18 m. The thawed layer extends to 24 cm. There is no ground water. Surface is hillocky (hills have a hight 20-40 cm and occupy 40-45 % of area). The flat areas covered by *Ledum*

palustre, *Rubus hamomorus* and *B.nana*, on the hillocks the lichen and mosses grow. Polygons are separated by thermo-cracks and that zones are occupied by hollow vegetation (brown mosses and sedges). There is a thawed layer extends deeper on a polygon (till 35 cm) and ground water has a weak acidity and medium mineralization (EC=43 µSm) and lies on 4 cm depth. Sometimes the part of the polygons degrades, disappears and combines to hollows.

Class 7 - Wet-sedge
This is a zone of heightened wetting which occupies the lowest sites of thermocarst origin. Vegetation cover is presented by mosses which covered almost 95-100 % of area except when open water appears (till 5 %). Sedges occupy till 65 % of area. Ground water stays on 10 cm depth, a frozen layer is on 39 cm. Ground water has a weak acidity and low mineralization (pH=4.5, EC=14 µSm). Area consists a thin peat deposit (35-40 cm) lying on a mineral ground.

Class 8 - Thaw (1st type)
This is a wet zone conjugated polygonal wetlands. There are the rest of thawed polygon structures spread around this class. It tells about a polygonal wetland degradation process and smooth transformation 6th class to 8th class. Thawed depth is 23 cm, and water has a weak acidity and low mineralization (pH=4.2, EC=20 µSm). Vegetation is presented by brown mosses (till 100 %), sedges and cotton-grass (90 %). Sometimes there are the shrubs (*Salix, B.nana*) appear on a local hills (10-15 cm). Soil is formed by peat till the frozen layer.

Class 9 - Thaw (2st type)
This class is different from 8th class because water flow. There is a water runoff appear there which supply the brooks. Water appears on surface and has pH=4.07, EC=16. Plant diversity is poorer and presents by brown mosses and sedges. There is the small hillocks (30-35 cm) compose 35 % of area and occupied by sedges (60 %) and Andromeda (15 %). The thawed layer extends to 38 cm.

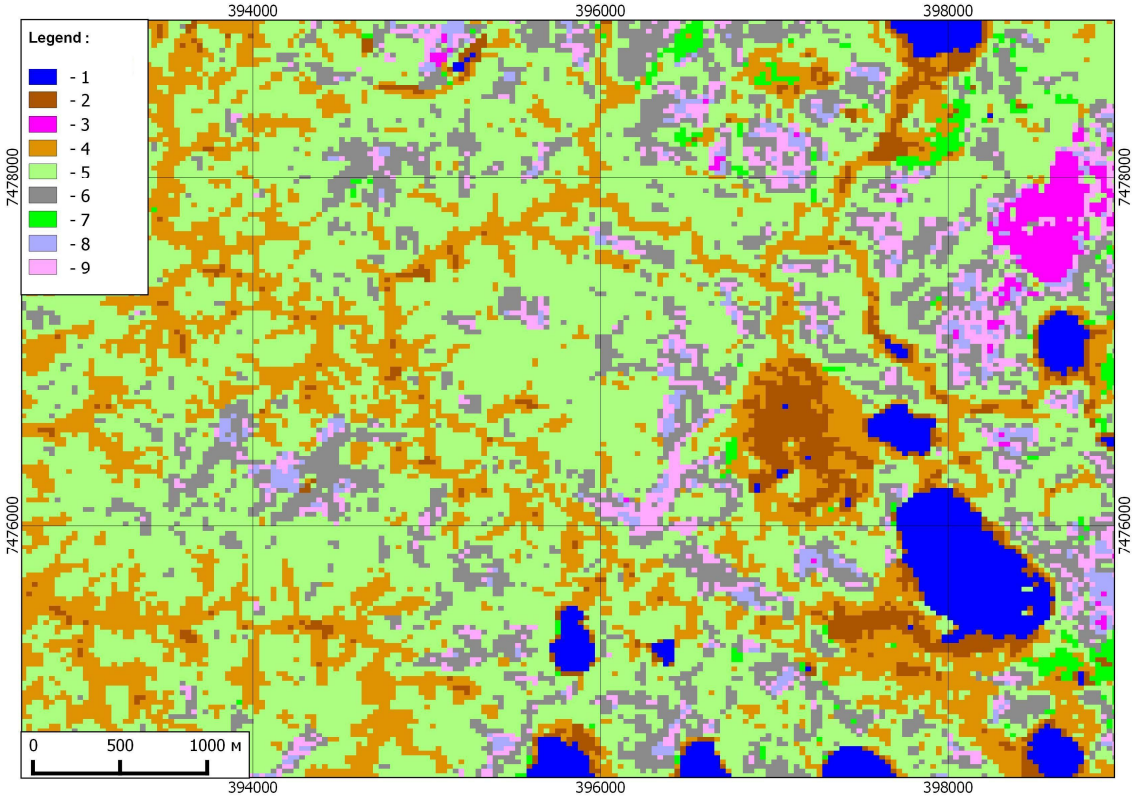

Figure 1. Classified map of key area. (Description of a legend in the text)

CONCLUSIONS

In this way, we have investigated a key area located in south tundra zone, within Pur-Taz watershed. The territory was subdivided for 9 different classes based on the results of expert assessment of satellite image and field survey. First-step criteria were chosen an image spectral brightness. Second-step criteria were description of each class during a fieldwork. There were measured the pH and EC, ground water and thawed layer depths, soil and botanical description and location of a class in general landscape structure. Result analysis based on listed parameters had proved the differences of chosen classes and gave preliminary material for constructing the model of landscape structure understanding of south-tundra key area.

ACKNOWLEDGEMENTS

This work was supported by the Russian fond of fundamental researches under grant 14-05-00193A and 14-05-91764 АФ_а.

REFERENCES

Bouman, Ch., Shapiro, M. (1992). Multispectral Image Segmentation using a Multiscale Model, *Acoustics, Speech, and Signal Processing* **3**, 565 – 568, ICASSP-92.

Congalton, R. G., Oderwald, R. G., and Mead, R. A. (1983). Assessing Landsat classification accuracy using discrete multivariate statistical techniques, Photogramm. *Eng. Remote Sens*. **49**(12):1671-1678.

Karen E. F., Smith, L.C. (2007). How well do we know northern land cover? Comparison of four global vegetation and wetland products with a new ground-truth database for West Siberia, *Global biogeochemical cycles* **21**, GB1016, doi:10.1029/2006GB002706

Kremenetski, K.V., Velichko, A.A., Borisova, O.K., MacDonald, G.M., Smith, L.C., Frey, K.E., Orlova, L.A., (2003). Peatlands of the Western Siberian lowlands: current knowledge on zonation, carbon content and late Quaternary history. *Quaternary Science Reviews* **22**, 703-723.

McCauley, J.D., Engel, B.A. (1995). Comparison of Scene Segmentations: SMAP, ECHO and Maximum Likelyhood. *Geoscience and remote sensing* **33**, no.6, 1313 - 1316

Peregon A., Maksyutov S., Kosykh N., Mironycheva-Tokareva N. (2008). Map-based inventory of wetland biomass and net primary production in western Siberia, *Journal of Geophysical Research* **113**, G011007. DOI:10.1029/2007JG000441.

Peteel, D., Andreev, A,, Bardeen, W. & Mistretta, F. (1998). Long-term Arctic peatland dynamics, vegetation and climate history of the Pur-Taz region, Western Siberia. *Boreus*, **27**, pp. 115- 126. Oslo. ISSN 0300-9483.

Romanova E.A., R.T. Bybina, E.F. Golitsyna, G.M. Ivanova, L.I. Usova, and L.G. Trushnikova (1977), Tipologicheskaya karta bolot Zapadno-Sibirskoi ravniny [Typological map of wetlands of West Siberian Lowland], GUGK, Leningrad, Scale 1:2,500,000.

Romanova, E.A., Wetland vegetation (1985). *Vegetation cover of West-Siberian flat*, (Novosibirsk: Nauka, Russia), (in Russian).

Sabrekov, A.F., Glagolev M.V., Kleptsova I.E., Maksyutov S.S. (2011). CH_4 emission from West Siberia tundra mires, *Environmental dynamics and global climate change* **2**, № 1(3), (in Russian).

Sabrekov, A.F., Glagolev M.V., Kleptsova I.E., Bashkin V.N., Barsukov P.A., Maksyutov S.S. (2011). Contribution of palsa to methane emission from west Siberian tundra wetlands, *Environmental dynamics and global climate change* **2**, № 2(4), (in Russian).

Sheng, Y., Laurence C. Smith, Glen M. MacDonald, Kremenetski, K.V., Frey, K.E. Velichko, A.A., Lee M., Beilman, D.W., Dubinin P. (2004). A high-resolution GIS-based inventory of the west Siberian peat carbon pool, *Global biogeochemical cycles* **18**, GB3004, doi:10.1029/2003GB002190

Tedrow, J. C. F., Harries, H. (1960). Tundra Soil in Relation to Vegetation, Permafrost and Glaciation, *Oikos* **11**, Fasc. 2, pp. 237-249

Zimov, S.A., Schuur, E.A.G., Chapin, F.S. (2006). Permafrost and the Global Carbon Budget, *Science* **312**, no. 5780 pp. 1612-1613 DOI: 10.1126/science.1128908

ON A POSSIBILITY TO IMPROVE OUR OBSERVATIONAL KNOWLEDGE ABOUT MESOSCALE AND SUB-MESOSCALE PROCESSES IN THE PEEX AREA

ZAYTSEVA N.A.

Department of Earth Sciences, Russian Academy of Sciences, ninaz@ras.ru

As shown in the circular letter, the 5th PEEX Meeting will address, among other important goals, "to coherent, coordinated Pan-Eurasian *in-situ* observation network including satellite observations and coordinated data systems". And this fully corresponds to the main goal of this interdisciplinary program i.e. to receive new data and findings for better understanding of the climate changes and consequences for Nature and Human society. Important point here is new materials of observations performed on either regular basis or in framework of special subprograms for specially organized complex field campaigns.

Atmospheric processes have different scales: global, continental, regional which are large-scale ones and we may recognize that our knowledge about these processes is rather adequate to general characteristics and variability of them on our planet. But, at the same time, we should agree that understanding of nature of mesoscale and, especially, sub-mesoscale atmospheric phenomena is still quite insufficient, however the low atmosphere where these phenomena take place is exactly our environment.

Long-term observations at standard observational network together with many field experiments had brought us great volume of data, results of analysis, and general understanding of the large-scale processes on the planet as the whole and in some specific regions like polar ones. It will suffice to mention the big international experiment of the last time – International Polar Year 2007-2008. And it would be rather reasonable if the PEEX could organize a special program of joint mesoscale observations at a wide observational network on territories of countries participating in the Experiment.

As concerns Russian institutes of the Russian Academy of Sciences (now they belong to new governmental unit – Federal Agency of Scientific Organizations but their scientific work is performed under the RAS methodical guidance), those working in the field of the Earth sciences have field bases or branches which are usually located at certain distances from an institute so that to observe an environment in its natural state, i.e. being not impacted by human activities. According to our analysis total number of such bases is about 65-68 ones. The latitudinal zone covered by stations extends from 33 to 71 degrees of the North, and the longitudinal one does from 24 to 170 degrees of the East. So, they can create a good network over the area under the PEEX interest. Some of them are very well instrumented for detailed observations of interaction between ecosystems and environment. Other countries-participants have similar bases too. They are able to present possibilities to organize simultaneous and highly coordinated observations on the ground and in some special cases the ground observations can be combined with measurements in the low troposphere using aircraft laboratories, etc. Data that can be obtained at this network will result in not only quite new knowledge about mesoscale and microscale processes in forests of boreal zone, in steppe and tundra zones, but will present new important data for perfecting already existing and for constructing new models of interaction between the surface and ecosystems within the atmospheric boundary layer/

More detailed analysis of possible observational programs will be presented in the report.

THE VERTICAL DISTRIBUTION OF DUST AEROSOL AND ITS SOURCE ANALYSIS IN BEIJING UNDER THE INFLUENCE OF DUST STORM

JIAHUA ZHANG[1], MEI DENG[2,1], FENGMEI YAO[3,1], HUADONG GUO[1]

[1] Lab. of Digital Earth Sciences, Institute of Remote Sensing and Digital Earth, Chinese Academy of Sciences, Beijing 100094,China.
[2] School of Resources and Environment, Anhui Agricultural University, Hefei 230036, China
[3] University of Chinese Academy Sciences, Beijing, 100049, China.

Keywords: Dust aerosol, CALIPSO, Depolarization ratio, Color ratio, Beijing region

INTRODUCTION

Dust aerosol can cause visibility impairment and pollution index increased in a region, and mix other contaminants to produce air quality hazards such as haze phenomena. During the transmission process, dust aerosol also make the atmospheric optical thickness (AOT) increase significantly, impact the atmospheric environment, and even cause international transportation (Forster *et al.*, 2007). Dust is an important source of aerosols, which could directly affect the radiation balance of earth and atmosphere by scattering, reflecting and absorbing solar radiation and other effects of the radiation, and through heating or cooling the entire earth-atmosphere system, thus influencing the whole climate change. In recent years, satellite data has been used to study the regional distribution of dust aerosols, the vertical profile on single point retrieved from AVHRR, MODIS, MIRS, and TOMS, has already made great progress. The Cloud-Aerosol Lidar and Infrared Pathfinder Satellite Observations (CALIPSO) mission was launched successfully in April 2006 (Winker *et al.*, 2007) and provided valuable information on detecting dust aerosols, and helps to clarify climatic role and radiative effects of dust aerosols on a global scale. Liu *et al*. (2008) used CALIPSO data to analyze optical properties of dust aerosols in a typical case of Saharan dust transmitted over a long-range. Huang *et al*. (2008) studied the long-distance transport and vertical structure of Asian dust during the Pacific Dust Experiment with CALIPSO data. This study adopted the CALIPSO satellite data on the analysis of vertical distribution of dust aerosols in Beijing under the influence of a dust storm via Xinjiang, Gansu, Inner Mongolia and other places on 8-11 March 2013. Moreover, the Backward trajectory analysis model (i.e., HYSPLIT) and global aerosol model (i.e., NAAPS) were used to track and simulate the transmission pathways of the dust storm.

METHOD

CALIPSO satellite data

The CALIPSO payload consists of the Cloud-Aerosol Lidar with Orthogonal Polarization (CALIOP), a two-wavelength polarization sensitive lidar, the Infrared Imaging Radiometer (IIR), which has three channels in the thermal infrared, and the Wide Field Camera (WFC) with a single channel at 650 nm. CALIOP provides global, vertically-resolved measurements of aerosol spatial distributions and aerosol

extinction coefficients, and an ability to perform height-resolved discrimination of aerosol into several types (Winker *et al*., 2006). After the calibration and distance correction, the return signal can be described as (Hostetler *et al*., 2006):

$$RCS_{\lambda}(z) = P_{\lambda}(z)z^2 / C_{\lambda} = \beta(z)T^2(z) = [\beta_{m,\lambda}(z) + \beta_{a,\lambda}(z)]\exp\{-2\int_0^z[\sigma_{m,\lambda}(z) + \sigma_{a,\lambda}(z)]dz\} \quad (1)$$

where $\beta_{m,\lambda}(z)$, $\sigma_{m,\lambda}(z)$, $\beta_{a,\lambda}(z)$ and $\sigma_{a,\lambda}(z)$ are the backscatter and extinction coefficients for the molecular and aerosols at the wavelength λ and altitude z, respectively .Echo signal from the laser distance atmosphere. $P_{\lambda}(z)$ is the backscatter signal at the wavelength λ from the altitude *z*. Besides, C_{λ} is the calibration constant. The range scaled, energy and gain normalized profiles for the 532 nm parallel, 532 nm perpendicular, and 1064 nm channels are defined, respectively, as follows:

$$\beta_{ABStot532} = \beta_{//} + \beta_{\perp} \quad T^2{}_{532(Z)} \quad (2)$$

$$\beta_{ABS\perp,532} = \beta_{\perp} T^2{}_{532(Z)} \quad (3)$$

$$\beta_{ABS,1064} = \beta_{1064} T^2{}_{1064(Z)} \quad (4)$$

Where $\beta_{//}$, $\beta_{\perp}$ and β_{1064} are the original scattering data of 532 nm parallel and perpendicular and channel 1064 nm respectively . T^2 is two-way atmospheric transmittance.

Depolarization ratio is the attenuated backscatter coefficient ratio of 532 nm perpendicular and parallel channel, reflecting the degree of irregular particles being measured, the greater value indicates more irregular particles; attenuation lidar color ratio (referred to as the color ratio) is the ratio of total attenuated scattering coefficient of the channel 1064 nm and 532 nm, reflecting the size of the particle measured, the higher number indicates larger particle size.

2.2 HYSPLIT model

The NOAA HYSPLIT (Hybrid-Single Particle Lagrangian Integrated Trajectory) model is the particle trajectory, diffusion and sedimentation integrated model system, can be used to calculate and analyze the transport and dispersion of air pollutants trajectory. This model has a deal with a variety of meteorological elements input field, a variety of physical processes and functions of different types transport, diffusion and deposition model of pollutant emission sources, adopting the global reanalysis data of the U.S. National Centers for Environmental Prediction (NCEP) and the National Center for Atmospheric Research (NCAR), with the horizontal resolution of $2.5^{\circ} \times 2.5^{\circ}$, and a total of 17 vertical layers from the ground to 10hPa height.

2.3 Aerosol model

In this study, NAAPS (Navy Aerosol Analysis and Prediction System) global aerosol model used is a modified form of that developed by Christensen (1997). The version uses global meteorological fields from the Navy Operational Global Atmospheric Prediction System (NOGAPS) to analyze and forecast the global spatial distribution of tropospheric aerosols on a 1 × 1 degree grid, at 6-hour intervals and 24 vertical levels (Maciszewska et al., 2010).

CONCLUSIONS

In this paper, the CALIPSO satellite data was used to analyze the vertical distribution of dust aerosol of Beijing which caused by a dust storm on 8-11 March 2013, and adopted the HYSPLIT model and the NAAPS to simulate the dust source and transmission process. The results showed that: (1) The

stratification, composition, distribution of the atmosphere and the height of each component can be visually illustrated in the spatial distribution of attenuated backscatter coefficient, depolarization ratio and color ratio and the other parameters detected by CALIPSO data. The distribution height of dust aerosols which belongs to the low-level aerosols in Beijing was lifted from 3 km to about 4 km due to the impact of rising air during the transmission process. The depolarization ratio of the dust aerosol is 0.1 - 0.4, and the color ratio is greater than 0.3. (2) The transmission path and process of the dust aerosol indicated that there were two sources of dust in this region, i.e., the southern Xinjiang basin, Midwest of Inner Mongolia. The dust transmitted in both east and south directions. (3) During the dust transmission, the main pollutant converted from PM2.5 formation of haze to the dust PM10.

However, the distribution of aerosols will decrease with the increase of altitude, and the corresponding space parameter such as attenuated backscatter coefficient, depolarization ratio and color ratio will also change. Therefore, further research is needed to determine the threshold at different heights.

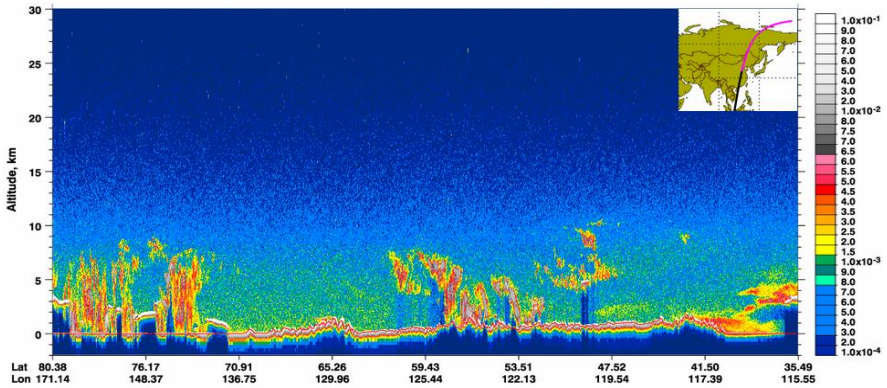

（a）532nm Total attenuated backscatter coefficient($km^{-1}\cdot sr^{-1}$)

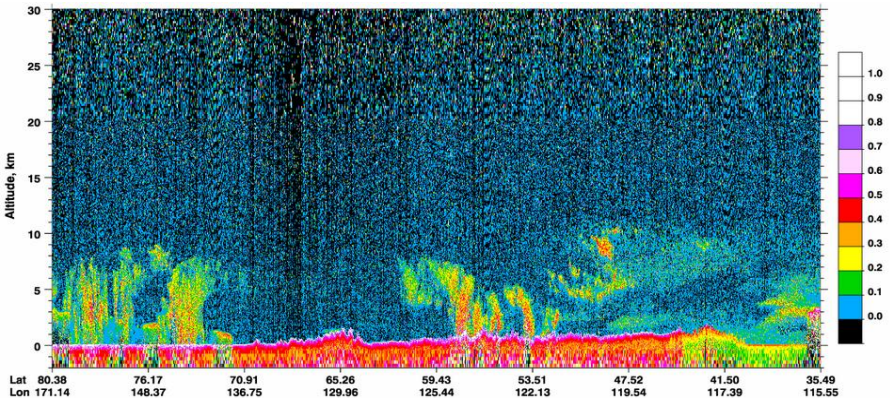

（b）Depolarization ratio

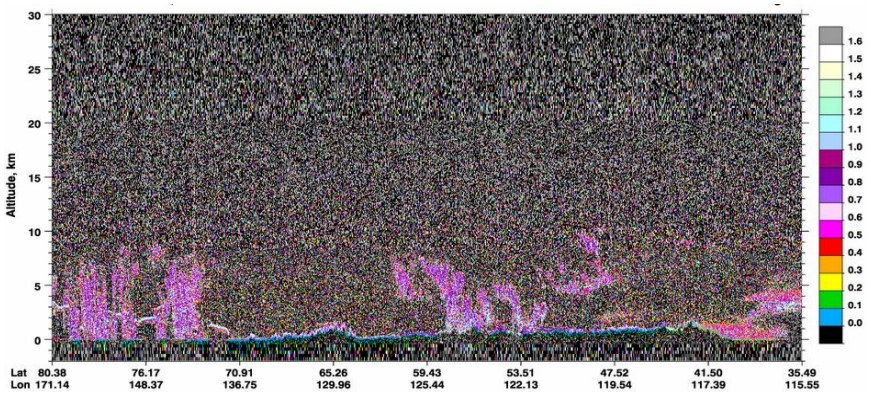

（c）Color ratio

Fig.1Total attenuated backscatter coefficient ($km^{-1}\cdot sr^{-1}$), polarization ratio and color ratio in the CALIPSO 532 nm channel in the rage of（35.5° N，115.5° E）～（80.4° N,171.2° E）between 18:12:34～18:26:03 in 10 March, 2013.

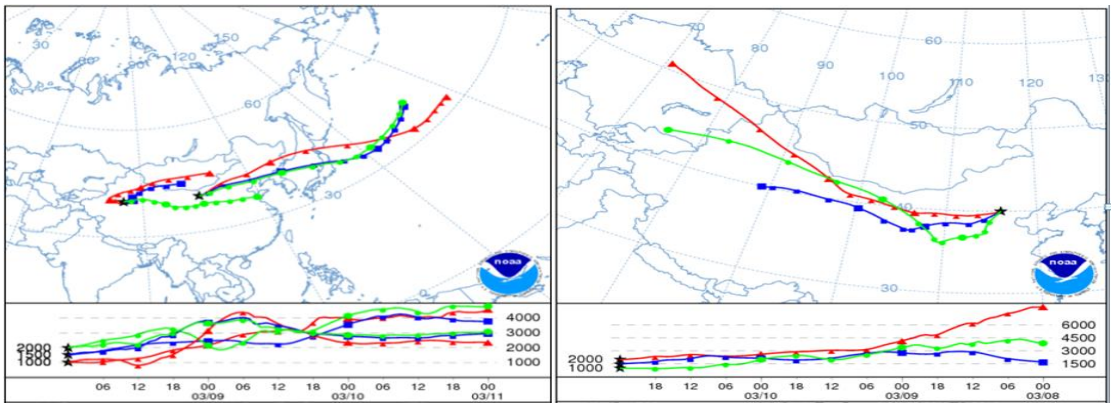

（a）Forward trajectory of source areas （b）Backward trajectory of Beijing area

Fig.2 Forward trajectory of source areas and backward trajectory of Beijing area with HYSPLIT model.

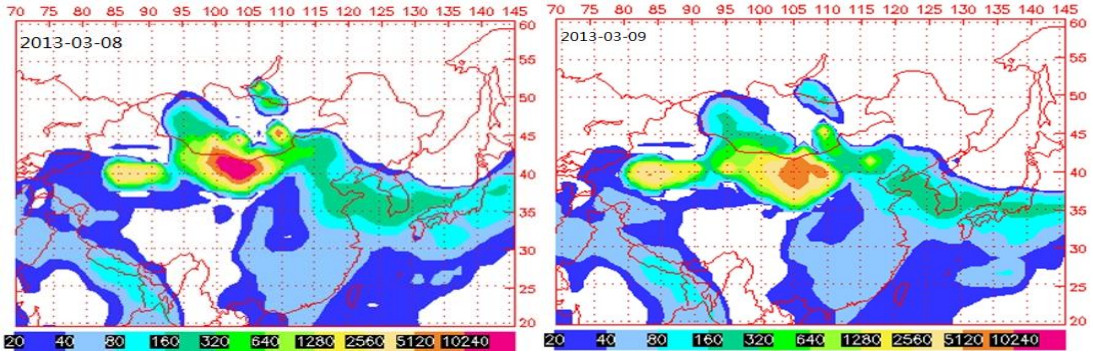

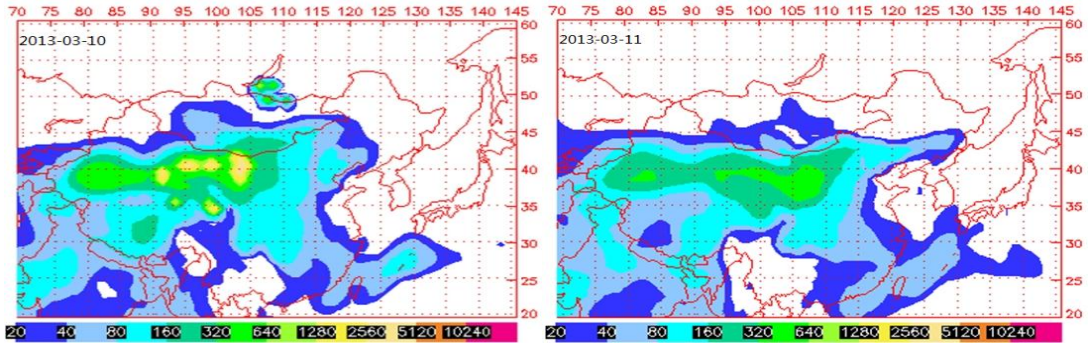

Fig.3. Spatial distribution of dust concentration（$mg \cdot m^{-3}$）from March 8 to 11, 2013 simulated using the Navy Aerosol Analysis and Prediction System (NAAPS) model

ACKNOWLEDGEMENTS

This study was supported by 100 Talent Program of Chinese Academy of Sciences (No.Y24002101A), the 1-3-5 Innovation Project of RADI_CAS (No. Y3ZZ15101A), the RADI Program (No.Y2EE26101B, No.Y1ZZ12101B), and CAS-TWAS Project for Drought Monitoring and Assessment (No. Y3YI2701KB), We would like thank the NASA Langley ASDC for distribution of CALIPSO data (http://eosweb.larc.nasa.gov), the NOAA Air Resources Laboratory (ARL) for the provision of the HYSPLIT transport and dispersion, and the Naval Research Laboratory for the NAAPS model.

REFERENCES

Christensen, J. H. (1997). The Danish eulerian hemispheric model—A threedimensional air pollution model used for the Arctic. *Atmos. Environ.*, **31**,4169 – 4191.

Hostetler, C. A., Liu, Z., Reagan, J., et al. (2006) CALIOP Algorithm Theoretical Basis Document–Part 1: Calibration and Level 1 Data Products. Doc. PC-SCI, 201.

Huang, J., Minnis, P., Chen, B., et al.(2008). Long-range transport and vertical structure of Asian dust from CALIPSO and surface measurements during PACDEX. *Journal of Geophysical Research* **113**, D23212.

Liu, Z., Omar, A., Vaughan, M., et al. (2008). CALIPSO lidar observations of the optical properties of Saharan dust: A case study of long‐range transport. *Journal of Geophysical Research* **113**, D07207.

Maciszewska, A. E., Markowicz, K. M.and Witek, M. L. (2010), A multiyear analysis of aerosol optical thickness over Europe and Central Poland using NAAPS model simulation. *Acta Geophysica* **58**(6): 1147-1163.

Winker, D.M., Pelon, J. and McCormick, M. (2006). Initial results from CALIPSO[C]//Reviewed and Revised Papers Presented at the 23rd International Laser Radar Conference. *Tokyo Metropolitan Univ.* 991-994.

Winker, D. M., Hunt, W. H. and McGill. M. J. (2007) Initial performance assessment of CALIOP. *Geophysical Research Letters*, **34**, L19803.

MODELLING NEW PARTICLE FORMATION AND GROWTH IN PLANETARY BOUNDARY LAYER

L. ZHOU[1, 2], R. GIENRES[1], A. RUSANEN[1], D. MOGENSEN[1], A. SOGACHEV[3], J. ORTEGA[4], P. C. HARLEY[4], A. TURNIPSEED[4], S. SMOLANDER[1], J. N. SMITH[4, 5], A. B. GUENTHER[6], M. KULMALA[1], T. KARL[7] and M. BOY[1]

[1]Department of Physics, University of Helsinki, P.O. Box 48, Helsinki, Finland,
[2]Helsinki University Centre of Environment, Helsinki, Finland
[3]Department of Wind Energy, Technical University of Denmark, Frederiksborgvej 399, P.O. Box 49, Building 118, 4000, Roskilde, Denmark
[4]National Center for Atmospheric Research, Boulder, Colorado, USA
[5]Department of Applied Physics, University of Eastern Finland, 70211 Kuopio, Finland
[6]Atmospheric Sciences and Global Change Division, Pacific Northwest National Laboratory, Richland, Washington, USA
[7]University of Innsbruck, Institute for Meteorology and Geophysics (IMGI), Innrain 52, 6020 Innsbruck, Austria

Keywords: boundary modelling, new particle formation

INTRODUCTION

Natural and anthropogenic aerosols may have a great impact on climate as they can directly interact with solar radiation and indirectly affect the Earth's radiation balance and precipitation by modifying clouds. In order to quantify the direct and indirect effect, it is essential to understand the complex processes that connect an aerosol particle to a cloud droplet. However, while modern measurement techniques are able to detect particle sizes down to nanometer all the way from ground up to the stratosphere, the data does not serve for all of our needs for understanding the processes. Hence we will demonstrate a modeling approach to investigate the complex processes of aerosols in the planetary boundary layer (PBL).

METHODS

SOSAA (model to Simulate the concentration of Organic vapors, Sulfuric Acid, and Aerosols) is a 1D chemical-transport model with detailed aerosol dynamics and two emission modules. It was constructed to study the emissions, transport, chemistry, as well as aerosol dynamic processes in the PBL in and above a canopy (Boy *et al*., 2011; Zhou *et al.*, 2014).

The SOSAA model was used to study the particle formation and growth in two different ecosystems. One is a boreal forest environment with occasional anthropogenic influence. The SMEAR II station at the boreal forest site has one of the longest data sets of land-atmosphere exchange observations, which includes particle number size distributions. Another site, Manitou Experimental Forest observatory (MEFO), is a mountainous site at Colorado Front Range, which is under is periodic anthropogenic influences.

CONCLUSIONS

The modeling activities at the two sites showed that SOSAA model is a good tool for studying various atmospheric processes including SOA formation. The large fraction of partly correct simulation days at SMEAR II station suggests that both kinetic and organic nucleation parameterizations are not suitable for all period. The growth studies at MEFO in western US revealed the compounds contributing for particle growth are related to MBO or the compounds responsible for the growth should have similar diurnal

pattern and concentration level as the oxidation products of MBO. While the growth of particles can be a crucial step linking atmospheric trace gases to cloud formation, it is crucial to gain more insight to particle growth.

ACKNOWLEDGEMENTS

We would like to thank the NCAR Advanced Study Program, Helsinki University Centre of Environment, and Academy of Finland Centre of Excellence program ACCC (Atmospheric Composition and Climate Change) and the Nordic Centers of Excellence CRAICC for their generous financial support. We would like to acknowledge NCAR BEACHON project for data sharing.

REFERENCES

Boy, M., A. Sogachev, J. Lauros, L. Zhou, A. Guenther, and S. Smolander (2011). SOSA – a new model to simulate the concentrations of organic vapours and sulphuric acid inside the ABL - Part1: Model description and initial evaluation, *Atmos. Chem. Phys.* 11, 43 - 51.

Zhou, L., T. Nieminen, D. Mogensen, S. Smolander, A. Rusanen, M. Kulmala and M. Boy (2014). SOSAA – a new model to simulate the concentrations of organic vapours, sulphuric acid and aerosols inside the ABL – Part 2: Aerosol dynamics and one case study at a boreal forest site, *Boreal Environ. Res.* 19, 237-256.

STABLY STRATIFIED PLANETARY BOUNDARY LAYERS: NATURE, THEORY AND ROLE IN ATMOSPHERE-LAND SYSTEMS

S. ZILITINKEVICH[1,2]

[1]Finnish Meteorological Institute, Helsinki, Finland

[2]Department of Physics, Division of Atmospheric Sciences, University of Helsinki, Finland

Historically, theoretical analysis of stably stratified atmospheric planetary boundary layers (PBLs) was limited to the nocturnal stable (NS) PBL typical of the night time over land at mid latitudes, where most meteorological observations were carried out. The NS PBL develops after sunset on the background of comparatively deep "residual layer". The latter remains at least weakly mixed during a few night hours due to residual motions originated by both velocity shear and turbulent convection in the strongly mixed day-time PBL. Such motions decay only gradually and maintain almost neutral stratification in the residual layer. The basic mechanism suppressing turbulence in the NS PBL is stable stratification in the lower part of the layer caused by radiative cooling of the land surface and characterised by the near-surface turbulent flux of buoyancy F_{bs} and the friction velocity u_*, which determine the Obukhov length-scale $L = -u_*^3 / F_{bs}$.

This scheme does not hold true in the high-latitudinal PBL typical of winter-time over both land and ocean. In this PBL, persistent stable or neutral stratification often continues during day and night. Hence, no residual layer develops, and the PBL directly interacts with strongly stable stratification sustained in the free troposphere by counteractions of general circulation, turbulent mixing and radiative heat transfer. Essential stratification in such long-lived stable (LS) PBL is maintained by its interaction with both Earth surface and free flow. Typical values of the Brunt-Väisälä frequency $N \sim 10^{-2}$ s^{-1} and baroclinic shear $S = \partial U / \partial z \sim 10^{-3}$ s^{-1} in the free troposphere correspond to the Richardson number $Ri = (N/S)^2 \sim 10^2$, which implies extremely strong static stability. For comparison, maximal values of Ri in the atmospheric surface layer practically never exceed 0.25. It is not surprising that LS and NS PBLs dramatically differ from one another. For example, LS PBLs are several times shallower, which makes it very sensitive to external impacts, such as global warming, land-use changes, air pollution, etc. This sensitivity is an important factor of the high vulnerability of the Arctic and sub-Arctic environment (Zilitinkevich and Esau, 2009).

LS PBLs have been identified and subjected to theoretical and experimental studies only recently (first publication dates 2002). They are still poorly reproduced in meteorological, air-quality and climate modelling. State of the art models, except recently developed Energy- and Flux-Budget (EFB) turbulence closure theory (2013), essentially overestimate the height of LS PBLs. In this paper we summarise our knowledge about nature, theory and parameterization of stable PBLs and outline prospects for realistic representation of LS PBLS in studies of atmosphere-land systems.

ACKNOWLEDGEMENTS

This work has been supported by the Academy of Finland project Atmosphere-hydrosphere interaction in the Baltic Basin and Arctic Seas (ABBA, 2014-2017); Russian Mega-grant "Interaction of the Atmosphere, Hydrosphere and Land Surface" (Contract No. 11.G34.31.0048); and Russian Federal Program "Research and development on priority directions of development of scientific-technological infrastructure of Russia for 2014-2020" (Contract No. 14.578.21.0033).

REFERENCES

Zilitinkevich S., 2002: Third-order transport due to internal waves and non-local turbulence in the stably stratified surface layer. *Quart, J. Roy. Met. Soc*. **128**, 913-925.

Zilitinkevich S., Baklanov, A., Rost, J., Smedman, A.-S., Lykosov, V., Calanca, P., 2002: Diagnostic and prognostic equations for the depth of the stably stratified Ekman boundary layer. *Quart, J. Roy. Met. Soc*., **128**, 25-46.

Zilitinkevich S.S., Perov, V.L., King, J.C., 2002: Near-surface turbulent fluxes in stable stratification: calculation techniques for use in general circulation models. *Quart, J. Roy. Met. Soc*. **128**, 1571-1587.

Zilitinkevich S.S., and Esau, I.N., 2002: On integral measures of the neutral, barotropic planetary boundary layers. *Boundary-Layer Meteorol*. **104**, 371-379.

Zilitinkevich S.S., Baklanov, A., 2002: Calculation of the height of stable boundary layers in practical applications. *Boundary-Layer Meteorol.* **105**, 389-409.

Zilitinkevich S.S., Esau I.N., 2003: The effect of baroclinicity on the depth of neutral and stable planetary boundary layers. *Quart, J. Roy. Met. Soc*. **129**, 3339-3356.

Zilitinkevich S.S., Esau I.N., 2005: Resistance and heat/mass transfer laws for neutral and stable planetary boundary layers: old theory advanced and re-evaluated. *Quart. J. Roy. Met. Soc*. **131**, 1863-1892.

Zilitinkevich, S.S., and Esau, I.N., 2009: Planetary boundary layer feedbacks in climate system and triggering global warming in the night, in winter and at high latitudes. *Geography, Environment and Sustainability* **1**, No. 2, 20-34.

Zilitinkevich S., Esau, I., Baklanov, A., 2007: Further comments on the equilibrium height of neutral and stable planetary boundary layers. *Quart. J. Roy. Met. Soc.* **133**, 265-271.

Zilitinkevich S.S., 2012: The height of the atmospheric planetary boundary layer. – Chapter 13 in "*National Security and Human Health Implications of Climate Change*", edited by H.J.S. Fernando, Z. Klaić, J.L. McKulley, NATO Science for Peace and Security Series – C: Environmental Security (ISBN 978-94-007-2429-7), Springer, 147-161.